Ross Large.

Studies of VHMS-related alteration: geochemical and mineralogical vectors to ore

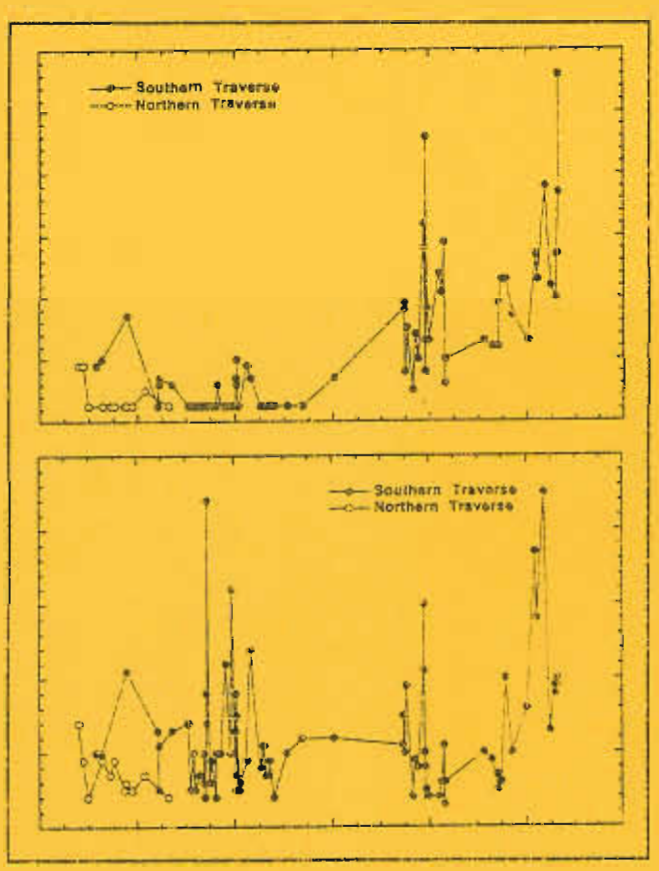

AMIRA/ARC project P439

Report 4
May 1997

Centre for Ore Deposit Research
University of Tasmania

Studies of VHMS-related alteration: geochemical and mineralogical vectors to ore

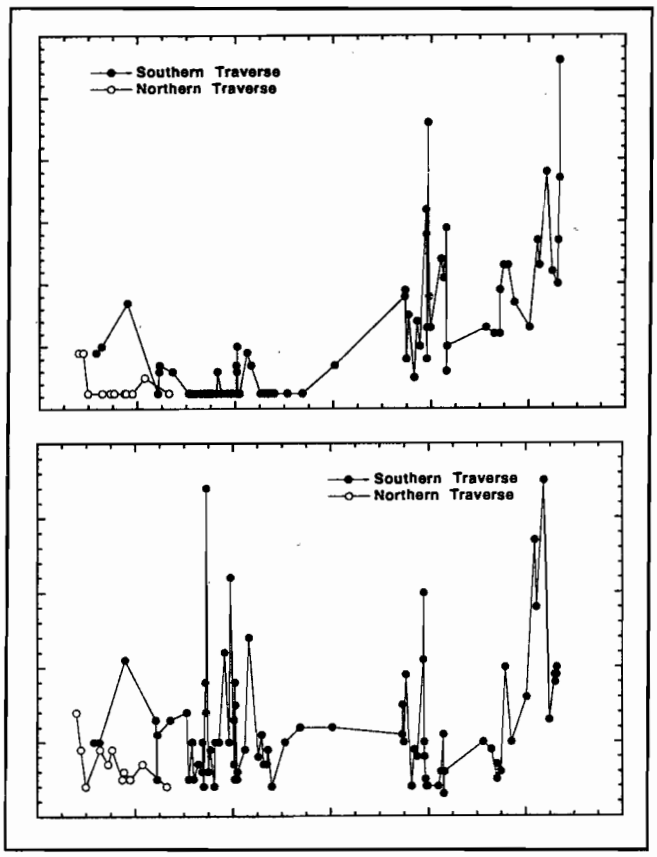

AMIRA/ARC project P439

Report 4
May 1997

Centre for Ore Deposit Research
University of Tasmania

Centre for Ore Deposit Research,
Geology Department,
University of Tasmania,
GPO Box 252-79,
Hobart, Tasmania,
Australia

http://www.geol.utas.edu.au/codes

another Pongratz Production 1997

Contents

Introduction v

Petrographic and geochemical characteristics of alteration from the Macintosh Dam–Anthony Road–Mt Black traverse, Mt Read Volcanic Belt
Joe Stolz, Rod Allen, Cathryn Gifkins, Jocelyn McPhie and Michael Blake 1

MRV geochemical database update
Michael D. Blake 27

Surface lithochemical responses of known VHMS deposits based on the MRV geochemical database
Ross R. Large and Michael D. Blake 93

Gossan Hill: relationship between mineralogy, alteration and geochemistry
Robina Sharpe 97

Volcanic facies analysis, alteration and geochemistry of the host rock sequence to VHMS-style mineralisation at Thalanga (north Queensland)
Holger Paulick 185

The alteration system of the Waterloo prospect, North Queensland
Thomas Monecke 223

Alteration associated with sub-seafloor replacement style massive sulfide deposits: evidence from the Cambro-Ordovician Highway–Reward deposit, Mount Windsor Subprovince
Mark G. Doyle 231

Preliminary report on the Rosebery lithochemical halo study
Ross Large and Rod Allen 259

Research program and preliminary results of alteration studies at the Western Tharsis deposit, Mt Lyell field
David L. Huston 331

Dobson Creek–White Spur area "step-out" traverses: preliminary report
Rod Allen, Jocelyn McPhie, Cathryn Gifkins and Michael Blake 343

Aims and Progress

Introduction

Volcanic-hosted massive sulphide deposits (VHMS) provide a significant contribution to the total zinc, copper, lead, silver and gold production in Australia and continue to be a major target for most base metal explorers. However, due to the geological complexity of ancient submarine volcanic terrains, new VHMS deposits are becoming extremely difficult to discover, especially deposits that are buried more than a few tens of metres below the surface. To complement the conventional multidisciplinary approach utilising geology, geophysics and geochemistry, a new attack to the problem is proposed here which involves the integration of volcanic facies analysis with alteration geochemical and mineral chemical studies to develop a set of vectors to guide explorers toward ore-grade mineralisation. The research has been concentrating on three productive submarine volcanic belts in Australia: the Mt. Read Volcanics (MRV) in western Tasmania, the Mt. Windsor Volcanics (MWV) in northern Queensland, and the Archean Murchison volcanic province in western Australia.

Project objectives

1. To characterise the mineralogy and geochemistry for the various styles of hydrothermal alteration throughout the Mount Read Volcanics (MRV) and the Mount Windsor Volcanics (MWV). This will be based on mapping supported by whole-rock and trace element geochemistry, mineral chemistry, REE and stable isotope geochemistry.

2. To determine the relationship between geochemical alteration patterns and sub-volcanic intrusions that are coeval with VHMS formation.

3. To undertake case studies of alteration halos related to specific VHMS deposits with particular emphasis on hangingwall alteration, and the relationship between alteration patterns and volcanic facies.

4. To develop a set of vectors towards ore, based on the regional studies and ore deposit specific studies, that can be applied in the exploration for VHMS deposits in submarine volcanic sequences throughout Australia. The vector matrix will include whole-rock, trace element, mineral chemistry, REE, isotope and volcanic facies factors.

Research framework

As there has been considerable research on alteration mineralogy and geochemistry of VHMS systems, our research is not to repeat previous work but will utilise a multi-disciplinary approach at both the regional volcanic belt scale and ore deposit scale, with emphasis on selective geochemical techniques.

This report

This is the fourth progress report on the project and covers the six-month period from November 1996 to May 1997. Very good progress has been achieved in to date.

Volcanic Facies and Regional Geochemistry/ Petrology Modules

- Joe Stolz reports on the alteration mineralogy and geochemistry of the Mt Black traverse.
- Jocelyn McPhie discusses the additional Mt Read traverses.
- Michael Blake gives an update on the Mt Read geochemical database.
- Joe Stolz summarises the regional alteration studies

Mineralisation and Alteration Module

- Robina Sharpe describes the volcaniclastic host rocks, alteration assemblages and geochemistry at the Gossan Hill deposit, WA.
- Holger Paulick discusses volcanic facies, alteration mineralogy and geochemistry at the Thalanga deposit, Qld.
- Thomas Monecke describes the alteration associated with the Waterloo prospect, Qld.
- Mark Doyle provides an update on the alteration research geochemistry at the Highway Reward deposit, QLD.
- Ross Large reports on the work he and Rod Allen are doing on petrology and geochemistry at Rosebery.
- Bruce Gemmell summarises the new findings from the deposit studies.

Important data and interpretations continue to emerge from this project which will have implications for exploration. Progress throughout of the project has been very encouraging and I would like to acknowledge the excellent work by the CODES research team and the cooperation provided by the sponsor companies.

Ross Large
Director

Petrographic and geochemical characteristics of alteration from the Macintosh Dam–Anthony Road–Mt Black traverse, Mt Read Volcanic Belt

Joe Stolz, Rod Allen, Cathryn Gifkins, Jocelyn McPhie and Michael Blake
Centre for Ore Deposit Research, Geology Department, University of Tasmania

Summary

Petrographic and geochemical studies of the samples from the Macintosh Dam–Anthony Road–Mt Black traverse indicate that albitisation and K-feldspar alteration resulting from diagenetic effects are relatively uncommon in the predominantly coherent rhyolite and dacite units of the Mt Black and Sterling Valley Volcanics. These styles of alteration produce distinctive chemical characteristics which are readily distinguishable from the more important and restricted hydrothermal alteration which produces the assemblage sericite ± pyrite ± chlorite. The chemical and mineralogical characteristics of the granitoid-related K-feldspar ± magnetite ± chlorite alteration in the Murchison Granite and Murchison Volcanics are also documented and discussed. The petrographic and geochemical studies on the samples from this traverse confirm the variety of alteration styles and timing relationships distinguished in the Hall Rivulet–Mt Read–Red Hills–Selina traverse.

Introduction

One of the principal objectives of undertaking the regional traverses in the Mt Read Volcanic belt was to characterise the 'background' alteration effects in the volcanics, i.e. those attributable to processes other than mineralising hydrothermal convection cells and to characterise their geochemical signature. These processes may include immediate post-depositional effects related to devitrification of glass, diagenetic modification by interaction with low-temperature seawater and rock-buffered fluids, as well as subsequent regional metamorphism and igneous intrusion-related effects.

Approximately 46 samples were collected along the Macintosh Dam–Anthony Road–Mt Black traverse (Fig. 1) during January 1996 and these have been examined petrographically and analysed for major elements and a wide range of trace elements. The results and interpretation of these data are presented in this report which supplements the report by Gifkins (1996) on the volcanology, geochemistry and alteration characteristics of the Mt Black Volcanics. Sampling of the Mt Black Volcanics and Sterling Valley Volcanics (principally from the Murchison Highway) was supplemented with material collected by Catherine Gifkins in the course of her PhD studies.

Lithofacies variation

Descriptions of field observations, principal lithofacies and field logs for this traverse were provided by Gifkins et al. (1996). The traverse was undertaken in four sections (Fig. 1) which encompassed the following important lithostratigraphic units of the Mt Read Volcanic Belt.

1. Macintosh Dam to Henty Fault: Murchison Granite and Murchison Volcanics (Tyndall Group).
2. Anthony Road: Murchison Volcanics.

3. Henty Fault to Rosebery along Murchison Highway: Sterling Valley Volcanics and Mt Black Volcanics, Central Volcanic Complex.
4. Mt Black summit to Rosebery : Mt Black Volcanics.

Murchison Granite

The Murchison Granite (MB96-1 to MB96-10 & MB96-12 to MB96-13b) is an important lithology in the eastern sector of the traverse where it has intruded the Murchison Volcanics or Eastern Quartz-phyric Sequence (Corbett, 1992). The Murchison Granite has been dated at 501 ± 5.7 Ma by Ar-Ar on hornblende (Perkins and Walshe, 1993). Despite moderate to strong hydrothermal alteration of the granite in the traverse area, preservation of the textural characteristics of the granite is reasonably good in most examples. The least altered examples of the granite (MB96-9, MB96-5) retain the interlocking igneous textures with subhedral alkali feldspar and plagioclase and anhedral quartz. Original hornblende and biotite have been completely replaced by aggregates of chlorite, magnetite and sphene. The biotite pseudomorphs have lamellae of Fe oxides parallel to the cleavage, whereas the hornblende pseudomorphs typically have aggregates of sphene oriented parallel to the cleavage. In these least altered examples the plagioclase displays weak to moderate replacement by sericite, whereas the K-feldspar displays only very minor clay alteration. With more intense sericite alteration of the feldspars (particularly the plagioclase), the textural integrity of the rock becomes progressively diminished.

Murchison Volcanics

The Murchison Volcanics from the Macintosh Dam Road (MB96-11 & MB96-14 to MB96-16) and Anthony Road (MB96-17 to MB96-34) sectors of the traverse (Fig. 2) are dominated by coherent rhyolitic lavas with subordinate volcaniclastic facies. The rhyolites are characterised by abundant resorbed quartz phenocrysts and subordinate K-feldspar and plagioclase phenocrysts in a fine grained quartz-feldspar-rich groundmass which is variably altered. The least altered examples display only weak sericite alteration of plagioclase phenocrysts and weak clay alteration of K-feldspar with minor chlorite and veinlets of sericite throughout the silicic groundmass.

Sterling Valley and Mt Black Volcanics

West of the Henty Fault, within the Central Volcanic Complex, rocks from the Mt Black and Sterling Valley areas (Fig. 3) vary from basalt to rhyolite in composition and include coherent lavas, sills and a range of volcaniclastic facies (Gifkins, 1996). The Sterling Valley Volcanics (M4, M6, M7, M9, M10) are dominantly basaltic to andesitic with subordinate dacites. The least altered basaltic rocks consist of relatively large, euhedral plagioclase phenocrysts, sometimes with euhedral clinopyroxene phenocrysts, in a finer groundmass of plagioclase laths with interstitial chlorite and sphene.

Coherent units in the Mt Black Volcanics are predominantly dacites, the least altered of which (e.g. MB96-35) consist of unaltered (or weakly sericitised) plagioclase phenocrysts in a recrystallised spherulitic groundmass composed of quartz, feldspar, minor chlorite, sphene, Fe oxides and sericite.

Styles of alteration

On the basis of the samples examined in the Hall Rivulet Canal–Mt Read–Red Hills–Selina traverse five major styles of alteration were distinguished (Stolz et al., 1996b):

1. Albite ± epidote ± sericite ± chlorite
2. K-feldspar
3. Carbonate
4. Sericite ± pyrite ± chlorite
5. K-feldspar ± magnetite ± chlorite

The first two alteration assemblages are characteristic of the regional alteration and, in general, appear to reflect very early diagenetic changes. Types 4 and 5 are hydrothermal alteration assemblages with type 5 specifically related to intrusive granitic magma bodies. The carbonate alteration (which is relatively minor in the regional traverse samples) may be largely

WESTERN TASMANIA

Mt Black Traverse

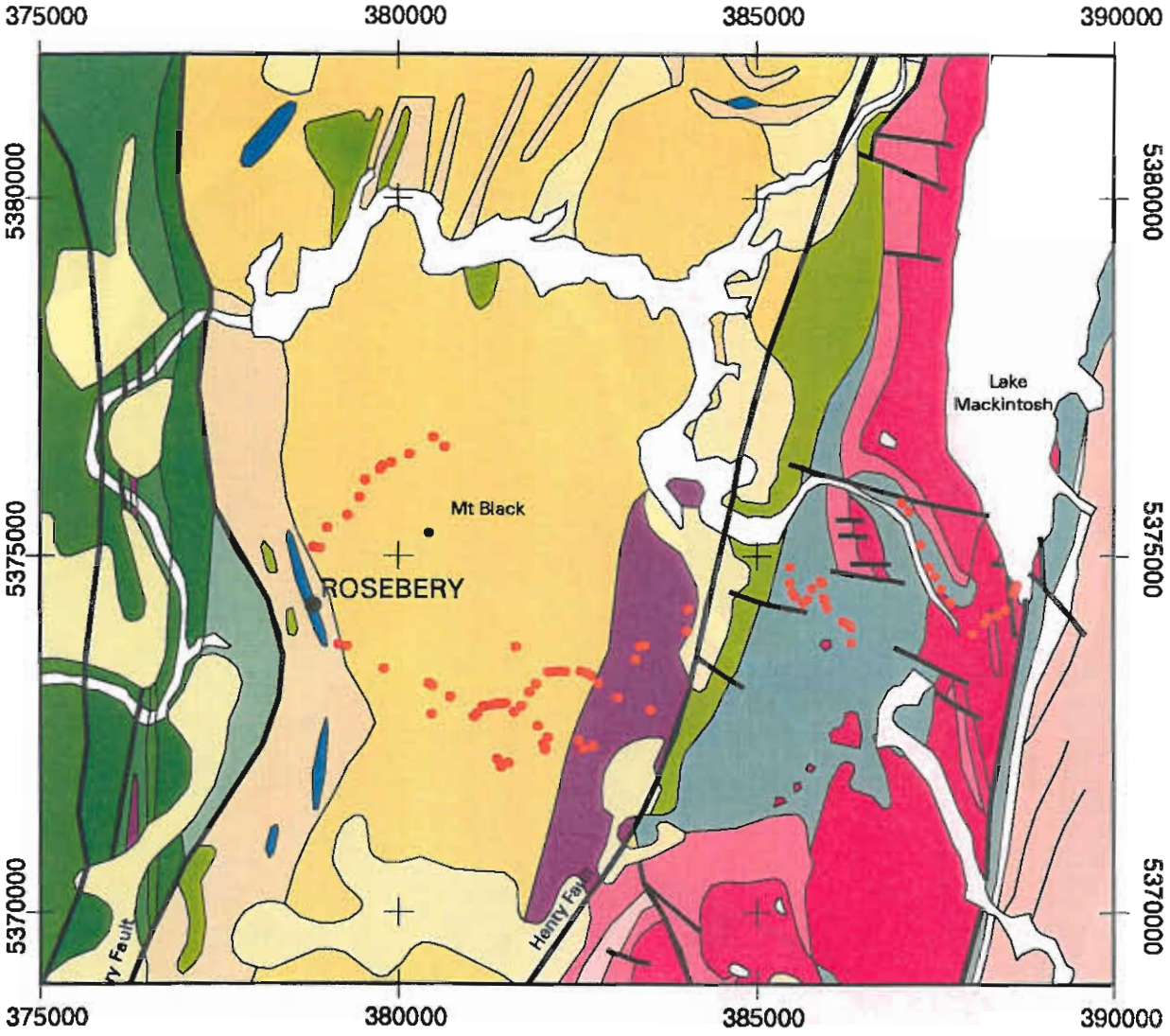

Owen Group
- QUATERNARY
- GRANITIC ROCKS
- INTERBEDDED SANDSTONE AND CONGLOMERATE
- VOLCANICLASTIC CONGLOMERATE, SANDSTONE, BRECCIA

Farrell Murchison Sequence
- FARRELL-MURCHISON SEQUENCE, SLATE, SANDSTONE AND TUFF
- FARRELL-MURCHISON SEQUENCE, FELSIC VOLCANICS

Central Volcanic Complex
- CENTRAL VOLCANIC COMPLEX
- CVC SHALE, SILTSTONE, SANDSTONE, MINOR TUFF
- ANDESITIC LAVAS, BRECCIAS, TUFFS AND INTRUSIVES
- FELSIC VOLCANICLASTICS

N

Scale: 1:100,000

0 1000 2000 3000 4000 5000

metres

WESTERN TASMANIA

Mt Read Traverse - Macintosh Dam Section

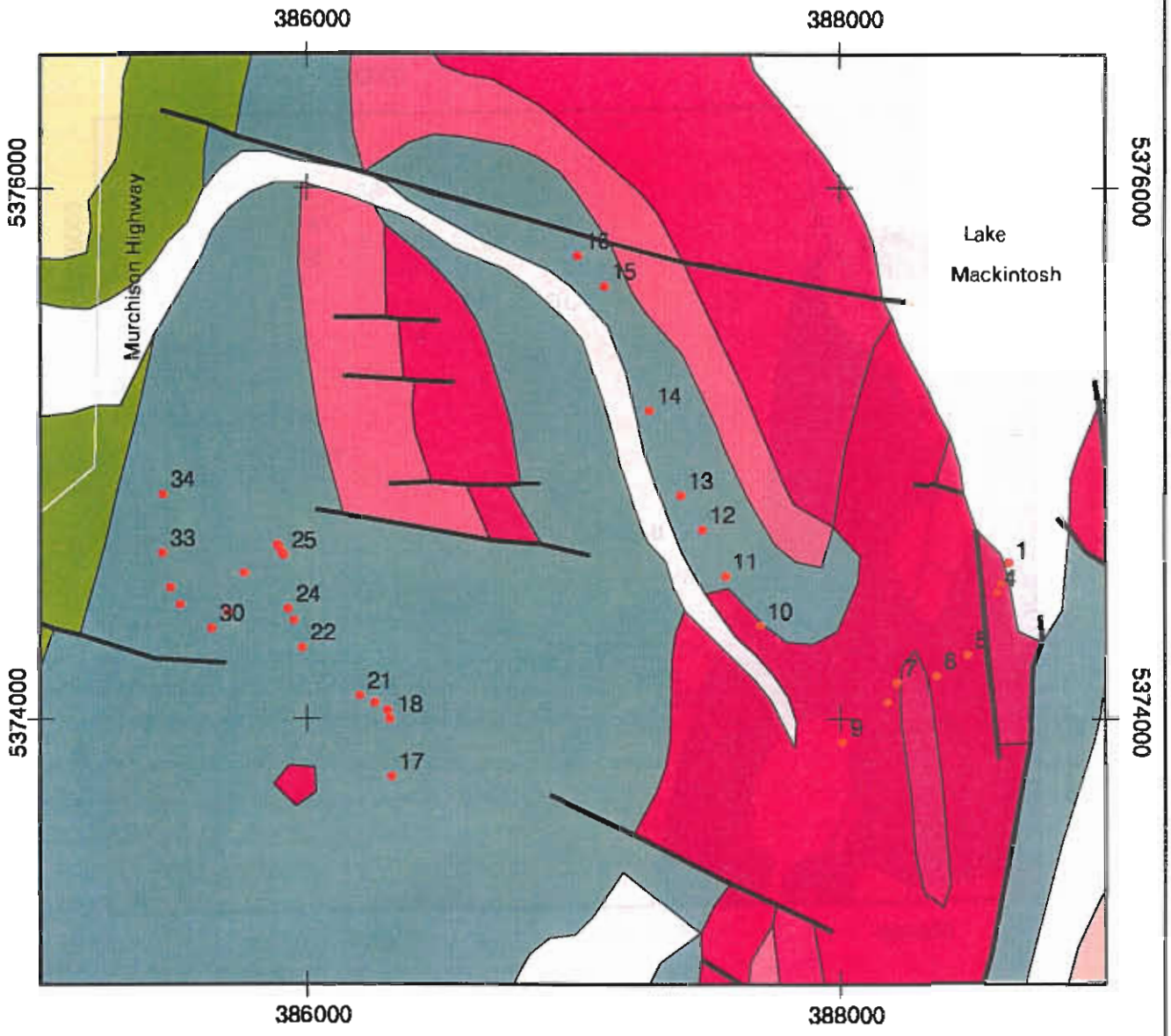

QUATERNARY

GRANITIC ROCKS

Owen Group
- INTERBEDDED SANDSTONE AND CONGLOMERATE
- VOLCANICLASTIC CONGLOMERATE, SANDSTONE, BRECCIA

Farrell Murchison Sequence
- FARRELL-MURCHISON SEQUENCE. SLATE, SANDSTONE AND TUFF
- FARRELL-MURCHISON SEQUENCE, FELSIC VOLCANICS

Central Volcanic Complex
- CENTRAL VOLCANIC COMPLEX
- CVC SHALE, SILTSTONE, SANDSTONE, MINOR TUFF
- ANDESITIC LAVAS, BRECCIAS, TUFFS AND INTRUSIVES
- FELSIC VOLCANICLASTICS

N

Scale: 1:25,000

0 200 400 600 800 1000

metres

WESTERN TASMANIA

Mt Black Volcanics

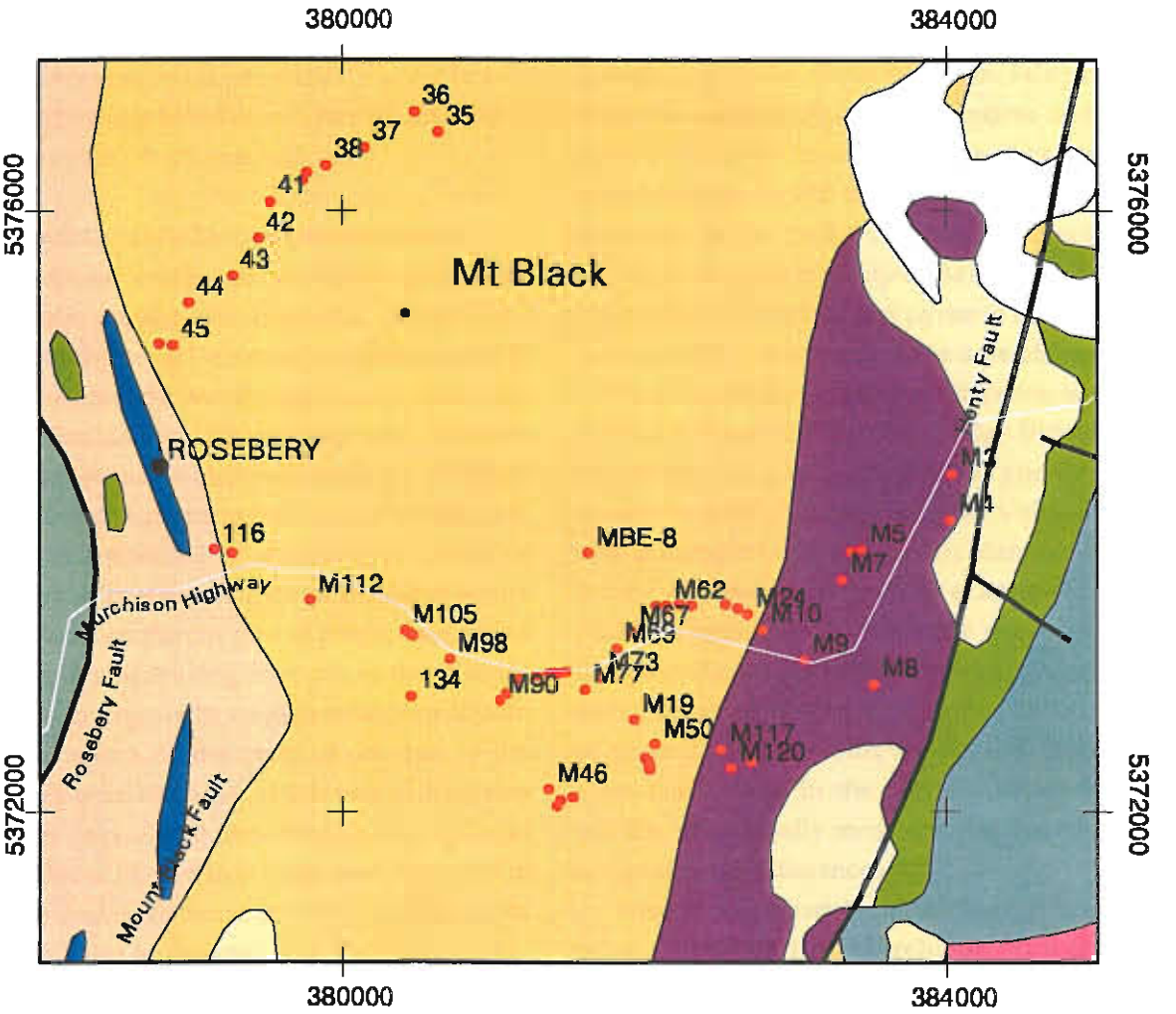

due to remobilisation of carbonate during the Devonian metamorphism.

The rocks from the Mt Black–Macintosh Dam traverse display broadly similar styles of alteration to those examined from the Hall Rivulet Canal–Mt Read–Red Hills–Selina traverse. The least altered samples (chemically and mineralogically) are dacitic to rhyolitic lavas and intrusives from the Mt Black Volcanics, whereas the most intensely altered rocks include parts of the Murchison Granite and several zones within the Murchison Volcanics.

Albite ±epidote ±sericite ±chlorite alteration

This assemblage, which was well developed in the volcaniclastic sandstones from the White Spur Formation and Central Volcanic Complex in the Hall Rivulet Canal traverse, is only occasionally developed in the predominantly coherent lava and intrusive dominated sequence which comprises the Mt Black Volcanics. In handspecimen this style of alteration is commonly characterised by a distinctive patchy or banded pink and green colouration. The albite occurs as overgrowths on the margins of plagioclase grains and as a replacement along fractures in the feldspar grains. These overgrowths are generally evident from the ragged nature of the margins, or due to the preferential partial alteration of the cores of the grains to sericite or clays. Albite also occurs in aggregates of decussate laths of varying grain size adjacent to plagioclase grains scattered through the matrix, or replacing pumice fragments.

K-feldspar alteration

This alteration style, which was recognised in the Hall Rivulet Canal rocks by high whole-rock K_2O/Na_2O values coupled with an obviously feldspar-rich assemblage, has been recognised in several samples (e.g. MB96-15, MB96-19 & MB96-25) from the Murchison Volcanics in this traverse. These rocks typically consist of abundant quartz phenocrysts with subordinate, relatively unaltered K-feldspar phenocrysts and weakly sericitised plagioclase phenocrysts in a fine groundmass of K-feldspar and quartz.

Sericite ±pyrite ±chlorite

This alteration type is commonly superimposed on the albite ± epidote ± sericite ± chlorite alteration and the diagenetic K-feldspar alteration and has gradational characteristics. It is typified by more extensive development of sericite initially in the matrix and also ultimately replacing the plagioclase crystals, whereas feldspar destruction is clearly not associated with the albitic alteration. Feldpar crystals may also become replaced by quartz in the more intensely altered examples. The development of sericite usually results in a significant cleavage being imparted to the rock. Chlorite is subordinate to sericite in the great majority of the samples displaying this style of alteration, and pyrite is also commonly only a minor component of the assemblage.

Weak to moderate sericite alteration is common in the Mt Black and Sterling Valley Volcanics. The sericite occurs replacing plagioclase phenocrysts and as veinlets through the groundmass. Volcanic breccias and pumiceous units typically display the most intense sericite alteration. The silicic rocks in these packages generally display only minor chlorite in the groundmass and as a replacement product of ferromagnesian phases, and pyrite is relatively rare or present in veins with quartz and chlorite. The more mafic units in the Sterling Valley Volcanics contain substantially more chlorite due to the bulk compositional differences.

Weak to strong sericite ± chlorite ± pyrite alteration occurs in both the Murchison Volcanics and Murchison Granite. In the volcanics the sericite commonly pseudomorphs plagioclase phenocrysts and occurs as veinlets throughout the groundmass which become more closely spaced and pervasive as the alteration becomes more intense. Similarly, in the granite samples, the least altered rocks display selective alteration of plagioclase and the K-feldspar remains unaffected. With increasing intensity, the plagioclase and K-feldspar become completely replaced by sericite and subsequent deformation has resulted in weak cleavage development that has largely destroyed the igneous textures.

Carbonate alteration

Weak, patchy, partial alteration of the albite-quartz-chlorite matrix and plagioclase grains is a relatively minor feature of the volcaniclastic and coherent silicic rocks from this traverse. Carbonate more commonly occurs in veins (associated with quartz) that appear to have been remobilised during the Devonian metamorphism.

K-feldspar ±magnetite ±chlorite alteration

This alteration style occurs at a number of localities within the MRVB including, Murchison Gorge (on this traverse), Red Hills and Lake Selina (on the Hall Rivulet Canal–Mt Read–Red Hills–Selina traverse), Mt Sedgwick, and the Jukes–Darwin area (Polya et al., 1986; Eastoe et al., 1987; Hunns, 1987; Doyle, 1990; Wyman, 1996; Stolz et al., 1996b).

The alteration associated with the Murchison Granite occurs extensively within the granite and the overlying volcanics, whereas at Red Hills and Selina only the altered overlying volcanics are readily available for examination. The well developed zonation at Red Hills involving an inner core of K-feldspar ± magnetite ± chlorite alteration surrounded by a zone of sericite ± pyrite ± chlorite alteration is not obviously developed within the granite, although such a zonation would be difficult to infer from a single traverse.

The K-feldspar alteration is characterised by an orange colour in handspecimen. In thin section the K-feldspar typically occurs as very fine grained aggregates that have pervasively replaced the rock. There may be some preservation of primary textures such as the outlines of feldspar phenocryts (now completely replaced by fine aggregates of K-feldspar) or original breccia textures. However, some of the latter may be hydrothermal breccias in which the chlorite-rich matrix alteration has overprinted the earlier K-feldspar alteration. There is widespread evidence in the K-feldspar altered rocks of retrogressive alteration of feldspar to sericite in veins that also commonly have chlorite and magnetite.

This style of alteration has only been confirmed in a few samples of this traverse from the Murchison Volcanics (e.g. MB96-27B & MB96-32). Samples of Murchison Granite that are characterised by a patchy pink and green alteration (e.g. MB96-10) have clearly experienced K addition when their compositions are compared with the least altered examples. Thin section examination showed that the K-feldspar in these rocks occurs both as large optically continuous, simply twinned crystals and as fine decussate aggregates pervasively replacing patches of feldspar and quartz. The incomplete replacement by K-feldspar presumably reflects relatively low water/rock values. Other granitoid samples (e.g. MB96-12) display stronger chlorite + sericite alteration which involves destruction of both feldspars.

Geochemistry

Major and trace element analyses for the samples from this traverse are presented in Table 1 (see p. 19). Details of the analytical methods and accuracy and precision of the data are provided by Stolz et al. (1996b). The geochemical data have been assessed with the objectives of:

- determining the chemical changes which characterise the different alteration types,
- distinguishing any differences in the intensity and styles of alteration in volcaniclastic and coherent rock types, and
- determining the distribution of the different alteration types along the traverse and how this relates to the geology.

Albite ± epidote ± sericite ±chlorite alteration

The most obvious chemical change associated with this alteration type is an increase in the Na_2O content above concentrations that would be regarded as the normal upper limit for unaltered modern volcanics of similar bulk composition. Petrographic evidence for albitic alteration has been noted in rhyolitic rocks with > 4.5 to 5 wt.% Na_2O and hence rocks with > 5 wt.% Na_2O have been generally designated as albite-altered. There are some samples with < 4.5 wt.% Na_2O that still display albite overgrowths on plagioclase grains but these rocks invariably exhibit substantial sericite alteration of their matrix which

has resulted in albite breakdown and some loss of Na_2O. The enrichment in Na_2O is reflected in low values for the Ishikawa (1983) Alteration Index (i.e. $100(MgO+K_2O)/(MgO+K_2O+Na_2O+CaO)$), and accompanied by substantial decreases in the K-group elements (K_2O, Rb, Cs, Ba; Figs. 4 & 5) compared with the least altered coherent rocks with similar SiO_2 contents and more normal Na_2O/K_2O values. Consistent with the observations from the Hall Rivulet Canal traverse (Stolz et al., 1996b) there is no significant enrichment in CO_2, S, Cu, Zn, Pb, As, Mo, Ag, Cd, Sb, Tl or Bi associated with the albitic alteration (Figs 4, 5). The Rb/Sr and K/Ba values for the albitised rocks are among the lowest for any of the rocks reflecting the stronger leaching of K_2O and Rb relative to Ba and Sr even though these elements have also been decreased compared with their original concentrations.

K-feldspar alteration

The samples from this traverse which display this style of alteration have the same chemical signature as similarly altered rocks from the Hall Rivulet Canal (Stolz et al., 1996b) and the Mt Windsor Volcanics (Stolz et al., 1996a). Typically these rocks have relatively high K_2O and very low Na_2O (<1%) resulting in high Alteration Indices (>90). They are also enriched in Ba, but generally have low concentrations of the chalcophile elements (e.g. Cu, Pb, Zn, Bi, As, Ag, Tl, Sb and Mo). An exception is MB96-19 (Table 1) which has moderately elevated concentrations of As, Sb, Tl and Pb that may be due to a weak overprinting sericitic alteration.

Sericite + pyrite ±chlorite alteration

As there is a wide range in the intensity of this alteration style among the samples from this traverse, the geochemical changes accordingly show substantial variation. The effects of this alteration style also appear to have been superimposed on the albitic alteration resulting in transitional chemical characteristics between the two groups. Alteration Index values for samples in which this style of alteration is significant range from about 55 to 99 (Figs 4, 5). The progressive increase in the Alteration Index accompanies depletion of CaO, Na_2O and Sr, and general enrichments in Cs, Sb, Tl, and higher Rb/Sr. In addition, there are sporadic enrichments in S, Cu, Pb, Zn, As, Mo, Ag, Cd and Bi in some of the sericite ± pyrite ± chlorite altered rocks. A few samples with high AI show a decrease in the Th/U value which appears to be an important indicator of strong hydrothermal alteration proximal to mineralisation (Stolz et al., 1996b; Large, 1996).

K-feldspar ±magnetite ±chlorite alteration

The chemical changes associated with this alteration style vary depending on the relative abundance of chlorite and K-feldspar. Strong enrichment in K_2O (up to 7.4 wt.%) reflecting K-feldspar-rich assemblages is generally accompanied by higher ΣFe as Fe_2O_3, Ba and Rb, and strong depletion of CaO, Na_2O resulting in high values for the Alteration Index (generally >90). These rocks generally have very low CO_2, S and loss on ignition, and concentrations of Pb, Zn, Bi, As, Ag, Cd, Mo, Tl and Sb that are only occasionally elevated above background values.

Sample MB96-27B is an exception being characterised by high concentrations of many of these elements. However, these elements may have been enriched in relatively late-stage quartz-chlorite-pyrite veins which cut this sample and the adjacent sericite-altered sample (MB96-27) which also has anomalous chemistry.

Variations in alteration chemistry along the traverse

As the traverses were undertaken in a broadly E–W orientation across the MRV belt, the geographical variability of the geochemical data has been evaluated by plotting the various elements as functions of easting (Figs 6–8). The data have been divided into two groups; one for the northern traverse which extends from near the top of Mt Black to the Mt Black Fault (Fig. 1), and the southern traverse which includes the remaining samples extending from the Macintosh Dam to the Henty Fault, and then to Rosebery along the Murchison Highway.

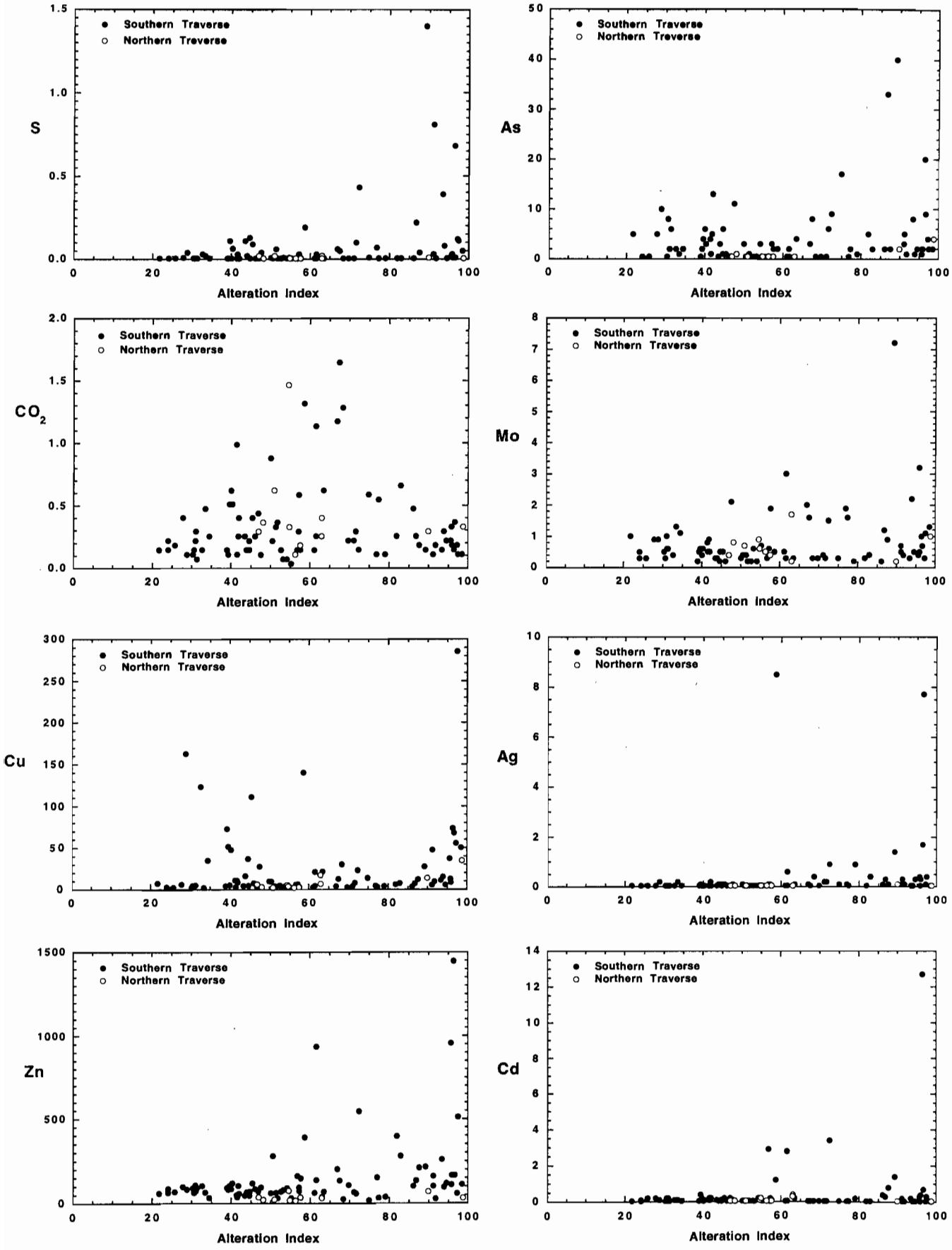

Figure 4. Variation of S, CO_2, Cu, Zn,As, Mo, Ag and Cd as functions of the Ishikawa Alteration Index.

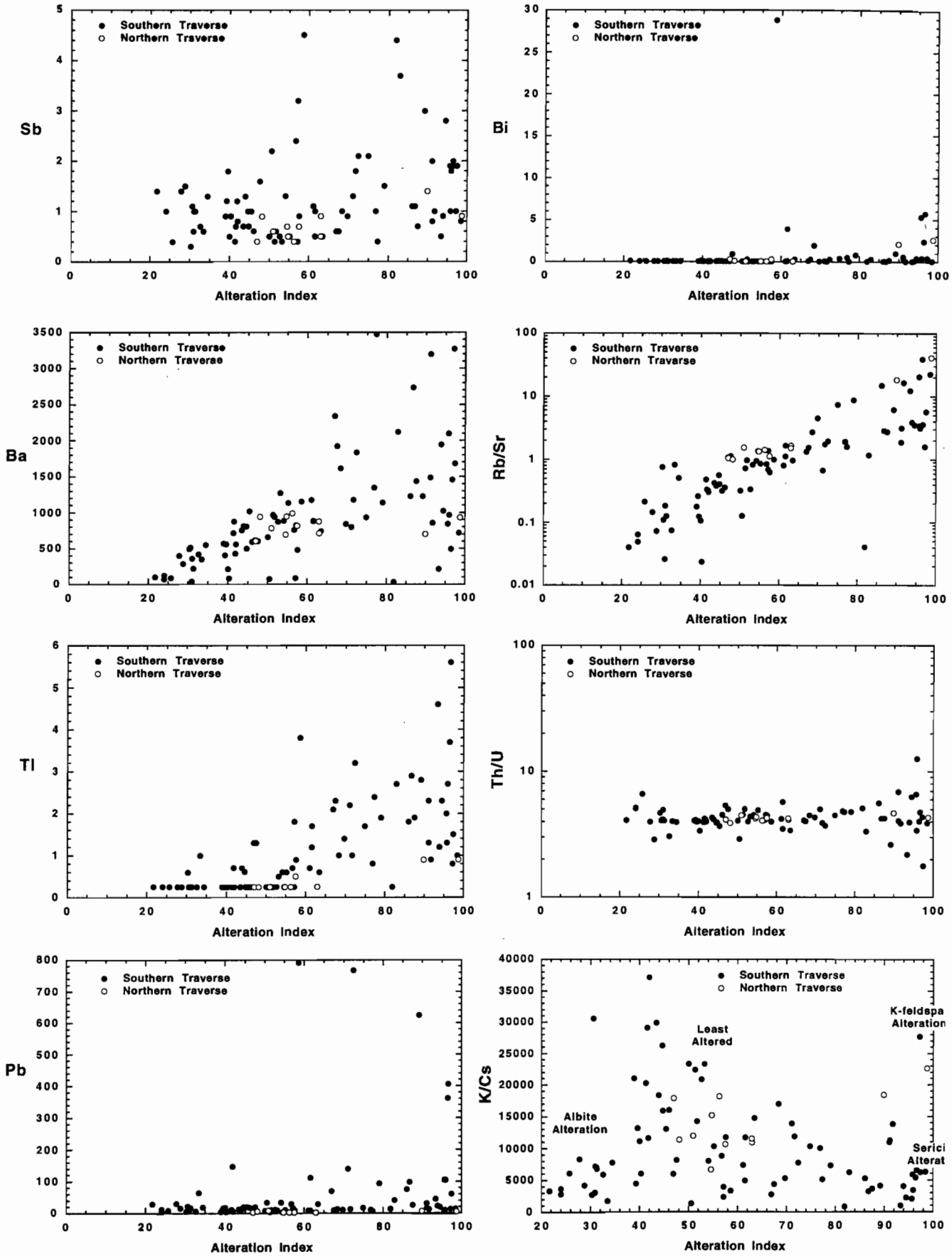

Figure 5. Variation of Sb, Ba, Tl, Pb, Bi, Rb/Sr, Th/U and K/Cs as functions of the Ishikawa Alteration Index.

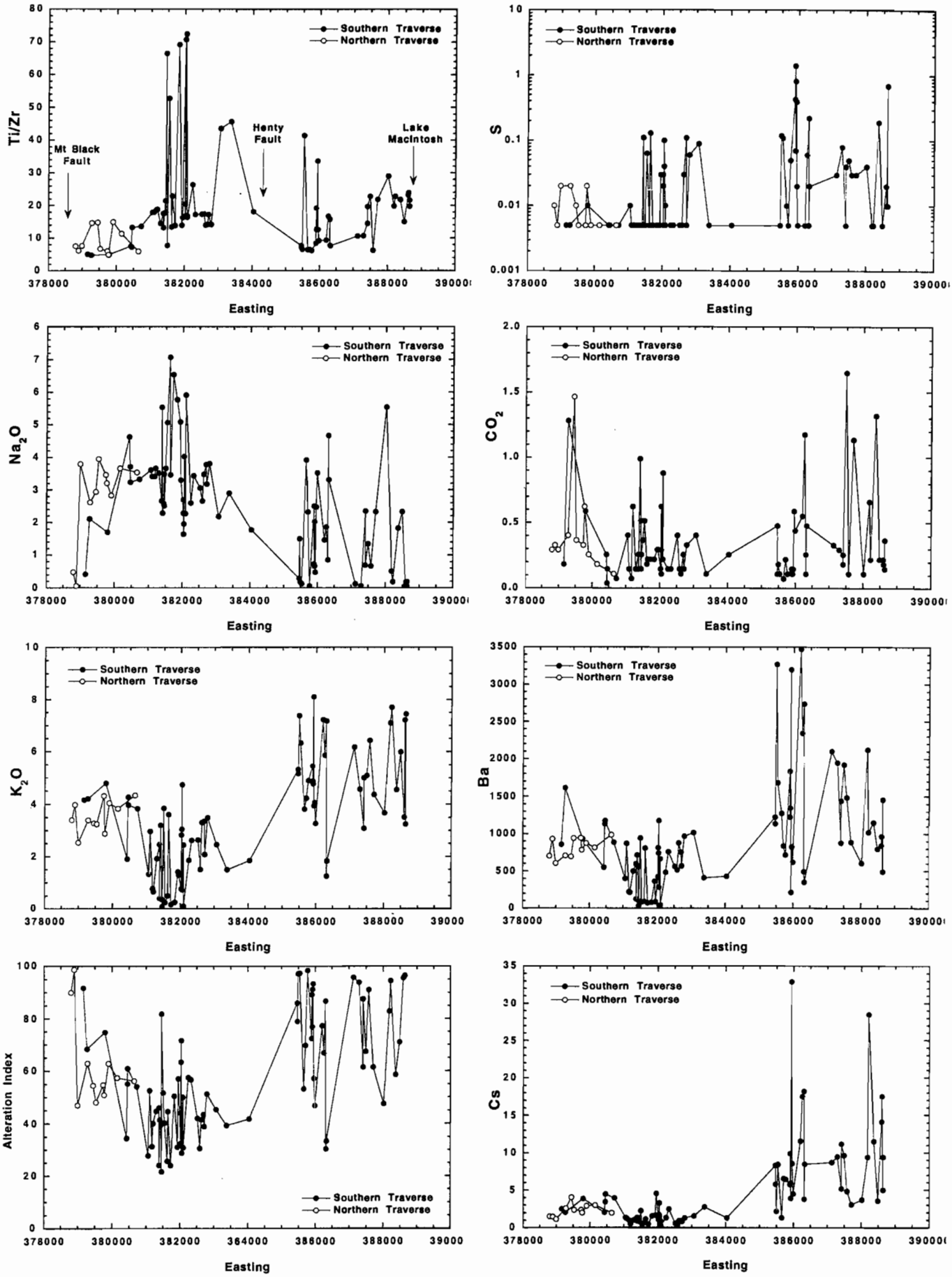

Figure 6. Variation of Ti/Zr, Na_2O, K_2O, Alteration Index, S, CO_2, Ba and Cs as functions of sample location (easting).

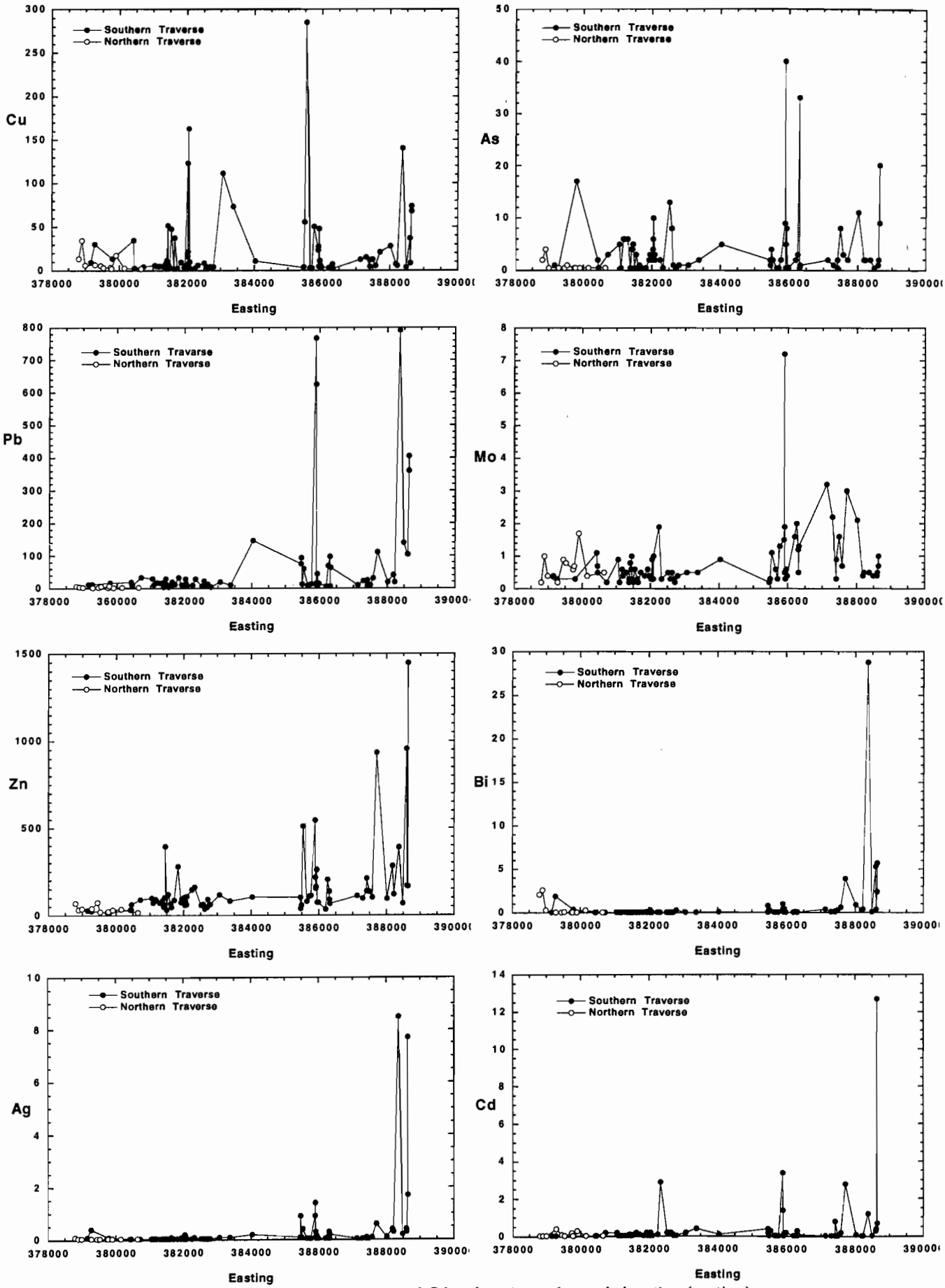

Figure 7. Variation of Cu, Pb, Zn, Ag, As, Mo, Bi and Cd as functions of sample location (easting).

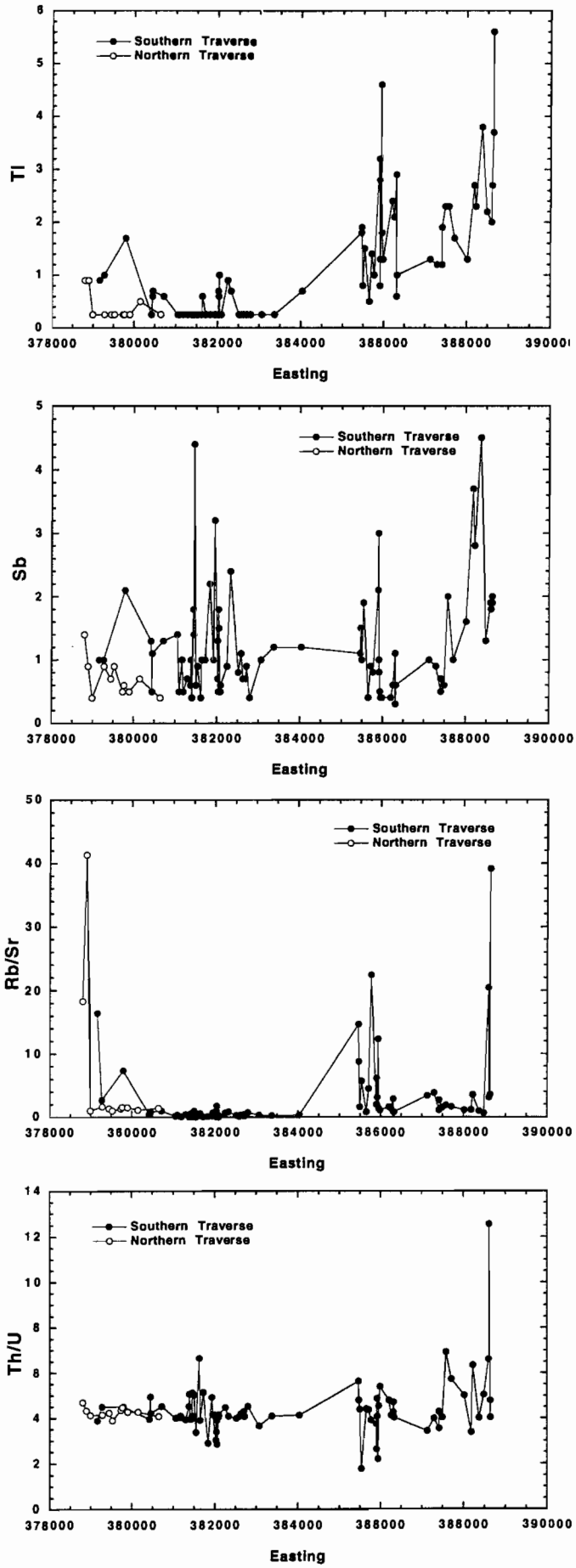

Figure 8. Variation of Tl, Sb, Rb/Sr and Th/U as functions of sample location (easting).

The Murchison Granite samples have Ti/Zr values in the range 15 to 30 with the majority close to 20. This contrasts with the rhyolitic rocks of the Murchison Volcanics which mostly have Ti/Zr <10. The highest Ti/Zr values (i.e. >40) are for the basaltic and andesitic rocks from the Sterling Valley Volcanics and Henty Dyke suite which intrude the Mt Black Volcanics. The latter display values typical of both dacitic (≥12) and rhyolitic (<12) rocks.

The traverse samples display a wide range of Na_2O, K_2O and Alteration Index values (Fig. 6) which partly reflect variation in the primary lithologies, and partly the different types of alteration. Zones of albite-dominated alteration are depicted by strong spikes in the Na_2O content, and are restricted to a specific region within the Mt Black Volcanics. Regions of strong Na-depletion correspond (as expected) with high values of the Ishikawa Alteration Index, and include both zones of sericite and K-feldspar alteration predominantly within the Murchison Granite and Murchison Volcanics. The last few (most westerly) samples, which occur adjacent to the Mt Black Fault in the Mt Black Volcanics also show evidence of strong sericite alteration.

The minor and trace element data are also very useful in delineating zones of hydrothermal alteration which have been superimposed on the regional background alteration. For example there are several significant spikes in the Ba, Cu, Pb, Zn, As, Ag, Cd, Sb and Tl data which correlate with zones of Na_2O depletion and enrichment in S. One of these anomalous zones within the Murchison Volcanics displays a coincident reduction in the Th/U value (Fig. 8).

Significance of different alteration styles

The observations on the samples from this traverse support those from the Hall Rivulet Canal–Mt Read–Red Hills–Selina traverse. The earliest alteration appears to be related to diagenesis and reflected by the present assemblage albite ± epidote ± sericite. As these rocks have recrystallised under prehnite-pumpellyite or lower greenschist facies conditions during the Devonian metamorphism, there is some uncertainty whether these phases were produced during diagenetic alteration or are the recrystallised metamorphic equivalents.

The development of K-feldspar instead of albite during diagenetic alteration apparently reflects subtle differences in the phase equilibria at low temperature controlled by Na/K of the fluid under neutral or slightly alkaline conditions.

The sericite±pyrite±chlorite alteration generally overprints earlier diagenetic alteration although it is not always clear where diagenetic alteration ends and hydrothermal alteration begins. The final breakdown of the feldspar grains is the best indicator of intense alteration and is reflected chemically by the strong depletion of Na_2O and CaO (unless carbonate is an associated alteration product).

The depletion of Na_2O, which is a common characteristic of many altered footwall volcanic packages to massive sulphide deposits, is frequently used as an exploration vector to ore. However, this should be exercised with some caution given that low-temperature diagenetic K-feldspar alteration also results in depletion of Na_2O through cation exchange processes rather than breakdown of primary Na-bearing phases by interaction with high temperature hydrothermal fluids.

Conclusions

- Petrographic and chemical data for the samples from the Murchison Dam–Anthony Road–Mt Black traverse confirm the 5 major styles of alteration distinguished in the Hall Rivulet–Mt Read–Red Hills–Selina traverse. Two of these (albite ± epidote ± sericite and low-temperature K-feldspar alteration) are regarded as the result of diagenetic processes that have been texturally modified by subsequent greenschist facies regional metamorphism.

- There is negligible enrichment of base or precious metals associated with the diagenetic albitic alteration, but these rocks have distinctive

compositions characterised by Na_2O> 5 wt% and substantial depletion of K_2O, Rb, Cs and Ba compared with unaltered equivalents.

- Diagenetic K-feldspar alteration is indicated by high K_2O/Na_2O, Rb, Ba and Cs, but negligible enrichment in base metals, S and CO_2.

- The effects of sericite ± pyrite ± chlorite hydrothermal alteration commonly overprint and are gradational to the albite ± epidote ± sericite alteration. The more intense variants of this alteration style are characterised by strong depletion of CaO, Na_2O and Sr, and commonly display significant enrichment of a wide range of trace elements including As, Sb and Tl. High Rb/Sr values are also a good indicator of this style of alteration, and because of the greater enhancement of values in the altered rocks is possibly more sensitive than the Ishikawa Alteration Index.

- K-feldspar ± magnetite ± chlorite alteration within the Murchison Granite and Murchison Volcanics is characterised by strong depletion of Na_2O and CaO, coupled with high K_2O and Ba in the feldspar-rich rocks, and higher Fe_2O_3, MnO, MgO and P_2O_5 together with lower K_2O and Ba in the chlorite-rich assemblages. The feldspar-rich alteration appears to be the earliest phase and is overprinted by chlorite-magnetite-rich veins and sericite-rich veins.

References

Doyle, M.G., 1990, The geology, mineralisation and alteration of the Jukes Proprietary prospect, Tasmania. Unpubl. BSc Hons Thesis, University of Tasmania, 114p.

Eastoe, C.J., Solomon, M. and Walshe, J.L., 1987, District-scale alteration associated with massive sulfide deposits in the Mt Read Volcanics, western Tasmania. Economic Geology, 82, 1239–1258.

Gifkins, C., 1996, Mount Black Volcanics: Preliminary volcanic facies and alteration, petrography and geochemistry. Studies of VHMS-related alteration: geochemical and mineralogical vectors to ore. AMIRA-ARC Project P439, Report 3, p321–349.

Hunns, S.R., 1987, Mineralisation in the west coast range, western Tasmania - The Lake Selina Prospect. MSc Q. Thesis, University of Tasmania, 49p.

Ishikawa, Y., Sawaguchi, T., Iwaya, S. and Horiuchi, M., 1976. Delineation of prospecting targets for Kuroko deposits based on modes of volcanism of underlying dacite and alteration haloes. Mining Geology, 26, 105–117.

Jenkins, D.R., 1991, Volcanology, mineralisation and alteration of the Red Hills, western Tasmania. Unpubl. BSc Hons. Thesis, University of Tasmania, 90p.

Large, R., 1996, The Hercules–Mt Read traverse: Relationships between volcanic mineralogy, alteration and geochemistry. Studies of VHMS-related alteration: geochemical and mineralogical vectors to ore. AMIRA-ARC Project P439, Report 3, p153–233.

Stolz, J., 1991, Stratigraphy and geochemistry of the Mt Windsor Volcanics and associated exhalites. Mt Windsor Project Research Report No. 2, 23–83.

Stolz, J., Davidson, G. and Blake, M., 1996a, 'Barren alteration systems: Example - Gydgie Central, Mt Windsor Volcanic Belt, north Queensland. Studies of VHMS-related alteration: geochemical and mineralogical vectors to ore. AMIRA-ARC Project P439, Report 3, p1–85.

Stolz, J., Allen, R., Gifkins, C., Davidson, G., McPhie, J. and Blake, M., 1996b, Petrographic and geochemical characteristics of alteration from the Hall Rivulet Canal–Mt Read–Red Hills–Anthony Dam traverse, Mt Read Volcanic Belt. Studies of VHMS-related alteration: geochemical and mineralogical vectors to ore. AMIRA-ARC Project P439, Report 3, p379–424.

Table 1. Major and trace element analyses of volcanic rocks from the Mt Black traverse.

	M4	M6	M7	M9	M10	M19	M24	M25	M29B	M3O	M33	M39
SiO2	62.51	53.86	50.66	50.49	65.89	59.68	66.52	67.63	68.15	49.22	62.93	52.39
TiO2	0.68	0.59	0.92	0.96	0.51	0.69	0.49	0.46	0.59	0.92	0.68	0.55
Al2O3	15.66	16.34	18.32	18.39	15.70	16.59	15.30	14.87	14.09	19.56	16.28	14.87
Fe2O3#	6.54	7.79	10.00	10.36	4.70	8.76	4.36	4.33	4.66	11.74	5.83	10.30
MnO	0.10	0.13	0.19	0.16	0.08	0.09	0.06	0.07	0.11	0.18	0.07	0.21
MgO	2.74	6.02	4.38	4.73	1.35	4.58	1.22	1.33	1.66	4.01	3.10	7.29
CaO	4.61	8.73	8.64	6.46	0.77	1.11	2.17	3.04	3.03	7.60	1.15	6.09
Na2O	1.78	2.90	4.03	2.19	3.81	3.30	3.78	3.48	2.70	2.28	1.96	5.07
K2O	1.85	1.50	0.73	2.46	3.49	1.29	3.35	3.30	2.83	0.76	4.74	0.24
P2O5	0.10	0.06	0.10	0.11	0.13	0.12	0.12	0.13	0.08	0.09	0.12	0.05
LOI	3.39	2.47	2.61	3.70	2.88	4.04	1.90	1.43	2.05	4.00	3.23	2.83
Total	99.96	100.39	100.58	100.01	99.33	100.25	99.27	100.07	99.95	100.36	100.09	99.89
S	<0.01	<0.01	0.04	0.09	0.06	0.03	0.11	0.03	0.02	0.03	0.10	0.06
Total C	0.07	0.03	0.03	0.11	0.09	0.08	0.07	0.03	0.04	0.04	0.08	0.14
CO2	0.26	0.11	0.11	0.40	0.33	0.29	0.26	0.11	0.15	0.15	0.29	0.51
Alteration Index	41.8	39.3	28.7	45.4	51.3	57.1	43.4	41.5	43.9	32.6	71.6	40.3
Trace Elements (ppm)												
Sc	17	33	35	29	9	19	8	7	15	33	15	35
V	129	176	292	271	65	159	60	54	114	300	133	201
Cr	43	67	83	61	4	50	5	5	46	107	28	67
Ni	9	34	54	31	2	11	2	2	7	47	5	36
Cu	11	73	163	112	4	6	5	3	17	123	8	48
Zn	104	81	82	118	63	95	47	38	67	104	58	119
As	5	2	10	1	1	3	<1	1	3	2	6	3
Rb	84	69	28	84	97	79	90	88	88	27	224	5
Sr	263	268	385	267	134	115	214	265	233	360	128	228
Y	34	24	24	26	36	32	26	32	28	23	33	19
Zr	225	77	76	132	213	253	206	197	211	78	242	62
Nb	12.0	3.4	2.2	5.3	12.4	12.6	11.8	11.8	11.0	3.2	12.5	2.3
Mo	0.9	0.5	0.9	0.5	0.4	0.4	0.3	0.5	0.3	0.4	0.3	0.6
Ag	0.2	0.1	0.2	0.1	<0.1	0.1	<0.1	<0.1	0.1	<0.1	0.2	<0.1
Cd	0.1	0.4	0.1	0.2	<0.1	<0.1	0.1	0.2	<0.1	0.1	<0.1	0.1
Sb	1.2	1.2	1.5	1	0.4	3.2	0.7	0.7	1.3	0.7	1.8	0.9
Cs	1.32	2.79	1.44	1.56	1.29	4.56	0.93	0.94	1.28	1.07	3.3	0.33
Ba	429	410	285	1017	968	88	755	878	813	423	1175	85
La	40	15	9	15	46	35	30	34	26	8	25	11
Ce	81	33	19	33	81	69	63	73	63	24	61	22
Nd	35	13	10	15	38	31	29	30	26	12	24	12
Tl	0.7	<0.5	<0.5	<0.5	<0.5	<0.5	<0.5	<0.5	0.7	<0.5	1	<0.5
Pb	147	10	16	20	4	6	13	11	10	7	13	5
Bi	0.1	<0.1	<0.1	<0.1	0.3	<0.1	<0.1	<0.1	0.1	<0.1	<0.1	<0.1
Th	13.4	4.39	3.37	6.81	16	15.6	15.3	14	12.6	3.46	15.1	3.97
U	3.24	1.07	1.18	1.86	3.54	3.76	3.56	3.33	3.04	1.14	3.86	1.18

Total Fe as Fe2O3; LOI = loss on ignition; Alteration Index = 100(MgO+K2O)/(MgO+K2O+CaO+Na2O)

Table 1. continued

	M45	M46	M50	M59	M60	M63	M67	M69B	M73	M77	M78	M79
SiO2	60.15	70.08	64.10	63.06	69.98	64.92	67.73	50.29	68.85	66.65	74.18	63.48
TiO2	0.73	0.44	0.65	0.71	0.80	0.65	0.48	0.81	0.49	0.48	<0.5	0.68
Al2O3	16.55	14.49	14.69	16.39	12.65	15.50	15.14	19.29	14.96	16.41	13.65	15.60
Fe2O3#	7.43	3.82	6.41	6.85	5.79	5.64	4.95	11.66	3.93	4.15	2.12	6.03
MnO	0.12	0.06	0.09	0.13	0.10	0.09	0.10	0.21	0.06	0.03	0.02	0.08
MgO	3.08	1.68	2.78	3.00	2.46	3.12	1.58	6.42	2.01	2.03	0.50	2.15
CaO	4.47	1.04	2.96	0.85	0.59	1.30	1.59	0.77	0.34	0.24	0.40	5.59
Na2O	2.58	5.54	2.27	3.44	2.60	5.91	5.09	5.77	6.54	7.07	3.66	3.49
K2O	1.53	0.40	2.45	2.62	1.86	0.10	1.42	0.25	0.16	0.50	3.85	0.36
P2O5	0.08	0.09	0.10	0.13	0.12	0.10	0.12	0.10	0.10	0.12	0.04	0.10
LOI	3.44	2.22	3.64	3.08	2.90	2.51	1.87	4.48	1.97	1.95	1.30	2.38
Total	100.16	99.86	100.14	100.26	99.85	99.84	100.07	100.05	99.41	99.63	99.97	99.94
S	0.11	<0.01	0.01	<0.01	<0.01	<0.01	<0.01	<0.01	<0.01	<0.01	<0.01	<0.01
Total C	0.14	0.04	0.24	0.04	0.04	0.06	0.08	0.06	0.06	0.05	0.10	0.04
CO2	0.51	0.15	0.88	0.15	0.15	0.22	0.29	0.22	0.22	0.18	0.37	0.15
Alteration Index	39.5	24.0	50.0	56.7	57.5	30.9	31.0	50.5	24.0	25.7	51.7	21.7
Trace Elements (ppm)												
Sc	21	7	16	19	20	18	8	45	10	10	4	15
V	158	45	120	149	147	136	61	318	61	63	13	139
Cr	37	5	49	24	227	49	4	11	6	5	5	30
Ni	12	2	10	5	43	10	2	29	3	2	2	10
Cu	52	3	10	6	3	3	4	10	3	2	4	8
Zn	104	64	61	162	147	108	75	280	87	68	32	60
As	4	<1	3	<1	2	2	2	<1	<1	<1	<1	5
Rb	47	21	62	119	69	4	46	19	7	20	118	16
Sr	377	325	192	141	111	160	253	152	147	94	121	406
Y	30	28	31	29	19	27	28	33	26	39	20	31
Zr	204	200	233	247	182	238	207	70	212	214	192	228
Nb	11.0	12.5	12.5	11.9	10.4	12.1	12.2	2.8	11.8	13.3	10.5	11.6
Mo	0.6	0.3	0.3	0.3	1.9	1	0.6	0.4	0.5	0.3	0.2	1
Ag	<0.1	<0.1	0.1	0.1	<0.1	<0.1	<0.1	<0.1	<0.1	<0.1	<0.1	<0.1
Cd	0.1	<0.1	<0.1	2.9	0.1	<0.1	0.2	<0.1	0.1	0.2	<0.1	<0.1
Sb	1.8	1	0.5	2.4	0.9	0.6	1	2.2	1	0.4	0.6	1.4
Cs	0.96	0.91	0.87	2.47	1.31	0.27	1.64	1.54	0.47	0.68	2.24	0.9
Ba	562	123	664	761	483	42	362	78	71	91	942	102
La	25	37	25	26	21	27	28	47	22	53	23	27
Ce	59	71	55	56	40	56	63	104	42	110	50	64
Nd	26	33	25	22	17	26	26	47	21	47	16	29
Tl	<0.5	<0.5	<0.5	0.7	0.9	<0.5	<0.5	<0.5	<0.5	<0.5	<0.5	<0.5
Pb	16	5	8	29	10	9	11	34	12	8	11	30
Bi	0.1	<0.1	<0.1	<0.1	<0.1	<0.1	0.1	<0.1	<0.1	<0.1	<0.1	0.1
Th	12.5	16.1	14.1	14.2	9.05	14.5	16	5.97	16.6	16	19.3	14.2
U	3.15	3.18	3.48	3.47	2.02	3.49	3.25	2.06	3.23	2.41	3.84	3.47

Total Fe as Fe2O3; LOI = loss on ignition; Alteration Index = 100(MgO+K2O)/(MgO+K2O+CaO+Na2O)

Table 1. continued

	M81	M84	M85	M86	M89	M90	M98	M103	M105	M112	M114	M116
SiO2	62.58	66.77	61.05	62.81	64.53	62.98	68.53	73.19	73.93	75.30	75.48	77.62
TiO2	0.65	0.56	0.72	0.65	0.63	0.69	0.50	<0.5	0.31	0.20	0.19	0.18
Al2O3	15.18	14.83	15.89	15.34	14.87	15.32	14.76	13.72	13.72	13.02	13.49	12.54
Fe2O3#	6.20	5.32	7.59	6.33	6.08	5.60	4.34	2.40	2.66	1.61	1.45	2.01
MnO	0.09	0.07	0.10	0.09	0.09	0.10	0.06	0.04	0.11	0.01	0.00	0.01
MgO	2.82	2.56	3.57	3.03	2.75	2.21	1.38	0.52	0.61	0.35	0.42	0.60
CaO	3.53	2.02	2.69	4.92	1.73	5.62	1.09	0.18	0.18	0.03	0.03	0.01
Na2O	2.66	3.52	3.66	3.42	3.42	3.61	3.33	3.71	4.63	1.70	2.11	0.42
K2O	2.46	1.92	0.66	0.77	2.97	1.33	3.83	4.26	1.91	4.79	4.20	4.16
P2O5	0.11	0.08	0.10	0.11	0.11	0.13	0.12	0.05	0.05	0.03	0.02	0.02
LOI	2.79	2.50	4.04	2.36	2.77	2.22	1.76	1.08	1.60	1.85	2.31	2.15
Total	99.07	100.15	100.07	99.83	99.95	99.81	99.70	99.40	99.71	98.89	99.70	99.72
S	<0.01	<0.01	<0.01	<0.01	<0.01	0.01	<0.01	<0.01	<0.01	0.01	<0.01	<0.01
Total C	0.07	0.04	0.17	0.02	0.04	0.11	0.02	0.01	0.07	0.16	0.35	0.05
CO2	0.26	0.15	0.62	0.07	0.15	0.40	0.07	0.04	0.26	0.59	1.28	0.18
Alteration Index	46.0	44.7	40.0	31.3	52.6	27.7	54.1	55.1	34.4	74.8	68.3	91.7
Trace Elements (ppm)												
Sc	17	12	16	15	16	13	10	4	4	4	4	3
V	132	109	145	132	143	113	68	8	6	<1.5	3	2
Cr	55	29	64	40	45	27	7	2	2	2	2	2
Ni	11	6	11	8	8	6	2	1	0	2	2	1
Cu	8	5	5	5	5	6	5	3	35	14	30	10
Zn	86	71	86	92	71	99	91	33	33	18	26	28
As	<1	6	6	6	<1	5	3	<1	2	17	<1	1
Rb	86	76	22	36	77	44	150	122	78	298	153	171
Sr	240	188	205	283	226	305	157	142	152	41	56	10
Y	32	29	30	32	35	37	32	40	44	42	47	37
Zr	222	231	230	209	211	231	220	207	244	238	241	214
Nb	11.5	12.2	11.3	11.0	11.4	12.4	12.6	14.7	15.1	15.8	16.5	14.8
Mo	0.2	0.5	0.4	0.6	0.2	0.9	0.2	0.7	1.1	0.3	0.3	0.4
Ag	<0.1	<0.1	<0.1	<0.1	<0.1	<0.1	<0.1	<0.1	<0.1	0.1	0.4	0.1
Cd	<0.1	<0.1	<0.1	<0.1	<0.1	0.2	0.2	<0.1	<0.1	<0.1	<0.1	<0.1
Sb	0.6	0.7	0.5	1	0.5	1.4	1.3	0.5	1.3	2.1	1	1
Cs	1.27	1	0.49	0.93	1.18	1.32	3.94	3.43	2.04	3.84	2.05	2.5
Ba	595	499	213	223	871	400	889	1133	551	932	1613	858
La	27	23	24	29	30	30	37	50	42	43	41	32
Ce	59	58	55	62	63	68	78	91	89	94	92	71
Nd	26	25	23	30	30	32	33	43	37	39	37	31
Tl	<0.5	<0.5	<0.5	<0.5	<0.5	<0.5	0.6	0.6	<0.5	1.7	1	0.9
Pb	19	16	18	18	11	30	34	11	19	17	13	12
Bi	<0.1	0.1	<0.1	<0.1	<0.1	<0.1	<0.1	<0.1	<0.1	0.4	1.9	<0.1
Th	8.57	15.3	13.5	13.5	13.3	14.2	18.4	20.1	18.4	21.6	21.2	16.9
U	1.9	3.89	3.36	3.31	3.32	3.56	4.08	4.07	4.65	4.8	4.71	4.35

Total Fe as Fe2O3; LOI = loss on ignition; Alteration Index = 100(MgO+K2O)/(MgO+K2O+CaO+Na2O)

Table 1. continued

	M120	M121	M134	MBE96-8	MY	MB96-1	MB96-2	MB96-3	MB96-4	MB96-5	MB96-6	MB96-7
SiO2	63.11	63.67	68.17	62.71	66.94	59.69	63.98	61.82	59.90	72.66	61.20	61.50
TiO2	0.66	0.65	0.51	0.71	0.64	0.72	0.74	0.75	0.65	0.29	0.68	0.80
Al2O3	14.95	15.12	15.04	15.01	14.11	14.61	16.39	16.36	14.90	13.47	14.20	16.76
Fe2O3#	6.12	5.92	4.83	5.96	5.82	12.46	4.99	8.61	12.13	2.18	7.57	7.97
MnO	0.10	0.12	0.03	0.10	0.08	1.03	0.20	0.06	0.68	0.06	0.53	0.03
MgO	2.43	2.61	1.67	2.62	2.81	2.88	1.97	1.40	3.46	0.75	2.32	1.51
CaO	6.29	4.19	0.36	4.29	1.74	0.18	0.14	0.19	0.24	0.42	3.03	0.35
Na2O	2.66	3.18	3.24	3.46	1.64	0.05	0.19	0.18	0.08	2.33	1.83	0.19
K2O	1.51	2.08	3.97	3.61	3.05	3.25	7.45	7.21	3.51	5.99	4.55	7.70
P2O5	0.09	0.10	0.12	0.11	0.10	0.18	0.18	0.19	0.18	0.06	0.19	0.27
LOI	2.40	2.29	1.71	1.77	3.18	4.14	3.41	2.91	3.86	1.76	3.47	2.46
Total	100.32	99.93	99.65	100.35	100.11	99.19	99.64	99.68	99.59	99.97	99.57	99.54
S	<0.01	<0.01	<0.01	0.13	<0.01	0.68	0.01	0.01	0.02	<0.01	0.19	<0.01
Total C	0.04	0.04	0.04	0.06	0.17	0.04	0.10	0.05	0.06	0.06	0.36	0.06
CO2	0.15	0.15	0.15	0.22	0.62	0.15	0.37	0.18	0.22	0.22	1.32	0.22
Alteration Index	30.6	38.9	61.0	44.6	63.4	96.4	96.6	95.9	95.6	71.0	58.6	94.5
Trace Elements (ppm)												
Sc	18	16	12	22	16	22	22	23	20	6	17	23
V	126	124	73	157	143	172	179	139	119	42	142	133
Cr	47	47	9	31	46	37	41	36	33	9	26	30
Ni	8	9	2	8	10	11	10	16	8	4	8	27
Cu	5	4	3	37	22	74	68	9	37	4	140	6
Zn	64	92	63	47	68	1447	165	168	956	67	390	119
As	8	<1	<1	1	4	20	9	2	1	<1	2	2
Rb	39	56	136	115	127	321	446	314	201	186	218	337
Sr	352	315	170	205	131	8	124	100	10	278	220	96
Y	33	36	33	33	26	27	24	30	21	15	29	31
Zr	228	227	231	186	188	200	225	188	168	116	187	211
Nb	12.0	11.7	12.8	9.7	10.7	14	14.9	13.7	12.9	14.2	14.7	14.9
Mo	0.3	0.2	0.5	0.2	0.3	1	0.7	0.5	0.4	0.4	0.5	0.5
Ag	<0.1	<0.1	<0.1	0.1	0.1	1.7	7.7	0.3	0.4	0.2	8.5	0.3
Cd	0.2	<0.1	<0.1	0.1	0.2	12.7	0.7	0.4	0.3	<0.1	1.2	<0.1
Sb	1.1	0.9	1.1	1	0.5	2	1.9	1.8	1.9	1.3	4.5	2.8
Cs	0.41	0.82	4.46	1.14	1.71	5	9.41	17.5	14.1	3.57	11.5	28.5
Ba	515	568	1176	809	742	492	1455	964	844	798	1151	1023
La	31	34	42	27	25	51	49	69	38	43	54	55
Ce	70	70	88	62	47	99	98	125	71	84	101	101
Nd	32	33	35	28	20	39	39	52	30	29	38	41
Tl	<0.5	<0.5	0.7	0.6	0.6	3.7	5.6	2.7	2	2.2	3.8	2.3
Pb	22	5	8	20	29	361	406	104	105	140	791	19
Bi	<0.1	<0.1	<0.1	<0.1	0.3	2.4	5.7	0.4	5.3	0.1	28.8	0.4
Th	13.9	13.6	17.9	10.3	11.4	26.2	23.7	22.6	21.2	44.4	25	21.6
U	3.41	3.34	4.25	2.64	3.36	6.52	4.97	1.8	3.21	8.84	6.26	3.41

Total Fe as Fe2O3; LOI = loss on ignition; Alteration Index = 100(MgO+K2O)/(MgO+K2O+CaO+Na2O)

Table 1. continued

	MB96-9	MB96-10	MB96-11	MB96-12	MB96-13	MB96-13B	MB96-14	MB96-15	MB96-17	MB96-18	MB96-19	MB96-20
SiO2	63.31	62.77	72.41	58.14	66.88	63.89	69.67	69.76	76.51	76.51	69.93	65.53
TiO2	0.84	0.68	0.28	0.62	0.56	0.62	0.50	0.49	0.33	0.33	0.44	0.54
Al2O3	16.44	13.19	12.95	13.82	14.02	14.43	12.56	12.32	12.35	12.52	13.77	14.05
Fe2O3#	5.53	7.54	3.97	10.77	7.23	8.74	7.23	6.42	1.38	1.78	3.58	4.77
MnO	0.09	0.72	0.09	0.17	0.19	0.16	0.10	0.23	0.06	0.05	0.13	0.16
MgO	2.09	2.85	1.62	3.10	2.03	2.71	2.15	1.53	0.80	0.90	1.46	1.97
CaO	0.82	2.19	0.12	2.61	0.86	0.41	0.38	0.22	1.94	0.28	0.46	2.02
Na2O	5.54	2.33	0.67	1.35	2.35	0.69	0.06	0.12	3.31	4.67	0.86	1.86
K2O	3.67	4.37	6.43	5.09	3.09	5.00	4.57	6.17	1.83	1.25	7.17	5.86
P2O5	0.21	0.17	0.05	0.14	0.10	0.13	0.10	0.09	0.05	0.03	0.10	0.11
LOI	1.71	3.07	1.80	3.82	2.47	2.89	2.57	1.99	1.33	1.39	2.01	2.73
Total	100.25	99.88	100.55	99.63	99.78	99.67	99.89	99.34	99.89	99.71	100.17	99.60
S	0.04	0.03	0.03	0.05	<0.01	0.04	0.08	0.03	0.02	<0.01	0.22	0.06
Total C	0.03	0.31	0.03	0.45	0.07	0.05	0.08	0.09	0.13	0.03	0.07	0.32
CO2	0.11	1.14	0.11	1.65	0.26	0.18	0.29	0.33	0.48	0.11	0.26	1.17
Alteration Index	47.5	61.5	91.1	67.4	61.5	87.5	93.9	95.8	33.4	30.3	86.7	66.9
Trace Elements (ppm)												
Sc	22	17	10	28	24	28	13	14	9	9	11	13
V	173	141	14	187	113	180	69	65	25	23	77	95
Cr	35	29	2	20	15	18	26	24	3	3	15	20
Ni	9	8	4	7	4	5	5	5	8	3	5	7
Cu	28	21	6	13	5	12	15	13	2	2	7	4
Zn	95	934	102	134	138	211	96	111	66	90	136	203
As	11	2	3	8	<1	2	1	2	1	<1	33	3
Rb	121	147	247	192	154	224	137	168	124	68	290	250
Sr	107	88	130	125	137	81	36	49	151	90	101	188
Y	24	27	46	33	43	33	37	38	47	34	29	32
Zr	174	187	269	163	232	189	280	276	258	254	167	195
Nb	13.6	11.2	19.3	10.9	12.5	13.2	14.1	13.5	13.9	13.9	13.6	14.4
Mo	2.1	3	0.7	1.6	0.3	0.9	2.2	3.2	1.3	0.5	1.2	2
Ag	0.1	0.6	0.1	<0.1	<0.1	0.1	<0.1	<0.1	0.2	<0.1	0.3	0.1
Cd	0.1	2.8	0.2	<0.1	<0.1	0.8	<0.1	<0.1	0.1	<0.1	0.3	<0.1
Sb	1.6	1	2	0.6	0.5	0.7	0.9	1	0.6	0.3	1.1	0.6
Cs	3.72	3.09	4.86	9.65	5.2	11.2	9.49	8.72	8.5	3.81	18.2	17.5
Ba	605	886	1485	1922	879	1440	1947	2097	353	496	2735	2342
La	36	37	126	31	51	38	39	39	39	35	42	47
Ce	72	72	269	61	96	74	91	84	95	88	91	99
Nd	32	30	92	24	39	30	40	36	41	36	30	37
Tl	1.3	1.7	2.3	2.3	1.2	1.9	1.2	1.3	1	0.6	2.9	2.1
Pb	20	112	31	10	9	25	23	10	64	7	98	70
Bi	0.9	3.9	0.6	0.3	0.1	0.2	0.1	0.4	<0.1	<0.1	<0.1	0.1
Th	15.6	13.6	29.9	10.9	15	12.3	19.6	18.9	20.9	20.8	24	21
U	3.12	2.38	4.33	2.72	4.26	2.88	4.93	5.54	5.2	4.43	5.65	5.11

Total Fe as Fe2O3; LOI = loss on ignition; Alteration Index = 100(MgO+K2O)/(MgO+K2O+CaO+Na2O)

Table 1. continued

	MB96-22	MB96-23	MB96-24	MB96-25	MB96-26	MB96-27	MB96-27B	MB96-28	MB96-29	MB96-30	MB96-31	MB96-32
SiO2	72.39	67.55	51.31	61.41	65.16	68.76	67.29	73.56	73.06	74.43	44.12	77.14
TiO2	0.34	0.56	0.56	0.54	0.58	0.52	0.56	0.29	0.32	0.30	0.79	0.19
Al2O3	13.09	13.79	15.10	15.38	14.21	15.07	14.07	12.91	13.46	12.89	17.11	10.05
Fe2O3#	2.30	4.44	14.34	8.54	6.86	3.97	5.34	4.77	3.13	2.45	21.49	2.99
MnO	0.06	0.08	0.39	0.11	0.09	0.11	0.06	0.05	0.05	0.03	0.22	0.07
MgO	1.14	2.50	8.22	2.87	3.04	1.78	2.44	1.23	1.34	0.82	4.90	0.60
CaO	1.48	2.45	0.39	0.40	0.34	0.26	0.16	0.04	0.10	0.16	0.17	0.05
Na2O	3.52	2.47	0.48	0.67	2.02	2.50	0.73	0.06	2.32	3.92	0.13	0.18
K2O	3.27	4.06	3.94	8.10	4.78	5.45	4.88	4.90	4.23	3.82	6.33	7.38
P2O5	0.05	0.09	0.10	0.11	0.10	0.11	0.09	0.05	0.05	0.05	0.13	0.04
LOI	1.51	2.01	4.65	2.46	2.47	2.17	3.71	2.18	1.76	0.94	3.45	0.82
Total	99.15	100.00	99.48	100.59	99.65	100.70	99.33	100.12	99.82	99.81	98.84	99.51
S	<0.01	0.02	0.39	0.81	0.07	0.43	1.40	0.05	<0.01	0.01	0.11	0.12
Total C	0.12	0.16	0.04	0.03	0.03	0.04	0.04	0.03	0.06	0.02	0.03	0.05
CO2	0.44	0.59	0.15	0.11	0.11	0.15	0.15	0.11	0.22	0.07	0.11	0.18
Alteration Index	46.9	57.1	93.3	91.1	76.8	72.4	89.2	98.4	69.7	53.2	97.4	97.2
Trace Elements (ppm)												
Sc	7	13	35	16	20	14	16	12	9	7	36	6
V	36	87	231	117	101	42	92	3	10	8	279	3
Cr	24	104	558	101	124	20	74	2	4	4	6	2
Ni	8	26	105	31	29	11	31	3	3	3	12	3
Cu	4	6	11	48	5	23	28	50	3	3	285	56
Zn	72	73	259	162	153	546	216	112	107	79	511	58
As	<1	<1	8	5	<1	9	40	2	<1	<1	2	4
Rb	149	206	478	209	141	193	229	231	211	78	257	150
Sr	139	150	39	66	73	98	37	10	47	95	45	94
Y	38	39	15	98	26	20	33	32	39	36	26	43
Zr	221	265	100	254	277	370	175	281	295	276	114	174
Nb	13.1	13.2	9.4	12.6	13.1	12	14.4	12.4	13.2	13.3	9.2	8.8
Mo	0.4	0.6	0.3	0.5	1.9	1.5	7.2	1.3	0.3	0.6	1.1	0.3
Ag	<0.1	<0.1	<0.1	0.3	0.1	0.9	1.4	<0.1	<0.1	<0.1	0.4	0.1
Cd	0.2	0.2	0.2	<0.1	<0.1	3.4	1.4	<0.1	<0.1	<0.1	0.3	<
Sb	0.4	0.4	0.5	0.8	1	2.1	3	0.8	0.9	0.4	1.9	1
Cs	4.52	8.6	32.9	5.97	3.95	5.78	9.91	6.46	6.57	1.36	8.45	2.21
Ba	620	827	215	3197	1346	1835	1226	719	840	1277	1684	3271
La	43	41	19	55	42	25	30	35	54	54	32	63
Ce	95	93	34	111	91	61	68	72	110	110	62	137
Nd	40	40	14	49	38	22	28	32	46	46	24	59
Tl	1.3	1.8	4.6	1.3	0.8	3.2	2.8	1	1.4	0.5	1.5	0.8
Pb	14	15	45	16	11	768	625	14	11	9	60	13
Bi	<0.1	0.1	<0.1	0.4	0.5	0.3	1	<0.1	<0.1	<0.1	0.2	0.4
Th	19.9	18	7.89	17.9	19.8	17	20.5	19.8	24.3	22.6	8.23	15.5
U	3.7	3.98	3.61	4.42	4.08	4.58	7.82	5.09	5.6	5.15	4.65	3.55

Total Fe as Fe2O3; LOI = loss on ignition; Alteration Index = 100(MgO+K2O)/(MgO+K2O+CaO+Na2O)

Table 1. continued

	MB96-34	MB96-35	MB96-37	MB96-38	MB96-39	MB96-40	MB96-41	MB96-42	MB96-43	MB96-44	MB96-45	MB96-46
SiO2	76.03	74.58	68.89	68.13	73.89	74.24	74.03	66.68	69.50	71.51	73.78	71.55
TiO2	0.15	0.27	0.46	0.53	0.27	0.23	0.30	0.49	0.51	0.36	0.26	0.30
Al2O3	13.09	13.85	15.12	14.98	13.70	13.93	13.74	14.21	14.95	15.00	13.10	13.87
Fe2O3#	1.43	2.08	4.11	5.50	2.22	2.15	2.38	6.09	4.60	3.15	4.79	5.74
MnO	0.02	0.01	0.02	0.10	0.02	0.01	0.01	0.37	0.14	0.02	0.02	0.12
MgO	0.53	0.38	1.23	1.18	0.37	0.49	0.46	1.34	1.42	0.89	0.64	1.06
CaO	0.02	0.13	0.08	0.25	0.41	0.04	0.04	0.90	0.21	0.06	0.00	0.02
Na2O	1.50	3.54	3.66	2.83	3.46	3.21	3.95	2.94	2.62	3.80	0.06	0.48
K2O	5.17	4.34	3.83	4.04	4.31	2.88	3.24	3.27	3.39	2.53	3.98	3.40
P2O5	0.03	0.03	0.09	0.14	0.04	0.02	0.05	0.13	0.13	0.05	0.03	0.04
LOI	1.44	1.11	2.12	2.22	1.25	2.71	1.79	3.23	2.42	2.23	3.09	2.94
Total	99.41	100.32	99.61	99.90	99.94	99.91	99.99	99.65	99.89	99.60	99.75	99.52
S	<0.01	<0.01	<0.01	<0.01	<0.01	0.02	<0.01	0.01	0.02	0.02	<0.01	0.01
Total C	0.03	0.03	0.05	0.07	0.09	0.17	0.10	0.40	0.11	0.08	0.09	0.08
CO2	0.11	0.11	0.18	0.26	0.33	0.62	0.37	1.47	0.40	0.29	0.33	0.29
Alteration Index	78.9	56.3	57.5	62.9	54.7	50.9	48.1	54.6	63.0	47.0	98.7	89.9
Trace Elements (ppm)												
Sc	5	4	11	11	3	5	4	11	11	6	4	4
V	6	4	60	83	3	3	12	77	81	12	7	18
Cr	3	2	11	8	2	3	3	7	7	3	2	4
Ni	2	1	3	3	2	2	1	3	3	1	1	1
Cu	4	2	3	18	4	3	3	6	7	6	35	14
Zn	39	17	36	32	19	23	21	75	40	38	33	70
As	1	<1	<1	<1	<1	<1	1	<1	<1	<1	4	2
Rb	256	136	138	157	140	121	112	135	129	103	170	154
Sr	29	96	122	103	104	78	112	100	78	98	4	8
Y	35	41	28	35	62	38	41	42	41	40	25	24
Zr	125	270	243	212	269	282	266	199	209	282	254	238
Nb	13.7	17	13.6	10.7	16.1	16.8	13.4	10.6	11.1	16	13.7	11.6
Mo	0.2	0.5	0.4	1.7	0.6	0.7	0.8	0.9	0.2	0.4	1	0.2
Ag	0.9	<0.1	<0.1	<0.1	<0.1	<0.1	<0.1	<0.1	<0.1	<0.1	<0.1	0.1
Cd	0.2	<0.1	<0.1	0.3	0.2	<0.1	<0.1	0.1	0.4	<0.1	<0.1	<0.1
Sb	1.5	0.4	0.7	0.5	0.5	0.6	0.9	0.7	0.9	0.4	0.9	1.4
Cs	5.82	1.98	2.98	2.9	2.35	1.99	2.36	4.06	2.57	1.17	1.46	1.53
Ba	1138	988	817	876	947	787	942	696	711	606	931	703
La	56	57	38	54	174	47	54	47	49	41	32	41
Ce	122	102	80	113	289	82	107	95	101	74	72	82
Nd	46	45	31	47	131	42	44	39	45	37	29	32
Tl	1.9	<0.5	0.5	<0.5	<0.5	<0.5	<0.5	<0.5	<0.5	<0.5	0.9	0.9
Pb	94	3	3	2	3	8	7	4	2	3	5	7
Bi	0.8	<0.1	0.3	<0.1	<0.1	<0.1	0.1	<0.1	<0.1	0.3	2.6	2.1
Th	28.2	22	21.4	19.6	22	23.3	22.3	18.4	19.3	20.6	25.1	18.4
U	5.9	5.4	5.01	4.59	5.05	5.21	5.73	4.35	4.66	4.98	5.79	3.91

Total Fe as Fe2O3; LOI = loss on ignition; Alteration Index = 100(MgO+K2O)/(MgO+K2O+CaO+Na2O)

MRV geochemical database update

Michael D. Blake
Centre for Ore Deposit Research, Geology Department, University of Tasmania

Database structure

Geochemical data along with locational, lithological and other descriptive data for AMIRA/ARC project P439 have been stored following the structure of the MRT (Mineral Resources Tasmania) geochemical database. This information takes the form of an ARC-INFO dataset stored on 'geo' in the Geology Department. The final integrated database will be available to sponsors at the end of the project. (A preliminary version is available on disk as an Excel file.)

Composition

The data so far compiled for the Mt Read Volcanics Database was sourced from data provided by MRT, CODES and Pasminco Exploration, and has the following breakdown:

• released ISM data	1576 samples
• UNITAS thesis data and other research projects	535 samples
• P439 Traverse data	216 samples
• Pasminco Exploration data	734 samples
Total	**3061 samples**

The MRT dataset is derived from information in the 'Rockchem' database taken from previously released 1:25000 sheet digital packages.

Pasminco Exploration data came from a file containing over 1400 analyses provided for this project. Unfortunately lithological information for many samples was incomplete, so over half of the data was excluded from the combined database. The Pasminco data does not contain S, Cu, Pb, Zn analyses.

Progress

Recent interpretation of the combined dataset involved the production of contoured geochemical images of the Mt Read Volcanics using GIS techniques.

Colour images of element distributions and various element ratios from the MRV database were created with the aim of visually enhancing anomalous data in a large dataset which relates to a large geographic area. In this case the contouring was done with ARC-INFO using IDW (Inverse Distance Weighted Interpolation) to produce a colour image based on located geochemical analyses. The resulting contoured geochemical images were used as a gridded overlay for topographic and geological digitised data.

All plots have been compiled in Appendix 1. The images show the distribution of : Cu, Pb, Zn, Na_2O, MnO, S, K_2O, Tl, Sb, Ba/K, S/Na_2O, TiO_2/Zr, Ishikawa Alteration Index, and Chlorite Index.

The images are designed to allow easy recognition of trends and anomalous areas from within the dataset.

Each of the contour plots has been generated from a subset of the main database in order to exclude unwanted data from the interpolation.The data was confined to those samples identified as being within

the Mt Read Volcanics. Samples excluded were classed as regional and contact metamorphics, biological and chemical precipitates, as listed in the Mineral Resources Tasmania database classification (MRT1996/06). Images have been coloured using a colour stretching method to remap colours over a particular range of concentrations in the data.

The following calculations were used in the production of images:

Chlorite Index (CI) =

$$100(MgO + FeO)/(MgO + FeO + Na_2O + K_2O)$$

$$FeO = Fe_2O_{3tot} * 0.8998$$

Ishikawa Alteration Index (AI) =

$$100 (K_2O + MgO)/(K_2O + MgO + Na_2O + CaO)$$

Titanium–Zirconium Ratio (TiZr) =

$$(TiO_2 * 5995)/Zr$$

IDW

IDW is a weighted distance average function used to interpret between known data points. The properties of the function are controlled by the following:

- The distance to a known data point
- The number of sample data points to be included in the interpolation can be set
- The power option: changes the interpolation from local to global. A larger power diminishes the effect of surrounding points.
- Radius option: A radius can be set, within which all data points will be included in the interpolation.
- Minimum Points: The minimum number of points for interpretation.
- Cellsize: The resolution produced in the output grid

The images contained in Appendix 1. were calculated with the following parameters: Radius = 500 m, Power = 2, Minimum Points = 0, Cellsize = 100 m

An important feature of IDW is that interpreted values will not exceed the highest, nor be less than the lowest input point because of the weighted distance average.

It is important to remember that contour maps are a visual guide designed for easy viewing of data and to draw attention to spatial variations. By their nature they are interpretive so reference to the original data must be made once areas of interest are identified to determine the real significance of the anomalies

Future developments

Further work to be done with the MRV dataset will involve the addition of geochemical data from the following:

- The Hellyer and Rosebery studies of P439
- Newly released data from ISM.

The complete dataset is and will be available (including MRT data) provided sponsors have individually purchased the MRT data. Otherwise, the same dataset minus the MRT data will be available.

References

Watson, D.F. and Phillip, G.M., *A Refinement of Inverse Distance Weighted Interpolation*, Geo - Processing, 2: 315-327, 1985.

McClenaghan, M.P., Bottrill, R.S., & Bird, K.G., *Structure of GIS Databases (Revision 1)*, Mineral Resources Tasmania - Tasmanian Geological Survey, Record 1996/06

Characteristics of mineralised centres — from contoured geochemical data

The following trends have been interpreted directly from contoured geochemistry maps. The characteristics are general as they were 'eyed' directly from the maps.

Hercules

- MnO in footwall and hangingwall > 0.28
- Manganese Carbonate Index > 60 at the ore position, and > 40 in footwall rocks
- Chlorite Index > 60 in footwall and immediate hangingwall

Rosebery

- Cu < 120 ppm
- Zn < 320 ppm
- Na_2O < 1.6
- Ishikawa Alteration Index > 70
- K_2O < 7
- S 0.8 - 4
- Ba/K_2O 400–760
- S/Na_2O > 0.8
- MnO not definitive
- Manganese carbonate Index not definitive
- Chlorite Index 40–60

Red Hills

- Cu > 120
- Pb > 120
- Zn > 120
- Na_2O < 1.6
- Ishikawa Alteration Index > 60
- K_2O > 4
- S Not anomalous, < 1.6
- Ba/K_2O > 520 and < 640, no anomaly although surrounding samples anomalous.
- S/Na_2O > 0.6
- MnO > 0.28
- Manganese Carbonate Index < 60, not anomalous
- Chlorite Index 40–60, not anomalous, although surrounding samples are.

Selina area

- Cu > 180
- Pb > 120
- Zn > 480
- Na_2O < 1.6
- Ishikawa Alteration Index > 70
- K_2O > 4
- S Not enough data
- Ba/K < 640, not anomalous
- S/Na_2O > 0.6 (v little data)
- Mno Not enough data in felsic rocks
- Manganese Index > 40 and < 60

Howards Anomaly

- Cu > 180
- Pb > 120
- Zn > 480
- Na_2O < 2.4
- Ishikawa Alteration Index > 60
- K_2O > 4
- Ba/K_2O Not anomalous although neighbouring anomalous sample
- S/Na_2O Not anomalous although neighbouring anomalous sample
- MnO < 0.2, Not anomalous
- Manganese Index Not anomalous
- Chlorite Index Some anomalous samples > 60

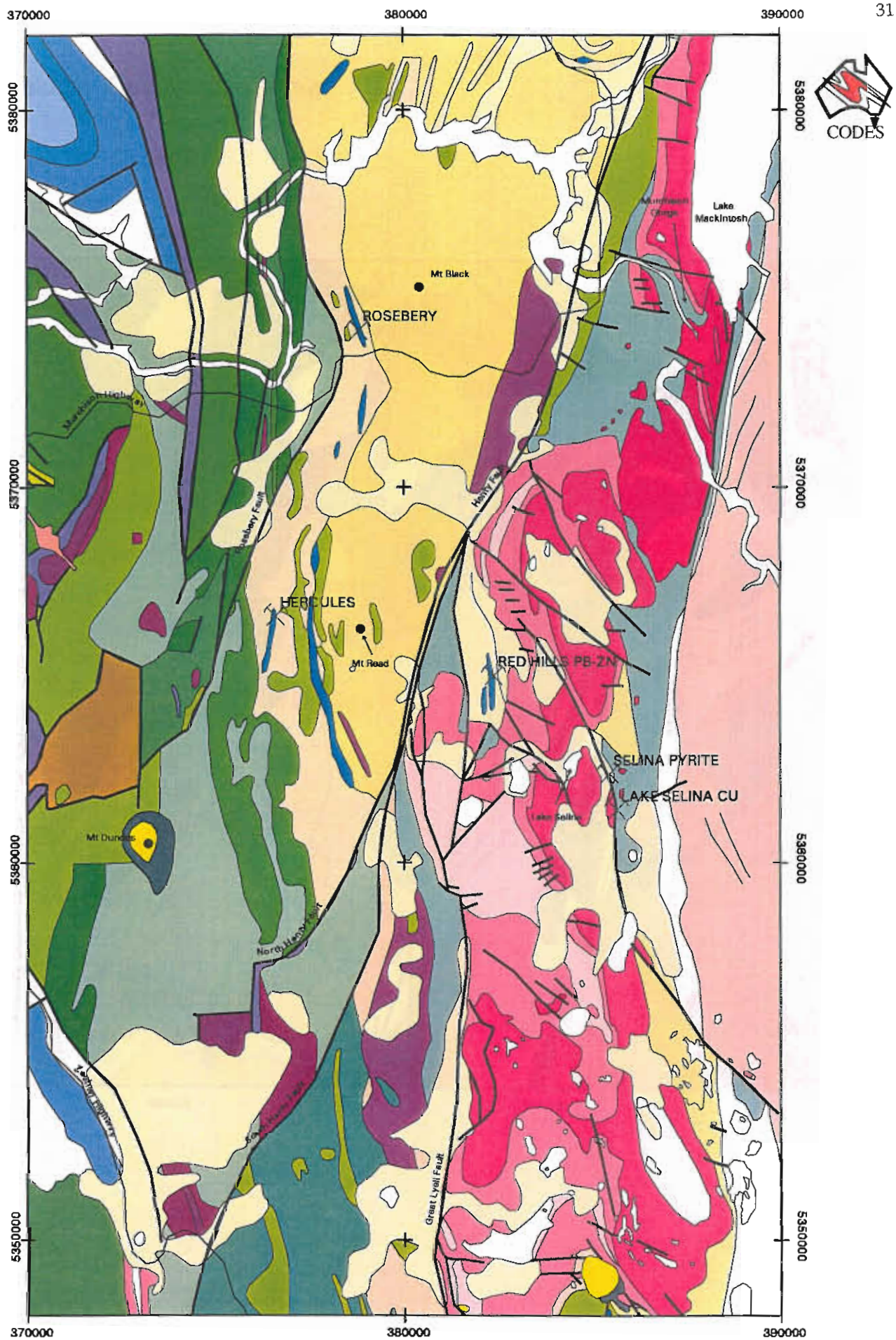

WESTERN TASMANIA

Geology : Mt Read Volcanics

Geology : Que - Hellyer Area

CODES

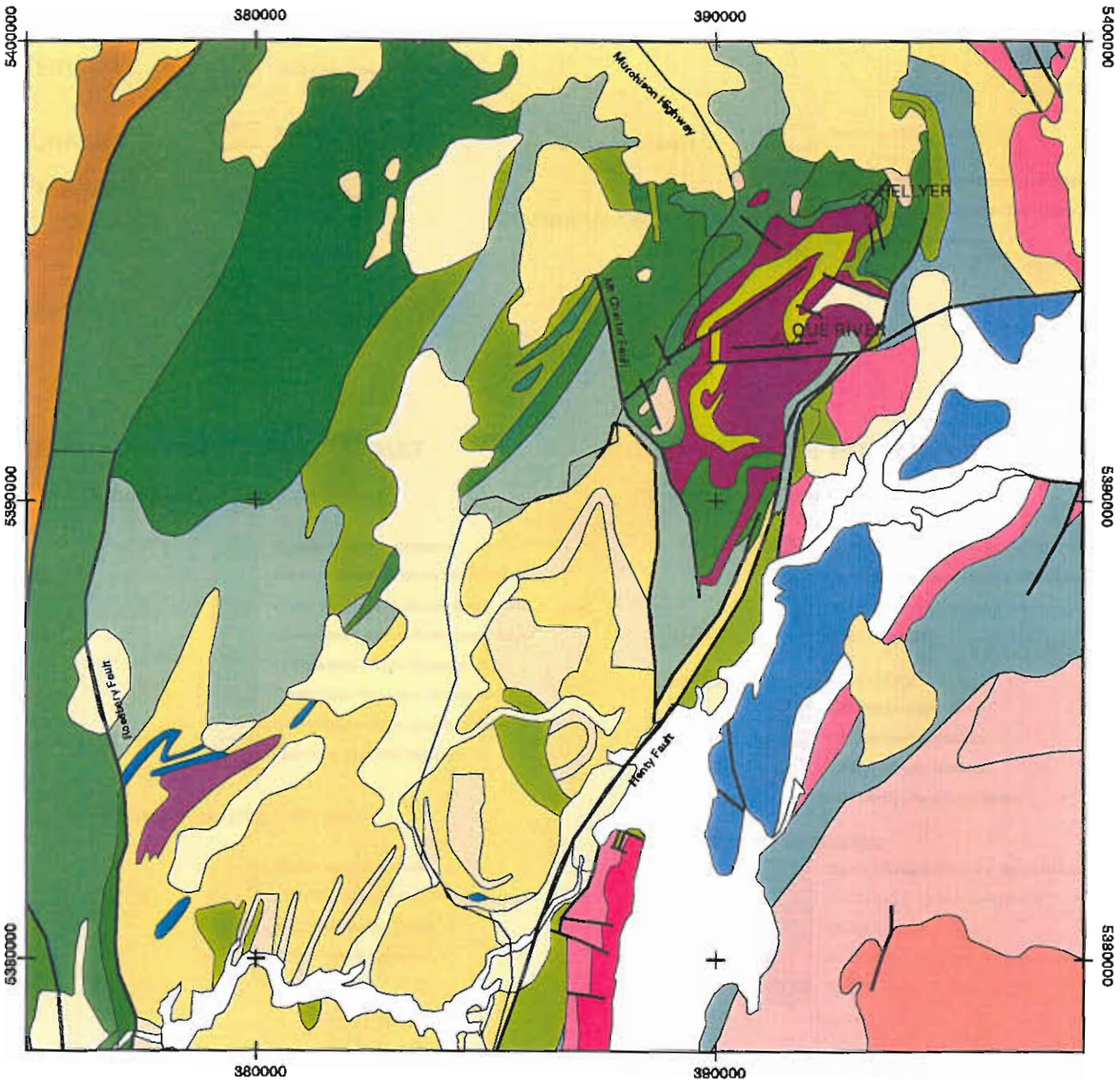

GEOLOGY KEY

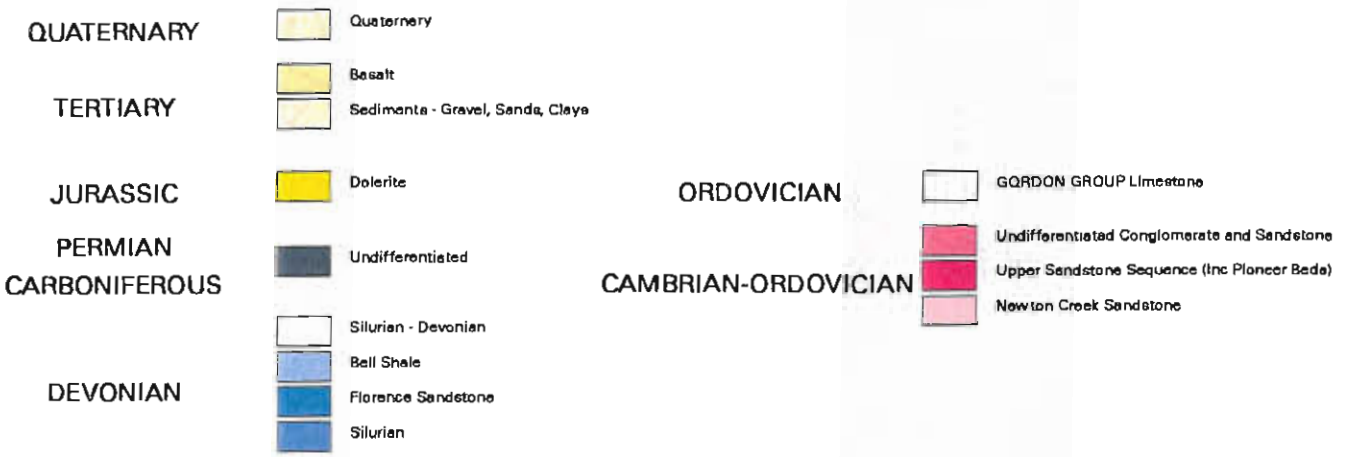

NORTH AND WEST OF HENTY FAULT

Dundas Group and Correlates

Central Volcanic Complex

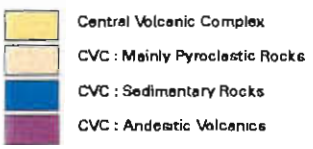

SOUTH AND EAST OF HENTY FAULT

Tyndall Group and Correlates

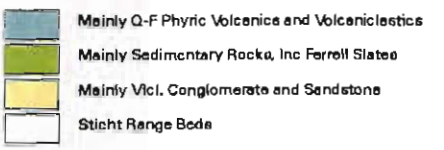

Central Volcanic Complex

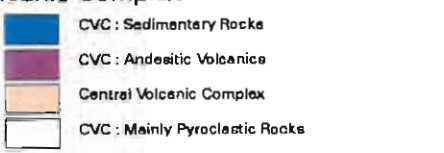

Western Sequence

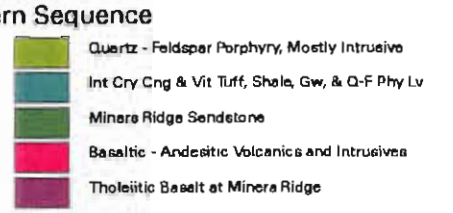

UNASSIGNED CAMBRIAN UNITS

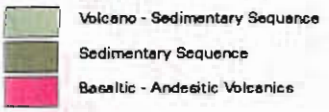

CAMBRIAN INTRUSIONS

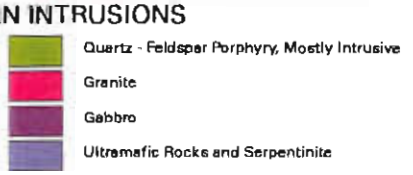

CRIMSON CREEK FORMATION

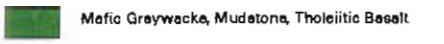

SUCCESS CREEK GROUP

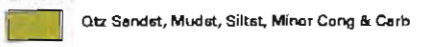

PRECAMBRIAN

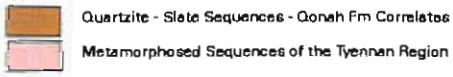

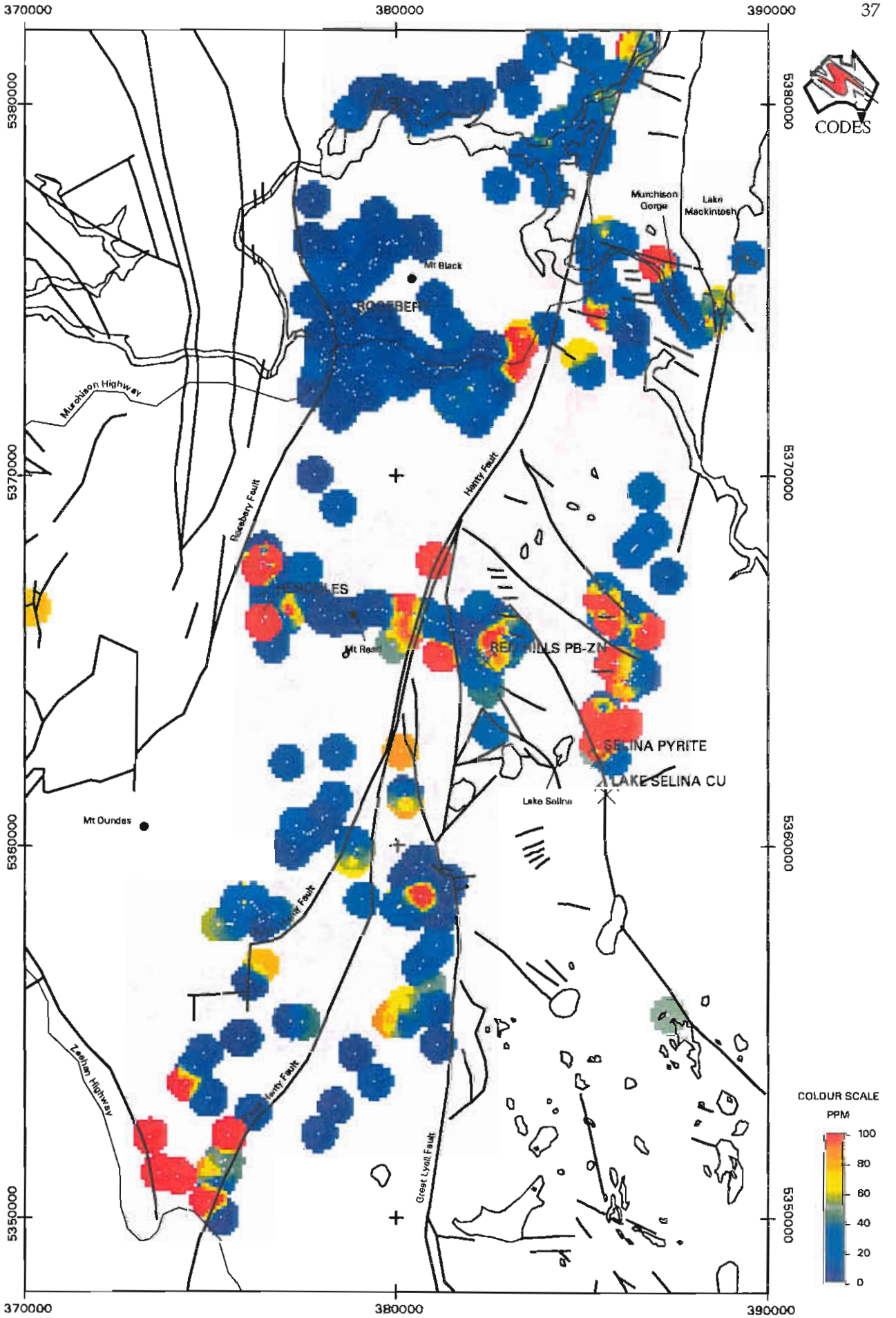
370000
380000
390000
5380000
5370000
5360000
5350000
CODES
Murchison Gorge
Lake Mackintosh
Mt Black
ROSEBERY
Murchison Highway
Rosebery Fault
Henty Fault
HERCULES
Mt Read
RED HILLS PB-ZN
SELINA PYRITE
LAKE SELINA CU
Lake Selina
Mt Dundas
Henty Fault
Zeehan Highway
Great Lyell Fault
A
A'
B
B'
COLOUR SCALE
PPM
100
80
60
40
20
0
Scale: 1:100,000
0 1000 2000 3000 4000 5000
metres
WESTERN TASMANIA
Contoured Cu Distribution : Mt Read Volcanics

Western Tasmania : Que - Hellyer Area

CODES

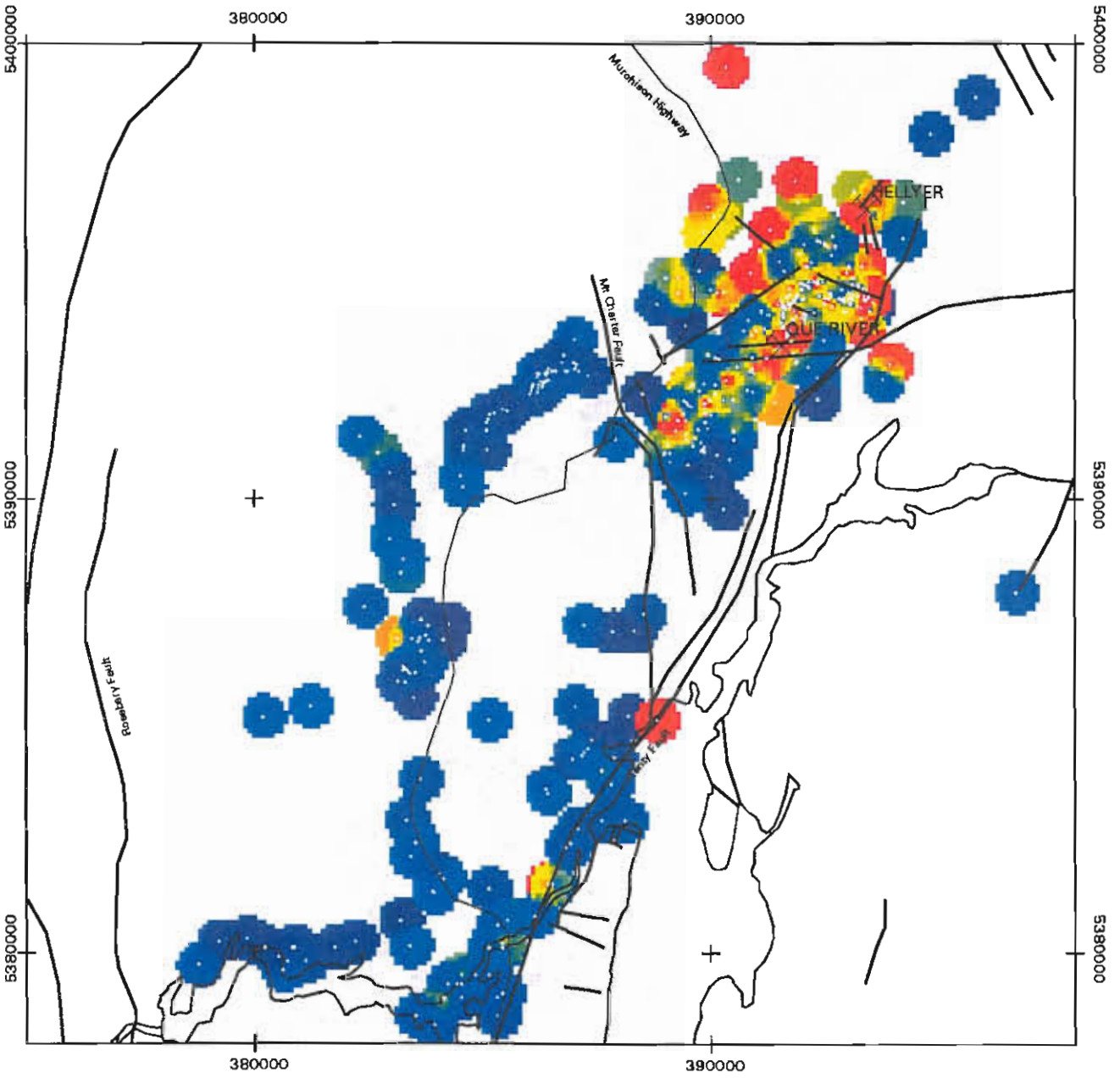

COLOUR SCALE
PPM
100
80
60
40
20
0

Scale: 1:100,000
0 1000 2000 3000 4000 5000
metres

Geochemical Database

Contoured Cu Distribution : Mt Read Volcanics

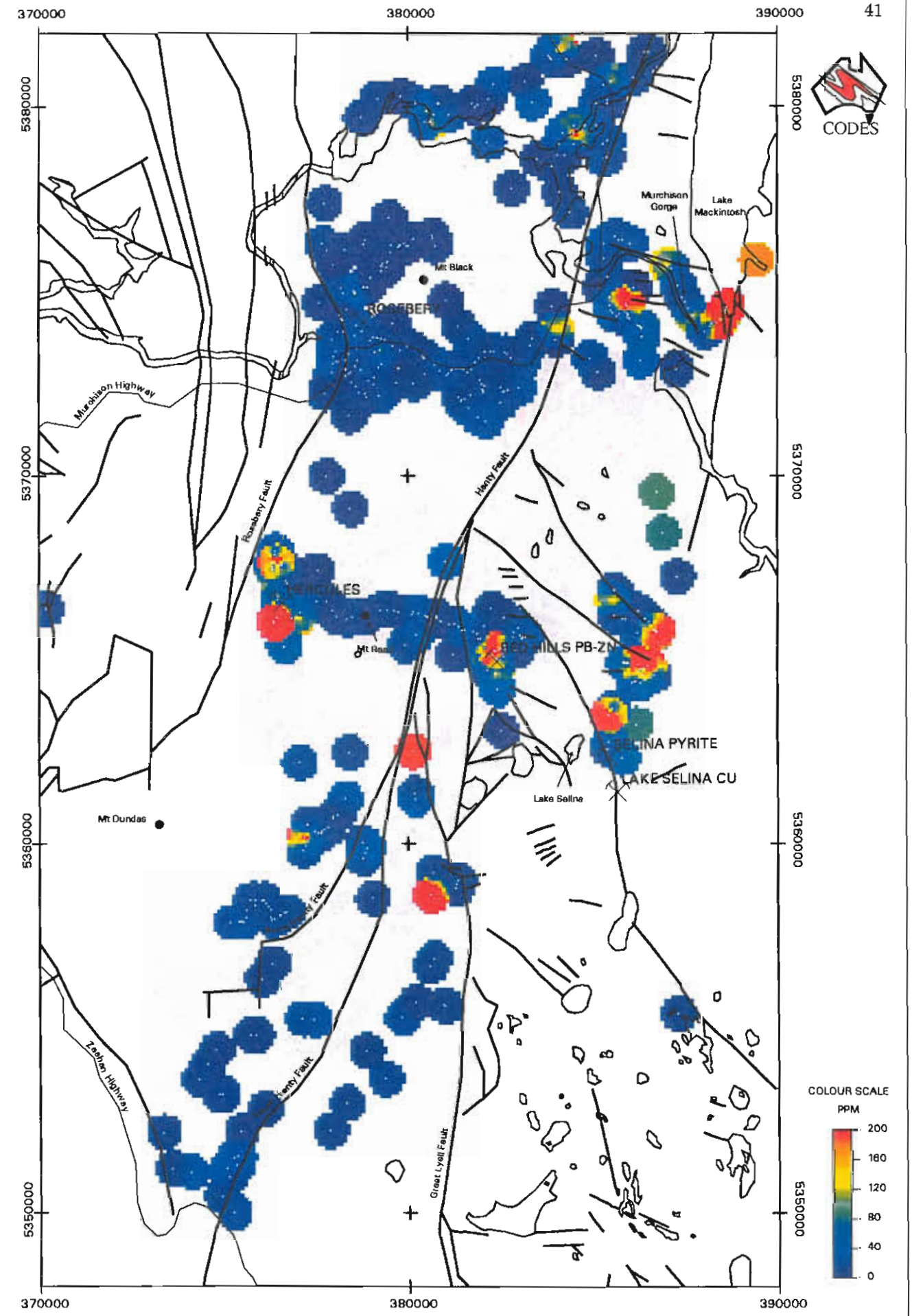

WESTERN TASMANIA

Contoured Pb Distribution : Mt Read Volcanics

Western Tasmania : Que - Hellyer Area

CODES

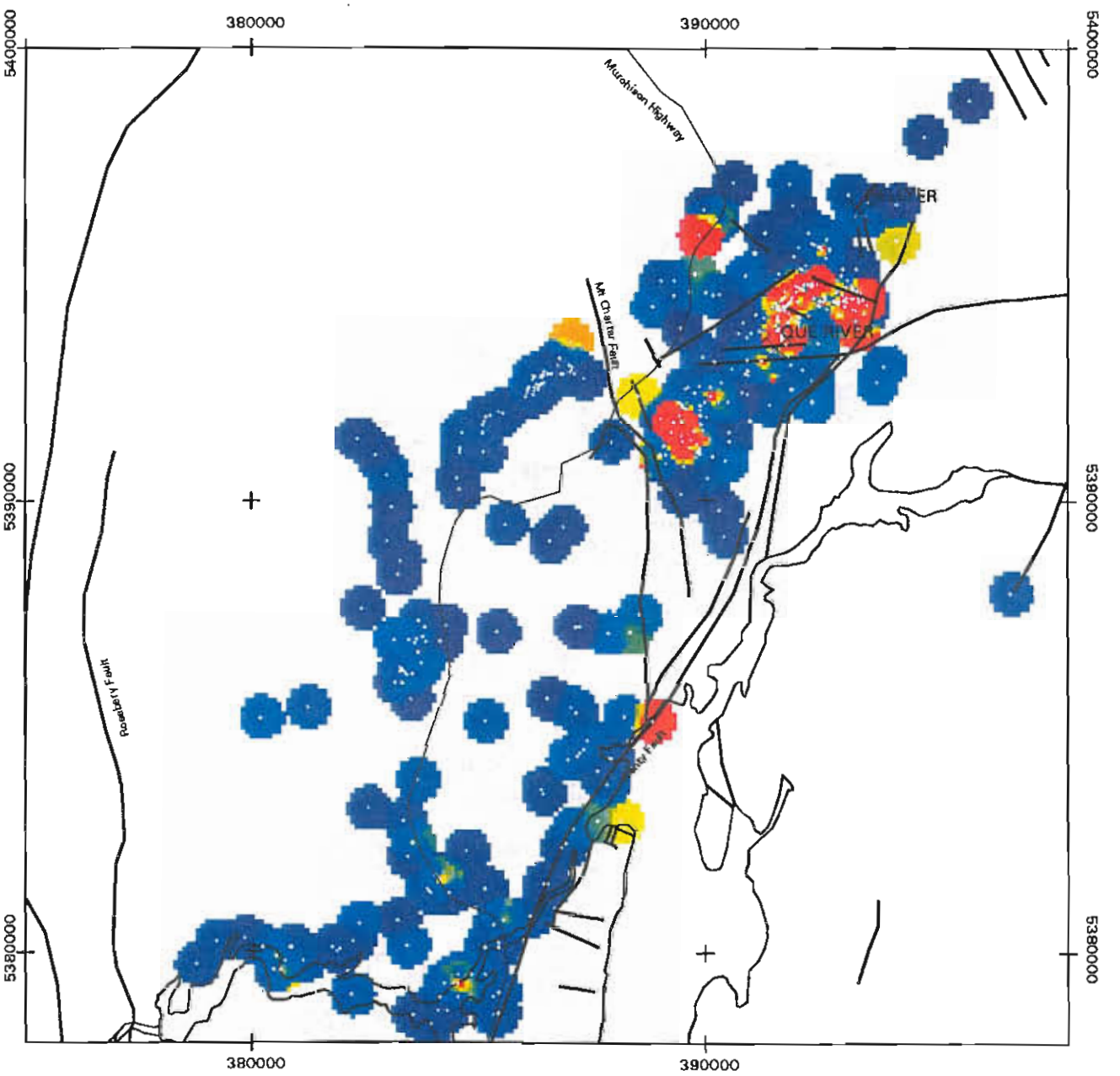

COLOUR SCALE
PPM
200
160
120
80
40
0

Scale: 1:100,000
0 1000 2000 3000 4000 5000
metres

Geochemical Database

Contoured Pb Distribution : Mt Read Volcanics

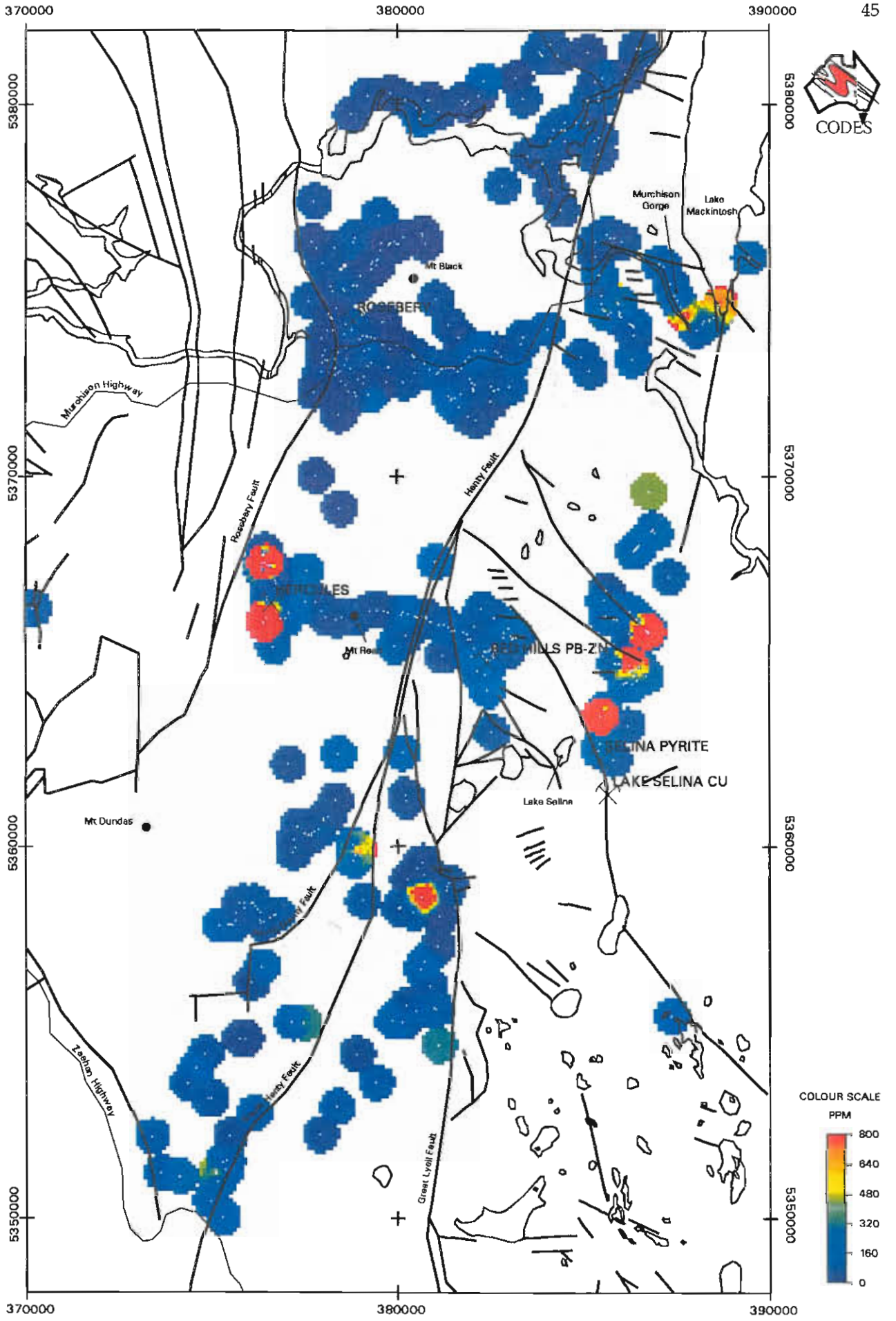

WESTERN TASMANIA

Contoured Zn Distribution : Mt Read Volcanics

Western Tasmania : Que - Hellyer Area

CODES

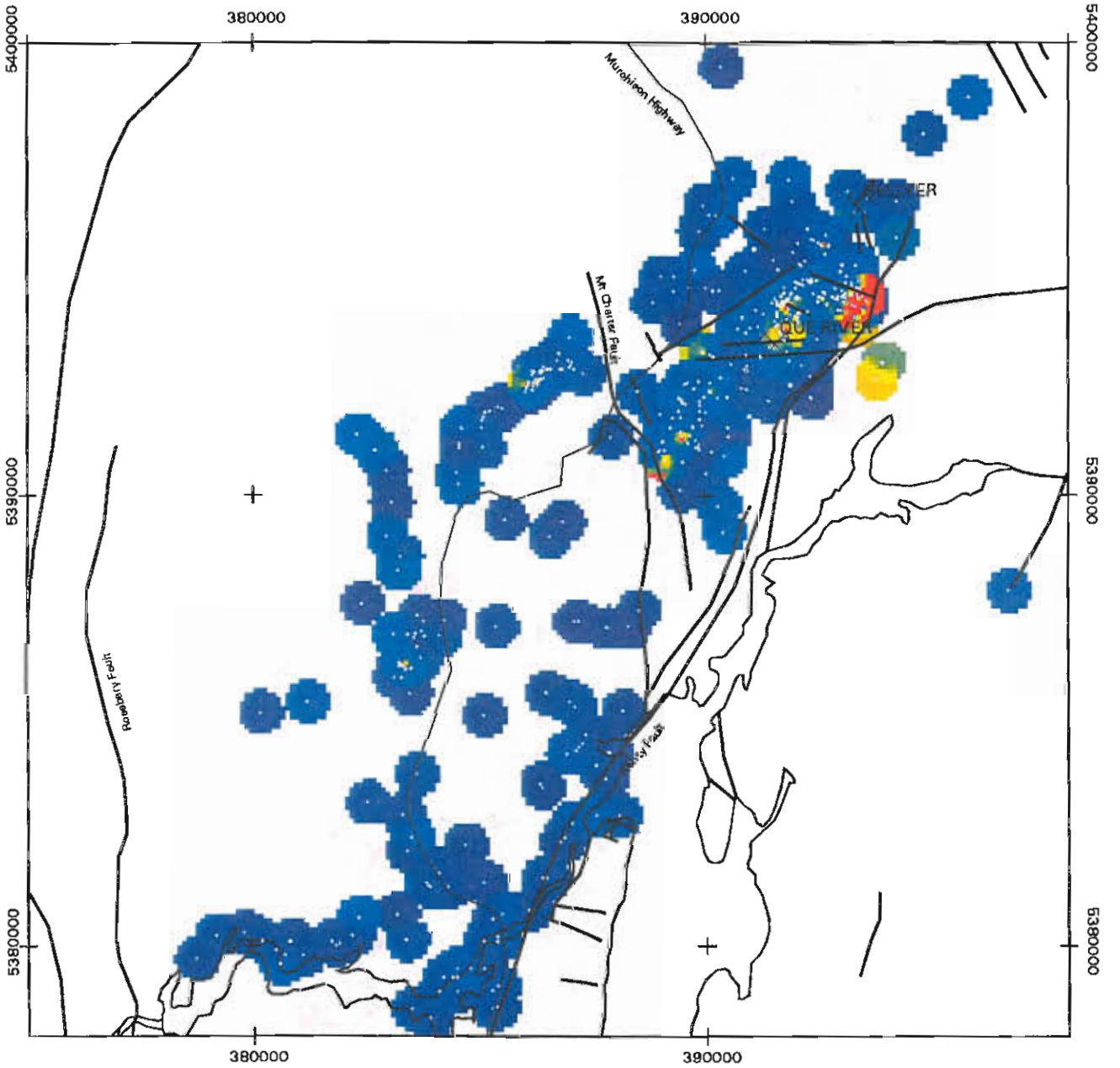

COLOUR SCALE
PPM
800
640
480
320
160
0

Scale: 1:100,000
0 1000 2000 3000 4000 5000
metres

Geochemical Database

Contoured Zn Distribution : Mt Read Volcanics

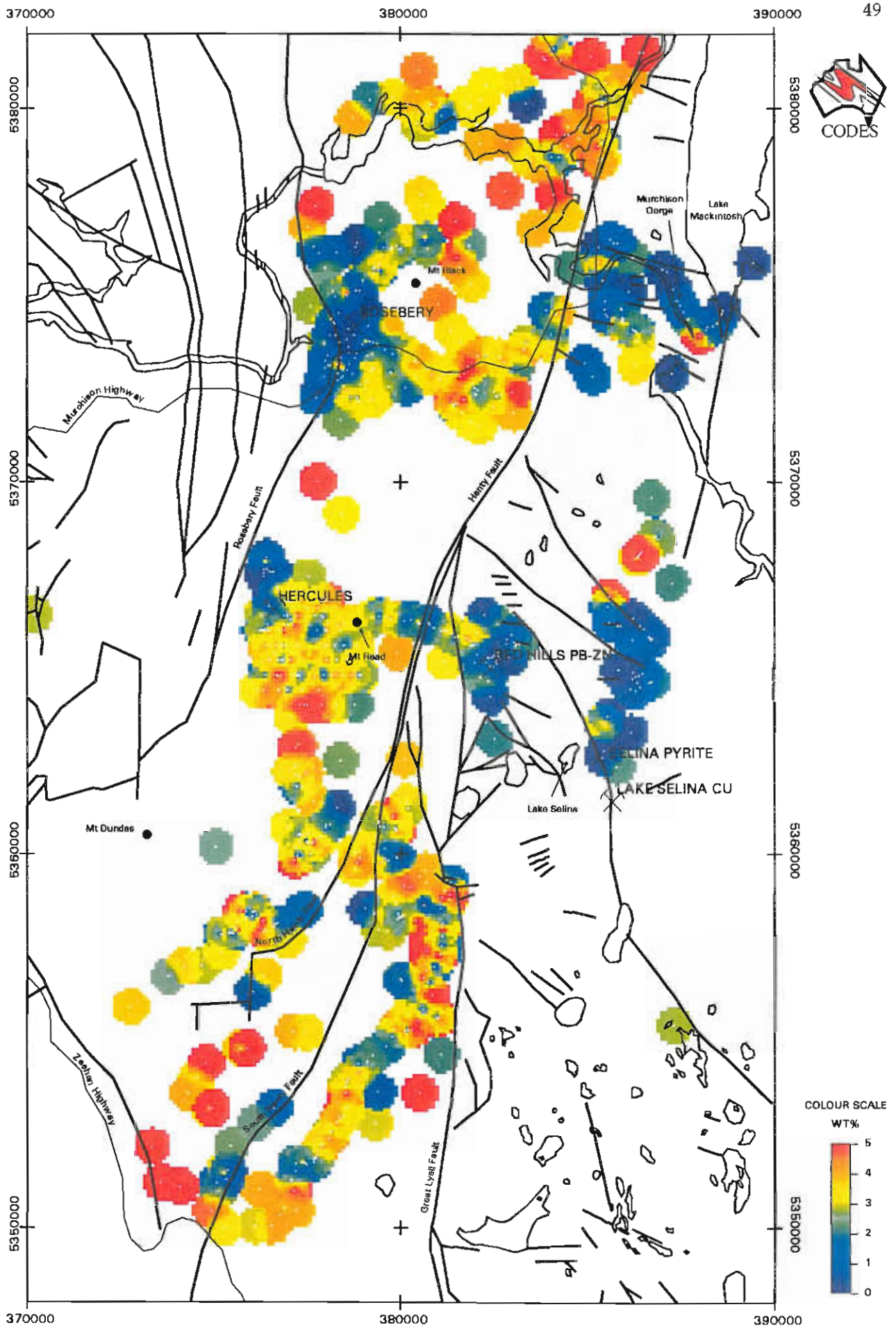
370000
380000
390000
5380000
5370000
5360000
5350000
CODES
Murchison Gorge
Lake Mackintosh
Mt Black
ROSEBERY
Murchison Highway
Rosebery Fault
Henty Fault
HERCULES
Mt Read
RED HILLS PB-ZN
SELINA PYRITE
LAKE SELINA CU
Lake Selina
Mt Dundas
North Head
Zeehan Highway
Great Lyell Fault
COLOUR SCALE
WT%
5
4
3
2
1
0
Scale: 1:100,000
0 1000 2000 3000 4000 5000
metres
WESTERN TASMANIA
Contoured Na2O Data : Mt Read Volcanics

Western Tasmania : Que - Hellyer Area

CODES

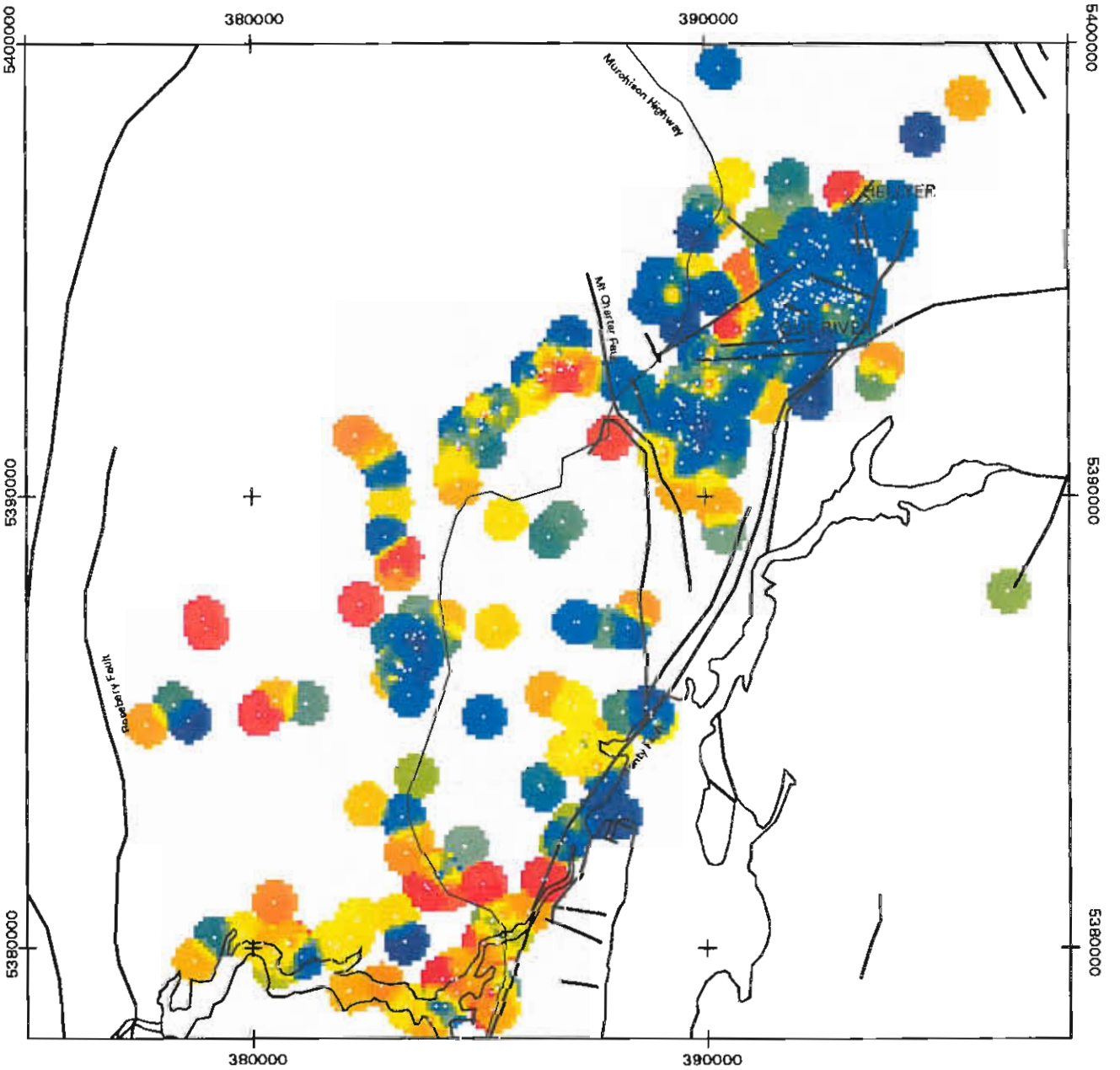

COLOUR SCALE
WT%
5
4
3
2
1
0

Scale: 1:100,000
0 1000 2000 3000 4000 5000
metres

Geochemical Database

Contoured Na2o Data : Mt Read Volcanics

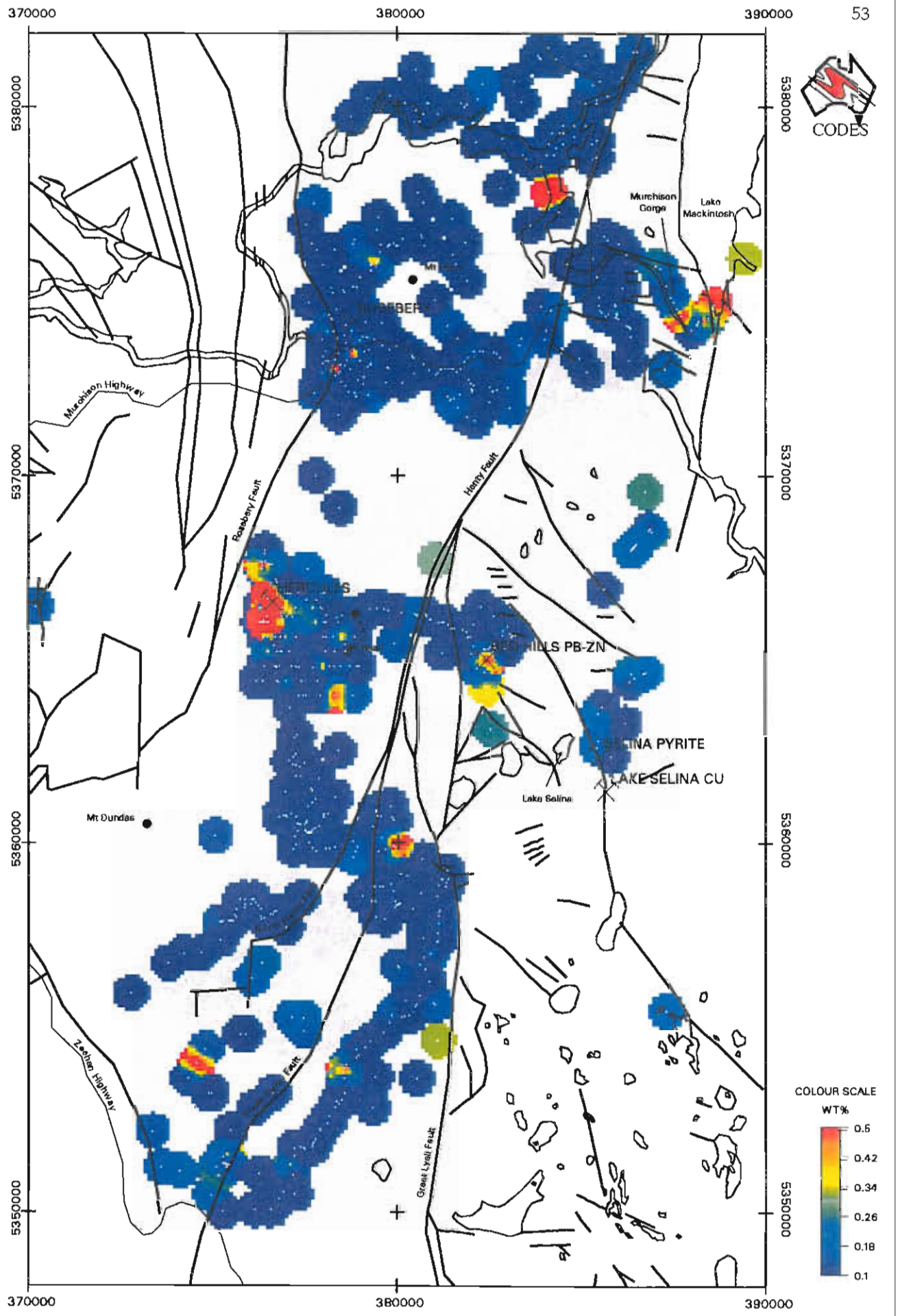

WESTERN TASMANIA

Contoured MnO Distribution : Mt Read Volcanics

Western Tasmania : Que - Hellyer Area

CODES

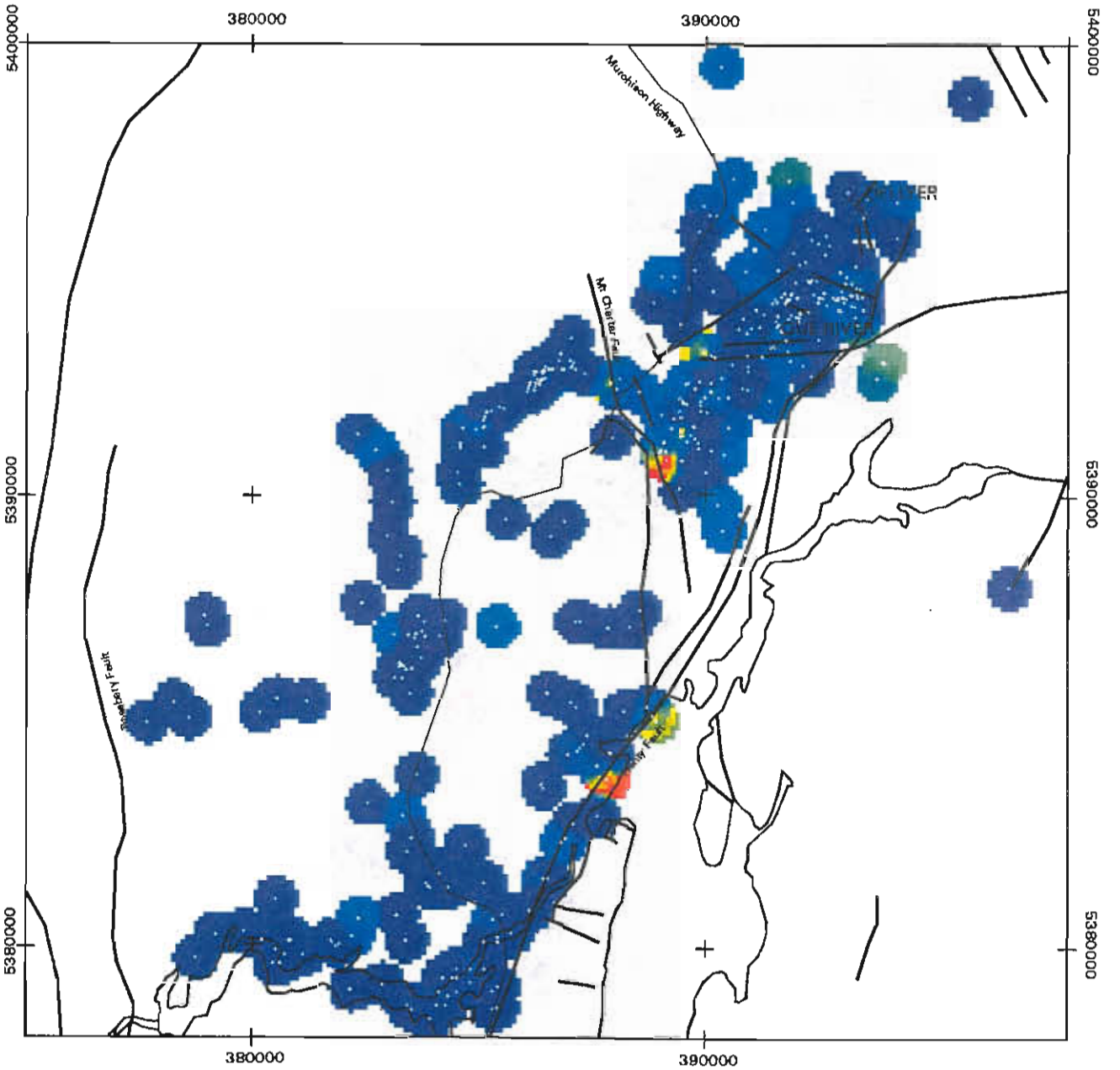

COLOUR SCALE
WT%
0.5
0.42
0.34
0.26
0.18
0.1

0 1000 2000 3000 4000 5000
metres

Geochemical Database

Contoured MnO Distribution : Mt Read Volcanics

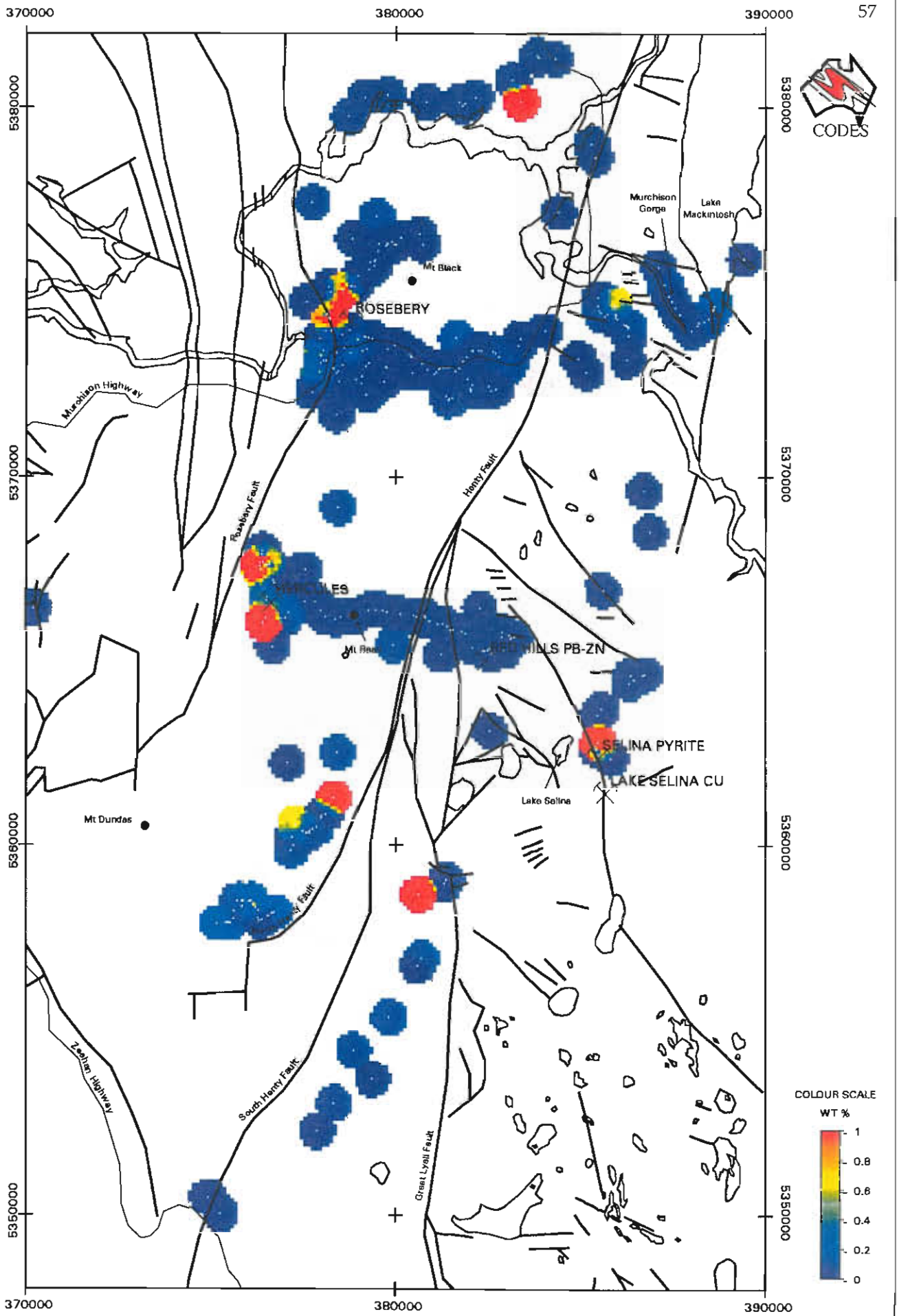

WESTERN TASMANIA

Contoured S Distribution : Mt Read Volcanics

Western Tasmania : Que - Hellyer Area

CODES

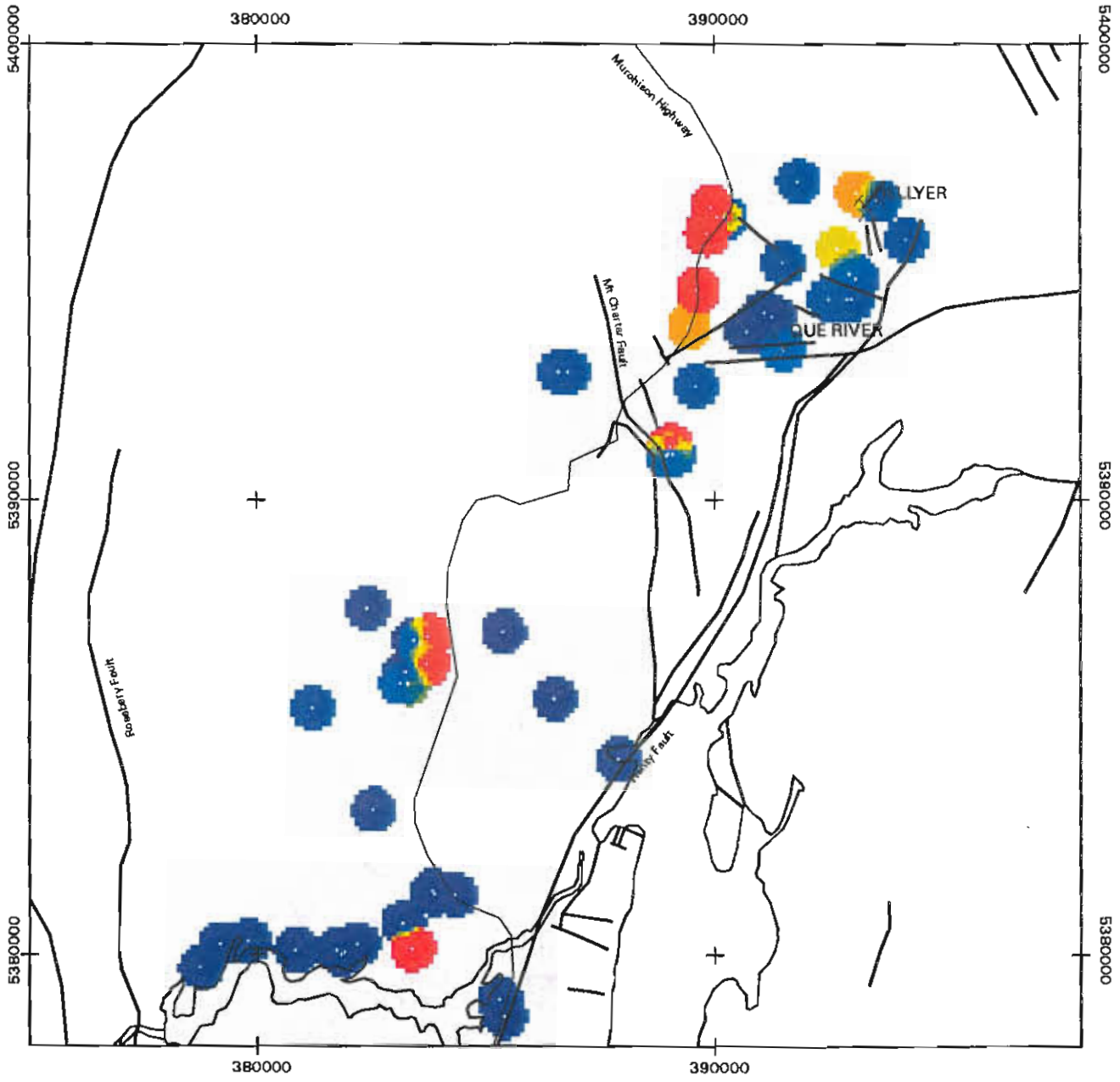

COLOUR SCALE
WT %
1
0.8
0.6
0.4
0.2
0

0 1000 2000 3000 4000 5000
metres

Geochemical Database

Contoured S Distribution : Mt Read Volcanics

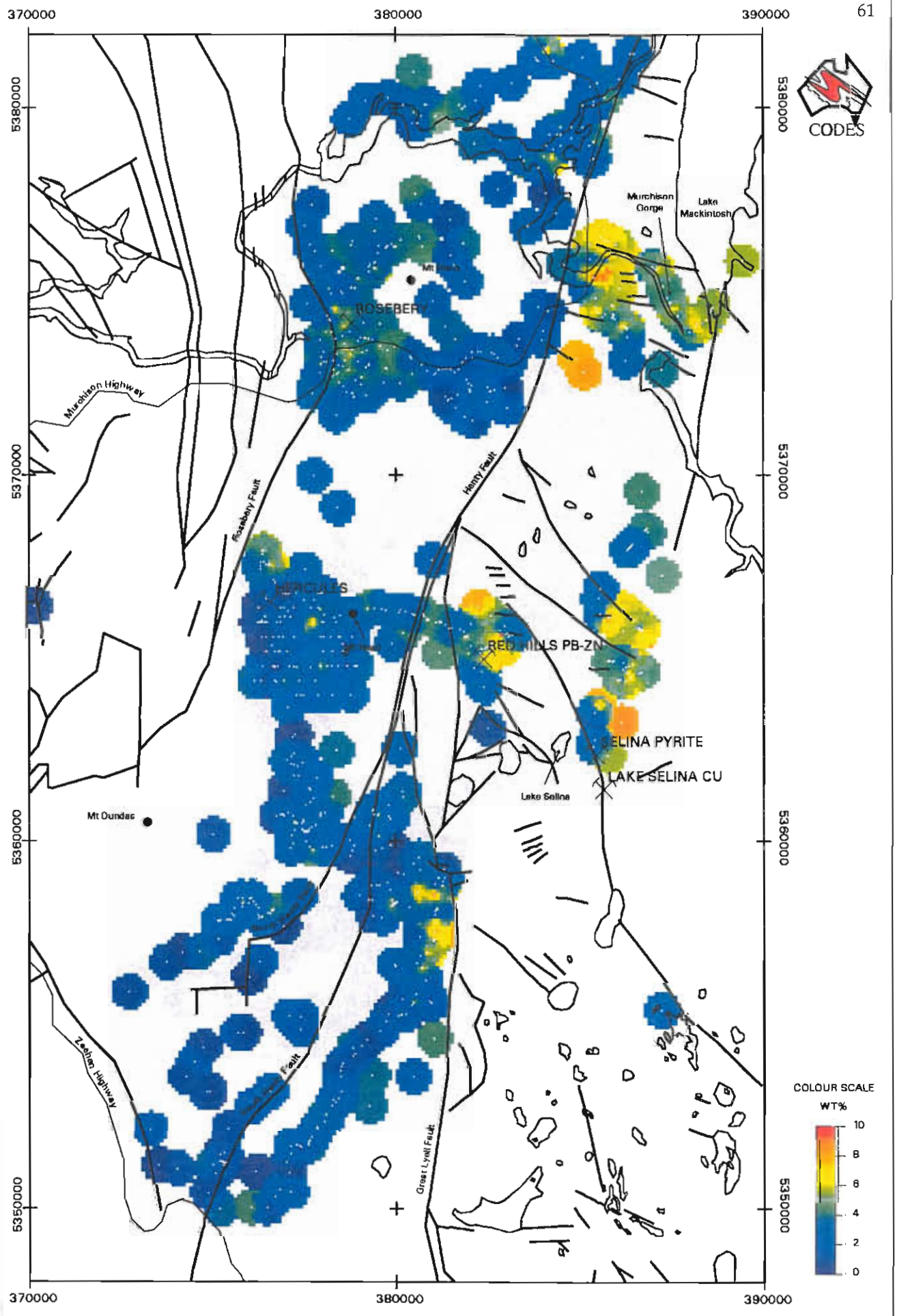
370000
380000
390000
5380000
5370000
5360000
5350000
CODES
Murchison Gorge
Lake Mackintosh
ROSEBERY
Mt Black
Murchison Highway
Rosebery Fault
Henty Fault
HERCULES
RED HILLS PB-ZN
SELINA PYRITE
LAKE SELINA CU
Lake Selina
Mt Dundas
Zeehan Highway
Great Lyell Fault
A
A'
B
B'
COLOUR SCALE
WT%
10
8
6
4
2
0
0 1000 2000 3000 4000 5000
metres
WESTERN TASMANIA
Contoured K2O Distribution : Mt Read Volcanics

Western Tasmania : Que - Hellyer Area

CODES

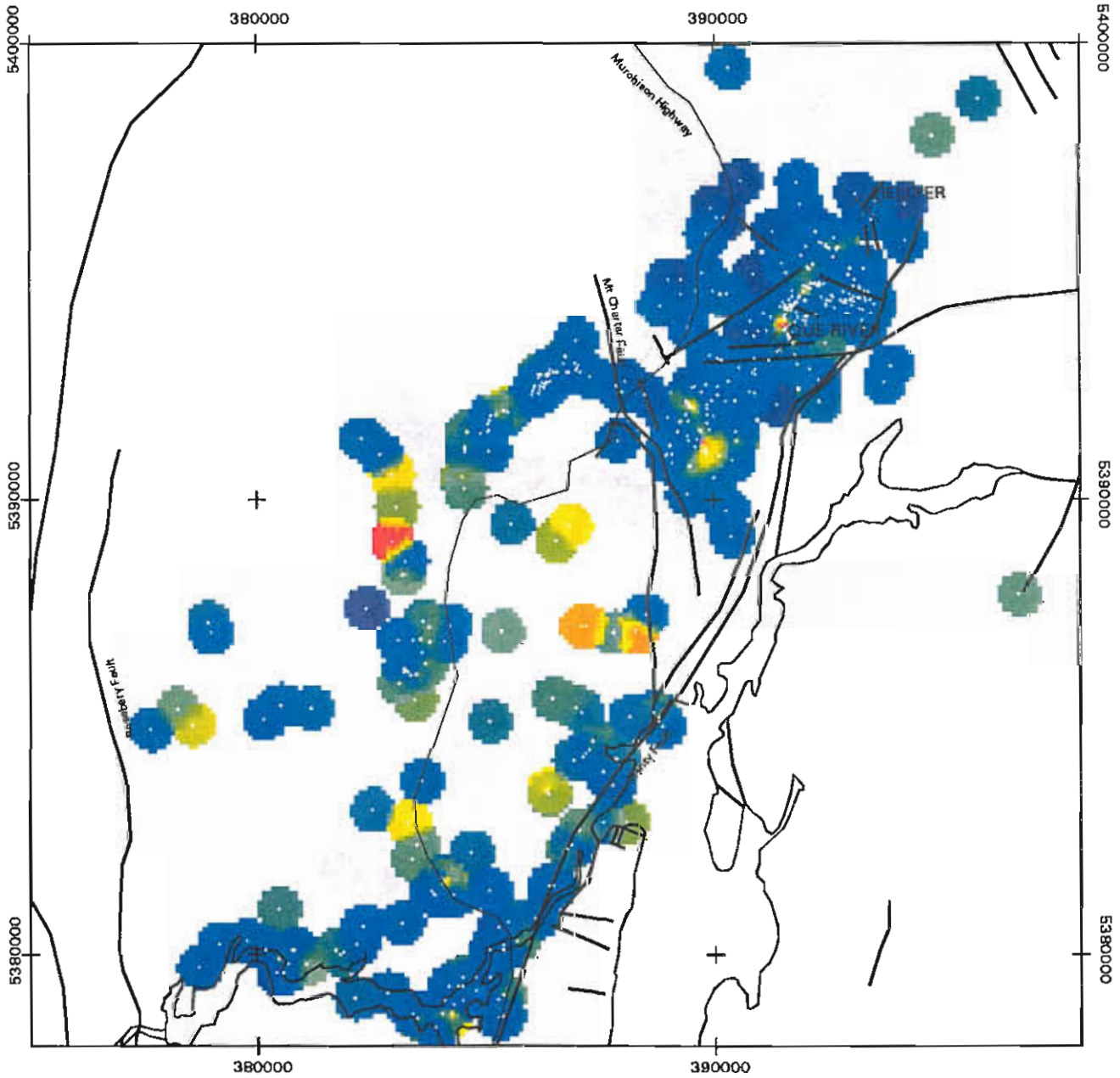

COLOUR SCALE
WT%
10
8
6
4
2
0

N

0 1000 2000 3000 4000 5000
metres

Geochemical Database

Contoured K2O Distribution : Mt Read Volcanics

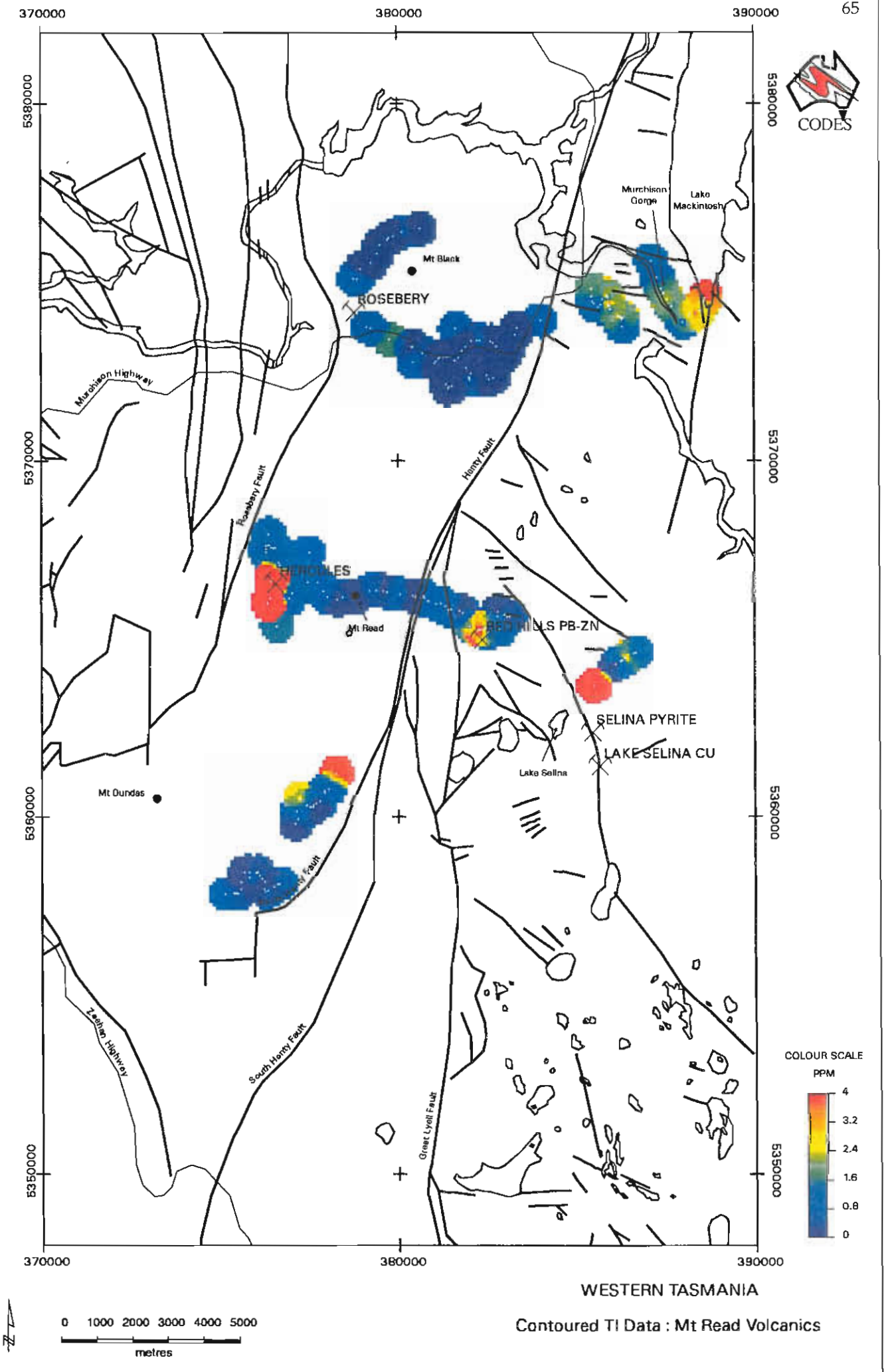
370000
380000
390000
5380000
5370000
5360000
5350000
CODES
Murchison Gorge
Lake Mackintosh
Mt Black
ROSEBERY
Murchison Highway
Rosebery Fault
Henty Fault
RENDLES
Mt Read
RED HILLS PB-ZN
SELINA PYRITE
LAKE SELINA CU
Lake Selina
Mt Dundas
Zeehan Highway
South Henty Fault
Great Lyell Fault
COLOUR SCALE
PPM
4
3.2
2.4
1.6
0.8
0
0 1000 2000 3000 4000 5000
metres
WESTERN TASMANIA
Contoured TI Data : Mt Read Volcanics

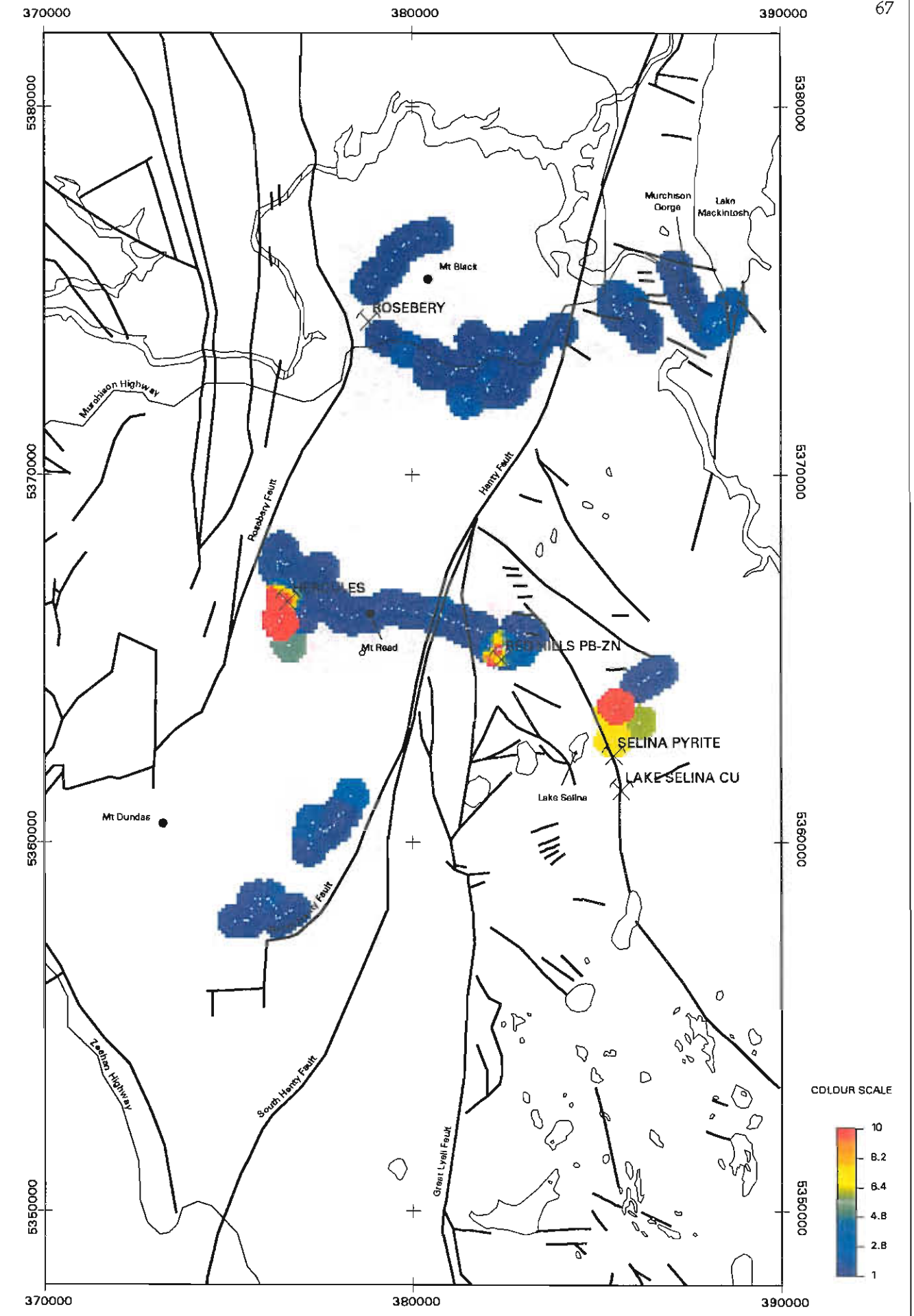

WESTERN TASMANIA

Contoured Sb Data : Mt Read Volcanics

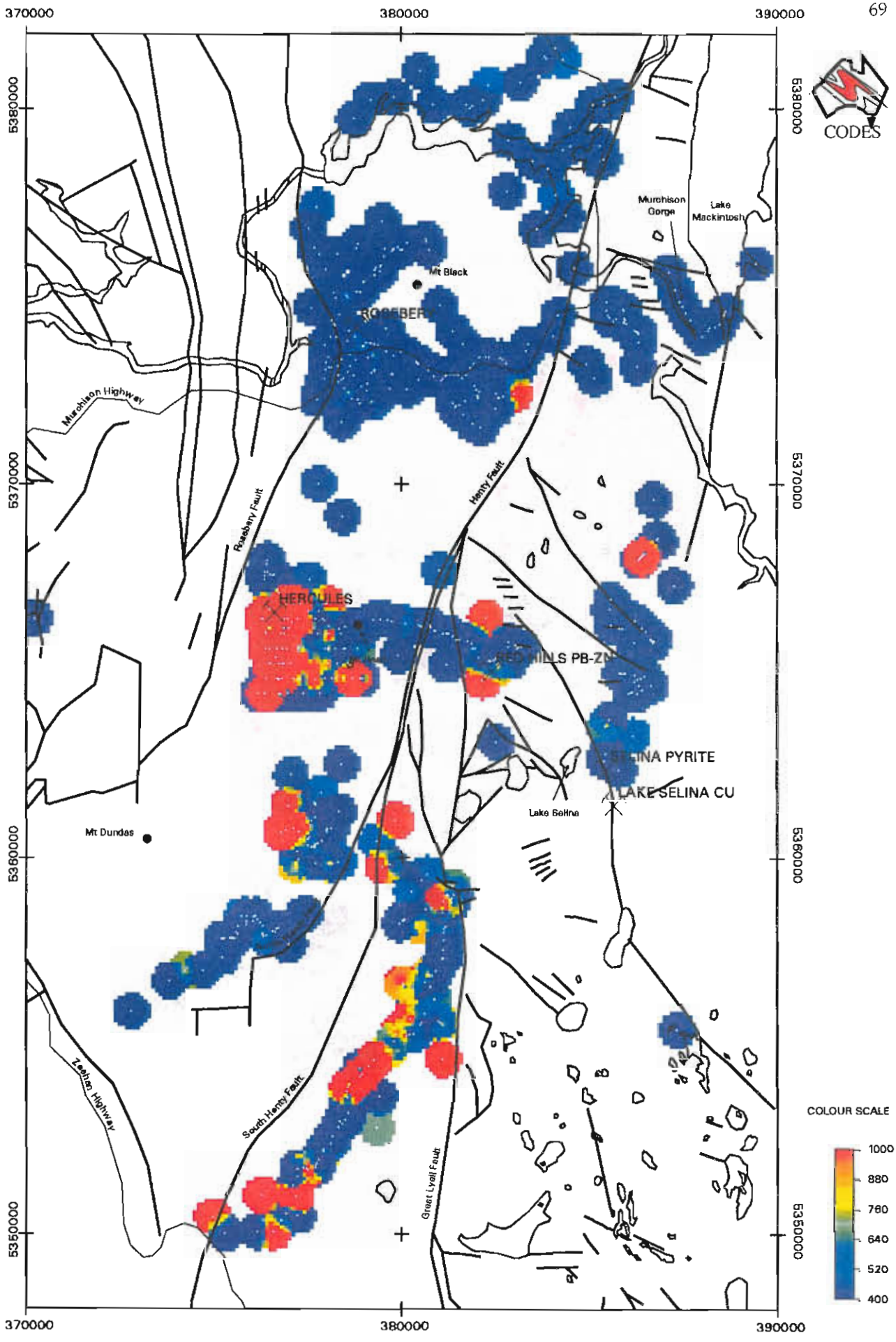

WESTERN TASMANIA

Contoured Ba/K Distribution : Mt Read Volcanics

Western Tasmania : Que - Hellyer Area

CODES

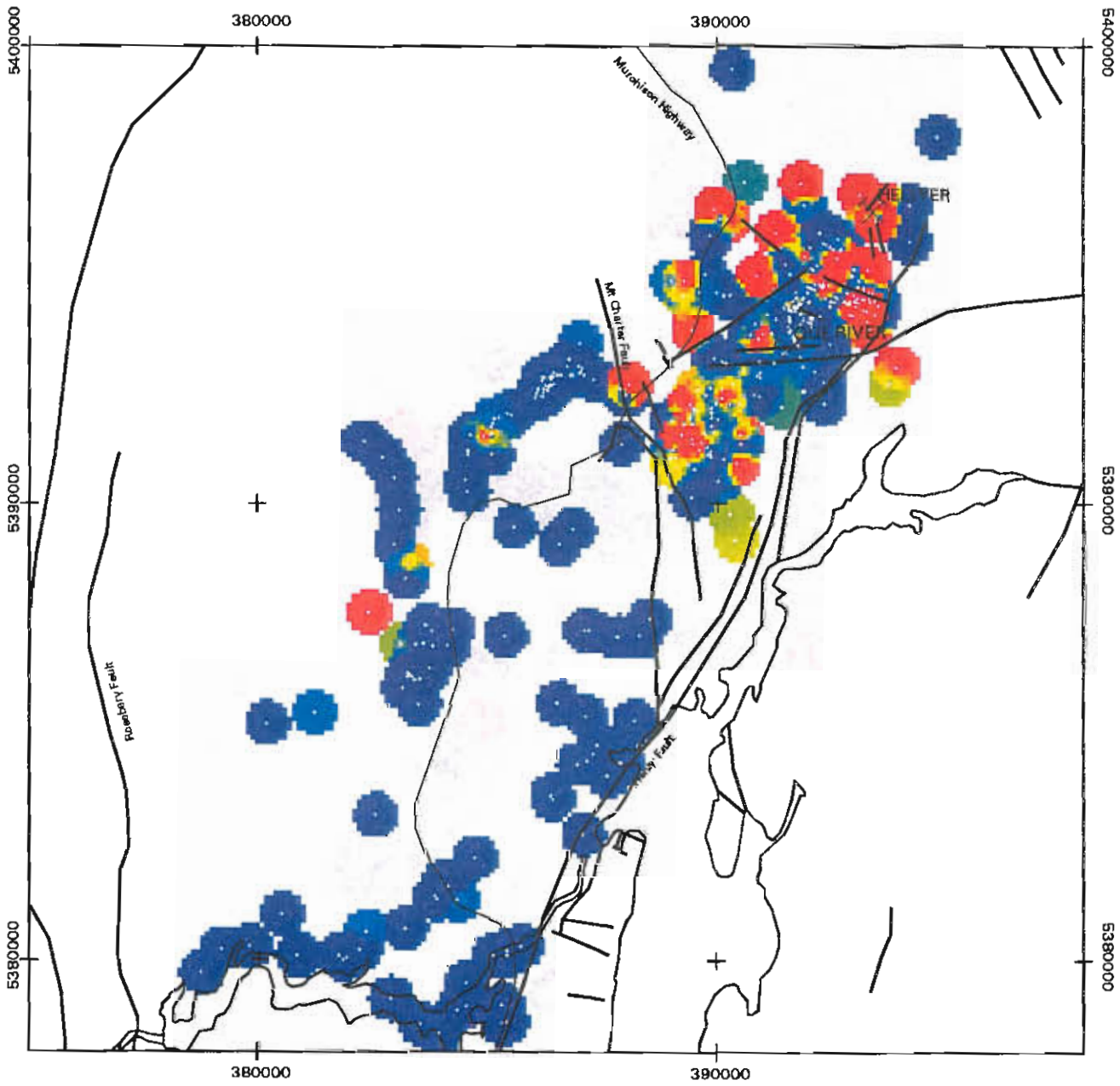

COLOUR SCALE

1000
880
760
640
520
400

N

0 1000 2000 3000 4000 5000
metres

Geochemical Database

Contoured Ba/K Distribution - Mt Read Volcanics

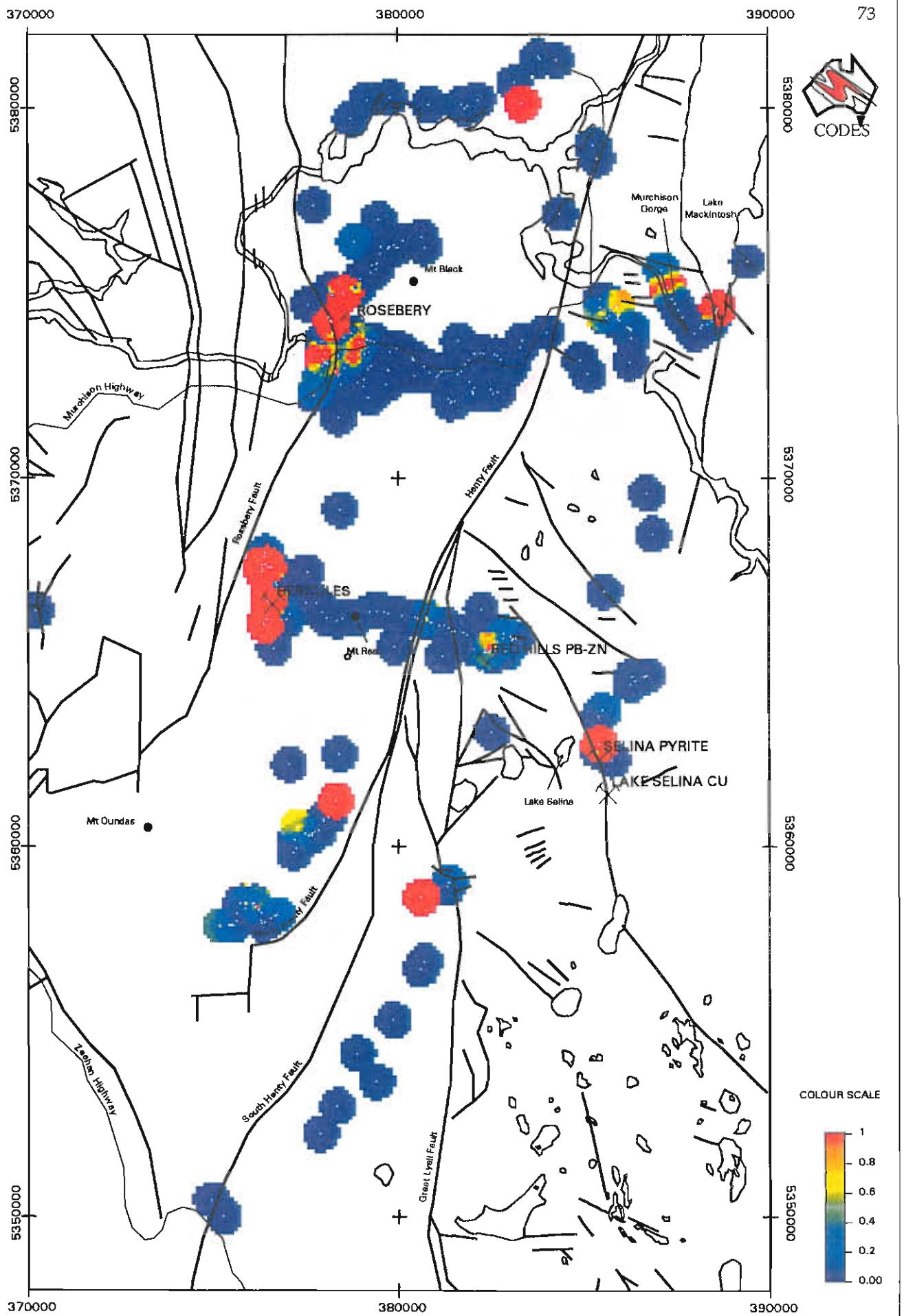

WESTERN TASMANIA

Contoured S/Na2O Distribution : Mt Read Volcanics

Western Tasmania : Que - Hellyer Area

CODES

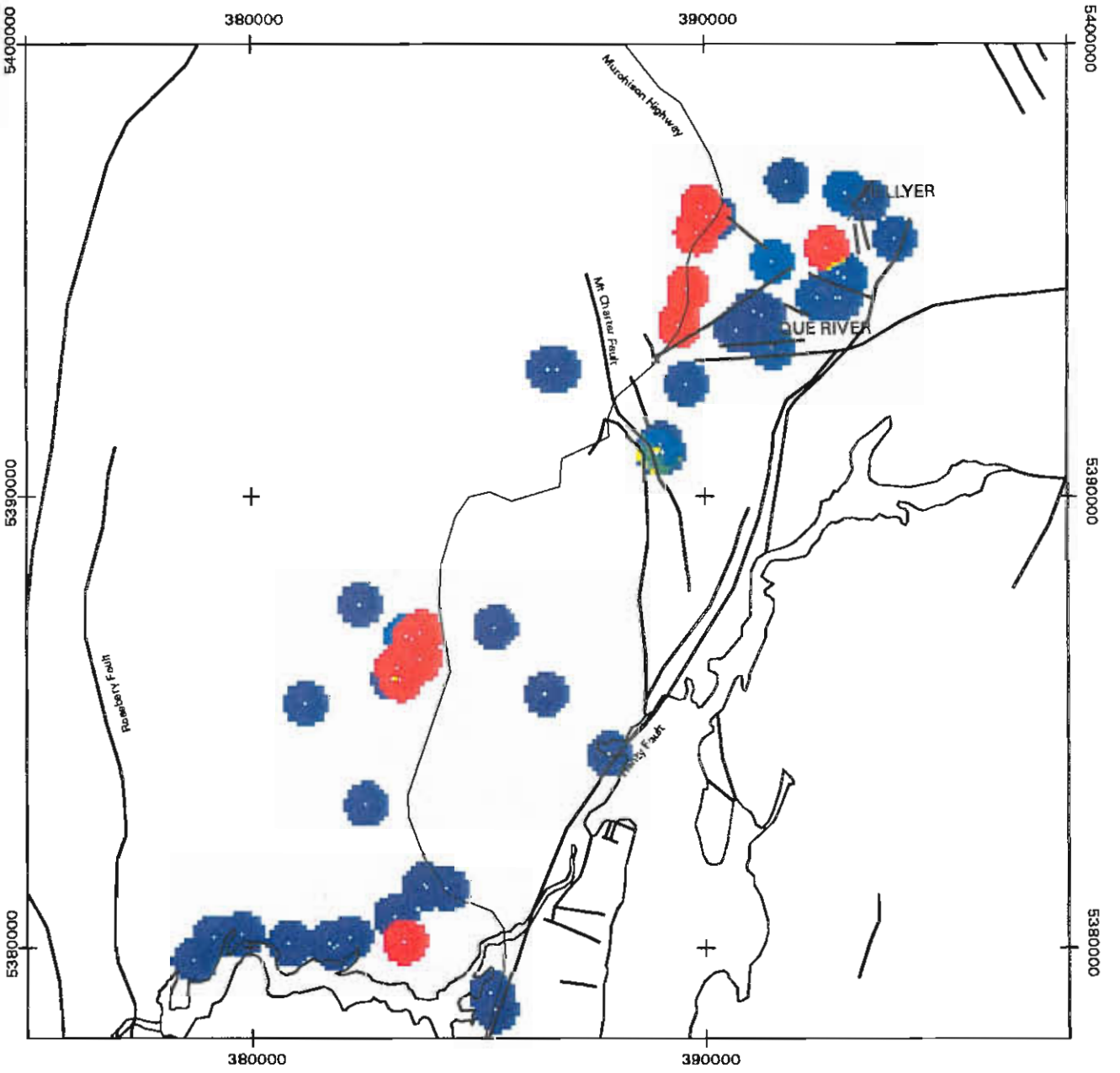

COLOUR SCALE

1
0.8
0.6
0.4
0.2
0.00

N

0 1000 2000 3000 4000 5000
metres

Geochemical Database

Contoured S/Na2O Distribution : Mt Read Volcanics

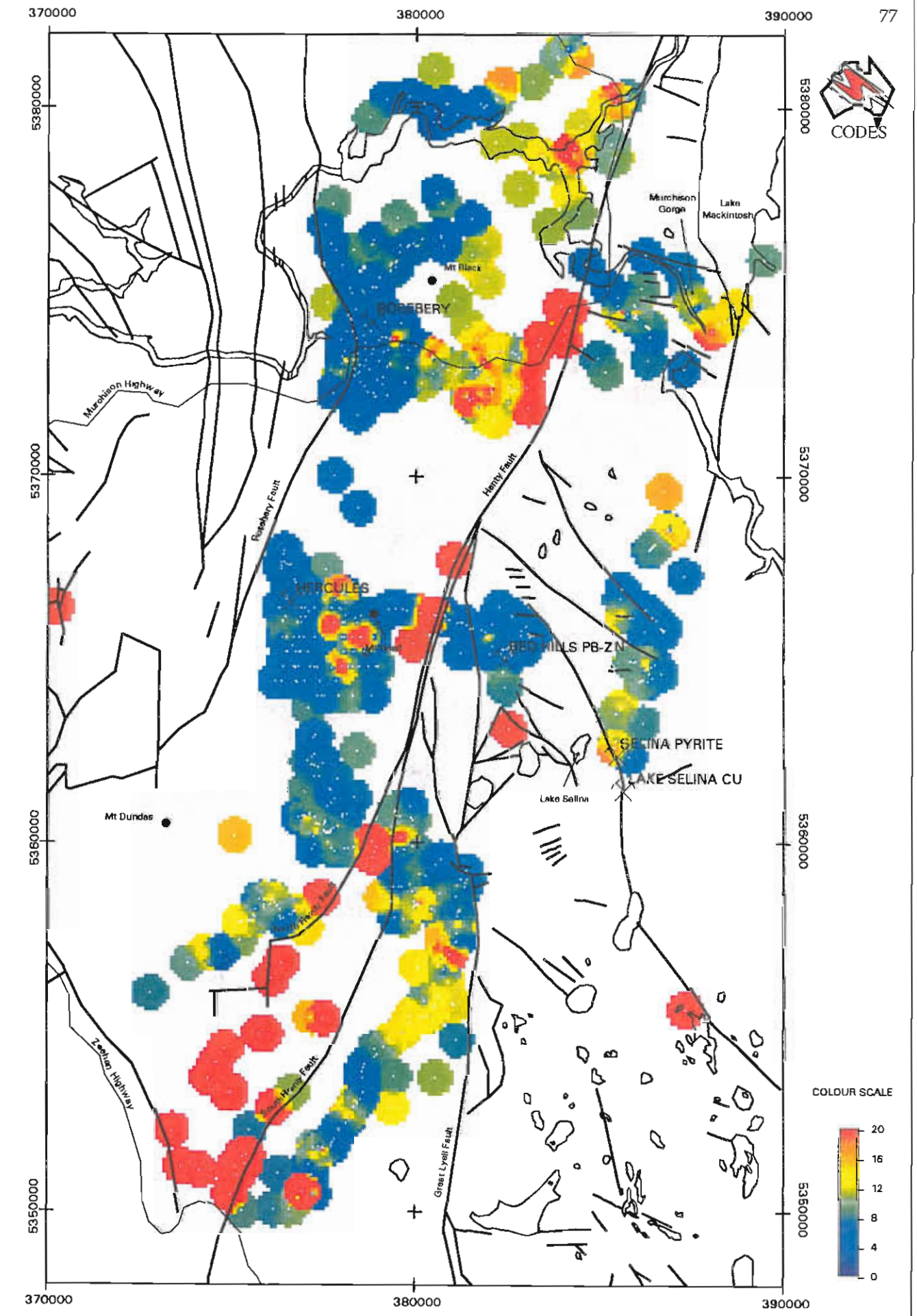
370000
380000
390000
5380000
5370000
5360000
5350000
CODES
Murchison Gorge
Lake Mackintosh
Mt Black
ROSEBERY
Murchison Highway
Rosebery Fault
Henty Fault
HERCULES
Mt Hall
RED HILLS PB-ZN
SELINA PYRITE
LAKE SELINA CU
Lake Selina
Mt Dundas
South Riverd Fault
Zeehan Highway
South Henty Fault
Great Lyell Fault
COLOUR SCALE
20
16
12
8
4
0
0 1000 2000 3000 4000 5000
metres
WESTERN TASMANIA
Tio2/Zr Ratios : Mt Read Volcanics

Western Tasmania : Que - Hellyer Area

CODES

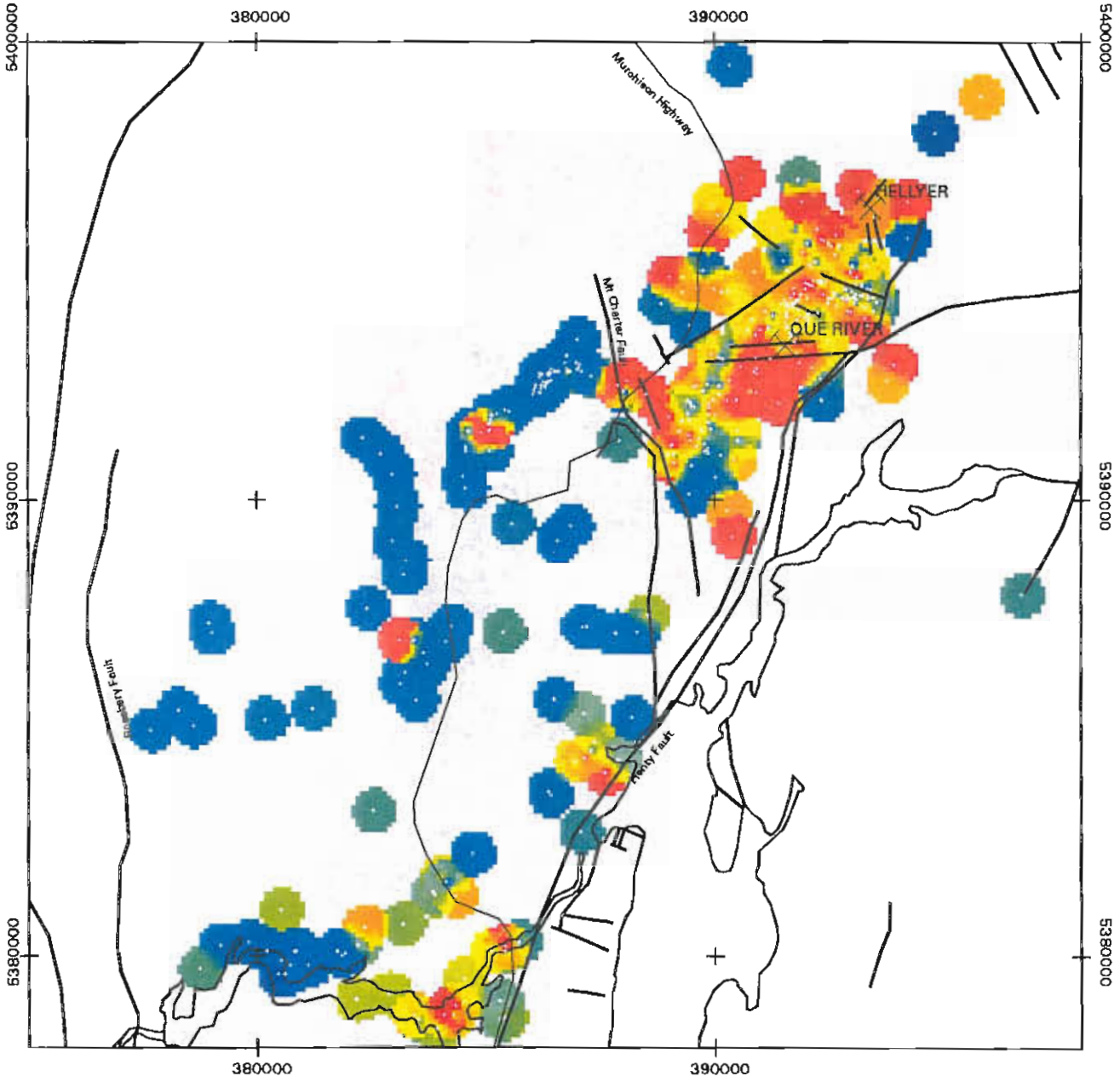

COLOUR SCALE

30
24
18
12
6
0

0 1000 2000 3000 4000 5000
metres

Geochemical Database

Contoured TiO2/Zr Distribution Mt Read Volcanics

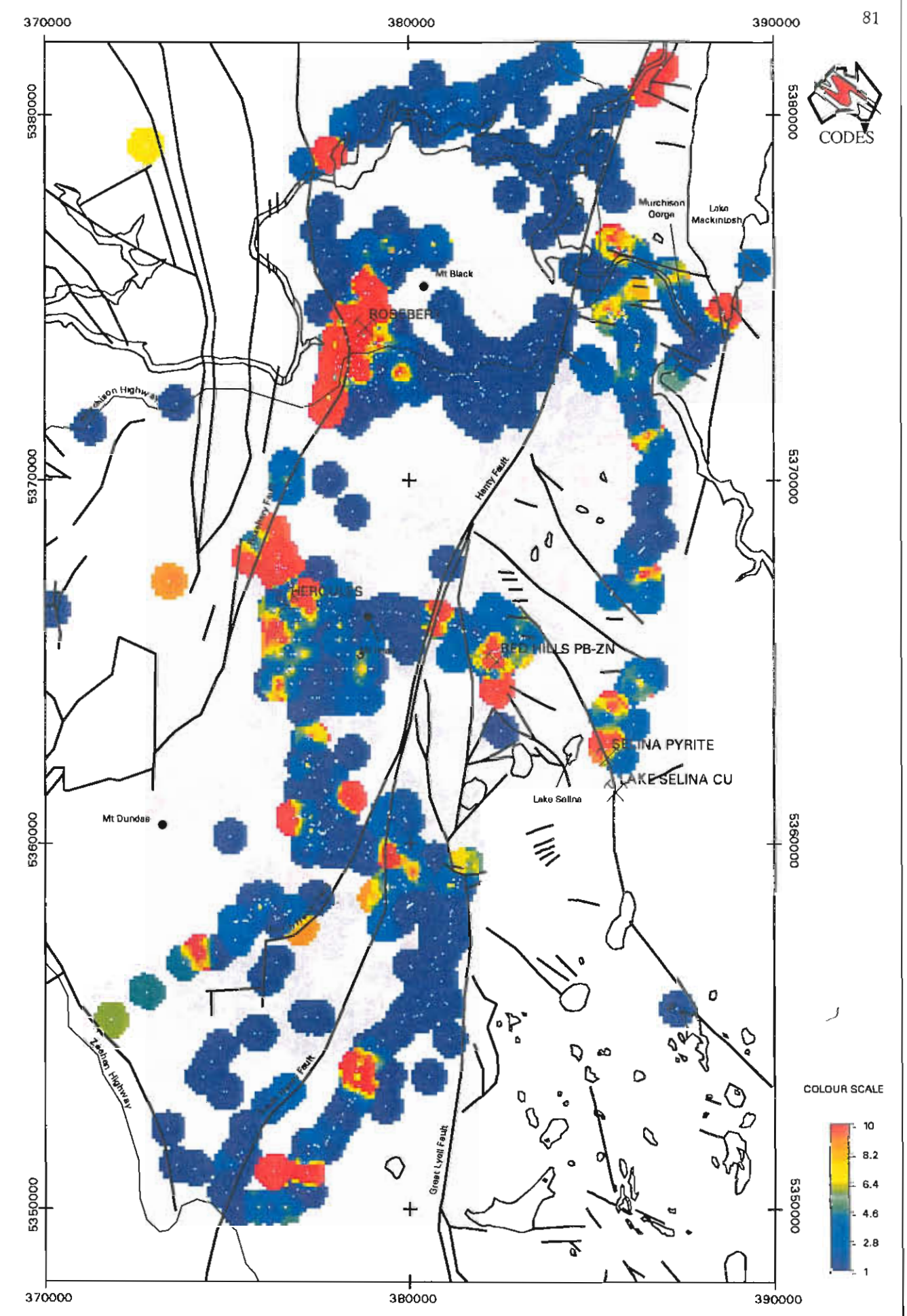

WESTERN TASMANIA

Rb/Sr Ratios : Mt Read Volcanics

All Data

Western Tasmania : Que - Hellyer Area

CODES

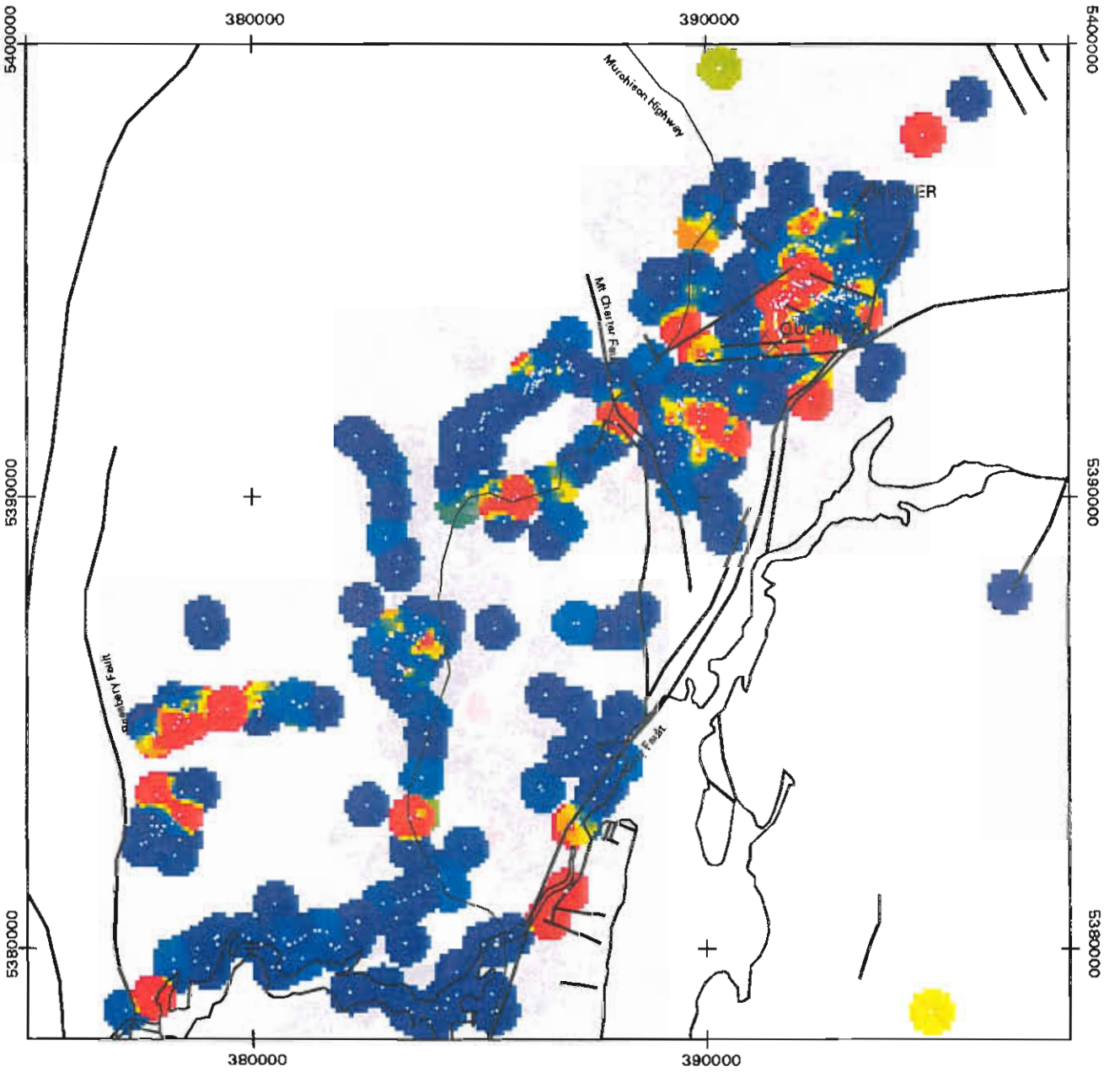

COLOUR SCALE

10
8.2
6.4
4.6
2.8
1

N

0 1000 2000 3000 4000 5000
metres

Geochemical Database

Contoured Rb/Sr Distribution Mt Read Volcanics

All Data

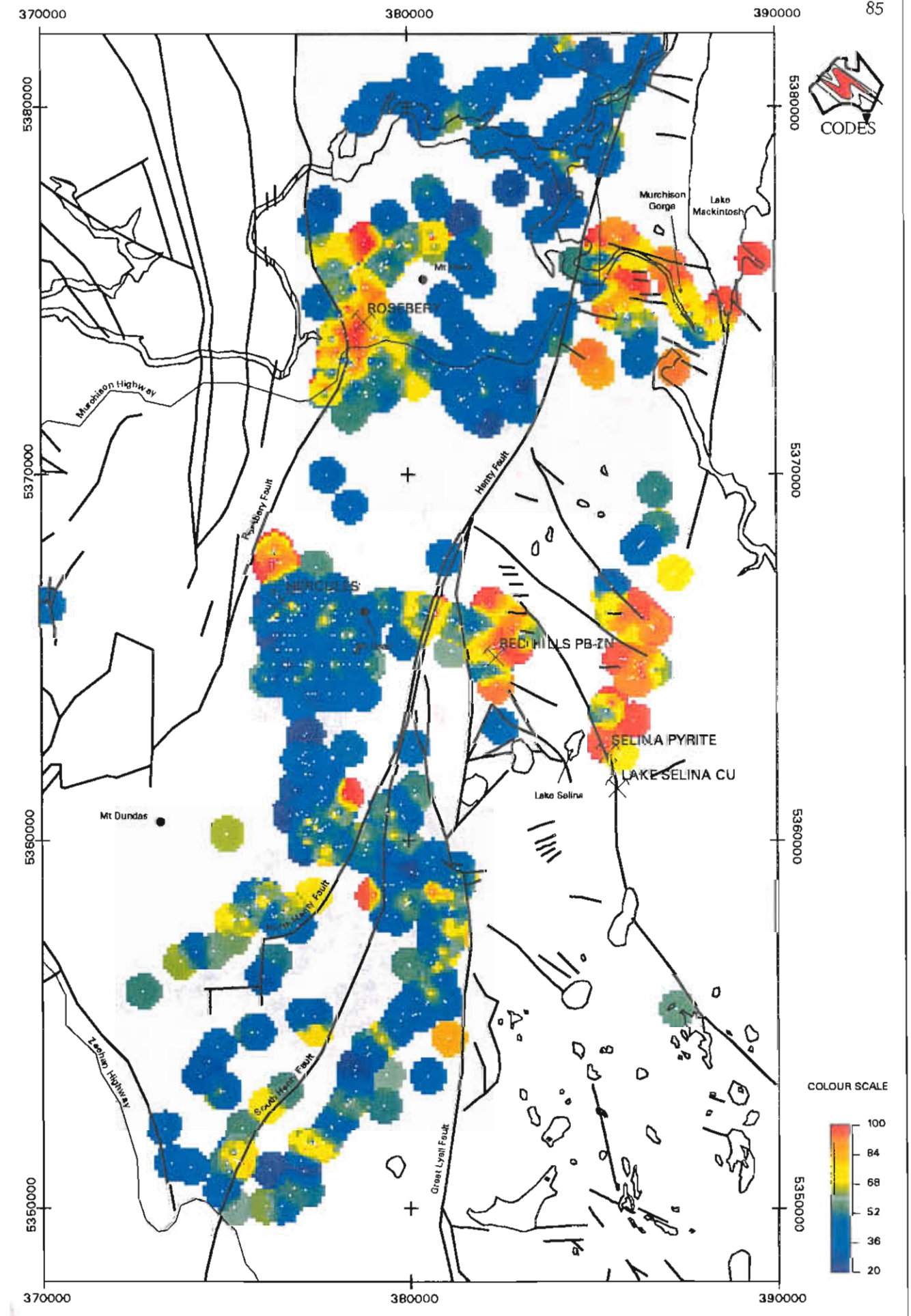

WESTERN TASMANIA

Alteration Index Distribution, Mt Read Volcanics

Western Tasmania : Que - Hellyer Area

CODES

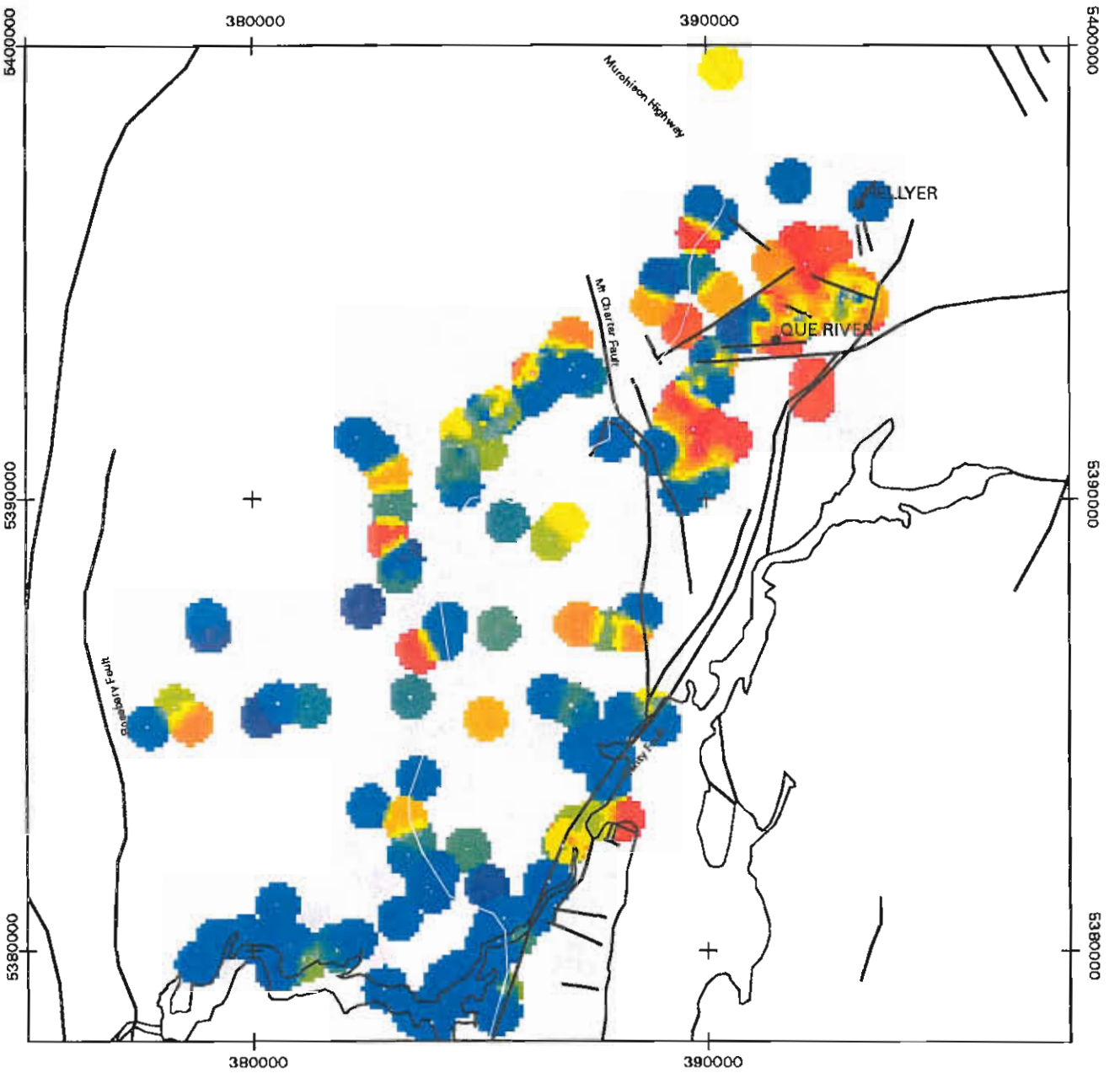

COLOUR SCALE

100
84
68
52
36
20

Scale: 1:150000

0 2500 5000 7500

metres

Grid: Australian Map Grid, Zone 55.

Geochemical Database

Alteration Index Distribution - All MRV Data

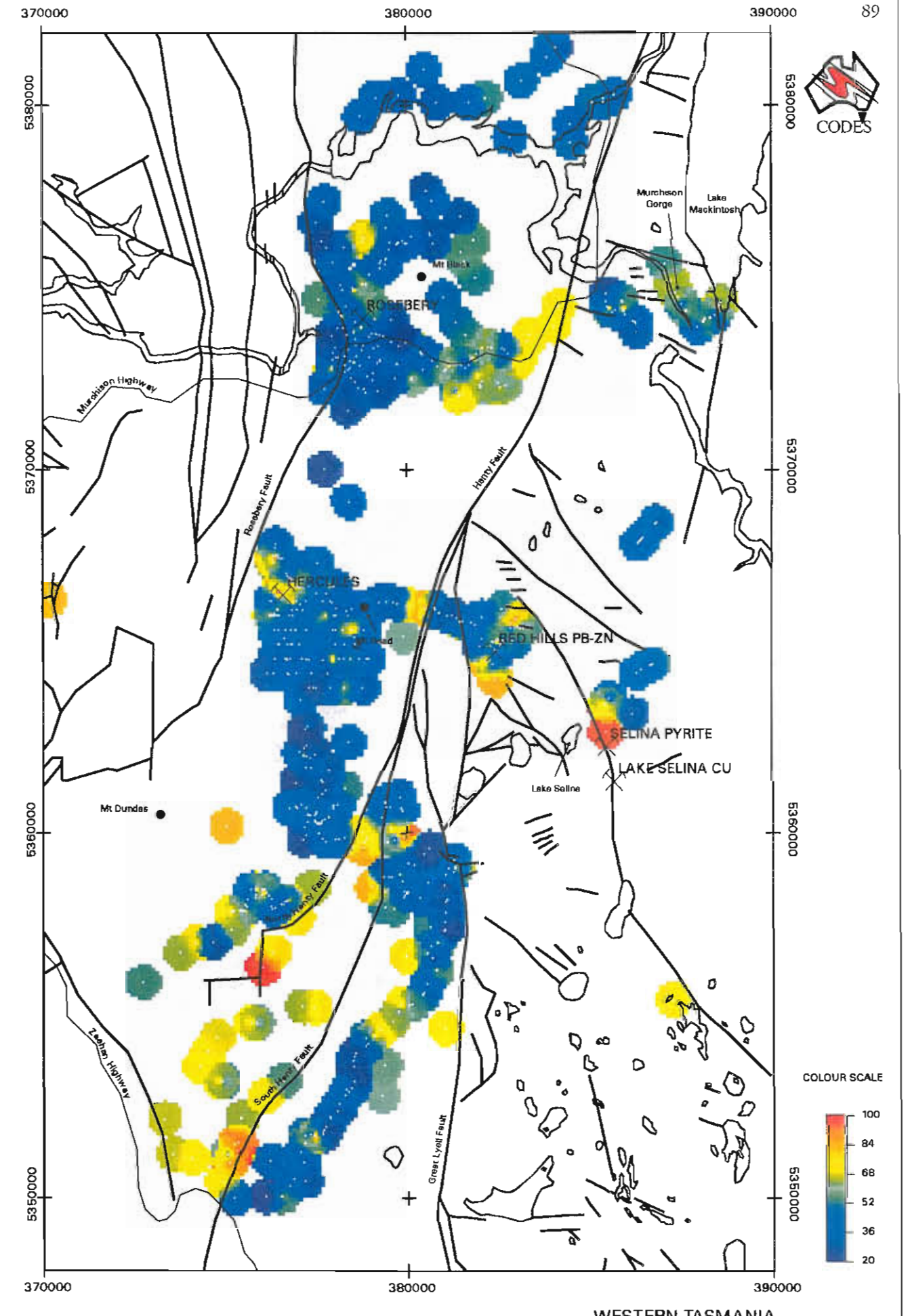
370000
380000
390000
5380000
5370000
5360000
5350000
CODES
Murchison Highway
Zeehan Highway
Rosebery Fault
Henty Fault
South Henty Fault
Great Lyell Fault
Mt Black
ROSEBERY
Murchison Gorge
Lake Mackintosh
HERCULES
Mt Read
RED HILLS PB-ZN
SELINA PYRITE
LAKE SELINA CU
Lake Selina
Mt Dundas
COLOUR SCALE
100
84
68
52
36
20
0 1000 2000 3000 4000 5000
metres
WESTERN TASMANIA
Chlorite Index Distribution, Mt Read Volcanics

Western Tasmania : Que - Hellyer Area

CODES

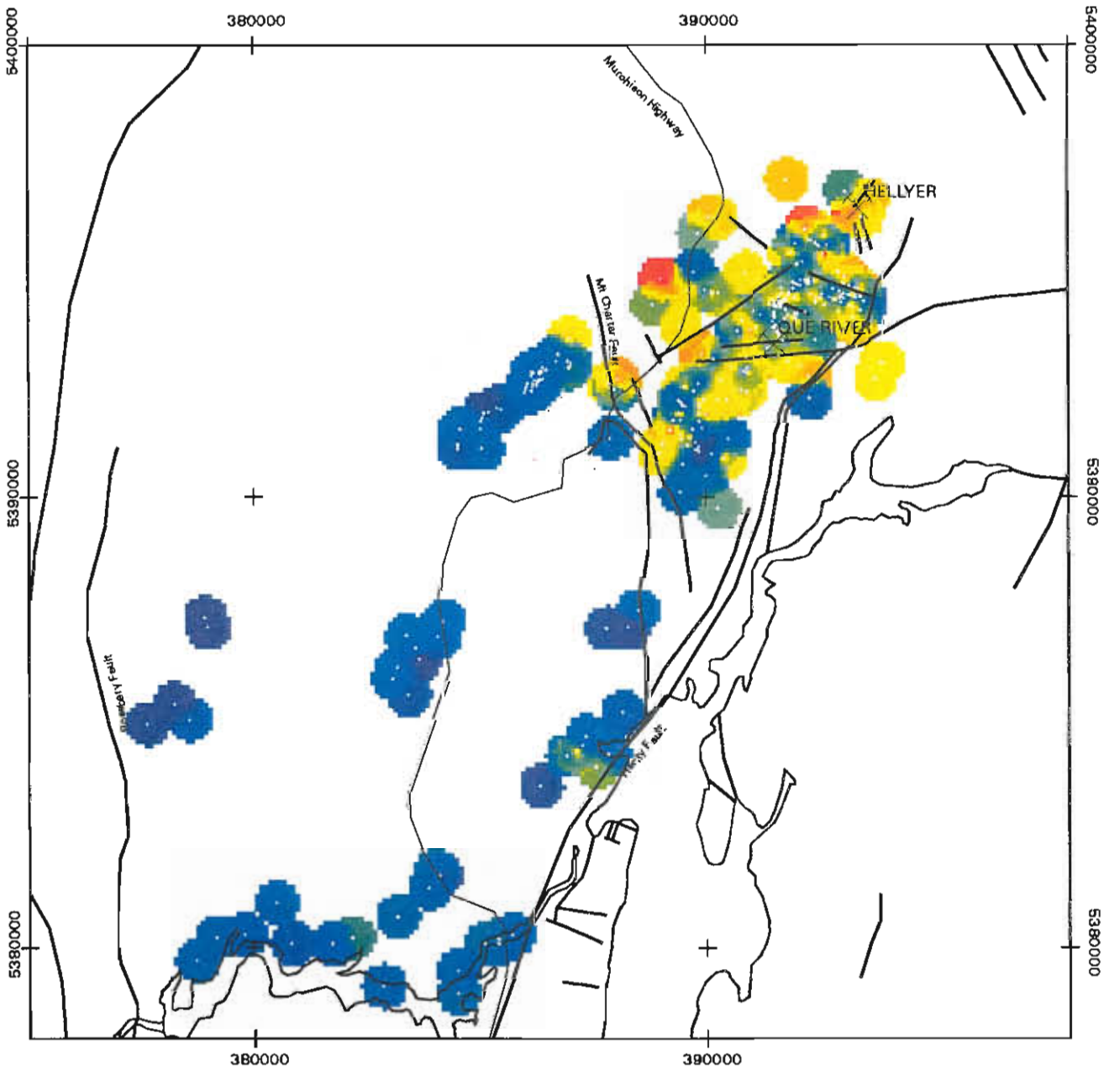

COLOUR SCALE

100
84
68
52
36
20

0 1000 2000 3000 4000 5000
metres

Geochemical Database

Chlorite Index Distribution : Mt Read Volcanics

Surface lithochemical responses of known VHMS deposits based on the MRV geochemical database

Ross R. Large and Michael D. Blake
Centre for Ore Deposit Research, Geology Department, University of Tasmania

Introduction

Using the lithochemical GIS plots provided in this report (Blake, 1997) it is possible to comment on the surface responses of the known mineralisation in the northern-central portion of the Mt Read Volcanics. Sufficient data is available to make comparisons between the surface lithochemical responses at Rosebery, Hercules, Que River and Hellyer. Comparisons are made with the Cambrian granite-related alteration zones at Lake Selina (AMG coords 385520E, 5362 400) and Murchison Gorge (AMG coords 387200, 5375 000).

Rosebery

A comprehensive data set is available for surface samples around Rosebery, based on previous data from Naschwitz (1985), combined with data from Pasminco and the current AMIRA traverse (Gifkins et al., 1996).

The surprising feature of this data is the complete lack of anomalous samples in Zn, Pb or Cu for both the footwall and hangingwall outcropping lithologies at Rosebery. All samples in the vicinity of Rosebery contain <300 ppm Zn, <80 pm Pb and <40 ppm Cu.

However there is a zone of strong Na_2O depletion (<2% Na_2O) extending 3 km north and 4 km south from Rosebery with an across strike width of about 2 km. This zone is accompanied by high Ishikawa AI values from 70 to 100. A strong sulphur anomaly (>0.6% S) and S/Na_2O ratio (>0.8) characterises the centre of the sodium depletion zone. No distinct anomalous zones of Chl/carb/py Index, manganese or Ba/K_2O ratios are apparent from the data. There are insufficient analyses of thallium or antimony on surface samples surrounding Rosebery to draw any conclusions.

Hercules

The deeply eroded nature and good exposure of the footwall alteration system at Hercules (Large, 1996) has resulted in a strong lithochemical response in most of the chosen chemical indicators.

Zn, Pb and Cu show a spotty regional response over the central alteration pipe and host rock package. The sodium depletion and AI zone is less extensive than Rosebery and concentrated over the footwall alteration pipe. Manganese exhibits a strong anomaly over the centre of the hydrothermal system, coincident with elevated S/Na_2O and Ba/K_2O ratios. Thallium and antimony show distinct anomalies in volcaniclastics at the ore position.

Que River

A zone of Pb anomalism (>180 ppm Pb) extends 2 km NNE of Que River, accompanied by weak erratic zinc and copper anomales. The pattern of copper in the volcanics in this area is difficult to interpret due to elevated background value in the andesitic and basaltic volcanics, compared with the rhyolitic volcanics at Rosebery and Hercules. A broad zone of sodium depletion is centred on Que River extending over 9 km from Mt Charter to Hellyer.

The Ishikawa AI shows an anomalous zone of values from 70 to 95 extending from Que River to Hellyer (5 km x 4 km) and a separate zone surrounding Mt Charter to the south. The Chl/carb/py Index exhibits erratic variation in the Que-Hellyer region probably related to the mixed mafic-felsic volcanic lithologies rather than variation in alteration. Manganese shows no anomalous response at Que River, and the Ba/K_2O ratio shows low values immediately surrounding the deposit, but elevated values elsewhere in the district.

Hellyer

Due to the lack of surface lithochemical data immediately surrounding Hellyer it is difficult to draw any firm conclusions. The limited data set shows an elevated Ba/K_2O ratio and Na_2O depletion halo in the overlying rocks at Hellyer.

Granite related alteration systems

As a comparison to the VHMS deposits, two Cambrian granite-related alteration systems; Lake Selina (Hunns, 1987) and Murchison Gorge (Polya et al., 1986) are worthy of discussion.

These two prospects are within the Eastern Quartz-phyric Sequence adjacent to intrusions of Cambrian granite. The lithochemical plots indicate strong anomalies in Cu, Pb, Zn, Tl, Sb with depletion in Na_2O and very broad AI halos.

The major differences between these granite-related alteration zones and the VHMS alteration zones is the K_2O level and Ba/K_2O ratio. The granite-related systems, have intense K-feldspar alteration with whole-rock K_2O values from 5 to 10 wt%, compared to the sericitic alteration in the VHMS systems with K_2O from 1 to 6 wt%. Due to the high K_2O and low Ba values in the granite-related systems Ba ppm/K_2O wt% ratios are always less than 500.

Discussion and conclusions

A summary of the lithochemical responses for the mineral deposits discussed above is provided in Table 1. From these data and the plots in the accompanying report, it is apparent that the level of erosion and exposure of the hydrothermal system at each deposit is a key factor controlling the responses.

At ***Hellyer***, based on limited data, the hydrothermal system is 90% buried, and the only lithochemical response is provided by a weak sodium depletion zone and elevated Ba/K_2O ratios.

At ***Rosebery***, the hydrothermal system is better exposed, giving rise to extensive sodium depletion, Ishikawa AI and S/Na_2O halos; but no anomalous metals (Tl and Sb data is not sufficient to draw conclusions).

At ***Hercules***, a large part of the hydrothermal system is exposed from the root zone (alteration pipe) to the ore horizon. Extensive anomalies in all the indicators are apparent; Zn, Pb, Cu, Mn, Tl, Sb, Na depletion, AI, CI, S/Na_2O and Ba/K_2O.

For comparison, the Cambrian granite-related alteration systems at Lake Selina and Murchison Gorge show similar base metal anomalies and AI halos. However they are distinguished from the VHMS hydrothermal systems by their strongly elevated K_2O values and low Ba/K_2O ratios.

References

Blake, M.D., 1997 - this volume.

Gifkins, C.C., 1996. Mount Black Volcanics: Preliminary volcanic facies and alteration, petrography and geochemistry. *AMIRA project P439, Report 3*, Oct. 1996:321-350.

Hunns, S.R., 1987. Mineralisation of the Lake Selina prospect. Unpublished MSc Preliminary Thesis, University of Tasmania.

Large, R.R., 1996. The Hercules-Mt Read traverse: relationships between volcanic mineralogy, alteration and geochemistry. *AMIRA project P439, Report 3*, Oct. 1996: 153-234.

Naschwitz, W., 1985. Geochemistry of the Rosebery Ore Deposit. Unpublished PhD Thesis, University of Tasmania, Hobart.

Table 1. Summary of surface lithochemical responses for some VHMS deposits and Cambrian granite-related prospects in the MRV. Based on the AMIRA P439 data base.

Vector	Rosebery	Hercules	Que River	Hellyer	Lake Selina	Murchison Gorge
Zn	0	2	1	0	2	2
Pb	0	2	2	0	2	2
Cu	0	2	2	2	3	1
Mn	0.5	3	0	0	0	1
Tl	0.5?	3	?	?	2	3
Sb	?	3	?	?	2	1
Na depletion	3	2	2	2?	3	3
K enrichment	0.5	0	1	0	3	3
Alteration Index	3	2	3	3	3	3
Chl/carb/py Index	0	2	b*	b*	1	1
S	3	3	?	?	2	0
S/Na	3	3	?	?	1	1
Ba/K_2O	0	3	1	2	0	0

0 = background; 1 = weak; 2 = moderate; 3 = strong; ? = insufficient data
b* = mafic volcanics with high background Cl

Gossan Hill: relationship between mineralogy, alteration and geochemistry

Robina Sharpe
Centre for Ore Deposit Studies, Geology Department, University of Tasmania

Introduction

The Gossan Hill deposit is an Archean Cu-Zn-magnetite VHMS deposit hosted in the Yalgoo-Singleton greenstone belt of the Murchison Province within the Yilgarn Craton, Western Australia. Gossan Hill shows both notable similarities and differences to many other Australian VHMS deposits. Perhaps the most exceptional differences at Gossan Hill are the presence of magnetite lenses and a felsic volcano-sedimentary host sequence of bedded pumiceous and tuffaceous facies with lesser epiclastics. These differences make Gossan Hill comparable to the Mattabi style Canadian VHMS deposits (Morton and Franklin, 1987).

Stratigraphy

Host strata to mineralisation is the Golden Grove Formation; a thick sequence of felsic volcaniclastics and minor intercalated lavas. Stratigraphic classification of the sequence is taken form Clifford (1992) and illustrated by Figure 1. The Golden Grove Formation consists of six Members, GG1 to GG6. The lowermost Members (GG1 to GG5) are a bedded succession of pumiceous and tuffaceous breccia and sandstone, whereas the uppermost Member (GG6) consists of epiclastic units. Hangingwall units at Gossan Hill are the lower stratigraphic Members of the Scuddles Formation and include coherent rhyodacite and dacite with associated breccia facies. Dacite in the hangingwall Scuddles Formation cross cut the Golden Grove Formation strata.

Footwall Stratigraphy–GG1

Golden Grove Formation Member 1 (GG1) is a volcaniclastic facies of tuffaceous origin that forms the footwall strata to copper-rich mineralisation and is termed the Stratified Rhyodacite Lithic Breccia Facies (Clifford, 1992). GG1 is a sequence of bedded, formerly pumice-rich breccia (>4mm) to granule breccia (2–4mm) (Plates 1, 2a, b, c) and is a laterally continuous stratigraphic horizon with a strike length of 15 km and a thickness of <170 m. GG1 is well bedded on a scale of centimetres to metres with both normal and reverse grading. Lithic constituents include relict pumiceous fragments and shard-rich debris. Volcanic quartz crystals form modal 2 to 7% of the GG1 breccia facies. Blocky quartz grains have variably reacted grain margins and quartz crystal reaction textures, which include: <0.05 mm quartz overgrowths with optical continuity, recrystallisation of volcanic quartz crystals to finer grained quartz mosaics, irregular reacted grain margins, embayment textures, grain fracture often with insitu crystal dissaggregation, recrystallisation of quartz along and outward from fracture planes and undulose extinction patterns. Angular quartz crystals range in size between 0.1 to 1 mm, have an abundance of up to 3% modal and are generally more embayed than blocky quartz grains.

Relict pumice clasts are the primary lithic constituent of GG1 forming in excess of modal 90% of the unit. Formerly glassy lithics include vesicular pumice fragments, bubble wall shards, curviplanar to arcuate shards and rod-like shards. Pumiceous textures are well preserved in this facies due to

Stratigraphic Framework of the Gossan Hill Deposit

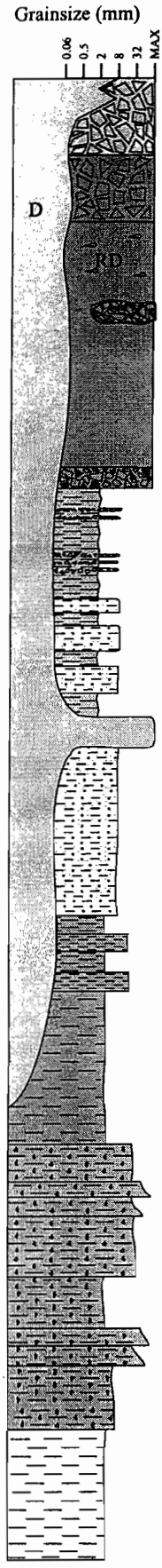

Scuddles Formation

Dacite (D) : Massive feldspar - quartz phyric lava/intrusion and associated breccia facies. Intrudes GG4 to GG6 and rhyodacite and sills parallel to the GG5 - GG6 contact (thickness 0 to 330 m).

Rhyodacite (RD) : Massive quartz - feldspar phyric lava and associated breccia facies. Large 5-8 mm quartz grains, fractured and embayed. Upper portions may be amygdaloidal. The lower breccia facies is polymict, poorly sorted and clast supported with a quartz - feldspar phyric rhyodacite matrix. Clasts include; rhyodacite, bedded sediment and sulphide clasts (thickness 0 to 300 m).

Golden Grove Formation GG6 Member

Thinly to thickly bedded siltstone, sandstone and polymict pebble breccias. Sandstone units are pumiceous - bearing with scoured basal contacts. Normal grading, syndepositional faulting and mantling are common. Lower portions of GG6 are interbedded with GG5 (thickness 0 to 180 m).

Golden Grove Formation GG5 Member

Massive, clast supported, closed framework, lithic - rich pebble breccias with minor volcanic quartz (<1%). Lithic include < 4mm, pumiceous and formerly glassy detritus including, tube pumice, vesicular glassy fragments, bubble wall fragments and shards (thickness 0 to 120 m).

Golden Grove Formation GG4 Member

Quartz - rich, clast supported granule breccia to bedded sandstone. Quartz forms 5 -10%, up to 1-2 mm angular quartz fragments. Formerly pumiceous - glassy lithics include relict tube pumice, vesicular glassy fragments and rod - like shards (thickness 50 to 140 m).

Golden Grove Formation GG1 Member

Massive, clast supported, poorly sorted pumice breccias interbedded with granule to pebble breccia and minor sandstone. A monomict lithic population of tube pumice fragments up to 100 mm, but generally <10-20 mm. Blocky quartz form 1-5%. Thinly bedded zones show normal to reverse grading, locally scoured basal contacts and cross bedding (thickness 100 to 170 m).

Gossan Valley Formation

Bedded quartz - rich sandstones. Quartz forms 5 - 8 % and 2-3 mm grains (thickness 50 to 660 m).

Figure 1. Stratigraphic framework of the Gossan Hill area in the Golden Grove Domain. The Golden Grove Formation hosts massive Zn - rich sulphide at Scuddles and Zn - Cu - magnetite in Members 4 and 6 at Gossan Hill.

complete quartz replacement of original glassy detritus and clasts by interlocking arrays of megaquartz and lesser microcrystalline quartz. Quartz-replaced pumiceous fragments have preserved textural affinities of the original fragment morphologies. Tube pumice is characterised by preserved delicate striations of sub-parallel alignment, imparting a fibrous texture. Pumiceous clasts show variable sizes from 8–10 mm up to 30–40 cm, but are generally smaller at < 1–2 mm. Pumice clast morphologies show a variation in size and shape with random orientations as denoted by differential orientation of preserved tube structures. Pumice clasts also host blocky subhedral quartz, indicating some pumice fragments were quartz phyric. The blocky to tabular morphologies of pumiceous show little evidence of flattening due to diagenetic compaction and confirm the non-welded nature of these units. The Stratified Rhyodacite Lithic Breccia Facies are closed framework, lithic (pumice) supported breccias with a relatively homogeneous juvenile provenance of lithic constituents.

GG2/3

GG2 and GG3 are not observed at Gossan Hill. Where present, they occur as narrow intervals, less than 2–3 m, of thinly bedded, fine grained epiclastics. In areas where GG2 and GG3 are absent, GG1 has an interbedded contact with overlying GG4 units. GG2 and GG3 have strong to intense silicification of thinly bedded units.

Host lithofacies — GG4

GG4 is termed the Stratified Rhyolite Pumice-Lithic Breccia Facies (Clifford, 1992), and are quartz-bearing lithic-rich breccias to granule breccias. The thickness of the Stratified Rhyolite Pumice-Lithic Breccia Facies is estimated between 75–140 m. A thickening of the GG4 facies to the north is coincident with extensive development of massive sulphide-magnetite mineralisation at Gossan Hill within this facies. Lower stratigraphic contacts are locally interbedded over 20 m with GG1. The upper contact between GG4 with GG5 is sharp and conformable. GG4 shows a broad transition from well bedded to thinly bedded quartz-rich volcaniclastics in stratigraphic lower zones, to lithic-rich granule and pebble breccia units in upper zones. GG4 is thinly to well bedded, <2 mm to 1 m, and hosts strongly to intensely developed chlorite alteration (Plate 2d) Abundant, variably sized, angular volcanic quartz crystals in a fine grained matrix is diagnostic of the GG4 facies (Plate 2e, g). Quartz forms 7 to 10%, and rarely up to modal 15%, with blocky to euhedral and an angular to sub-angular morphologies. In zones of extreme alteration, quartz is the only relict grain phase and bedding is often depicted by changes in quartz crystal sizes, abundances and distributions.

Preserved pumiceous lithics include tube pumice clasts that may be quartz-phyric. Tube pumice clasts maybe tabular to blocky and up to 4 mm, but generally smaller than 2 mm (Plate 2f). Tube striations are present as delicate, thin, sub-parallel lineations with chlorite alteration of pumiceous lithics generally parallel to tube striations and bubble walls. Pumice clasts are composed of megaquartz and microcrystalline quartz mosaics with chlorite alteration superimposed. Preserved lithic pumiceous fragments are not flattened and have random orientations. Formerly glassy fragments also include vesicular fragments (Plate 2h), bubble wall and cuspate fragments, rod-like shards up to 0.6 mm in length, smaller pumice fragments and spherulites all recrystallised to megaquartz and microcrystalline quartz. These glassy indicators form a closely packed and randomly oriented array where preserved, but are poorly preserved in strong chlorite alteration. Finer grained volcanic textures are best preserved within siliceous nodular alteration zones disseminated throughout chlorite altered host. The matrix of GG4 is interpreted to be a formerly glassy mixture of shard, pumice and bubble wall fragments, randomly oriented and tightly packed, indicating a poorly sorted and closed framework.

Host facies — GG5

GG5 is defined as the Massive Rhyolite Pumice Breccia Facies (Clifford, 1992). The GG5 Member is a dark grey, massive unit with minor volcanic quartz (modal <1%) and fine grained lithics (Plate 3a, b).

The unit is universally chlorite altered, with chlorite forming a moderate to strong and locally intense pervasive alteration that masks subtle bedding indicators. GG5 is characterised by its massive nature and relatively homogeneous appearance. The upper contact of GG5 is locally interbedded with GG6 over a thickness of 50 m.

Volcanic quartz crystals form up to modal 1%, with an angular to sub-angular quartz crystal phase and a blocky quartz crystal phase. Relict pumice lithics have a blocky to tabular morphology, and a grain size up of <1 to 4 mm (Plate 3c). Tube striations are often preserved in quartz replaced pumice, showing random tube striation orientations. Other preserved volcanic textures within GG5 include quartz replaced vesicle structures of former vesicular pumice fragments, quartz replaced shard textures including small cuspate fragments, rod-like fragments and bubble wall fragments (Plate 3d). Relict pumiceous textures indicate GG5was a pumice-rich breccia. A closed framework is indicated by the pumice supported, poorly sorted array of glassy, shardy and pumiceous lithic constituents and unfragmented blocky quartz grains. No evidence for diagenetic compaction or flattening of the pumiceous constituents is observed.

Host facies — GG6

GG6 is characterised by intense silicification of thinly bedded to laminated units with interbedded pebble breccia horizons. A large portion of GG6 consist of thinly bedded to laminated formerly glassy to granule breccia horizons that are chlorite, quartz or carbonate altered. Some units show preservation of pumiceous and shard textures and may indicate that the finer grained zones of GG6 were composed of finer fractions of formerly glassy debris. Volcanic textures are generally not preserved in intensely silicified zones. Breccia horizons within GG6 are polymict, poorly sorted and clast supported. The occurrence of polymict clasts including clasts of thinly bedded sandstone and siltstone is supportive of a multiple provenance source.

Alteration and Mineral Geochemistry

GG1: A semi-conformable footwall alteration zone

The Stratified Rhyodacite Lithic Breccia Facies (GG1) contains two alteration phases : quartz and chlorite. Both chlorite and quartz alteration phases are ubiquitous throughout GG1and the alteration is intense and domainal (Plate 1). Domainal quartz-chlorite alteration appears to be the result of alteration controlled largely by host rock and its pumiceous lithic constituents and formerly glassy detritus.

GG1 chlorite alteration

Chlorite is generally fine grained and ubiquitous throughout GG1. Fine grained portions of pumiceous and glassy detritus are chlorite altered. Chlorite is also a preferential alteration of former pumiceous-glassy lithic fragments. In these examples, chlorite occurs as a fine grained domainal alteration. These chlorite domains may be blocky or tabular, reflecting the original morphology of the replaced pumice clast or irregular curviplanar to cuspate domains, reflecting replacement of interstitial formerly glassy shard-rich material. Pumiceous fragments and clasts with tube vesicle structures frequently show preferential chlorite development parallel to preserved tube vesicle structures.

Chlorite domains range in size and occurrence and reflect the size of pumiceous lithics. In GG1, chlorite abundances vary between modal 15% in least altered units and 30–40% modal in intensely altered samples. Cleavage fabrics are preferentially well developed in chlorite-rich domains and reflect the more ductile nature of the phyllosilicate altered domains compared to siliceous zones. The contacts between chlorite and quartz domains are sharp and enhance the original breccia textures in the GG1. Such domainal chlorite textures have previously been interpreted as fiamme and used to infer welded fabrics (Ashley et al., 1988; Ashley, 1983; Frater, 1983). Chlorite patches or domains were interpreted by Clifford (1992) to represent differentially replaced and recrystallised devitrification features. Preferential chlorite development within pumice clasts may

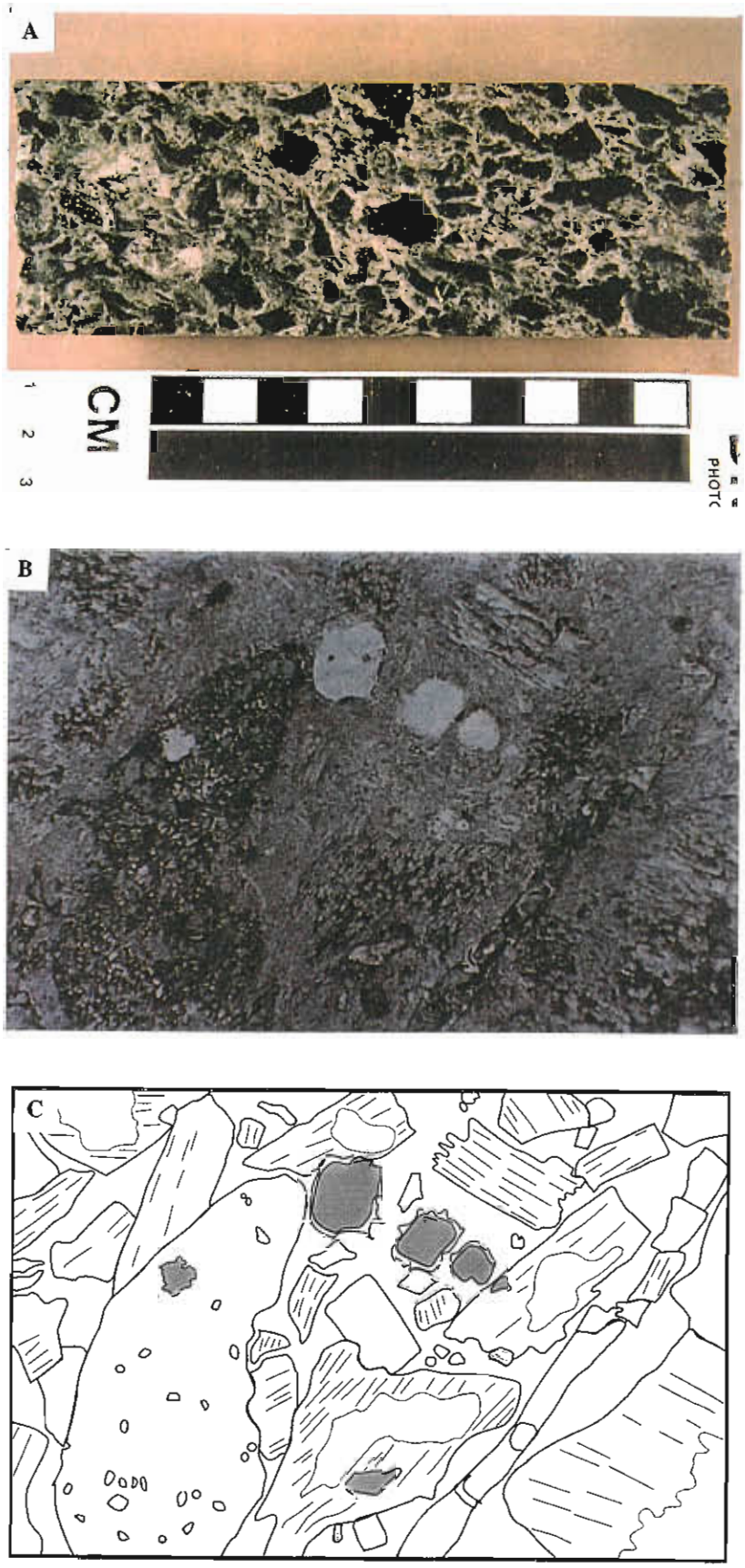

Plate 1: DDH GG157 at 157.1m (sample 769146) representing GG1 units proximal to magnetite - pyrite - chalcopyrite mineralisation at Gossan Hill on transform section 18438N. A) Hand specimen showing a clast supported monomict breccia units with chlorite altered pumiceous clasts (dark green) and quartz altered pumice clasts (grey). Quartz grains are abundant and disseminated throughout the unit. B) Thin section from A showing variably sized, randomly oriented tube pumice and vesicular pumice fragments that are replaced by chlorite and quartz. Volcanic quartz grains are rounded to blocky with micro - sized quartz overgrowths. Also note that the large vesicular pumice clast is quartz - phyric (field of view = 2.5mm). C) Interpretation of plate B showing the clast supported nature of the GG1 and preferential chlorite alteration within pumiceous clasts.

BLANK

Plate 2

A) Sample from DDH GG157 at 198.6m (769148). Pervasive strong chlorite altered quartz - pumice breccia/sandstone from GG1 units on transform section 18438 N. Quartz crystals form up to 1mm in both rounded to blocky populations. Pumiceous lithics are <1-2 mm and maybe grey (silica altered) or green (chlorite - quartz altered) and blocky to angular. Some of the clasts are quartz - phyric.

B) Sample of chlorite - quartz altered, pumice quartz crystal - rich breccia of GG1 from DDH GG162 at 200m (769166). This alteration is a domainal alteration of lithic and matrix constituents, with some chlorite altered pumice clasts having grey haloes composed of fine grained quartz. Quartz grains are abundant, forming modal 8% and are <1mm.

C) Sample of chlorite - quartz altered GG1 from DDH GG157 at 121m (769143). Example of a pumice breccia with chlorite and quartz domainal alteration developed. Former pumice clasts are generally chlorite altered and show haloes or quartz. The pumiceous fragments have cuspate grains margins and well preserved shapes through the chlorite alteration and some of the former pumice clasts are quartz - phyric.

D) Sample from DDH GG038 at 275.1m (769095). A dark green bedded quartz sandstone to fine grained siltstone showing abundant angular volcanic quartz crystals. Changes in abundance of quartz, as well as size and distribution of quartz illustrate bedding. Pervasive, strong chlorite alteration is developed through both sandstone and siltstone units in this sample. Minor disseminated rutile and ilmenite is associated with chlorite observed in hand specimen.

E) Sample of a volcanic quartz crystal - rich horizon typical of coarse sandstone/breccia units of GG4. Sample is from DDH GG157 at 211.7m (769150). Dark green colour is the result of pervasive, intense chlorite alteration that has destroyed the majority of relict pumice textures with the only remaining volcanic texture present being volcanic quartz crystals. Quartz grains are up to 4-5 mm and show a wide distribution in size and angularity. Quartz has blocky to angular forms often with preserved curvi-planar grain margins.

F) A sample from DDH GG157 at 157.1m (769146) showing a lithic - rich (pumice), quartz crystal breccia unit similar to units from upper zone in GG4. This sample has pervasive moderate chlorite alteration and shows well preserved, formerly pumiceous fragments hosted in finer grained, formerly glassy groundmass.

G) An example of the preservation of angular to blocky quartz grains within pervasive intense altered quartz crystal - rich sandstones of GG4, similar to E above. The quartz crystals are hosted by fine grained chlorite and show local recrystallisation and overgrowths on quartz margins and an insitu fracture pattern. Foliation wraps around quartz grains and disseminated opaques in the chlorite are ilmenite and rutile. Plane Polarised Light. Field of view = 1.2mm, sample form DDH GG118 at 262.1m (760357) on transform section 18141 N

H) Sample from DDH GG027 at 517.3m (769072) on transform section 18288N showing partially preserved vesicular pumice fragment. The former pumice fragment is replaced by mosaics of quartz and is hosted within a fine grained pervasive chlorite - altered former glassy groundmass. Sample from GG5. Plane polarised light. Field of view = 1.2 m.

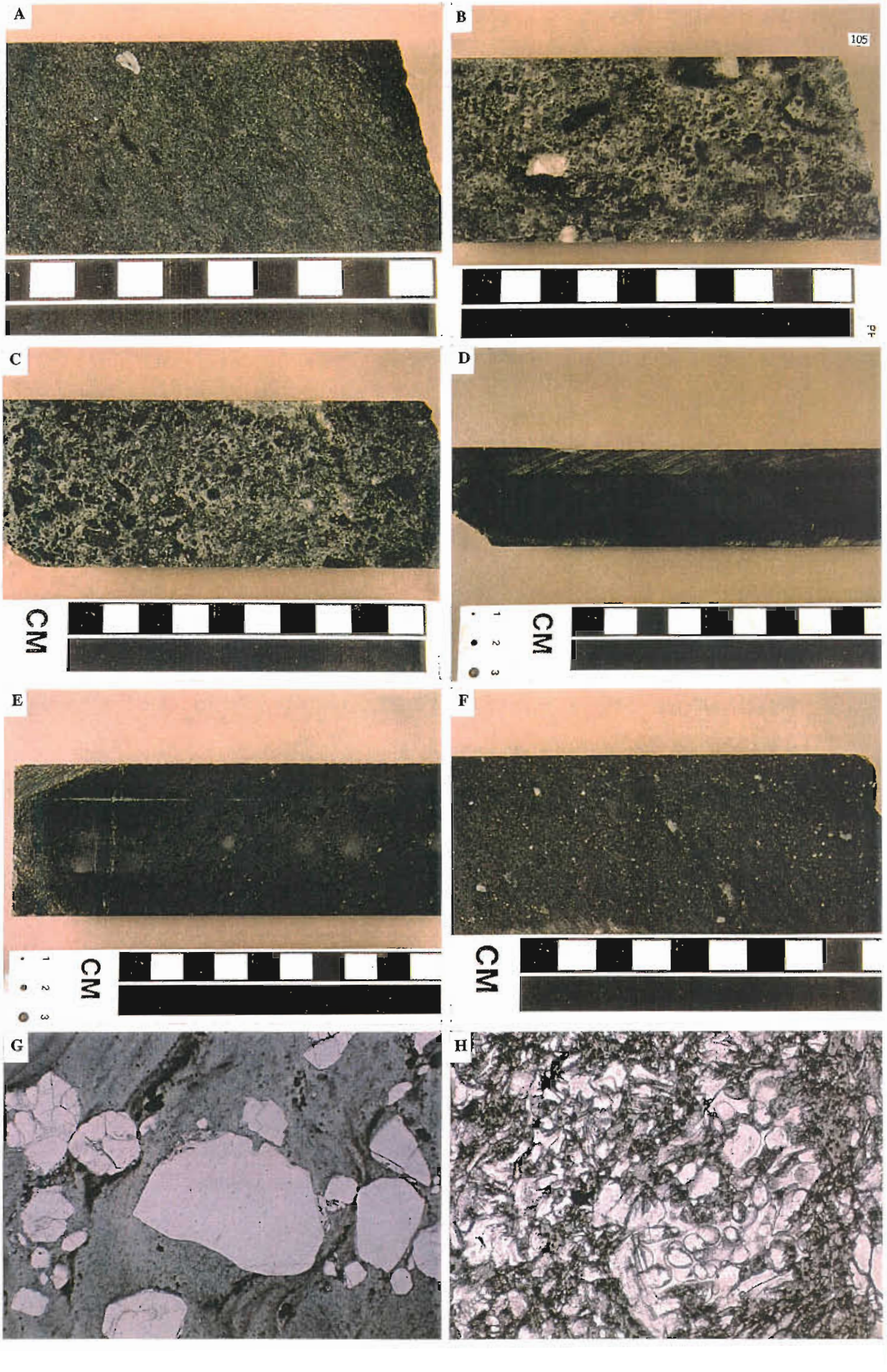
A
B
105
C
CM
D
CM
1
2
3
E
CM
1
2
3
F
CM
G
H

BLANK

Plate 3

A) Hand specimen sample from DDH GG027 at 517.3 (769072) showing a dark grey - green unit from GG5. GG5 is a relatively massive homogeneous unit with strong chlorite alteration. Pumiceous clasts are <0.5 mm set in a matrix is of fine grained, formerly glassy debris (scale bar in cm).

B) Sample of GG5 from DDH GG157 at 279.4m (769162). Massive fine grained sandstone with visible pumiceous lithics and quartz crystals in hand specimen. The unit consists almost entirely of altered, relatively well preserved, fine grained pumiceous debris and formerly shard sized glassy debris. Pervasive chlorite alteration occurs throughout the sample.

C) Example of well preserved tube pumice, bubble wall fragments and shardy debris of the massive GG5 unit. The sample is taken from DDH GG139 at 261.2m (769214). Plane polarised light. Field of view 1.2mm.

D) Example of fine grained formerly pumiceous - glassy shard rich material from GG5. Note the rounded patches in the groundmass which are rounded aggregates of quartz replaced shard - rich material. The sample is taken from DDH GG139 at 261.2m (769214). Plane polarised light. Field of view 2.5mm.

E) Sample from DDH GG038 at 275.1m (769105) shows an example of a moderate to strong chlorite altered formerly pumiceous sandstone/breccia with 2-3 mm rounded siliceous nodules. The nodules have chlorite cores and silicified rims.

F) Pictomicrograph of siliceous nodules from E. The nodules consist of meshworks of fine grained microcrystalline quartz. Relict shard and pumiceous textures are preserved through the replacement of shardy material by quartz. Quartz - chlorite alteration is ubiquitous through the matrix and the shard textures are not as well preserved as those from within the nodules. Sample DDH GG038 at 275.1m (769105). Plane polarise light. Field of view = 1.2 mm).

G) Siliceous nodular texture from GG5 in DDH GG148 at 219.7m (760499). In this sample the siliceous nodules consist of microcrystalline quartz with a strong to intense, pervasive chlorite altered matrix. Quartz aggregates of the siliceous nodules have good preservation of formerly glassy - shard textures and are indicative of the chlorite altered groundmass. The large nodule has a chlorite altered core, the preserved shape and texture of this chlorite core suggests that the core to the nodule was a vesicular pumice clast. Plane polarised light. Field of view = 1.2mm.

H) A deformed siliceous nodule in intensely altered GG4. The nodule has been recrystallised and textural preservation of former glassy - shard is poor. The nodule shows wrapping of foliation, internal cracking and pressure solution shadows. The matrix is fine grained chlorite with some angular quartz fragments present. Sample from DDH GG048 at 328.6m (769238). Plane polarised light. Field of view = 3mm.

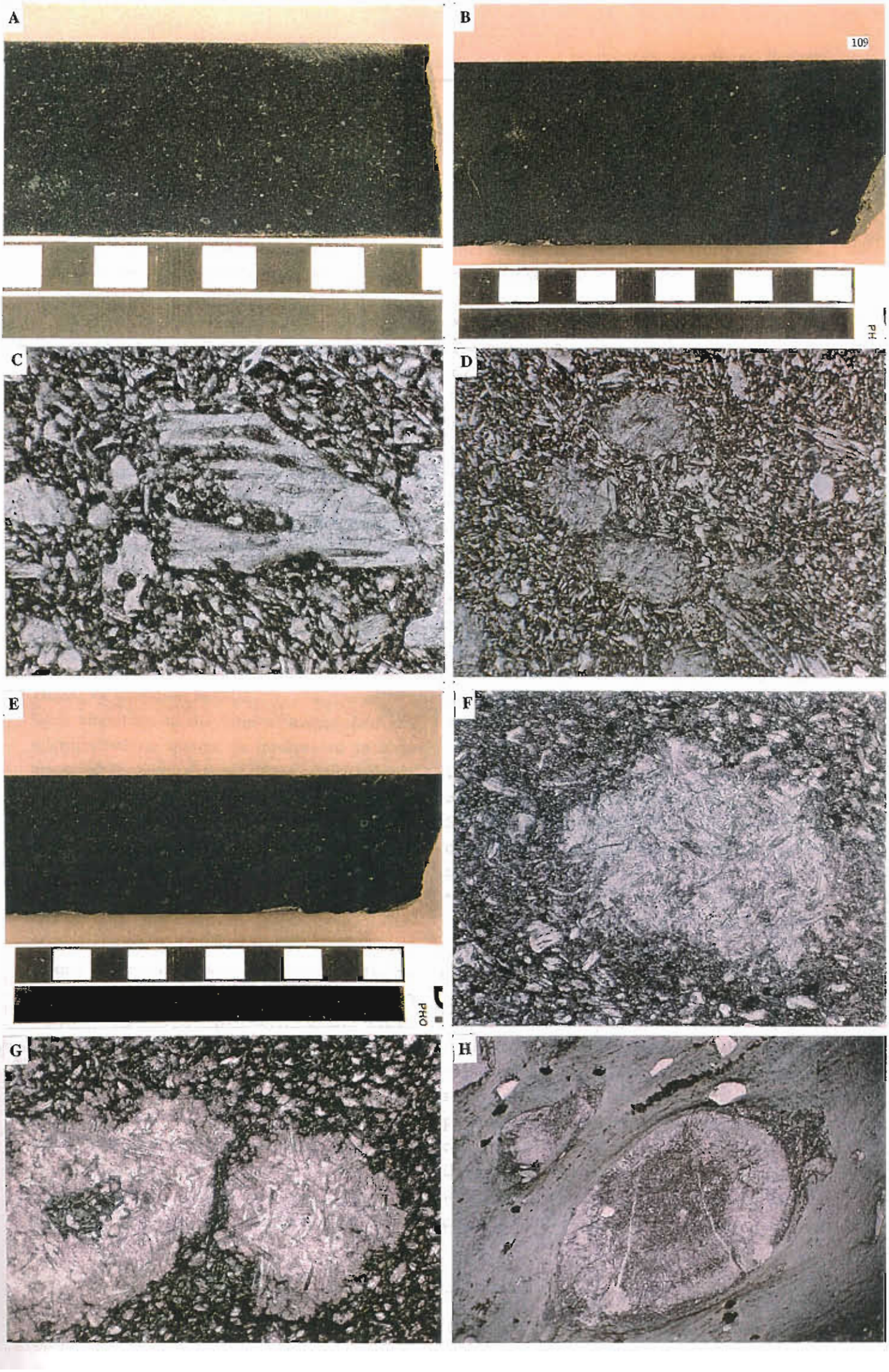
A
B
109
C
D
E
F
G
H

reflect, however the chlorite may just reflect variable alteration intensity.

Distribution of alteration

GG1 is ubiquitously altered. The distribution of hydrothermal alteration is locally intense below the mineralisation at Gossan Hill and laterally continuous throughout the 17 km strike length of the facies (Clifford, 1992). Alteration is also locally intense developed within specific beds or zones within GG1, with the distribution irregular. Alteration intensity increases towards the contact with GG4 and the alteration boundary may be sharp, reflecting a sharp stratigraphic boundary, or the interbedded reflecting the interbedded GG1-GG4 contact. Clifford (1992) proposed the chlorite-quartz alteration present in GG1 to be a footwall semi-conformable alteration zone underlying mineralisation. Evidence for the non-compacted nature of the pumice breccias and intense pervasive alteration indicate GG1 to have been a porous and permeable medium for migrating hydrothermal fluids.

Timing of alteration in GG1

Silica alteration, in the form of megaquartz and microcrystalline quartz, is interpreted to have preserved the textural forms of the original glassy-pumiceous breccias. Recrystallisation of pumice and glassy fragments to megaquartz is interpreted to have occurred soon after mass flow emplacement. This conclusion is based on the absence of flattened and compacted pumice indicates quartz-chlorite alteration was prior to diagenetic processes. Some devitrification is interpreted from rare relict feldspar-quartz textures. This devitrification may have occurred either prior to, during or soon after transportation and mass flow emplacement. The majority of units within GG1 were of a glassy composition at the onset of alteration due to the absence of preserved devitrification textures. Chlorite alteration is interpreted to be partially synchronous with the silicification. It is possible that preferential alteration of some lithic clasts, as well as glassy material in the matrix, to chlorite-rich assemblages was synchronous to silicification resulting in a domainal chlorite-quartz alteration. Another consideration is the alteration of pumice and glass to zeolite-illite assemblages. Zeolites form a common alteration product in pumiceous deposits associated with VHMS deposits (for example the Kuroko deposits; Iijima, 1973) and that during superseding alteration processes clays were transformed to chlorite.

Silica alteration

The Golden Grove Formation, incorporating GG1, GG2/3, GG4, GG5 and GG6, is universally silicified. The intensity of silicification varies between members, as well as units within members. Silicification proximal to mineralisation is intense. GG4, GG5 and GG6 have variably intense to weak quartz alteration, but do not show the distinctive domainal alteration textures diagnostic of GG1. Silicification of GG6 is intensely developed, with finer grained units composed entirely of quartz. Pebble breccia units in GG6 are however, weakly quartz altered. The transformation of formerly glassy detritus to quartz has preserved many volcanic textures. The timing of quartz alteration due to the well preserved volcanic textures is pre-diagenetic compaction and pre-to syn-mineralisation.

Siliceous nodular alteration

Siliceous nodular alteration occurs in GG4 and GG5. Siliceous nodular zones consist of microcrystalline quartz with lesser megaquartz and chlorite. The morphology of siliceous nodules is spheroidal, rounded, ovate or hourglass and range betweem 0.2 to 6 mm nodules disseminated the host rocks (Plate 3e). Relict volcanic textures maybe preserved within the siliceous nodules and can show quartz replacing former glassy-pumiceous textures. Textures include well preserved tube pumice, spherulites, shards and bubble wall fragments and angular volcanic quartz crystals (Plate 3f, g). These textures indicate that the siliceous nodules formed around aggregates of pumiceous and formerly glassy matter and in some cases have a discrete grain or lithic phase in the core. Deformation of siliceous nodules includes foliation wrapping, stretching parallel to the foliation and pressure solution shadows around nodules. These

effects indicate the brittle deformation of siliceous nodules compared to the ductile deformation within the chlorite altered host (Plate 3h).

The occurrence and distribution of siliceous nodules in hydrothermally altered and mineralised zones indicate the formation is associated with early alteration. Silicification, associated with formation of nodular alteration phases is interpreted to have formed pre-diagenetic, likely associated with the early hydrothermal-mineralising system. The distribution of siliceous nodules they formed via nucleation of quartz outward from a nucleation point, encapsulating glassy, pumiceous and quartz crystal debris.

Chlorite alteration and composition

Chlorite is a major alteration mineral within host and footwall units and shows variable textures and occurrences. Chlorite in GG6 is associated with zinc mineralisation and occurs with sphalerite and pyrite or as a alteration phase disseminated through GG6. Chlorite alteration in GG5 is a pervasive alteration phase of very fine grained chlorite forming generally less than modal 20%, in least altered zones, and up to modal 40% in strongly altered zones. GG5 units contain chlorite interstitial to silicified pumiceous lithics. GG4 contains intense chlorite alteration, although the distribution of chlorite is variable between individual units. Chlorite in GG4 occurs as very fine grained (<10m) interlocking meshworks of chlorite, to coarser grained chlorite proximal to sulphide and magnetite zones. Chlorite is a major constituent of sulphide stringer veins in GG4, GG5 and GG6, and occurs as coarse grained fibrous aggregates. GG1 footwall has domainal development of chlorite in which chlorite is forms interlocking, fine grained meshworks.

The composition of chlorite has proved to be a useful parameter in the study of hydrothermal alteration (Urabe et al., 1983). The chlorite classification proposed by Hey (1954) is a two fold classification of chlorite into an oxidised (Fe_2O_3 > 4%) and unoxidised (Fe_2O_3 < 4%) series. A solid solution series exist, with limited substitution of Al for Si and more abundant substitution of Mg for Fe. Morton and Franklin (1987) subdivided massive sulphide deposits into a Noranda-type and a Mattabi-type classification. Noranda-type deposits are associated with Mg-rich chlorite and Mattabi-type deposits are associated with Fe-rich chlorite.

Analysis of chlorite phases from Gossan Hill are plotted in Figure 2 and given in Table 1. A positive correlation exists between Fe-Mg and Al-Si substitution. Footwall chlorite is pynochlorite to ripidolite in composition and host chlorites are ripidolite to psudoethuringite in composition. This chang in mineralogy corresponds to increased Mg and decreased Fe contents in chlorite with depth into the footwall. The highest concentrations of Fe in chlorite are associated with zinc-rich sulphides in the hangingwall and the lowest concentrations of Fe (highest Mg) in stringer veins, host units GG5, GG4 and footwall GG1. Al levels decrease (increasing Si/Al ratio) with increasing depth to the footwall. Chlorites analysed from Scuddles (Ashley, 1983; Potter, 1991) show a similar systematic variation. The footwall is relatively Mg enriched and Fe depleted ($Fe^*/Fe^* + Mg$ = 0.55–0.45) and the hangingwall enriched in Fe (Fe^*/Fe^*+Mg = 0.65).

The chlorites at Gossan Hill are therefore Fe-rich chlorites, consistent with the classification of Morton and Franklin (1987). Morton and Franklin (1987) suggest that the differences in chlorite compositions between Noranda and Mattabi-type deposits are due to the relative amount of cold unreacted seawater drawn down into the discharge zone. The composition of the host units prior to mineralisation is also an important consideration. At Gossan Hill, large amounts Fe and Mg were introduced to the host units as their original felsic composition and the presence of abundant magnetite and pyrite suggests the mineralising system to was relatively enriched in Fe with respect to the mineralising fluids. Mg sources may have included cold, unreacted seawater as a result of drawn down or alternatively seawater permeating down in to the volcaniclastic pile.

Carbonate alteration and composition

Carbonate minerals at Gossan Hill are ankerite to siderite in composition and have a widespread occurrence that is closely associated with massive

Table 1. Microprobe Analysis of chlorite and chloritoid from altered and mineralised samples at Gossan Hill

AVERAGE CHLORITE COMPOSITIONS		WO3	SiO2	TiO2	SnO2	Al2O3	MgO	CaO	MnO	FeO	CuO	ZnO	Na2O	K2O	H2O	F	Cl	Total
Intense chlorite alteration	GG4	0.00	24.81	0.05	0.01	19.71	14.30	0.01	0.07	28.47	0.01	0.03	0.01	0.01	11.03	0.17	0.02	98.736
Qz rich pumiceous breccias	GG4	0.00	24.51	0.05	0.01	20.28	14.03	0.02	0.06	28.52	0.02	0.02	0.02	0.02	11.03	0.18	0.02	98.797
Footwall chlorite - quartz alteration	GG1	0.00	24.01	0.03	0.02	23.17	13.09	0.02	0.09	27.83	0.02	0.04	0.03	0.02	11.27	0.07	0.02	99.736
Andalusite-chloritoid-chlorite	GG6	0.01	22.27	0.04	0.03	22.28	6.06	0.02	0.24	37.62	0.05	0.04	0.01	0.02	10.68	0.02	0.02	99.397
Carbonate nodular alteration	GG5	0.00	28.47	0.04	0.07	21.87	22.26	0.04	0.05	16.22	0.01	0.07	0.01	0.00	12.16	0.12	0.01	101.39
Sphalerite mineralisation	GG6	0.03	22.45	0.04	0.12	23.49	7.77	0.01	0.24	34.98	0.06	0.51	0.01	0.00	10.95	0.04	0.00	100.69
Stringer vein chlorite	GG5/GG6	0.00	23.07	0.04	0.03	23.58	12.38	0.02	0.25	28.67	0.06	0.06	0.02	0.01	11.17	0.05	0.02	99.421
Siliceous nodular-chlorite alteration	GG4/GG5	0.00	25.35	0.05	0.02	18.73	13.68	0.01	0.02	30.22	0.01	0.01	0.00	0.01	11.06	0.08	0.03	99.281
Chlorite - apatite alteration	GG4	0.00	23.34	0.19	0.01	20.91	9.18	0.02	0.15	33.98	0.07	0.06	0.02	0.01	10.78	0.08	0.02	98.825
OVERALL		0.00	23.71	0.06	0.03	21.65	11.57	0.02	0.15	30.80	0.04	0.09	0.02	0.01	11.01	0.09	0.02	99.288

Sample	Host Rock	Position	Char	Other	WO3	SiO2	TiO2	SnO2	Al2O3	MgO	CaO	MnO	FeO	CuO	ZnO	Na2O	K2O	H2O	F	Cl	Total
762040	Andalusite-chloritoid-chlorite alteration	GG4	euhed	ctd1	0.00	23.25	0.00	0.09	39.46	1.23	0.00	0.42	26.90	0.00	0.00	0.00	0.00		0.03	0.00	91.39
762040	Andalusite-chloritoid-chlorite alteration	GG4	euhed	ctd2	0.00	23.27	0.00	0.00	39.71	1.34	0.00	0.62	26.35	0.08	0.10	0.01	0.01		0.00	0.02	91.49
762040	Andalusite-chloritoid-chlorite alteration	GG4	euhed	ctd3	0.00	23.83	0.06	0.04	40.20	1.47	0.00	0.59	27.00	0.00	0.04	0.04	0.01		0.00	0.00	93.27
762040	Andalusite-chloritoid-chlorite alteration	GG4	euhed	ctd4	0.00	23.69	0.02	0.00	39.85	1.17	0.02	0.39	27.26	0.04	0.03	0.00	0.00		0.03	0.00	92.50
762040	Andalusite-chloritoid-chlorite alteration	GG4	euhed	ctd5	0.00	23.70	0.00	0.00	39.69	1.33	0.00	0.60	27.54	0.01	0.07	0.00	0.00		0.02	0.03	92.99
762040	Andalusite-chloritoid-chlorite alteration	GG4	euhed	ctd6	0.00	23.76	0.02	0.10	39.49	1.36	0.02	0.41	27.04	0.00	0.15	0.00	0.01		0.08	0.00	92.44
762040	Andalusite-chloritoid-chlorite alteration	GG4	relict lath	ctd7	0.00	23.95	0.00	0.02	39.97	1.45	0.00	0.58	26.55	0.00	0.15	0.00	0.00		0.00	0.00	92.66
762040	Andalusite-chloritoid-chlorite alteration	GG4	relict lath	ctd8	0.00	23.90	0.00	0.05	39.94	1.36	0.02	0.67	26.88	0.01	0.04	0.01	0.00		0.00	0.01	92.88
762040	Andalusite-chloritoid-chlorite alteration	GG4	dis lath	ctd9	0.00	23.35	0.00	0.07	39.06	1.56	0.03	0.45	26.81	0.00	0.00	0.00	0.01		0.00	0.00	91.33
762040	Andalusite-chloritoid-chlorite alteration	GG4	dis lath	ctd10	0.00	17.75	0.65	0.00	29.02	2.46	0.08	0.28	38.54	0.07	0.05	0.00	0.00		0.00	0.00	88.90
762040	Andalusite-chloritoid-chlorite alteration	GG4	euhedral	ctd11	0.00	23.68	0.03	0.00	39.86	1.46	0.00	0.49	26.36	0.07	0.16	0.02	0.00		0.03	0.01	92.16
762040	Andalusite-chloritoid-chlorite alteration	GG4	suhed	ctd12	0.00	23.24	0.02	0.00	39.83	1.33	0.01	0.52	26.50	0.05	0.00	0.04	0.00		0.03	0.00	91.56
762040	Andalusite-chloritoid-chlorite alteration	GG4	suhed	ctd13	0.00	23.59	0.00	0.06	39.58	1.46	0.03	0.45	26.20	0.00	0.13	0.00	0.00		0.00	0.00	91.50
762040	Andalusite-chloritoid-chlorite alteration	GG4	euhedra;	ctd14	0.00	22.99	0.05	0.04	37.77	1.14	2.29	0.45	26.67	0.09	0.01	0.00	0.02		0.04	0.02	91.58
760473	Chloritoid chlorite alteration	GG4	lath	ctd1	0.00	23.34	0.00	0.00	38.94	1.08	0.00	0.47	27.39	0.00	0.12	0.03	0.00		0.00	0.00	91.36
760473	Chloritoid chlorite alteration	GG4	lath	ctd2	0.00	23.42	0.00	0.00	39.24	0.98	0.00	0.58	27.31	0.01	0.15	0.00	0.02		0.02	0.01	91.73
760473	Chloritoid chlorite alteration	GG4	lath	ctd3	0.00	23.37	0.00	0.01	39.30	0.96	0.00	0.59	27.95	0.00	0.17	0.01	0.01		0.00	0.00	92.38
760473	Chloritoid chlorite alteration	GG4	lath	ctd4	0.00	23.27	0.05	0.00	37.92	1.09	0.00	0.64	28.19	0.00	0.06	0.03	0.01		0.02	0.00	91.28
760473	Chloritoid chlorite alteration	GG4	lath	ctd5	0.00	23.71	0.00	0.00	39.09	0.94	0.00	0.58	27.53	0.03	0.16	0.02	0.02		0.08	0.00	92.16
760473	Chloritoid chlorite alteration	GG4	lath	ctd6	0.00	23.47	0.00	0.00	39.16	0.81	0.00	0.49	27.79	0.00	0.12	0.01	0.00		0.01	0.00	91.86
760473	Chloritoid chlorite alteration	GG4	lath	ctd7	0.00	23.51	0.01	0.00	39.85	0.88	0.00	0.53	27.51	0.03	0.06	0.00	0.01		0.00	0.02	92.41
760473	Chloritoid chlorite alteration	GG4	lath	ctd8	0.00	23.45	0.04	0.02	39.08	1.21	0.00	0.55	27.48	0.00	0.12	0.02	0.00		0.00	0.02	91.98
760473	Chloritoid chlorite alteration	GG4	lath	ctd9	0.00	23.53	0.00	0.00	39.44	1.02	0.00	0.46	27.42	0.00	0.13	0.00	0.00		0.00	0.00	92.01
760473	Chloritoid chlorite alteration	GG4	lath	ctd10	0.00	23.61	0.00	0.00	39.59	0.71	0.00	0.52	27.70	0.00	0.07	0.01	0.00		0.00	0.01	92.22
AVERAGE CHLORITOID COMPOSITION																					
	chloritoid-chlorite alteraton	GG4			0.00	23.52	0.01	0.02	39.39	1.19	0.11	0.52	27.14	0.02	0.09	0.01	0.01	0.00	0.02	0.01	92.05

*Note H2O not included in chloritoid microprobe analysis

sulphide and stringer mineralisation. The occurrence of carbonate is irregular within altered rocks of the host sequence, but is pervasive in hangingwall units. In host units carbonate occurs as a disseminated alteration phase hosted by intensely chlorite altered GG4 proximal to massive magnetite and pyrite-chalcopyrite mineralisation. Carbonate forms irregular disseminated grains to well formed rhombs, up to 1 mm, and hosted by chlorite. Disseminated carbonate may also form anastomosing zones. Carbonate is also a minor to major constituent of sulphide stringer vein phases. Hangingwall dacite and rhyodacite units have a pervasive, disseminated, carbonate alteration, either in the matrix or as an alteration of relict feldspar phases within the dacite and rhyodacite units. The composition of carbonates from Gossan Hill are presented in Table 2 and Figure 3. Carbonate compostions vary, becoming increasingly Fe and Mg-rich in the hangingwall-host GG6 units.

Minor alteration minerals and occurrences

A number of other alteration minerals are present in alteration zones associated with mineralisation at Gossan Hill. These minerals occur in the chlorite and siliceous alteration zones peripheral to mineralisation, having trace to minor abundances.

Ilmenite-rutile

Rutile and ilmenite are common accessory minerals in the host Members GG1, GG4, GG5 and GG6. Textural forms vary from acicular, lath, tabular to blebby shapes, which consist of generally poorly formed skeletal to spongy grain aggregates. Exsolution textures may be developed between rutile and ilmenite mineral phases indicating that rutile was partially transformed to ilmenite. Ilmenite-rutile are best developed within strong chlorite (± carbonate) alteration and are also present in disseminated, sub-massive and massive magnetite zones. The Ti-bearing phase is rutile in footwall GG1 hosted by quartz-chlorite alteration minerals. Comparatively, in GG4, Ti phases have cores of rutile enclosed in blebby ilmenite grain aggregates with exsolution textures developed. Rutile-ilmenite grains are observed in magnetite zones and may be encapsulated by magnetite. The occurrence of rutile-ilmenite as relict grains hosted within paragenetically later magnetite support the formation of rutile-ilmenite laths as an early alteration of the footwall-host stratigraphy prior to the main phase of magnetite deposition. Rutile-ilmenite compositions are presented in Figure 4 and in Table 3. The data show that rutile and ilmenite phases have endmember compositions. Microprobe results for magnetite indicate that magnetite does not contain Ti. Levels of Mn within rutile and ilmenite vary from 0.4 to 1.1 wt.% and Mg levels are less than 0.6 wt.%.

Jiang et al. (1996) contend that the presence of Mn-rich ilmenite may provide an additional record of either a brine pool environment or sub seafloor precipitation at the Sullivan Pb-Zn-Ag deposit in Canada. The source of Ti at Sullivan is considered to be derived locally from clastic sediments prior to alteration and mineralisation, whereby Ti is enriched through the leaching of alkalis and other elements. Ti sources may also include the breakdown of original Ti-bearing minerals such as rutile and ilmenite, during hydrothermal alteration and thereby providing the Ti necessary for formation of the ilmenite and other Ti-bearing phases at Sullivan. Hutchinson and Searle (1971) demonstrated that syngenetic exhalative mineralisation contains little Ti, whereas intense epigenetic stringer mineralisation retains the signature of the footwall lithology due to the immobility of Ti. Huston (1988) implicated that Ti-rich staurolite alteration in the footwall developed from intense epigenetic mineralisation compared with Ti-poor staurolite associated with syngenetic mineralisation at Balcooma. Huston (1988) thereby infers a seawater interface at the time of mineralisation based on the break in Ti contents of staurolite. The origin of these rutile-ilmenite aggregates at Gossan Hill is similarly ascribed to formation resultant from locally remobilised Ti from source minerals in the host and potentially from alteration of glass to quartz during early silicification, pre-magnetite-sulphide deposition

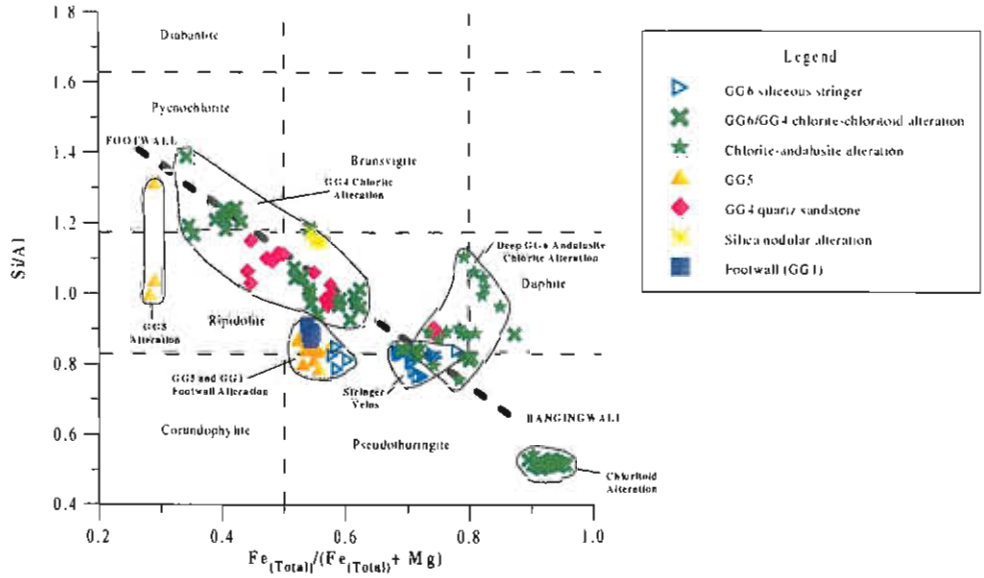

Figure 2. Chlorite compositions at Gossan Hill. The selected samples include alteration zones, mineralised zones and stringer veins. Chlorite shows a range in compositian from Fe - rich chlorite assoicated with zinc - rich mineralisation and a gradual decrease in Fe and increase in Mg contents with depth into the footwall. Chloritoid compositions from GG4 and GG6 alteration zones show a well constrained composition.

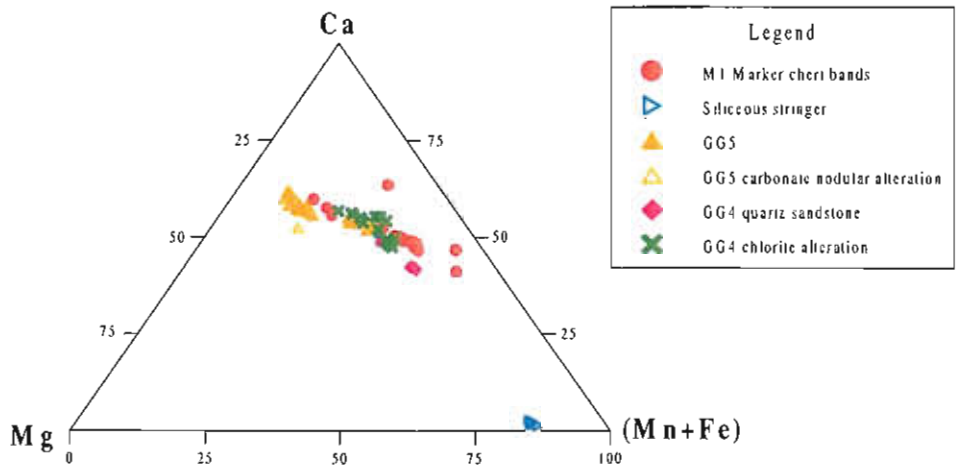

Figure 3. Microprobe analysis of carbonate from selected carbonate alteration zones at Gossan Hill. Carbonate compositions show a trend to increased levels of Fe + Mn and Mg in carbonate with depth into the footwall. Stringer veins show a distinct composition.

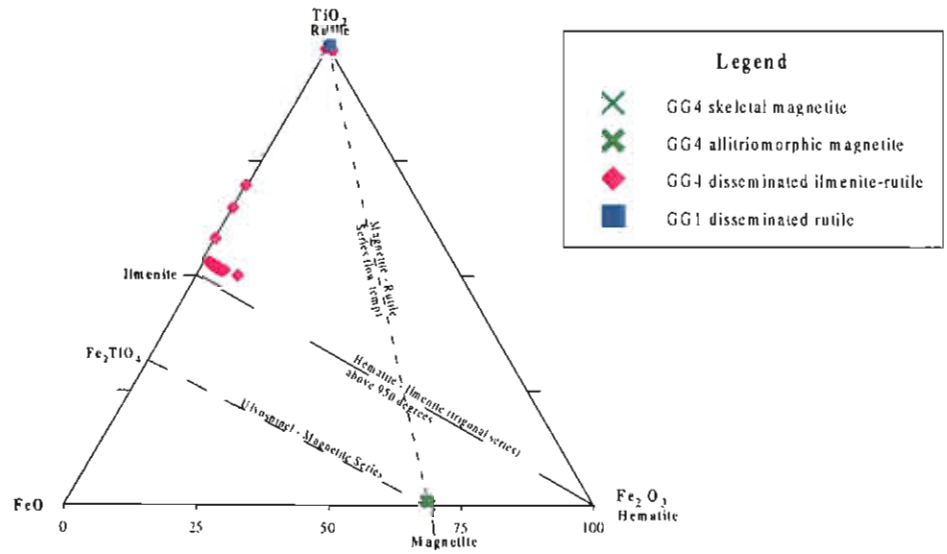

Figure 3. Composition of rutile, ilmenite and magnetite from microprobe results. The Ti - rich phases are assoicated with chlorite - quartz alteration minerals and show endmember compositions of rutile and ilmenite. Magnetite analysis show that magnetite assoicated with mineralisation does not contain elevated levels of Ti.

Apatite

Disseminated apatite occurs with chlorite-quartz alteration, as grains <0.4 mm and up to modal 2%. Apatite forms euhedral to corroded grains hosted by chlorite. Ashley et al. (1988) reported high F anomalism in the footwall at Scuddles. Apatite analysed from alteration and mineralised zones at Gossan Hill contain high levels of F, between 4.8 and 6.2% (Table 4). The F in apatite is responsible for F anomalism as reported by Ashley et al. (1988).

Summary of timing and alteration styles

Alteration mineralogy at Gossan Hill is defined by the presence of two minerals; chlorite and quartz. Both chlorite and quartz form extensive and intensely developed alteration zones that encompass mineralisation. Early silicification of the stratigraphic pile encompassed units GG1, GG2/3, GG4, GG5 and GG6 and is a widespread alteration that affected the entire Golden Grove stratigraphy over the strike length of the Golden Grove Domain (Clifford, 1992). The silicification of the pile was not a homogeneous alteration as shown by the domainal quartz-chlorite alteration in GG1 and the presence of silica alteration nodules in GG4 and GG5. Quartz alteration has preserved former volcanic textures within the original host lithology, including pumiceous and shard textures. The silicification of the footwall and host units is thought to be an early hydrothermal alteration, possibly the onset of hydrothermal alteration. Mass silicification of the host units may also have reduced permeability and porosity of the original host mediums such that hydrothermal fluid migration may have been relatively more focused through fractures. The main phase of sulphide deposition occurred post carbonate-magnetite formation as indicated from vein and mineralogical paragenesis. Sulphide veining cross cuts zones of disseminated and massive magnetite but forms zones of massive pyrite-chalcopyrite proximal to zones of massive magnetite. The temporal association between the magnetite zones and pyrite-chalcopyrite zones clearly indicate sulphide-bearing zones and veins to overprint magnetite zones. Broadly, Gossan Hill shows semi-conformable alteration zones and the association between stratigraphy and alteration mineralogy is given in Table 5a.

Geochemical studies

Introduction

Geochemical studies at Gossan Hill focus on the immediate ore forming environment and include footwall, host and hangingwall strata as well as differing alteration types and styles. In a volcano-sedimentary succession, such as the Golden Grove Formation at Gossan Hill, the application and effectiveness of geochemical techniques has been limited due to the absence of unaltered stratigraphic equivalents, as well as the potential heterogeneous nature of the volcaniclastic sediments. This study addresses these problems and examines geochemical signatures of hydrothermal alteration with emphasis on geochemical variation imposed by physical constraints such as mineralogical and mineral geochemical variation.

Aims

The aim of geochemical investigations is to examine immobile and mobile element distributions in order to characterise elemental variations attributed to primary lithofacies, hydrothermal alteration and regional metamorphism and assess the homogeneity of footwall and host volcano-sedimentary lithologies at Gossan Hill. Alteration geochemistry also examines elements considered mobile in the ore forming environment. These elements can be used to determine the depletion and addition of elements associated with hydrothermal alteration-mineralisation as well as regional metamorphism. Geochemical investigations aim to delineate element associations diagnostic of alteration associated with mineralisation and to characterise these element distributions.

Table 2. Electron microprobe analysis of carbonate minerals from altered and mineralised host lithologies

Sample	Host Rock	Position	Co host	Char	MgCO3	CaCO3	MnCO3	FeCO3	ZnCO3	SrCO3	BaCO3	CO2	Total
760411	Nodular carbonate alteration	GG5	quartz	Disseminated Groundmass	37.24	51.99	0.81	10.29	0.01	0.05	0.01	0.00	100.38
760411	Nodular carbonate alteration	GG5	quartz	Disseminated Groundmass	35.12	51.17	0.96	11.53	0.01	0.08	0.00	0.00	98.87
760411	Nodular carbonate alteration	GG5	quartz	Nodular	36.19	52.73	2.88	8.25	0.04	0.00	0.00	0.00	100.09
760411	Nodular carbonate alteration	GG5	quartz	Nodular	35.39	50.69	1.70	9.73	0.03	0.00	0.01	0.00	97.54
760411	Nodular carbonate alteration	GG5	quartz	Nodular	35.35	52.43	0.95	11.25	0.02	0.09	0.00	0.00	100.09
760411	Nodular carbonate alteration	GG5	quartz	Nodular	35.09	51.09	0.95	11.62	0.04	0.08	0.06	0.00	98.93
760411	Nodular carbonate alteration	GG5	quartz	Nodular	36.95	51.77	1.03	10.31	0.00	0.04	0.00	0.00	100.09
760411	Nodular carbonate alteration	GG5	quartz	Nodular	35.36	51.60	0.88	12.22	0.03	0.02	0.00	0.00	100.10
760411	Nodular carbonate alteration	GG5	quartz-chlorite	Zoned lath	36.00	53.39	1.81	8.84	0.00	0.00	0.05	0.00	100.09
760411	Nodular carbonate alteration	GG5	quartz-chlorite	Zoned lath	35.85	51.73	1.16	9.87	0.00	0.03	0.00	0.00	98.64
760411	Nodular carbonate alteration	GG5	quartz-chlorite	Zoned lath	34.64	53.49	3.46	8.49	0.00	0.00	0.02	0.00	100.09
760411	Nodular carbonate alteration	GG5	quartz-chlorite	Zoned lath	36.95	51.85	1.72	8.77	0.00	0.00	0.02	0.00	99.31
760411	Nodular carbonate alteration	GG5	quartz-chlorite	Zoned lath	36.56	52.31	0.76	10.39	0.03	0.04	0.01	0.00	100.09
760411	Nodular carbonate alteration	GG5	quartz-chlorite	Zoned lath	36.52	50.90	0.80	10.33	0.04	0.05	0.00	0.00	98.62
760411	Nodular carbonate alteration	GG5	quartz-chlorite	Zoned lath	38.47	52.40	1.07	8.12	0.00	0.04	0.00	0.00	100.09
760411	Nodular carbonate alteration	GG5	quartz-chlorite	Zoned lath	37.28	51.83	0.93	8.38	0.00	0.01	0.01	0.00	98.43
760411	Nodular carbonate alteration	GG5	quartz-chlorite	Zoned lath	35.85	55.50	0.76	6.91	0.07	0.02	0.02	0.00	99.12
760411	Nodular carbonate alteration	GG5	quartz-chlorite	Zoned lath	38.07	53.26	0.77	7.12	0.00	0.03	0.00	0.00	99.25
760411	Nodular carbonate alteration	GG5	quartz-chlorite	Zoned lath	38.74	45.93	0.91	11.31	0.07	0.02	0.01	0.00	96.99
760411	Nodular carbonate alteration	GG5	quartz-carbonate	Zoned lath	36.21	55.29	0.87	7.92	0.02	0.00	0.07	0.00	100.38
760411	Nodular carbonate alteration	GG5	quartz-carbonate	Zoned lath	36.02	53.48	1.82	8.00	0.03	0.03	0.01	0.00	99.39
760411	Nodular carbonate alteration	GG5	quartz-carbonate	Zoned lath	35.98	51.61	1.34	10.43	0.02	0.00	0.00	0.00	99.39
760411	Nodular carbonate alteration	GG5	quartz-carbonate	Zoned lath	37.00	54.74	0.79	7.48	0.00	0.03	0.05	0.00	100.09
760411	Nodular carbonate alteration	GG5	quartz-carbonate	Zoned lath	37.07	51.54	0.82	9.71	0.00	0.07	0.00	0.00	99.21
760411	Nodular carbonate alteration	GG5	quartz	Groundmass	35.33	51.34	0.94	12.89	0.05	0.00	0.03	0.00	100.59
760411	Nodular carbonate alteration	GG5	quartz	Groundmass	35.97	52.08	1.18	10.50	0.00	0.04	0.00	0.00	99.78
762057	Intense carbonate alteration	GG5	chlorite-carbonate	Sub massive carbonate	24.93	50.18	0.52	23.61	0.00	0.01	0.02	0.00	99.25
762057	Intense carbonate alteration	GG5	chlorite-carbonate	Sub massive carbonate	25.30	51.69	0.39	24.05	0.00	0.03	0.00	0.00	101.46
762057	Intense carbonate alteration	GG5	chlorite-carbonate	Sub massive carbonate	28.62	51.19	0.59	19.75	0.02	0.02	0.01	0.00	100.20
762057	Intense carbonate alteration	GG5	chlorite-carbonate	Sub massive carbonate	24.69	52.09	0.40	23.47	0.00	0.04	0.00	0.00	100.69
762057	Intense carbonate alteration	GG5	chlorite-carbonate	Sub massive carbonate	24.01	50.73	0.19	25.23	0.00	0.04	0.00	0.00	100.20
762057	Intense carbonate alteration	GG5	chlorite-carbonate	Sub massive carbonate	24.43	51.40	0.41	24.32	0.00	0.02	0.00	0.00	100.58
762057	Intense carbonate alteration	GG5	carbonate	Zoned lath	28.16	52.64	0.50	19.37	0.02	0.01	0.00	0.00	100.70
762057	Intense carbonate alteration	GG5	carbonate	Zoned lath	27.39	52.37	0.54	19.85	0.00	0.04	0.01	0.00	100.20
762057	Intense carbonate alteration	GG5	carbonate	Zoned lath	27.84	52.42	0.63	19.56	0.00	0.03	0.03	0.00	100.50
762057	Intense carbonate alteration	GG5	carbonate	Zoned lath	27.27	51.69	0.48	20.11	0.07	0.00	0.00	0.00	99.62
762057	Intense carbonate alteration	GG5	chlorite-carbonate	Sub massive carbonate	22.70	51.47	0.24	26.10	0.00	0.04	0.01	0.00	100.55
762057	Intense carbonate alteration	GG5	chlorite-carbonate	Sub massive carbonate	25.79	50.10	0.33	23.61	0.00	0.02	0.07	0.00	99.92
762057	Intense carbonate alteration	GG5	chlorite-carbonate	Sub massive carbonate	24.88	51.06	2.58	22.09	0.03	0.00	0.00	0.00	100.64
762057	Intense carbonate alteration	GG5	chlorite-carbonate	Sub massive carbonate	23.44	51.90	0.48	24.06	0.00	0.02	0.03	0.00	99.93
762057	Intense carbonate alteration	GG5	chlorite-carbonate	Sub massive carbonate	23.47	51.57	0.69	24.40	0.05	0.04	0.00	0.00	100.21
762057	Intense carbonate alteration	GG5	chlorite-carbonate	Sub massive carbonate	27.10	51.62	0.63	21.14	0.05	0.02	0.00	0.00	100.55
762057	Intense carbonate alteration	GG5	chlorite-sphalerite	Rhomb	21.32	50.39	1.99	27.40	0.02	0.02	0.01	0.00	101.15
762057	Intense carbonate alteration	GG5	chlorite-sphalerite	Rhomb	24.05	50.89	1.40	24.29	0.07	0.04	0.04	0.00	100.80
762057	Intense carbonate alteration	GG5	chlorite-sphalerite	Rhomb	16.96	49.67	2.22	31.16	0.01	0.00	0.00	0.00	100.01

Table 2. Electron microprobe analysis of carbonate minerals from altered and mineralised host lithologies

Sample	Host Rock	Position	Co host	Char	MgCO3	CaCO3	MnCO3	FeCO3	ZnCO3	SrCO3	BaCO3	CO2	Total
762057	Intense carbonate alteration	GG5	chlorite-sphalerite	Well formed	19.26	50.43	2.04	28.80	0.01	0.01	0.00	0.00	100.55
760432	Mgt-co-po-sph stringer vein	GG6	sphalerite	Well formed	21.41	49.60	11.45	19.14	0.39	0.00	0.00	0.00	101.99
760432	Mgt-co-po-sph stringer vein	GG6	sphalerite	Well formed	21.03	49.82	11.48	18.77	0.24	0.00	0.03	0.00	101.38
760432	Mgt-co-po-sph stringer vein	GG6	magnetite	Isolated rhomb	21.82	48.99	12.84	18.33	0.02	0.00	0.03	0.02	102.05
760432	Mgt-co-po-sph stringer vein	GG6	chlorite-magnetite	Isolated rhomb	20.98	1.85	25.09	53.35	0.05	0.00	0.00	0.22	101.54
760432	Mgt-co-po-sph stringer vein	GG6	chlorite-magnetite	Isolated rhomb	21.70	1.59	24.62	52.86	0.08	0.00	0.01	0.22	101.07
760432	Mgt-co-po-sph stringer vein	GG6	chlorite-magnetite	Interlocking aggregates	21.61	48.74	11.47	18.64	0.05	0.00	0.01	0.22	100.74
760432	Mgt-co-po-sph stringer vein	GG6	chlorite-magnetite	Interlocking aggregates	20.32	49.25	11.25	19.00	0.29	0.00	0.00	0.22	100.33
760432	Mgt-co-po-sph stringer vein	GG6	chlorite-magnetite	Interlocking aggregates	21.18	1.19	23.91	54.22	0.31	0.00	0.03	0.22	101.05
760432	Mgt-co-po-sph stringer vein	GG6	chlorite-sphalerite	Well formed	20.33	49.31	11.30	19.91	0.11	0.00	0.03	0.01	100.99
760432	Mgt-co-po-sph stringer vein	GG6	chlorite-sphalerite	Well formed	19.87	0.75	22.41	56.57	0.31	0.00	0.02	0.01	99.94
760432	Mgt-co-po-sph stringer vein	GG6	chlorite-sphalerite	Well formed	24.45	48.01	10.80	16.96	0.07	0.00	0.05	0.01	100.35
760490	M1 Marker cherty sediments	GG6	chlorite	Rhomb	17.76	49.11	4.02	28.65	0.02	0.00	0.02	0.00	99.57
760490	M1 Marker cherty sediments	GG6	chlorite	Rhomb	17.32	46.50	4.10	29.24	0.04	0.00	0.02	0.00	97.21
760490	M1 Marker cherty sediments	GG6	chlorite	Rhomb	18.70	47.80	3.52	26.14	0.00	0.04	0.01	0.00	96.21
760490	M1 Marker cherty sediments	GG6	chlorite	Rhomb	19.22	49.47	3.80	27.87	0.00	0.00	0.00	0.00	100.36
760490	M1 Marker cherty sediments	GG6	quartz-carbonate	Rhomb	19.64	49.97	4.29	26.80	0.01	0.00	0.00	0.00	100.70
760490	M1 Marker cherty sediments	GG6	chlorite	Rhomb	12.38	45.50	5.75	42.15	0.02	0.00	0.05	0.00	105.85
760490	M1 Marker cherty sediments	GG6	chlorite	Rhomb	7.77	47.71	3.85	38.05	0.00	0.00	0.00	0.00	97.38
760490	M1 Marker cherty sediments	GG6	quartz-carbonate	Rhomb	19.28	50.04	3.79	27.91	0.01	0.00	0.00	0.00	101.03
760490	M1 Marker cherty sediments	GG6	quartz	Disseminated Groundmass	18.70	49.54	4.30	28.46	0.06	0.00	0.03	0.00	101.08
760490	M1 Marker cherty sediments	GG6	chlorite-carbonate	Rhomb	16.53	44.61	3.80	30.02	0.06	0.00	0.00	0.00	95.03
760490	M1 Marker cherty sediments	GG6	chlorite-carbonate	Rhomb	19.71	50.15	4.13	27.07	0.00	0.00	0.00	0.00	101.06
760490	M1 Marker cherty sediments	GG6	chlorite-ilmenite	Rhomb	30.77	53.49	3.93	11.26	0.04	0.00	0.00	0.00	99.49
760490	M1 Marker cherty sediments	GG6	chlorite-ilmenite	Rhomb	16.36	48.30	4.22	30.12	0.00	0.00	0.07	0.00	99.06
760490	M1 Marker cherty sediments	GG6	chlorite-ilmenite	Rhomb	31.64	54.07	3.26	8.95	0.00	0.00	0.01	0.00	97.92
760490	M1 Marker cherty sediments	GG6	chlorite-ilmenite	Rhomb	30.40	50.92	3.48	13.00	0.03	0.00	0.06	0.00	97.90
760490	M1 Marker cherty sediments	GG6	carbonate-chlorite	Bedded carbonate bands	21.93	51.10	2.44	24.21	0.01	0.00	0.03	0.00	99.73
760490	M1 Marker cherty sediments	GG6	carbonate-chlorite	Bedded carbonate bands	16.85	47.35	4.26	28.12	0.00	0.00	0.00	0.00	96.58
760490	M1 Marker cherty sediments	GG6	carbonate-chlorite	Bedded carbonate bands	20.28	49.00	2.76	26.41	0.00	0.00	0.00	0.00	98.45
760490	M1 Marker cherty sediments	GG6	carbonate-chlorite	Bedded carbonate bands	19.48	48.33	3.18	27.82	0.00	0.00	0.04	0.00	98.84
760490	M1 Marker cherty sediments	GG6	carbonate-chlorite	Bedded carbonate bands	16.89	49.98	4.53	30.28	0.00	0.00	0.05	0.00	101.73
760490	M1 Marker cherty sediments	GG6	carbonate-chlorite	Bedded carbonate bands	13.05	62.95	3.25	20.03	0.05	0.00	0.04	0.00	99.38
769091	Quartz pumiceous lithic breccia	GG4/GG1	chlorite-magnetite	Disseminated grains	24.98	50.03	1.84	27.00	0.08	0.05	0.02	0.00	104.00
769091	Quartz pumiceous lithic breccia	GG4/GG1	chlorite-magnetite	Disseminated grains	22.06	42.37	1.43	34.16	0.00	0.06	0.00	0.00	100.08
769091	Quartz pumiceous lithic breccia	GG4/GG1	chlorite-magnetite	Disseminated grains	21.44	42.05	1.61	34.97	0.02	0.00	0.00	0.00	100.08

Avearge Carbonate Compositons		MgCO3	CaCO3	MnCO3	FeCO3	ZnCO3	SrCO3	BaCO3	CO2	Total
Nodular Carbonate Alteration	GG5	36.35	52.16	1.23	9.64	0.02	0.03	0.01	0.00	99.45
Stringer Veins	GG6/GG5	24.58	51.27	0.86	23.62	0.02	0.02	0.01	0.00	100.39
Carbonate-Magnetite	GG4	21.34	31.74	16.06	31.61	0.18	0.00	0.02	0.10	101.04
M1 Marker	GG6	19.27	49.80	3.84	26.31	0.02	0.00	0.02	0.00	99.26
Disseminated Carbonate	GG4	22.83	44.82	1.62	32.04	0.03	0.04	0.01	0.00	101.39
OVERALL		26.48	48.28	3.84	21.23	0.04	0.02	0.02	0.01	99.92

Table 3. Electron microprobe analysis of ilmenite, rutile and mangetite within altered and mineralised lithologies at Gossan Hill

Ilmenite and Rutile

Sample	Host Rock	Position	Host	Occurrence	Form	MgO	Al2O3	TiO2	Cr2O3	MnO	FeO	Fe2O3	SiO2	Total
769174	Quartz lithic sandstone	GG4	Quartz-chlorite	Groundmass	spongy	0.22	0.00	49.93	0.00	0.57	43.93	3.60	1.13	99.38
769174	Quartz lithic sandstone	GG4	Quartz-chlorite	Groundmass	spongy	0.03	0.00	49.51	0.00	0.51	43.95	4.41	0.16	98.55
769174	Quartz lithic sandstone	GG4	Quartz-chlorite	Groundmass	spongy	0.02	0.00	49.78	0.00	0.52	44.21	3.87	0.11	98.49
769174	Quartz lithic sandstone	GG4	Quartz-chlorite	Groundmass	spongy	0.30	0.00	50.02	0.00	0.57	43.87	2.66	0.54	97.96
769174	Quartz lithic sandstone	GG4	Magnetite	Groundmass	spongy	0.03	0.00	50.53	0.00	0.55	44.82	2.72	0.08	98.74
769174	Quartz lithic sandstone	GG4	Chlorite	Groundmass	spongy	0.04	0.00	49.61	0.01	0.54	43.99	4.17	0.06	98.42
769174	Quartz lithic sandstone	GG4	Chlorite-quartz	Groundmass	spongy	0.01	0.00	49.88	0.00	0.56	44.27	3.55	0.06	98.32
769174	Quartz lithic sandstone	GG4	Chlorite-quartz	Groundmass	spongy	0.00	0.00	49.89	0.02	0.57	44.30	3.31	0.00	98.08
769175	Quartz lithic sandstone	GG4	Chlorite	Disseminated	spongy	0.05	0.00	49.93	0.02	0.78	44.04	3.69	0.05	98.55
769175	Quartz lithic sandstone	GG4	Chlorite	Disseminated	spongy	0.01	0.00	50.12	0.01	0.81	44.23	3.70	0.00	98.89
769175	Quartz lithic sandstone	GG4	Magnetite	Disseminated	spongy	0.00	0.00	49.27	0.00	0.77	43.52	4.67	0.00	98.24
769175	Quartz lithic sandstone	GG4	Ilmenite	Disseminated	skeletal	0.01	0.00	49.66	0.00	0.74	43.89	4.32	0.00	98.61
769091	Quartz lithic sandstone	GG4/GG1	Chlorite	Disseminated	spongy	0.02	0.00	95.47	0.00	0.03	0.86	0.00	0.08	96.46
769091	Quartz lithic sandstone	GG4/GG1	Chlorite	Disseminated	spongy	0.16	0.00	49.71	0.00	0.93	43.46	3.70	0.34	98.31
769091	Quartz lithic sandstone	GG4/GG1	Chlorite	gmas, ds	spongy	0.00	0.00	50.04	0.03	0.90	44.10	3.87	0.05	98.99
769091	Quartz lithic sandstone	GG4/GG1	Chlorite	Groundmass	spongy	0.04	0.00	51.06	0.00	0.93	44.91	2.39	0.04	99.37
769091	Quartz lithic sandstone	GG4/GG1	Chlorite	Groundmass	spongy	0.03	0.00	51.21	0.00	0.89	45.10	1.54	0.02	98.78
769091	Quartz lithic sandstone	GG4/GG1	Chlorite	Groundmass	spongy	0.02	0.00	96.21	0.01	0.02	1.03	0.00	0.26	97.54
769091	Quartz lithic sandstone	GG4/GG1	Chlorite	Groundmass	needle	0.11	0.00	50.16	0.03	0.90	44.02	3.18	0.31	98.69
769091	Quartz lithic sandstone	GG4/GG1	Chlorite	Groundmass	needle	0.02	0.00	51.45	0.02	0.91	45.32	1.16	0.10	98.99
769091	Quartz lithic sandstone	GG4/GG1	Chlorite	Groundmass	spongy	0.05	0.00	51.43	0.00	0.87	45.27	1.63	0.08	99.33
769091	Quartz lithic sandstone	GG4/GG1	Chlorite	Groundmass	spongy	0.01	0.00	50.57	0.00	0.91	44.55	2.86	0.05	98.94
769091	Quartz lithic sandstone	GG4/GG1	Chlorite	Groundmass	needle	0.03	0.00	50.62	0.01	0.87	44.60	2.65	0.04	98.82
769091	Quartz lithic sandstone	GG4/GG1	Chlorite	Groundmass	needle	0.13	0.17	63.01	0.00	0.69	35.12	0.00	0.34	99.46
769091	Quartz lithic sandstone	GG4/GG1	Chlorite	Groundmass	needle	0.02	0.00	96.66	0.02	0.03	0.93	0.00	0.19	97.85

Magnetite

Sample	Host Rock	Position	Mgt host	Mgt type	Mgt Char	MgO	Al2O3	TiO2	Cr2O3	MnO	FeO	Fe2O3	Total
760432	Mgt-co-po-sph stringer vein	STZ	Sphalerite-carbonate	Disseminated	skeletal	0.00	0.08	0.02	0.01	0.00	31.45	69.70	101.25
760432	Mgt-co-po-sph stringer vein	STZ	Chlorite	Disseminated	skeletal	0.00	0.04	0.06	0.02	0.00	31.39	69.45	100.95
760432	Mgt-co-po-sph stringer vein	STZ	Chlorite	Disseminated	skeletal	0.01	0.04	0.11	0.01	0.05	31.52	69.67	101.41
760432	Mgt-co-po-sph stringer vein	STZ	Chlorite	Disseminated	skeletal	0.00	0.04	0.04	0.05	0.00	31.46	69.64	101.23
760432	Mgt-co-po-sph stringer vein	STZ	Chlorite	Disseminated	skeletal	0.11	0.06	0.02	0.02	0.01	30.28	67.56	98.06
760432	Mgt-co-po-sph stringer vein	STZ	Chlorite	Disseminated	skeletal	0.00	0.04	0.03	0.01	0.00	31.32	69.42	100.82
760432	Mgt-co-po-sph stringer vein	STZ	Chlorite	Disseminated	skeletal	0.00	0.00	0.01	0.01	0.05	31.40	69.83	101.30
760432	Mgt-co-po-sph stringer vein	STZ	Chlorite-carbonate	Disseminated	skeletal	0.01	0.13	0.04	0.00	0.06	31.44	69.68	101.36
760432	Mgt-co-po-sph stringer vein	STZ	Chlorite-carbonate	Disseminated	skeletal	0.00	0.15	0.05	0.00	0.00	31.42	69.43	101.05
760432	Mgt-co-po-sph stringer vein	STZ	Chlorite-carbonate	Disseminated	skeletal	0.00	0.06	0.05	0.06	0.06	31.51	69.80	101.53
769174	Quartz lithic sandstone	GG4	Chlorite-quartz	Groundmass	well formed	0.09	0.17	0.03	0.02	0.01	31.17	69.25	100.73
769174	Quartz lithic sandstone	GG4	Chlorite-quartz	Groundmass	well formed	0.00	0.01	0.11	0.00	0.05	31.59	69.87	101.63

Table 3. Electron microprobe analysis of ilmenite, rutile and mangetite within altered and mineralised lithologies at Gossan Hill

Sample	Host Rock	Position	Mgt host	Mgt type	Mgt Char	MgO	Al2O3	TiO2	Cr2O3	MnO	FeO	Fe2O3	Total
769174	Quartz lithic sandstone	GG4	Chlorite-quartz	Groundmass	well formed	0.01	0.02	0.02	0.00	0.00	31.56	70.08	101.69
769174	Quartz lithic sandstone	GG4	Chlorite-quartz	Groundmass	well formed	0.01	0.03	0.05	0.00	0.06	31.64	70.23	102.02
769174	Quartz lithic sandstone	GG4	Chlorite-quartz	Groundmass	well formed	0.16	0.29	0.07	0.04	0.00	31.34	69.52	101.42
769174	Quartz lithic sandstone	GG4	Chlorite-quartz	Groundmass	well formed	0.02	0.05	0.04	0.02	0.00	31.49	69.81	101.43
769174	Quartz lithic sandstone	GG4	Chlorite-quartz	Groundmass	well formed	0.01	0.02	0.08	0.00	0.01	31.54	69.81	101.47
769174	Quartz lithic sandstone	GG4	Chlorite-quartz	Groundmass	well formed	0.01	0.09	0.09	0.03	0.00	31.57	69.67	101.45
769174	Quartz lithic sandstone	GG4	Chlorite-quartz	Groundmass	well formed	0.03	0.06	0.21	0.00	0.03	31.40	69.03	100.76
769174	Quartz lithic sandstone	GG4	Chlorite-quartz	Groundmass	well formed	0.00	0.00	0.02	0.00	0.02	31.25	69.44	100.73
769174	Quartz lithic sandstone	GG4	Chlorite-quartz	Groundmass	well formed	0.02	0.03	0.04	0.00	0.00	31.53	70.00	101.62
769174	Quartz lithic sandstone	GG4	Chlorite-quartz	Groundmass	well formed	0.00	0.03	0.05	0.01	0.03	31.70	70.24	102.06
769174	Quartz lithic sandstone	GG4	Chlorite-quartz	Groundmass	well formed	0.00	0.02	0.05	0.00	0.00	31.48	69.76	101.30
769174	Quartz lithic sandstone	GG4	Carbonate	Disseminated	well formed	0.00	0.07	0.02	0.00	0.04	31.25	69.34	100.72
769174	Quartz lithic sandstone	GG4	Carbonate	Disseminated	well formed	0.00	0.06	0.17	0.03	0.00	31.58	69.41	101.24
769174	Quartz lithic sandstone	GG4	Chlorite-quartz	Groundmass	well formed	0.00	0.02	0.38	0.00	0.00	31.75	69.00	101.17
769174	Quartz lithic sandstone	GG4	Chlorite-quartz	Groundmass	well formed	0.04	0.04	0.06	0.04	0.00	31.67	70.17	102.02
769174	Quartz lithic sandstone	GG4	Chlorite-quartz	Groundmass	well formed	0.00	0.01	0.01	0.00	0.00	31.38	69.70	101.10
769175	Quartz lithic sandstone	GG4	Magnetite-chalcopyrite	Disseminated	idiomorphic	0.00	0.04	0.03	0.00	0.06	30.52	67.81	98.46
769175	Quartz lithic sandstone	GG4	Magnetite-chalcopyrite	Disseminated	idiomorphic	0.00	0.01	0.06	0.01	0.00	31.84	70.52	102.43
769175	Quartz lithic sandstone	GG4	Chlorite-ilmenite	Disseminated	idiomorphic	0.01	0.00	0.04	0.00	0.00	31.79	70.52	102.35
769175	Quartz lithic sandstone	GG4	Chlorite-ilmenite	Disseminated	idiomorphic	0.02	0.00	0.03	0.02	0.02	31.55	70.08	101.71
769175	Quartz lithic sandstone	GG4	Chlorite-talc	Disseminated	idiomorphic	0.00	0.03	0.06	0.00	0.00	31.47	69.65	101.21
769175	Quartz lithic sandstone	GG4	Chlorite-talc	Disseminated	idiomorphic	0.02	0.04	0.05	0.02	0.00	31.60	70.03	101.75
769175	Quartz lithic sandstone	GG4	Chlorite-talc	Disseminated	idiomorphic	0.06	0.23	0.05	0.00	0.01	31.23	69.11	100.68
769238	Siliceous nodular alteration	GG4	Chlorite-pyrrhotite	Isolated	idiomorphic	0.00	0.03	0.01	0.01	0.04	31.70	70.45	102.24

Table 4. Electron microprobe analysis of Apatite from chlorite alteration in copper - magnetite zones at Gossan Hill

Sample	Host Rock	Position	Host	Occurrence	Form	F	MgO	SiO2	SrO	P2O5	Cl	CaO	BaO	FeO	H2O	Total
769266	Quartz pumiceous sandstone	GG4	chlorite-quartz	Disseminated	Euhedral	5.10	0.00	0.00	0.00	42.00	0.02	54.94	0.00	0.10	0.00	102.15
769266	Quartz pumiceous sandstone	GG4	chlorite-quartz	Disseminated	Euhedral	5.13	0.00	0.01	0.00	41.87	0.01	55.08	0.02	0.05	0.00	102.16
769266	Quartz pumiceous sandstone	GG4	chlorite-quartz	Disseminated	Euhedral	5.31	0.00	0.00	0.00	41.97	0.02	54.92	0.00	0.02	0.00	102.24
769266	Quartz pumiceous sandstone	GG4	chlorite-quartz	Disseminated	Euhedral	5.47	0.00	0.00	0.00	41.55	0.15	55.05	0.01	0.11	0.00	102.34
769266	Quartz pumiceous sandstone	GG4	chlorite-quartz	Disseminated	Euhedral	5.94	0.00	0.01	0.00	41.97	0.03	54.48	0.00	0.09	0.00	102.51
769266	Quartz pumiceous sandstone	GG4	chlorite-quartz	Disseminated	Euhedral	5.97	0.00	0.01	0.00	41.61	0.02	54.72	0.00	0.18	0.00	102.52
769266	Quartz pumiceous sandstone	GG4	chlorite-quartz	Disseminated	Euhedral	5.72	0.00	0.00	0.01	41.85	0.03	54.71	0.01	0.09	0.00	102.42
769266	Quartz pumiceous sandstone	GG4	chlorite-quartz	Disseminated	Euhedral	5.44	0.00	0.00	0.00	41.89	0.03	54.79	0.03	0.12	0.00	102.30
769266	Quartz pumiceous sandstone	GG4	chlorite-quartz	Disseminated	Euhedral	4.88	0.00	0.02	0.00	41.96	0.02	55.03	0.01	0.15	0.00	102.06
769266	Quartz pumiceous sandstone	GG4	chlorite-quartz	Disseminated	Euhedral	5.00	0.00	0.01	0.00	42.16	0.02	54.83	0.01	0.08	0.00	102.11
769266	Quartz pumiceous sandstone	GG4	chlorite-quartz	Disseminated	Euhedral	5.83	0.00	0.01	0.00	41.97	0.01	54.45	0.00	0.18	0.00	102.46
769266	Quartz pumiceous sandstone	GG4	chlorite-quartz	Disseminated	Euhedral	5.59	0.00	0.02	0.00	42.23	0.02	54.41	0.00	0.10	0.00	102.36
769266	Quartz pumiceous sandstone	GG4	chlorite-quartz	Disseminated	Euhedral	6.24	0.00	0.00	0.00	41.60	0.00	54.62	0.00	0.17	0.00	102.63
769266	Quartz pumiceous sandstone	GG4	chlorite-quartz	Disseminated	Euhedral	5.36	0.00	0.01	0.00	42.08	0.01	54.64	0.00	0.17	0.00	102.26
769266	Quartz pumiceous sandstone	GG4	chlorite-quartz	Disseminated	Euhedral	5.58	0.00	0.00	0.00	41.93	0.01	54.69	0.00	0.15	0.00	102.35
769266	Quartz pumiceous sandstone	GG4	chlorite-quartz	Disseminated	Euhedral	5.87	0.00	0.01	0.00	42.05	0.01	54.43	0.00	0.11	0.00	102.47
769266	Quartz pumiceous sandstone	GG4	chlorite-quartz	Disseminated	Euhedral	5.78	0.00	0.01	0.00	41.50	0.01	54.80	0.02	0.31	0.00	102.44
769228	Apatite-andalusite-chloritoid-chlorite alteration	GG4	chlorite	Disseminated	Euhedral	5.72	0.00	0.03	0.00	41.77	0.00	54.73	0.00	0.17	0.00	102.41
769228	Apatite-andalusite-chloritoid-chlorite alteration	GG4	chlorite	Disseminated	Euhedral	6.12	0.00	0.04	0.00	41.59	0.01	54.43	0.00	0.39	0.00	102.58
769228	Apatite-andalusite-chloritoid-chlorite alteration	GG4	chlorite	Disseminated	Euhedral	4.28	0.71	3.26	0.01	36.23	0.04	46.94	0.00	7.77	0.00	99.23
769228	Apatite-andalusite-chloritoid-chlorite alteration	GG4	chlorite	Disseminated	Euhedral	5.24	0.00	0.00	0.00	41.83	0.02	55.01	0.00	0.12	0.00	102.21
769228	Apatite-andalusite-chloritoid-chlorite alteration	GG4	chlorite	Disseminated	Euhedral	6.05	0.00	0.03	0.00	41.94	0.05	54.41	0.00	0.08	0.00	102.56
769228	Apatite-andalusite-chloritoid-chlorite alteration	GG4	chlorite	Disseminated	Euhedral	6.18	0.10	1.11	0.01	40.26	0.03	52.83	0.01	2.08	0.00	102.61
769228	Apatite-andalusite-chloritoid-chlorite alteration	GG4	andalusite	Disseminated	Euhedral	5.64	0.00	0.02	0.00	42.09	0.03	54.50	0.00	0.11	0.00	102.38
769228	Apatite-andalusite-chloritoid-chlorite alteration	GG4	chlorite	Disseminated	Euhedral	5.98	0.00	0.00	0.00	41.93	0.00	54.41	0.00	0.20	0.00	102.52
769228	Apatite-andalusite-chloritoid-chlorite alteration	GG4	chlorite	Disseminated	Euhedral	6.26	0.00	0.00	0.00	41.70	0.03	54.62	0.00	0.04	0.00	102.64

Table 5. Major and trace element analyses of coherent and volcaniclastic units from the Golden Grove Formation and Scuddles Formation

	GGF M6 : Breccias and Siltstones								GGF M6 : Tuffaceous units				GGF Member 5		
SAMPLE	**760364ii**	**760364i**	**769162**	**769341**	**769343**	**760231**	**769336**	**Average**	**760491(i)**	**760491(ii)**	**760445**	**Average**	**760233**	**760376**	**769065**
NORTH	18134.0	18134.0	18400.0	18782.0	18790.2	17804.1	18762.3		18225.8	18225.8	18283.9		17799.8	18096.4	18288.9
EAST	4935.4	4935.4	5008.8	4943.3	4932.8	4925.6	4967.5		4787.2	4787.2	4842.9		4935.8	5001.3	5008.5
R.L.	10265.4	10265.4	10161.8	10138.1	10138.0	10032.1	10139.6		10141.7	10141.7	10008.6		10016.8	10168.8	10071.4
SECTION	18095	18095	18438	18778	18778	17766	18778		TF #4	TF #4	TF #4		17766	18095	18288
SiO2	55.76	64.36	59.71	63.54	70.64	83.84	84.05	68.84	55.22	59.31	66.14	60.22	71.32	66.82	66.77
TiO2	0.35	0.31	0.25	0.32	0.07	0.18	0.08	0.22	0.63	0.68	0.13	0.48	0.30	0.36	0.24
Al2O3	12.96	9.22	10.88	8.87	1.28	4.85	2.87	7.28	12.41	12.43	5.40	10.08	11.41	9.96	10.38
FeO*	19.80	16.96	17.21	15.25	6.91	7.19	7.30	12.95	17.44	16.93	18.48	17.62	6.26	13.54	13.7
MnO	0.14	0.11	0.03	0.08	0.03	0.06	0.07	0.07	0.22	0.17	0.05	0.15	0.15	0.05	0.05
MgO	5.30	3.78	7.39	3.40	0.33	1.44	0.70	3.19	5.45	5.65	1.74	4.28	1.43	5.46	4.85
CaO	0.06	0.17	-0.01	0.19	0.33	0.08	0.09	0.13	2.12	0.30	0.05	0.82	1.89	0.09	<0.01
Na2O	<0.05	<0.05	<0.03	<0.05	<0.05	0.03	0.11	0.02	0.05	0.05	<0.05	0.03	0.11	0.03	0.03
K2O	0.00	0.00	0.00	0.01	0.06	0.14	0.22	0.06	0.20	0.06	0.01	0.09	2.41	0.01	0.02
P2O5	0.03	0.05	0.01	0.05	0.01	0.02	0.04	0.03	0.08	0.07	0.01	0.05	0.04	0.08	0.01
TOTAL	98.89	100.14	99.84	98.75	97.90	99.57	98.72	99.12	98.62	99.83	98.12	98.86	99.06	100.12	99.62
LOI	4.43	4.71	4.35	4.18	5.55	1.74	3.00	3.99	4.80	4.18	6.06	5.01	3.74	3.72	3.58
S	0.21	2.48	<0.01	2.36	8.55	0.06	2.44	2.30	0.89	0.03	6.82	2.58	0.09	<0.01	<0.01
Ti/Zr	7.6	13.2	4.9	15.3	40.4	31.5	12.5	17.9	33.4	48.9	6.0	29.4	5.6	9.8	4.9
La	30	21	36	10	<2	7	5	16	6	3	17	9	26	23	30
Ce	57	40	67	19	<4	9	11	29	14	9	33	19	55	43	63
Nd	26	19	34	9	<2	4	3	14	7	3	16	9	28	23	40
Nb	9.0	4.9	10.7	5.6	<2	1.4	1.7	4.8	5.5	3.2	4.6	4.4	12.0	7.5	10.5
Zr	277	141	304	126	10	34	38	133	113	83	131	109	321	221	295
Sr	2	1	<1	1	4	2	6	2	4	1	2	2	24	2	<1
Cr	14	65	3	30	6	17	7	20	80	88	4	57	3	3	2
Ba	5	7	7	<4	<4	8	21	7	33	12	6	17	357	6	11
Sc	23	18	7	21	<2	8	4	12	37	36	9	27	10	21	7
V	64	53	2	92	22	44	16	42	205	209	6	140	4	2	<1.5
Sn	7.3	7.1	7.0	32.1	151.7	4.0	3.0	30.3	5.0	4.0	2.5	3.8	3.0	3.0	5.0
Cu	21.0	925.0	5.0	266.0	210.0	10.0	240.0	239.6	56.0	21.0	135.0	70.7	19.0	4.0	5.0
Pb	29.0	213.0	4.0	25.0	226.0	8.0	533.0	148.3	38.0	10.0	19.0	22.3	27.0	4.0	3.0
Zn	445	445	187	22700	101600	730	858	18138	453	425	194	357	491	133	230
Ni	23	23	2	Zn intf.	Zn intf.	5	12	9	46	52	2	33	1	3	2
Y	47	25	59	26	2	7	9	25	15	15	26	19	66	48	69
Rb	<1	<1	<1	<1	2	4	5	2	5	1	<1	2	82	<1	<1
Ag	2.7	24.0	0.2	1.1	5.2	0.3	4.1	5.4	1.4	0.3	0.4	0.7	0.4	0.1	0.1
As	28	58	1	26	61	3	40	31	50	48	24	41	4	<	1
Bi	0.6	5.4	<	3.0	7.8	0.2	10.2	3.9	0.8	0.1	1.7	0.9	<	<	<
Mo	1.0	1.0	1.3	0.8	0.4	0.4	1.3	0.9	0.6	<	0.5	0.4	0.3	0.8	1.1
Cd	0.8	9.1	0.2	72.8	323.0	2.6	5.0	59.1	0.2	0.1	0.2	0.2	1.2	<	0.1
Sb	0.8	4.0	1.9	2.2	3.0	0.7	2.5	2.2	2.9	1.6	1.7	2.1	1.4	0.6	1.1
Cs	0.07	0.07	0.21	0.09	0.06	0.09	0.18	0.11	0.17	0.15	0.08	0.13	0.63	0.26	0.21
Tl	<	<	<	<	1.5	0.6	0.7	0.4	0.6	<	<	0.2	1.3	<	<
Th	6.87	3.78	6.52	2.87	0.20	1.24	0.93	3.20	2.97	1.74	2.87	2.53	6.29	4.98	6.12
U	1.42	0.80	1.56	0.65	0.06	0.30	0.27	0.72	0.62	0.41	0.61	0.55	1.39	1.02	1.35
Th/U	4.84	4.73	4.18	4.42	3.33	4.13	3.44	4.43	4.79	4.24	4.70	4.62	4.53	4.88	4.53
Zr/TiO2	0.08	0.05	0.12	0.04	0.01	0.02	0.05	0.05	0.02	0.01	0.10	0.04	0.11	0.06	0.12
Nb/Y	0.19	0.20	0.18	0.22	-	0.20	0.19	-	0.37	0.21	0.18	0.25	0.18	0.16	0.15
Cu Ratio	4.5	67.5	2.6	1.2	0.2	1.4	21.9	1.3	11.0	4.7	41.0	16.5	3.7	2.9	2.1
Zn Ratio	93.9	67.6	97.9	99.9	99.8	98.9	61.7	99.2	92.3	97.7	91.1	94.1	94.8	97.1	98.7

FeO* indicates total Fe; Analysis un-normalised, < indicated below detection; Zn intf = not determined due to zinc interference

						GGF Member 4: breccia			GGF M4 : GG4 Quartz Sandstones						
SAMPLE	**769286**	**769288**	**769331**	**:lled 769277**	**Average**	**769056**	**769155**	**Average**	**769150**	**769072**	**760375**	**769089**	**769269**	**760357**	**Average**
NORTH	18679.1	18698.0	18727.8	18646.9		18268.7	18389.4		18386.1	18349.2	18099.1	18374.3	18629.2	18177.2	
EAST	5005.8	4982.4	5004.5	5048.2		5036.8	5037.4		5046.9	4924.0	4997.1	5088.4	5073.4	5010.2	
R.L.	10023.5	10003.6	10145.8	10067.2		10129.6	10202.5		10216.0	9961.0	10174.8	10187.3	10108.5	10158.3	
SECTION	18688	18688	18778	18688		18288	18438		18438	18288	18095	18438	18688	18141	
SiO2	68.92	65.6	63.04	64.83	66.75714286	29.57	69.23	49.4	45.69	66.96	77.05	49.55	27.40	38.23	50.81
TiO2	0.28	0.28	0.27	0.22	0.278571429	0.81	0.13	0.47	0.34	0.23	0.17	0.57	0.42	0.43	0.36
Al2O3	11.37	10.54	11.23	9.31	10.6	16.4	5.07	10.735	12.93	9.34	6.9	14.85	18.14	16.93	13.18
FeO*	11.17	14.21	17.33	13.9	12.87285714	26.3	10.17	18.235	24.59	13.95	11.44	20.54	28.78	31.85	21.86
MnO	0.05	0.07	0.05	0.02	0.062857143	0.05	0.01	0.03	0.03	0.04	0.03	0.05	0.03	0.06	0.04
MgO	3.74	5.19	3.95	7.09	4.53	13.28	10.75	12.015	8.52	5.18	2.2	7.67	15.86	5.52	7.49
CaO	0.03	0.1	0	0.03	0.304285714	2.59	0.18	1.385	0.06	0.03	0	0.21	0.03	0.00	0.06
Na2O	0.14	0.03	<0.03	0.05	0.055714286	0.06	0.03	0.045	0.05	0.02	0	<0.05	<0.05	<0.05	0.01
K2O	0.82	0.01	0.03	0	0.471428571	0	0	0	0	0.01	0.03	0.01	0.00	0.00	0.01
P2O5	0.03	0.04	0.01	0.01	0.031428571	0.05	0.01	0.03	0.01	0.01	0.01	0.16	0.00	0.01	0.03
TOTAL	99.71	99.72	99.6	99.58	99.63	99.6899168	99.39	99.5399584	99.172448	99.5	100.16	99.07	99.80	98.40	99.35
LOI	3.16	3.65	3.67	4.12	3.662857143	10.56	3.81	7.185	6.94	3.73	2.33	5.46	9.13	5.36	5.49
S	<0.01	<0.01	<0.01	<0.01	0.012857143	<0.01	0.02	0.01	<0.01	<0.01	<0.01	<0.01	<0.01	<0.01	0.00
Ti/Zr	5.4	5.9	5.3	5.4	6.0	36.1	5.7	20.9	7.1	5.3	5.7	11.3	5.3	7.0	7.0
La	30	23	29	34	28	22	14	18	33	22	23	19	38	30	27
Ce	58	45	56	61	54	43	25	34	56	43	43	39	74	53	51
Nd	29	22	29	27	28	18	14	16	27	19	19	20	36	25	24
Nb	11.0	9.7	10.4	8.3	9.9	3.8	4.8	4.3	9.6	9.6	7.0	10.4	16.2	11.8	10.8
Zr	308	286	305	246	283	135	137	136	287	260	179	302	472	366	311
Sr	8	2	<1	<1	5	9	<1	5	2	2	2	4	3	2	3
Cr	2	2	3	2	2	42	2	22	3	3	2	3	4	3	3
Ba	170	4	11	5	80	7	<4	3	10	9	8	7	9	10	9
Sc	10	9	9	9	11	38	6	22	15	7	4	32	14	12	14
V	2	4	<1.5	<1.5	2	242	<1.5	121	<2	2	<1.5	13	<2	<2	2
Sn	4.0	3.0	5.0	4.0	3.9	9.8	3.0	6.4	1.7	5.0	4.0	18.0	7.7	6.3	7.1
Cu	5.0	5.0	5.0	15.0	8.3	30.0	97.0	63.5	12.0	5.0	51.0	8.0	10.0	11.0	16.2
Pb	9.0	12.0	6.0	3.0	9.1	<1.5	2.0	1.0	<1.5	9.0	7.0	2.0	3.0	2.0	3.8
Zn	74	212	211	451	257	157	68	113	84	379	162	46	93	73	140
Ni	1	1	<1	2	1	37	2	20	2	2	1	3	3	3	2
Y	67	59	71	59	63	34	27	31	51	56	42	59	52	64	54
Rb	17	<1	<1	<1	14	<1	<1	0	<1	<1	<1	<1	<1	<1	0
Ag	0.1	0.2	0.1	<	0.1	<	<	0.0	0.2	0.1	0.1	0.2	0.2	0.1	0.2
As	4	4	<	<	2	5	<	3	4	2	<	1	20	8	6
Bi	<	<	<	<	0.0	0.5	0.2	0.4	0.5	<	0.2	0.3	<	<	0.2
Mo	0.9	0.9	0.9	4.2	1.3	2.7	2.3	2.5	2.3	2.0	0.9	6.3	0.1	1.8	2.2
Cd	0.2	<	<	0.2	0.2	0.3	0.1	0.2	0.2	0.2	0.2	0.2	0.2	0.2	0.2
Sb	1.0	0.8	1.5	0.8	1.0	1.7	0.7	1.2	0.6	0.9	0.6	0.9	1.3	1.6	1.0
Cs	0.60	0.70	0.26	0.13	0.40	1.67	0.14	0.91	0.15	0.32	0.18	0.43	0.35	0.20	0.27
Tl	<	<	<	<	0.2	<	<	0.0	<	<	<	<	<	<	0.0
Th	6.65	5.95	6.41	5.48	5.98	5.50	2.87	4.19	6.43	5.58	3.83	7.58	11.40	8.47	7.22
U	1.37	1.28	1.33	1.18	1.27	1.45	0.73	1.09	1.42	1.16	0.97	1.80	3.64	2.05	1.84
Th/U	4.85	4.65	4.82	4.64	4.70	3.79	3.93	3.84	4.53	4.81	3.95	4.21	3.13	4.13	3.92
Zr/TiO2	0.11	0.10	0.11	0.11	0.10	0.02	0.11	0.06	0.08	0.11	0.11	0.05	0.11	0.09	0.09
Nb/Y	0.16	0.16	0.15	0.14	0.16	0.11	0.18	0.14	0.19	0.17	0.17	0.18	0.31	0.18	0.20
Cu Ratio	6.3	2.3	2.3	3.2	3.1	16.0	58.8	36.1	12.5	1.3	23.9	14.8	9.7	13.1	10.4
Zn Ratio	89.2	94.6	97.2	99.3	96.6	-	97.1	99.1	-	97.7	95.9	95.8	96.9	97.3	97.3

FeO* indicates

	GGF M2 : GG1 Footwall volcaniclastics											SCF M2 : Hangingwall dacites (VDAC)			
SAMPLE	**769049**	**769142**	**769146**	**769148**	**769254**	**769255**	**769258**	**769259**	**762018**	**769325**	**Average**	**760206**	**760207**	**760214**	**760486**
NORTH	18257.5	18367.5	18376.1	18383.6	18576.2	18588.6	18609.9	18611.2	18169.3	19258.5		17843.2	17834.2	17817.7	18204.9
EAST	5055.2	5101.8	5077.2	5054.3	5152.0	5131.8	5101.1	5099.1	5043.8	5122.5		4829.7	4853.0	4893.4	4768.1
R.L.	10168.9	10300.1	10260.3	10226.6	10273.7	10229.5	10163.5	10159.3	10044.7	9886.2		10187.7	10148.2	10081.5	10190.7
SECTION	18288	18438	18438	18438	18688	18688	18688	18688	18187	19350		17766	17766	17766	TF #4
SiO2	75.55	73.64	78.48	51.69	74.34	78.29	83.69	57.7	80.11	73.05	72.654	65.68	68	71.86	64.3
TiO2	0.26	0.27	0.2	0.51	0.33	0.19	0.19	0.49	0.29	0.32	0.305	0.44	0.43	0.45	0.39
Al2O3	7.21	8.53	6.35	15.23	8.58	6.54	4.91	13.52	8.94	9.76	8.957	14.39	13.92	14.75	14.02
FeO*	10.29	10.1	8.14	18.8	9.18	8.58	6.5	16.46	4.42	9.21	10.168	4.18	3.87	5.71	4.07
MnO	0.03	0.04	0.02	0.06	0.03	0.02	0.02	0.05	0.02	0.05	0.034	0.06	0.07	0.04	0.08
MgO	3.44	4.13	3.2	7.73	3.71	3.09	2.25	6.35	2	3.52	3.942	2.32	1.92	1.27	2.47
CaO	0.04	-0.01	0.06	-0.01	0.08	0.03	0.01	0.04	0.05	0.14	0.04	3.48	3.19	0.15	5.16
Na2O	0.04	0.04	0.05	0.06	0.06	0.03	0.04	0.07	0.21	0.11	0.071	2.53	0.59	0.64	1.11
K2O	0	0	0	0	1	0	0	0	1	1	0	2	3	2	1
P2O5	0.0	0.0	0.0	0.0	0.1	0.0	0.0	0.0	0.0	0.0	0.0	0.1	0.1	0.1	0.1
TOTAL	99.6	99.9	99.4	99.8	99.5	99.4	99.6	99.7	99.6	99.7	99.6	99.7	99.5	99.6	99.4
LOI	2.7	3.0	2.7	5.4	2.6	2.6	1.9	4.6	2.1	2.9	3.0	4.5	4.7	2.7	6.5
S	<0.01	<0.01	0.5	0.1	<0.01	0.1	<0.01	<0.01	0.0	0.0	0.1	<	0.2	0.2	0.0
Ti/Zr	10.3	8.6	8.6	13.1	12.2	8.7	11.7	18.1	9.8	10.2	11.1	17.0	17.0	17.5	16.2
La	13	22	20	36	15	14	33	25	14	23	21	17	21	10	21
Ce	25	39	40	57	28	26	50	38	27	40	37	34	39	22	37
Nd	12	17	16	26	13	12	22	17	13	19	17	15	14	10	15
Nb	5.8	6.7	5.1	7.6	5.6	4.1	3.4	6.2	5.7	6.4	5.7	4.9	5.7	5.4	4.3
Zr	152	189	139	233	162	131	98	162	178	188	163	155	152	155	145
Sr	<1	2	3	5	5	2	2	5	42	5	7	132	78	38	86
Cr	2	3	3	104	4	2	2	29	3	6	16	51	46	47	64
Ba	5	48	34	59	277	17	17	78	246	136	92	712	578	166	218
Sc	10	10	8	25	13	8	6	27	13	14	13	12	10	12	12
V	7	13	3	72	11	5	9	103	8	12	24	72	69	71	76
Sn	3.0	2.0	2.0	5.0	2.0	2.0	1.0	5.0	2.0	3.0	2.7	1.0	1.0	1.0	2.0
Cu	4.0	6.0	19.0	10.0	7.0	11.0	4.0	9.0	9.0	4.0	8.3	21.0	13.0	34.0	16.0
Pb	4.0	1.5	5.0	5.0	3.0	4.0	4.0	4.0	7.0	3.0	4.1	7.0	7.0	15.0	26.0
Zn	45	38	22	61	29	22	30	93	24	31	40	64	45	194	249
Ni	2	3	2	17	2	2	3	12	2	3	5	46	33	39	47
Y	21	28	22	36	22	21	12	50	28	39	28	13	13	14	12
Rb	<1	4	3	4	13	2	2	8	31	15	8	62	74	48	31
Ag	<	0.1	0.1	0.2	<	<	<	<	0.1	<	0.1	<	0.1	0.3	0.1
As	<	<	4	2	<	<	<	2	<	<	1	<	1	48	2
Bi	0.1	<	0.5	1.1	<	0.1	0.1	0.2	0.2	3.3	0.6	<	0.3	0.1	<
Mo	3.2	12.5	1.6	42.9	2.6	1.0	3.9	2.0	1.6	1.1	7.2	0.7	0.2	1.1	0.7
Cd	<	<	<	0.2	0.1	<	<	4.4	<	<	0.5			0.2	0.1
Sb	0.6	0.2	1.0	0.7	0.2	0.2	0.2	0.6	0.4	0.3	0.4	0.6	1.1	1.6	1.4
Cs	0.13	0.13	0.31	0.77	0.41	0.19	0.18	0.45	0.63	0.72	0.39	1.12	1.37	0.97	1.09
Tl	<	<	<	<	<	<	<	<	<	<	0.0	<	<	0.5	1.0
Th	4.27	5.04	4.01	6.07	4.32	3.71	2.72	4.01	4.77	5.07	4.40	6.12	5.93	6.33	5.27
U	0.99	1.35	0.88	1.66	1.07	0.89	0.75	1.06	1.17	1.31	1.11	1.46	1.41	1.67	1.18
Th/U	4.31	3.73	4.56	3.66	4.04	4.17	3.63	3.78	4.08	3.87	3.95	4.19	4.21	3.79	4.47
Zr/TiO2	0.06	0.07	0.07	0.05	0.05	0.07	0.05	0.03	0.06	0.06	0.06	0.04	0.04	0.03	0.04
Nb/Y	0.28	0.24	0.23	0.21	0.25	0.20	0.28	0.12	0.20	0.16	0.22	0.38	0.44	0.39	0.36
Cu Ratio	8.2	13.6	46.3	14.1	19.4	33.3	11.8	8.8	27.3	11.4	17.4	24.7	22.4	14.9	6.0
Zn Ratio	91.8	96.2	81.5	92.4	90.6	84.6	88.2	95.9	77.4	91.2	90.7	90.1	86.5	92.8	90.5

FeO* indicates

										Dacite Intrusive			SCF M2 : Hangingwall Rhyodacite		
SAMPLE	**760447**	**769073**	**769074**	**769075**	**769279**	**769294**	**769328**	**769347**	**Average**	**769076**	**769278**	**Average**	**760211**	**760215**	**760217**
NORTH		18372.1	18379.4	18398.6	18653.2	18745.8	18697.2	18809.8		18415.6	18646.9		17822.5	17815.5	17811.7
EAST		4883.6	4870.0	4833.8	5039.6	4924.8	5038.1	4907.7		4802.6	5048.2		4881.9	4898.5	4907.8
R.L.		9934.3	9927.8	9914.3	10056.4	9961.4	10156.7	10138.9		9905.6	10067.2		10100.1	10073.4	10059.1
SECTION	TF #4	18288	18288	18288	18688	18688	18778	18778		18288	18688		17766	17766	17766
SiO2	63.75	66.09	66.78	66.43	65.92	60.62	65.21	58.65	65.27	68.07	66.85	67.46	81.98	80.7	71.81
TiO2	0.36	0.39	0.35	0.38	0.37	0.53	0.35	0.4	0.40	0.43	0.38	0.405	0.39	0.35	0.39
Al2O3	14.06	14.58	14.37	14.57	14.26	14.21	13.97	13.46	14.21	14.8	14.81	14.805	11.95	11.23	12.29
FeO*	3.92	3.47	3.96	3.4	3.85	4.94	3.8	5.2	4.20	3.54	3.68	3.61	0.11	2.17	4.73
MnO	0.14	0.06	0.1	0.08	0.14	0.08	0.1	0.21	0.10	0.02	0.04	0.03	0	0.01	0.11
MgO	3.07	2.03	2.58	2.38	2.69	3.68	2.59	2.77	2.48	2.53	2.32	2.425	0.05	0.63	1.34
CaO	3.64	3.88	2.93	2.93	2.86	4.63	3.37	6.21	3.54	0.99	2.67	1.83	0.15	0.12	2.36
Na2O	0.61	0.8	0.84	0.64	0.63	1.16	0.55	0.82	0.91	6.35	2.04	4.195	0.91	0.62	0.42
K2O	3	3	2	3	3	2	3	2	2	0	2	1	2	2	2
P2O5	0.1	0.1	0.1	0.1	0.1	0.2	0.1	0.1	0.1	0.1	0.1	0.1	0.1	0.1	0.1
TOTAL	99.9	99.7	99.9	99.6	99.5	99.7	99.9	99.9	99.7	99.6	99.5	99.6	99.3	99.8	99.6
LOI	7.5	5.6	5.4	5.7	5.9	7.9	6.9	9.8	6.1	2.6	4.6	3.6	1.6	1.8	3.9
S	0.1	<	<	0.1	0.2	0.0	<	0.1	0.1	0.5	0.1	0.3		0.2	0.1
Ti/Zr	14.6	15.4	14.5	15.0	14.7	19.1	14.4	15.3	15.9	16.4	15.0	15.7	8.9	9.0	8.9
La	17	17	17	19	19	20	14	17	17	19	18	18	8	25	24
Ce	32	32	34	35	32	38	29	32	33	39	34	37	18	57	46
Nd	12	13	11	14	12	16	11	13	13	14	14	14	9	27	22
Nb	5.2	5.4	4.8	5.0	5.4	6.5	4.1	5.4	5.2	6.2	5.0	5.6	10.2	8.9	9.7
Zr	148	151	145	152	150	166	145	156	152	157	152	154	262	234	264
Sr	54	60	53	41	43	66	43	57	63	192	56	124	56	41	39
Cr	27	28	28	30	30	89	30	54	44	62	32	47	6	6	7
Ba	380	337	343	434	534	443	509	387	420	1288	411	850	220	261	269
Sc	9	10	9	9	8	14	9	12	10	10	9	10	11	12	14
V	51	51	51	51	49	86	49	58	61	65	52	58	35	22	25
Sn		2.0	1.0	1.0	2.0	2.0	2.0	2.0	1.4	<	1.0	0.5	<	2.0	2.0
Cu	7.0	15.0	5.0	5.0	13.0	21.0	11.0	20.0	15.1	18.0	70.0	44.0	5.0	28.0	24.0
Pb	17.0	19.0	25.0	22.0	7.0	11.0	9.0	13.0	14.8	8.0	7.0	7.5	16.0	23.0	43.0
Zn	108	79	120	168	51	92	31	122	110	47	53	50	3	82	220
Ni	20	20	23	18	16	57	19	32	31	52	19	36	14	5	7
Y	10	11	10	11	10	13	9	13	12	11	10	11	57	43	48
Rb	77	79	70	81	68	49	75	57	64	5	52	29	49	49	54
Ag		<	<	<	<	<	<	0.1	0.1	0.2	<	0.1	0.1	0.7	0.5
As	4	<	<	2	3	<	<	7	6	4	2	3	30	14	10
Bi	<	<	<	<	0.1	<	<	<	0.0	0.1	0.1	0.1	<	<	<
Mo	0.1	1.8	0.1	0.8	0.7	2.0	0.7	0.5	0.8	0.2	0.6	0.4	2.5	0.9	1.1
Cd	0.1	0.2	0.2	0.1	<	0.1	<	0.1	0.1	<	<	0.0	<	<	0.4
Sb	0.7	0.7	0.8	1.2	0.5	1.2	0.9	1.8	1.0	2.0	0.6	1.3	1.0	3.3	2.0
Cs	1.18	1.21	1.13	1.30	1.09	1.91	1.15	1.15	1.22	0.43	0.94	0.69	1.28	1.05	0.96
Tl	1.0		<	0.6	<	<	<	<	0.3	<	<	0.0	<	0.7	1.2
Th	5.35	5.61	5.38	5.62	5.40	5.21	5.07	4.51	5.48	6.58	5.73	6.16	7.89	6.70	6.74
U	1.28	1.31	1.33	1.33	1.27	1.16	1.25	1.10	1.31	1.52	1.34	1.43	1.96	1.54	1.78
Th/U	4.18	4.28	4.05	4.23	4.25	4.49	4.06	4.10	4.18	4.33	4.28	4.30	4.03	4.35	3.79
Zr/TiO2	0.04	0.04	0.04	0.04	0.04	0.03	0.04	0.04	0.04	0.04	0.04	0.04	0.07	0.07	0.07
Nb/Y	0.52	0.49	0.48	0.45	0.54	0.50	0.46	0.42	0.45	0.56	0.50	0.53	0.18	0.21	0.20
Cu Ratio	6.1	16.0	4.0	2.9	20.3	18.6	26.2	14.1	12.0	27.7	56.9	46.8	62.5	25.5	9.8
Zn Ratio	86.4	80.6	82.8	88.4	87.9	89.3	77.5	90.4	88.1	85.5	88.3	87.0	15.8	78.1	83.7

FeO* indicates

	s (VRDA)								Dolerite Intrusives		
SAMPLE	760218	760219	760487	760488	769302	769303	769346	Average	769144	769145	Average
NORTH	17808.8	17807.8	18216.7	18221.0	19386.7	19356.1	18799.6		18372.6	18373.5	
EAST	4914.7	4917.1	4778.8	4782.8	4946.4	4990.1	4920.8		5087.6	5084.9	
R.L.	10048.5	10045.0	10163.0	10152.8	10070.2	10007.0	10138.4		10276.6	10272.4	
SECTION	17766	17766	TF #4	TF #4			18778		18438	18438	
SiO2	64.08	72.26	75.36	65.57	69.98	78.47	74.54	73.475	48.35	47.06	47.71
TiO2	0.48	0.4	0.36	0.33	0.38	0.38	0.41	0.387	0.83	1.36	1.10
Al2O3	15.38	12.21	11.43	10.46	11.3	12.14	12.81	12.12	14.85	13.66	14.26
FeO*	6.4	7.71	3.51	5.05	2.25	0.65	5.22	3.78	12.59	16.66	14.63
MnO	0.17	0.1	0.06	0.17	0.15	0.05	0.04	0.086	0.19	0.22	0.21
MgO	2.6	1.66	1.61	2.56	0.65	0.12	1.25	1.247	8	5.15	6.58
CaO	2.33	0.31	1.48	6.08	5.90	1.65	0.21	2.06	10.62	10.93	10.78
Na2O	0.37	0.31	0.38	0.27	0.64	0.53	0.48	0.493	1.51	0.22	0.87
K2O	3	2	2	2	2	3	2	2	0	0	0
P2O5	0.1	0.1	0.1	0.1	0.1	0.1	0.1	0.1	0.1	0.1	0.1
TOTAL	99.8	99.6	99.7	99.9	99.7	99.7	99.7	99.7	99.9	99.2	99.5
LOI	5.2	2.8	3.3	7.6	6.1	2.8	2.6	3.8	2.9	3.8	3.4
S	0.2	0.6	0.0		0.0	0.1	0.1	0.1	0.1	0.3	0.2
Ti/Zr	8.5	9.3	9.0	8.4	9.0	9.0	9.0	8.9	107.0	96.5	101.8
La	29	26	23	20	20	20	30	22	2	8	5
Ce	62	51	47	41	42	44	63	47	7	17	12
Nd	29	25	22	20	20	22	29	22	4	15	9
Nb	13.9	10.6	9.9	8.8	9.7	10.3	10.9	10.3	1.9	6.9	4.4
Zr	337	259	241	237	252	254	272	261	47	85	66
Sr	26	19	20	22	53	41	28	35	138	347	242
Cr	8	13	7	8	6	6	8	8	418	25	221
Ba	252	168	386	318	434	300	343	295	9	<4	4
Sc	15	15	11	12	13	11	13	13	41	23	32
V	28	26	21	21	21	23	26	25	261	254	257
Sn	3.0	6.0	3.0	3.0	3.0	2.0	2.0	2.6	2.0	3.0	2.5
Cu	19.0	7.0	70.0	8.0	19.0	11.0	45.0	23.6	101.0	211.0	156.0
Pb	128.0	94.0	23.0	23.0	26.0	25.0	16.0	41.7	3.0	6.0	4.5
Zn	250	207	118	148	112	12	161	131	103	126	115
Ni	11	4	4	6	9	6	9	8	151	91	121
Y	107	46	35	37	43	45	45	51	18	25	22
Rb	66	43	51	45	64	77	49	55	<1	<1	0
Ag	1.3	0.9	0.4	0.2	0.4	1.4	0.3	0.6	<	0.2	0.1
As	32	82	4	1	<	18	7	20	3	3	3
Bi	<	<	<	<	<	<	0.1	0.0	<	0.2	0.1
Mo	2.9	0.3	0.6	0.2	0.6	1.5	0.8	1.1	0.2	0.3	0.3
Cd	0.3	0.2	<	0.1	0.4	<	<	0.1	0.2	0.3	0.3
Sb	3.2	2.9	1.6	1.6	0.5	1.9	2.5	2.1	0.8	0.6	0.7
Cs	1.06	0.64	0.89	0.64	1.05	0.94	0.97	0.95	0.11	0.15	0.13
Tl	2.5	2.3	2.1	1.7	<	0.6	0.5	1.2	<	<	0.0
Th	8.75	7.03	6.40	5.87	6.47	5.92	7.22	6.90	0.33	0.97	0.65
U	2.31	1.62	1.54	1.41	1.51	1.50	1.74	1.69	0.07	0.23	0.15
Th/U	3.79	4.34	4.16	4.16	4.28	3.95	4.15	4.08	4.71	4.22	4.33
Zr/TiO2	0.07	0.06	0.07	0.07	0.07	0.07	0.07	0.07	0.01	0.01	0.01
Nb/Y	0.13	0.23	0.28	0.24	0.23	0.23	0.24	0.22	0.11	0.28	0.19
Cu Ratio	7.1	3.3	37.2	5.1	14.5	47.8	21.8	15.2	49.5	62.6	57.7
Zn Ratio	66.1	68.8	83.7	86.5	81.2	32.4	91.0	75.9	97.2	95.5	96.2

FeO* indicates

Table 5a. Alteration mineralogy of stratigraphic Members at Gossan Hill. The alteration mineral assemblages show major (+)and minor (±) mineral phases and their association to sulphide or magnetite mineralisation.

Stratigraphic Member	Alteration Minerals	Associated Mineralisation
SC2 (dacite)	sericite + chlorite + carbonate + quartz	minor disseminated pyrite ± sphalerite
SC2 (rhyodacite)	sericite + chlorite + carbonate + quartz	minor disseminated pyrite ± sphalerite
M1 Marker	quartz + carbonate + pyrite ± magnetite ± chlorite (chert)	pyrite ± magnetite
	chlorite + carbonate + quartz ± ilmenite (lithic)	pyrite ± magnetite
GGF M6	quartz	massive sphalerite -pyrite
	quartz ± chlorite ± ilmenite	stringer vein mineralisation
GGF M5	quartz + chlorite ± ilmenite	none
	chlorite + quartz + carbonate ± ilmenite	weak stringer mineralisation
	quartz ± chlorite ± ilmenite	intense stringer mineralisation
	quartz + chlorite + carbonate (nodules) ± sericite	minor disseminated pyrite
GGF M4	quartz (± nodules) + chlorite ± carbonate ± apatite	minor disseminated pyrite
	chlorite ± carbonate ± ilmenite	massive magnetite ± pyrite
	chlorite + carbonate + magnetite + talc + pyrite/pyrrhotite ± rutile ± ilmenite	massive magnetite ± massive Cpy and sulphides
	chlorite ± chloritoid ± andalusite + pyrite/pyrrhotite + magnetite ± rutile ± ilmenite	massive magnetite ± massive Cpy and sulphides
GGF M1	quartz + chlorite ± sericite ± rutile	trace disseminate pyrite

Previous geochemical investigations

Regional lithogeochemistry is the focus of company reports (Radford, 1994), detailed studies (Clifford, 1992) as well as ongoing exploration activity in the Golden Grove district. The Scuddles deposit has been the focus of geochemical studies by Ashley (1983), Potter, (1991) and Whitford and Ashley (1992). The results from these studies provide a broad framework for comparison with the results of this study. Although broad characterisation of geochemical trends at Gossan Hill were made by Frater (1978), many associations were hindered by the absence of stratigraphic control at the time of this study. The present geochemical study has the advantage of stratigraphic orientation and alteration paragenesis, which was unavailable to past researchers and provides a necessary context from which alteration and geochemical trends can be interpreted.

Sample details

Geochemistry was conducted on 88 samples from unweathered drill core, selected from specific stratigraphic Members and zones of alteration. The suite of samples represent least altered and altered samples from footwall, host and hangingwall units and their locations are given in Figure 5. Limitations from the orientation and placement of drill holes together with the stratigraphic separation of zinc and copper mineralised zones in a steeply dipping terrain precluded detailed investigation on any single section.

Immobile elements

Immobile element characterisation of stratigraphic units at Gossan Hill was conducted on samples from least altered lithotypes (Table 6). Immobile elements that have been used by various authors in previous studies include; Ti, Zr, Y, Nb, Ga, P, REE, V, Cr, Sc, Hf Ta, Th (Winchester and Floyd, 1977; Floyd and Winchester, 1978). Ashley (1983) demonstrated the relative immobility of Ti, V, Zr, Nb and Y at the Scuddles deposit and concluded that these elements best delineate original compositional variation. Linear trends on binary variation diagrams reflect immobility of the elemental components due to preservation of primary ratios (Whitford, et al., 1992). Evidence of immobility of the elements Nb, Zr, and Y at Gossan Hill are shown in Figure 6, using data normalised to volatile free contents. Hangingwall dacite, dacite intrusives and GG1 have lower Y, Nb and Zr values than hangingwall rhyodacite, GG4 and GG5 units. Dolerite intrusives have very low Nb and Zr values. A wide variation in Y/Nb and Nb/Zr ratios is observed for samples from GG6 breccias and sandstones and reflects the multi-provenance origin of these units. Whitford and Ashley (1992) identify similar trends at Scuddles, with the mineralised horizon have lower Zr/Nb ratios to footwall or hangingwall units.

Al_2O_3 and TiO_2 are generally considered immobile except under extreme hydrothermal alteration conditions where the mobility of Al_2O_3 and TiO_2 has been determined by a number workers on VHMS mineralisation (Larson, 1984). An Al_2O_3 vs. TiO_2 plot (Figure 7) shows a positive linear correlation for samples from footwall, host and hangingwall zones with the exception of late stage dolerite intrusive which has elevated TiO_2 values and GG6 and GG4 units which lie off the linear trend. The scatter of data from GG4 and GG6 suggests limited Al and Ti mobility. Petrographic support includes the occurrence of intense phyllosilicate-chlorite-chloritoid alteration and rare andalusite, ilmenite and rutile. The approach of assessing the composition of hydrothermally altered volcanics based on the immobility of TiO_2 and Al_2O_3 is offered by Whitford et al. (1989) from the Que River deposit. Clifford (1992) reviewed the mobility TiO_2 and Al_2O_3 to the Golden Grove district on a regional scale, concluding that the approach was not applicable due to the mobility of Al_2O_3 during hydrothermal alteration. The results from Gossan Hill show a relatively constant TiO_2/Al_2O_3 ratio indicating these ratios have not been substantially modified, but that some localised mobility of Al_2O_3 and TiO_2 under extreme hydrothermal alteration occurred in GG4 and GG6. Winchester and Floyd (1977) devised a discrimination diagram based on immobile elements to characterise differing rock types and magmatic affinity. Data from

Table 6 Major and trace element data from altered volcaniclastic units in the Golden Grove Formation

	GGF M6 : M1 Marker chert					GGF M6 : M1 Marker Lithic							GGF M6 : STRINGER
SAMPLE	**SCD007II**	**SCD005II**	**760490II**	**762064II**	**Average**	**SCD007I**	**SCD005III**	**SCD005I**	**760490I**	**760366**	**762064I**	**Average**	**760230**
NORTH	Scuddles	Scuddles	18224.4	18066.3		Scuddles	Scuddles	Scuddles	18224.4	18124.9	18066.3		17805.5
EAST			4786.0	4982.1					4786.0	4952.7	4982.1		4922.5
R.L.			10144.8	10257.5					10144.8	10238.8	10257.5		10036.8
SECTION			TF#4	18049					TF#4	18095.00	18049.00		17766
SiO2	79.84	86.86	76.09	81.31	81.03	39.24	48.28	35.53	16.65	61.56	71.73	45.50	60.74
TiO2	<0.01	<0.01	0.02	0.00	0.01	0.16	0.65	0.46	0.32	0.27	0.16	0.34	0.24
Al2O3	0.06	0.08	0.35	0.20	0.17	3.62	13.16	11.33	6.08	6.72	5.20	7.69	3.03
FeO*	5.23	2.89	5.86	10.17	6.04	34.49	18.42	24.00	24.39	23.34	13.94	23.10	8.39
MnO	0.20	0.13	0.32	0.07	0.18	0.80	0.19	0.38	1.02	0.32	0.04	0.46	0.03
MgO	2.01	0.66	1.88	0.36	1.23	5.13	4.14	5.99	7.62	2.67	2.13	4.61	0.95
CaO	4.47	3.70	5.86	0.35	3.60	4.77	4.45	7.75	16.64	0.08	0.04	5.62	0.03
Na2O	<0.03	<0.03	<0.03	<0.05	0.00	0.08	0.17	0.12	0.12	<0.05	<0.05	0.08	<0.05
K2O	<0.01	<0.01	<0.01	0.00	0.00	0.00	1.52	0.29	0.00	0.00	0.00	0.30	0.06
P2O5	<0.01	<0.01	0.01	0.01	0.01	0.18	0.19	0.12	0.13	0.04	0.02	0.11	0.02
TOTAL	99.22	99.32	99.23	98.54	99.08	97.62	99.54	98.85	95.46	99.30	98.47	98.21	97.80
LOI	7.39	4.99	8.84	4.99	6.55	9.11	8.32	12.81	22.42	4.15	3.86	10.11	6.22
S	0.21	0.16	0.26	6.41	1.76	0.80	0.04	0.17	0.28	0.77	3.40	0.91	9.97
Ti/Zr	-	bd	13.2	0.0	3.3	42.1	17.1	43.6	37.3	22.9	67.1	38.3	38.1
La	<2	<2	4	<2	1	7	17	7	15	8	<2	9	7
Ce	<4	<4	7	<4	2	28	34	16	27	14	<4	20	12
Nd	<2	<2	2	<2	0	4	16	7	12	3	<2	7	4
Nb	<1	<1	<1	<1	0.0	<2	9.7	2.4	1.7	2.1	<1	2.7	<2
Zr	3	2	9	2	4	23	228	63	52	71	14	75	38
Sr	9	31	7	2	12	15	52	70	22	1	2	27	4
Cr	3	2	4	26	9	25	12	242	26	44	1521	312	11
Ba	<4	<4	3	13	4	8	290	64	9	7	14	65	<4
Sc	<2	<2	2	<2	1	12	29	45	22	16	10	22	5
V	3	2	15	3	6	49	58	177	113	49	83	88	62
Sn	2.0	1.0	1.0	16.6	5.2	<1	2.1	<1	2.8	4.9	25.2	5.8	124.7
Cu	64.0	132.0	176.0	8300.0	2168.0	101.0	110.0	43.0	386.0	39.0	10620.0	1883.2	1500.0
Pb	9.0	170.0	4.0	20.0	50.8	3.0	11.0	30.0	7.0	<2	28.0	13.2	688.0
Zn	39	553	39	235	217	206	288	531	228	1255	205	452	143240
Ni	6	9	3	46	16	22	14	45	25	25	65	33	Zn intf
Y	4	8	6	2	5	17	50	23	29	8	5	22	8
Rb	<1	<1	<1	<1	0	<1	35	6	<1	<1	<1	7	2
Ag	0.2	0.7	1.1	7.1	2.3	0.3	0.3	0.3	2.5	0.5	8.8	2.1	33.8
As	91	32	10	54	47	5080	21	8	150	596	43	983	192
Bi	<	0.4	<	8.2	2.2	<	0.2	0.2	0.1	<	2.6	0.5	17.2
Mo	0.2	0.3	0.4	0.3	0.3	0.2	1.0	0.4	0.4	0.2	1.0	0.5	0.4
Cd	<	5.0	0.1	1.3	1.6	0.2	0.3	1.7	0.3	4.6	1.0	1.4	473.0
Sb	4.5	2.1	1.1	3.1	2.7	7.7	1.8	2.0	2.2	1.4	1.9	2.8	11.6
Cs	<	<	<	<	0.00	0.12	0.62	0.35	<	<	<	0.18	0.05
Tl	<	<	<	<	0.0	<	2.7	0.6	<	<	<	0.6	8.0
Th	<	<	0.12	<	0.03	0.63	5.53	1.45	1.70	2.06	0.38	1.96	1.19
U	<	<	<	<	0.00	0.18	1.09	0.34	0.26	0.46	0.09	0.40	0.30
Th/U	-	-	-	-	-	3.50	5.07	4.26	6.54	4.48	4.22	4.86	3.97
Zr/TiO2	-	-	0.05	-	-	0.01	0.04	0.01	0.02	0.03	0.01	0.02	0.02
Nb/Y	-	-	-	-	-	-	0.19	0.10	0.06	0.26	-	-	-
Chl-Co Index													
Cu Ratio	62.1	19.3	81.9	97.2	90.9	32.9	27.6	7.5	62.9	3.0	98.1	80.6	1.0
Zn Ratio	81.3	76.5	90.7	92.2	81.0	98.6	96.3	94.7	97.0	-	88.0	97.2	99.5

FeO* indicates total Fe; Analysis un-normalised, < indicated below detection; Zn intf = not determined due to zinc interference

Chl-Co index defined as 100*(0.5*FeO*+MgO)/(0.5*FeO*+MgO+2*CaO+2*MnO), Zn Ratio as 100*Zn/(Pb+Zn) and Cu Ratio as 100*Cu/(Cu+Zn)

	GGF M6 : CHLORITE ALTERATION				GGF M5 : CARBONATE NODULAR ALTERATION					GGF M4 : CHLORITE ALTERATION			
SAMPLE	**760436**	**760373**	**760433**	**Average**	**760411**	**SCDOO1**	**760410**	**769066**	**Average**	**769151**	**769061**	**769053**	**Average**
NORTH	18267.0	18105.9	18259.5		18107.3		18107.3	18290.4		18397.9	18280.2	18266.2	
EAST	4825.9	4985.9	4818.7		5014.7		5014.4	5006.3		5014.2	5020.1	5040.7	
R.L.	10047.5	10190.7	10064.6		10242.3		10242.6	10067.2		10169.5	10095.1	10137.8	
SECTION	TF #4	18095	TF #4		18095		18095	18288		18438	18288	18288	
SiO2	29.09	56.77	54.05	46.64	54.72	58.07	60.42	71.08	61.07	22.10	18.72	33.30	24.71
TiO2	0.08	0.07	0.36	0.17	0.19	0.30	0.29	0.16	0.24	0.38	0.09	0.62	0.36
Al2O3	2.38	2.13	12.44	5.65	7.25	11.81	11.31	9.35	9.93	14.63	3.26	18.23	12.04
FeO*	42.25	21.75	24.23	29.41	7.67	5.74	9.50	11.74	8.66	37.56	68.28	31.15	45.66
MnO	0.09	0.30	0.30	0.23	0.13	0.01	0.03	0.05	0.06	0.07	0.02	0.06	0.05
MgO	1.21	2.25	3.16	2.21	11.13	15.21	11.91	3.81	10.52	12.67	7.23	8.98	9.63
CaO	0.03	3.56	0.09	1.23	6.37	1.12	0.35	0.00	1.96	0.02	0.60	0.31	0.31
Na2O	<0.05	<0.05	<0.05	0.00	0.04	0.05	0.03	0.06	0.05	<0.05	<0.05	<0.05	0.00
K2O	0.01	0.01	0.00	0.01	0.00	0.00	0.00	0.22	0.06	0.00	0.00	0.00	0.00
P2O5	0.03	0.01	0.05	0.03	0.03	0.01	0.03	0.01	0.02	0.02	0.02	0.19	0.08
TOTAL	95.14	96.69	99.71	97.18	98.43	99.39	99.63	99.66	99.28	98.36	99.73	99.64	99.24
LOI	19.53	9.03	4.44	11.00	10.90	7.07	5.76	3.18	6.73	9.63	1.51	6.73	5.96
S	27.66	7.75	1.36	12.26	0.23	0.01	<0.01	<0.01	0.06	4.19	0.00	0.02	1.40
Ti/Zr	71.6	6.5	7.9	28.7	5.2	5.3	5.5	3.9	5.0	6.2	6.5	18.7	10.5
La	<2	10	35	15	20	26	30	24	25	48	12	41	34
Ce	<4	23	63	28	43	52	57	48	50	60	19	73	51
Nd	<2	9	26	12	23	25	30	22	25	26	10	36	24
Nb	<2	2.5	9.0	3.8	8.2	11.5	10.9	8.9	9.9	12.5	<2	8.5	7.0
Zr	7	64	275	115	217	339	315	243	279	365	83	199	216
Sr	3	14	3	7	50	4	3	4	15	4	4	4	4
Cr	552	2	16	190	2	2	3	2	2	4	5	10	6
Ba	6	8	11	8	3	12	4	67	21	16	<4	10	9
Sc	6	<2	12	6	12	12	9	5	9	15	7	36	19
V	47	3	34	28	4	7	7	<1.5	4	2	<2	47	16
Sn	3.7	73.3	20.9	32.6	3.0	3.0	3.0	4.0	3.3	10.8	9.0	7.4	9.0
Cu	2800.0	2077.0	3830.0	2902.3	32.0	4.0	4.0	4.0	11.0	10070.0	18.0	41.0	3376.3
Pb	231.0	14.0	59.0	101.3	8.0	2.0	4.0	4.0	4.5	8.0	<2	2.0	3.3
Zn	1062	4420	835	2106	161	27	217	208	153	151	63	612	275
Ni	87	Zn intf	12	33	2	1	2	2	2	3	1	4	3
Y	3	17	71	30	60	73	72	58	66	45	19	41	35
Rb	<1	<1	<1	0	<1	<1	<1	4	1	<1	1	<1	0
Ag	9.1	7.5	7.9	8.2	0.6	0.1	0.2	0.1	0.3	1.0	<	0.1	0.4
As	454	24	21	166	3	5	<	<	2	5	<	<	2
Bi	49.6	1.5	0.5	17.2	0.3	<	<	<	0.1	11.3	0.1	7.5	6.3
Mo	4.3	0.9	6.3	3.8	0.1	<	0.3	1.2	0.4	3.1	3.2	10.4	5.6
Cd	3.0	33.5	1.9	12.8	0.1	<	<	0.1	0.1	1.0	0.3	0.8	0.7
Sb	13.9	2.4	4.0	6.8	1.2	1.9	0.7	1.4	1.3	0.9	4.2	1.5	2.2
Cs	0.06	0.06	0.17	0.10	0.19	2.43	0.24	0.24	0.78	0.22	0.19	0.59	0.33
Tl	0.6	<	<	0.2	<	<	<	<	0.0	<	<	<	0.0
Th	0.08	1.41	6.63	2.71	4.26	6.45	6.36	5.18	5.56	8.37	1.83	4.65	4.95
U	0.08	0.32	1.66	0.69	0.87	1.46	1.33	1.12	1.20	2.02	0.42	1.31	1.25
Th/U	1.00	4.41	3.99	3.94	4.90	4.42	4.78	4.63	4.65	4.14	4.36	3.55	3.96
Zr/TiO2	0.01	0.09	0.08	0.06	0.11	0.11	0.11	0.15	0.12	0.10	0.09	0.03	0.07
Nb/Y	-	0.15	0.13	-	0.14	0.16	0.15	0.15	0.15	0.28	-	0.21	-
Chl-Co Index													
Cu Ratio	72.5	32.0	82.1	58.0	16.6	12.9	1.8	1.9	6.7	98.5	22.2	6.3	92.5
Zn Ratio	82.1	99.7	93.4	95.4	95.3	93.1	98.2	98.1	97.1	95.0	-	99.7	98.8

FeO* indicates t

Chl-Co index def

	GGF M4 : CHEMICAL/MAGNETITE			GGF M6/4 : ANDALUSITE ALTERATION				GGF M4 : SILICA ALTERATION NODULES		
SAMPLE	**760356**	**769077**	**Average**	**760465**	**760441**	**760434**	**Average**	**769174**	**769267**	**Average**
NORTH	18178.4	18264.4		18287.6	18275.4	18260.3		18632.8	18627.6	
EAST	5002.7	5043.6		4848.9	4834.3	4819.4		5066.9	5075.7	
R.L.	10167.1	10143.8		10068.6	10028.1	10062.8		10135.7	10112.8	
SECTION	18141	18288		TF #4	TF #4	TF #4		18688	18688	
SiO2	42.11	14.95	28.53	18.03	10.92	17.68	15.54	55.04	49.75	52.40
TiO2	0.07	0.10	0.09	0.51	0.13	0.75	0.46	0.25	0.33	0.29
Al2O3	2.49	3.25	2.87	18.19	4.49	11.35	11.34	10.39	12.74	11.57
FeO*	41.04	57.52	49.28	45.00	56.11	52.68	51.26	17.53	20.10	18.82
MnO	0.11	0.20	0.16	0.16	0.20	0.25	0.20	0.04	0.04	0.04
MgO	4.43	5.31	4.87	4.94	3.62	5.14	4.57	9.49	8.89	9.19
CaO	1.59	5.91	3.75	0.01	0.55	0.20	0.25	0.91	0.77	0.84
Na2O	<0.05	<0.05	0.00	<0.05	<0.05	<0.05	0.00	0.04	0.06	0.05
K2O	0.00	0.00	0.00	0.00	0.00	0.00	0.00	0.00	0.00	0.00
P2O5	0.02	0.17	0.10	0.03	0.03	0.13	0.06	0.01	0.01	0.01
TOTAL	98.55	98.78	98.67	97.35	94.84	98.05	96.75	99.31	99.16	99.24
LOI	6.66	11.37	9.02	10.39	17.69	7.17	11.75	5.61	6.46	6.04
S	0.85	0.09	0.47	12.39	24.19	7.17	14.58	0.02	0.01	0.02
Ti/Zr	6.9	9.0	8.0	6.2	6.8	45.1	19.3	5.6	6.3	5.9
La	8	21	14	54	35	40	43	25	28	26
Ce	8	29	19	97	53	68	73	46	54	50
Nd	3	15	9	48	23	33	35	21	25	23
Nb	2.0	<2	1.0	16.5	3.0	2.0	7.2	9.3	11.3	10.3
Zr	61	66	64	495	115	100	237	270	312	291
Sr	12	26	19	4	4	2	3	6	5	5
Cr	4	4	4	9	11	8	9	2	3	3
Ba	4	<4	2	4	<4	<4	1	5	8	6
Sc	6	10	8	24	7	48	26	9	11	10
V	2	6	4	13	4	213	77	<1.5	<2	0
Sn	4.4	11.6	8.0	1.0	4.2	138.0	47.7	4.0	1.8	2.9
Cu	204.0	37.0	120.5	347.0	4390.0	377.0	1704.7	217.0	6.0	111.5
Pb	<2	2.0	1.0	19.0	315.0	2662.0	998.7	5.0	<1.5	2.5
Zn	55	31	43	361	4970	18900	8077	53	81	67
Ni	<2	2	1	3	Zn intf	Zn intf	1	1	2	2
Y	19	18	19	118	32	26	59	55	53	54
Rb	<1	<1	0	<1	<1	<1	0	<1	<1	0
Ag	0.1	<	0.1	1.0	16.4	9.2	8.9	0.2	0.1	0.2
As	<	21	11	43	844	8	298	1	12	7
Bi	0.6	17.5	9.1	6.4	123.0	23.6	51.0	0.3	0.1	0.2
Mo	0.3	28.4	14.4	2.7	5.0	0.3	2.7	5.1	2.4	3.8
Cd	0.2	0.2	0.2	0.3	15.1	67.8	27.7	0.3	0.1	0.2
Sb	3.9	5.5	4.7	3.8	12.0	4.8	6.9	1.0	1.2	1.1
Cs	0.06	0.10	0.08	0.42	0.07	0.08	0.19	0.15	0.25	0.20
Tl	<	<	0.0	<	<	1.6	0.5	<	<	0.0
Th	1.25	1.42	1.34	11.30	2.71	2.55	5.52	5.81	6.83	6.32
U	0.30	0.46	0.38	3.10	0.91	0.50	1.50	1.54	1.55	1.55
Th/U	4.17	3.09	3.51	3.65	2.98	5.10	3.67	3.77	4.41	4.09
Zr/TiO2	0.09	0.07	0.08	0.10	0.09	0.01	0.07	0.11	0.09	0.10
Nb/Y	0.11	-	-	0.14	0.09	0.08	0.10	0.17	0.21	0.19
Chl-Co Index										
Cu Ratio	78.8	54.4	73.7	49.0	46.9	2.0	17.4	80.4	6.9	62.5
Zn Ratio	-	93.9	97.7	95.0	94.0	87.7	89.0	91.4	-	96.4

FeO* indicates t

Chl-Co index def

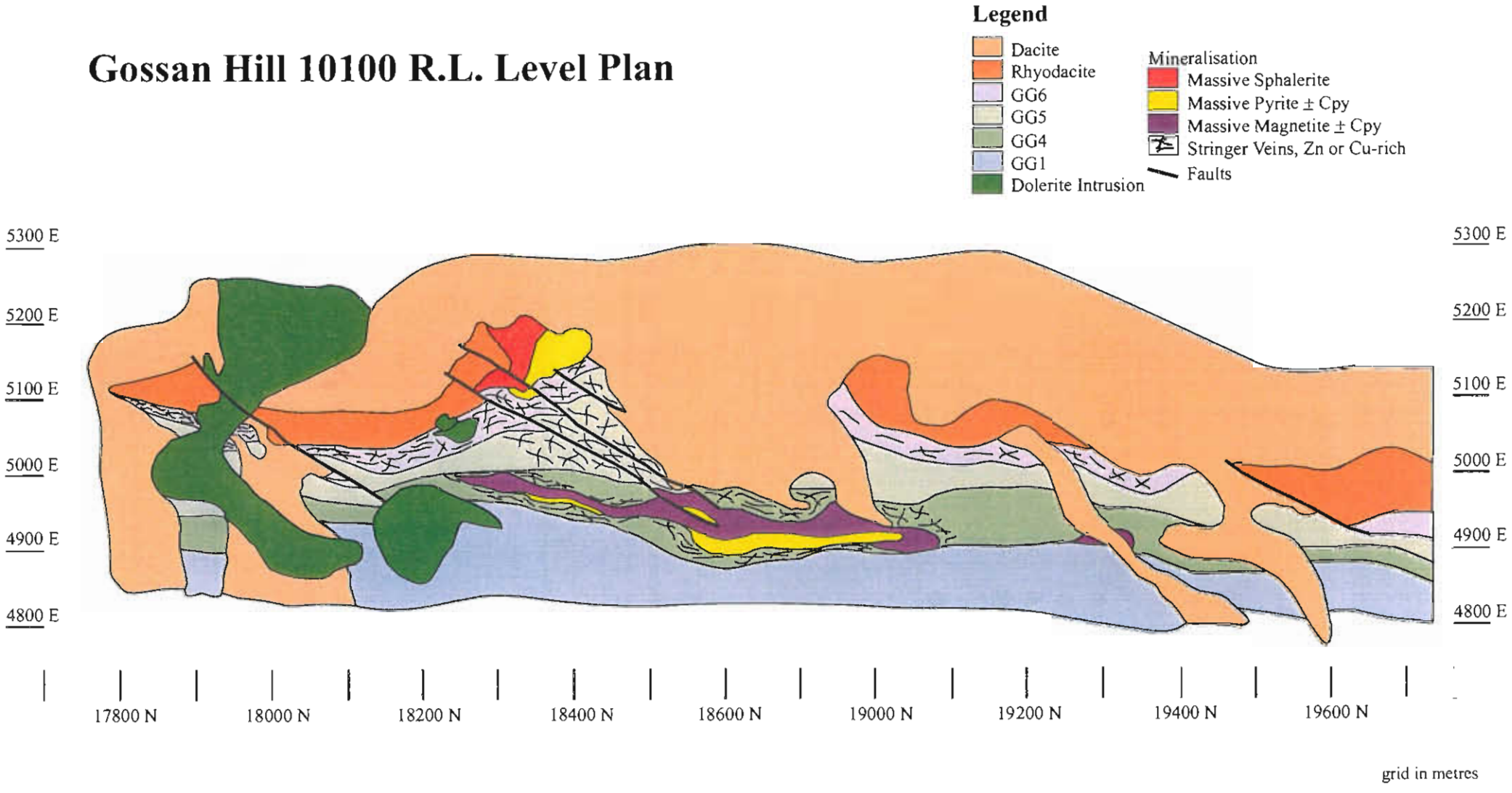

Figure 5: Composite level plan for 10100 R.L illustrating the distribution of stratigraphic Members and context of mineralisation. Interpretation is compiled from transform east-west and plan interpretation work completed from the diamond drilling database. Drill data is from a 25 m window above and below the R.L. The distribution of geochemical samples from this study are shown on the overlay.

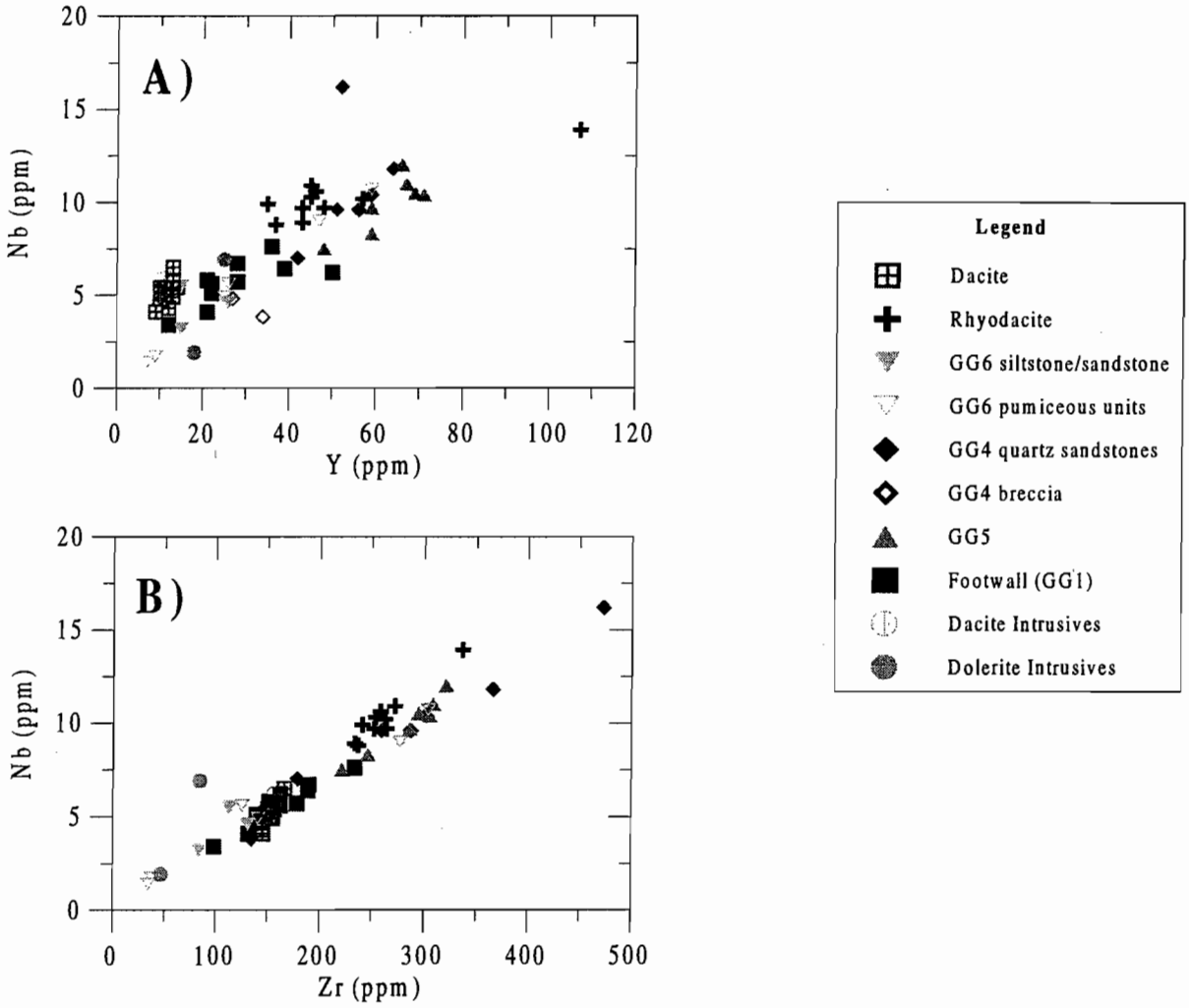

Figure 6. A) Y vs. Nb and B) Zr vs. Nb. Graphs show a positive linear which indicates preservation of primary Y/Nb and Zr/Nb ratios.

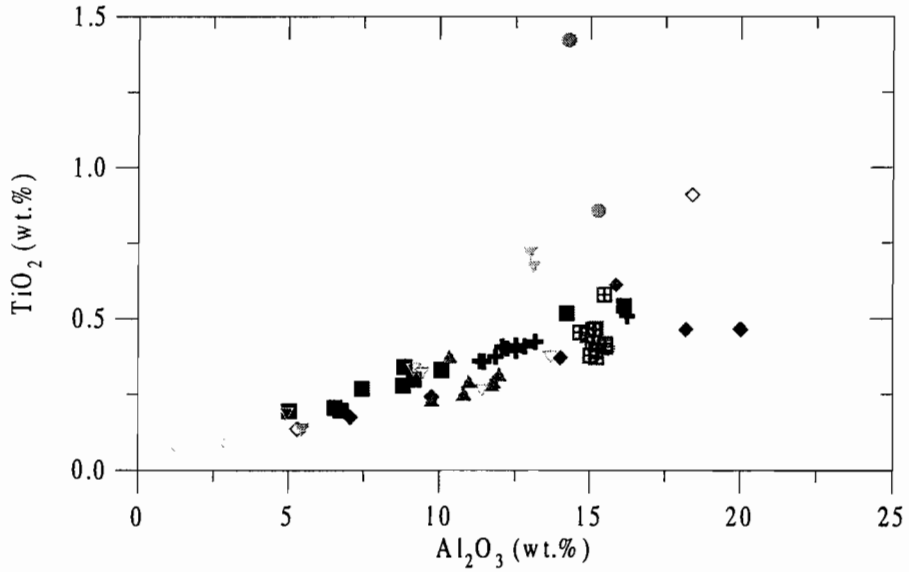

Figure 7: Al_2O_3 vs. TiO_2, showing a broad positive linear trend indicating the preservation of primary ratios. Variation from this trend indicates limited mobility of Al and Ti, particularly in GG6 siltstone/sandstone and GG4 breccia units. Refer to legend in Figure 6.

Gossan Hill (Table 6), normalised to volatile free contents, is plotted in Figure 8. Footwall, host and hangingwall show dacite to rhyodacite compositions. Tight clustering of data points is observed in the hangingwall dacites, rhyodacites, footwall GG1 and host GG5 and GG4 units. GG4 breccias and GG6 sandstones and breccias show a spread in data. Whitford and Ashley (1992) interpreted a correlation of increasing Zr with decreasing TiO_2 to indicate a fractional crystallisation trend. The distribution of TiO_2 and Zr values from Gossan Hill (Figure 9) have very different trends from those observed by Whitford and Ashley (1992) at Scuddles. At Gossan Hill hangingwall units are geochemically distinct and GG1 footwall units and GG5 are also well clustered.

Immobile element summary

Hangingwall rhyodacite and dacite units are geochemically distinct. The hangingwall dacite has a composition that is transitional to an andesite composition. Dacite in the hangingwall and dacite from syn-volcanic intrusions cannot be distinguished on the basis of geochemistry. The interpretation that syn-volcanic dacite intrusions represent feeder zones to hangingwall dacites is supported by compositional similarities. Primary composition is well constrained for the GG1, GG4 and GG5, with Nb/Y values similar for all three Members. The tight cluster in data points for GG5, GG1 and GG4 supports a relatively homogeneous provenance for these units. A broad trend from lower Zr/ TiO_2 ratios in the footwall to higher Zr/ TiO_2 ratio corresponds to the transition from dacitic/andesitic composition in footwall units to rhyodacite-rhyolitic units in host horizons. However, compositional variation is reflected in GG6 and GG4 breccias due to the spread in immobile elements, supporting variation in source material supporting a polymictic provenance. Hangingwall rhyodacites and footwall units are andesitic to dacitic in composition, implying that the hangingwall rhyodacites and footwall units are geochemically similar.

Two dolerites are geochemically distinct from the host sequences and each other. A coarse grained dolerite has an andesite/basalt composition due to lower Nb/Y ratio compared to the fine grained dolerite which has a sub-alkaline basalt composition.

Alteration geochemical studies

Alteration geochemistry identifies elements enriched or depleted by reaction of hydrothermal fluids with the rocks. At Gossan Hill, the effects of alteration are obscured by more than one hydrothermal event and by the long duration of hydrothermal activity. In addition regional metamorphic effects overprint the hydrothermal alteration. The bulk rock geochemistry therefore represents the superposition of these chemical changes on the original composition of the rock. Mineral geochemical constraints are an important aid towards understanding these changes associated with alteration and mineralisation and are documented in Table 7.

Major element variations

Major elements considered mobile during hydrothermal alteration and metamorphism are SiO_2, FeO, MgO, MnO, CaO, Na_2O, K_2O and S. The complexity of the alteration system at Gossan Hill is reflected by differential alteration of stratigraphic components at bedding scale. Heterogeneous alteration patterns mean broad alteration zones are difficult to define and characterise mineralogically and consequently, geochemically.

Alteration at Gossan Hill is typified by the abundance of quartz and chlorite, with variation in alteration styles reflecting the relative abundances of these two mineral phases. Other alteration minerals including; carbonate, sericite and apatite, may form locally abundant mineral phases within zones or beds, however the occurrence of these minerals is sporadic rather than defining broad zones. The distribution of major alteration minerals, quartz and chlorite, is reflected by the wide range and a broad linear negative correlation between SiO_2 and FeO* shown in Figure 10. The linear trend is interpreted (Figure 10b) to delineate the footwall, host volcaniclastic sequence and hangingwall alteration. Hangingwall rhyodacites and dacites directly below the main trend indicating a different alteration style. Hangingwall

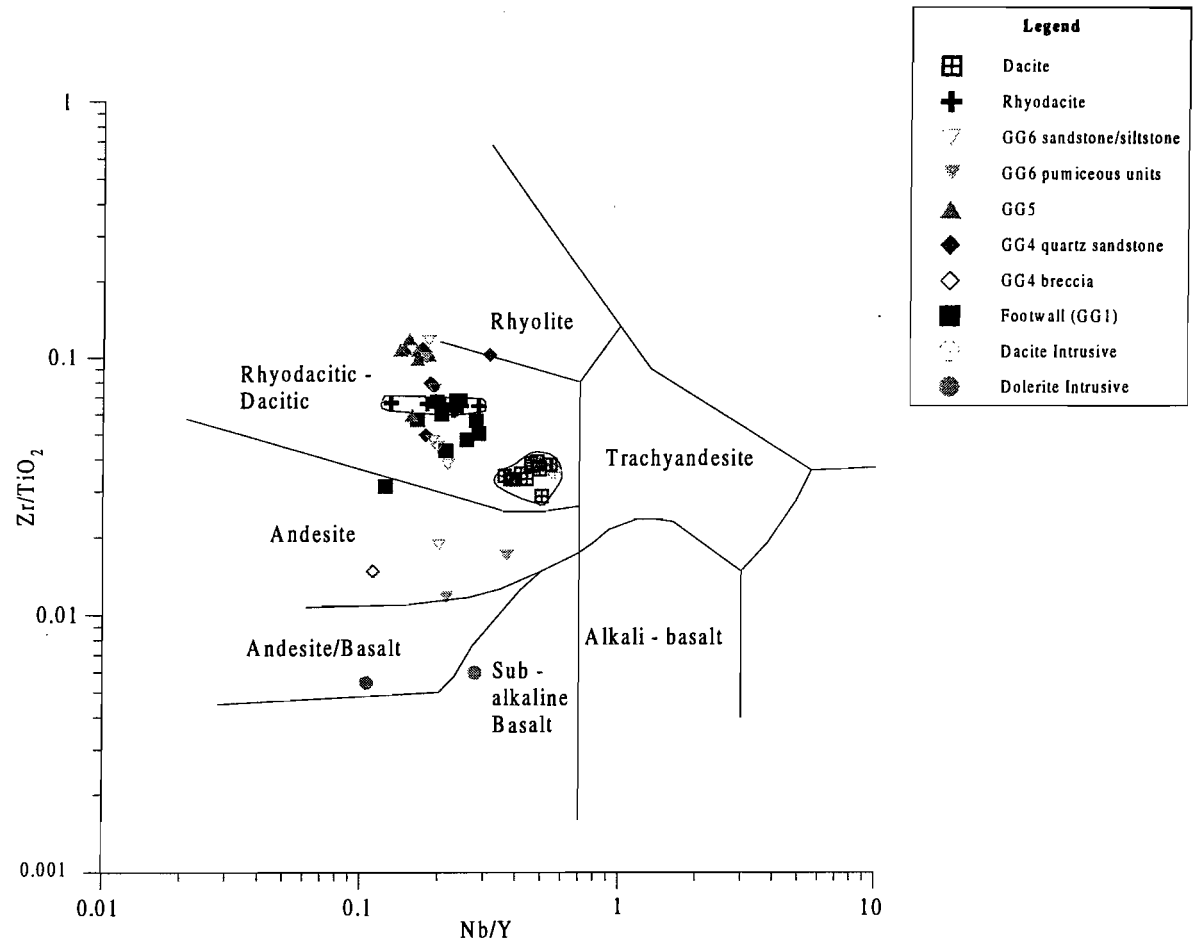

Figure 8. Nb/Y vs. Zr/TiO_2, after Winchester and Floyd (1977), showing the composition of lithofacies from the Golden Grove Formation and Scuddles Formation at Gossan Hill. Hangingwall rhyodacites and dacite units show tightly clustered data points. Variation in composition is observed for GG6 units.

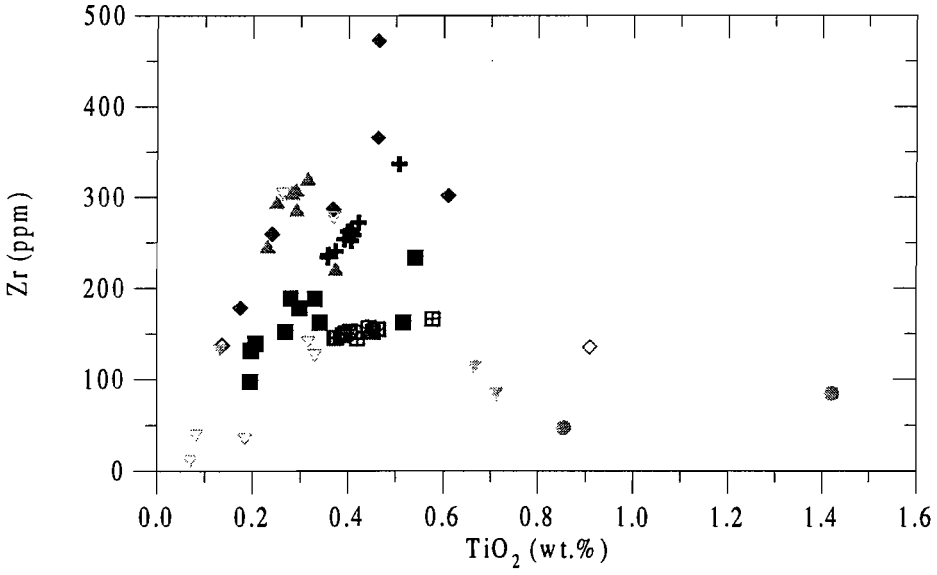

Figure 9. TiO_2 vs. Zr showing a broad linear distribution of data points. Variation in GG6 units and GG4 units is attributed to local mobility in TiO_2 as evidenced by the presence of ilmenite and rutile in these units. Legend as for Figure 8.

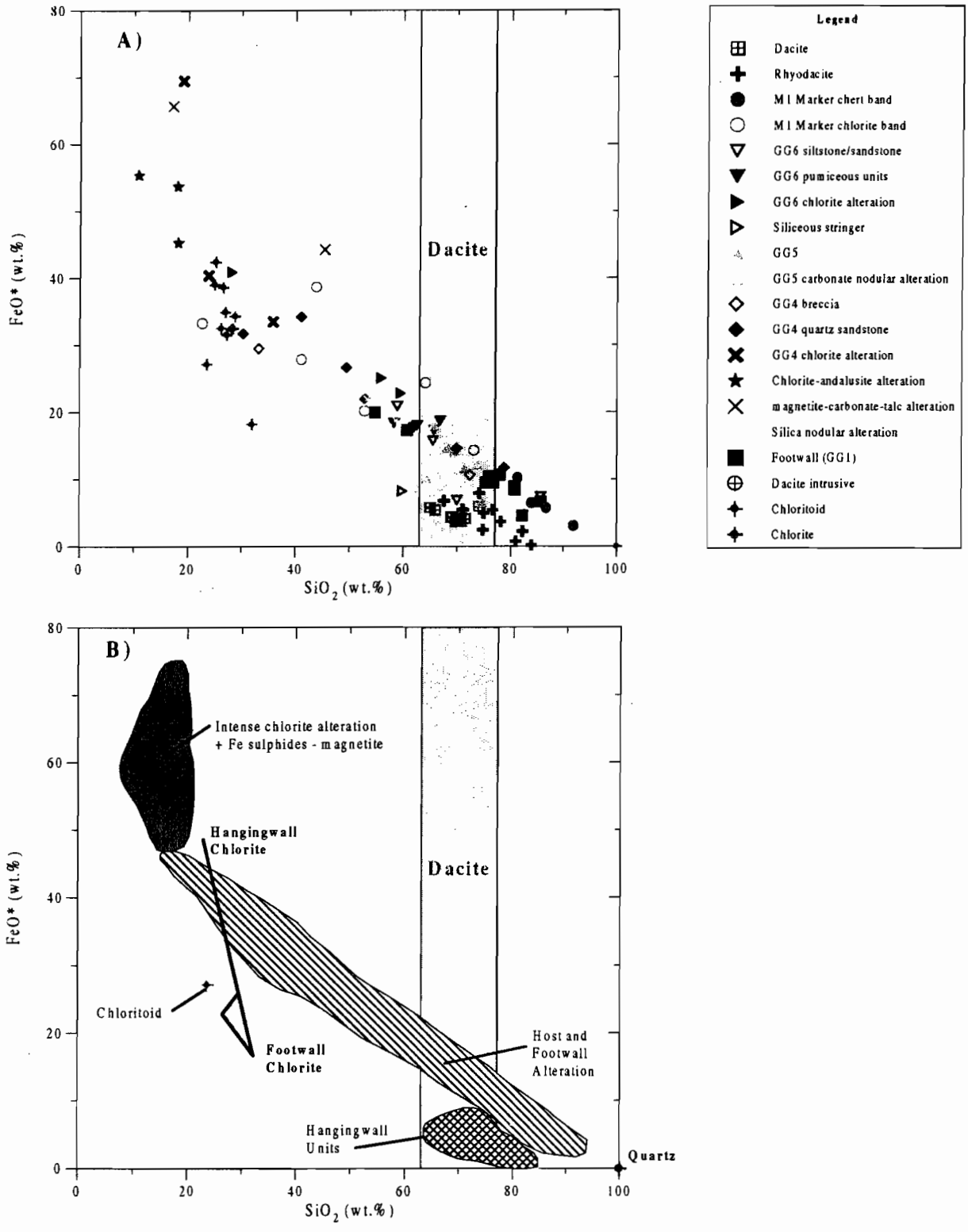

Figure 10: A) SiO_2 vs. FeO, showing the distribution of SiO_2 and FeO* of data normalised to volatile free contents from altered and litho-stratigraphic samples at Gossan Hill. FeO* indicates total iron contents. B) Interpretation of SiO_2 vs. FeO*. Footwall (GG1) and host units (GG6, GG5 and GG4) define a negative trend reflecting relative proportions of FeO* in chlorite and SiO_2 in quartz (and chlorite). The compositions of chlorite and chloritoid from Gossan Hill are plotted and show variation in FeO contents from hangingwall units to footwall units.*

units do no have chlorite as a major alteration which is reflected by relatively constant levels of FeO*. The most intensely silicified units are GG1 footwall units, host horizon GG6 and the M1 Marker and the most intensely chloritised units are GG4 units. A group of altered samples from GG4 plot above the main trend due to elevated FeO* contents associated with sulphide or magnetite alteration. The composition of chlorite is also plotted in Figure 10 and defines a sub-vertical line, reflecting variation in the abundance of FeO* and MgO within the chlorite minerals. The chlorite trend defines progressive enrichment in FeO* from host to footwall, where chlorite compositions are Mg enriched. The chlorite compositional trend differs from the broad SiO_2 vs. FeO* trend defined for host and footwall samples with the latter trend controlled by the relative abundance of chlorite to quartz in the altered host rock and contributed to by other elemental components in the rock.

MgO levels range between 0.05 and 15.86 wt.% (Figure 11a) and the broad negative correlation between SiO_2 and MgO is consistent with the negative correlation previously identified between SiO_2 and FeO under the assumption that the majority of MgO is contained in chlorite. Hangingwall rhyodacites, GG1 footwall and GG6 units have elevated SiO_2 corresponding to low MgO levels and GG4 units show elevated MgO levels associated with intensely chlorite altered GG4 units. The composition of chlorites (Figure 11a) defines a subvertical trend with variations in MgO contents of chlorite ranging from 6.8 to 25.9 wt.% MgO. The range in the MgO content of chlorite approximates the range in whole rock MgO contents. The negative correlation of MgO vs. SiO_2 reflects changes in the composition of chlorite from MgO-rich in GG4 units to decreasing MgO content in chlorite towards the hangingwall contact. Scatter in whole rock MgO values is also contributed to be the presence of carbonate minerals that show a range in MgO compositions between 9.2 and 17.4 wt.% MgO. Average carbonate contents are also plotted on Figure 11a for comparison.

MnO has relatively low concentrations between the detection limit (<0.01) and 1.02 wt.% throughout the suite of Gossan Hill sample and does not correlate with SiO_2 levels (Figure 11b). Elevated MnO is only present in the M1 Marker lithic units (up to 1.02 wt.% MnO). Mn is present in carbonate and chlorite alteration minerals which contribute to the scatter in data points observed from the whole rock data. The compositions of chlorite and carbonate are plotted on Figure 11b and show MnO content of chlorite between 0.02 to 0.29 wt.% and a MnO variation in carbonate of 0.7 to 12.7 wt.%.

A positive broad linear correlation between FeO* vs. MgO (Figure 11c, d) supports the composition of chlorite to be a major mineralogical variable controlling distribution of elements. Sample with elevated FeO* contents do not lie on this positive trend and reflect Fe enrichment due to sulphide and magnetite phases. Samples which plot above the linear trend are identified as having elevated MgO levels and lower FeO levels due to the presence of Mg-bearing carbonates. Hangingwall units of rhyodacite, dacite and dacite intrusives have low MgO and FeO* levels. The compositional variation in chlorite and carbonate are also plotted (Figure 11c and d). Chlorite compositions show a systematic linear decrease in the abundance of MgO in chlorite with increasing FeO, representing the change in the composition of chlorite from footwall to hangingwall. Samples adjacent to this line on Figure 11d are intensely chlorite altered samples. Carbonate compositions are transitional from Mg-rich in the hangingwall to relative Fe-enrichment in carbonates from lower stratigraphic levels.

CaO levels are generally low for samples from host strata, with levels from below the detection limit (<0.01) to 6.37 wt.% (Figure 11e). Elevated CaO occur in GG4 units associated with magnetite and disseminated carbonate alteration, the M1 Marker horizon in cherty and lithic components and hangingwall dacite and rhyodacite units. The variation observed in CaO contents is a reflection of the distribution of carbonate alteration throughout the host and hangingwall. Carbonate alteration is not present in footwall GG1 units and may be patchy or disseminated in host rocks associated with sulphide mineralisation and magnetite. The M1 Marker horizon shows abundant carbonate alteration

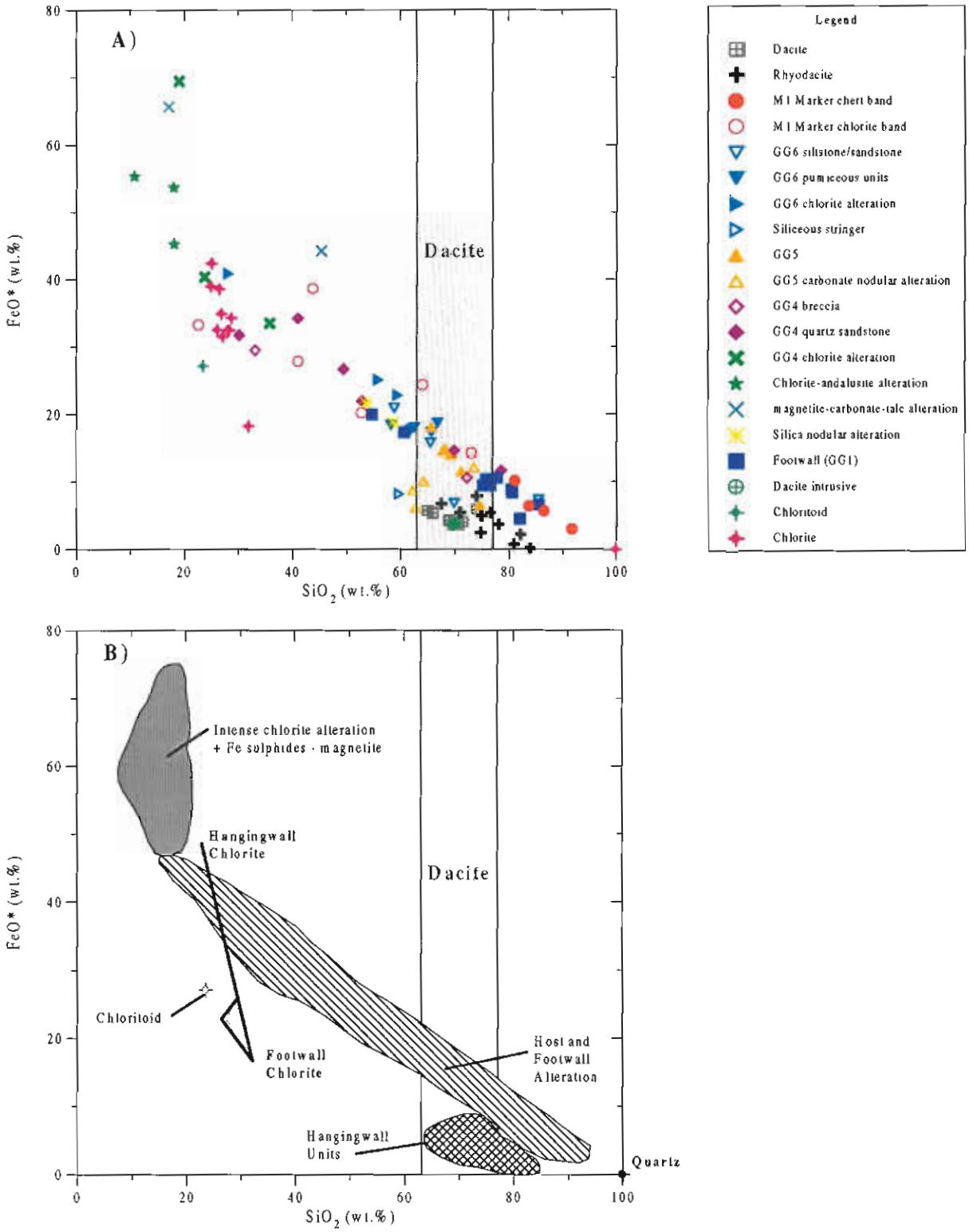

Figure10: A) SiO_2 vs. FeO, showing the distribution of SiO_2 and FeO* of data normalised to volatile free contents from altered and litho-stratigraphic samples at Gossan Hill. FeO* indicates total iron contents. B) Interpretation of SiO_2 vs. FeO*. Footwall (GG1) and host units (GG6, GG5 and GG4) define a negative trend reflecting relative proportions of FeO* in chlorite and $SiO_2$2 in quartz (and chlorite). The compositions of chlorite and chloritoid from Gossan Hill are plotted and show variation in FeO contents from hangingwall units to footwall units.*

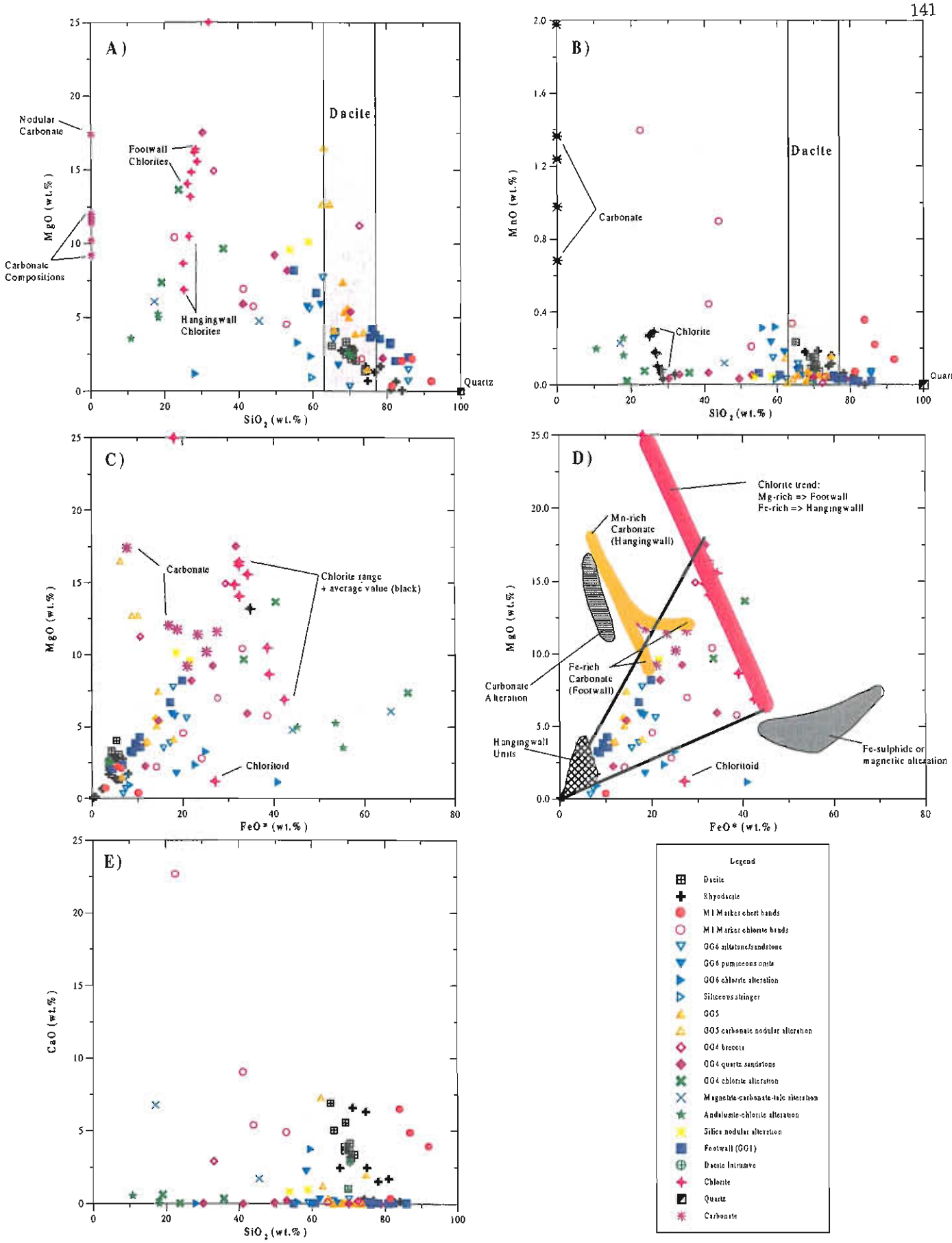

Figure 11. A) SiO_2 vs. MgO, showing a negative correlation. Scatter in data points reflect variation in MgO. Compositions of chlorite and carbonate are plotted B) SiO_2 vs. MnO. No correlation indicated. The variation in MnO levels is comparable to the variation of MnO in chlorite (also plotted). C) FeO vs. MgO. Positive linear correlation. D) FeO* vs. MgO. Interpretation of C) indicating the variation in FeO* and MgO can be explained in terms of the compositional variation of chlorite and carbonate. Chlorite becomes increasing Mg - rich toward the hangingwall. E) CaO vs. SiO_2 showing strongly depleted CaO levels throughout the footwall and host. Elevated CaO reflects patchy carbonate alteration assoicated with sulphide - magnetite and strong carbonate alteration in the hangingwall.*

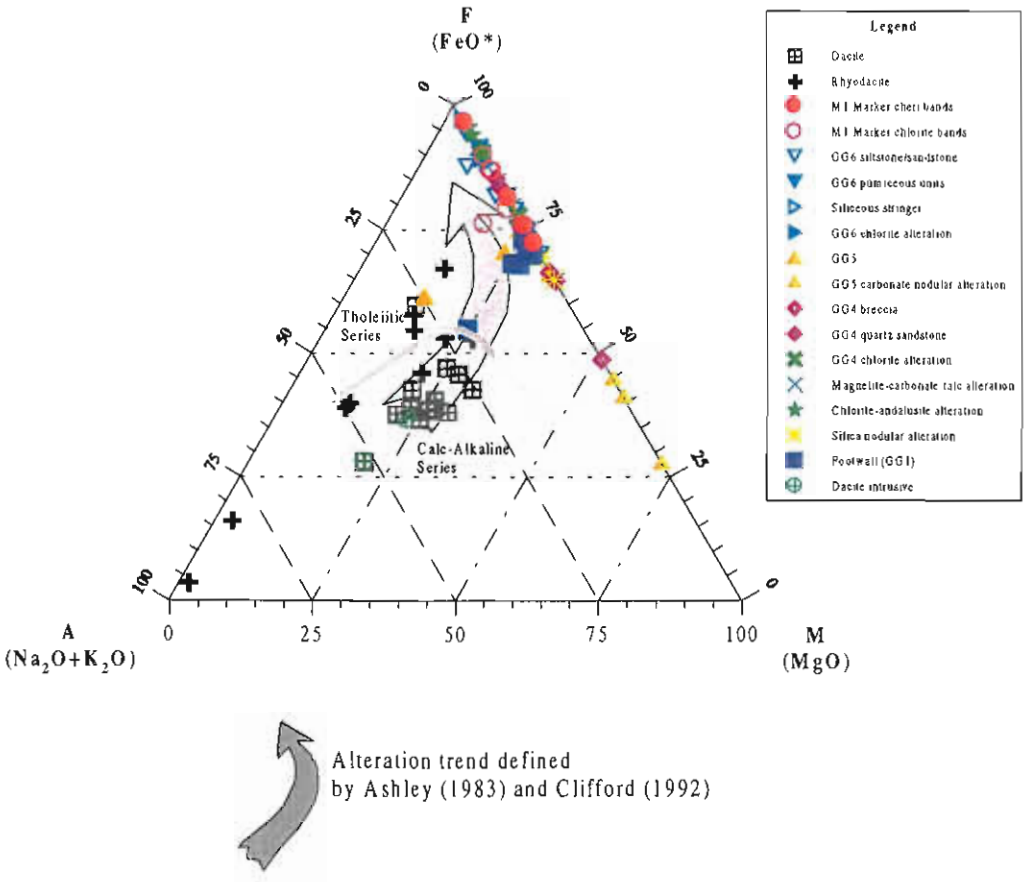

Figure 12. AFM diagram used by Ashley (1983) and Clifford (1992) to infer alteration trends at the Scuddles VHMS deposit. Data from Gossan Hill is plotted and shows widespread depletion in Na2O and K2O with relative intense FeO enrichment. The alteration trend defined by Ashley (1983) is indicated but does not apply to lithofacies and alteration at Gossan Hill. The trend indicates gradual enrichment in FeO* in host units however samples from Gossan Hill lie at the endmembers of this trend. The calc-alkaline and tholeiitic series trend is defined from Irvine and Baragar (1971).*

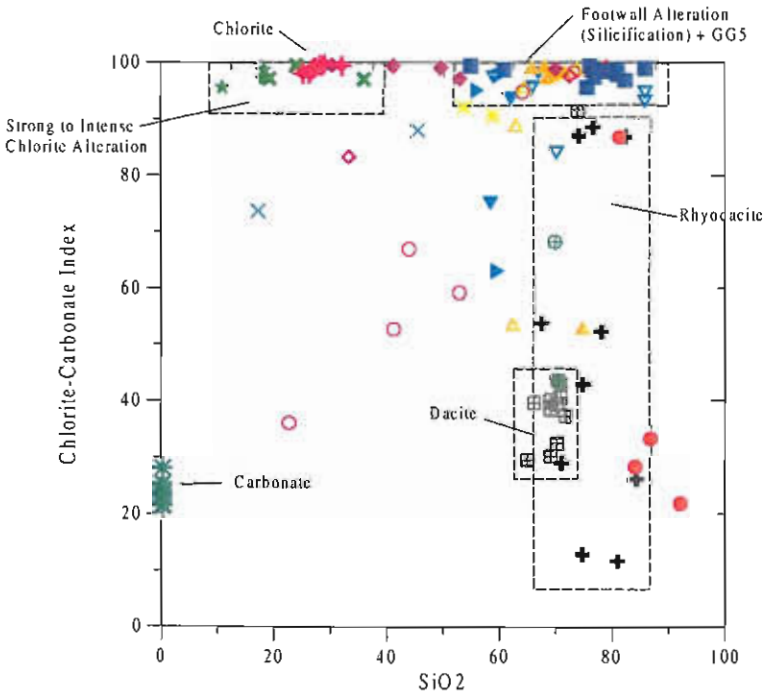

Figure 13. Distribution of Chlorite-Carbonate Index vs SiO_2. The chlorite carbonate index is defined as: 100(0.5*FeO+MgO)/((0.5*FeO)+MgO+2*CaO+2*MnO) and distinctly define footwall, GG5, chlorite and carbonate alteration patterns. The hangingwall dacites form a well constrined field, however the rhyodacites are clearly more altered and show more variation in the chlorite - carbonate index. Legend as for Figure 12.*

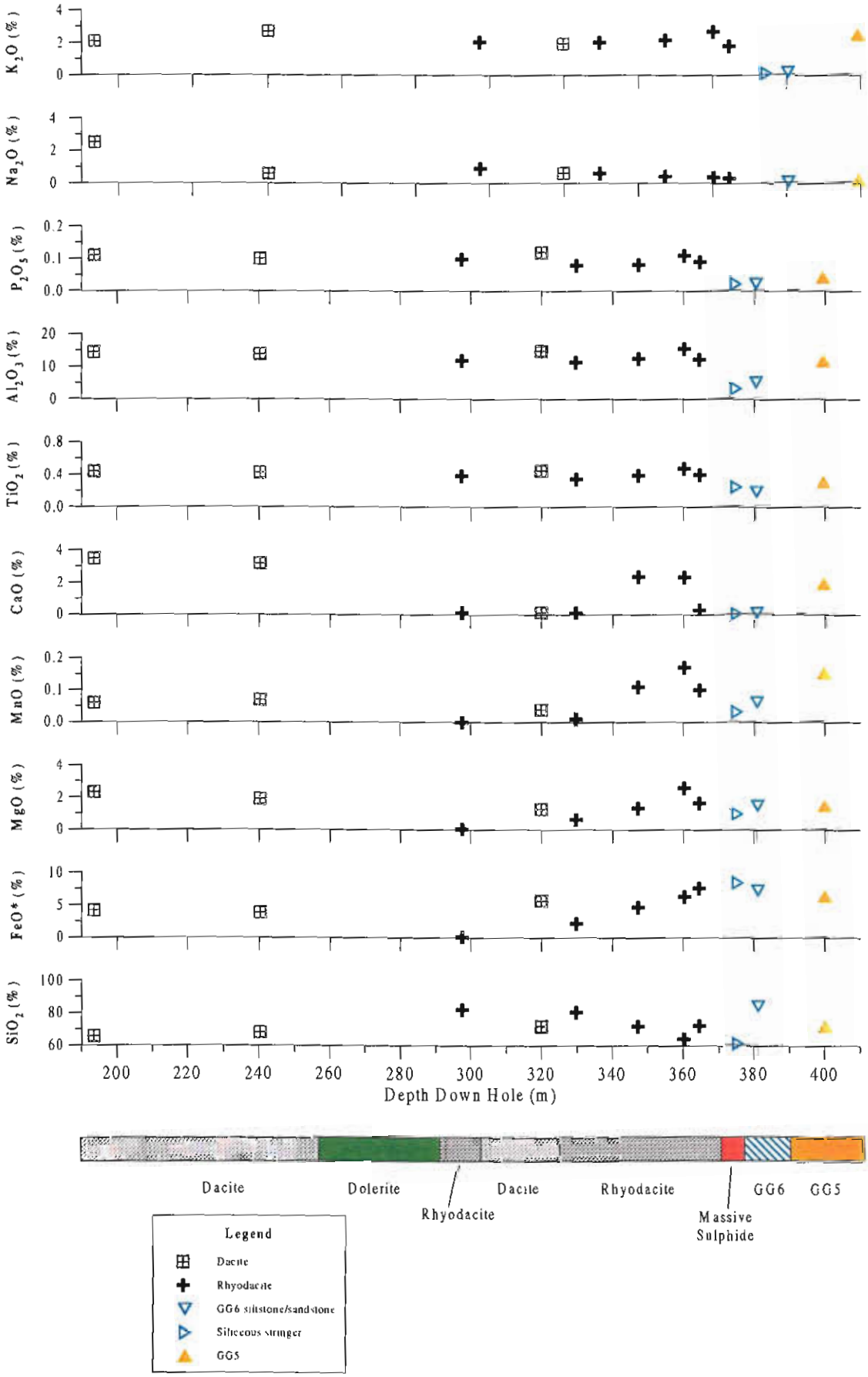

Figure 14. Down hole variation of major elements through drill intercept GG132, section 17868 N at the south end of Gossan Hill.

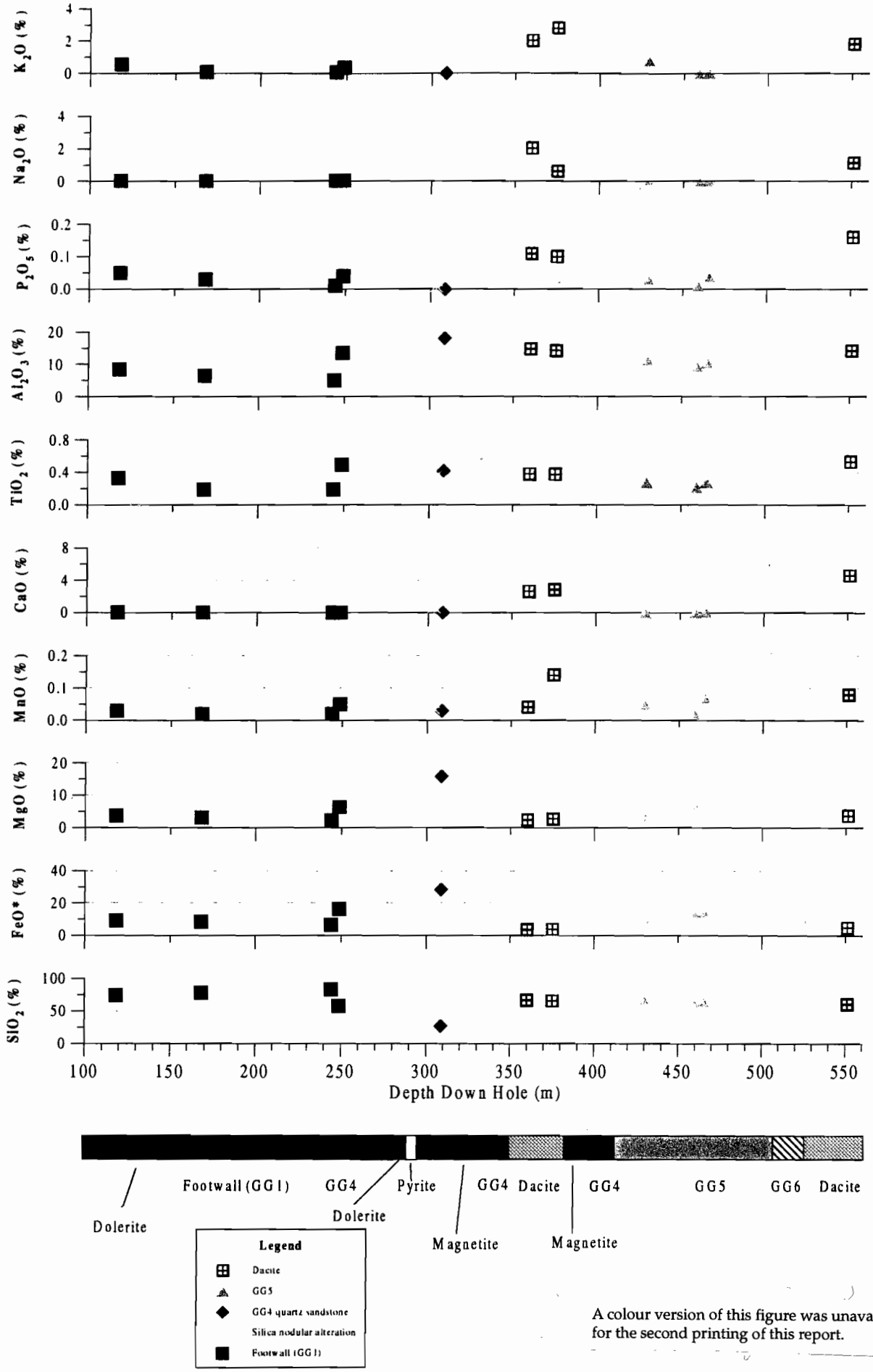

Figure 15. Down hole variation of major elements in GG070, section 18688 N at the north end of Gossan Hill through copper - bearing pyrite - magnetite mineralisation.

Mineral	Origin	Composition	Abundance	Occurrence
Quartz	primary and alteration	SiO_2	Ubiquitous	Ubiquitous through host package : strong to intense Variable alteration of hangingwall lavas Strong to intense alteration of footwall
Chlorite	alteration veining metamorphic	$(Mg,Fe,Mn,Al)_{12}$ $(Si,Al)_8O_{20}OH_{16}$	ubiquitous	Intensely developed throughout GG4 Strong to moderate in GG5 and GG1 patchy with quartz in GG6 minor occurrence in hangingwall units
Carbonate	alteration. veining metamorphic	$Ca(Mg,Fe,Mn)$ $(CO_3)_2$	abundant/ patchy	patchy occurrence: disseminated to veining; associated with magnetite and Fe-sulphides
Chloritoid	alteration	$(Fe,Mg,Mn)_2(Al,$ $Fe)(OH)_4Al_3O_2$ $(SiO_4)_2$	minor patchy	associated with andalusite alteration, sporadic occurrence in GG4 and GG6 units
Andalusite	alteration, metamorphic	Al_2SiO_5	minor patchy	sporadic occurrence in chlorite altered ± Fe-sulphides ± magnetite alteration GG4
Apatite	alteration	$Ca_5(PO_4)_3$ (OH,F,Cl)	minor	sporadic occurrence GG4 associated with quartz - chlorite alteration
Sericite	alteration, metamorphic	$K_2Al_4(Si_6Al_2O_{20})$ $(OH,F)_4$	minor to major	minor constituent of footwall; metamorphic major constituent of hangingwall units
Sulphides	alteration veining	FeS, FeS_2	major	disseminated to massive, GG4 and GG6 also stringer veins
Magnetite	alteration veining	Fe_3O_4	major	associated with carbonate in GG4 units, vein stringer occurrence
Rutile/Ilmenite	alteration	TiO_2,$FeTiO_3$	minor	disseminated alteration of footwall (GG1), host GG4,GG5, GG6 units; transition from rutile to ilmenite from hangingwall to footwall
Talc	alteration, metamorphic	$Mg_{16}(Si_8O_{20})OH_4$	minor to major	Patchy strong to weak alteration associated with magnetite - carbonate - chlorite alteration of GG4

Table 8: Alteration minerals adjacent to and within mineralised and altered zones at Gossan Hill. Minerals of both major and minor occurrences are listed, together with compositional variation and mineral association within specific units of the Golden Grove Formation stratigraphy. Alteration minerals have three origins; either hydrothermal pervasive alteration, hydrothermal vein hosted or metamorphic.

14). Figure 15 shows footwall GG1 to have ubiquitous elevated SiO_2. Comparatively, the level of oxides in GG4 quartz sandstones and silica nodular altered zones are similar to levels identified in GG1 proximal to the GG4 contact, with the exception of enrichment in FeO* and Al_2O_3 and depletion in SiO_2. GG5 units shows relatively constant levels of SiO_2, MgO, CaO, TiO_2, Al_2O_3 with an increase in MnO, FeO and P_2O_5 with increasing distance from the GG4 contact and copper-bearing mineralisation.

Summary of major element geochemistry

Major element geochemistry at Gossan Hill strongly reflects the distribution of alteration minerals. Universal blanket depletion of Na_2O and K_2O in footwall and host rocks reflects intense alteration of the primary lithofacies and the complete alteration of glass and feldspar to quartz-chlorite dominated assemblages. The depletion in K_2O also reflects limited sericite alteration in the footwall and host rocks to mineralisation. A quartz-chlorite alteration is reflected by the correlation of the SiO_2, FeO, MgO and to a lesser extent MnO. Strong correlation between FeO and MgO is largely the result of chlorite compositional variation from MgO-rich chlorite in the footwall and lower host units (GG4) to FeO-rich chlorites in the hangingwall host rocks (GG6). Carbonate minerals also contribute to the variation in the major oxide minerals FeO*, MgO and MnO. Strong FeO* enrichment is identified in alteration zones adjacent to mineralisation due to the Fe-sulphides, magnetite and intense chlorite alteration. Hangingwall rhyodacite, dacite and dacite intrusive units do not show the enriched levels of FeO*, reflecting the absence chlorite as a dominant alteration phase in the hangingwall. Hangingwall alteration is characterised by elevated CaO and K_2O due to carbonate and sericite alteration. SiO_2 levels are elevated in GG6, GG5, M1 Marker and footwall zones (GG1) indicating intense silicification within the host and footwall strata.

Trace element variations

Unlike many VHMS deposits, Ba is depleted throughout the host and footwall at Gossan Hill. Elevation of Ba in the hangingwall lavas corresponds with elevated Sr and Rb levels (Figures 16a, b), and elevated CaO levels (Figure 16). The levels of Ba, Sr and Rb in the hangingwall likely reflect feldspar phases. Rb is depleted throughout the host units and corresponds with low or below detection levels of Sr and Ba.

Metal associations between Cu, Zn, Pb, Ni and Sn are shown in Figures 16d–e. At Gossan Hill the average zinc grade is 12 %, however in siliceous alteration enclosing high grade mineralisation the level of Zn reaches 850 ppm. Similarly, copper zones shows an average grade of 2 % in ore zones and up to 612 ppm in altered host. Cu and Zn (Figure 16d) are elevated throughout GG6 and associated siliceous alteration, the M1 Marker and andalusite-chlorite alteration. Hangingwall lavas, chlorite alteration associated with massive copper, GG5 all have levels below 100 ppm Cu and variable Zn up to 1000 ppm in GG4 units. Pb values (Figure 16e and 16f) have a similar distribution to that observed for Zn, with anomalous Pb values recorded in siliceous alteration associated with zinc-rich mineralisation, corresponding with elevations in Cu and Zn.

Ratios such as the Zinc Ratio (Huston and Large, 1987) or the Copper Ratio, are used to display relative associations of metal values and have been implemented as a guide to alteration at many VHMS deposits. At Gossan Hill the Zinc Ratio, defined as (100*Zn/ (Zn+Pb)), have elevated values above 75 for all host rocks with the exception of two data points from the hangingwall lavas, and indicates elevated Zn relative to Pb throughout the altered and host units (Figure 16g). The copper ratio, defined as (100*Cu/(Cu+Zn)), indicates the association between Cu and Zn at Gossan Hill to be more variable than that for Pb and Zn. Elevated Copper Ratios are associated with the M1 Marker, chlorite alteration, GG4 host and magnetite alteration. Elevated Zn levels also correspond to elevated Sn levels in GG6 siliceous alteration (Figure 16h). Figure 16i shows the distribution of Cu and Ni, suggesting that elevated

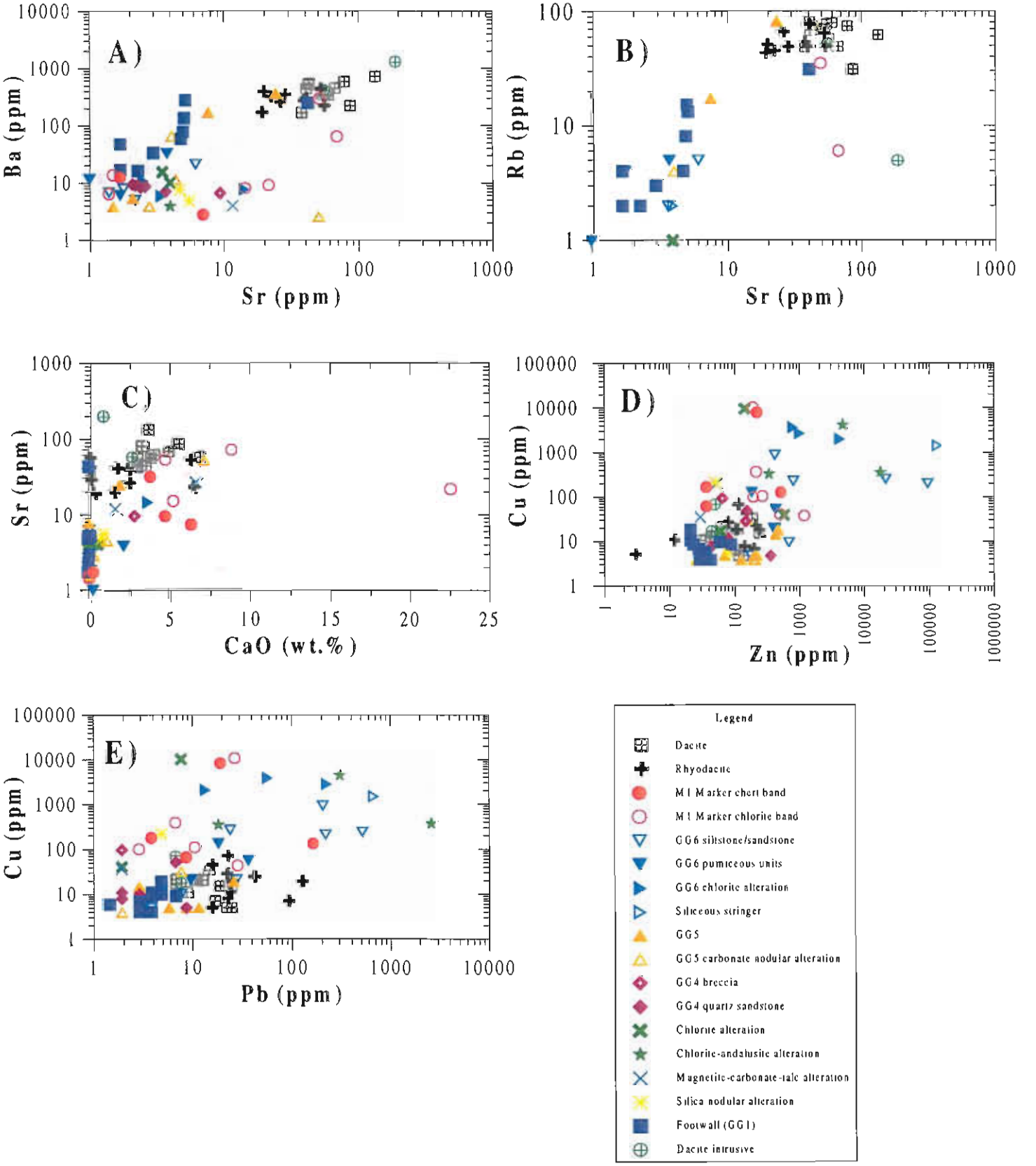

Figure 16. Distribution of trace element data analysed from host stratigraphic and alteration sample peripheral to mineralisation at Gossan Hill. A) Sr vs. Ba B) Sr vs. Rb C) CaO vs. Sr D) Zn vs. Cu E) Pb vs. Cu F) Pb vs. Zn G) Cr Ratio vs. Zn Ratio H) Zn vs. Sn I Cu vs. Ni.

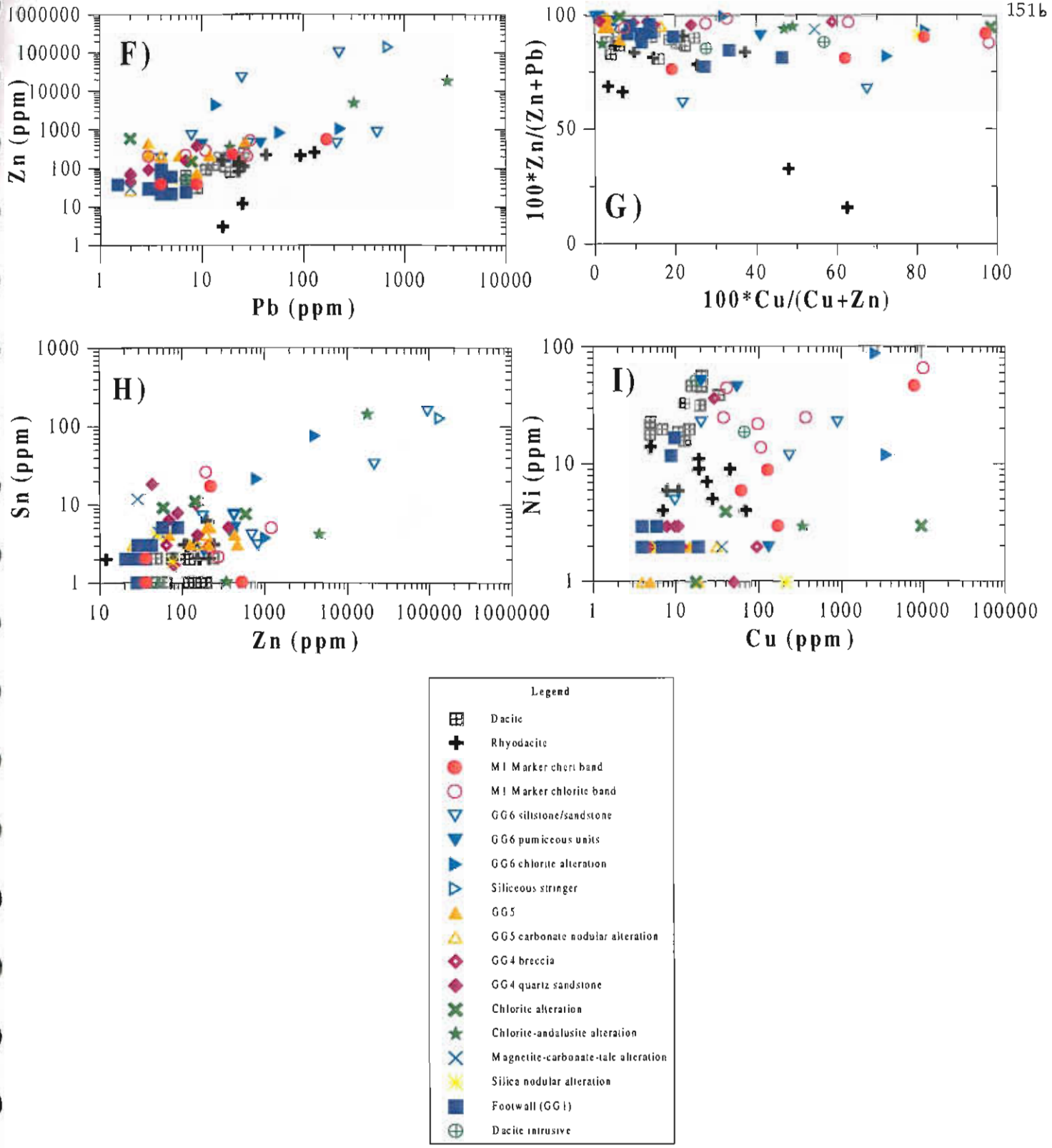

Figure 16 cont. Distribution of trace element data analysed from host stratigraphic and alteration sample peripheral to mineralisation at Gossan Hill. A) Sr vs. Ba B) Sr vs. Rb C) CaO vs. Sr D) Zn vs. Cu E) Pb vs. Cu F) Pb vs. Zn G) Cr Ratio vs. Zn Ratio H) Zn vs. Sn I Cu vs. Ni.

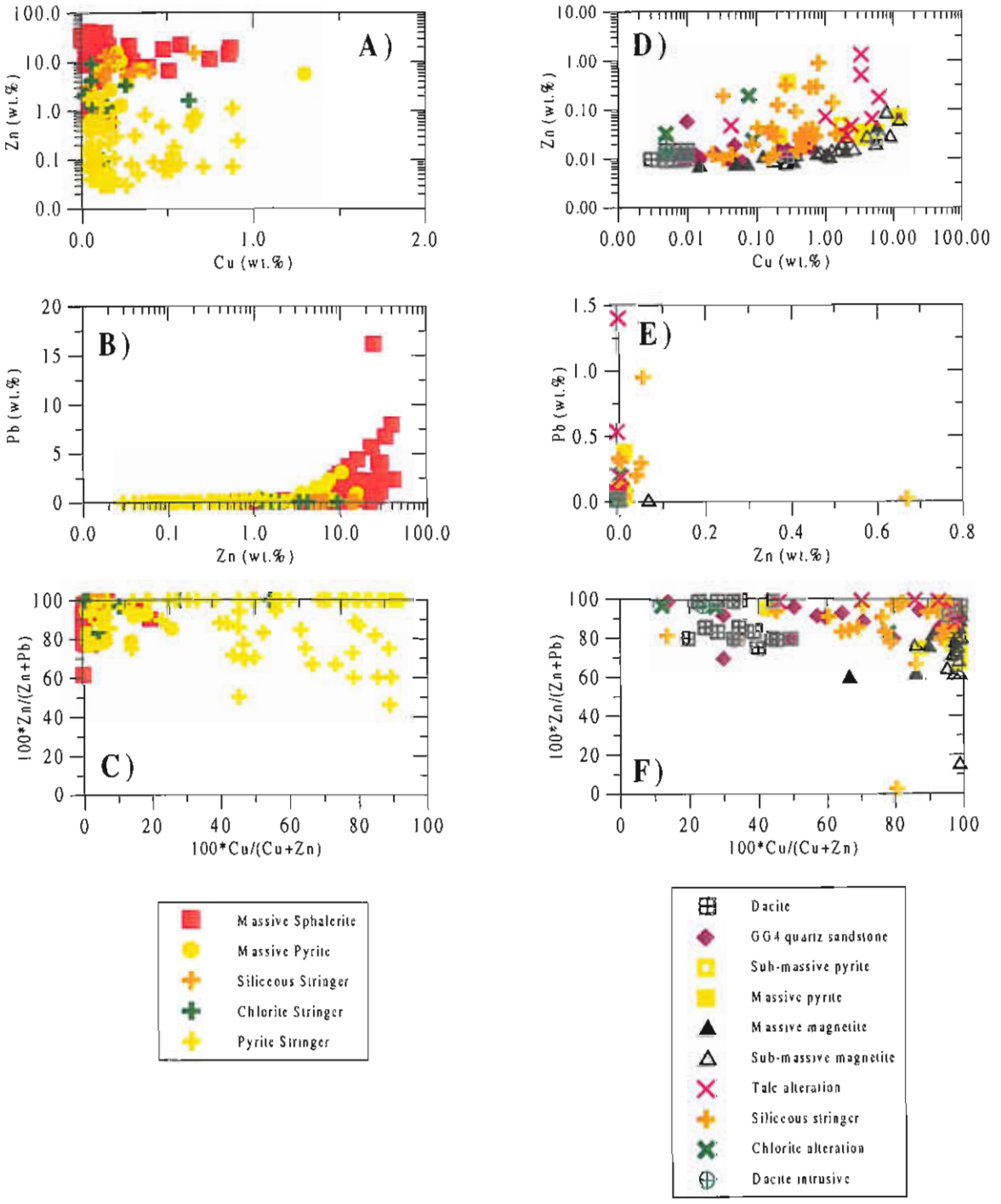

Figure17. Metal concentrations and element associations from two drill hole intercepts through sulphide mineralisation at Gossan Hill. An example of zinc - rich sulphide mineralisation from drill intercept GG165 (transform section 4) shows the aassociation for A) Cu vs. Zn B) Zn vs. Pb and C) Cu Ratio vs. Zn Ratio through massive zinc and assaciated stringer mineralisation. Copper - rich mineralisation, thraugh drill intercept GG070 (section 18688 N) at the north end of Gossan Hill shows element distributions for D) Cu vs. Zn E) Zn vs. Pb and F) Cu Ratio vs Zn Ratio. The metal associations are very different between the two mineralised zones.

Ni is also present in GG6 units, M1 Marker and hangingwall dacites.

A comparison of metal distributions in sulphide and alteration zones associated with zinc and copper mineralisation is shown in Figure 17. The two intersections are from GG165 through massive sphalerite mineralisation and GG070 through copper-magnetite mineralisation and highlight the differing metal associations within each of the mineralised zones. Zn is elevated in massive sphalerite mineralisation and lowest in pyrite stringer mineralisation (Figure 17a). Cu has a wide range of values for all ore types, with no correlation evident between Zn and Cu (Figure 17a). Pb values correlate well with Zn (Figure 17b), the highest values occurring in massive sphalerite mineralisation. Cu and Zn Ratios through sphalerite mineralisation show similar trends to those observed from host strata and alteration zones (Figure 17c). Comparatively, copper-magnetite mineralisation shows no association between the levels of Cu and Zn, with Zn less than 1% and a wide range of Cu levels (Figure 17d). Pb is generally below detection, but may form up to 1% and Pb values show no correlation to elevated Zn levels (Figure 17e). The Cu and Zn Ratio (Figure 17f) have a wide range in Cu Ratio values and Zn Ratios that are predominantly elevated associated with the absence of Pb in this mineralised zone. The sporadically elevated levels of Cu reflected by Cu Ratio values reflect vein controlled mineralisation.

Down hole variation of trace elements

Down hole variation of trace elements at the south end of Gossan Hill is shown in Figure 18. Ba, Sr, Rb and Ni levels decrease with proximity to the GG6 host and mineralisation over 150 m. Elevated Sn, Zn, Pb, Cu and Zn Ratio are hosted by GG6 units proximal to the hangingwall contact. Weak anomalism of Pb and Zn in the hangingwall rhyodacite and dacite units over 50 m adjacent to the host contact is clearly defined by the Zn Ratio. Figure 19, at the northern end of mineralisation (GG070), indicates that the footwall GG1 is depleted in Sr and Rb, with a slight increase in Ba with proximity to the GG4 contact. Ni, Sn, Zn, Pb, Cu all have increased abundances within 30 m of the footwall contact and are relatively depleted away from this zone. GG4 has variable metal concentrations with some enrichment in Sn.

Trace element summary

Levels of Ba, Sr, Rb are elevated in the hangingwall and reflect the presence of feldspar in these units. With increasing alteration associated with proximity to hangingwall contact the levels of Sr decreases in the hangingwall, reflecting the alteration of feldspar. In footwall units, a weak enrichment of Ba, Sr and Rb is observed, however these elements are depleted throughout the host sequence. Elevated values of Cu and Zn are associated with M1 Marker units and andalusite-chlorite alteration. The GG4 units show anomalous Zn levels comparative to Cu despite the association of these units with Cu mineralisation. Anomalous Pb, Cu, Zn, Sn and Ni values in siliceous alteration are associated with zinc-rich mineralisation. The lowest Pb values are recorded in the GG1 footwall. The distribution of Zn Ratio values reflect the general depletion in Pb throughout the Gossan Hill system.

ICPMS — Data

ICP-MS analysis of the elements Ag, As, Bi, Mo, Cd, Sb, Cs, Tl, Th, U were completed Analabs in conjunction with funding provided by the AMIRA alteration project. Results from ICP-MS analysis show Tl to have low levels for host stratigraphic and hydrothermally altered units. Th/U ratios (Figure 20a) show relatively constant levels, with depletion in the Th/U ratio only associated with chlorite-andalusite alteration. Above background levels of Sb (Figure 20b) occur in andalusite, chlorite and GG6 siliceous alteration, corresponding to high FeO* (Figure 20c). Mo levels (Figure 20d) are only elevated in footwall GG1 rocks, chlorite alteration and GG4 rocks. Ag values are low in the majority of units, however elevated values up to 33.8 ppm are recorded in siliceous altered GG6 and stringer associated lithologies (Figure 20e). Arsenic (Figure 20f) correlates to the distribution of Ag, with the most elevated values up to 5040 ppm recorded in siliceous rocks of GG6 and the M1 Marker. Bi (Figure 20g) correlates

with FeO* showing elevated values in siliceous altered GG6 and a trend of increasing Bi with increasing FeO* contents. Cd (Figure 20h) is sporadic throughout alteration zones, the most elevated values corresponding to siliceous alteration in GG6 and Cs (Figure 20i) levels are generally low.

Strong inter-element correlation within the suite of ICPMS are shown in the bivarate plots in Figure 21. Positive correlation between Bi-Sb, Bi-As and As-Sb (Figure 21a, b, c) reflect the association of these elements to siliceous alteration in GG6 units and M1 Marker units. Bi also shows a broad positive correlation with Cu (Figure 21d) and a strong correlation with Zn (Figure 21e), particularly in siliceous altered GG6 and chlorite-andalusite alteration. The distribution of Cd is similar to that of Bi, with a strong positive correlation between Cd and Sn (Figure 21f), Cd and Zn (Figure 21g) and Cd vs. Ag (Figure 21h). Elevated values of Cd corresponding to elevated Sn, Zn and Ag in GG6 and the M1 Marker. Ag levels (Figure 21i) have a strong association with Cu levels in GG6 siliceous alteration.

Down hole variation

Th/U ratios in all drill intercepts show relatively constant levels. Gradual anomalism in Sb and As is observed in hangingwall rhyodacites with proximity to the hangingwall contact (Figure 22). A decrease in Cs levels in rhyodacite units is observed proximal to the hanginwall contact. Mo levels in the hangingwall rhyodacite are elevated but erratic (Figure 22). Few trends from the down hole variation of elements Sb, Mo, Cd, As and Ag are present, however decreasing Cs toward the contact with mineralisation is present. Stringer associated alteration however show elevated levels of Sb, Mo and Ag and sporadic distributions in As, and localised enrichment in Cs, Sb and Cd in the 30 m adjacent to the footwall contact. Elevated Mo values are recorded in GG1 footwall units (Figure 23).

ICPMS trace element discussion

Siliceous alteration hosted by GG6 units and andalusite-chlorite alteration is well characterised by ICP-MS trace element data. GG6 siliceous alteration is host to massive sphalerite-pyrite and stringer mineralisation and shows universally elevated levels of Bi, As, Sb, (Cu, Zn) Sn, all of which show positive inter-element associations and correspond to anomalous elements associated with massive sphalerite-rich mineralisation. Footwall units (GG1) show low levels of trace elements with the exception of elevated levels of Mo and Cs. Low trace elemental abundances are recorded in the host units GG5, GG4, and the hangingwall units. However, hangingwall lavas show slight enrichment in Sb depletion in Cs toward the hangingwall contact. GG4 may show elevated Cu and depleted Zn levels but does not indicate the same elemental association of zinc-rich mineralisation and is not well characterised from the suite of ICP-MS data analysed.

M1 Marker

The M1 Marker horizon was initially defined by Ashley (1983) and mine geologists at Scuddles who recognised these distinctive units as a stratigraphic marker horizon at the top of the Scuddles ore position. The M1 Marker unit is characterised by distinctive bedded chert and chlorite bands with magnetite-pyrite and forms a 2 to 5 m zone overlying massive zinc mineralisation at Scuddles. A similar horizon, with bedded chert and chlorite ± sulphides has been identified at Gossan Hill. The mineralogy and geochemistry of these units is of particular interest as the Gossan Hill Group lacks stratigraphic marker units. The presence of an M1-type horizon at Gossan Hill has ramifications for future exploration activities as well as constraints on ore formation. The presence of a semi-continuous or locally discontinuous marker horizon at the top of the Scuddles and Gossan Hill zinc mineralisation presents an opportunity for development of exploration criteria in the Golden Grove district. Similar interbedded chert-lithic horizons have been noted in association with many other VHMS deposits; for example Kuroko (Kalogeropoulos and Scott, 1983), New Brunswick (Peter and Goodfellow, 1996) and Thalanga (Duhig et al., 1992; Doyle, 1996).

Geochemistry has proved advantageous in the

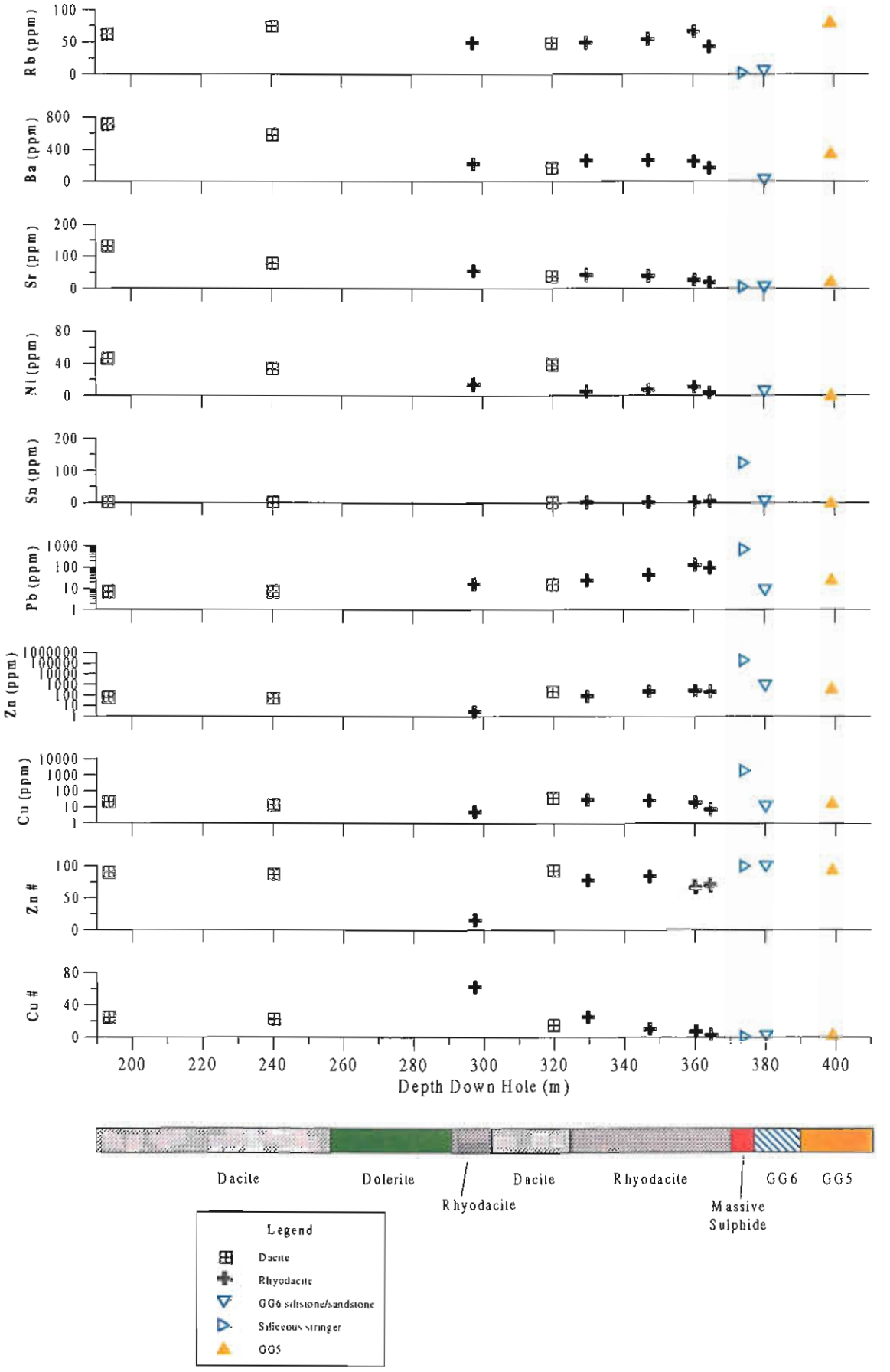

Figure 18. Down hole variation of trace elements along drill intercept GG132, section 17868 N at the south end of Gossan Hill.

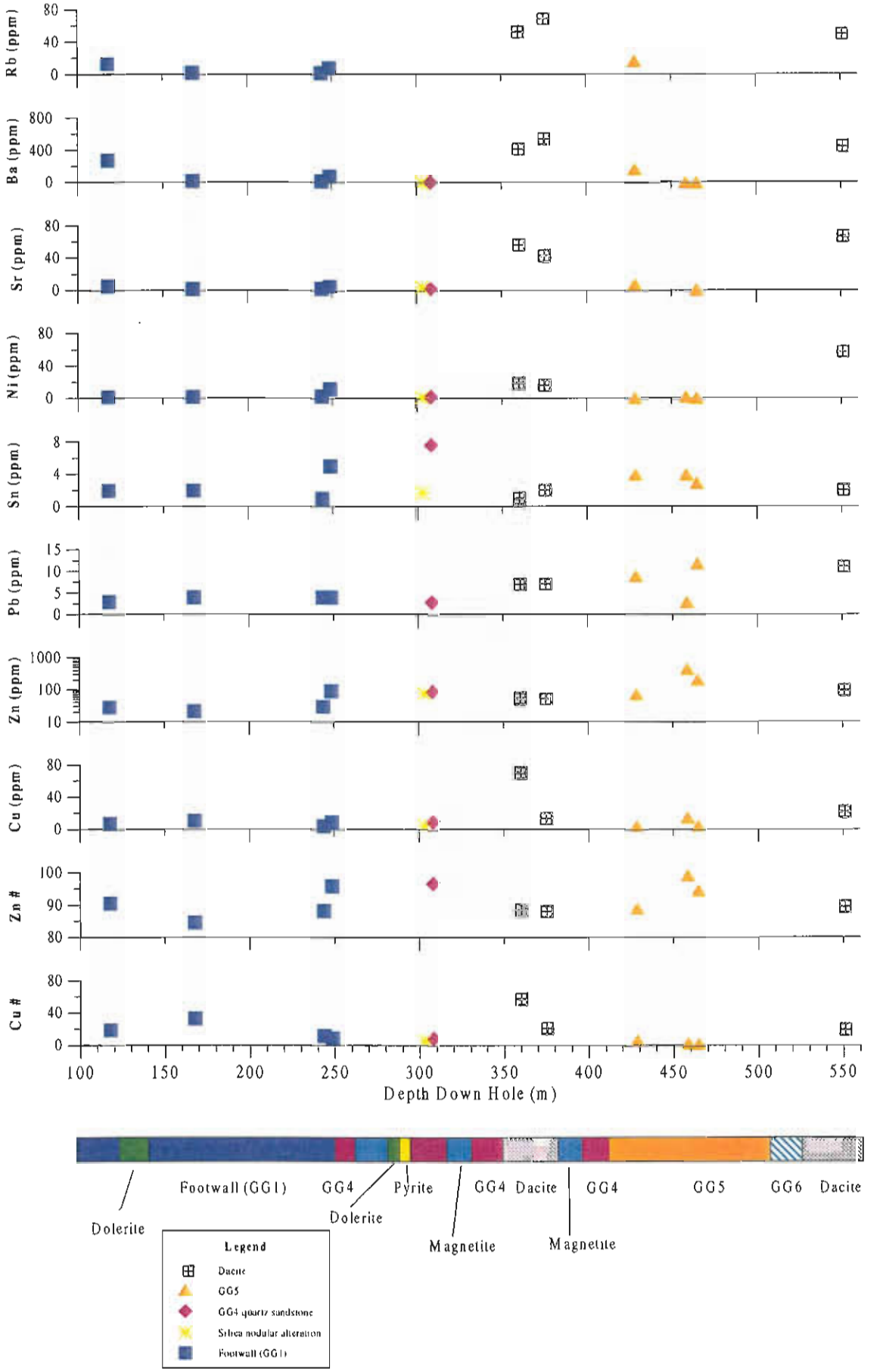

Figure 19. Down hole variation of trace elements in GG070, section 18688 N at the north end of Gossan Hill through copper - bearing pyrite - magnetite mineralisation.

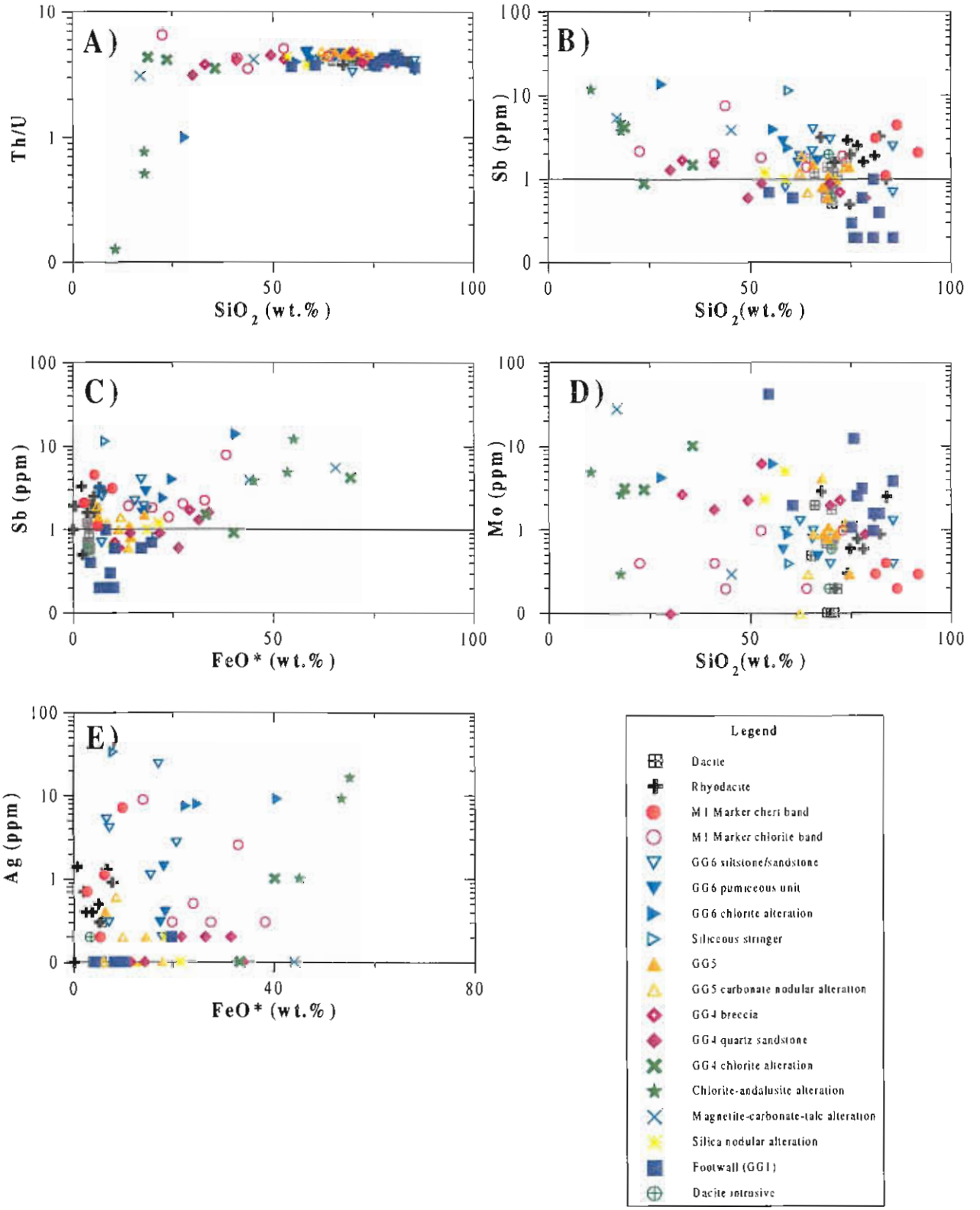

Figure 20. Trace element data from trace elements analysed by ICP-MS. A) SiO_2 vs. Th/U B) SiO_2 vs. Sb C) FeO vs. Sb D) SiO_2 vs. Mo E) FeO* vs. Ag and figures F) FeO* vs. As G) FeO* vs. Bi H) FeO* vs. Cd and I) FeO* vs. Cs shown on next page*

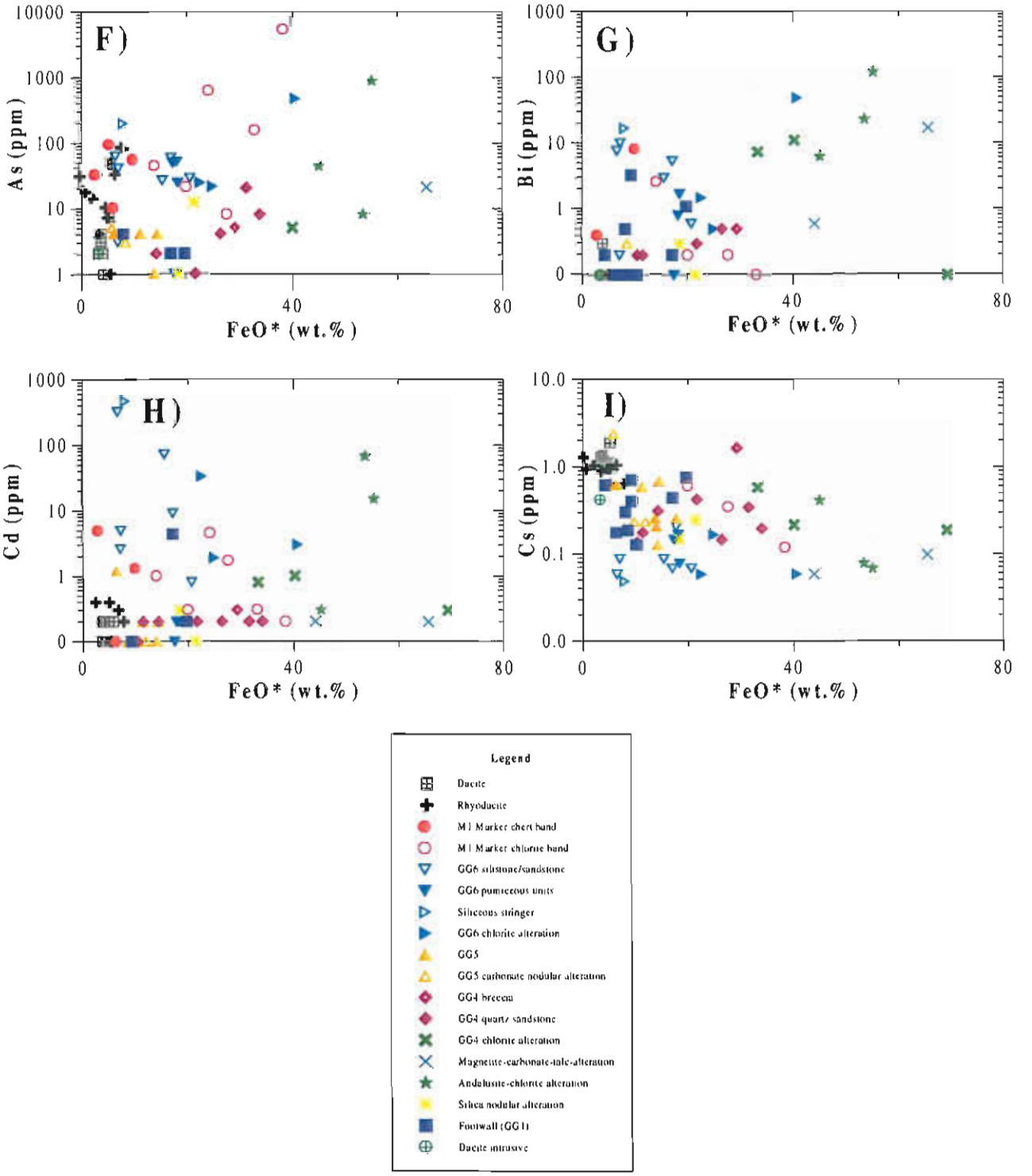

Figure 20 cont. Trace element data from elements analysed by ICP-MS. Continued from previous page F) FeO vs. As G) FeO* vs. Bi H) FeO* vs. Cd I) FeO* vs. Cs*

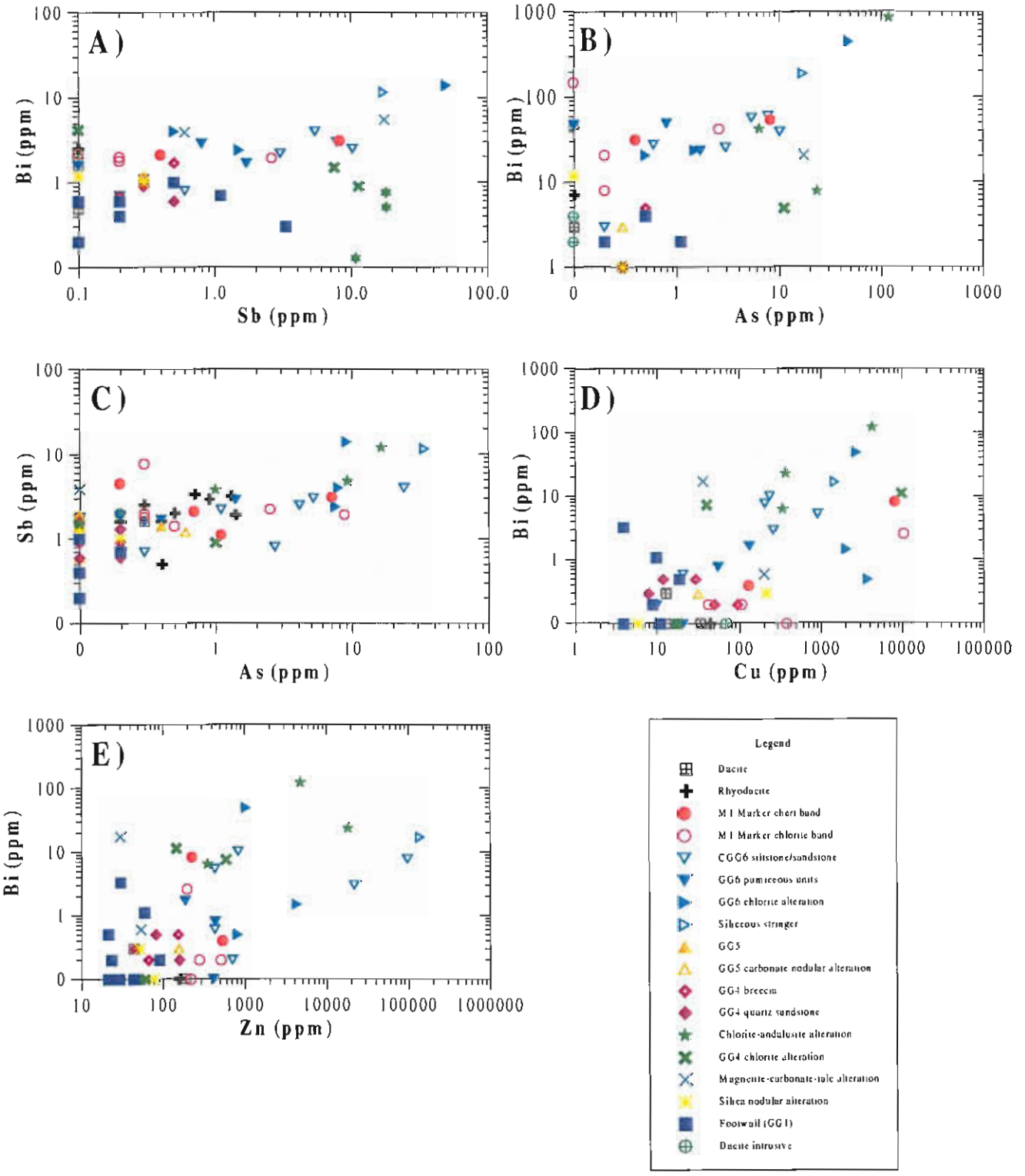

Figure 21. Inter-element assoication of trace element data analysed by ICPMS with correlated elements A) Sb vs. Bi B) As vs. Bi C) As vs. Sb D) Cu vs. Bi E) Zn vs. Bi

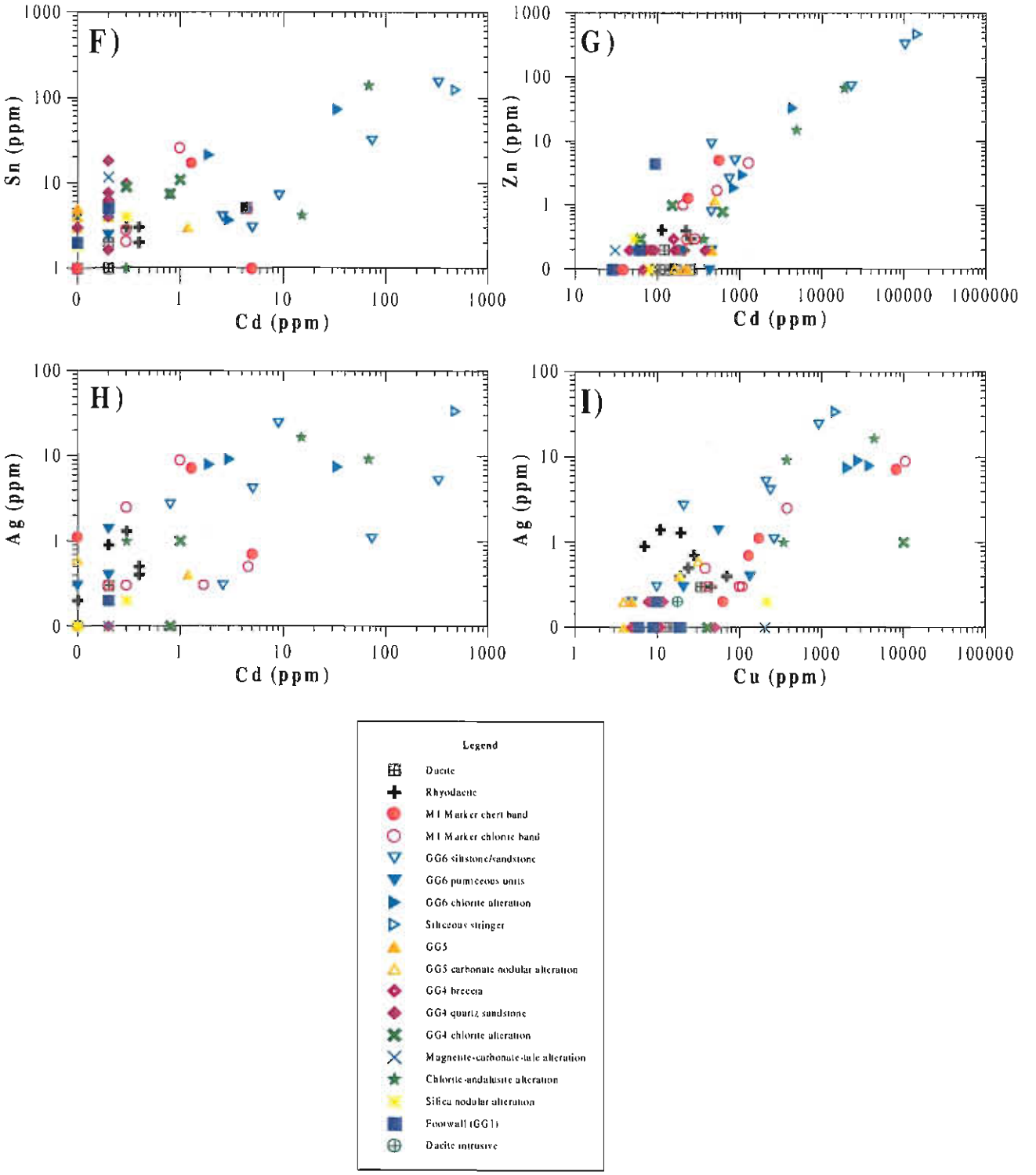

Figure 21 cont. Distribution of trace element data analysed by ICPMS with correlated elements F) Cd vs. Sn G) Cd vs. Zn H) Cd vs. Ag I) Cu vs. Ag

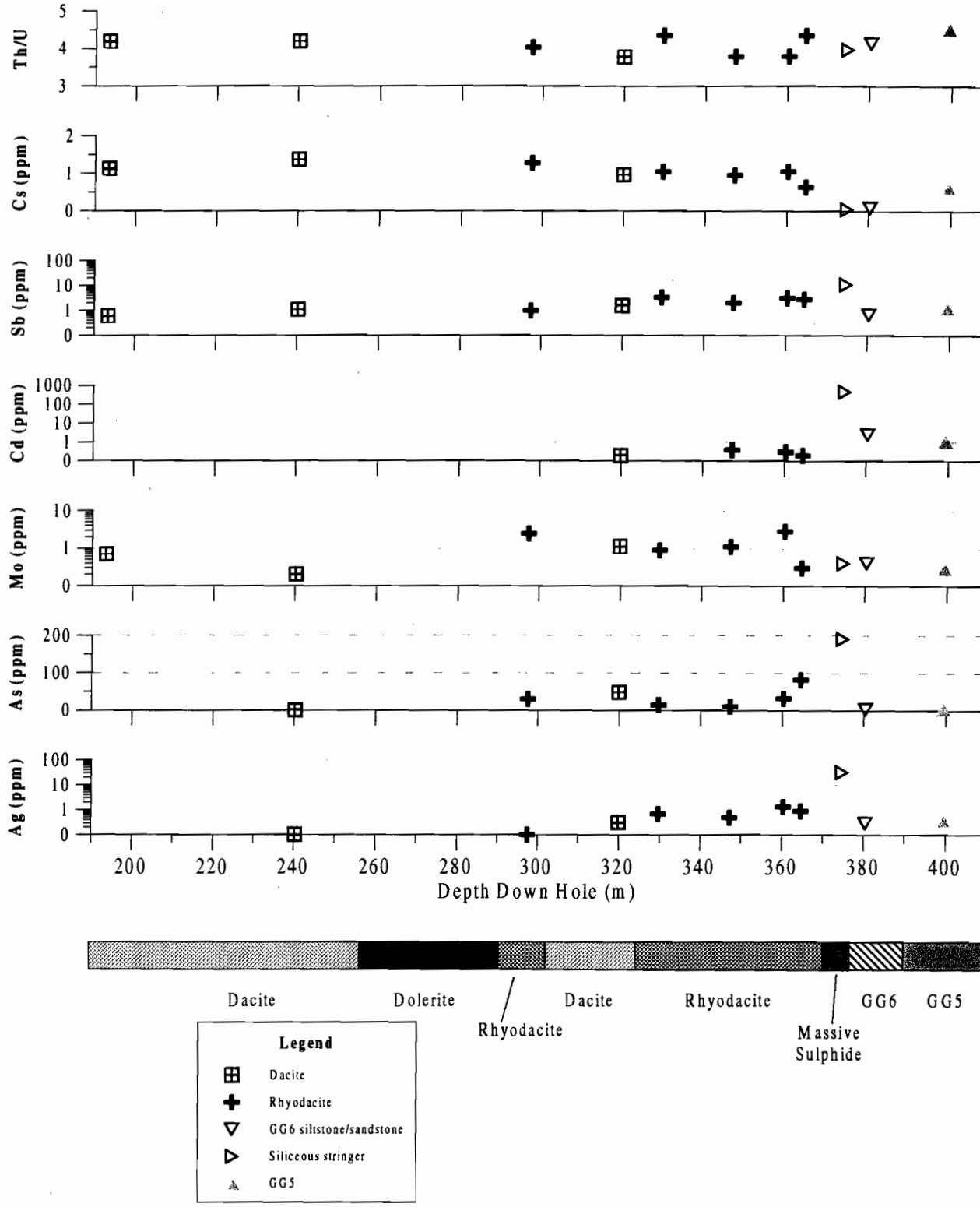

Figure 22. Down hole variation of trace elements analysed by ICP-MS in drill intercept GG132, section 17868 N at the south end of Gossan Hill.

A colour version of this figure was unavailable for the second printing of this report.

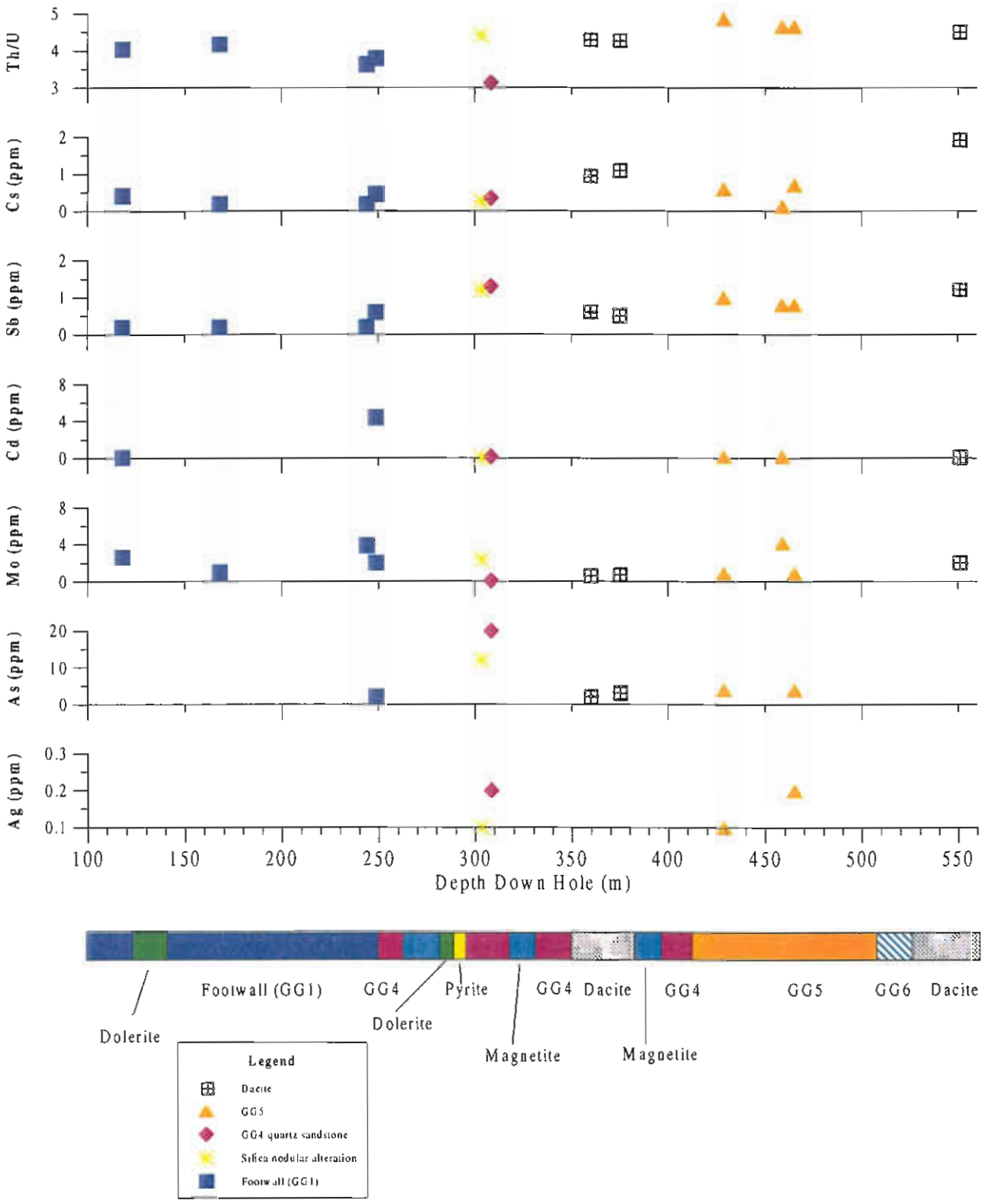

Figure23. Down hole variation of trace elements analysed by ICP-MS in GG070, sectian 18688 N at the north end af Gossan Hill through copper - bearing pyrite - magnetite mineralisotion.

study of "exhalative" units and it is possible to geochemically characterise hydrothermal and lithic constituents. Geochemistry was completed on 10 samples from the M1 Marker, including samples from Gossan Hill and Scuddles. Of these samples, two are from Scuddles and three from Gossan Hill, had chert and lithic bands analysed separately. Chlorite-rich bands are thought to represent beds deposited from ongoing background sedimentation during hydrothermal processes and represent the lithic component. Chert bands, consist of quartz and carbonate, are interpreted to represent deposition from SiO_2-rich hydrothermal fluids on the seafloor. Geochemical investigations will address the degree of hydrothermal contribution to both the chert and lithic bands, resultant from mineralising processes associated VHMS mineralisation at Scuddles and Gossan Hill.

Peter and Goodfellow (1996) use immobile elements to separate detrital material from that sourced by direct hydrothermal contribution. Immobile elements associations of the M1 Marker at Scuddles and its equivalent at Gossan Hill are plotted in Figure 24 and indicate chert bands to be geochemically distinct from chlorite bands. TiO_2 vs. Al_2O_3 (Figure 24a) show chert bands at Gossan Hill and Scuddles with low Al_2O_3 and TiO_2 values and chlorite bands with TiO_2 levels greater than 0.4 wt.% and Al_2O_3 greater than 4 wt.%. Al_2O_3 in the Scuddles chlorite bands are more elevated than those at Gossan Hill. Similar associations are observed between TiO_2 and Zr in Figure 24b. Zr contents for chert horizons are less than 10 ppm (Scuddles) compared to 228 ppm Zr in chlorite bands (Gossan Hill). MgO contents (Figure 24c) are less than 0.21 wt.% for chert horizons from both Gossan Hill and Scuddles and variable between 0.1 and 10 wt.% in chlorite bands and correspond to low levels of SiO_2 and FeO*. P_2O_5 contents are very low in chert horizons (<0.01 ppm) and elevated in lithic zones (Figure 24d) and Zr vs. Al_2O_3 (Figure 24e) show levels similar to P_2O_5. Chert bands have low Al_2O_3 and Zr, whilst chlorite bands show higher but variable Zr and Al_2O_3 contents. Cr levels (Figure 24f) for chert bands are lower than chlorite bands, with Cr contents between 25 ppm to 1520 ppm in chlorite horizons. A positive correlation between Ni and Cr levels for the M1 Marker (Figure 24g) is present with Ni contents in chert bands lower than chlorite bands. FeO* in chert bands is up to 10.1 wt.% compared with the FeO* range of 13 to 43 wt.% for chlorite bands (Figure 24h). Elevated FeO* in the chlorite bands is attributed to the intense chlorite alteration, as well as common sulphide minerals and magnetite phases. Sr and V levels (Figure 24i) are variable for both chert and chlorite bands. Figure 24 illustrates the different immobile element signatures of the chlorite and chert bands in the M1 Marker units and shows that the chlorite bands from Gossan Hill or Scuddles deposits are indistinguishable.

The distribution of major elements (Figures 25, 26) reflects differing mineralogy of chert and chlorite horizons. FeO* and SiO_2 (Figure 25a) show a negative linear correlation similar to that observed in host and footwall units at Gossan Hill. The trend indicates chlorite horizons to have lower SiO_2 (22 to 73 wt.%) than the chert units (81 to 91 wt.%). The high proportion of SiO_2 in chert bands is a reflection of the microcrystalline quartz meshwork of which these samples are composed. A positive correlation also occurs between FeO* and MgO (Figure 25b) and FeO and MnO (Figure 25c) for chert and chlorite bands. Minor chlorite occurs in chert horizons and thus the MgO content is below 2.1 wt.% and MnO content below 0.2 wt.%. Comparatively, MgO and MnO contents in chlorite bands are higher between 2.2 to 10.4 wt.% for MgO, and between 0.21 and 4.8 wt.% for MnO. The higher MgO and MnO contents in these chlorite bands is a result of abundant chlorite in these units. No distinction can be made between the composition of the Scuddles and Gossan Hill chlorite bands on the basis of FeO, MgO and MnO. CaO levels in chert and lithic bands (Figure 25d) is variable between 0.4 to 22.7 wt.%, reflecting a variable proportion of carbonate in both, which contribute to the elemental variations in MnO, MgO and FeO*. Irregular distributions of Zn, Sr, Ag and Cu are also observed and no clear distinction between chlorite or chert horizons can be made based on variation of these elements. Zn (Figure 25e) have low and high values for chert and chlorite units as does Sr (Figure

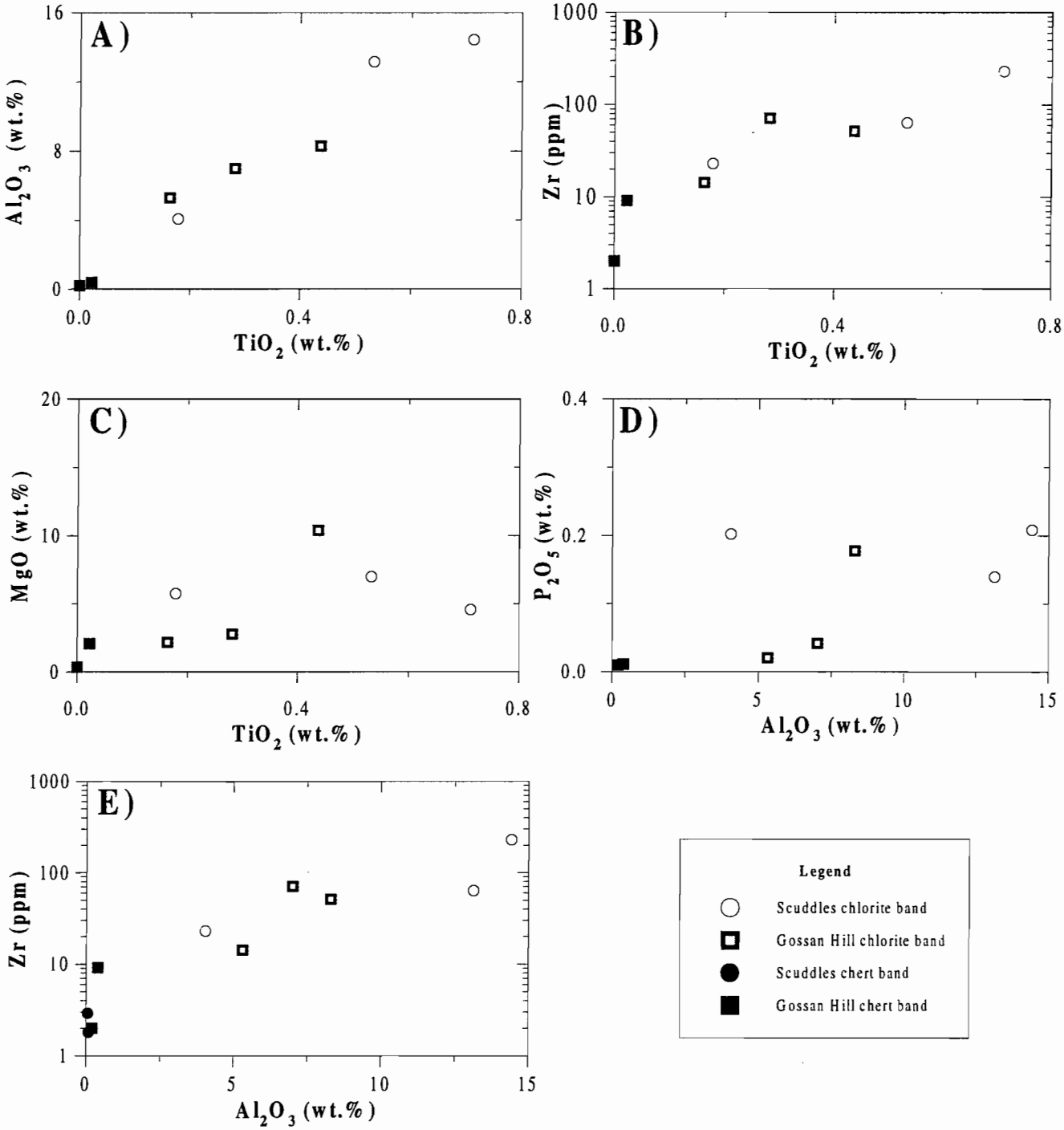

Figure 24. Immobile element distributions from chert and chlorite bands in the M1 Marker at Scuddles and Gossan Hill A) TiO_2 vs. Al_2O_3 B) TiO_2 vs. Zr C) TiO_2 vs. MgO D) Al_2O_3 vs. P_2O_5 E) Al_2O_3 vs. Zr *- continued on next page*

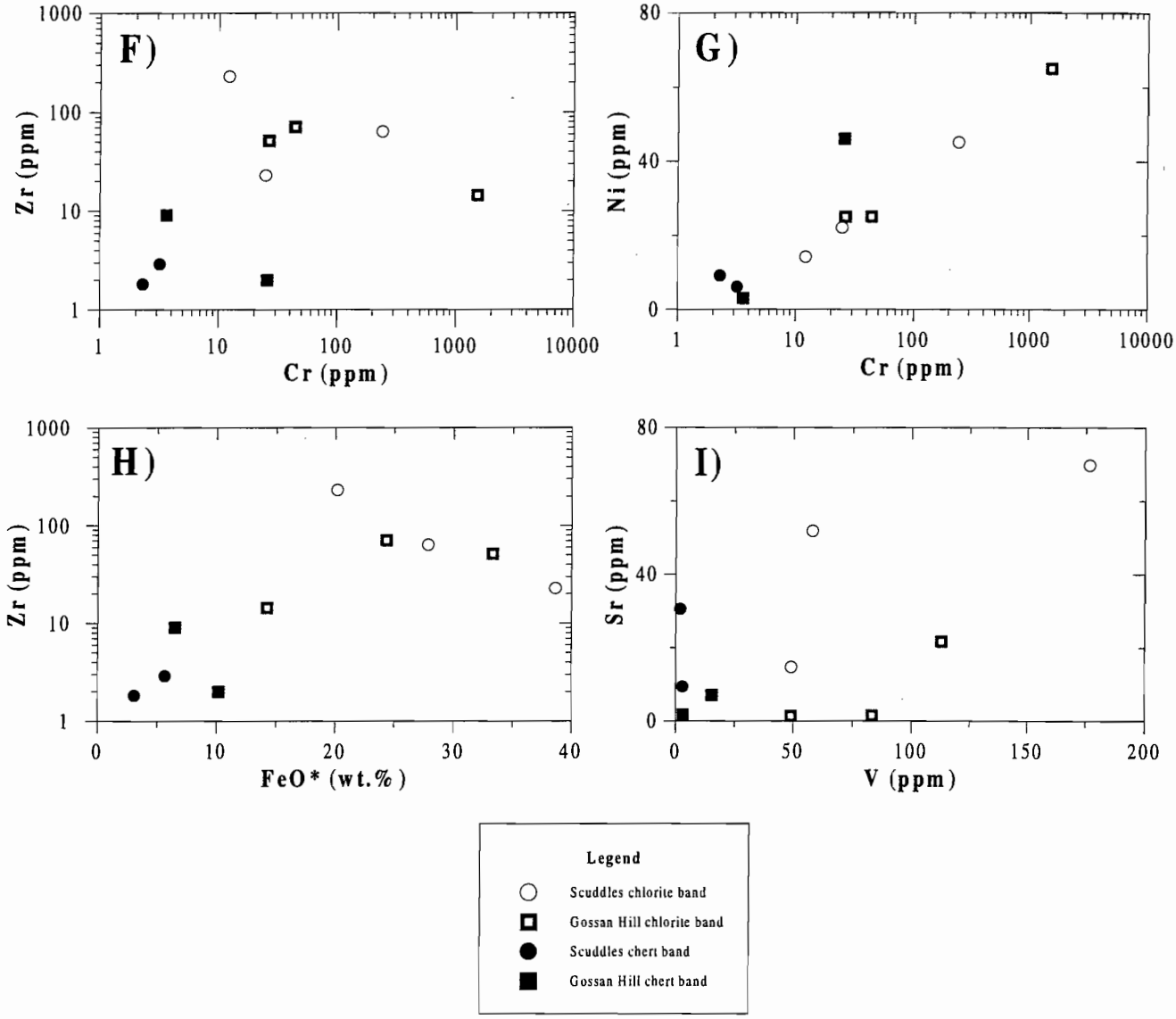

Figure 24 cont. Immobile element distributions from chert and chlorite bands in the M1 Marker at Scuddles and Gossan Hill F) Cr vs. Zr G) Cr vs. Ni H) FeO vs. Zr I) V vs. Sr*

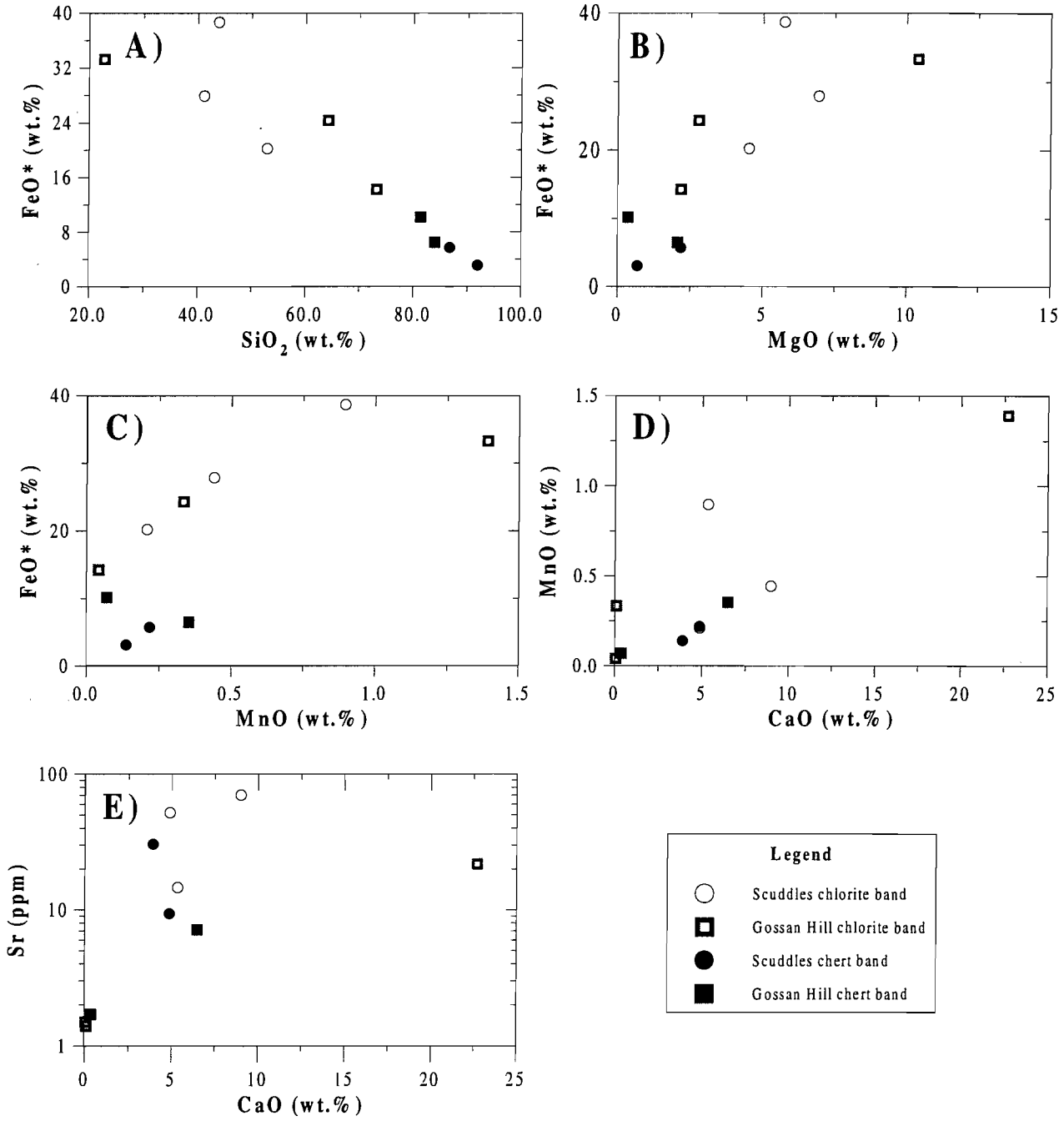

Figure 25. Distribution of mobile major and trace element data from chert and chlorite bands in the M1 Marker units from Gossan Hill and Scuddles. A) SiO_2 vs. FeO B) MgO vs. FeO* C) MnO vs. FeO* D) CaO vs. MnO E) CaO vs. Sr*

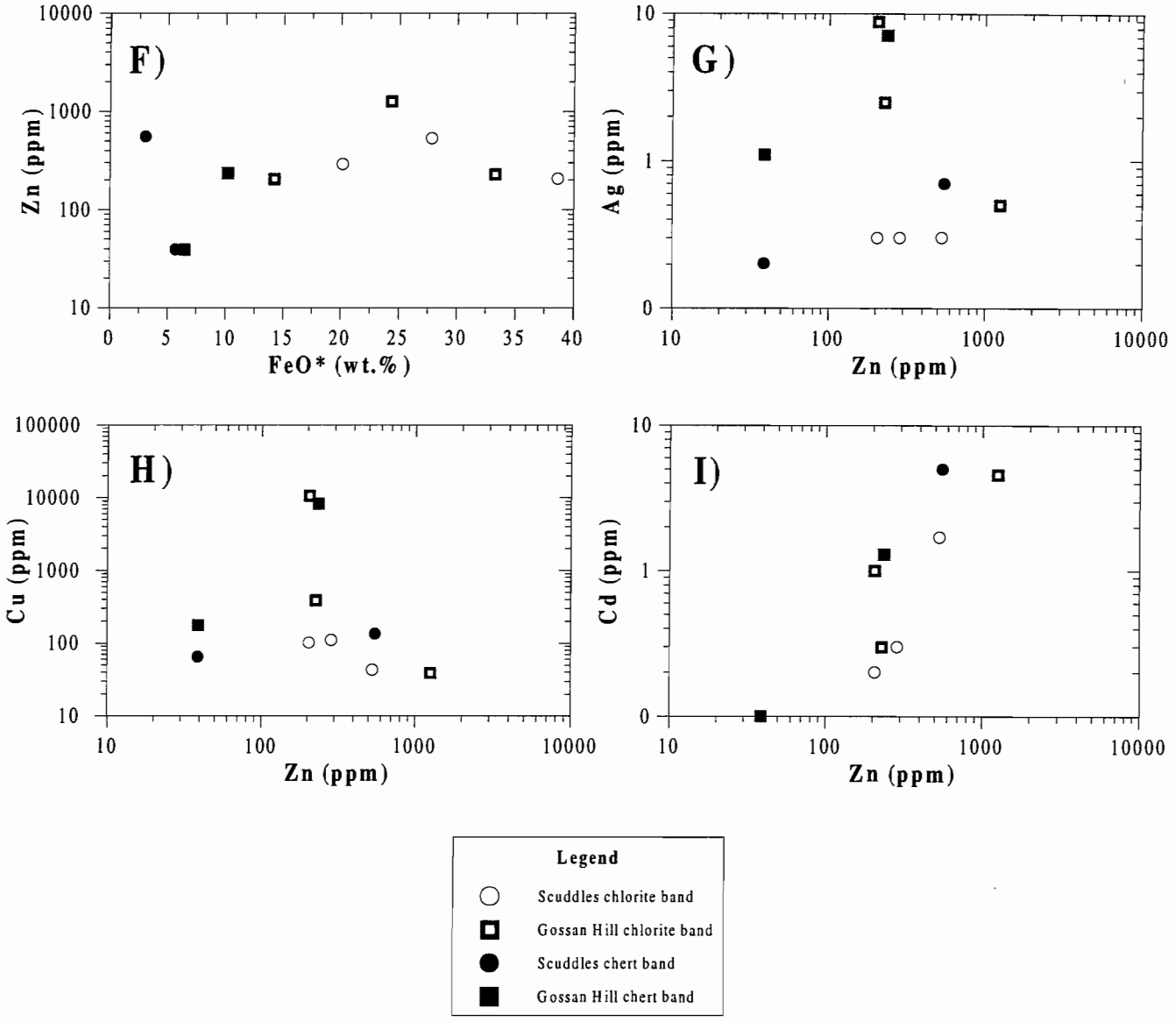

Figure 25. Distribution of mobile major and trace element data from chert and chlorite bands in the M1 Marker units from Gossan Hill and Scuddles. F) FeO vs.Zn G) Zn vs. Ag H) Zn vs. Cu I) Zn vs. Cd*

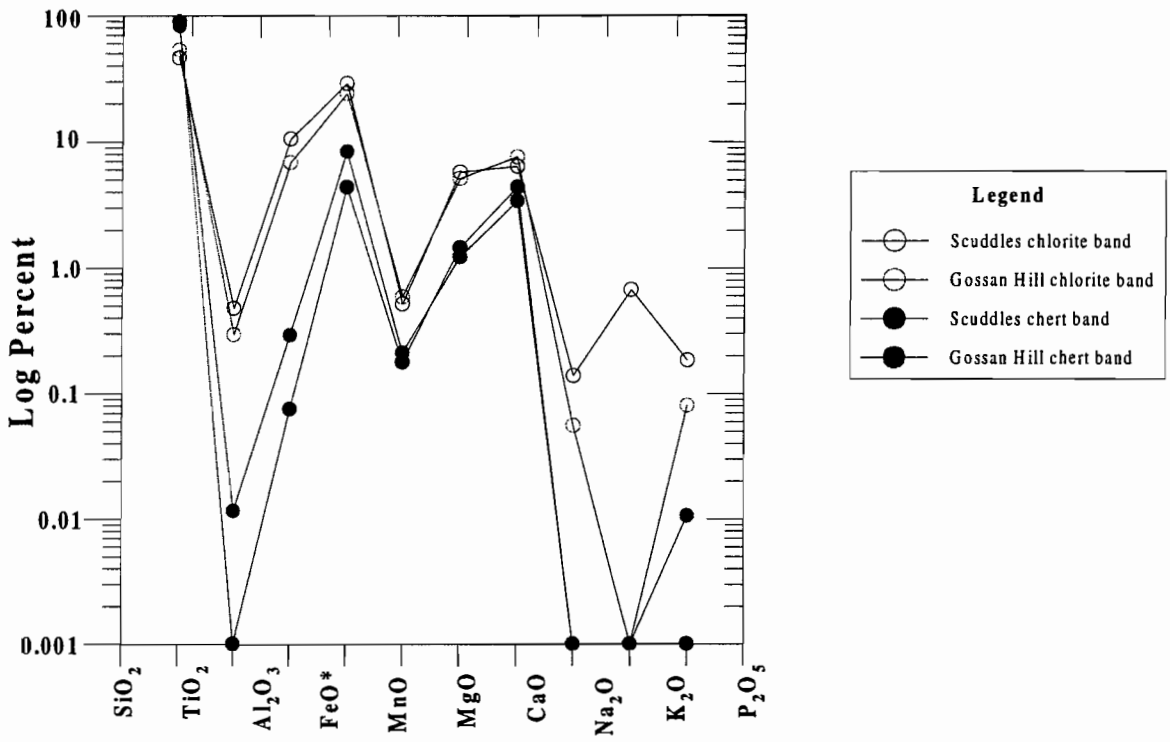

Figure 26. Spiderdiagram plot of major oxide elements from avearge values of the M1 Marker horizon at Scuddles and equivalent unit at Gossan Hill

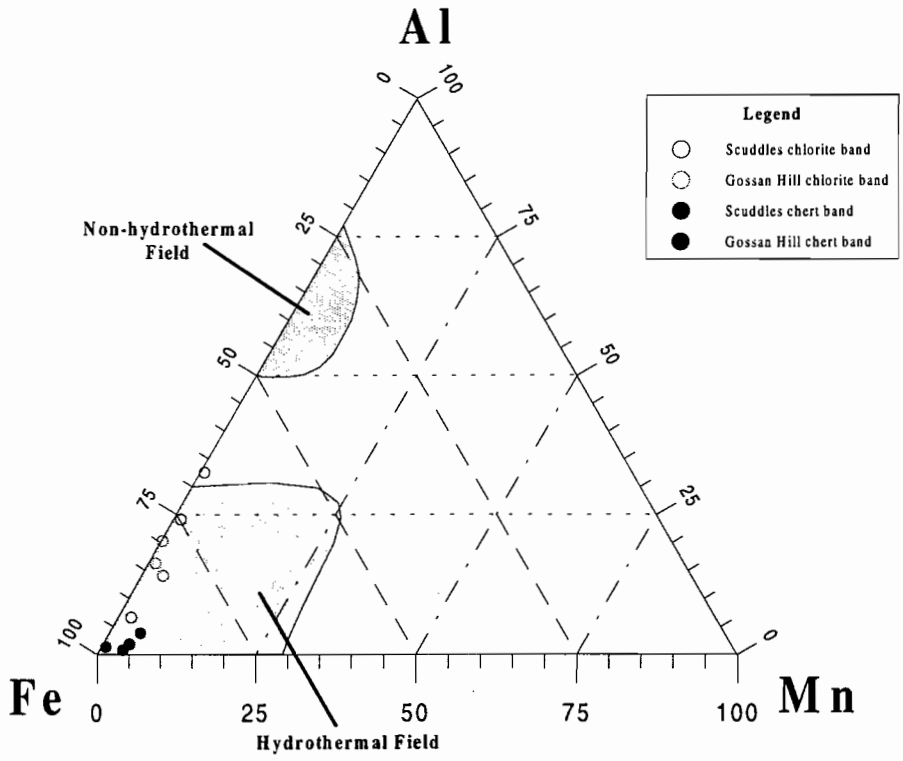

Figure 27. Al-Fe-Mn ternary plot showing the distribution of the M1 Marker samples from Gossan Hill and Scuddles. Both chert and lithic horizons from Scuddles and Gossan Hill plot in the hydrothermal field as defined by Adachi et al. (1986).

25f), Ag (Figure 25g) and Cu (Figure 25h). Positive correlation is observed between Cd and Zn (Figure 25i) and suggests Cd and Zn contained in minor disseminated sphalerite. Many elements, including Na_2O, K_2O, La, Ce, Nd, Nb, Ba, Sc, Sn, Rb, Bi, Mo, Cs, Tl,, Th and U, have low abundances in both the chert and chlorite bands.

The elements Ti, Al, Zr, Cr are relatively immobile under hydrothermal conditions and as such the source of these minerals is likely to have been detrital in origin. By contrast the elements Fe, Mn, Pb, Zn, Cd, Ca, Sr, Ba, P, Si are mobile and present as iron oxides, carbonate, quartz and sulphide minerals. Immobile, detrital originating elements (Figure 24) in chlorite bands are higher than those observed in chert bands at both Scuddles and Gossan Hill, reflecting a detrital component to the chlorite bands. Chert horizons show low levels of immobile elements and are interpreted to have a significant hydrothermal component, particularly SiO_2. It is however, clear from Figures 25 and 26, that both units show some degree of hydrothermal contribution, but that the hydrothermal contribution to the chert horizons is greater than the chlorite horizons.

Previous workers on hydrothermal cherts and iron formation utilise an Al-Fe-Mn ternary diagram to define the hydrothermal contribution to these horizons. The implementation of the ternary diagram discriminates between components derived mainly from hydrothermal sources, represented by Mn and Fe, and that of detrital origin, namely Al. Application to the M1 Marker horizon (Figure 27) shows data conforms to the hydrothermal field as defined by Adachi et al. (1986). Cherts from Gossan Hill and Scuddles reflect Fe enrichment with low levels of Mn and Al. Chlorite horizons of the M1 Marker show higher levels of Al and Mn and lower levels of Fe. These data indicate that the chert and, to a lesser extent, the chlorite bands of the M1 Marker have a significant hydrothermal contribution.

M1 Marker discussion

Geochemical analysis from chert and chlorite layers of the M1 Marker defined at Scuddles show similar characteristics to banded chert and chlorite horizons identified at Gossan Hill. The similarity in mineralogy and chemistry between these units supports the conclusion that they are of similar origin. The hydrothermal component of chert horizons is estimated to be significantly greater than that of the chlorite horizons. It is proposed, based on geochemical investigations, that chlorite-rich horizons in the M1 Marker units were derived largely from background sedimentation during hydrothermal activity associated with the Gossan Hill and Scuddles mineralisation. Chlorite bands represent periods of sedimentation during which fine grained clay-rich horizons were deposited. Interstitial chert bands were deposited in periods of low sedimentation derived principally from hydrothermal precipitates and take the form of quartz-rich horizons with sulphide and magnetite. The layered nature of the M1 Marker indicates repetition of pulses of sedimentation and hydrothermal chert precipitation. Pulsation during M1 Marker formation likely contributed to substantial hydrothermal modification of the precursor detrital (chlorite) and chert horizons, associated with elevated FeO*, MgO, MnO and CaO levels, due to precipitation of sulphides, magnetite, chlorite and carbonate minerals.

The geochemistry of the M1 Marker unit units are directly associated with ore forming processes and that the M1 Marker from Scuddles and Gossan Hill represent units formed under similar conditions due to proximity to mineralisation at similar stratigraphic levels. The recognition of these units in exploration has widespread ramifications to identifying stratigraphic position relative to mineralisation the Golden Grove district.

Summary of alteration zonation at Gossan Hill

Hangingwall alteration

The rhyodacite that overlies GG6 is and altered to sericite, carbonate and minor chlorite. Feldspar in rhyodacite units is poorly preserved and altered to sericite-chlorite-carbonate. Disseminated sulphides, predominantly pyrite and lesser sphalerite, may be

locally abundant. The rhyodacite units are ubiquitously altered, however the intensity of alteration, particularly sericite and pyrite, increases with proximity to GG6 host-hangingwall contact. Hangingwall dacite units have geochemically indistinct feeder zones which intrude host and footwall strata. Dacites in the hangingwall overly rhyodacite units. Alteration of dacite includes carbonate, sericite, quartz and minor chlorite mineral phases, with strong to intense carbonate alteration of feldspar phases. In both dacite and rhyodacite units the levels of Ba, Sr, Rb reflect the presence and alteration of feldspar. Decreasing levels of Ba, Sr and Rb, particularly in rhyodacite units, occurs proximal to the host-hangingwall contact over 150 m from the contact. Hangingwall rhyodacite and dacite units do not show the elevated levels of FeO* but do show slight enrichment in FeO*, MgO and MnO with increasing proximity to host GG6 and mineralised zones. This enrichment occurs over 50 m adjacent to the hangingwall contact and likely reflects increased abundance in carbonate and sulphides adjacent with proximity to the hangingwall contact. These trends differ from those observed within host and footwall strata and reflect the absence chlorite as a dominant alteration phase. Hangingwall alteration is characterised by elevated CaO and K_2O due to carbonate and sericite alteration, particularly of feldspar phases. Metal contents in the hangingwall do not show elevated values. Other trace elements which show variation in the hangingwall are Cs, As and Sb, with Cs having slight depletion and As and Sb low level enrichment. The hangingwall alteration at Gossan Hill is summarised below.

Host alteration

The volcaniclastic host units GG4 and GG5 have a relatively homogeneous rhyodacite to rhyolite composition based on immobile elements. GG6 and GG4 breccia units have comparatively wider variation in immobile element geochemistry indicating an inhomogeneous source consistent with a multiple provenance origin. Na_2O and K_2O are universally depleted throughout the host units GG4, GG5 and GG6. The depletion in K_2O reflects absence of sericite alteration in the host sequence. Quartz-chlorite (± carbonate) alteration is characterised by the correlation of SiO_2, FeO, MgO and to a lesser extent MnO. Strong correlation between FeO and MgO is the result of progressive changes in chlorite compositions from MgO-rich chlorite in GG4 to FeO-rich chlorites in the GG6. CaO distributions in the host units are sporadic due to patchy carbonate alteration but is broadly strongly depleted again reflecting the intense alteration of primary glass precursors in these units. Strong FeO* enrichment is

HANGINGWALL ALTERATION — Gossan Hill

Unaltered lithotype:	dacite	feldspar, quartz	
rhyodacite	quartz, feldspar		
Alteration mineralogy:	carbonate, sericite, quartz, ± chlorite, ± pyrite, ± sphalerite		
Geochemistry:	Depletion	Strong & ubiquitous	Na_2O, K_2O
	Depletion	200-150m from hangingwall contact	Sr, Ba, (Rb), Cs, SiO_2
	Enrichment	<100 m from hangingwall contact	FeO, MgO, MnO, As, Sb, CaO

identified in alteration zones adjacent to mineralisation and is due to Fe- sulphides, magnetite and chlorite. SiO_2 levels are elevated in GG6, GG5, M1 Marker indicating intense silicification within the host and footwall strata.

Data indicates that the siliceous alteration associated with GG6 units is best characterised by trace element data. GG6 siliceous alteration, associated with sphalerite-rich mineralisation , has elevated levels of Bi, As, Sb, Cu, Zn, Pb, Sn, Cd and Ag with positive inter-element correlation. Anomalism in these elements reflects mineralogical contents of galena, arsenopyrite, bismuthanite, tetrahedrite and cassiterite of the massive sphalerite mineralisation in GG6. Cu mineralisation in GG4 does not show this elemental correlation or association.

GG6-HOST ALTERATION

Unaltered lithotype:	siltstone-sandstone-breccia pumiceous units		mixed provenance, quartz quartz, pumice-glassy debris
Alteration mineralogy:	quartz, ± chlorite, ± carbonate, ± sphalerite, ± pyrite, ± magnetite,		
Geochemistry:	Depletion	strong & ubiquitous	Na_2O, K_2O
	Enrichment	sporadic distribution	Cd, As, Pb, Fe, Zn, Ag, Bi, Sb, Sn
Enrichment	strong to intense		SiO_2, (± FeO, MgO, CaO, MnO)

GG5-HOST ALTERATION

Unaltered lithotype:	sandstone	quartz, pumiceous lithics, glassy debris	
	lithic pebble breccia	quartz, pumiceous lithics, glassy debris	
Alteration mineralogy:	quartz, chlorite, ± carbonate, ± pyrite		
Geochemistry:	Depletion	strong & ubiquitous	Na_2O, K_2O
	Depletion	strong	CaO
	Enrichment	weak anomalism	Pb, Zn, ±Rb, ±Sr, ±Cs, ±Sb
	Enrichment	pervasive strong	SiO_2, FeO, MgO, MnO
	Enrichment	sporadic	CaO

GG4-HOST ALTERATION

Unaltered lithotype:	sandstone to pebble breccia breccia	quartz, pumiceous lithics, glassy debris mixed provenance, quartz	
Alteration mineralogy:	quartz, chlorite, ± carbonate, ± pyrite, ± magnetite ± chloritoid, ± apatite, ± andalusite, ± pyrrhotite, ± talc		
Geochemistry:	Depletion	strong & ubiquitous	Na_2O, K_2O
	Depletion	strong	CaO
	Enrichment	weak anomalism	TiO_2, MnO ,Al_2O_3, ± Zn, ± Pb, Mo, ± Bi, ± Sb
	Enrichment	pervasive strong to intense	SiO_2, FeO, MgO, CaO, Cu
	Enrichment	pervasive intense	FeO

Footwall alteration (GG1) — semiconformable alteration

The footwall GG1 has a relatively homogeneous provenance based on immobile elements. Ubiquitous depletion of Na_2O and K_2O throughout the footwall reflects the absence of feldspar and sericite and intense alteration of the primary lithofacies. Footwall GG1 units have low levels of all trace elements with the exception of slightly elevated levels of Mo and Cs. Mo tends to be adsorbed by silica in a weak alkaline solution such as seawater (Ichikuni, 1968). Thererfore Mo may be associated with quartz resulting from the intense silicification process which has affected the footwall. Sources for silica alteration may be derived from within the host from clays (eg smectite), from the devitrification of glass. Alternatively silica may have been added by the hydrothermal fluid.

Gibson et al. (1983) report silicification of the Amulet Rhyolite Formation which host VHMS deposits in the Noranda area. This silicification is interpreted to be early and widespread and contemporaneous with volcanism. The silicification reported by Gibson et al. (1983) was associated with increased Si and Ca contents of the host and decreased Fe, Mg, Ti, Al and Zn contents. Geochemical variations for alteration of the GG1 footwall at Gossan Hill are shown below.

Summary

The alteration at Gossan Hill forms broad zones of mineralogically simple arrays; being predominantly chlorite and quartz alteration. As interpreted from petrographic work, much of the host and footwall units have undergone early widespread silicification. Silicification has resulted in widespread depletion of mobile elements Na and K and Ca throughout the footwall. This alteration is not limited to the Gossan Hill area, but represents a regional-scale depletion in Na and K and Ca through the Golden Grove Formation (Clifford, 1992; Ashley, 1983; Frater 1978). Limited mobility of Ti is identified in the footwall and host rock sequence at Gossan Hill. There is a transition in Ti-bearing minerals from rutile in the footwall to ilmenite in the host rock sequence.

The host sequence at Gossan Hill has a correlation between SiO_2, FeO, MgO and MnO. The correlation of these elements reflect not only relative abundance of quartz and chlorite as the dominant phases of alteration, but also changes in the composition of chlorite. Chlorite has a progressive change from an Mg-rich chlorite to Fe-rich chlorite, corresponding to the transition from the footwall to the hangingwall. Carbonate alteration is sporadically associated with mineralised zones is siderite to ankerite in composition. Intense Fe-enrichment is associated with sulphide and magnetite mineralisation.

GG1-FOOTWALL ALTERATION

Unaltered lithotype:	pumiceous pebble breccia	quartz, pumiceous lithics, glassy debris	
Alteration mineralogy:	quartz, chlorite, ±pyrite, ±rutile ± ilmenite,		
Geochemistry:	Depletion	strong & ubiquitous	Na_2O, K_2O, CaO
	Enrichment	weak anomalism	TiO_2, MnO , Mo, Cs
	Enrichment	pervasive strong to intense	SiO_2, FeO, MgO

Alteration trace element geochemistry of GG6, which hosts massive sphalerite-pyrite mineralisation, show anomalism in Cd, As, Pb, Fe, Zn, Ag, Bi, Sb and Sn. These elements are also enriched in sphalerite mineralised zones. Comparatively, GG5 shows weak to minor enrichment in Pb, Zn and Sb. GG4, which hosts copper-magnetite mineralisation, shows weak to sporadic anomalism in Zn, Pb, Mo, Bi and Sb.

References

Adachi, M., Yamamoto, K. and Sugisaki, R., 1986. Hydrothermal cherts and associated siliceous rocks from the northern Pacific: Their geological significance as indication of ocean ridge activity. *Sedimentary Geology*, 47, 125-148.

Ashley, P. M., 1983. Geochemistry and wallrock alteration phenomena at the Scuddles deposit, golden Grove district, Western Australia, with application to volcanogenic massive sulphide exploration. *Regional Studies Group, Minerals Department, ESSO* Australia Limited.

Ashley, P. M., Dudley, R. J., Lesh, R. H., Marr, J. M., and Ryall, A. W., 1988. The Scuddles Cu-Zn prospect, an Archean volcanogenic massive sulfide deposit, Golden Grove District, Western Australia. *Economic Geology*, 83, 918-951.

Clifford, B. A., 1992. Facies and palaeoenvironment analysis of the Archean volcanic-sedimentary succession hosting the Golden Grove Cu-Zn massive sulphide deposits, Western Australia.. *PhD Thesis*, Department of Earth Sciences, Monash University.

Doyle, M., 1996. Volcanic influences in the formation of iron oxide-silica deposits in a volcanogenic -massive sulfide terrain, Mount Windsor Volcanic Belt, Queensland in Studies of VHMS -related alteration: geochemical and mineralogical vectors to ore. AMIRA/ARC project P439, *October 1996 Progress Report*, Centre for Ore deposits and Exploration Studies, University of Tasmania.

Duhig, N. C., Stoltz, J., Davidson, G.J., and Large, R.R., 1992. Cambrian microbial and silica gel textures in silica iron exhalites from the Mount Windsor volcanic belt, Australia: their petrography, chemistry, and origin. *Economic Geology*, 87, 764-784.

Floyd, P.A. and Winchester, J.A., 1978. Identification and discrimination of altered and metamophosed volcanic rocks using immobile elements. *Chemical Geology*, 21, 291-306.

Frater, K. M., 1978. The Golden Grove copper-zinc deposit, Western Australia-an Archean exhalative, volcanogenic occurrence. *PhD Thesis*, University of Newcastle.

Frater, K. M., 1983. Geology of the Golden Grove prospect, Western Australia: A volcanogenic massive sulfide-magnetite deposit. *Economic Geology*, 78, 875-919.

Gibson, H. L., Watkinson, D.H. and Comba, C.D.A., 1983. Silicification: hydrothermal alteration in an Archean geothermal system within the Amulet Rhyolite Formation, Noranda, Quebec. *Economic Geology*, 78, 954-971.

Hey, M. H., 1954. A new review of the chlorites. *The mineralogical magazine*, 30, 277-292.

Huston, D. L., 1988. Aspects of the geology of massive sulfide deposits from the Balcooma district, northern Queensland and Rosebery, Tasmania: implication for ore genesis. *PhD Thesis*, University of Tasmania.

Huston, D.L. and Large, R.R., 1987. Genetic and exploration significance of the Zinc Ratio (100 Zn/(Zn+Pb)) in massive sulfide systems. *Economic Geology*, 82, 1521-1539.

Hutchinson, R. W. and Searle, D. L. 1971. Strata bound pyrite deposits in Cyprus and relation to other sulphide ores *in Takkeuchi, Y. Ed., Proceedings of the IMA_IAGOD Meetings, 70.* Mining Geology Special Issue 3, p. 198-205

Ichikuni, M., 1968. Chemistry of siliceous deposits formed from hot spring waters. *Journal of the Society for Engineering Mineralogy*, Japan, 5, 48-53, English abstract only

Iijima, A., 1973. Clay and zeolite alteration zones surrounding Kuroko deposits in the Hokuroku district, Northern Akita, as submarine hydrothermal-diagenetic alteration products. *Mining Geology Special Issue*, 6, 267-289.

Ishikawa, Y., Sawaguchi, T., Iwaya, S. and Horiuchi, M., 1976. Delineation of prospecting targets for Kuroko deposits based on modes of volcanism of underlying dacite and alteration halos: *Mining Geology*, 26,105,117, English abstract.

Jiang, S. Y. and Palmer, M. R., 1996. Mn-rich ilmenite for the Sullivan Pb-Zn-Ag deposit, British Columbia. *The Canadian Mineralogist*, 34, 29-36.

Kalogeropoulos, S. I. and S. D. Scott, S.D., 1983. Mineralogy and geochemistry of tuffaceous exhalites (Tetsusekiei) of the Fukazawa Mine, Hokuroku district, Japan. The Kuroko and related volcanogenic massive sulphide deposits. H. Ohmoto and B. J. Skinner, *Economic Geology Monograph.* 5: 412-432.

Large, R.R., 1996. The Hercules-Mt Read traverse: relationships between volcanic mineralogy, alteration and geochemistry In Studies of VHMS -related alteration: geochemical and mineralogical vectors to ore. AMIRA/ARC project P439, *October 1996 Progress Report*, Centre for Ore deposits and Exploration Studies, University of Tasmania

Larson, P. B., 1984. Geochemistry of the alteration pipe at the Bruce Cu-Zn volcanogenic massive sulphide deposit, Arizona. *Economic Geology*, 79, 1880-1896.

Morton, R. L. and Franklin, J. M., 1987. Two fold classification of Archean volcanic associated massive sulfide deposits. *Economic Geology*, 82, 1057-1063.

Peter, J. M. and Goodfellow, W.D., 1996. Mineralogy, bulk and rare earth element geochemistry of massive sulphide-associated hydrothermal sediments of the Brunswick Horizon, Bathurst Mining Camp, New Brunswick. *Canadian Journal of Earth Science*, 33, 252-283.

Potter, B. K., 1991. Chemical and physical effects of wall rock alteration around volcanogenic massive sulphide deposits. *Honours Thesis*, University of Western Australia.

Radford, N., 1994. Scuddles lithogeochemistry. Internal memorandum. Normandy Exploration.

Urabe, T., Scott, S.D. and Hattori, K., 1983. A comparison of footwall-rock alteration and geothermal systems beneath some Japanese and Canadian volcanogenic massive sulphide deposits in Ohmoto H. and Skinner, D.J. Eds. Kuroko and related volcanogenic massive sulphide deposits. *Economic Geology Monograph 5*, p. 507-522.

Whitford, D. J. and Ashley, P.M., 1992. The Scuddles volcanic-hosted massive sulfide deposit, Western Australia: geochemistry of the host rocks and evaluation of lithogeochemistry for exploration. *Economic Geology*, 87, 873-888.

Whitford, D.J., McPherson, W.P.A. and Wallace, D.B., 1992. Geochemistry of the host rocks of the volcanogenic massive sulfide deposit at Que River, Tasmania. *Economic Geology*, 84, 1-21.

Winchester, J. A. and Floyd, P.A., 1977. Geochemical discrimination of different magma series and their differentiation products using immobile elements. *Chemical geology*, 20, 325-343.

Volcanic facies analysis, alteration and geochemistry of the host rock sequence to VHMS-style mineralisation at Thalanga (north Queensland)

Holger Paulick
Centre for Ore Deposit Studies, Geology Department, University of Tasmania

Introduction

Regional geology

The Thalanga VHMS deposit is located ~180 km west of Townsville (north Queensland) and contains 6.35 Mt of ore with an average grade of 12.4% Zn, 3.9% Pb, 2.2% Cu, 99 g/t Ag and 0.6 g/t Au (Gregory et al, 1990). The mineralisation occurs close to the western end of the E–W striking Mount Windsor Subprovince which consists of a Cambro-Ordovician succession of marine sediments and volcanics (Henderson, 1986; Berry et al, 1992). The succession has a subvertical dip and consists of 4 conformable formations with a combined stratigraphic thickness of ~10 000 m maximum.

The lowermost unit is the Puddler Creek Formation (PCF), which consists of continental derived, lithic sandstones and greywackes interbedded with siltstones and basaltic volcanics with alkaline affinities (Stolz, 1995). It is overlain by rhyolitic lavas and intrusion of the Mount Windsor Formation (MWF) which constitute the footwall to the Thalanga VHMS deposit. Rhyolite from the railway cutting through the Thalanga Range (Fig. 1) have been dated by SHRIMP U-Pb analysis of zircons (Perkins, 1993) and yield a crystallisation age of about 480 Ma (lower Ordovician). The overlying volcano-sedimentary Trooper Creek Formation (TCF), the hangingwall to the Thalanga mineralisation, shows prominent lateral facies variations. It contains andesitic, dacitic and rhyolitic volcanics, mudstones, crystal-rich sandstones and volcaniclastic gravity flow deposits. Graptolites of lower Ordovician age have been identified by Henderson (1983) from several localities. Additionally, silica ironstones and massive sulphide lenses occur at several stratigraphic levels within the TCF throughout the Mount Windsor Subprovince. Massive sulphide mineralisation of economic grade includes the prospects of Liontown, Highway–Reward and Waterloo. The overlying Rollston Range Formation (RRF) marks the cessation of volcanic activity in the Mount Windsor Subprovince. It consists of sandstones, siltstones and cherty sediments which yield graptolite and trilobite fauna of a slightly younger age than the Trooper Creek Formation.

Aims

The principal aims of this project are to:

- integrate volcanic facies analysis and alteration studies in order to constrain the volcanological and hydrothermal processes involved in the mineral deposition at Thalanga,
- determine the metamorphic history of the Thalanga mine area and the effect on textures, mineral assemblages and composition and;
- define systematic changes in whole rock geochemistry and mineral composition with distance from the ore horizon which may serve as vectors to ore in exploration for VHMS deposits.

CODES: AMIRA Project P439 — Studies of VHMS-related alteration: geochemical and mineralogical vectors to ore. May 1997

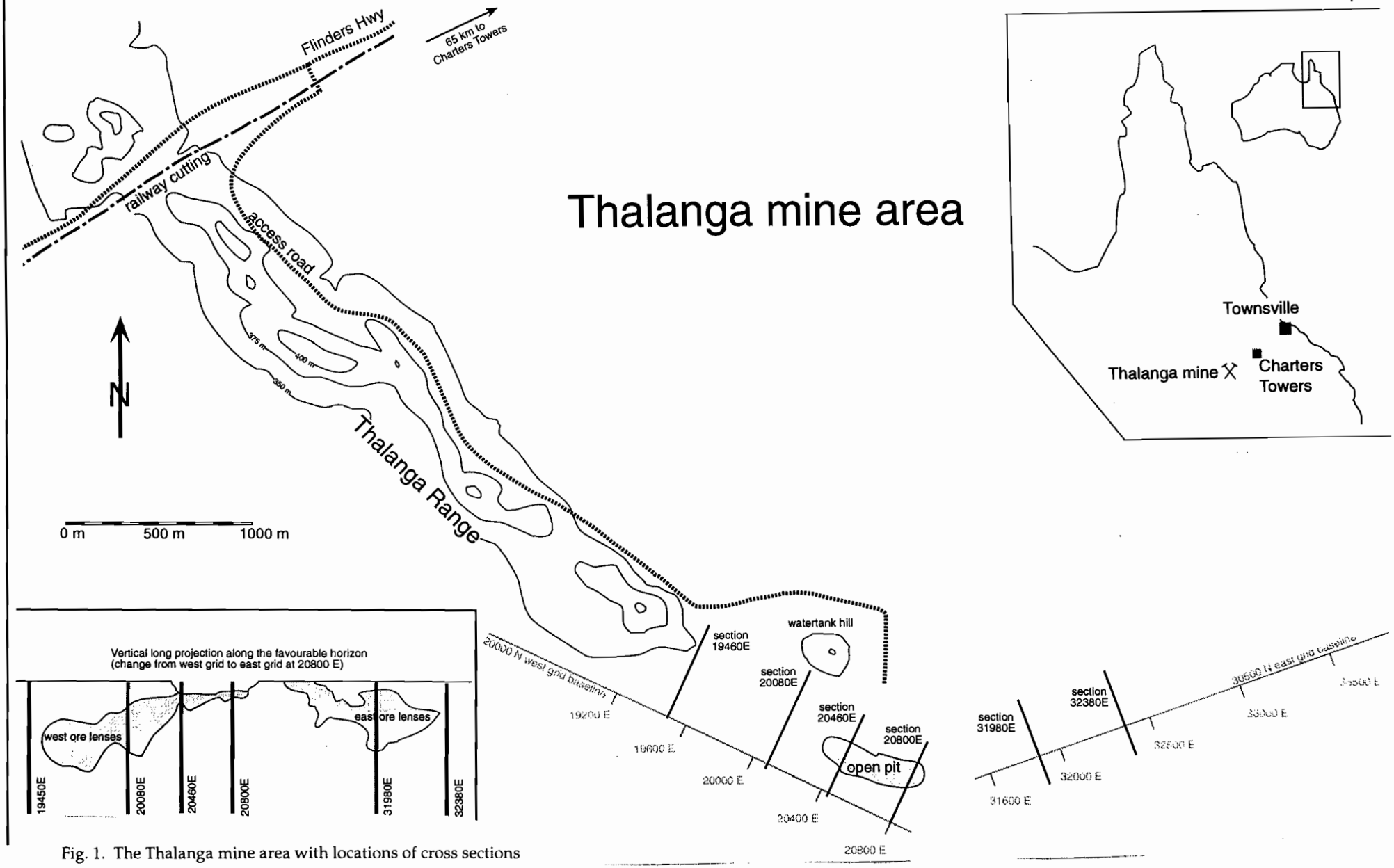

Fig. 1. The Thalanga mine area with locations of cross sections

Geology of the Thalanga mine area

Stratigraphy

The Thalanga Zn-Cu-Pb deposit is a stratiform, sheet-like VHMS deposit with extensively altered quartz ± feldspar phyric rhyolite of the MWF in the footwall (Fig. 2). The hangingwall sequence (TCF) consists of a diverse volcano-sedimentary succession dominated by weakly to moderately altered, feldspar phyric dacites. The stratigraphic position between the rhyolite and the first occurrence of hangingwall dacite is refered to as the ore horizon or favourable horizon hosting the massive sulphide lenses. It varies in thickness from a few meters to a few tens of meters and consists of a laterally variable lithofacies association including medium to coarse, quartz crystal-rich sediments ('Quartz Eye Volcanicastics', 'QEV'), medium to coarse quartz-feldspar porphyries ('QFP' or 'QEP' for 'quartz-eye porphyry'), polymict rhyolite-dacite mass flow deposits ('Hangingwall Fragmental', 'HWF'), carbonate-tremolite-chlorite rocks, massive barite, mudstones and silica-ironstones. These immediate host rocks to the Thalanga mineralisation have been studied in detail by Hill (1996). The term 'Thalanga sequence' has been chosen to refer collectively to the footwall rhyolites, the lithologies of the favourable horizon and the hangingwall sequence.

Because of the paucity of surface outcrop, diamond drill core logging provides the main source of geological information in the Thalanga mine area. Upto 500 m of stratigraphy have been intersected by diamond drilling at several localities along strike of the mineralisation.

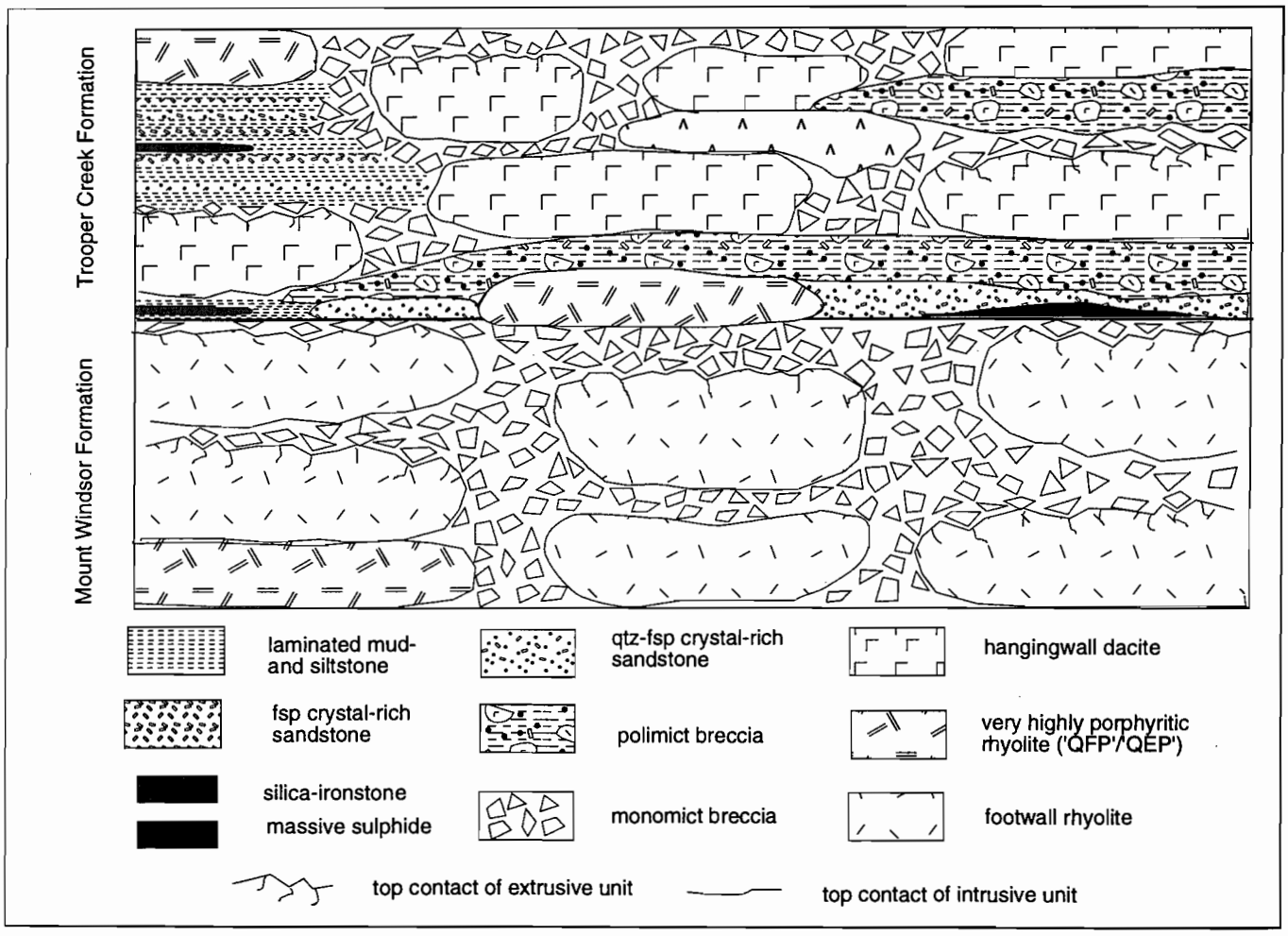

Fig. 2. Schematic illustration of the facies association in the Thalanga sequence

Large-scale intrusions, deformation and metamorphism

The Thalanga mine sequence has a sub-vertical dip and has been interpreted as the south facing limb of an east–west fold (Berry et al, 1992, Hill, 1996). The principal deformation event (D_2) imparted a strong regional foliation onto incompetent lithofacies. The abundance of biotite oriented parallel to S_2 indicates that P/T conditions reached upper greenschist metamorphic grade during D_2 deformation.

On the basis of aeromagnetic data, two distinctive, large-scale intrusive bodies have been interpreted in the subsurface of the Thalanga mine area. A granite intrusion to the north of Thalanga mine has been intersected in RC drill holes (eg. THRC8) and was sampled for textural and geochemical studies in 1996. It has a porphyritic texture and consists mainly of quartz and feldspar which occur as coarse phenocrysts and also dominate the groundmass. However, biotite and sericite are also important components. Textural observations (strained quartz phenocrysts, recrystallisation, foliation) indicate that the granite has been deformed and therefore predates D_2. According to textural and geochemical criteria proposed by Hutton & Crough (1993; p.6) it can be inferred that the granite was probably emplaced during the Ordovician. Given that zircon ages from the footwall rhyolite yield an early Ordovician age (480 Ma; Perkins, 1993), it is possible that a temporal link may exist between granite emplacement and mineralisation at Thalanga.

A diorite intrusion with a north–south elongation cuts through the footwall and hangingwall to the east of the Orient ore lens and has been intersected by DDH TH471 (collar: 33600N 30670E). It has a granular texture dominated by plagioclase, hornblende and biotite and shows no signs of alteration or deformation. It is clearly younger than the Thalanga mine sequence and has apparently been emplaced after D_2. Adjacent to the diorite an unusual abundance of garnet porphyroblasts in the altered footwall rhyolite has been noted which may be interpreted as the products of contact metamorphism.

Progress to date

During the course of this project ~14000 m of drill core from 6 cross section through the Thalanga mine sequence have been logged and sampled (Tables 1, 2). Additionally, a section of the MWF in the railway cutting (~5 km to the west of Thalanga mine) and several outcrops along the Thalanga Range immediately to the west of the mine have been examined in order to document the lithofacies, petrography and geochemical composition of weakly altered footwall rhyolite. Geochemical data and petrographic slides have been compiled from previous studies to complement the samples collected during this project collection (Table 2). In total, ~290 XRF analyses (including 180 prepared during this project) and ~400 thin sections are available for geochemical and petrographic examination covering the entire range of lithofacies in the Thalanga sequence.

Volcanic facies analysis

The lithofacies association of the Thalanga sequence has been examined with the aim to correlate individual units between drill holes, interpret their mode of emplacement and develop a general facies model for the volcanological evolution of the Thalanga area. This part of the project is primarily based on textural observations on hand specimen and thin sections documenting contact relationships and textural information. The descriptive terminology scheme proposed by McPhie et al (1993, pp. 9, 10) has been applied to record the textural features of lithofacies. However, the Ti/Zr ratio may also be used as a discriminator of footwall rhyolite and hangingwall dacite and between individual dacite emplacement units.

Lithofacies association in the footwall

Individual rhyolite emplacement units within the MWF have been interpreted based on contact relationships and consistent differences in phenocryst assemblages. The footwall rhyolite units can be poorly (<3 %), moderately (3–10 %) of highly (10–20 %)

Table 1: Summary of logged drill core and mapped surface exposure in the Thalanga area

Sections through the Thalanga mine sequence											
cross section		stratigraphic thickness intersected		diamond drill holes (footwall)		total for footwall	diamond drill hole (hangingwall)		total for hangingwall	total for section
mine grid	location	footwall	hangingwall	name	length [m]		name	length [m]		
19450E ± 80[1)]	just west of main western ore lens	~270m	~250m	TH148	550		TH37	500		
				TH410	440		TH40	590		
				TH410A	300	Σ1290m	TH62C	950	Σ2040m	Σ3330m
20080E ± 80[1)]	through main west Thalanga ore lens	~230m	~230m	TH234A	350		TH28	530		
				TH245	550		TH29	320		
				TH247	310	Σ1210m	TH41/A	600	Σ1550m	Σ2760m
20460E ± 50[2)]	western part of central Thalanga mineralisation	~280m	~120m	part of TH5	300		part of TH5	200		
				TH112	650		TH334	150		
				TH238	260	Σ1210m	C2047SD46	120	Σ470m	Σ1680m
20800E ± 100[1)]	eastern part of central Thalanga mineralisation	~300m	~100m	TH3	200		part of TH18	170		
				part of TH18	230		part of TH38	100		
				part of TH38	300					
				TH412A	580					
				TH412B	750	Σ2060m			Σ270m	Σ2330m
31980E ± 50[2)]	through main east Thalanga ore lens	~250m	~200m	TH85	600		TH382A	500		
				TH85A	300		TH401	130		
				TH270	380	Σ1280m			Σ630m	Σ1910m
32380E ± 50[2)]	just east of main eastern ore lens	~200m	~220m	TH61	280		TH402	400		
				TH144B	700					
				TH394	500	Σ1480m			Σ400m	Σ1880m
										Σ13890m

Sections through the Thalanga Range			
		thickness	stratigraphy exposed
	railway cutting[2)]	~400m	complete section through Mt Windsor Formation
19200E	Thalanga Range[2)]	~300m	surface exposure of Mt Windsor rhyolites

[1)] : logged in 1995

[2)] :logged/mapped in 1996

Table 2: Compilation of XRF data and thin sections

Section	DDH	Paulick		Herrmann (1994)		Hill (pers. com.)		Stolz (1991)		Wills (1985)		total	
		XRF	slides	XRF	slides	XRF	slides	XRF	slides	XRF	slides	XRF	slides
19450E (west)	TH37	2	7	-	-	-	-	10	10	10	12	22	29
	TH40	3	14	1	1	-	-	-	-	2	5	6	20
	TH62C	5	19	-	-	-	-	-	-	3	9	8	28
	TH148	6	5	-	-	-	-	-	-	-	-	6	5
	TH410	11	22	-	-	-	-	-	-	-	-	11	22
	TH410A	-	4	-	-	-	-	-	-	-	-	-	4
												Σ53	Σ108
20080E (west)	TH28	3	3	-	-	-	-	-	-	3	2	6	5
	TH29	1	2	-	-	-	-	-	-	2	4	3	6
	TH41/A	5	4	-	-	-	-	-	-	-	2	5	6
	TH243A	2	6	-	-	-	-	-	-	-	-	2	6
	TH245	1	3	14	4	-	-	-	-	-	-	15	7
	TH247	3	3	-	-	1	1	-	-	-	-	4	4
												Σ35	Σ34
20460E (central)	TH5	11	15	1	1	1	-	5	10	8	32	26	58
	TH112	8	14	9	-	-	-	6	6	1	2	24	22
	TH238	8	11	-	-	-	-	-	-	-	-	8	11
	TH334	2	4	-	-	-	-	-	-	-	-	2	4
	C2047SD46	7	14	-	-	-	-	-	-	-	-	7	14
												Σ67	Σ109
20800E (central)	TH3	1	1	-	-	-	-	-	-	-	4	1	5
	TH18	3	2	-	-	-	-	-	-	3	7	6	9
	TH38	4	4	-	-	-	-	-	-	8	8	12	12
	TH412A	3	3	-	-	-	-	-	-	-	-	3	3
	TH412B	3	3	-	-	-	-	-	-	-	-	3	3
												Σ25	Σ32
31980E (east)	TH85	11	11	-	-	-	-	-	-	-	-	11	11
	TH85A	7	9	-	-	-	-	-	-	-	-	7	9
	TH270	7	11	2	-	-	-	-	-	-	-	9	11
	TH382A	8	12	4	1	-	-	-	-	-	-	12	13
	TH401	5	4	-	-	-	-	-	-	-	-	5	4
												Σ44	Σ48
32380E (east)	TH61	8	11	-	-	-	-	-	-	-	-	8	11
	TH144B	6	7	10	-	-	-	-	-	-	-	16	7
	TH394	7	11	3	1	-	-	-	-	-	-	10	12
	TH402	8	10	-	-	-	-	-	-	-	-	8	10
												Σ42	Σ40

Other samples			
surface samples:			
railway cutting	12	15	
Thalanga Range (19200E)	2	3	
watertank hill area	3	4	Σ17 Σ22
miscellaneous:			
TH471 (33600E, contact to diorite intrusion)	2	3	
THRC-008 (north of Thalanga, contact to granite)	1	1	Σ3 Σ4
			Σ287 Σ397

porphyritic with fine to medium grained phenocrysts. Intrusions of very highly porphyritic rhyolites (> 20 % phenocrysts) with medium to coarse grained quartz and feldspar phenocrysts occur in the footwall, and the favourable horizon, and locally in the hanging-wall, however, extrusive units may also be present in the Favourable Horizon (Hill, 1996, pp. 122–124). These rocks have been refered to as 'QFP' (quartz - feldspar porphyries) or 'QEP' (quartz eye porphyries) in previous studies (Gergory et al, 1990; Herrmann, 1994; Hill, 1996). However, if a more descriptive terminology is applied it becomes apparent that there are more than one lithofacies that fits into the 'QFP/QEP' category (Fig. 3: railway cutting section). This is an important observation in the light of a proposed genetic link between base metal mineralisation and the emplacement of 'QFP/QEP' and 'QEV' units in the favourable horizon (Sainty and Hill, 1996) and the apparent geochemical heterogeneity of the 'QFP/QEP' group (see below).

Massive, non graded, monomict rhyolite breccia with gradational contacts into coherent facies are the principal clastic lithofacies in the MWF (Fig. 4) and are interpreted as in-situ or re-sedimented hyaloclastites (Fig. 4). Their positive identification requires at least one of the following textural observations: preserved clast outlines, heterogeneous phenocryst distribution (variably porphyritic clasts, crystals concentrated in matrix, differences in crystal size between clasts and matrix) or the presence of rotated, flow laminated clasts.

The discrimination of coherent and clastic facies and the identification of individual emplacement units is a very challenging task in the strongly altered, deformed and metamorphosed parts of the footwall rhyolite below the mineralisation. The original groundmass of the rhyolite and the feldspar phenocrysts have been extensively replaced by variable proportions of phyllosilicates (sericite and chlorite) during hydrothermal alteration. Domainal alteration with gradational or sharp contacts between siliceous domains and phyllosilicate-rich domains is very common, resulting in pseudoclastic textures of the rhyolite (Fig. 4). Therefore, the distribution, size range and abundance of quartz phenocrysts are crucial observations as these are the only components of the rocks that are unlikely to have been affected by hydrothermal alteration. However, thin section examinations are essential in order to confirm field observations in highly altered parts of the sequence, because the abundance of quartz phenocrysts can sometimes easily be misjudged. For example, in strongly silicified domains the abundance of quartz phenocrysts may be substantially underestimated because they are often virtually undistinguishable from the groundmass in hand specimen. Conversely, phyllosilicate altered domains may contain abundant small siliceous kernels (relicts of perlite?) superficially resembling quartz crystals, causing phenocryst abundances to be overestimated in hand specimen (Fig 4).

The railway cutting: a section through the MWF in a distal position to the Thalanga mineralisation

A complete section of the MWF is exposed in the railway cutting through the Thalanga Range (Figs 1, 3). The top part of the PCF and the base of the TCF are exposed in outcrops along the Flinders Highway adjacent to the railway line.

The base of the MWF is occupied by very highly quartz -feldspar phyric intrusions. The older one is moderately chlorite/biotite-sericite altered and contains ~15% quartz phenocrysts and ~15% feldspar phenocrysts with 1–4 mm diameter. The younger intrusion is unaltered and has a higher feldspar to quartz phenocryst ratio and the phenocrysts are medium to coarse grained (1–6 mm). The moderately porphyritic fine to medium rhyolite lavas on top of these intrusions can be divided into two principal units based on contact relationships and differences in phenocryst assemblages. Both units have 3–5% quartz phenocrysts, and while the lower one also contains significant amounts of feldspar phenocrysts, the upper one is very feldspar phenocryst poor (<< 1%). These rhyolite units are dominantly coherent with minor intervals of monomict rhyolitic breccia which commonly have gradational contacts into coherent facies and can be interpreted as in-situ and resedimented hyaloclastites.

Fig. 3: Stratigraphy of the Mount Windsor Formation in the railway cutting (Thalanga Range) (upper part)

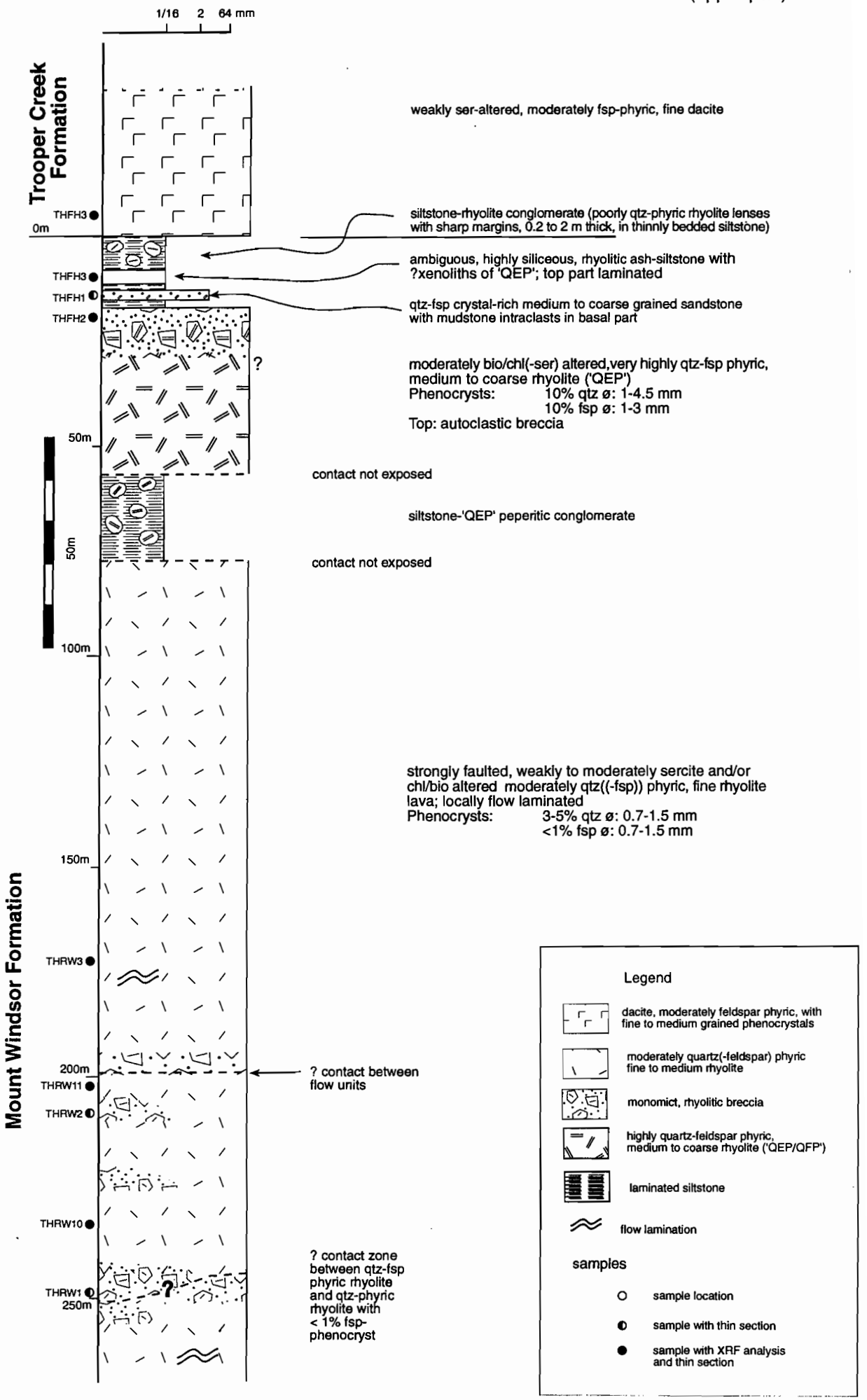

Fig. 3: Stratigraphy of the Mount Windsor Formation in the railway cutting (Thalanga Range) (lower part)

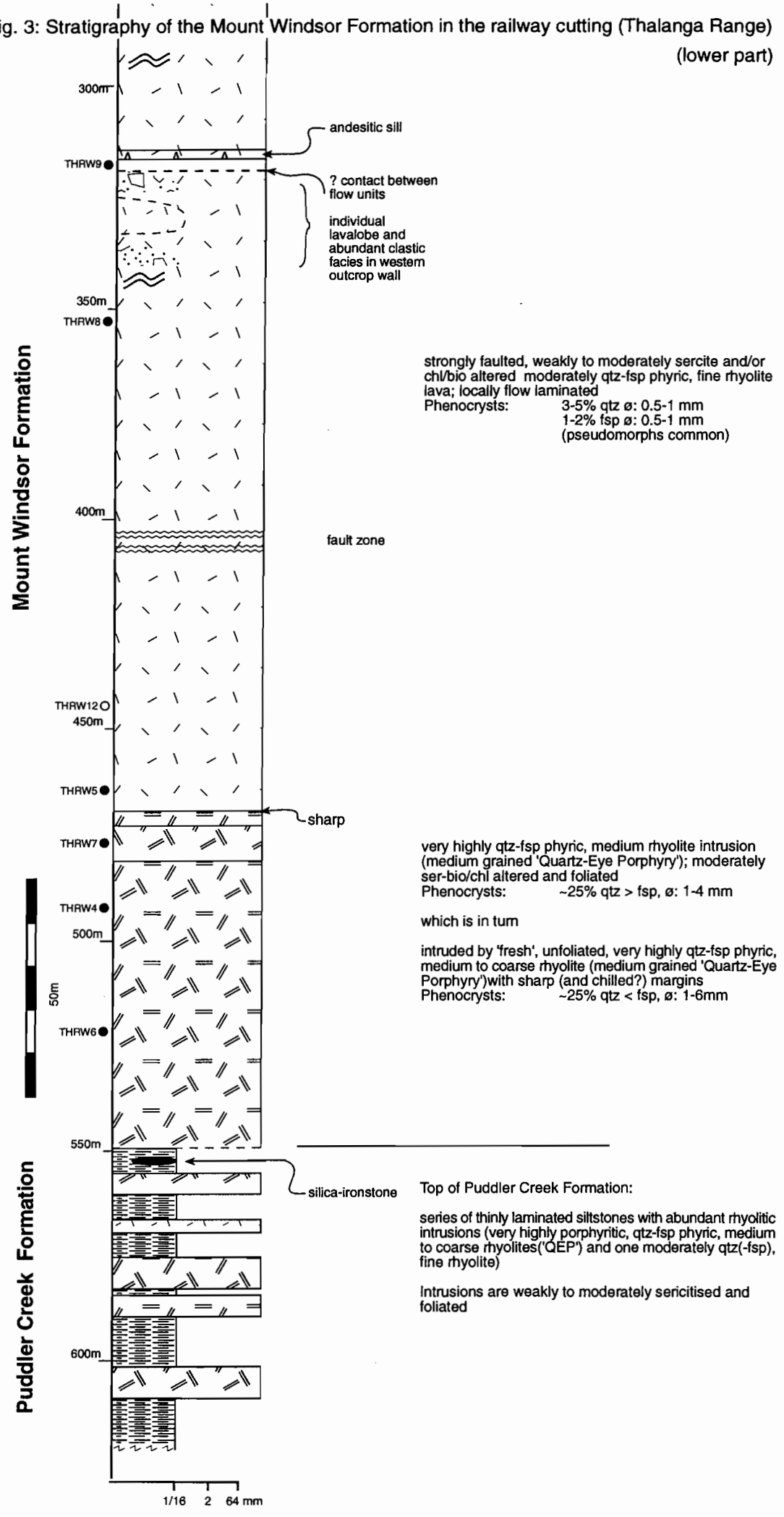

The favourable horizon is exposed in gullies and outcrops along the Flinders Highway and has a stratigraphic thickness of ~70 m. It consists of a diverse lithofacies association comprising siltstones, siltstone-rhyolite peperitic conglomerate, very highly quartz-feldspar-phyric medium-coarse rhyolite in coherent and monomict clastic facies, quartz-feldspar crystal-rich sandstone and an ambiguous, highly siliceous, very poorly quartz -phyric rhyolitic ash-siltstone. The top contact of the favourable horizon with feldspar-phyric dacite (TCF) is sharp and conformable.

Some important conclusions can be drawn from the observations in the railway cutting section. Weakly altered, essentially feldspar phenocryst-free rhyolite lavas have been recognised immediately below the ore position in this section. This suggests that the absence of feldspar phenocrysts in strongly altered rhyolite below the Thalanga mineralisation does not necessarily indicate that they must have been destroyed beyond recognition. The presence of three discrete units of very highly porphyritic rhyolite in the railway cutting section reinforce the conclusion that a number of units with 'QEP/QFP' characteristics were emplaced in the Thalanga sequence over a period of time (cf. Paulick, 1996). A period of reduced volcanic activity may be indicated by the accumulation of siltstones in the favourable horizon. The highly siliceous ash-siltstone may be interpreted as a distal ash deposit from a rhyolitic, explosive eruption elsewhere in the region.

Lithofacies association in the hangingwall

The hangingwall consists of a variable volcano-sedimentary sequence dominated by weakly to moderately altered feldspar-phyric dacite lavas and intrusions (Fig. 2 and Fig. 5). The abundance and size of feldspar phenocrysts varies substantially and the texture of the dacite units ranges from aphyric to moderately and highly porphyritic. One unaltered highly feldspar -phyric, medium to coarse dacite intrusion has been intersected in the footwall (DDH TH85, section 31980E) which probably represents a feeder dyke to the hangingwall dacite. Andesitic lavas and intrusions are abundant in sections through the central part of Thalanga. One very highly quartz-feldspar-phyric, coarse rhyolite unit occurs in the upper part of the hangingwall in west Thalanga (section 19460E). Moderately porphyritic rhyolite clasts and fine to medium quartz crystals occur in some mass flow deposits in the hangingwall. This indicates that rhyolite with similar textural characteristics to the rhyolite in the Thalanga footwall were eroded in the source area of these volcaniclastic units.

The sedimentary lithofacies association of the hangingwall sequence comprises monomict dacite breccia (in-situ and resedimented hyaloclastites), polymict dacite-rhyolite breccia, quartz-feldspar crystal-rich, coarse sandstone (± mudstone intraclasts), mudstone-siltstone commonly punctuated by beds of normal graded feldspar crystal-rich turbidites, and minor occurrences of silica-ironstone. The facies arrangement varies substantially between cross sections. The quartz-feldspar crystal-rich coarse sandstone facies and the mudstone/siltstone-turbidite facies appear to be restricted to the western sections possibly indicating a more proximal position to the source areas of these deposits.

Alteration of the Thalanga sequence

Alteration of the Thalanga sequence is most intense in the immediate footwall to the mineralisation where the rhyolites of the MWF have been intensely modified in texture and composition compared to the rhyolites in the railway cutting (Fig. 4). The most abundant alteration minerals are sericite and chlorite, however, due to the metamorphic overprint, biotite is also common. The abundance and proportion of sericite, chlorite and biotite vary widely over short core intervals and even on a cm-scale, resulting in apparent clastic textures of the rocks (cf. Allen, 1988). The texture of such domainal altered parts of the footwall rhyolites is often superficially similar to textures of pyroclastic deposits (Fig. 4). Such 'pseudoclastic' textures have not been observed in the hangingwall dacite, where phyllosilicate alteration occurs mainly as fine interconnected networks in the groundmass (Fig. 5). Massive white

BLANK

Figure 4:

a) monomict rhyolite breccia (sample THRW2, railway cutting)

b) pseudoclastic texture in coherent rhyolite, chlorite and biotite-rich domains appear as apparent clasts in a quartz-rich groundmass (sample TH410-312.80, section 19460E, west Thalanga)

c) patchy to vein-controlled epidote alteration in coherent dacite (sample TH62C-825.20, section 19460E, west Thalanga)

d) gradational contact between massive 'white silica' alteration and domainal phyllosilicate-silica alteration in coherent rhyolite (sample TH410-323.0, section 19460E, west Thalanga)

e) core interval of coherent dacite with variations in alteration facies (fresh, epidote alteration and 'red rock' alteration). Samples (from left to right) TH112-420.0, TH112-404.0, TH112-388.60, TH112-370.0 (section 20460E, central Thalanga)

f) dacite tube pumice clact from a politmict dacite-rhyolite breccia in the hangingwall (sample TH38-404.50, section 20800E , central Thalanga; clast diameter ~2 mm)

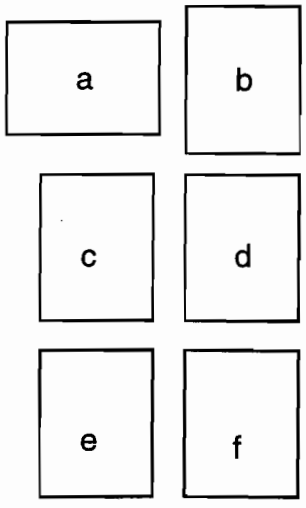

BLANK

Figure 5:

a) strongly sericite-chlorite-biotite altered, coherent rhyolite with strong foliation. Siliceous kernels between phylosilicate bands can easily be misidentified as quartz phenocrysts in hand-specimen leading to an overestimation of phenocryst abundance. Sample TH243A-249.20, section 20800E, PPL)

b) same picture as a) with nicols crossed. Some siliceous kernels contain quartz phenocrysts while others may be relicts of silicious groundmass or kernels of perlite.

c) phyllosilicate alteration commonly occurs as interconnected, network-shaped domains of biotite ± chlorite in coherent dacite (sample TH40-68.79, section 19460E, PPL)

d) the intergrowth of chlorite and biotite in altered coherent rhyolite suggests that biotite was formed by a reaction involving chlorite during metamorphism (sample TH85-214.80, section 31980E, PPL)

e) the outline of a rhyolite clast in a monomict rhyolite breccia in preserved by an hematite coating (sample THRW2, railway cutting, PPL)

f) disseminated epidote crystals in the groundmass of coherent dacite (sample TH62C-825.25, section 19460E, PPL).

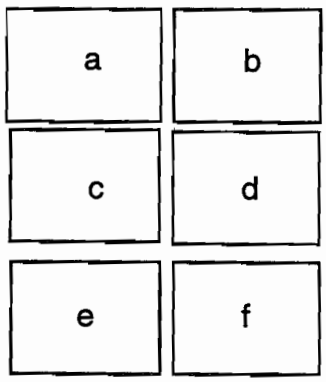

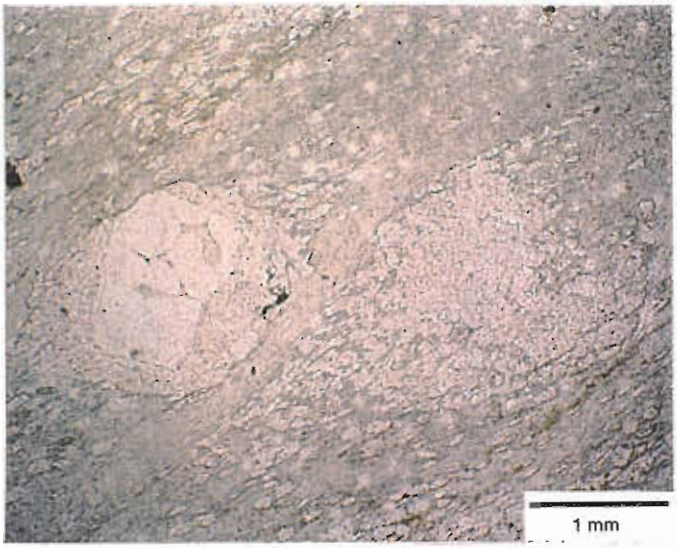
1 mm

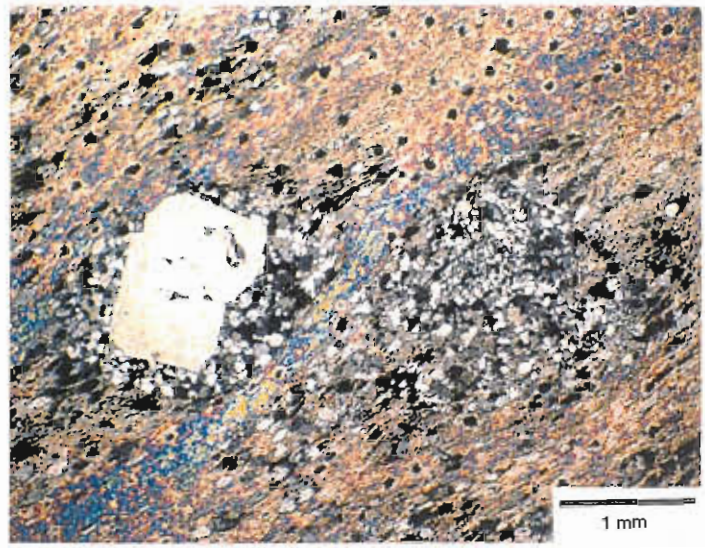
1 mm

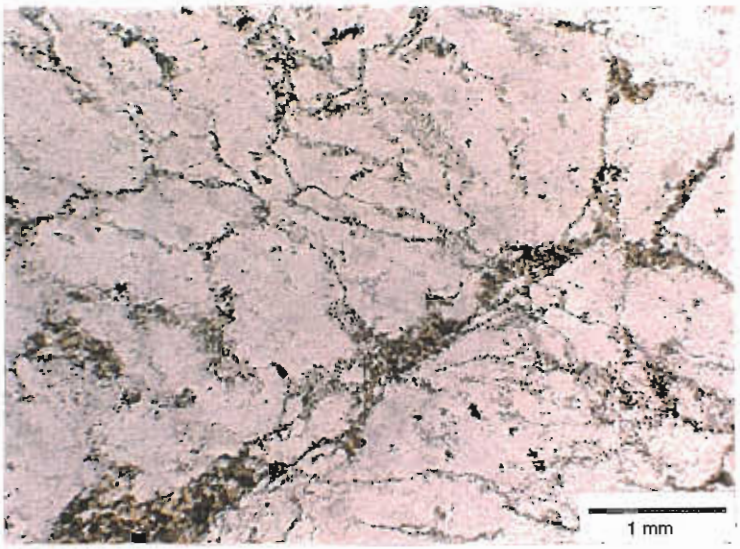
1 mm

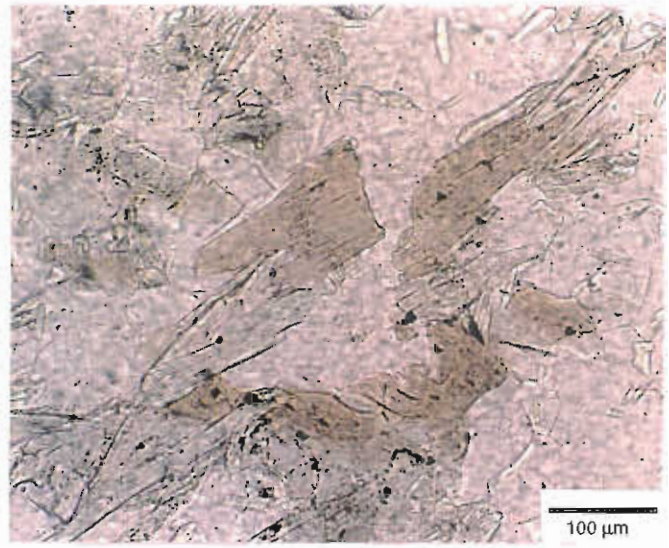
100 µm

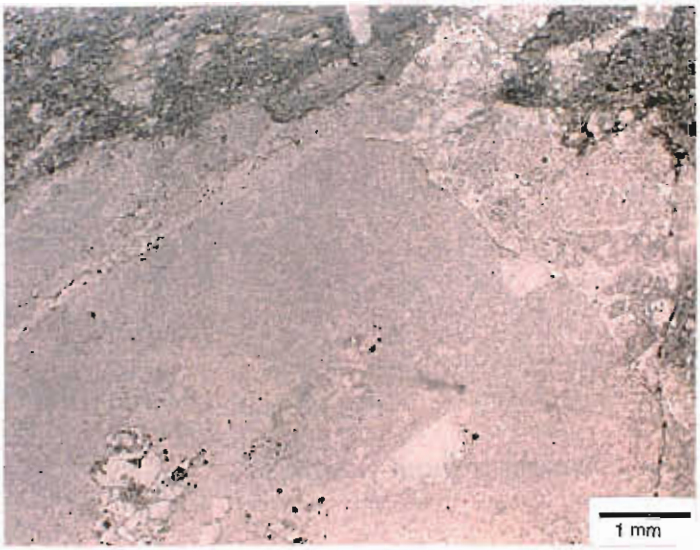
1 mm

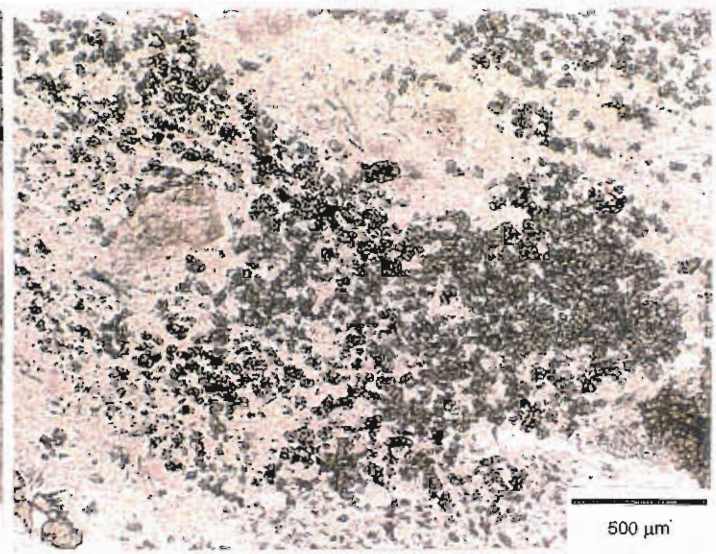
500 µm

Fig. 6: Example of a graphic log representing lithofacies and alteration facies (DDH TH270: section 31980E)

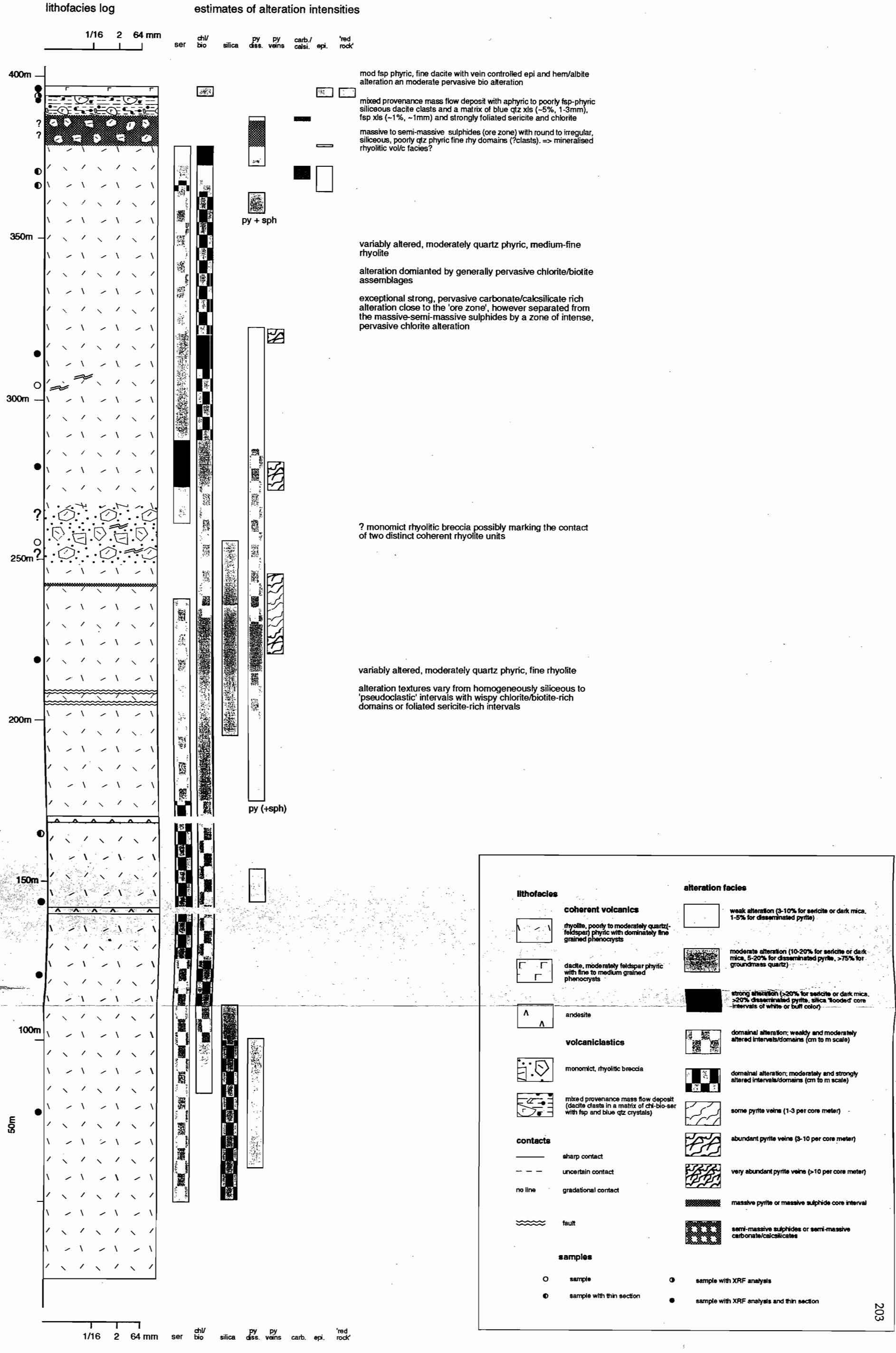

silica alteration occurs as core intervals of 1–10 m length or as irregular to lensoidal shaped domains of 5–20 cm diameter. Pyrite has been observed as disseminated crystals within the groundmass and as veins or veinlets (0.1 cm – 1 cm wide). Carbonate-calcsilicate alteration in the footwall can be patchy or massive but is generally restricted to the uppermost part of the footwall, locally grading into massive carbonate-chlorite-tremolite 'pseudo-exhalite' (Herrmann, 1994). Patchy to vein controlled epidote alteration (Fig. 5) occurs sporadically in the footwall but is widespread and prominent in the dacite of the hangingwall. An enigmatic patchy-vein controlled to pervasive 'red rock' alteration facies (Fig.5) is also common in the hangingwall dacite and rare in the footwall. It has previously been assumed that the red staining was indicative of albite alteration and the geochemical data for the dacites indicate that Na-metasomatism did indeed occur in the hangingwall (Fig. 10b). However, the albite altered dacites are not necessarily red and the red stained dacites are not necessarily albite altered. Further work is required to constrain the cause and significance of 'red rock' alteration in the Thalanga area. Therefore, at present this alteration facies is best refered to in purely descriptive terms.

Estimates of the abundance of alteration minerals provide important information on the type and the intensity of alteration. However, the mineralogy of the altered rocks has been substantially modified due to the metamorphic overprint on the Thalanga sequence, which has to be taken into account. In order to visualise the variation in alteration type and intensity in diamond drill cores logged during this project, the relative abundance of several alteration facies have been plotted along side the graphic logs (Fig. 6).

The abundance of sericite, chlorite+biotite, disseminated pyrite and epidote have been estimated while logging the core and in thin sections. Chlorite and biotite are assigned to one alteration facies because textural evidence indicates that biotite has formed by metamorphic reactions involving chlorite (Fig.4). Furthermore, it is usually not possible to obtain reliable separate estimates of the abundance of chlorite and biotite in hand specimen due to the intimate intergrowth of these two minerals. Even though biotite contains significant amounts of potassium, it can be assumed that the combined abundance of chlorite and of biotite represents an approximate measure of Mg(-Fe) metasomatism in the footwall during hydrothermal alteration.

Estimates for the intensity of silicification, pyrite veining, carbonate-calcsilicate alteration and 'red rock' alteration were recorded during logging of the drill core. Divisions of weak, moderate and strong alteration, and two categories of domainal alteration, have been assigned to the abundance of the individual alteration facies.

The geometry of the hydrothermal system should be reflected in systematic variation in the alteration facies along strike, down dip and with stratigraphic depth. The spatial arrangement of alteration facies in cross section can be assessed by plotting the alteration logs along the drill hole traces. Such plots have been prepared for section 31980E (Fig. 8).

The geology of section 31980E is relatively simple and can be summarised as follows (Fig 7). The footwall consists of a moderately quartz-phyric fine rhyolite lava with a minimum stratigraphic thickness of 120 m. The rhyolite is locally topped by a coarse quartz-feldspar crystal-rich sandstone which is in turn overlain in one case (DDH TH85A) by another coherent rhyolite. Massive sulphide mineralisation occurs within the top part of the rhyolite, and within the overlying crystal-rich sandstone. An extensive polymict rhyolite-dacite mass flow deposit, devoid of sulphides, covers this sequence. It is strongly foliated and contains lensoidal (deformed) siliceous dacite clasts which commonly show normal grading. Rhyolite clasts with quartz and feldspar phenocrysts have been observed in DDH TH85. The matrix consists of strongly foliated sericite-chlorite-biotite, blue quartz crystals (1–3 mm, 3–5%) and feldspar crystals (≤1 mm, 2–5%). The mass flow deposit is overlain by an aphyric to poorly feldspar phyric, fine coherent dacite in the hangingwall.

About 200 m of hangingwall stratigraphy have been intersected in DDH TH382A, exposing a sequence dominated by variably porphyritic dacite

units with feldspar phenocrysts mainly in the 0.3 to 0.8mm size range. The abundance of feldspar phenocrysts increases from ≤ 1% at the base of the sequence to up to 30% higher up in the stratigraphy. In the upper part of DDH TH382A, a complex facies association is exposed. Based on contact relationships and the arrangement of clastic and coherent facies the interval is best interpreted as a normal graded, monomict dacitic mass flow intruded by poorly pyroxene-phyric andesite. The andesite (Ti/Zr ~50) is strongly biotite-chlorite altered and contains siliceous, feldspar-phyric dacite clasts, suggesting that significant peperitic mixing of fluidal andesitic magma and unconsolidated sediment occurred during emplacement.

The alteration intensity logs have been plotted onto the cross section alongside the drill hole traces (Fig. 8). It is apparent that the intensity of alteration in the footwall does not steadily increase towards the ore horizon, rather a 'waxing and waning' in the abundance of sericite, chlorite, biotite, groundmass quartz (silicification), disseminated pyrite and pyrite veins can be observed. However, a qualitative correlation between the abundance of chlorite-biotite and disseminated pyrite and pyrite veins can be observed, whereas the abundance of sericite does not seem to be correlated with the abundance of sulphides. The intensity of chlorite/biotite and pyrite alteration is particularly high just below the ore zone in the top ~20 m of the rhyolite. It drops to moderate levels in an apparently stratabound zone about 50 m below the dacite contact. Another zone of intense chlorite/biotite-pyrite alteration at about 70 m to ~90 m below the dacite contact also seem to have a stratabound geometry. Below this stratigraphic level the footwall rhyolite is only weakly to moderately altered. Carbonate alteration and epidote alteration are mainly confined to the immediate host rocks of massive and semi-massive sulphide mineralisation. The dacites in the basal part of the hangingwall are moderately to strongly epidote (+ actinolite) altered and contain very minor sericite, chlorite or biotite. Epidote is absent from ~50 m above the base of the hangingwall where variable amounts of sericite, chlorite and biotite become the dominate alteration phases. The hangingwall sequence shows a consistent decrease of 'red rock' alteration up stratigraphy.

The observed variations in alteration intensity may indicate that the hydrothermal system had zones of preferred fluid flow causing intense alteration in selected stratabound zones. However, the spacing of drill core is not dense enough for definite conclusions to be drawn and the distribution of alteration facies may also be interpreted as individual patches of intense alteration which are not connected with each other. Furthermore, the foliation of incompetent, phyllosilicate-rich parts of the altered footwall indicates that shearing did occur during regional folding. Therefore, it must be taken into account that the original geometry of the alteration system has probably been modified during deformation possibly even to a degree where original 'pipe-like' structures are sheared into positions with a low angle to stratigraphy.

Geochemistry

The chemical composition of the felsic volcanics in the Thalanga sequence varies widely indicating that most elements have been mobile during hydrothermal alteration. Nevertheless, TiO_2 and Zr values for the footwall rhyolite and the hangingwall dacite plot on radial alteration lines (Fig. 9a) satisfying the test for chemical immobility of MacLean & Barrett (1993). The narrowly constrained Ti/Zr ratios (~4, range 3–5) of the rhyolite units in the footwall indicate that they were derived from a large, homogeneous, high-silica magma source. A likely process to produce large volumes of high-silica magma with a fairly uniform composition is extensive melting of continental lithosphere (cf. Stolz, 1995). The data for the hangingwall dacite units defines two radial lines except for a sample of a dacite dyke from the footwall with an exceptionally high Ti/Zr ratio. One group has an average Ti/Zr ratio of ~11 while the other has a more mafic composition with an average Ti/Zr ratio of ~18.5 (Fig. 9a). The identification of two petrogenetically distinct dacite groups in the hangingwall is a new development and future

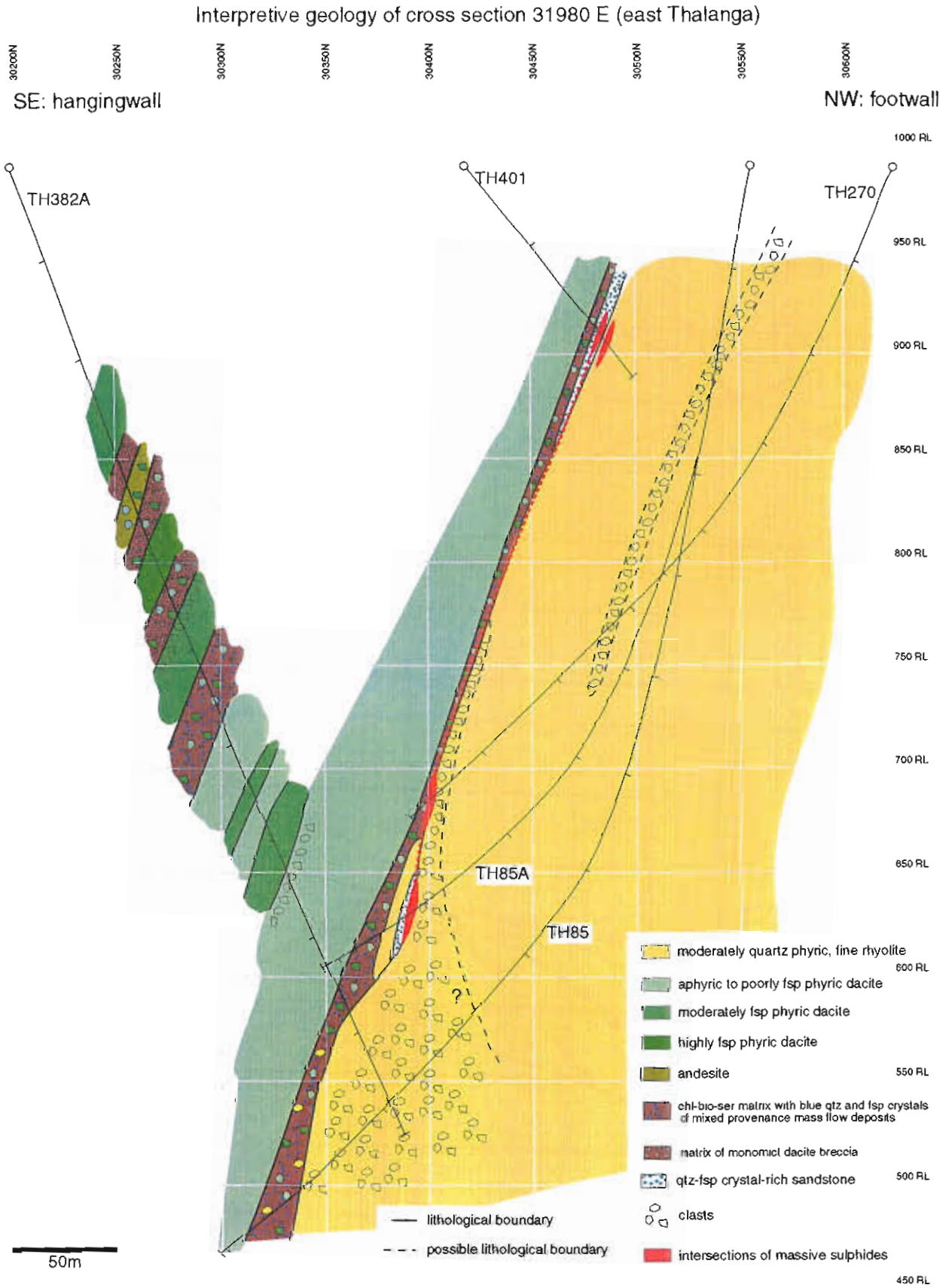

Fig 7. Interpretive geology of section 31980E (east Thalanga)

Fig. 8: Geometry of alteration facies at Thalanga - cross section 31980 E

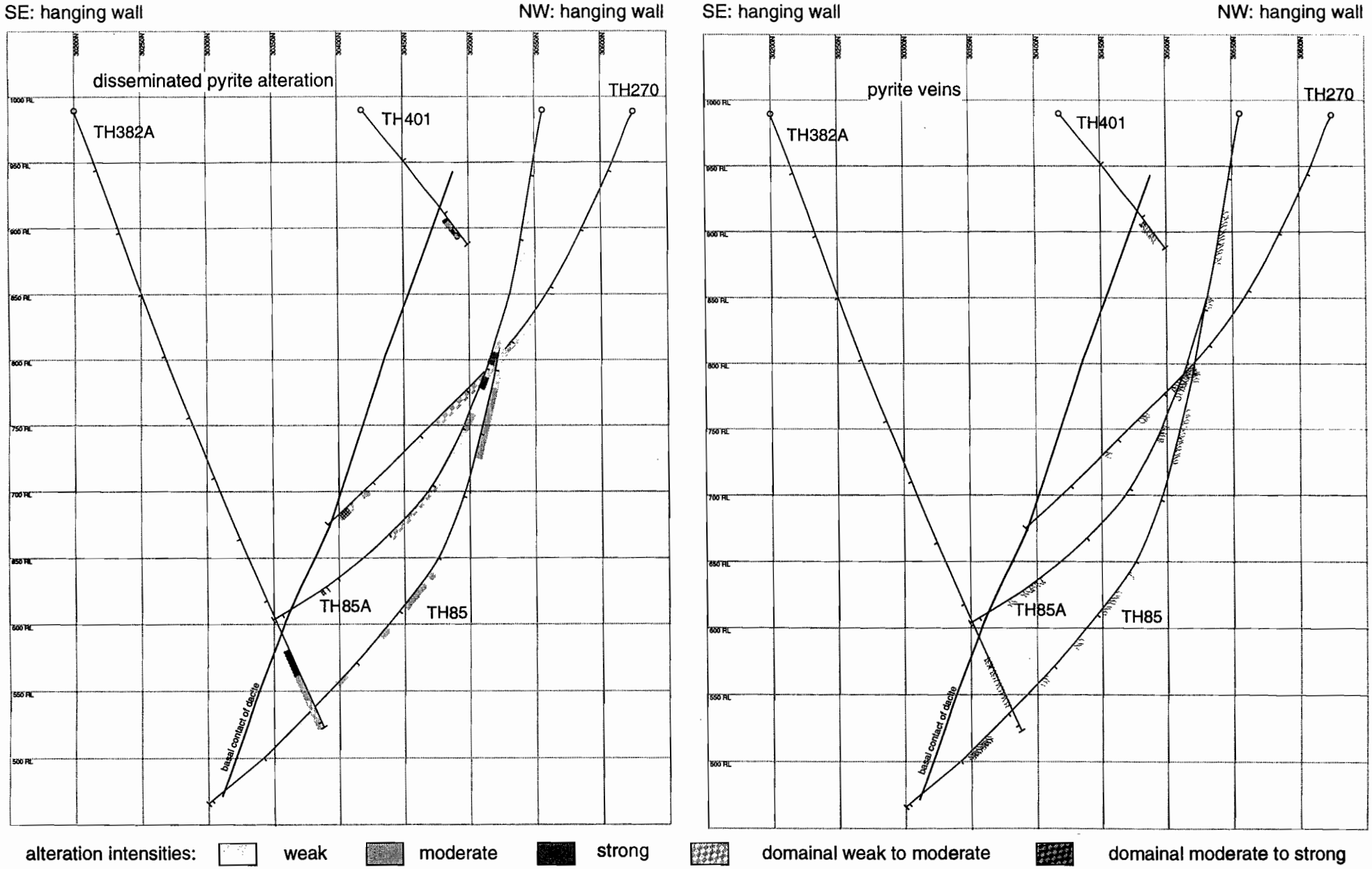

Fig. 8: Geometry of alteration facies at Thalanga - cross section 31980 E

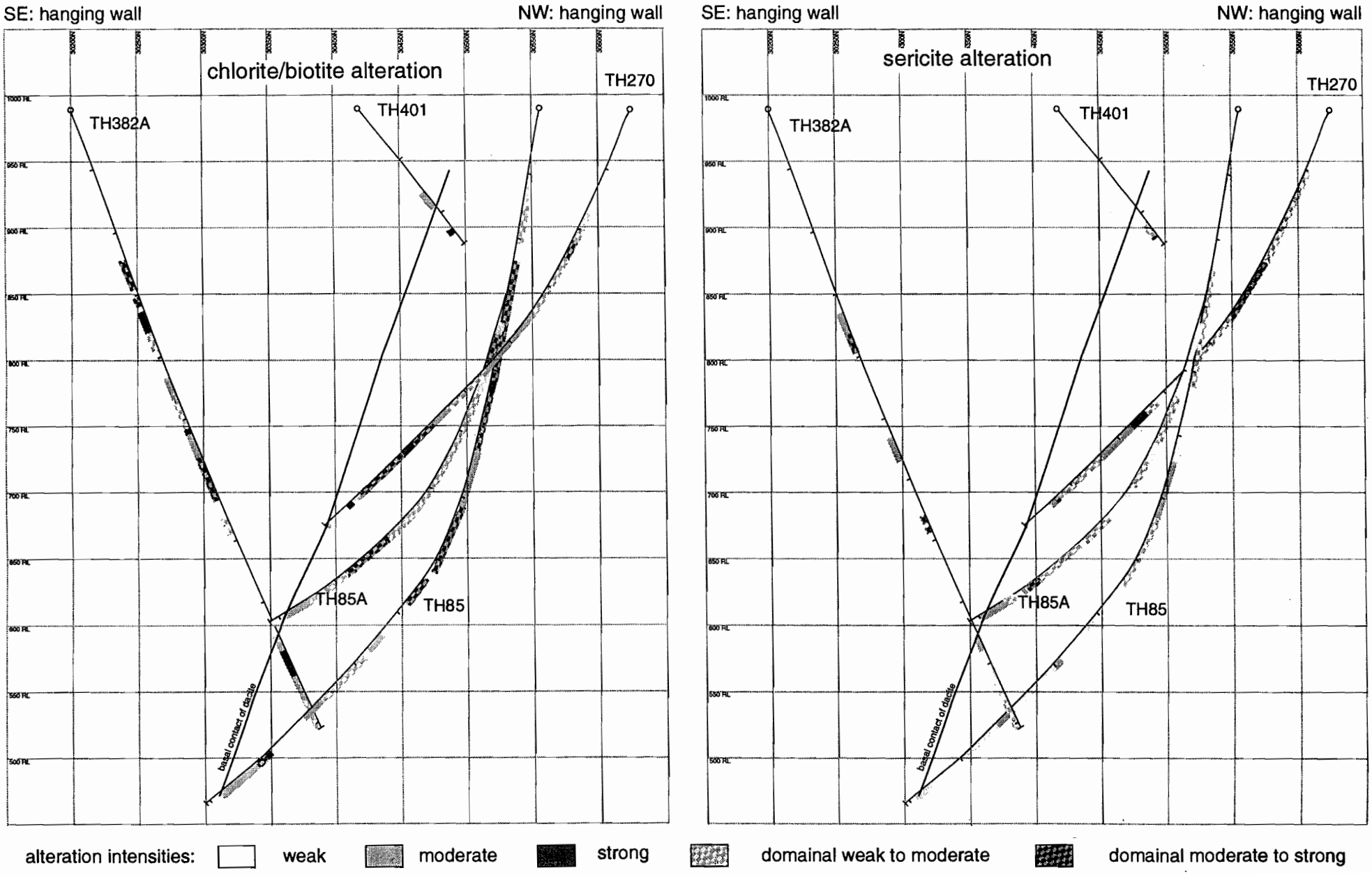

Fig. 8: Geometry of alteration facies at Thalanga - cross section 31980E

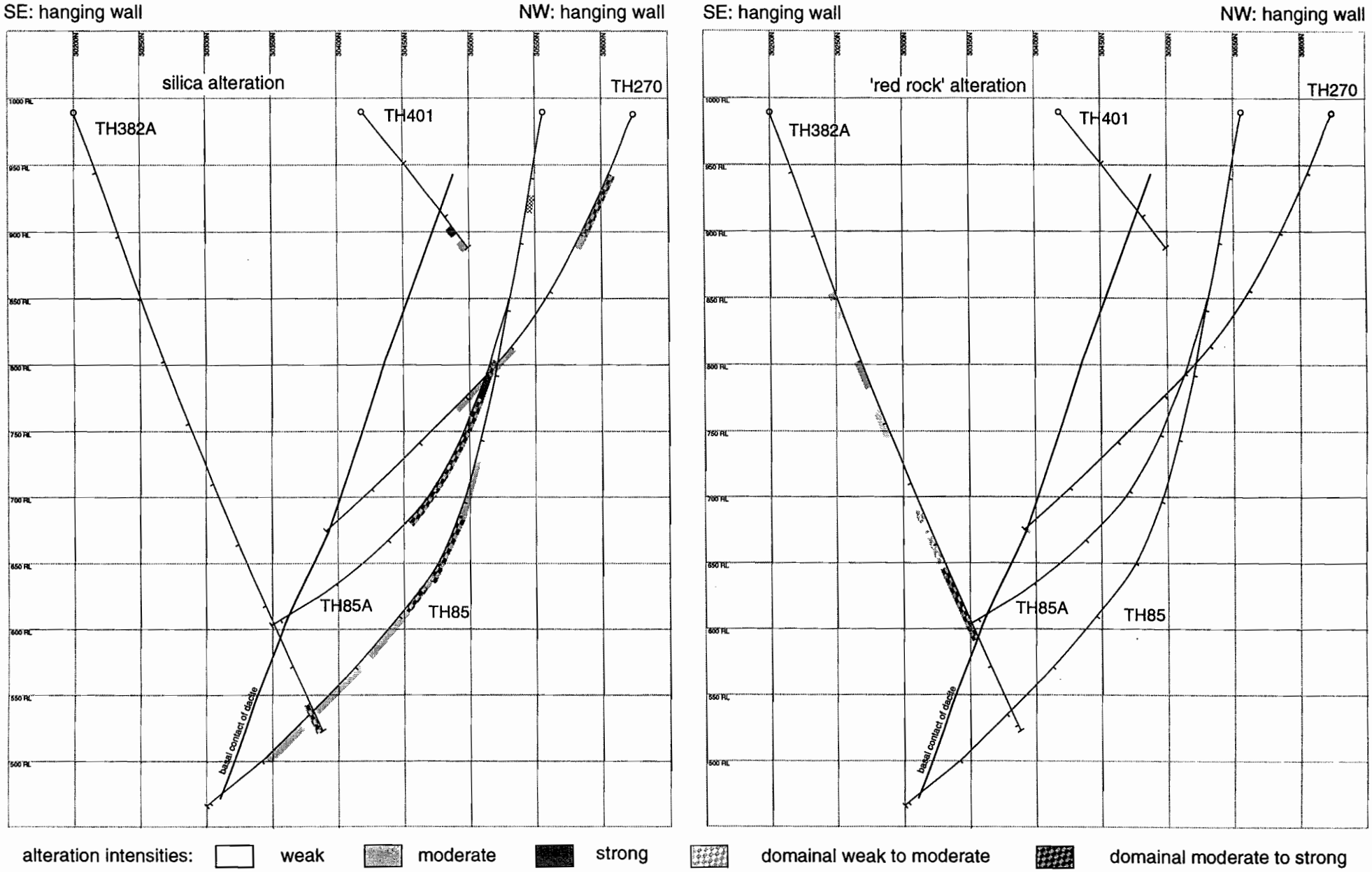

Fig. 8: Geometry of alteration facies at Thalanga - cross section 31980 E

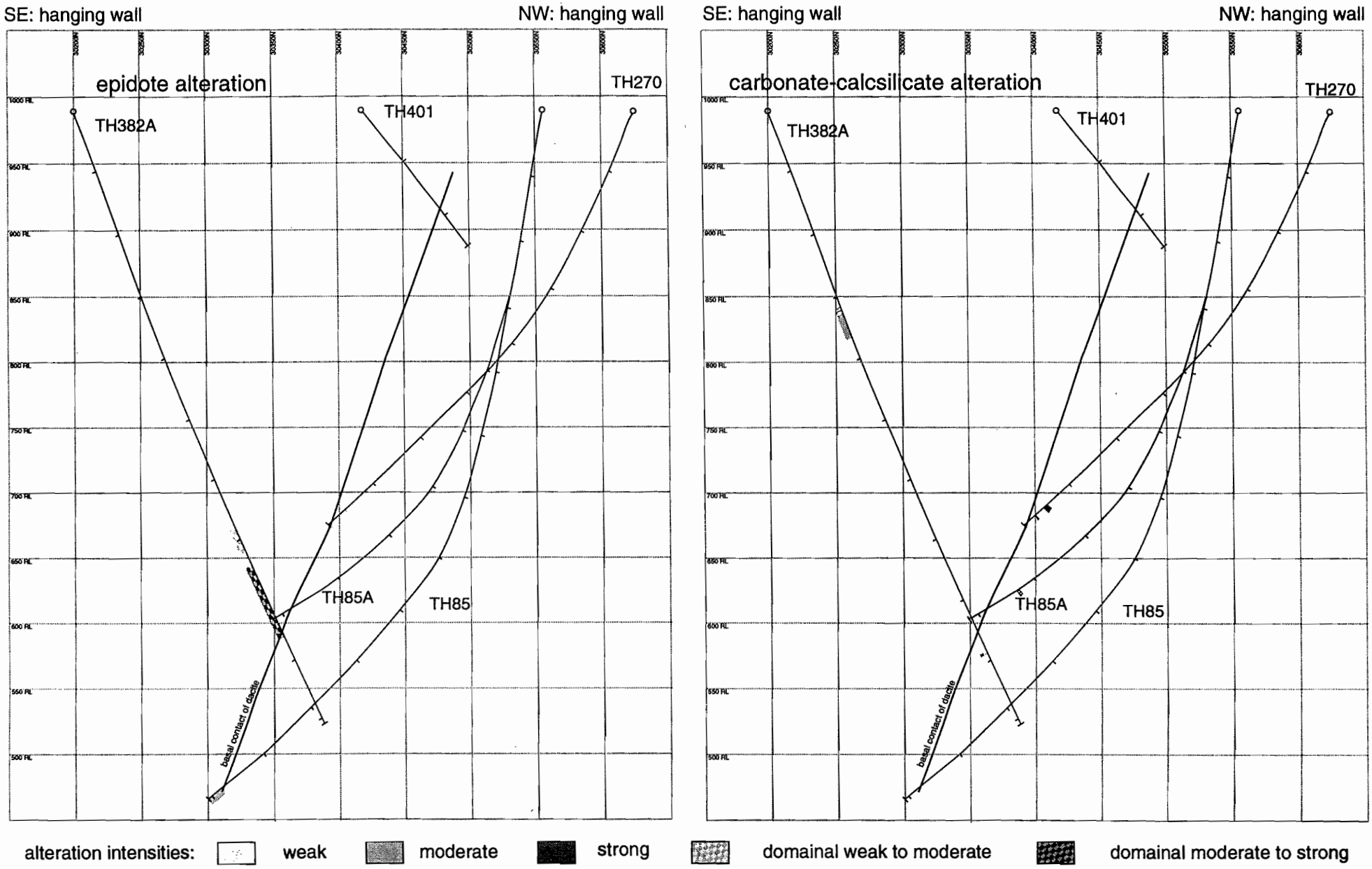

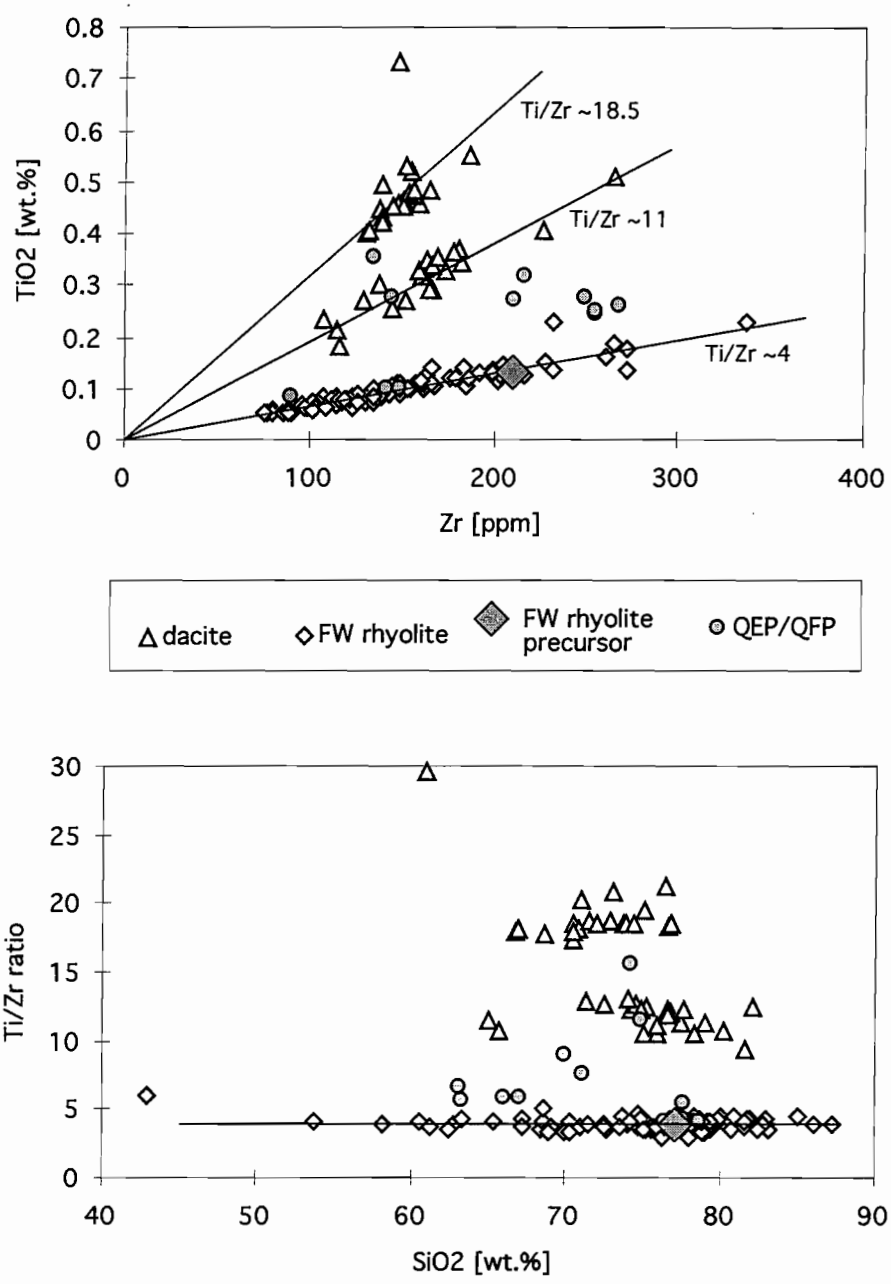

Fig. 9. (A) The TiO2 and Zr values for footwall rhyolite and hangingwall dacite plot on radial lines. Analyses of 'QEP/QFP' rocks do not show systematic variations. (data: this study). (B) Ti/Zr vs SiO2 scatter plot for footwall rhyolites hangingwall dacites and 'QEP/QFP' rocks. (data: this study)

research will address the question wether they represent temporally and/or spatially discernible phases of volcanic activity. The existence of two distinct dacite groups was not obvious previously because XRF data from several sources were combined (Paulick, 1996). Apparently, this caused significant 'artificial' scatter attributable to differences in preparation and measurement methods applied by different XRF laboratories. The distribution of analyses for 'QEP/QFP' does not provide evidence for a straightforward interpretation. However, a 'low Ti' group (≤ 0.1 wt.% TiO_2) with Ti/Zr ratios of ~4 and a 'high Ti' group (> 0.2 wt.% TiO_2) with Ti/Zr ratios ranging from 6 to 16 may be distinguished.

The constant Ti/Zr ratio of the footwall rhyolite indicates that geochemical modifications due to hydrothermal alteration can be assessed in a single precursor system. Therefore, it is justified to calculate one approximate precursor composition from the moderately quartz(-feldspar) porphyritic rhyolite units in the railway cutting which are inferred to represent the direct stratigraphic equivalent to the altered footwall rhyolite units below the Thalanga mineralisation. Samples with minimal alteration were selected to calculate the average composition of the 'least altered footwall rhyolite' in the Thalanga area (Table 3). This average composition is similar to the compositional range of modern, unaltered, high-silica arc volcanics (Stolz, 1996). The slightly higher MgO and SiO_2 values and lower CaO contents of the least altered Thalanga rhyolite is probably due to some degree of low temperature alteration. The base metal concentrations are well within the range of modern, unaltered high-silica arc volcanics.

The hangingwall dacite units represent two petrogenetic groups with distinct precursor compositions. These will be defined during the course of this project in order to assess the geochemical effects of alteration in the hangingwall.

The 'QEP/QFP' units represent a geochemically diverse group. Their variability in Ti/Zr ratios is not correlated with SiO_2, indicating that the Ti/Zr decrease of the samples is not a result of continuous fractionation of one parental magma (Fig. 9b). It is unclear wether they are petrogenetically related to the rhyolite or dacite units in the Thalanga sequence or wether they represent independent magma batches.

The SiO_2 contents of the footwall rhyolites range from 42 to 87 wt.% while the Ti/Zr ratios are narrowly constrained (Fig. 9b). This demonstrates that silica was mobile during hydrothermal alteration causing significant SiO_2 depletion and enrichment relative to the inferred precursor value of 77.5 wt.%. The SiO_2 values for the two dacite groups are less variable indicating that silica was significantly less mobile during hangingwall alteration (Fig. 9b). On average, the low Ti/Zr group has a higher SiO_2 concentration than the high Ti/Zr group. This is broadly consistent with a magmatic fractionation process causing concurrent SiO_2 increase and Ti/Zr ratio decrease.

The footwall rhyolites show very pronounced geochemical changes which correlate with the observed alteration facies and are therefore interpreted to represent the geochemical effects of hydrothermal alteration (Fig. 10a). In a plot of the Alteration Index (A.I., Ishikawa et al., 1976) versus the Chlorite-Carbonate-Pyrite Index (CCP, Large,

Fig 10 (opposite). Scatter diagrams illustrating the effects of alteration on the composition of footwall rhyolites and hangingwall dacites (data: this study). (A) CCP vs AI scatter plot for footwall rhyolites and hangingwall dacites. The rhyolites are shown in variable colour corresponding to alteration facies. (B) Na_2O+K_2O vs $K_2O/(K_2O+Na_2O)*100$ (K_2O ratio) variation diagram with fields for unaltered volcanics (igneous spectrum), K-metasomatism and Na- metasomatism(adopted from Bromley-Challenor, 1988). The dacites are shown in variable colour corresponding to alteration facies. (C) Mn carbonate index versus CCP for hangingwall dacites illustrating the different trends induced by epidote and chlorite/biotite alteration.

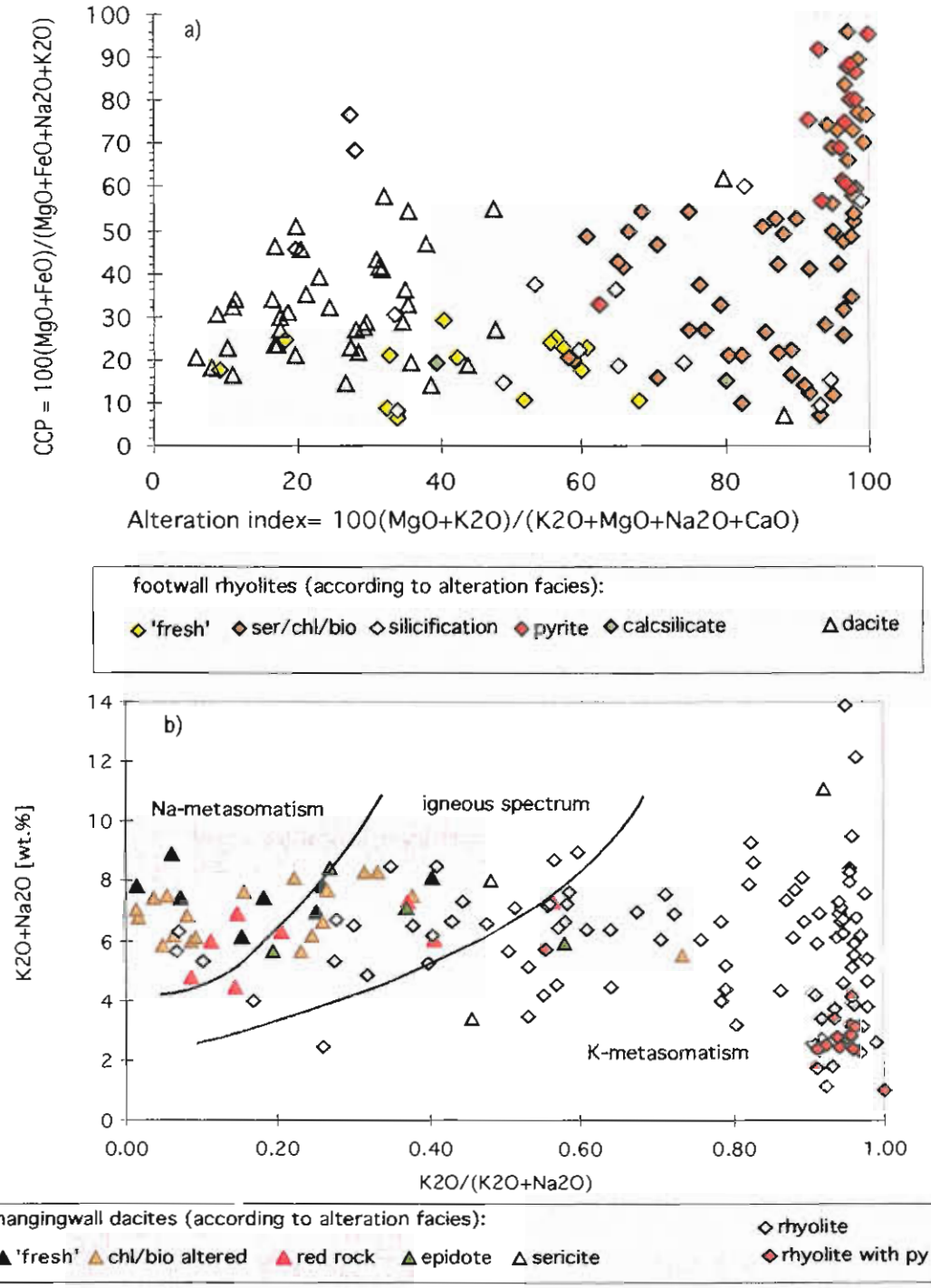
a)
CCP = 100(MgO+FeO)/(MgO+FeO+Na2O+K2O)
Alteration index= 100(MgO+K2O)/(K2O+MgO+Na2O+CaO)
footwall rhyolites (according to alteration facies):
'fresh'
ser/chl/bio
silicification
pyrite
calcsilicate
dacite
b)
Na-metasomatism
igneous spectrum
K-metasomatism
K2O+Na2O [wt.%]
K2O/(K2O+Na2O)
hangingwall dacites (according to alteration facies):
'fresh'
chl/bio altered
red rock
epidote
sericite
rhyolite
rhyolite with py
c)
Mn carbonate index = 100(caO+10MnO)/(CaO+10MnO+K2O+Na2O
CCP = 100(MgO+FeO)/(MgO+FeO+Na2O+K2O)

Tab. 3: XRF analyses of samples from the railway cutting and calculated average composition of a least altered footwall rhyolite in the Thalanga area.

XRF number	THFH4	THFH3	THFH2	THRW3	THRW11	THRW10	THRW9	THRW8	THRW5	THRW7	THRW4	THRW6	composition of least altered footwall rhyolite (MWF) in the Thalanga area		approx. values for modern, unaltered, high-silica arc volcanics (after Stolz, 1996)
sample bag no.	THFH4	THFH3	THFH2	THRW3	THRW11	THRW10	THRW9	THRW8	THRW5	THRW7	THRW4	THRW6	Average composition of weakly altered, moderately qtz(-fsp) porphyritic rhyolite in the railway cutting (average of samples: THRW3, THRW8, THRW9 and THRW10)		
DDH	surface	surface	surface	surface	surface	surface	surface	surface	surface	surface	surface	surface			
interval	Flinders Hwy	Flinders Hwy	Flinders Hwy	RW cutting	RW cutting	RW cutting	RW cutting	RW cutting	RW cutting	RW cutting	RW cutting	RW cutting			
source	Paulick 96	Paulick 96	Paulick 96	Paulick 96	Paulick 96	Paulick 96	Paulick 96	Paulick 96	Paulick 96	Paulick 96	Paulick 96	Paulick 96			
rock type	dac mtfi	rhy silica ?ash	vol/c rhy-QEP	rhy mqm-fi	rhy mqm-fi	rhy mqm-fi	rhy mqtfi	rhy mq(f)fl	rhy mqtfi	rhy-QEP q<f	rhy-QEP q>f	rhy-QEP q>f			
alteration	fresh	silica	wsermbiowchl	wsermbio	wserbio,silica	m-strser	wser,silica	mbio,wchl	msermbiowchl	msermbiowchl	mserwbio/chl	msermbiowchl			
group													average	deviation	
SiO2 %	75.93	82.38	74.99	74.03	80.64	76.69	80.36	78.74	76.27	70.03	71.16	77.66	77.46	2.73	75 to 77
TiO2 %	0.34	0.09	0.28	0.18	0.13	0.13	0.11	0.14	0.14	0.32	0.27	0.08	0.14	0.03	0.15
Al2O3 %	13.40	10.38	13.64	13.64	11.17	13.51	11.30	11.37	12.35	15.43	15.18	12.23	12.45	1.30	12
Fe2O3 %	1.34	0.79	2.68	1.97	0.62	1.32	0.67	1.64	2.26	3.20	3.50	0.91	1.40	0.56	0.5 to 1.5
MnO %	0.01	0.00	0.03	0.05	0.01	0.02	0.00	0.04	0.05	0.06	0.04	0.02	0.04	0.02	
MgO %	0.13	0.39	0.88	0.80	0.29	0.46	0.22	0.64	0.72	1.17	2.23	0.48	0.53	0.25	0.3
CaO %	0.59	0.40	0.85	0.50	0.07	0.10	0.12	0.10	1.44	2.15	1.24	0.05	0.21	0.20	0.5
Na2O %	4.82	5.23	5.70	3.78	2.27	3.18	3.48	3.02	3.78	4.63	2.49	1.88	3.36	0.33	2.5 to 4.5
K2O %	3.27	0.29	0.80	4.91	4.69	4.46	3.65	4.19	2.86	2.83	3.72	6.38	4.30	0.52	2.5 to 5
P2O5 %	0.06	0.01	0.06	0.02	0.01	0.02	0.01	0.02	0.02	0.05	0.05	0.02	0.02	0.01	
Ba ppm	582	225	297	580	540	506	540	651	594	674	602	1387	569	62	10 to 1000
Cu ppm	3	4	4	5	2	3	1	5	2	3	3	11	3	2	<10
Pb ppm	4	22	12	6	6	5	7	6	6	11	6	37	6	1	5 to 25
Zn ppm	43	25	43	66	24	31	9	37	37	71	53	65	36	24	20 to 40
Nb ppm	11	8	11	18	15	16	12	13	13	11	11	10	15	3	
Zr ppm	183	97	145	272	198	200	159	209	273	216	211	90	210	47	
Sr ppm	48	77	203	84	38	43	61	38	79	143	84	43	57	21	
Th ppm	9	16	11	16	13	12	11	11	10	16	17	16	12	2	
Y ppm	32	27	29	47	38	39	25	30	45	32	34	27	35	10	
Rb ppm	84	8	38	146	117	120	67	93	67	89	130	164	106	34	
V ppm	<1	2	20	<1	<1	<1	<1	<1	<1	19	14	4	<1		
Cr ppm	2	2	3	<1	3	<1	<1	6	<1	2	5	<1	<1		
Ni ppm	2	2	1	1	1	<1	1	1	2	3	4	2	<1		
Bi ppm	<1	<1	<1	<1	<1	<1	<1	<1	<1	<1	<1	<1	<1		
	100	100	100	100	100	100	100	100	100	100	100	100	100.00		
Loss %	0.64	0.39	0.93	0.57	0.76	0.94	0.58	0.62	0.63	0.72	1.68	0.75	0.68	0.18	
S %	<0.01	<0.01	<0.01	<0.01	<0.01	<0.01	0.19	0.14	0.01	<0.01	<0.01	0.19	0.08	0.08	
Ti/Zr	11.2	5.6	11.5	3.9	3.9	3.9	4.1	4.0	3.0	8.9	7.6	5.4	3.97	0.13	
ΣNa2O+K2O	8.09	5.52	6.50	8.68	6.96	7.65	7.13	7.21	6.64	7.46	6.21	8.27	7.66		
K2O-ratio	40	5	12	57	67	58	51	58	43	38	60	77	56		
A.I.	39	11	20	57	68	60	52	61	41	37	61	78	58		
CCP-index	14	17	33	23	11	18	10	22	29	35	46	14	19		
MCI	8	7	15	10	2	4	2	7	23	27	21	3	7		

1996) the 'least altered' rhyolite samples plot in a field of moderate values for both indices, however a trend towards higher A.I. is apparent. The CCP values for the rhyolite range mainly between 10 and 60 except for rhyolite with an A.I. > 90 were CCP ranges between 5 and 95. This broad range of CCP values represents variable proportions of chlorite, biotite and sericite in strongly phyllosilicate altered footwall rhyolite. Samples with significant pyrite content have A.I. > 90 and CCP values > 55. By contrast, the analyses of the hangingwall dacite units plot in the opposite area of the diagram with CCP values ranging between 10 and 60 and A.I. between 50 and 0. This indicates that significant enrichment of alkalis over MgO, FeO and CaO is an important alteration feature of the hangingwall.

Diverging trends for the footwall rhyolites and hangingwall dacites can also be observed in a plot of K_2O+Na_2O versus K_2O–ratio ($K_2O/(K_2O+Na_2O)$; Fig. 10b). The analyses for the rhyolites stretch from the field of the igneous spectrum towards K-metasomatism. At K_2O–ratios >90 the total alkali content varies between 1 and 14 wt.% which approximates the respective K_2O concentration. The increase in K_2O ratio and enrichment in K_2O is inferred to reflect sericite alteration while the K_2O depletion is probably correlated with chlorite/biotite alteration. Samples with pyrite alteration have less K_2O than the precursor (4.3 wt.%) indicating that pyritisation is associated with K_2O depletion. The dacites occupy a field ranging from the igneous spectrum towards Na-metasomatism with values for K_2O+Na_2O mainly in the range between 4 to 9 wt.%. However, some samples show signs of K-metasomatism. The field for Na-metasomatism (i.e. albitisation of feldspar crystals) is occupied by dacite samples with chlorite/biotite alteration, 'red rock' alteration and samples that appear unaltered in hand specimen. Dacites samples with 'red rock' alteration also plot in the field for the igneous spectrum. The data indicate that albitisation is more wide spread in the hangingwall dacites than previously thought and that red rock alteration is not a reliable indicator of Na-metasomatism in the hangingwall of Thalanga.

A Mn-carbonates index (MCI) has been defined by Large (1996) which, in the case of the dacite samples from Thalanga, effectively separates epidote alteration and chlorite/biotite alteration (Fig 10c). In a plot of MCI versus CCP the epidote altered dacites plot on a fairly steep positive trend while the chlorite/biotite altered dacites are confined to MCI values of 20 to 30 for high CCP values. Two samples with red rock alteration also contain significant amounts of epidote. These trends reflect the inclusion of calcium, manganese and iron in the crystal structure of epidote while magnesium, iron and manganese fit into the crystal structures of chlorite and biotite. Both, epidotisation and chlorite alteration are associated with relative depletion of Na_2O and K_2O.

Some interesting conclusions can be drawn from plots of Fe_2O_3 versus S and Fe_2O_3 versus MgO (Fig. 11). The positive correlation of Fe_2O_3 and S for the rhyolite samples indicates that Fe-enrichment in the footwall is dominantly related to pyritisation. The dacites contain very little S and Fe_2O_3 has a well constrained correlation with MgO. This relationship seems to indicate that the enrichment of MgO and Fe_2O_3 in the hangingwall is due to common process such as the formation of Fe-Mg chlorites and that hangingwall alteration took place under oxidised conditions. The Fe_2O_3 versus MgO plot shows no consistent trend for the rhyolite samples suggesting that Mg-enrichment and Fe-enrichment are caused by different processes such as pyritisation and Mg-chlorite alteration.

Systematic variations in Zn and MgO contents of rhyolite and dacite samples can be observed (Fig 12). While Zn values of several hundred ppm to > 1000 ppm are most likely due to sphalerite crystals in the samples the increase of Zn from ~10 ppm to ~300 ppm appears to be correlated with MgO enrichment. This suggests that Zn is partially correlated with chlorite/biotite alteration. The concentration of Zn in chlorite and biotite might change systematically with distance from the massive sulphides and provide a new tool for base metal exploration. Therefore, measurements of the Zn content in chlorite and biotite from several stratigraphic positions within the

Thalanga sequence will be a priority for microprobe analyses.

References

Allen, R. L., 1988, False pyroclastic textures in altered silicic lavas, with implications for volcanic-associated mineralisation: Economic geology, v. 83, p. 1424-1446.

Berry, R. F., Huston, D.L., Stolz, A.J., Hill, A.P., Beams, S.D., Kuronen, U. & Taube, A., 1992, Stratigraphy, structure and volcanic hosted mineralisation of the Mt. Windsor Subprovince, North Queensland, Australia: Economic Geology, v. 87, p. 739-763.

Bromley-Challenor, M.D., 1988, The Falun supracrustal belt. part 1: primary geochemical characteristics of Proterozoic metavolcanics and granites: Geologie en Mijnbouw, v. 67 (2-4), pp. 279-291.

Gregory, P. W., Hartley, J.S. & Wills, K.J.A., 1990, Thalanga zinc-lead-copper-silver deposit, in Hughes, F. E., ed., geology of the mineral deposits of Australia and Papua-New Guinea: Melbourne, AIMM, p. 1527-1537.

Herrmann, W., 1994, Immobile element geochemistry of altered Volcanics and Exhalites at the Thalanga Deposit, North Queensland: Unpub. M. Econ. Geol. thesis, University of Tasmania.

Henderson, R.A. 1983, Early Ordovician faunas from the Mount Windsor Subprovince, northeastern Queensland: Mem. Ass. Austalas. Palaeontols, 1, 145-175.

Henderson, R. A., 1986, Geology of the Mt Windsor Subprovince - a lower Palaeozoic volcano-sedimentary terrane in the northern Tasman Orogenic Zone: Australian Journal of Earth Science, v. 33, p. 343-364.

Hill, A. P., 1996, Structure, volcanic setting, hydrothermal alteration and genesis of the Thalanga massive sulphide deposit. Unpub. PhD thesis, University of Tasmania.

Hutton, L. J., and Crouch, S. B. S., 1993, Geochemistry and Petrology of the Western Ravenswood Batholith, Department of minerals and energy Queensland.

Ishikawa, Y., Sawaguchi, T., Iwaya, S. & Horiachi, M., 1976: Delineation of prospecting targets for Kuroko deposits based on modes of volcanism of underlying dacite and alteration halos. Mining Geology 26: 105-117. (in Japanese with English abstract)

Large, R.R. 1996, The Hercules-Mount Read traverse: Relationships between volcanic mineralogy, alteration and geochemistry: AMIRA/ARC project P439, report 3, pp. 153-234.

MacLean, W. H., and Barrett, T. J., 1993, Lithogeochemical techniques using immobile elements: Journal of Geochemical Exploration, v. 48.

McPhie, J., Doyle, M., and Allen, R., 1993, Volcanic Textures. A guide to the interpretation of textures in volcanic rocks: Hobart, Codes, University of Tasmania, 198 p.

Paulick, H. 1996, Facies architecture, alteration and metamorphism of the volcanic host rock sequence at the Thalanga massive sulphide deposit, north Queensland, Australia. AMIRA/ARC project P439, report 2, pp. 147-154.

Perkins, C., 1993, Isotopic dating of precious and base metal deposits and their host rocks in Eastern Australia, AMIRA, project P334.

Sainty R. A. and Hill, A. P., 1996, Thalanga: A Dome-type VMS deposit related to explosive eruption of a quartz-eye porphyry and its fluids. Eos, Transactions, American Geophysical Union Vol. 77, No. 22, May 28, 1996; abstracts of 1996 Western Pacific Geophysical Meeting.

Stolz, A. J., 1995, Geochemistry of the Mount Windsor Volcanics: Implications for the tectonic setting of Cambro-Ordovician volcanic-hosted massive sulfide mineralization in Northeastern Australia: Economic Geology, v. 90, p. 1080-1097.

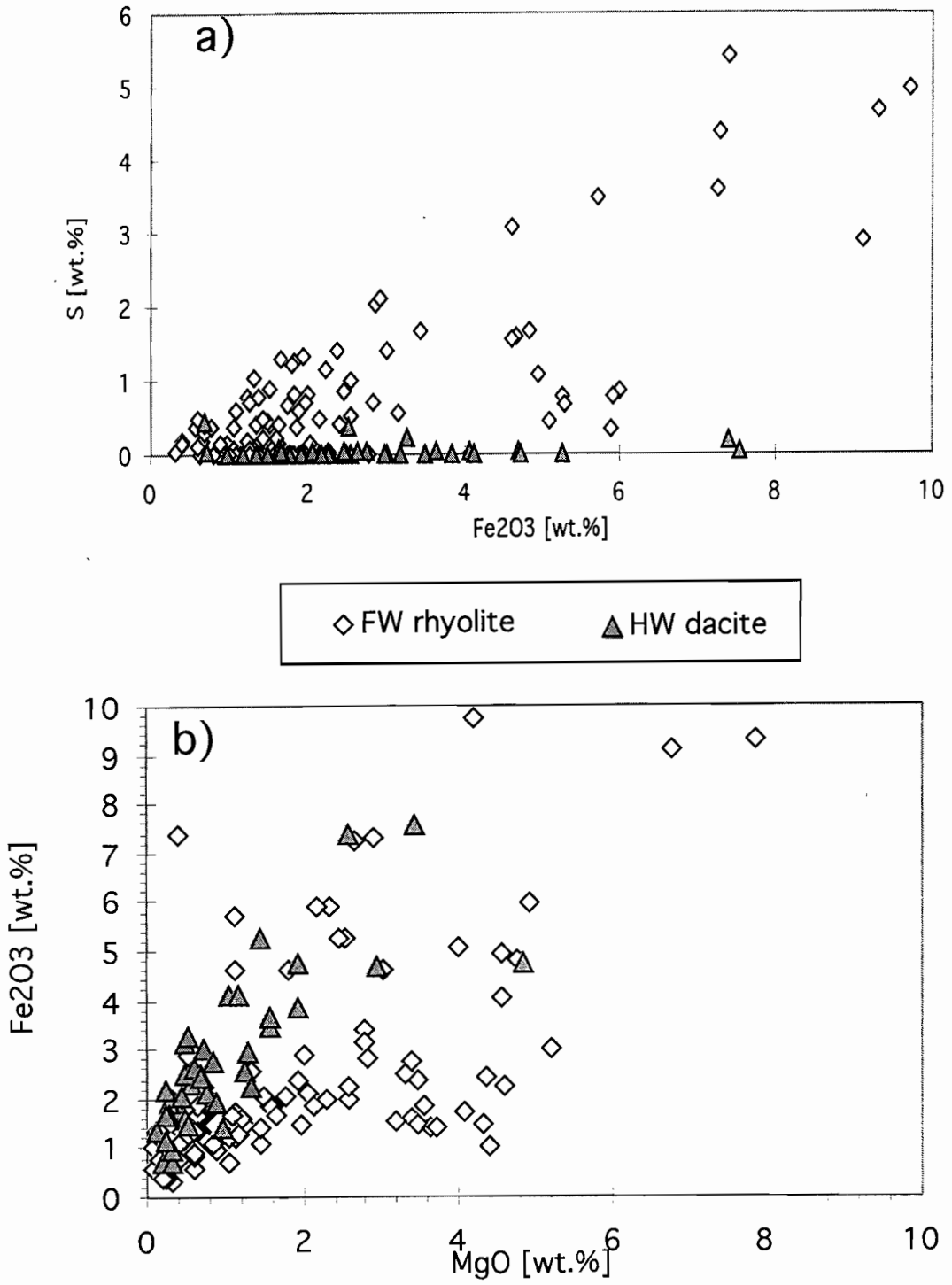

Fig 11. (A) MgO vs Fe_2O_3 scatter plot for footwall rhyolites and hangingwall dacites (data: this study). (B) Fe_2O_3 vs S scatter plot for footwall rhyolites and hangingwall dacites (data: this study)

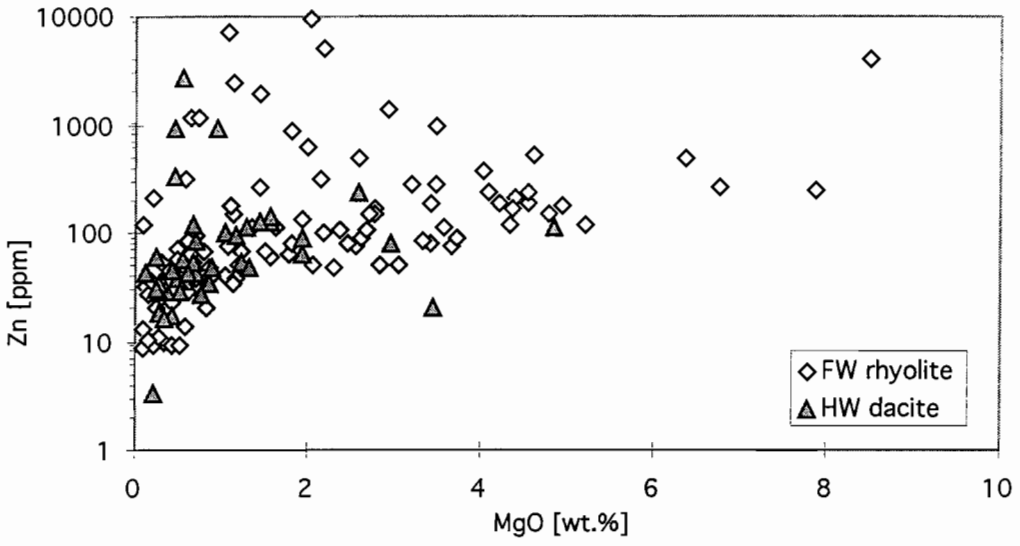

Fig 12. Zn vs MgO scatter plot for footwall rhyolites and hangingwall dacites (data: this study).

The alteration system of the Waterloo prospect, North Queensland

Thomas Monecke

Centre for Ore Deposit Research, Geology Department, University of Tasmania

Summary

A brief overview on the geology of the Waterloo prospect, the lithologies and the types of alteration is given in this report. Since the field work, undertaken between December 1996 and February 1997, two hundred samples have been prepared for geochemical analysis, and thin sections have been made from half the samples.

Styles of alteration of the least altered footwall andesites include disseminated pyrite, epidote, carbonate and silicification. The footwall alteration zone is characterized by assemblages of sericite ± chlorite ± pyrite and quartz-sericite ± chlorite ± pyrite. Alteration assemblages in the hangingwall include sericite ± chlorite, carbonate, hematite-quartz, epidote, albite, and silicification. The high-grade zinc-copper-rich base metal mineralisation of the Waterloo prospect occurs in two distinct lenses of massive sulphide. New metal distribution maps have been prepared. The distribution of metals changes within the prospect from east to west; the alteration system beneath the West Waterloo mineralised zone shows abundant low grade (Cu> 0.05% and Zn>0.05%) disseminated mineralisation compared to East Waterloo. The Waterloo mineralisation is characterized by anomously high Zn ratios (>80) and by Cu ratios <25.

Introduction

This study forms part of the ongoing CODES SRC research activities on VHMS-related alteration and part of a PhD project being undertaken at the Freiberg University of Mining and Technology (Germany). The study is focused on the Waterloo prospect (Mt. Windsor subprovince, North Queensland) (Fig. 1), which contains a geological reserve of 0.372 Mt at 3.8 % Cu, 19.7% Zn, 2.8% Pb, 94 g/t Ag, and 2 g/t Au (Berry et al. 1992).

Field work was conducted between December 1996 and February 1997 and included the re-logging of selected drill core from the Waterloo (WT1A, WT2, WT6, WT5, WT7, WT9A, WT16, WT17, WT18, WT21, WT22, WT23, WT24, WT25, WT26, WT27) and Agincourt (AGDD1, AGDD5, AGDD7B) prospects. Agincourt is located only 1 km west of Waterloo and occurs at about the same stratigraphic level. Approximately 400 core samples were taken at 15 m intervals through the foot- and hangingwall packages and at 5 m intervals in the hangingwall adjacent to the hangingwall-footwall contact. Whole rock major and trace element analyses (200 samples), thin section work (100 thin sections) and a statistical examination of the company assay data are in progress.

Prospect geology

The Waterloo prospect is located in the central portion of the Trooper Creek Formation within the volcano-sedimentary succession of the Mount Windsor

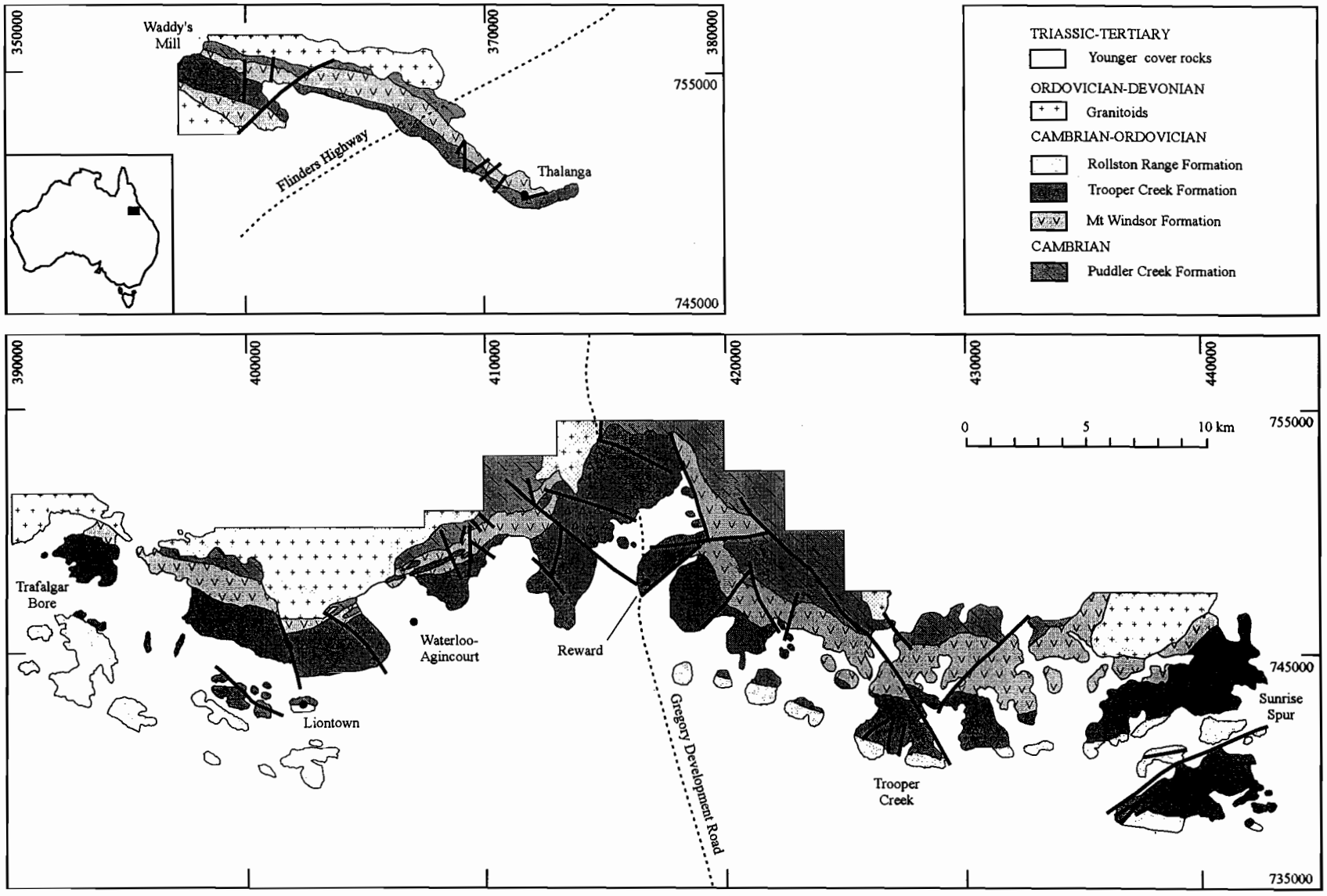

Figure 1. Geological map of the Mount Windsor subprovince between Waddy's Mill and Sunrise Spur showing the distribution of the principal units and younger granitoid intrusions (Stolz, 1995).

subprovince (Fig. 2). The regional geology and the prospect geology have been previously described by Henderson (1986), Berry (1989), Huston (1991), Berry et al. (1992), Stolz (1995), and Huston et al. (1995). As the prospect is covered by 30-60 m of Tertiary sediments, the geology is inferred from the detailed drill logs. The drill hole location plan of the Waterloo prospect is given in Figure 3a.

Base metal mineralisation occurs near the contact of a subvertical sequence of pyritic sericite±chlorite and pyritic quartz-sericite±chlorite schists (footwall alteration zone) to the north with an overlying sequence of volcaniclastic rocks (rhyolitic sandstone, siltstone, greywacke, and shale) and andesitic to dacitic lavas (hangingwall sequence) to the south. Massive andesitic lavas occur stratigraphically below the zone of pyritic sericite ± chlorite and pyritic quartz-sericite ± chlorite schists. The footwall and hangingwall sequences are commonly cut by andesitic dykes (Figs 3b, 4; Fig. 4 in back pocket).

The footwall alteration zone below the massive sulphide mineralisation at 19800mE is 20 to 30 m (drill holes WT5 and WT9A) thick and thickens towards the west to over 100 m (section 19300mE). The true thickness of the footwall alteration zone also seems to increase with depth, although no reliable data can be obtained from the drill holes WT23, WT24, and WT25 because they did not penetrate through the alteration zone. In some places, the less altered footwall andesites contain zones of 0.5 to 2 m wide pyritic sericite±chlorite schists (e.g. WT16).

Lithologies

Footwall andesites

The footwall is dominated by coherent aphyric to moderately plagioclase-phyric andesitic lavas, subordinate andesitic autobreccias, and andesitic volcaniclastic rocks. The lavas are sparsely to moderately vesicular with quartz- and/or carbonate ± chlorite-filled vesicles. Phenocrysts of plagioclase and chlorite-epidote pseudomorphs of original pyroxene phenocrysts are evenly distributed through a fine groundmass by flow-aligned plagioclase laths, with interstitial chlorite and patchy epidote. Commonly, there are traces of sericite, disseminated pyrite cubes and patchy carbonate alteration in the groundmass.

Hangingwall sediments

The footwall alteration zone is overlain by a mixture of volcano-sedimentary rocks. The most abundant sediments are volcaniclastic sandstones and siltstones. The former are typically composed of abundant angular plagioclase and quartz grains (0.5 to 2 mm in size) with subordinate lithic fragments, while the latter are composed of tiny angular quartz and feldspar grains in a very fine grained matrix of quartz and feldspar. Blue quartz has been recognised in the volcaniclastic sandstones, usually in the immediate hangingwall of massive sulphides (e.g. WT9A).

Hangingwall dacites and andesites

The hangingwall dacitic to andesitic lavas are aphyric to moderately plagioclase-phyric. Peperites occur in a few places and indicate the mixing of coherent lava with unconsolidated wet sediment.

Styles of alteration

There are several styles of alteration in both footwall and hangingwall at Waterloo:

Styles of footwall alteration:

(1) sericite±chlorite alteration
(2) disseminated and vein pyrite alteration
(3) carbonate alteration
(4) epidote alteration
(5) silicification

Styles of hangingwall alteration:

(1) sericite±chlorite alteration
(2) carbonate alteration
(3) epidote alteration
(4) albite alteration
(5) hematite-quartz alteration
(6) silicification

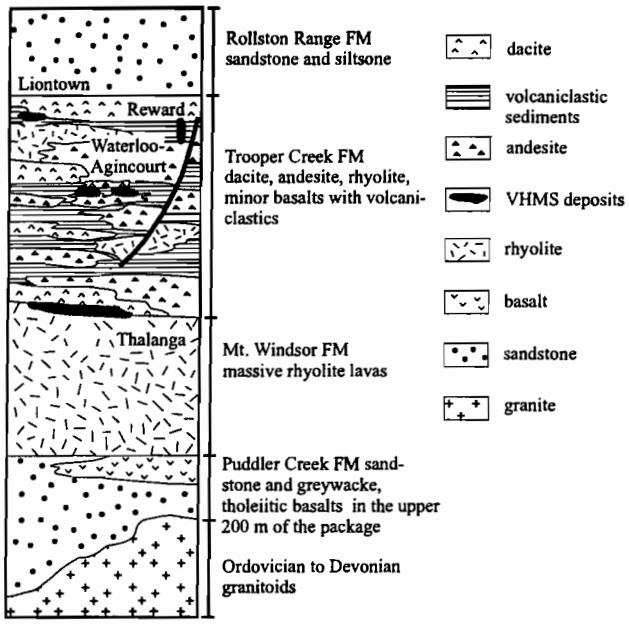

Figure 2. Schematic volcano-stratigraphic section of the Mount Windsor subprovince (after Large, 1992).

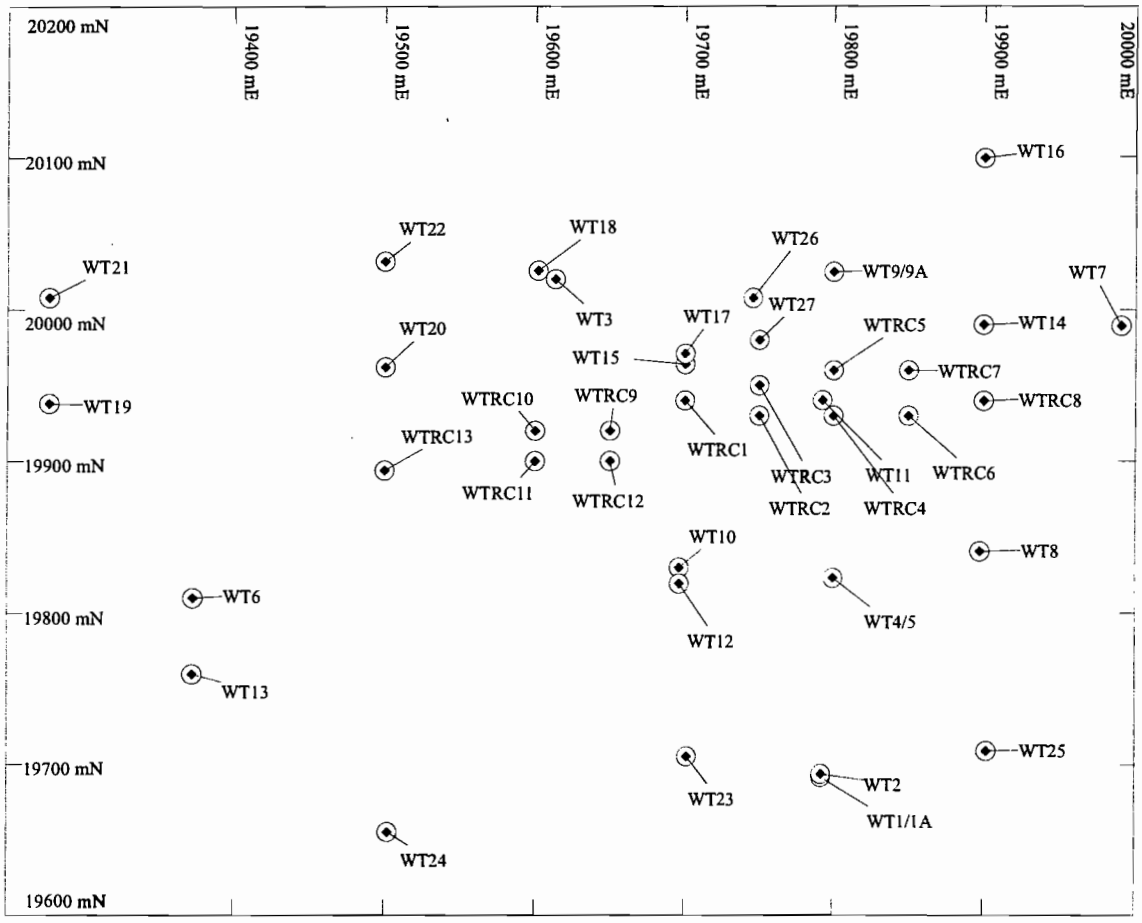

Figure 3a. Drill hole location plan of the Waterloo prospect (scale = 1:5000).

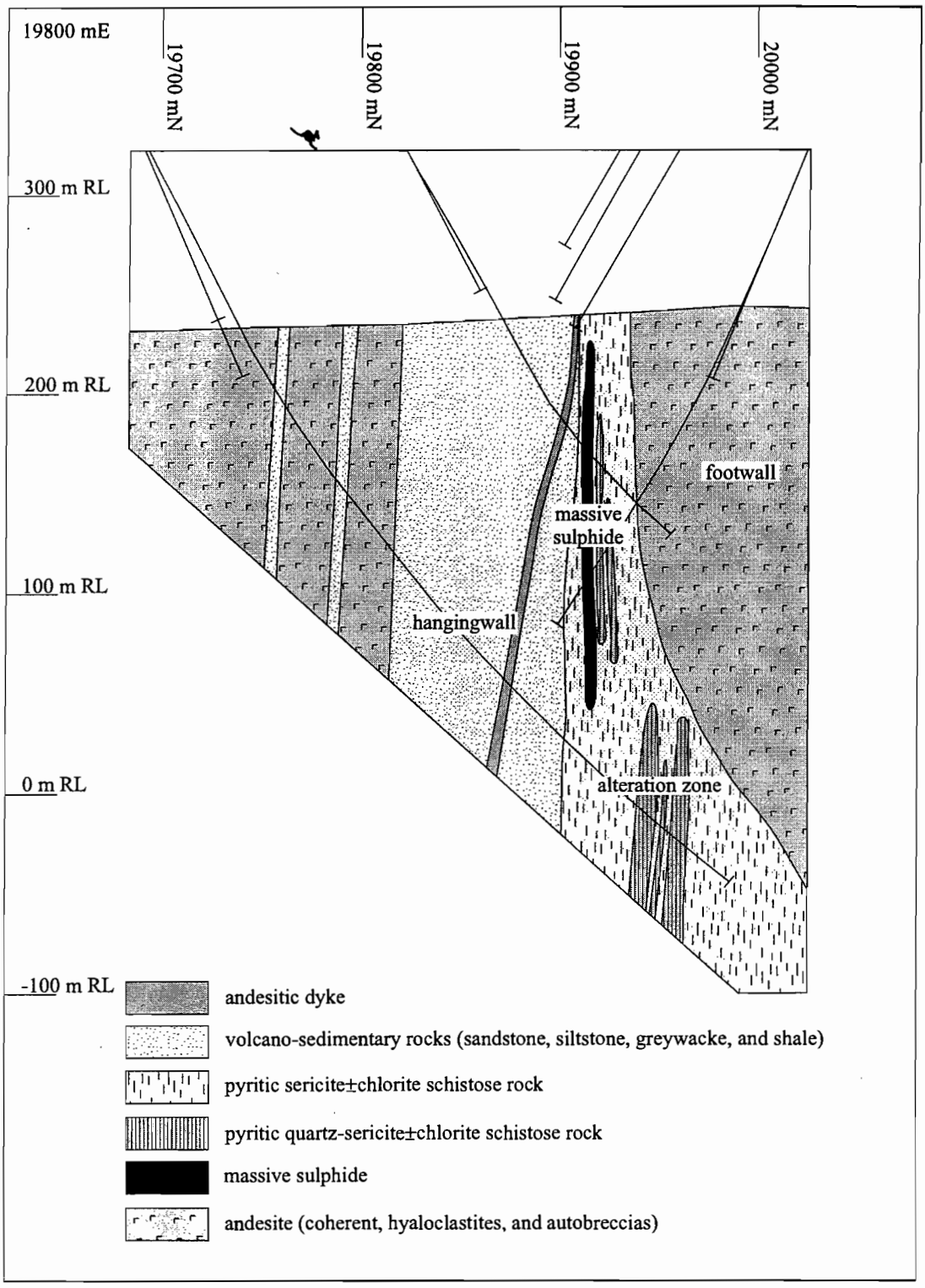

Figure 3b. Cross-section showing the interpreted geology at 19800 mE.

Sericite±chlorite alteration

The most widespread and obvious alteration is an assemblage of sericite±chlorite which makes up most of the footwall alteration zone at Waterloo. A weak pervasive sericite±chlorite alteration is widespread in the groundmass of most of the footwall andesites and feldspar phenocrysts show partial replacement by sericite±chlorite. Contacts between the less altered lavas and the strongly altered pyritic sericite±chlorite schists in the footwall are sharp to gradational. Within the more strongly altered zones primary volcanic textures are largely destroyed. The pyritic sericite ± chlorite and pyritic quartz-sericite ± chlorite schists are strongly cleaved. Pyrite grains exhibit significant flattening parallel to the cleavage. Large grains have pressure shadows which are filled with quartz and chlorite, hence the alteration predates the development of the cleavage (which is D_2, as D_1 is not recognised in the Waterloo area — Berry, 1989). Due to pyrite breakdown and acid attack much of the core from the footwall alteration zone is in an advanced state of oxidation and deterioration. The sericite ± chlorite alteration commonly penatrates a few metres (5-10 m) into sediments in the hangingwall above the ore position.

Disseminated and vein pyrite alteration

This style of alteration is widespread and the pyrite contents varies from traces to about 20%. The pyrite typically forms cubes (0.1 mm to 1 mm), but there is some remobilisation of pyrite into narrow (2 mm) veins.

Carbonate alteration

This alteration is widespread and pervasive. Carbonate replaces plagioclase grains, and occurs in patches or aggregates in the volcano-sedimentary units and coherent lavas in both footwall and hangingwall. Mobilisation of carbonates into narrow veins (1 mm) is very common.

Epidote alteration

Epidote is common in most of the weakly altered footwall andesites and the hangingwall extrusives. Epidote occurs in the groundmass of the andesites, partially replacing plagioclase phenocrysts and forms up to 4 cm patches. Epidote alteration in the least altered footwall andesites appears to be more intense than in the hangingwall andesites.

Albite, hematite-quartz alteration and silicification

Due to its pink color, albite has been recognised in hand-specimens at several locations in the hangingwall sediments. Hematite-quartz alteration is observed in some of the hangingwall dacites and hangingwall sediments. Silicification is weak to moderate, widespread and pervasive, and occurs in the footwall andesites and hangingwall andesites and dacites.

The styles of alteration and their spatial distribution will be described in more detail in a subsequent report when geochemical data and more thin sections are available.

Metal distribution

Metal distribution studies at Waterloo have been carried out previously by Kuronen (1989), Huston (1991) and Huston et al. (1995). Metal values were contoured on long sections and level plans. Cu, Zn and Pb data for almost all 200 samples of this study were available, and new metal distribution maps have been prepared.

Methodology

Figures 5 to 7 (see back pocket) show the distributions of Cu, Zn and Pb, respectively. The downhole distribution patterns are based on company assay data, analytical data obtained by Stolz (1991), and from this study, and represent the element concentrations over the length of the samples at the locations of the samples in the drill cores. These diagrams only contain the "spot" analysis with no interpolation between the assayed intervals. The metal value catagories have been selected *empirically* and not by applying a statistical method.

Results

This metal distribution study broadly confirms a similar study by Huston (1991):

(1) Significant base metal mineralisation occur in two centers: (1) 19300mE to 19400mE at 0 mRL to 250 mRL (thereafter referred as West Waterloo) and (2) 19600mE to 19800 mE at 0 mRL to 250 mRL (thereafter referred as East Waterloo).

(2) Copper enrichment (>0.5%) is largely restricted to the West Waterloo and East Waterloo massive sulphide lenses. Elevated copper concentrations (0.05 to 0.5%) in the alteration zone are more widespread in the West Waterloo than in the east.

(3) Zinc enrichment (>10%) is restricted to the West Waterloo and East Waterloo massive sulphide lenses. Both centers are separated by a zone (19500mE) of mainly low Zn concentrations (<1%). The alteration zone underlying the West Waterloo lens has elevated Zn concentrations (>0.05%), while the Zn concentrations of the alteration zone at East Waterloo are usually lower (<0.05%). Zinc has been leached from the weathered zones.

(4) Lead enrichment is restricted to the massive sulphide lenses of West Waterloo and East Waterloo, and there is no significant lead enrichment in the alteration zone.

(5) Zinc ratios (100Zn/[Zn+Pb]) in the Waterloo massive sulphide lenses (Fig. 8) (only samples with a total base metal content exceeding 1% were considered) are anomalously high for VHMS deposits (Huston and Large, 1987). The distribution of Zn ratios is a right hand distribution and most samples show Zn ratios in the range of 80 to 100. Zinc ratios of less than 60 occur in weathered samples, hence the Zn ratio can be used as a criterion to identify samples from the weathered zone in a set of data as already noted by Huston et al. (1995).

(6) The distribution of Cu ratios (100Cu/[Cu+Zn]) for samples with base metal concentrations exceeding 1% is given in Figure 9. The distribution of Cu ratios shows one main mode which is a left hand distribution (log-normally distributed). Most samples have Cu ratios below 25, although a possible second mode occurs in the range from 85 to 100.

Conclusions

The following preliminary conclusions can be drawn from this study to date: the Waterloo mineralisation contains two high-grade zinc-copper-rich VHMS lenses which occur near the contact of a subvertical sequence of andesite lavas and breccias which have been altered to pyritic sericite±chlorite and pyritic quartz-sericite±chlorite schists (footwall alteration zone) and an overlying sequence of volcaniclastics, including andesite to dacite lavas. The footwall andesites exhibit epidote and weak to strong sericite ± chlorite ± carbonate ± pyrite alteration. Alteration surrounding the ore zone is dominated by sericite ± chlorite. Styles of alteration in the hangingwall include the assemblages sericite±chlorite, carbonate, hematite-quartz, epidote and albite. Silicification is common both footwall and hangingwall. Base metal mineralisation occurs in two distinct lenses of massive sulphide. The distribution of metals changes from east to west; the alteration system beneath West Waterloo contains abundant low grade (Cu> 0.05% and Zn>0.05%) disseminated mineralisation compared to East Waterloo. The zinc ratio of highly mineralised samples from the Waterloo prospect are anomalously high (>80). Cu-ratios of most samples are below 25.

Further work will be carried out to characterise the mineralogy and geochemistry of the various styles of alteration.

References

Berry R.F. (1989) Structure of the Mount Windsor Subprovince initial report - September 1989: Centre for Ore Deposit and Exploration Studies, University of Tasmania, Mount Windsor Project Research Report No. 1, pp. 51-73.

Berry R.F., Huston D.L., Stolz A.J., Hill A.P., Beams S.D., Kuronen U., and Taube A. (1992) Stratigraphy, structure, and volcanic-hosted mineralization of the Mount Windsor Subprovince, North Queensland, Australia: Economic Geology v. 87, pp. 739-763.

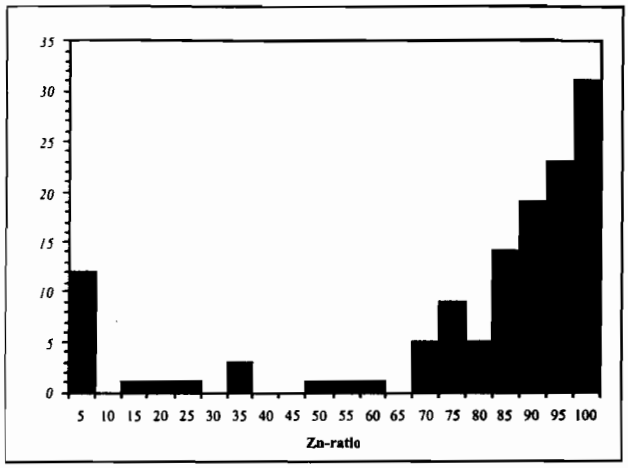

Figure 8. Histogram showing the distribution of Zn-ratios in highly mineralised samples (total base metal content > 1%).

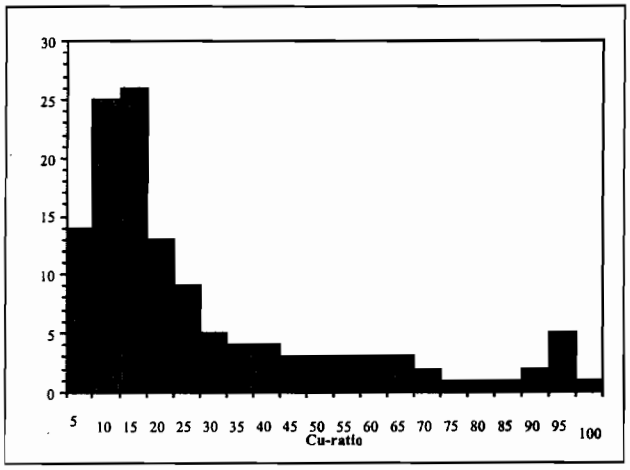

Figure 9 Histogram showing the distribution of Cu-ratios in highly mineralised samples (total base metal content > 1%).

Henderson R.A. (1986) Geology of the Mount Windsor subprovince-a lower Palaeozoic volcano-sedimentary terrane in the northern Tasman orogenic zone: Australian Journal of Earth Sciences v. 33, pp. 343-364.

Huston D.L. (1991) Metal zonation and mineralogy of the Waterloo and Agincourt prospects: Centre for Ore Deposit and Exploration Studies, University of Tasmania, Mount Windsor Project Research Report No. 2, pp. 109-144.

Huston D.L and Large R.L. (1987) Genetic and exploration significance of the zinc ratio (100Zn/Zn+Pb)) in massive sulfide systems: Economic Geology v. 82, pp. 1521-1539.

Huston D.L., Kuronen U., and Stolz J. (1995) Waterloo and Agincourt prospects, northern Queensland: contrasting styles of mineralization within the same volcanogenic hydrothermal system: Australian Journal of Earth Sciences v. 42, pp. 203-221.

Kuronen U. (1989) Report on drilling at Waterloo (ATP 3798M-Balfes Creek) and Agincourt (ATP4066M-Dione) prospects during 15.11.1988-15.7.1989: Unpub. Pancontinental Mining Ltd. Report 89/44.

Large R.R. (1992) Australian volcanic-hosted massive sulfide deposits: Features, styles, and genetic models: Economic Geology v. 87, pp. 471-510.

Stolz A.J. (1991) Stratigraphy and geochemistry of the Mt. Windsor volcanics and associated exhalites: Centre for Ore Deposit and Exploration Studies, University of Tasmania, Mount Windsor Project Research Report No. 2, pp. 23-83.

Stolz A.J. (1995) Geochemistry of the Mount Windsor Volcanics: Implications for the tectonic setting of Cambro-Ordovician volcanic-hosted massive sulfide mineralization in northeastern Australia: Economic Geology v. 90, pp. 1080-1097.

Alteration associated with sub-seafloor replacement style massive sulfide deposits: evidence from the Cambro-Ordovician Highway–Reward deposit, Mount Windsor Subprovince

Mark G. Doyle
Centre for Ore Deposit Research, Geology Department, University of Tasmania

Introduction

There is emphasis in the literature that volcanic-hosted massive sulfide deposits form on the seafloor by accumulation of sulfides precipitated from exhaling hydrothermal fluids. The principal lines of evidence to support a seafloor exhalative origin initially came during studies of pristine ancient examples from uplifted and eroded subaqueous volcanic successions (see reviews by Solomon, 1976 and Franklin et al., 1981 for the early history of the concept). The discovery of sulfide chimney-mound deposits on the modern seafloor not only provided corroboration of the hydrothermal exhalative model for the genesis of VHMS deposits, but raised questions as to the viability of mineral precipitation by exhalation at the seawater–sediment interface. Sulfide accumulation from buoyant hydrothermal plumes exiting black smokers is a highly inefficient process. It has been estimated that more than 99% of the metal carried by hydrothermal fluids is dispersed in the water column by the black smoker plume and incorporated into distal sediments (Rona, 1984). Studies of the structure of modern sulfide chimneys and mounds (e.g. Goldfarb et al., 1983; Koski et al., 1984) and the texture and metal zonation in ancient analogues (e.g. Large, 1977) have highlighted the importance of sulfide accumulation by open space filling and replacement in the sulfide mound. There is increasing evidence to suggest that these processes may extend into the sub-seafloor environment and that large parts of some VHMS deposits are replacements of the host volcanic and sedimentary rocks.

There are very few detailed or convincing descriptions of sub-seafloor replacement deposits in modern and ancient volcanic successions. Youthful sub-seafloor deposits have been mapped at Middle Valley, a sediment covered ridge located along the Juan de Fuca spreading centre (Goodfellow and Blaise, 1988; Goodfellow and Franklin, 1993). The deposit is expressed on the seafloor by a small sulfide mound, but it passes down into a discordant pipe-like body of massive sulfide extending more than 93 m into the underlying siltstone. The best studied examples of sub-seafloor replacement style VHMS deposits are confined to ancient volcanic successions. These include deposits hosted by silicic-intermediate sequences (Allen, 1988, 1992; Khin Zaw and Large, 1992; Doyle and McPhie, 1994; Bodon and Valenta, 1995; Galley et al., 1995; Allen et al., 1997b) and mafic volcanic successions (Zierenberg et al., 1988). The paucity of examples is probably a reflection of the difficulty of recognising these deposits, rather than their abundance.

The principal intention of this research is to consider more fully the problems associated with distinguishing exhalative and sub-seafloor replacement style VHMS deposits. In particular I consider the evidence for sub-seafloor replacement, and the role of lithofacies in determining the character of the resulting deposit. A second aim is to examine the characteristics of alteration associated with Highway–Reward type massive sulfide deposits.

Highway–Reward massive sulfide deposit

The Highway Member (Trooper Creek Formation) at Highway–Reward hosts two spatially associated copper–gold-rich massive sulfide orebodies; Highway and Reward. After Thalanga, the Highway–Reward deposit is the largest known volcanic-hosted massive sulfide deposit in the Mount Windsor Subprovince. The Highway orebody is located approximately 200 m NNW of the Reward orebody beneath the abandoned Highway open pit (Fig. 1). The massive sulfide deposit consist of sub-vertical pipe-like bodies of massive pyrite-chalcopyrite that are associated with minor marginal zones of pyrite-sphalerite-galena±barite mineralisation. Supergene and oxide ores overlie the primary ores at both Highway and Reward. Most of the oxide resource at Highway was mined from the Highway open cut by North Queensland Resources in the period 1986 to 1988. A significant primary resource remains at Highway and the Reward deposit is presently undeveloped (Table 1).

Previous investigations have briefly addressed various aspects of the Highway–Reward deposit: geophysics and discovery (Kay, 1982; Beams et al., 1989; Beams et al., 1993; Beams and Dronseika, 1995), geology of the mineralisation and host rocks (Kay, 1987; Berry et al., 1992; McPhie and Large, 1992; Large, 1992; Doyle, 1994), sulfur and lead isotope geochemistry of the massive sulfide (Huston, 1992; Dean and Carr, 1992), deformation style and strain partitioning around the orebodies (Laing, 1988; Berry, 1989); and exploration geochemistry (Beams and Jenkins, 1995). The interpretations presented here are based on detailed diamond drill core logging (61

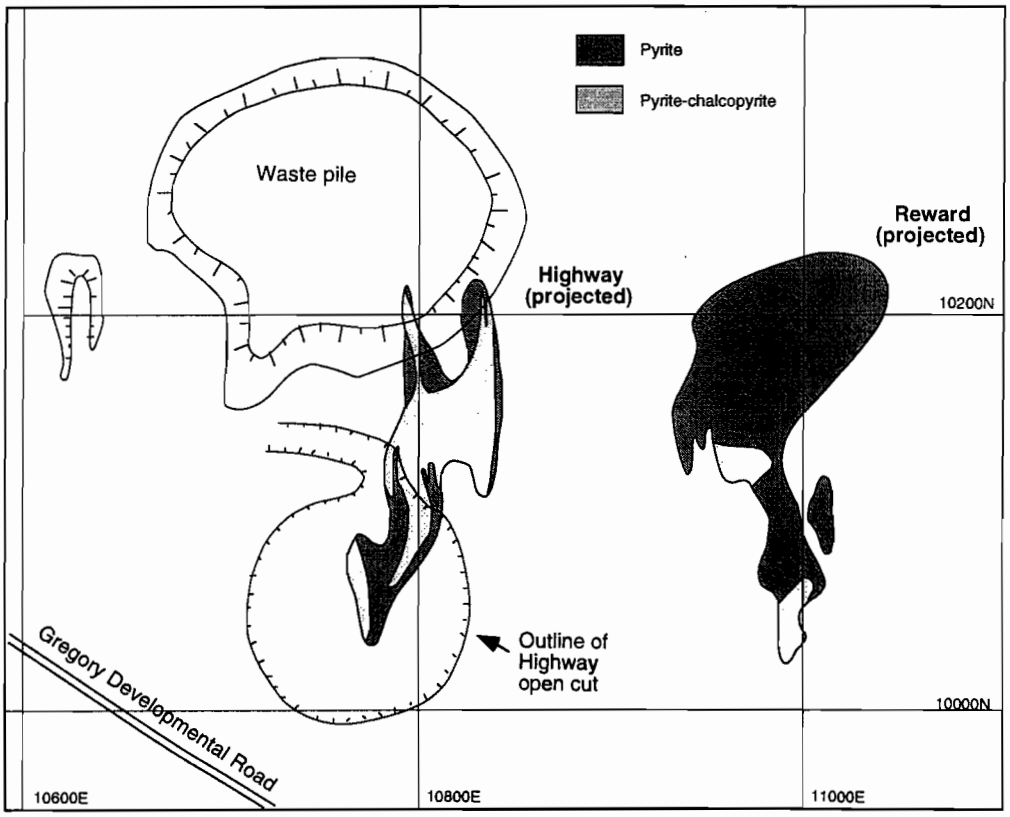

Figure 1. Surface projection of the Highway and Reward orebodies from approximately 175 m RL (150 m below surface). Stippling highlights the distribution of Cu-rich massive sulfide. Modified from Aberfoyle Resources Limited.

holes), 1:250 scale mapping of the Highway open pit and the few available surface outcrops, and detailed petrography of the host lithofacies.

Local geology

The Highway–Reward deposit are hosted by a silicic intrusive and volcanic sequence intercalated with sedimentary facies that indicate a submarine, below-storm-wave-base environment of deposition. Contact relationships and phenocryst mineralogy, size and percentages indicate the presence of more than thirteen distinct porphyritic units in an area of 1 x 1 x 0.5 km (Figs 2, 3). The peperitic upper margins to many porphyries demonstrate their intrusion into wet unconsolidated-sediment. Syn-sedimentary sills, cryptodomes, partly extrusive cryptodomes, and associated in situ and resedimented autoclastic deposits have been recognised. These are the principal facies in the environment of mineralisation and represent a proximal facies association from intrabasinal, non-explosive, syn-sedimentary intrusion dominated magmatism.

Porphyries intruded or were overlain by a volcaniclastic and sedimentary facies association comprising suspension-settled siltstone, graded turbiditic sandstone and thick, non-welded pumice- and crystal-rich sandstone-breccia units. Pumiceous and crystal-rich deposits record episodes of explosive silicic volcanism in an extrabasinal or marginal basin environment, and were emplaced by cold, water-supported, high-concentration turbidity currents. Andesite dykes cut across the massive sulfide and altered host rocks.

Volcanic host rocks in the Highway–Reward area are weathered to depths in excess of 100 m. The weathered and oxidised zone is better developed at Reward and extends below the top of the massive sulfide orebody on most sections. Prior to development the Highway gossan cropped out at surface. The Reward deposit occurs under 100 m combined thickness of Tertiary fluviatile sediments (Campaspe Formation) and deeply weathered gossanous volcanics. Structural readings from drill core indicate a shallow dip of 10° south east in the subsurface volcanics (Laing, 1988). Flow banding in rhyolites from the Highway open pit has steeper dips (18–55°) but may be at a high angle to bedding.

The massive sulfide orebodies

The mineralisation can be divided into five principal types on the basis of mineralogy, textures and the relationships to the host rocks. These are: (1) pyrite-chalcopyrite pipes; (2) pyrite-sphalerite-galena ± barite; (3) footwall stringer; (4) hangingwall stringer; and (5) gossanous breccia.

Pyrite-chalcopyrite pipes

The Highway and Reward pyrite-chalcopyrite pipes are discordant to bedding, but parallel to S3, and have a plunge subparallel to a sub-vertical mineral lineation (cf. Berry et al., 1992). The Highway pipe is a NE trending, chalcopyrite-rich massive pyrite body that is approximately 175 m long. To the south, the pipe is less than 20 m wide and 200 m in depth (section 10050N; Fig. 2). The central and northern parts of the deposit comprise two to three pipes

Table 1 Grade and tonnage data for the primary, oxide, and supergene ore zones at Highway–Reward. The Highway oxide resource is an estimate of the pre-mining resources. Data from Beams and Dronseika (1995).

	Highway	Reward
Primary	1.2 m.t. @ 5.5% Cu, 6.3 g/t Ag, 1.2 g/t Au	0.2 m.t. @ 3.5 Cu, 13 g/t Ag, 1 g/t Au
Supergene		0.3 m.t Cu, 11.6% Cu, 21 g/t Ag, 1.8 g/t Au
Oxide	0.07 m.t. @ 6.04 g/t Au	0.1 m.t 33 g/t Ag, 6.49 g/t Au

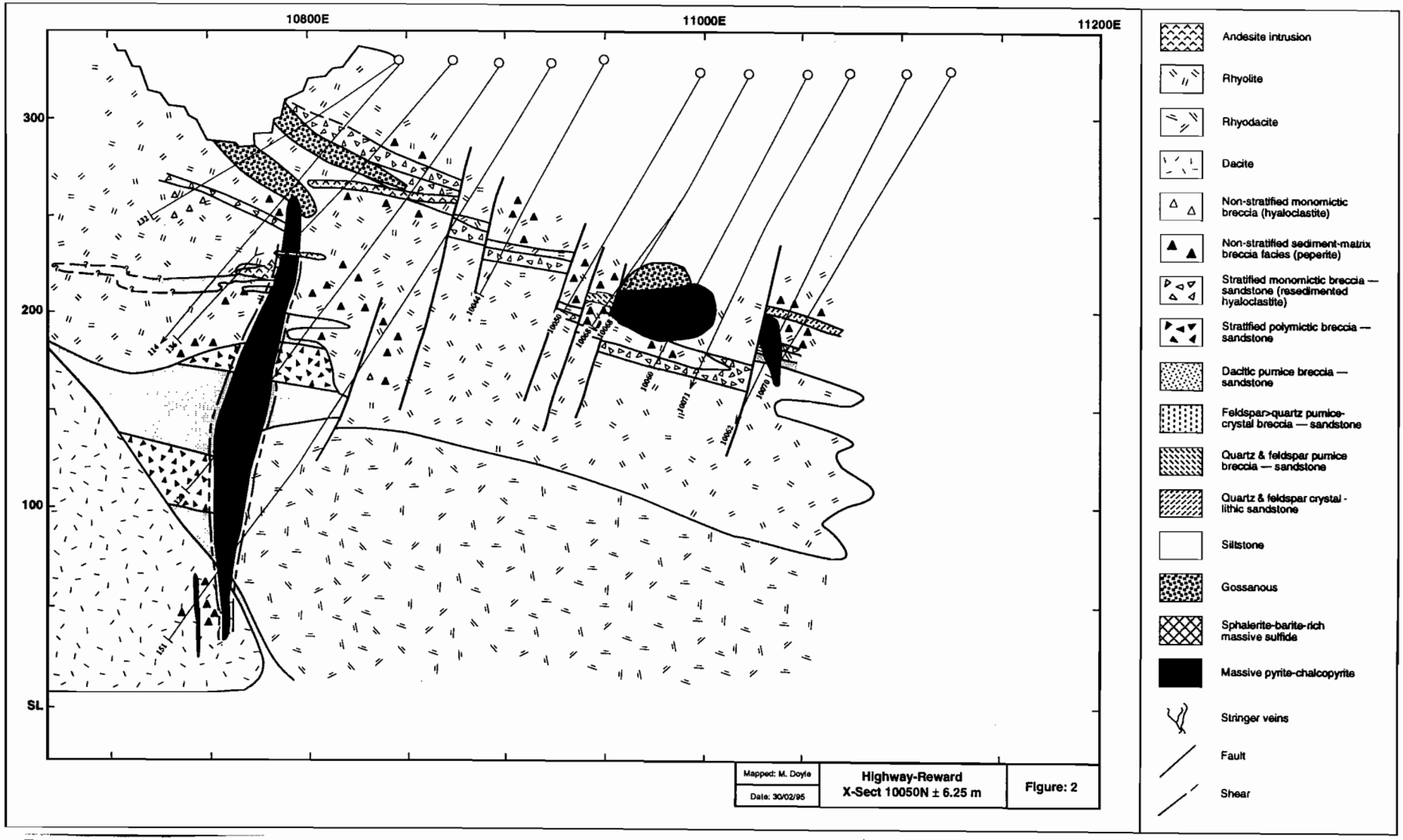

Figure 2. Simplified geological cross-section of the Highway–Reward deposit at 10050N. RL = relative position above sea level.

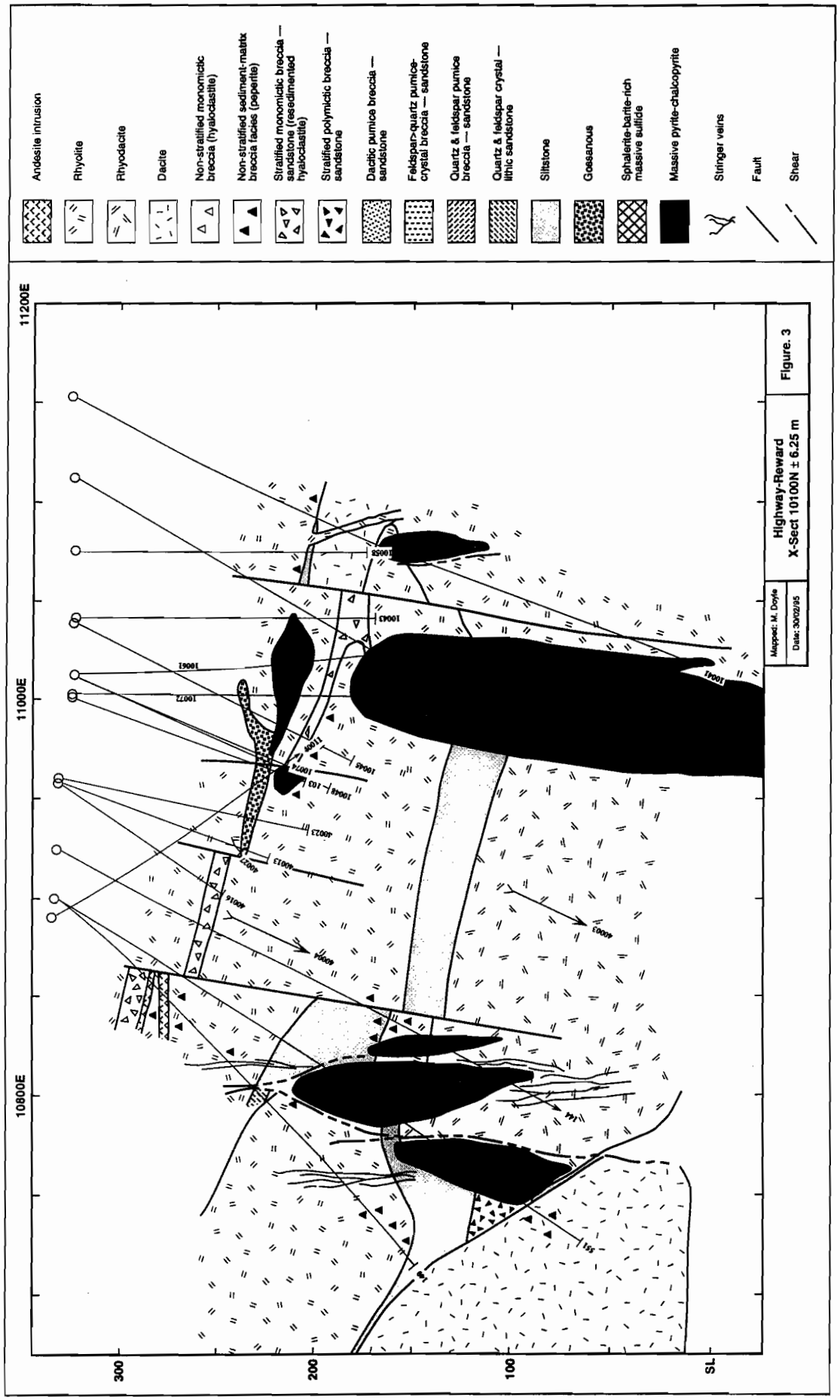

Figure 3. Simplified geological cross-section of the Highway–Reward deposit at 10100N. RL = relative position above sea level.

spaced less than 3 to 10 m apart (section 10100N; Fig. 3) or a single "dome" or "tooth-shaped" massive sulfide body. The Reward orebody consists of one main and several smaller subvertical, NNE trending, massive pyrite pipes (Fig. 3). The largest pipe is saddle-shaped in plan, with a bulbous top (Fig. 1). The pipe is 100 m x 150 m in plan and up to 250 m in depth. It contains around 5 million tonnes of massive pyrite (Beams et al., 1989), which includes a small chalcopyrite-rich zone.

Mineralogy, textures, and contact relationships

The massive pyrite-chalcopyrite pipes comprise a relatively simple mineralogy of pyrite and chalcopyrite, with minor tennantite, sphalerite, quartz and sericite. Trace minerals include chlorite, aikinite, carbonate, galena, barite, hematite and rutile (Huston, 1992). Pyrite is typically subhedral to euhedral and fine to medium grained (20–300 μm). Patches of coarse grained (2–5 mm) pyrite are often associated with shear zones. Rarely pyrite has a lath-like habit (e.g. REM 150, 159.3 m) and may be pseudomorphing an earlier mineral such as hematite, barite, or anhydrite (cf. Large, 1992). Pyrite can also be spongy, shreddy, framboidal, or exhibit snowflake texture (Huston, 1992). Chalcopyrite flecks, veinlets (< 1 mm wide), and patches cut across massive pyrite. Fine grained annealed chalcopyrite fills the interstices between pyrite crystals. Barite, quartz-carbonate, and anhydrite veins cut across the pyrite-chalcopyrite mineralisation. In some drill cores, barite occurs as tabular laths interstitial to pyrite and is pseudomorphed by quartz (e.g. REM 147, 140m).

In the massive sulfide, matrix gangue is generally absent except locally along the margins of the pipes where quartz or sericite ± quartz±pyrite altered volcanic rock is abundant. The exception is a small segment of the Highway pipe (e.g. REM 551, 228–285) where interstitial sericite (now clay) comprises around 10% of the pipe. In most other holes, semi-massive and massive pyrite with 30–60% relict patches and segments of altered coherent and peperitic rhyolite to dacite occur within a 1 to 10 m wide zone at the margins and top of the pipes. Relict quartz phenocrysts are rarely preserved within the sulfide, but quartz and/or feldspar are common in relict volcanic intervals. The rhyolitic-dacitic component of peperite is often more pyritic than siltstone in the matrix or filling fractures (e.g. REM 142, 170–177). Interstial anhedral quartz constitutes up to 20–30% of the pipe along some of these contacts. The quartz is intergrown with pyrite, forms patches up to 2 cm across, or occurs in bands of pyrite-quartz ± barite (e.g. REM 554). Contacts vary from sharp to finely bulbous, and many are sheared. A halo of disseminated and patchy pyrite extends out into the surrounding altered rhyolite-dacite or peperite.

Sphalerite-galena mineralisation

The pyrite-chalcopyrite pipes are surrounded by a halo of Pb–Zn-rich mineralisation up to 500 m wide in an east–west direction and around 225 m long. Within this zone there are four styles of Pb-Zn mineralisation. They are: (1) veins and veinlets of sphalerite-galena-barite within altered volcanics along the margins and top of the pyrite pipes; (2) disseminated, patchy and spotty sphalerite ± galena within sericite-quartz-chlorite altered rocks at the top of the pipes; (3) lenses of stratabound massive pyrite-sphalerite-chalcopyrite-barite closely associated with volcaniclastic mass flow deposits in the hanging wall to the Reward deposit; (4) massive to semi-massive pyrite-sphalerite-chalcopyrite ± barite at the margins of the pyrite pipes.

The first style consists of low grade Pb-Zn and can be found throughout the host succession above and adjacent to the walls of the pipes. However, the strongest vein development occurs along the margins of the Reward pipe. Disseminated and patchy sphalerite and galena form a halo above the Highway pipe and extends around 5 m into the peperitic base of the hangingwall rhyolite (e.g. REM 155, 554). Above Reward, supergene clay, sphalerite, bornite and covellite occur as disseminations and patches in near surface, partially oxidised samples. The halo of Pb-Zn mineralisation extends up to 20 m into the hangingwall, 80 m laterally and includes a small stratiform pyrite-sphalerite-chalcopyrite-barite lens around 60 m in length. The massive sulfide lens is spatially associated with, but physically separated

from, the main Reward pipe. Drilling to date suggests that southern part of the lens comprises massive and finely banded sphalerite-rich massive sulfide. Banded sulfide textures are common towards the base of the interval, and comprise thin sulfide bands and siltstone bands which are deformed by small F3 folds. The up dip and northern part of the lens has a progressively thickening pyrite-rich base and grades into a discordant massive pyrite pod (Fig. 4). The pod occurs around 20 m above the southern margin of the Reward pipe. Sphalerite-barite-rich massive sulfide intersected at a similar stratigraphic position in drill holes further to the east is interpreted as continuation of the pyrite pod. Thin (3 m) intervals of sphalerite-rich massive sulfide intersected lower in the stratigraphy (e.g. REW 808, 470–473 m) may be of a similar style. Their geometry and distribution is poorly constrained. The forth style of massive sulfide occurs within a thin (<1 m) zone at the margins of the pyrite-chalcopyrite pipes (e.g. REM 150, 224–228m). It consists of massive to finely banded pyrite-chalcopyrite-sphalerite-barite replacing peperite. The bands are 1–2 mm wide, strongly contorted, and mimic contacts between the massive sulfide and altered volcanic. (e.g. REM 116, 182–190 m).

Mineralogy and textures

This mineralisation style consists of varying proportions of pyrite, sphalerite, chalcopyrite, and galena with a gangue dominated by quartz, sericite, and barite. Minor and trace minerals include tennantite, carbonate, chlorite, bismuth minerals, marcasite, hematite and electrum (Huston, 1992). Supergene clay, bornite and covellite occur in near surface, partially oxidised samples. Pyrite is euhedral or exhibits snowflake, colloform, or spongy textures (Huston, 1992). Sphalerite occurs as anhedral to annealed intergroths with pyrite and chalcopyrite, and often exhibits chalcopyrite disease. Barite laths are often pseudomorphed by quartz.

Fine lamination in the stratabound pyrite-sphalerite-chalcopyrite-barite mineralisation closely resemble bedded sulfide sediments. A limited microscopic study (REM 122, 157.7 m) suggests that laminae consist of 1–2 mm microcrystalline bands of anhedral quartz intergrown with pyrite, alternating with 1–20 mm bands of pyrite-sphalerite-chalcopyrite with interstitial coarse grained (0.05–0.2 mm) anhedral quartz and minor sericite. The grainsize of pyrite decrease from the base to the top of the thicker bands and resembles sedimentary grading. Pyrite is euhedral to subhedral and generally associated with sphalerite. Chalcopyrite occurs as anhedral grains and as chalcopyrite disease in sphalerite. Banding in the stratabound interval is cross-cut, and partially replaced, by diffusely bound veins and veinlets of pyrite and quartz. Similar veins dissect massive sphalerite mineralisation at the margins of the pyrite pipes.

Footwall and hangingwall stringer veins

Stringer vein style pyrite ± quartz ± sericite occurs below the Highway and Reward pipes and adjacent to the walls of the pipes. On some sections, stringer pyrite ± covellite ± chalcopyrite veins also occur in sericite-quartz altered volcanics above the pyrite pipes (e.g. REM 140, 60–220; Fig. 3). Small veins are dismembered in the cleavage and larger veins are fractures internally. Fibre quartz fills the fractures or forms a selvedge surrounding a pyrite ± sericite ± quartz core. A few veins comprise discontinuous, finely bulbous bands of quartz and pyrite. In general, disseminated fine to coarse grained euhedral to subhedral pyrite accounts for 10–20% of the wall rock beneath the pyrite pipes and veins vary from 0.5 to 15 cm across, but are mostly around 1 cm wide. Towards the centre of the stringer zone, vein spacing decreases from 0.5–1 m to 15–30 cm (e.g. REM 142, 275–290 m). In the hangingwall, stringer veins are thinner (0.1–1 cm wide) and spaced 30 to 40 cm apart (e.g. REM 560, 101–120; REM 147, 102–116 m). The wall rock typically contains only 6–10 % disseminated pyrite.

Gossanous breccia zones

Gossanous zones occur within volcaniclastic deposits and coherent rhyolite overlying the pyrite pipes and crop out in the base of the Highway pit. They comprise heavily silicified and/or clay weathered volcanic rock with iron oxide filled veinlets and cubic

hollows after disseminated pyrite. Relict quartz phenocrysts are preserved in intervals of gossanous rhyolite. Some quartz bearing zones contain cherty seams and patches and may be altered peperite. Veins and patches of tabular barite crystals (1–2 mm long) are abundant in a few cores (e.g. REM 132, 58–69m).

Effects of deformation on the massive sulfide orebodies

The host lithofacies, mineralisation and associated alteration have the same tectonic fabric although the intensity of the fabric varies. The massive pyrite pipes have been fractured and dilated by the deformation and include local domains of cataclasite (e.g. HMO 60, 133–151 m). The alteration halo has sheared parallel to the subvertical S4 cleavage. Shearing has been focussed along the margins of the pyrite pipes and porphyries. Spotty and disseminated sphalerite have been drawn out into the cleavage while bands in stratiform pyrite-sphalerite lenes are folded. Fibre quartz has grown in the pressure shadows of disseminated euhedral pyrite grains. Stringer veins have been dismembered in the cleavage, whereas gypsum veins are crenulated by S4 (e.g. REM 149, 169.8 m). Chalcopyrite was mobilised into the cleavage, which cuts across primary quartz-pyrite banding at the margins of the pipes.

Alteration mineralogy and distribution

Detailed drill core logging of alteration- and volcanic-facies allow for investigation of the interplay between primary volcanic texture, the texture and mineralogy of each alteration stage, and mineralisation. Graphic lithological logs are and effective way of recording this information as the nature and positions of contacts, volcanic textures and facies, alteration mineralogy, and mineralisation are visible at a glance (Doyle, 1995). Textural relationships between each alteration stage and the pre-alteration texture, mineral abundances and associations, and chronology have been recorded using a code system developed by Doyle (1995).

The Highway and Reward orebodies occur within a well developed discordant alteration envelope. The envelop extends from at least 150 m below the orebodies to over 80 m above the Highway pipe. At Reward, intense weathering and oxidation obscure the hangingwall alteration on most sections. Footwall alteration occurs along the entire length of the deposit in a 500 m by 250 m postdeformational elliptical shape. Small zones of footwall-style alteration also occur peripheral to the orebodies, at Gateway (200–250 m west of Highway) and 200 m east of Reward.

Hydrothermal alteration at Highway–Reward is very irregular, reflecting primary heterogeneity modified by superimposed faulting. Broadly the alteration envelope has a spatial mineralogical zoning which is defined by assemblages of sericite, chlorite-sericite, chlorite ± anhydrite, quartz-chlorite-sericite, quartz-sericite ± pyrite, albite ± sericite-chlorite-quartz, and hematite ± chlorite-sericite-quartz. Disseminated pyrite is a common accessory in all but the latter two assemblages. Although the stringer veining and sulfide orebodies at Highway and Reward are spatially distinct, the alteration zones associated with each overlap, and some alteration zones partially envelop both orebodies. A quartz-sericite±pyrite zone is centred beneath the pyrite pipes and extend along the margins of the orebodies into the hangingwall succession (Figs 5, 6). Small domains of intense chlorite±anhydrite alteration occur within the footwall quartz-sericite zone, and along some margins of the pipes (Fig. 5). Sericite-quartz alteration gives way laterally and vertically to domains of sericite-chlorite ± quartz and chlorite-sericite alteration. Beyond the hydrothermal alteration halo, rocks of rhyolitic to dacitic composition contain various assemblages of albite, carbonate, sericite, chlorite, quartz, and hematite ± chlorite-sericite-quartz (Fig. 6). Contacts between the alteration zones are typically gradational. Less intense alteration, as indicated by variable preservation of feldspar and volcanic textures, occurs more commonly marginal to the orebodies and in the hangingwall. By contrast, the most intense alteration occurs in the stringer zone beneath the pyrite pipes, and on some sections, in quartz-sericite altered hangingwall rocks.

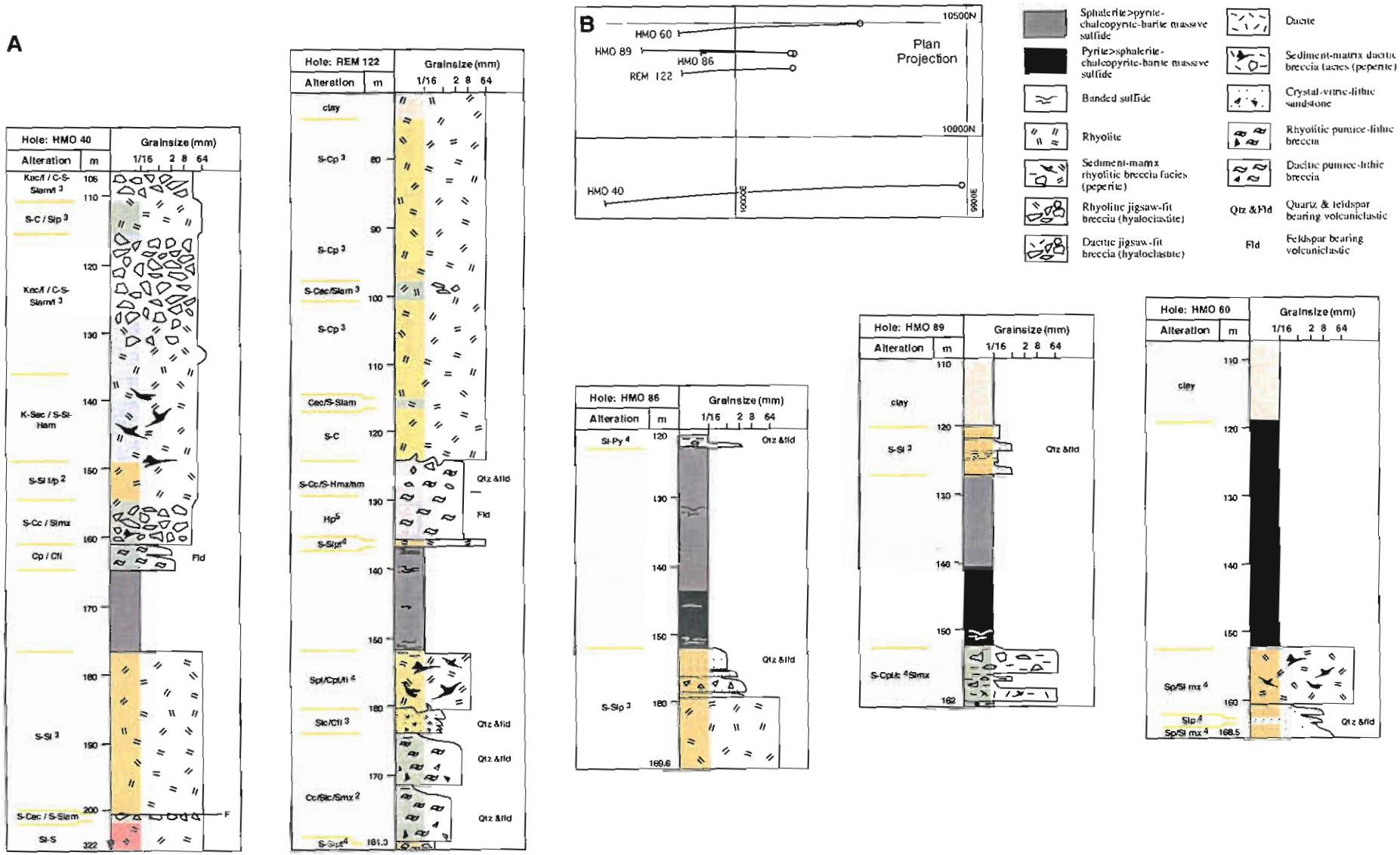

Figure 4. (A) Selected drill logs showing important internal textural variations and contact relationships of sphalerite-rich mineralisation and volcanic facies to the south of the Reward pipe. Alteration as in Fig. 7. (B) Plan projection of diamond drill holes in (A).

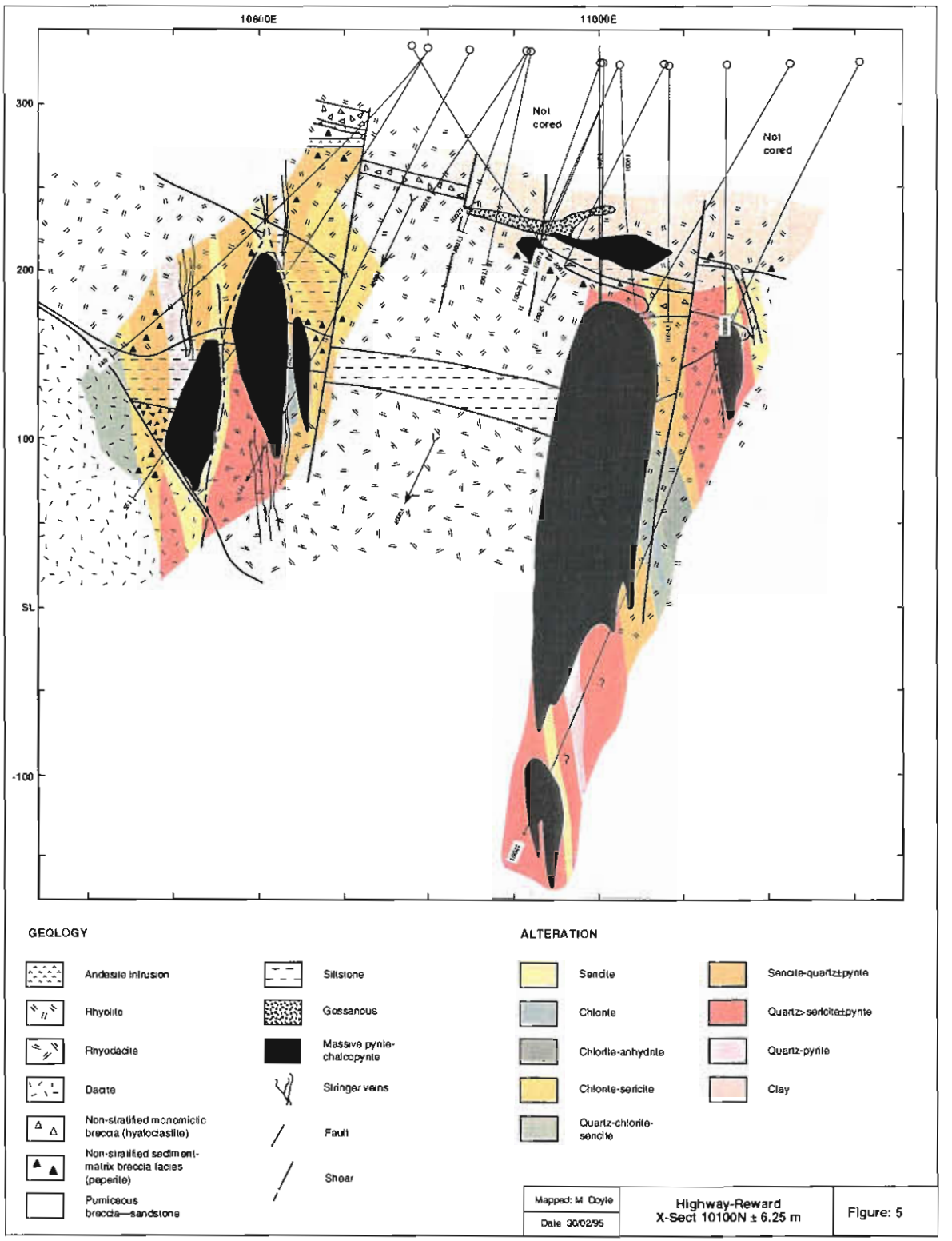

Figure 5. Simplified geological cross section showing the distribution of volcanic facies, alteration, and mineralisation at 10100N. RL = relative position above sea level.

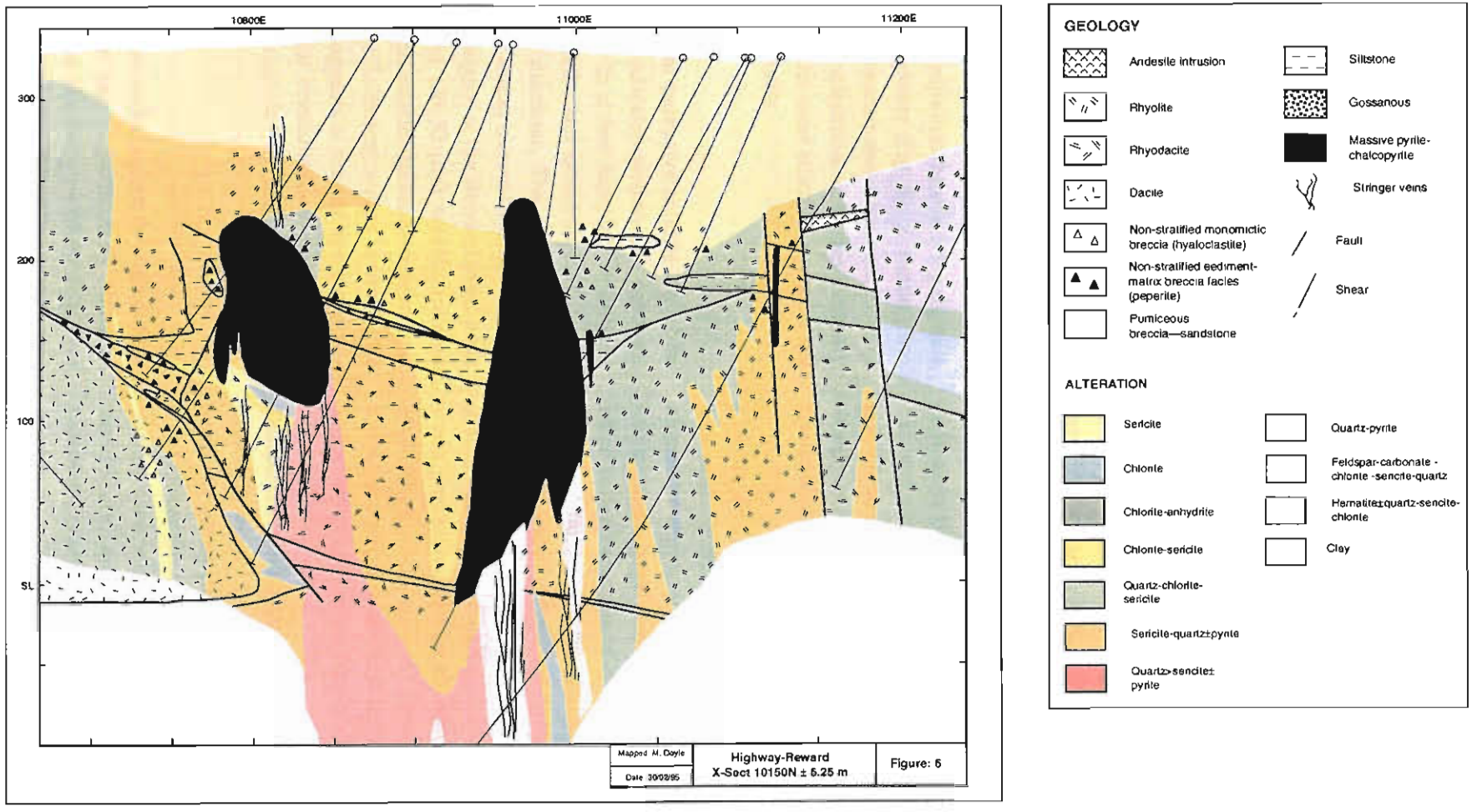

Figure 6. Simplified geological cross section showing the distribution of volcanic facies, alteration, and mineralisation at 10100N. RL = relative position above sea level.

Quartz-sericite ± pyrite zone

Within this zone, the relative proportions of quartz and feldspar varies considerably, and either can be the dominant phase. Quartz dominant alteration is more common in beneath the pipes domains of intense pervasive silicification are associated with strong quartz-pyrite stringer vein development (Fig. 6). In the footwall, alteration is pervasive or patchy, and often has often destroys original volcanic textures and created apparent clastic textures. Relict quartz phenocrysts are occasionally recognisable along the margins of the zone, particularly in sericitic apparent clasts enclosed by more intensely silicified wall rock. In some samples, disseminated pyrite preferentially replaced the sericitic component. In the hangingwall, a discordant zone of strong quartz-sericite±pyrite alteration extends up to more than 80 m above the Highway pipe into the overlying rhyolite and volcaniclastic deposits (Fig. 5). A similar, but poorly preserved zone occurs above the main Reward pipe. This style of alteration obscures primary textures, but only in the most silicified domains are lithofacies indeterminable.

Chlorite zone

Small zones of intense pervasive chlorite alteration are developed sporadically within the footwall quartz-sericite zone. In a few samples, chloritised wall rock contains lath- and ovoid-shaped quartz spots, 0.5–2 mm in diameter. The quartz may be pseudomorphing an earlier mineral such as barite or carbonate. At the margins of the Reward pipe, pods of very fine grained (30–50 μm) weakly foliated chlorite contain abundant euhedral anhydrite crystals up to 1.5 cm. The foliation wraps around the anhydrite, which suggests a pre- or syn-kinematic timing for anhydrite crystallisation, not the late-kinematic timing suggested by Beams et al. (1989, 1990).

Sericite alteration

This style of alteration is distributed through out the alteration envelope, but is particularly common within shear zones at the margins of the Highway and Reward orebodies. Sericitised wall rock also occurs as the gangue in semi-massive pyrite-chalcopyrite at the margins of the pyrite pipe. Subsequent strong tectonic foliation has concentrated on the sericitic domains and obscured or destroyed primary textures in the volcanic rock.

Quartz-chlorite-sericite zone

Outward from the quartz-sericite zone is a widespread quartz-chlorite-sericite zone. The zone comprises a complex alteration assemblage in which the dominant phase can be chlorite, sericite-quartz, or chlorite-sericite. Alteration within this zone is strongly controlled by primary volcanic textures, particularly fracture and matrix permeability. Early pervasive alteration phases often comprise pale to dark phyllosilicate-rich assemblages. Subsequent quartz-sericite alteration was often strongly controlled by fracture and matrix permeability or has overprinted earlier alteration assemblages. The polyphase alteration has resulted in the widespread development of patchy, motley, wispy and apparent clastic textures.

Chlorite-sericite alteration

Low intensity chlorite-sericite, with minor carbonate, alteration characterises this alteration zone. The assemblage is largely restricted small domains within more widespread quartz-chlorite-sericite alteration and is common towards the northern end of the Highway orebody. Near the hangingwall contact of the Highway pipe, quartz-sericite alteration passes gradationally out through a chlorite-sericite zone into weak pervasive chlorite alteration (e.g. REM 562, 100–197 m). Moderate to strong quartz-sericite alteration overprints earlier chlorite-sericite alteration at the contact of the two zones.

Feldspar (albite & K-feldspar) ± carbonate-chlorite-sericite-quartz alteration

Formerly glassy rhyolitic to dacitic volcanic rocks in the Trooper Creek Formation have often altered to various assemblages of feldspar, carbonate, chlorite, sericite and quartz. At Highway–Reward, these assemblages are restricted to hangingwall lithofacies greater than 200 m form the orebodies (Fig. 6). The

alteration is a pervasive-selective style, being regionally distributed but selectively replacing glassy parts of lavas and intrusions, pumiceous units, and crystal-vitric breccia–sandstone beds. This style of alteration was very heterogeneous, forming pale feldspar ± quartz-rich domains and green chlorite-sericite-rich areas. In pumiceous and shard-rich deposits, secondary feldspar or carbonate nucleated around feldspar phenocrysts and moved out as nodular zones, infilling vesicles and replacing former glassy wall. The feldspar alteration was incomplete, leaving weakly altered domains, which were subsequently altered to more phyllosilicate-rich compositions. The phyllosilicate altered domains are often strongly flattened and define a bedding parallel diagenetic compaction foliation (S1; cf. Allen and Cas, 1990). In the glassy parts of lavas and intrusions, early feldspar-carbonate-chlorite alteration was typically pervasive or fracture controlled. More advanced phyllosilicate dominated alteration generally spread outward from fractures or the matrix, overprinting earlier feldspar alteration.

Hematite±quartz-sericite-chlorite

A second common alteration style in the Trooper Creek Formation, as well illustrated in lithofacies 50–200 m from the Highway–Reward deposit, is widespread hematite ± quartz-sericite-chlorite alteration. Occasionally, small zones of hematite-rich alteration are preserved along the margins of the orebodies (e.g. REM 122, 125–136 m). The alteration is pervasive or overprinting domains of hematite, chlorite-sericite and chlorite-carbonate alteration generate patchy, motley or pseudoclastic textures. Formerly glassy, porous, and permeable facies (e.g. pumice breccia–sandstone, fractured glassy lava) are particularly susceptible to this styles of alteration. In other cases, hematite overprints lamination and bedding within siltstone which was probably relatively poorly porous. The alteration is generally restricted to single depositional units or only a few beds.

Alteration paragenesis

The regional distribution of the feldspar-carbonate-chlorite-sericite-quartz alteration assemblage is consistent with an early diagenetic or regional metamorphic origin. The albitic alteration protected some pumice from diagenetic compaction suggesting alteration occurred prior to or during diagenesis. The diagenetic compaction foliation is crenulated by the regional cleavage indicating that the alteration was complete prior to regional metamorphism. The domainal feldspar-carbonate-chlorite-sericite-quartz alteration is similar to that documented by Allen and Cas (1990) in pumiceous breccia units at Rosebery and Hercules, in western Tasmania, Australia. Allen and Cas (1990) suggest that two phase albite–K-feldspar and chlorite alteration occurred prior to tectonic deformation during the onset of diagenetic compaction. Elements such as Na, K, Al and Si necessary to form the widespread albite–K-feldspar alteration were probably derived by dissolution of glassy pyroclasts and/or hydrothermal leaching of glass deeper in the volcanic pile. In the Trooper Creek Formation, the widespread development of a bedding parallel stylolitic dissolution foliation in the pumice breccia beds is good evidence for leaching and dissolution of glass in the volcanic pile. It is uncertain whether albite and K-feldspar were the first alteration minerals formed or if they replaced earlier minerals such as zeolite and clay.

Hematite-rich alteration and quartz-hematite veins are also regionally distributed and not preferentially associated with mineralisation. The hematite alteration appears to be associated with small, local hydrothermal systems in the proximal facies association of intrusion- and lava-dominated volcanic centres and shallow marine volcanoes (cf. Sigurdsson, 1977). Convective circulating porewaters leached Fe, Si, and other elements from the glassy volcanic rocks and reprecipitated the iron and silica by conductive cooling and mixing with seawater in the enclosing volcanic package. The same hydrothermal systems were probably important in contributing elements for regional diagenetic feldspar alteration.

From drill core, it appears that hydrothermal alteration associated with massive sulfide deposition started with sericite-chlorite which was subsequently

overprinted by quartz-sericite and chlorite ± anhydrite alteration.

Interrelationships between lithofacies, mineralisation, and alteration

The geometry and distribution of the Highway and Reward orebodies were strongly influenced by the position of cryptodomes in the host succession (Figs 2, 3). The Highway pipe is bound by four distinct porphyries; dacite 1 (western margin), rhyodacite 2 (eastern margin and footwall), and rhyolites 3 and 4 (hangingwall). Rhyodacite 2 hosts most of the pyrite-chalcopyrite pipe and it's associated stringer mineralisation. The upper contact of the pipe has partially replaced the peperitic lower margin of a rhyolitic partly extrusive cryptodome (rhyolite 4). The two rock types are discrete and show no indications of mixing. Weak disseminated and semi-massive pyrite-sphalerite-barite mineralisation has replaced the sedimentary and rhyolitic components of the peperite. Intense quartz-sericite alteration and associated disseminated and stringer pyrite mineralisation extends for at least 60 m into the cryptodome. The Highway oxide resource occurs within this alteration zone, along the top of rhyolite 3 (cryptodome) below an onlapping margin of rhyolite 4 (Fig. 1). The southern extent of the Highway pipe is limited by a substantial thickening of rhyolite 4, and termination of rhyodacite 2. Both rhyodacite 2 and significant pyrite-chalcopyrite mineralisation are absent north of 10200N.

The main Reward pyrite-chalcopyrite pipe straddles the boundary between two cryptodomes; rhyodacite 2 (western margin) and rhyolite 2 (eastern margin; Fig. 3). An underlying syn-sedimentary sill (rhyodacite 1) transgresses the boundary between rhyodacite 2 and rhyolite 2 implying that they are not in faulted contact. Stringer veins extend beneath the pyrite pipe into rhyodacite 1, the top of which is partially replaced by massive pyrite-chalcopyrite. As at Highway, rhyolite 4 forms the hangingwall to the main Reward pipe. On many sections the upper margin of the pipe corresponds to the extrusive top of rhyolite 4 (Fig. 3). Several smaller pyrite bodies cut across the overlying volcaniclastic units and intrusions (rhyolites 5–6; Fig. 3). The down-dip and southern extension of one small pyrite pipe comprises stratiform sphalerite-pyrite-barite. The stratiform mineralisation overlies resedimented hyaloclastite of rhyolite 4 and a distinctive syn-sedimentary sill (rhyolite 5) which intruded the breccia while it was wet and poorly consolidated. As at Highway, the northern extent of the Reward pyrite-pipe is marked by the boundary between rhyodacite 2 and a northerly thickening cryptodome (rhyolite 9). The southern limit of the Reward pipe is poorly constrained. Stringer vein-style mineralisation extends for at least 90 m north and 150 m south of the Highway and Reward pyrite pipes.

Evidence for a syn-volcanic origin

Laing (1988) and Beams et al. (1989, 1990) proposed two episodes of ore deposition at Highway–Reward: a Cambro-Ordovician event which deposited syngenetic sphalerite-rich mineralisation, and a Siluro-Devonian syn-deformational episode which produced discordant pyrite-chalcopyrite pipes. Occasional patches of sulfide that crosscut cleavage occur in parts of the Highway–Reward deposit. However, most of the mineralisation and alteration have the same tectonic fabric as their host rocks. S4 cleavage and faults are the most prominent structures suggesting the ore predates the Siluro-Devonian deformation.

The pyrite-chalcopyrite pipes and sphalerite-galena-barite-rich mineralisation display a strong stratigraphic and lithofacies control which is inconsistent with a multistage mineralising system. In addition, the distribution of alteration minerals and textures are closely related to initial patterns of permeability and compositional contrast in the volcanic succession. Alteration associated with syn-deformational mineralisation is more likely to be controlled by fracture and fault patterns than volcanic texture.

Textures observed within both the pyrite-chalcopyrite pipes and marginal sphalerite-rich mineralisation provide strong evidence for a syngenetic origin (Huston, 1992). Pyrite with colloform, framboidal, spongy, and "snowflake" textures is

common within VHMS deposits. In particular, colloform pyrite is characteristic of growth in open space (e.g. Guilbert and Park, 1986), which is inconsistent with a syn-deformational model for mineralisation. Chalcopyrite diseased sphalerite is characteristic, but not diagnostic, of syn-genetic VHMS deposits.

Further evidence consistent with a VHMS origin for Highway–Reward is the occurrence of the deposits in a regionally altered submarine volcanic succession hosting other VHMS-style deposits (e.g. Thalanga, Liontown, Berry et al., 1992). The regional stratigraphy, depositional setting, and alteration style of the deposit is also similar to successions that contain relatively undeformed VHMS deposits.

Evidence for sub-seafloor replacement

The lithofacies characteristics of the host succession provide important insights into the origins of the Highway and Reward orebodies. With the exception of the stratiform Pb–Zn ores, mineralisation and associated alteration are discordant to local bedding, and enclosed by rapidly emplaced intrusions and volcaniclastic deposits. Relicts of the host lithofacies are often preserved within the mineralisation. The massive sulfides must therefore be interpreted to postdate their host rock and have formed by sub-seafloor replacement and/or infiltration. The stratiform sphalerite-pyrite-barite mineralisation also probably formed sub-seafloor as it passes up dip into a discordant massive pyrite body. The mineralisation contains siltstone laminae and significant interstitial sericite and quartz that is presumably an alteration of former volcanic (vitric ?) detritus. The enclosing volcaniclastic beds display bedforms which suggest they were rapidly emplaced as sediment gravity flows (turbidites). The evidence suggests that the stratiform mineralisation is a replacement of a precursor permeable and porous vitric-rich horizon. Apparent graded bedding within some parts of the lens may pseudomorph primary grading in the volcanic precursor. The grading (normal) is defined by pyrite and unlikely reflect reworking of sulfides on the seafloor because: (1) the pyrite is euhedral and displays no textural evidence of reworking; (2) spongy pyrite overgrows sericite (Huston, 1992), indicating that mineralising fluids passed through the sediments after they were deposited; (3) pyrite is mixed with former volcaniclastic material which probably had a significantly lower density. If the mass flows were turbulent, pyrite would have been concentrated in the base of the units and volcanic detritus towards the top. Rather, altered volcanic material occurs throughout the graded intervals and was partially replaced by sulfides.

The distance below the seafloor at which replacement occurred is difficult to interpret. At Highway, strong quartz-sericite alteration and pyrite veining extends more than 80 m into the hangingwall without any abrupt breaks in intensity. Consequently, the palaeoseafloor position at the time of mineralisation is not preserved. Prior to mining, barite-rich laterite cropped out at surface (Kay, 1987). In VHMS systems, barite typically forms at the interface between ascending hydrothermal solutions and cold seawater and/or seawater saturated strata. This suggests that the barite-rich mineralisation marks a near seafloor position.

At Reward, intense weathering and oxidation obscure and destroy alteration and lithofacies above the main pipe hampering the interpretation. On some sections, the top of the main pyrite-chalcopyrite pipe coincides with the extrusive top of rhyolite 4. It is possible therefore that the top of the resedimented hyaloclastite units overlying rhyolite 4 was the seafloor at the time of ore formation, and replacement occurred right up to (and/or down from) the seafloor. Above the main pyrite pipe, small discordant pyrite pipes cut across the hangingwall volcaniclastic deposits and intrusions. Consequently, replacement and infiltration may have taken place beneath successive seafloor positions as the host succession evolved. Alternatively, all of the host rocks were deposited prior to significant hydrothermal activity, and replacement occurred at a number of stratigraphic positions below a seafloor position which is not preserved.

A genetic model for the formation of the Highway–Reward deposit.

The Highway–Reward deposit formed in the proximal region of a submarine, syn-sedimentary intrusion dominated volcanic centre which evolved over its extended history. Figure 7 is a schematic reconstruction showing successive stages in the evolution of the volcanic centre. At the onset of significant hydrothermal activity the centre had the configuration shown in frame B or D. Intensification of the hydrothermal system followed the main phase of intrusion dominated volcanism. The magmatism may have acted as a heat engine during seawater convection causing metals to be leached from the volcanic pile and/or contributed to the ore forming fluid. Initially, hydrothermal fluids ascended growth faults beneath the Highway and Reward positions. Within a few hundreds of metres of the sea floor, hydrothermal fluid flow was complicated by the intersection of faults and stratigraphic zones of lower permeability. Hydrothermal fluids were focussed along the steep margins of cryptodomes that intruded the host volcanosedimentary deposits while they were wet and poorly consolidated. Emplacement of the syn-sedimentary intrusions had transformed the sediments into relatively impermeable rocks compared to the fractured glassy parts of the rhyolites to dacites. The indurated sediments may have prevented the development of broad convection cells and focussed ascending hydrothermal fluids into faults and fractures within the host sequence and along the glassy margins of the cryptodomes. The porosity and permeability of the cryptodomes allowed infiltration of cold seawater which mixed with the high temperature (300–350°C) hydrothermal fluid, promoting precipitation of pyrite-chalcopyrite in the developing pipes. An advancing pyrite front gradually moved out through the host succession replacing rhyolite-dacite, volcaniclastic deposits and sediment. At Highway, a rhyolitic partly extrusive cryptodome (rhyolite 4) formed a barrier to ascending ore fluids and replacement occurred below and within it's peperitic base. Although massive sulfide deposition was largely limited by the contact zone, fluid flow extended into cryptodome producing strong hangingwall quartz-sericite alteration enclosing pyritic stringer and disseminated styles of mineralisation.

At Reward, it is possible that the hydrothermal system remained active during a small hiatus in volcanism, and the pyrite pipes form a stack system beneath two successive seafloor positions. If so, the extrusive top of rhyolite 4 was the seafloor position at the time the main pyrite pipe was forming, and replacement occurred up to near the seafloor (Fig. 7B–C). The Highway deposit may have formed beneath the same seafloor position, although it is not preserved above the orebody. Metals carried by the hydrothermal fluids to the seafloor were dispersed in the water column and incorporated into distal sediments. Volcaniclastic deposits and intrusions emplaced above rhyolite 4 during renewed magmatism, were replaced by small discordant pyrite pipes below a new seafloor position (Fig. 7D). Alternatively, all of the mineralisation was emplaced within a single alteration pipe that extended through pre-existing volcanic units, beneath a palaeoseafloor position which is not preserved or is marked by pumiceous mass flow deposits at the top of the sequence (Fig. 7D). Poorly focussed fluid flow to the west and east of the Highway and Reward deposits produced zones of weak to moderate sericite-silica alteration.

Dispersed fluids which escaped out from the margins of the pyrite pipes into the fractured and glassy host rock, mixed with seawater and deposited broad halo of disseminated and patchy sphalerite-galena-barite mineralisation. A small stratiform sphalerite-pyrite-barite-rich lens formed above the main pyrite pipe by lateral migration of low temperature (150°–250°C) hydrothermal fluids through permeable volcaniclastic deposits (Fig. 7D). The northern extent of the lens becomes progressively more pyrite-rich and deposited from higher temperature (300°–350°C) fluids. An advancing pyrite-chalcopyrite front gradually moved through the sphalerite-barite-rich lens. The common development of chalcopyrite disease suggests that lead and zinc leached at the advancing copper front were reprecipitated within the volcanic precursor along a Pb-Zn-Ba front.

In the waning stages of hydrothermal activity the fluids cooled from a peak of 300°–350°C down to 200°–250°C, with the resulting emplacement of late stage sphalerite-galena-barite veins. Anhydrite deposited in zones of intense chlorite alteration as hydrothermal fluids mixed with seawater along the margins of the pipes.

This model suggests that there are four principal controls on the location and formation of Highway–Reward type VHMS deposits: (1) a progressively evolving submarine intrusion- and lava-dominated volcanic centre. The magmatism drives hydrothermal fluid flow, and the lavas and intrusions focus hydrothermal fluids along discrete mineralising pathways; (2) growth faults that focus hydrothermal fluids and act as conduits for rising magma; (3) an impermeable barrier promoting ponding of hydrothermal fluids and sub-seafloor replacement; (4) a long lived hydrothermal system that remains active despite continued volcanism, dewatering of the sediment pile by syn-sedimentary intrusions, and a moderately rapid sedimentation rate.

Discussion

The importance of lithofacies in sub-seafloor replacement

Sub-seafloor deposition of massive sulfides involves dissolution, replacement, infilling of pore space, and precipitation of minerals along fluid pathways. Consequently, the shapes, dimensions, and distribution of hydrothermal circulation and mineralisation are closely related to initial patterns of permeability and compositional contrast formed in the volcanic host rock by eruption, fragmentation, devitrification and possibly diagenesis.

Many sub-seafloor replacement ores occur within rapidly emplaced mass-flow deposits, particularly pumiceous facies (e.g. Khin Zaw and Large, 1992; Allen, 1994; Allen et al., 1997b). The originally highly porous, permeable, water saturated, and glassy nature of these deposits make them favourable host rocks for sub-seafloor replacement deposits. Ascending hydrothermal fluids will be poorly focussed (e.g. Large, 1992) and permeate through the substrate to produce widespread stratabound alteration and lens- or sheet-style massive sulfide mineralisation. Sulfide replacement of this type probably commences at the interface between the ascending hydrothermal fluid and overlying cold seawater-saturated strata (e.g. Khin Zaw and Large, 1992; Allen et al., 1997b).

Within less permeable, syn-sedimentary intrusion- and lava-dominated volcanic piles fluids are likely to by focussed along faults, local autoclastic breccia zones, or within the fractured glassy margins of lavas and intrusions. Under these circumstances, well focussed fluid flow gives rise to lens- or pipe-shaped massive sulfide mineralisation and well developed, zoned alteration pipes. Massive sulfide deposition probably commences beneath a relatively impermeable barrier (e.g. massive lava) and grows downward by mixing with convective seawater circulating through the glassy, porous and permeable margins of lavas and shallow intrusions. In the absence of a barrier, ascending hydrothermal fluids are more likely to reach the seafloor, and may well form a seafloor massive sulfide deposit.

The distance below the seafloor at which infiltration and replacement take place is rarely well constrained. In some cases, mass-flow deposits directly overlying the host rocks to sub-seafloor replacement deposit contain clasts of the massive sulfide (e.g. Hercules deposit), suggesting that replacement and infiltration probably occurred within a few metres of the seafloor. The upper few tens of metres in the volcanosedimentary pile is probably the favoured position for replacement, as sediments are wet and poorly consolidated in this zone, and at greater depths become progressively more compacted, and less amenable to replacement and infiltration by hydrothermal fluids. Ascending hydrothermal fluids will mix with cold seawater in the unconsolidated strata and precipitate some of their metals before reaching the seafloor.

Models for sub-seafloor replacement

Consideration of known published cases of sub-seafloor replacement deposits, together with evidence

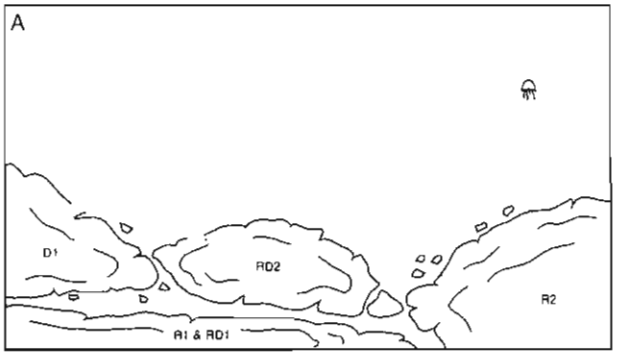

Subaqueous emplacement of feldspar±quartz-bearing pumiceous mass-flow deposits and overlying siltstone. Intrusion of rhyolitic to dacitic syn-sedimentary sills (R1, RD1) and cryptodomes (D1, RD2, R2). The intrusions influenced seafloor topography and partially dewatered the host succession.

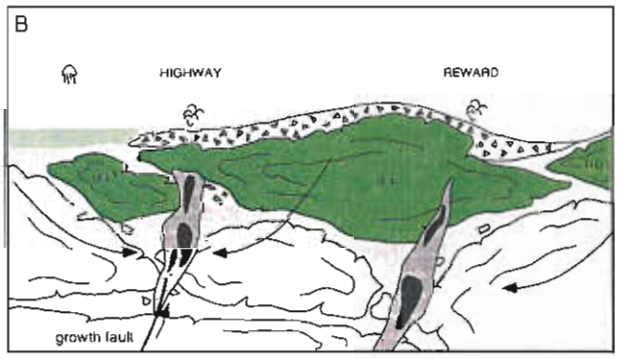

Intrusion of a rhyolitic cryptodome (R3) and partial extrusion of a rhyolitic cryptodome (R4) through the seafloor. Onset of significant hydrothermal activity. Hydrothermal fluids ascend growth faults and are focussed along the margins of the overlying cryptodomes. Fluids mix with seawater circulating through the glassy, porous and permeable margins of the cryptodomes and volcaniclastic deposits. Sulfides replace the enclosing strata within a strongly altered and veined zone.

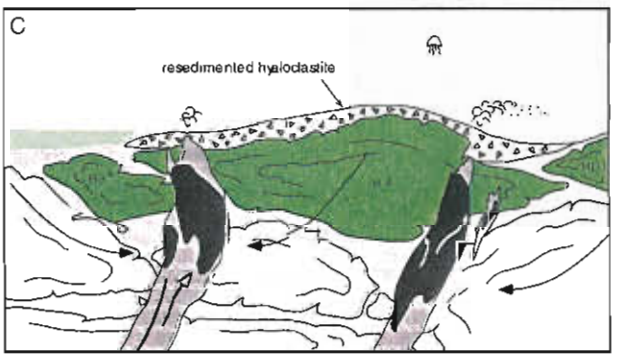

Intensification of the hydrothermal system to a maximum of 300-350°C. An advancing pyrite-chalcopyrite replacement front moves through the host strata overprinting earlier sulfide minerals. Ponding of hydrothermal fluids beneath rhyolite 4 promotes sulfide deposition. Vented hydrothermal fluids were dispered in the water column.

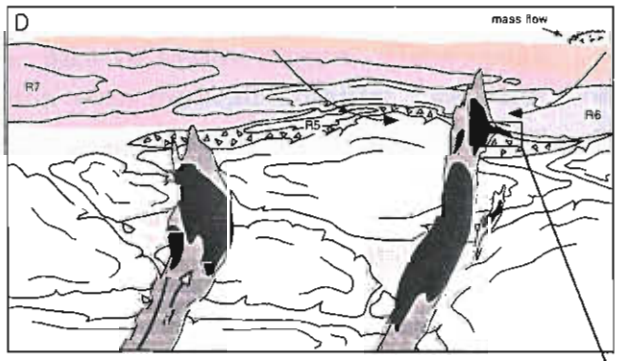

Intrusion of syn-sedimentary sills (R5-R7) into resedimented hyaloclastite of rhyolite 4, and the overlying deposits. At Reward, the pyrite pipe eventually penetrated rhyolite 4. Continued hydrothermal activity deposits pipe- and vein-style mineralisation above the main pipes. Hydrothermal fluids moving out from the margins of the pipes ,mix with seawater, and deposit a broad Pb-Zn-Ba halo. Minor stratiform Pb-Zn-Ba-rich lenses deposited by sub-seafloor replacement of permeable volcaniclastic deposits. Waining hydrothermal activity deposits minor sphalerite-galena-barite and anhydite.

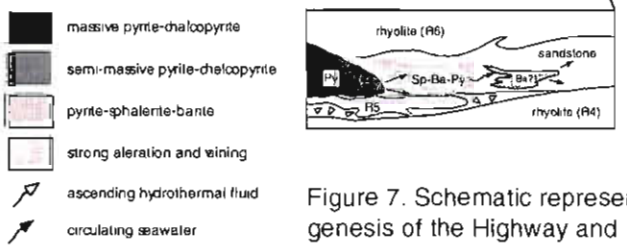

An advancing pyrite-chalcopyrite front progressively replaces earlier low-temperature (200-250°C) sphalerite (Sp)- and barite (Ba)-rich mineralisation.

Figure 7. Schematic representation of successive stages in the genesis of the Highway and Reward orebodies.

from Highway–Reward, allows some constrained speculation on the various circumstances under which sub-seafloor replacement and infiltration may develop, and the character of the resulting mineralisation. The various scenarios depend on the sedimentation rate and whether or not the host succession is dominated by relatively poorly porous rocks (e.g. lavas and shallow intrusions) or incompetent, very porous deposits (e.g. pumiceous units). Figure 8 summaries the main attributes of each of a range of possible sub-seafloor replacement style deposits. It does not aim to present a comprehensive account of all the possible scenarios for sub-seafloor replacement but simply to highlight the spectrum of deposit styles possible and their relationship to the enclosing strata.

Implications for mineral exploration

Pipes or plumes of intense hangingwall alteration are characteristic of sub-seafloor massive sulfide deposits, and can extend form tens to hundreds of metres into the hangingwall volcanic package. At Highway–Reward, this style of alteration hosts significant disseminated and stringer vein-style mineralisation and several small massive sulfide lenses. These characteristic are more typical of footwall alteration and stringer zones beneath seafloor massive sulfide deposits. Hangingwall alteration with footwall affinities has major implications for mineral exploration. Exploration requires consideration of: (1) the possibility of massive sulfides beneath alteration that would other wise be regarded as the footwall alteration pipe of an unpreserved seafloor massive sulfide deposit. The exploration history of the Highway–Reward deposit highlights the potential problems and benefits in distinguishing between the eroded remnants of a seafloor massive sulfide deposit and blind sub-seafloor ore deposit; (2) that massive sulfide lenses, pipes, veins, and/or disseminations may form a stacked system; and (3) the geochemical halo for sub-seafloor massive sulfide deposits may be more pronounced than for seafloor massive sulfide deposits located at a similar depth beneath the surface.

In many submarine volcanic successions, the localisation and shape of massive sulfide deposits has been related to fluid focussing along syn-volcanic growth faults (e.g. Large and Both, 1980). Berry et al., (1992) consider that syn-volcanic growth faults were important in controlling the distribution of the Reward deposits. The present research supports their interpretation, but highlights the importance of volcanic facies in focussing ascending hydrothermal fluids in sear seafloor environments. It is possible that the Truncheon and associated D3 faults reactivated pre-existing structures that controlled the initial deposition of the pyrite pipes. This possibility is supported by the elongation of the Highway and Reward pipes parallel to the trend of the Truncheon fault (mine grid north). An alternative interpretation is that the pyrite-chalcopyrite pipes were rotated into these structures during D3. In the Trooper Creek Formation, extensions of the Truncheon fault and other similar growth are favourable sites for the localisation of massive sulfide mineralisation.

This analysis reveals that the seafloor hydrothermal systems responsible for the massive sulfide mineralisation operated within a small non-explosive, syn-sedimentary intrusion-dominated volcanic centre. The Handcuff massive sulfide mineralisation is hosted by a similar but separate lava- and intrusion-dominated volcanic centre. The volcanic facies associations which dominate these centres are as prospective as parts of the Trooper Creek Formation dominated by lavas, sediments and volcaniclastic deposits. The spatial and temporal relationship of the massive sulfide mineralisation and volcanic centres, suggests that the mineralising hydrothermal systems were intimately and genetically related to the magmatism associated with emplacement of the volcanic centres.

Summary

The Highway–Reward deposit is hosted in the proximal facies association of a submarine (below storm wave base) silicic, syn-sedimentary intrusion dominated volcanic centre. The characteristic facies

associations of these volcanoes can be used as facies vectors to locate prospective proximal vent areas. Pyrite-chalcopyrite pipes and marginal pyrite-sphalerite-galena-barite mineralisation are syn-volcanic, sub-seafloor replacements of the host sediment, syn-volcanic intrusions, partly extrusive cryptodomes, and volcaniclastic deposits. Alteration associated with mineralisation is zonally arranged around the pipes so that alteration in the footwall and hangingwall is similar. Intense quartz-sericite alteration and pyrite veining extends more than 80 m above the Highway orebody. The location, distribution, form and shape of massive sulfide mineralisation and alteration are closely associated with syn-volcanic faults and initial patterns of permeability in the host rocks. pipe-shaped deposits are more likely to form if the host succession is dominated by relatively poorly porous rocks (e.g. lava and intrusion dominated volcanic centres), whereas lens- and sheet-shaped sub-seafloor replacement style-deposits are hosted by relatively incompetent, very porous deposits (e.g. pumiceous units).

References

Allen P.L., Weihed P. and Svenson S.Å., 1997. Setting of Zn-Cu-Au-Ag massive sulfide deposits in the evolution and facies architecture of a 1.9 Ga Marine Volcanic Arc, Skellefte District, Sweden. Econ. Geol., 1997: 1022-1053.

Allen R.L., 1988. False pyroclastic textures in altered silicic lavas, with implications for volcanic-associated mineralization. Econ. Geol., 83: 1424-1446.

Allen R.L., 1992. Reconstruction of the tectonic, volcanic and sedimentary setting of strongly deformed Zn-Cu massive sulfide deposits at Benambra, Victoria. Econ. Geol., 87: 825-854.

Allen R.L., 1994. Syn-volcanic, subseafloor replacement model for Rosebery and other massive sulfide ores. In: Contentious issues in Tasmania Geology, Hobart, Tasmania, 107-108.

Allen R.L. and Cas R.A.F., 1990. The Rosebery controversy: distinguishing prospective submarine ignimbrite-like units from true subaerial ignimbrites in the Rosebery-Hercules ZnCuPb massive sulphide district, Tasmania. In: Geological Society of Australia Abstracts, 31-32.

Beams S., Laing W. and O'Neill D., 1989. The exploration history and geology of the polymetallic Reward deposit, Mt Windsor Volcanic Belt, north Queensland. In: North Queensland Gold '89 Conference, Townsville, Queensland, 95-102.

Beams S., Laing W. and O'Neill D., 1993 The exploration history and geology of the polymetallic Reward deposit, Mt Windsor Volcanic Belt, north Queensland. In: Henderson, R. (eds.) Guide to the economic geology of the Charters Towers region, northeastern Queensland. 81-91.

Beams S., Laurie J. and O'Neill D., 1990. Reward polymetallic sulfide deposit. In: F.E. Hughes (ed.), Geology of the mineral deposits of Australia and Papua New Guinea, v. 1. The Australasian Inst. Mining and Metallurgy. Mon., 14: 1339-1543.

Beams S.D. and Dronseika E.V., 1995. The exploration history, geology and geochemistry of the polymetallic Reward and Highway deposits, Mt Windsor Subprovince. In: 17th International Geochemical Exploration Symposium. Mineral deposits of northeast Queensland: Geology and geophysics, Townsville, Queensland, 137-153.

Beams S.D. and Jenkins D.R., 1995. Regional exploration geochemistry and the regolith of northeast Queensland. In: 17th International Geochemical Exploration Symposium. Mineral deposits of northeast Queensland: Geology and geophysics, Townsville, Queensland, 33-53.

Berry R.F., 1989. Structure of the Mount Windsor Sub-province. CODES, University of Tasmania

Berry R.F., Huston D.L., Stolz A.J., Hill A.P., Beams S.D., Kuronen U. and Taube A., 1992. Stratigraphy, structure, and volcanic-hosted mineralisation of the Mount Windsor Subprovince, north Queensland, Australia. Econ. Geol., 87: 739-763.

Bodon S.B. and Valenta R.K., 1995. Primary and tectonic features of the Currawong Zn-Cu-Pb(-Au) massive sulfide deposit, Benambra, Victoria: Implications for ore genesis. Econ. Geol., 90: 1694-1721.

Dean J.A. and Carr G.R., 1992. Final report to Aberfoyle Resources Limited on the Pb isotopic compositions of mineralisation from Highway/Reward, Mt Windsor Joint Venture Project, NE Queensland. CSIRO Australia

Doyle M.G., 1994 Facies architecture of a submarine volcanic centre: Highway-Reward, Mount Windsor Volcanics, Canbro-Ordovician, Northern Queensland. In: Henderson, R. A. and Davis, B. K. (eds.) New developments in geology and matallogeny: Northern Tasman Orogenic Zone. EGRU Contribution, 50: 149-150.

Doyle M.G., 1995. Preliminary investigation of alteration at the Highway and Reward deposits, Mount Windsor Volcanics, Queensland. Australian Mineral Industries Research Association Limited - P439, report 1.

Doyle M.G. and McPhie J., 1994. A silicic submarine syn-sedimentary intrusive-dome-hyaloclastite host sequence to massive sulfide mineralisation: Mount Windsor Volcanics, Cambro-Ordovician, Australia. In: International Volcanological Congress, IAVCEI, Ankara, Turkey, Theme 10.

Franklin J.M., Sangster D.F. and Lydon J.W., 1981. Volcanic-associated massive sulfide deposits. Econ. Geol., 75th Aniv. Vol.: 485-627.

Galley A.G., Watkinson D.H., Jonasson I.R. and Riverin G., 1995. The subsea-floor formation ov volcanic-hosted massive sulfide: Evidence from the Ansil deposit, Rouyn-Noranda, Canada. Econ. Geol., 90: 2006-2017.

Goldfarb M.S., Converse D.R., Holland H.D. and Edmond J.M., 1983. The genesis of hot spring deposits on the East Pacific Rise, 21¡N. Econ. Geol. Mon., 5: 184-197.

Goodfellow W.D. and Blaise B., 1988. Sulfide formation and hydrothermal alteration of hemipelagic sediment in Middle Valley, Northern Juan de Fuca Ridge. Canadian Mineralogist, 26: 675-696.

Goodfellow W.D. and Franklin J.M., 1993. Geology, mineralogy, and chemistry od sediment-hosted clastic massive sulfides in shallow cores, Middle Valley, Northern Juan de Fuca Ridge. Econ. Geol., 88: 2037-2068.

Guilbert J.M. and Park C.P., 1986. The geology of ore deposits. Freedman, New York, 985 pp.

Huston D.L., 1992. Geological and geochemical controls on mineralisation at the Reward deposit: detailed studies of the Highway pipe. CODES, University of Tasmania

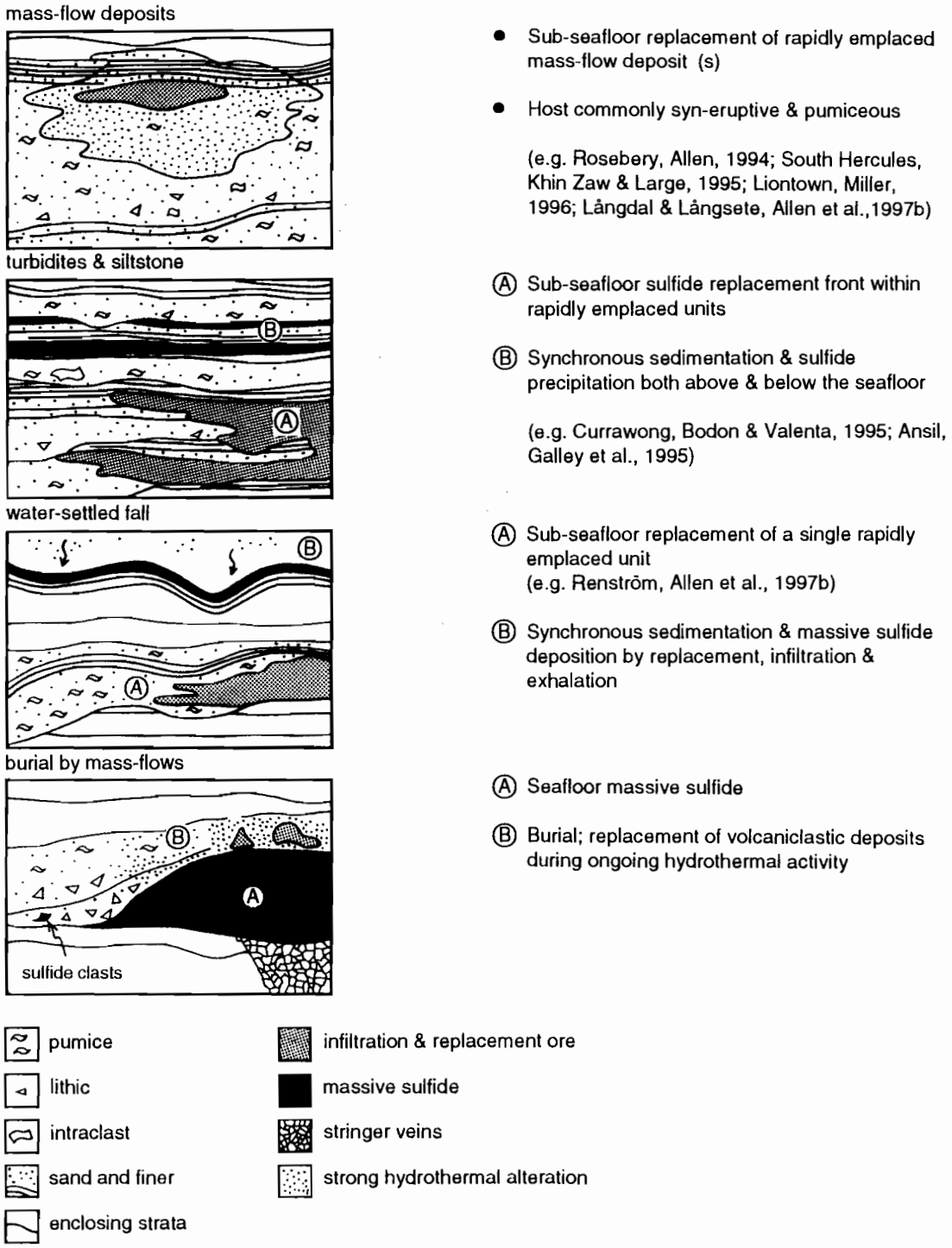

Figure 8. Schematic representation of the various scenarios in which ascending hydrothermal fluids can interact with the enclosing seawater-saturated strata to form a sub-seafloor replacement deposit.

syn-sedimentary sill

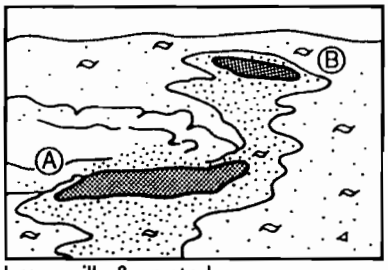

Ⓐ Ponding of hydrothermal fluids beneath a syn-sedimentary sill. Sub-seafloor replacement of the sill margin & host

Ⓑ Ascending fluids form a stacked system

(e.g. Rosebery, Allen, 1994)

lavas, sills & cryptodomes

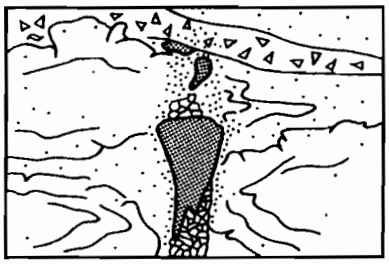

- Sub-seafloor replacement within a discordant alteration envelope
- Stacked massive sulfide pipes & stratiform lenses

(e.g. Highway-Reward)

lava

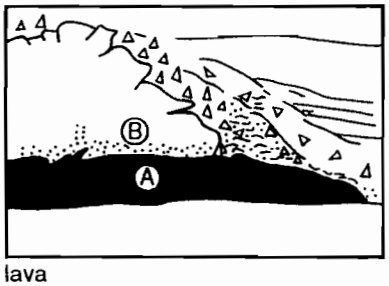

Ⓐ Seafloor massive sulfide mineralisation

Ⓑ Burial by lavas. Hanging-wall alteration develops during continued hydrothermal activity. May form a stacked system

(e.g. Fukazawa, Sato et al., 1979)

lava

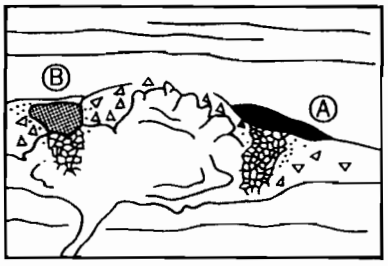

Ⓐ Seafloor massive sulfide

Ⓑ Replacement of in situ & resedimented autoclastic breccia units

pumice
lithic
sand and finer
autoclastic breccia
resedimented autoclastic breccia
glassy lava - intrusion
enclosing strata
infiltration & replacement ore
massive sulfide
stringer veins
strong hydrothermal alteration

Figure 8 cont. Schematic representation of the various scenarios in which ascending hydrothermal fluids can interact with the enclosing seawater-saturated strata to form a sub-seafloor replacement deposit.

Kay J.R., 1982. Notes on the geology of the Highway gold mine, Charter Towers. In: Geol. Soc. Aust. 1982 Field Conference, Charters Towers:Greenvale area,

Kay J.R., 1987. The Highway gold mine, Charters Towers:submarine volcanogenic gold-barite stringer mineralisation, modified by lateritic weathering. University of Queensland, Department of Geology Paper, 12: 111-125.

Koski R.A., Clague D.A. and Oudin E., 1984. Mineralogy and chemistry of massive sulfide deposits from the Juan de Fuca Ridge. Geol. Soc. Am. Bull., 95: 930-945.

Laing W., 1988. Structure of the Reward deposit, north Quensland.

Large R.R., 1977. Chemical evolution and zonation of massive sulfide deposits in volcanic terrains. Econ. Geol., 72: 549-572.

Large R.R., 1992. Australian volcanic-hosted massive sulfide deposits: features, styles, and genetic models. Econ. Geol., 87: 471-510.

Large R.R. and Both R.A., 1980. The volcanogenic ores at Mount Chalmers, eastern Queensland. Econ. Geol., 75: 992-1009.

McPhie J. and Large R., 1992. The Highway-Reward prospect: a brief description of the volcanic facies and nature of mineralisation. CODES, 11 pp.

Miller C.R., 1996. Geological and geochemical aspects of the Liontown VHMS deposit, NE Queensland [M. Econ. Geol.]. University of Tasmania, 90 pp.

Rona P.A., 1984. Hydrothermal mineralization at seafloor spreading centres. Earth Sci. Rev, 20: 1-104.

Sato Y., Ohmori Y. and Miyamoto H., 1979. Recent exploration of the Fukazawa kuroko deposit and some interesting modes of occurrences of the ores. Mining Geology, 29: 175-185.

Sigurdsson H., 1977. Chemistry of the crater lake during the 1971-72 Soufriere eruption. J. Volcanol. Geotherm. Res., 2: 165-186.

Solomon M., 1976 "Volcanic" massive sulfide deposits and their host rocks—a review and an explaination. In: Wolf, K. A. (eds.) Handbook of strata-bound and stratiform ore deposits, II, Regional studies and specific deposits. Elsevier, 21-50.

Zaw K. and Large R.R., 1992. The precious metal-rich South Hercules mineralisation, western Tasmania: A possible subsea-floor replacement volcanic-hosted massive sulfide deposit. Econ. Geol., 87: 931-952.

Zierenberg R.A., III W.C.S., Jr W.E.S., Koski R.A. and Strickler M.D., 1988. Mineralisation, alteration, and hydrothermal metamorphism of the ophiolite-hosted Turner-Albright sulfide deposit, southwestern Oregon. J. Geophys. Res., 93, B5: 4657-4674.

Preliminary report on the Rosebery lithochemical halo study

Ross Large and Rod Allen
Centre for Ore Deposit Studies, Geology Department, University of Tasmania

Introduction

Since the last report, the remaining two drill holes of the Rosebery alteration study (46R, 131R) have been logged and sampled, petrographic description of thin sections has continued, and whole rock and trace element geochemical analyses have been completed. Interpretation of the geochemical data, and microprobe analysis of individual mineral compositions, are in progress.

This report outlines the first batch of lithochemical results. Major and trace element data is reported on two drill holes through the orebody DDH 120R (K lens), R4452 (A-B lens) and three holes (DDH 131R, 113RDI and 109R) which lie to the north and outside the ore limits (Fig. 1).

The purpose of this preliminary report is to discuss the relationship between volcanic stratigraphy and alteration lithochemistry, with particular emphasis on DDH 120R which provides a good section through the hangingwall and footwall lithologies. This work will form the basis for more detailed studies on carbonate textures, carbonate distribution, carbonate chemistry and carbonate isotopes, which is the main focus of the research at Rosebery.

Chemostratigraphy using Ti/Zr ratios

Studies by Allen et al. (1996 a and b) have established the volcanic stratigraphy at the Rosebery north-end (Table 1).

Table 1. Volcanic stratigraphy of the Rosebery north-end.

Volcanic facies	Composition	Thickness (m)	Ti / Zr
Top		down hole thickness	
dacite lava (Mt. Black Volcanics)	rhyodacitic to dacitic		
Mt. Black Fault		1-3	
volcaniclastic mass flows	rhyolitic (+ mafic clasts)	190-230	7-18
black slate	mafic derived?	40-60	30-40
volcanic sandstone & siltstone	mixed	0-50	10-30
quartz porphyry sill	dacitic	0-95	12-14
pumice breccia **(host to ore)**	dacitic	0-20	12-14
pumice breccia mass flows	rhyolitic	>200	7-9
bottom			

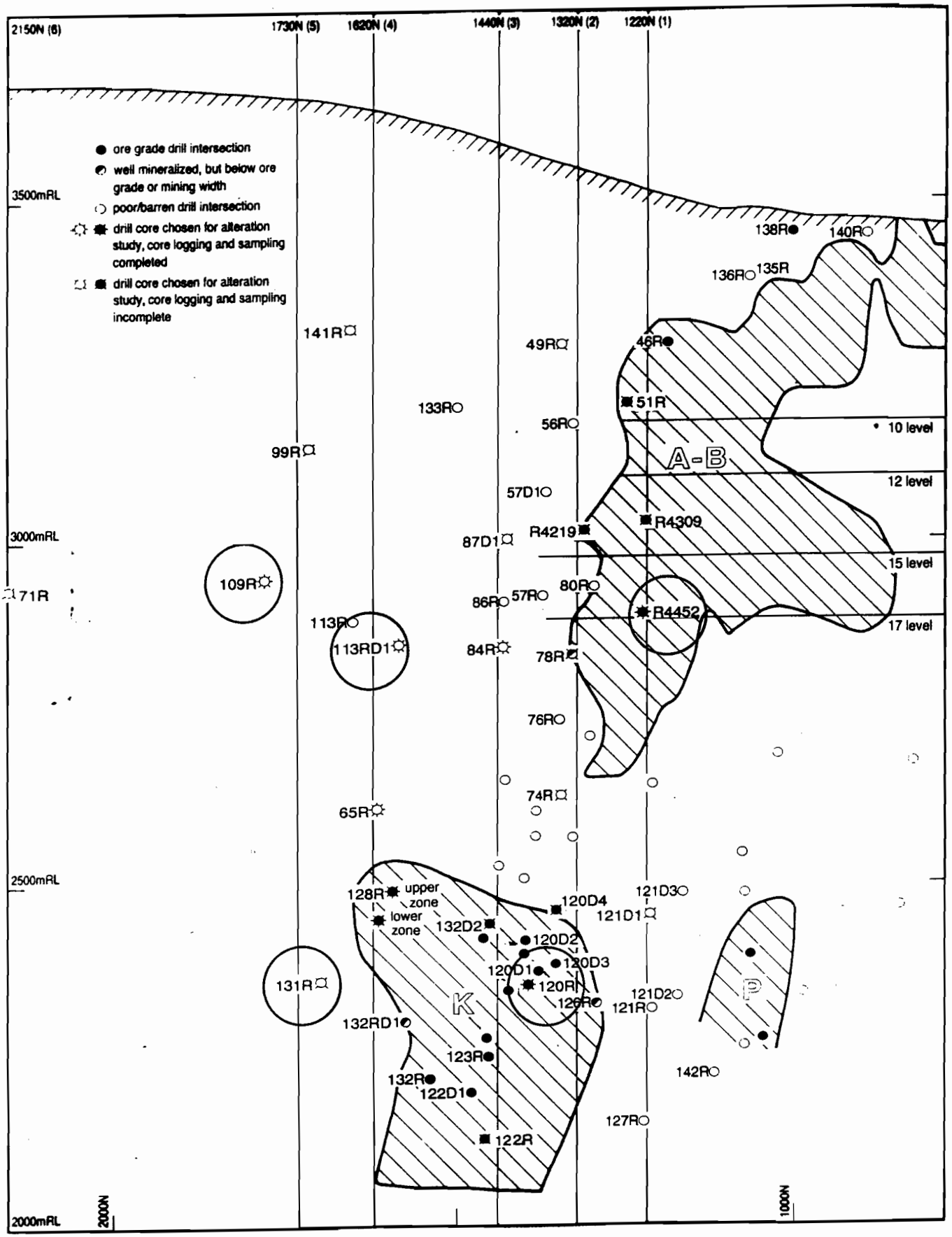

Figure 1. Location of drill holes sampled for the Rosebery alteration study. The holes discussed in this report are circled: DDH 120R, 131R, R4452, 113R, 109R.

Volcanic facies correlations in the five drill holes studied have been tested using the down hole Ti/Zr ratio, which is generally a good guide to primary volcanic composition. This is because Ti and Zr are immobile elements, and the Ti/Zr is unaffected by hydrothermal alteration or metamorphism. Previous work by Berry (1992) and Reid (1993) suggested that a subtle contact between the ore-bearing strata and the footwall could be defined by Ti/Zr ratios.

Using the Ti/Zr down hole plot from DDH 120R (Fig. 2), as an example, it is apparent that the major stratigraphic contacts are marked by abrupt changes in Ti/Zr. This is because each stratigraphic unit is characterised by a different volcanic composition.

By plotting Ti against Zr for the feldspar-phyric pumice breccias that underlie and locally enclose the ore (Fig. 3a), it is possible to show, that although the samples are altered and therefore have variable Ti and Zr contents, they fall into two groups each with a consistant Ti/Zr ratio, plotting along lines that extend through the origin (see discussion by Barrett and MacLean, 1994). This suggests that although the pumice breccias are strongly altered, they represent two compositionally distinct units, a feature which is only apparent in the geochemistry and was not discernible in the drill hole logging program or the thin section petrography. The fact that one of the data points in Figure 3a plots on the wrong line, suggests that it has been misclassified on the log. This sample in fact occurs at the contact between the two units.

In Figure 3b samples from the quartz-feldspar-biotite porphyritic sill which overlies Rosebbery Bank K ore lenses, are shown to plot along the same line as those from the host feldspar-phyric pumice breccia. The Ti/Zr ratio of 12–14 for both the pumice breccia and the sill suggest that both units are dacitic in composition, even though they have different pherocryst assemblages and the sill is quartz-rich. On the other hand the footwall pumice breccias are distinctly more rhyolitic with a Ti/Zr = 7 to 9. Our previous work on the Hercules–Mt Read regional traverse showed the same relationships. The host horizon at Hercules has Ti/Zr values of 12 to 14 (Large, 1996, Fig. 2) identical to the dacitic pumice breccia host horizon at Rosebery. This suggests that towards the end of the huge rhyotic pumic-breccia eruption that formed the Rosebery-Hercules footwall, the eruption tapped a more dacitic magma. Possible the source magma chamber was chemically zoned (as is typical of many large magma chambers), and toward the end of the eruption rhylite at the top of the chamber was depleted and underlying more mafic magma was tapped.

The Black Slate in DDH 120R exhibits much higher Ti/Zr ratios, from 30 to 40 (Figs 2, 3c), because the ratio will be affected by fractionation of Ti and Zr during sedimentary processes. A less likely alternative is that the slates were derived from a mafic source. The volcanic sandstones and siltstones underlying the Black Slate have variable Ti/Zr ratios from 10 to 30 indicating a mixed and variable composition (mixed provenance?) This is consistent with the interpretation that these rocks represent a reworked facies. The uppermost volcaniclastic mass flows also exhibit a variable Ti/Zr ratio. Typically the Ti/Zr ratio decreases upwards in each normal graded, subaqueous mass flow unit. Consequently, the variable Ti/Zr ratio probably reflects the physical fractionation of crystals and lithres from pumice and shards during deposition of each bed.

Summary — chemostratigraphy

The key conclusions from this part of the study are:

- The host pumice breccia and the quartz-feldspar-b? porphyry sill both have a dacitic composition with a characteristic Ti/Zr ratio of 12 to 14.
- These dacitic units (host pumice breccia and porphyry sill) form a distinct dacitic package that is relatively thin (0–140 m) and which could be related to the main mineralising episode (at least the K lens and A/B lens at the North end of Rosebery).
- The footwall pumice breccia and hangingwall mass flows are products of more rhyolitic volcanism which predated and post dated a more dacitic package that hosts and/or overlies the B and K lens ore bodies.
- The hangingwall volcanic sandstones have variable Ti/Zr ratios due to variable reworking and mixing of felsic and subordinate mafic components.

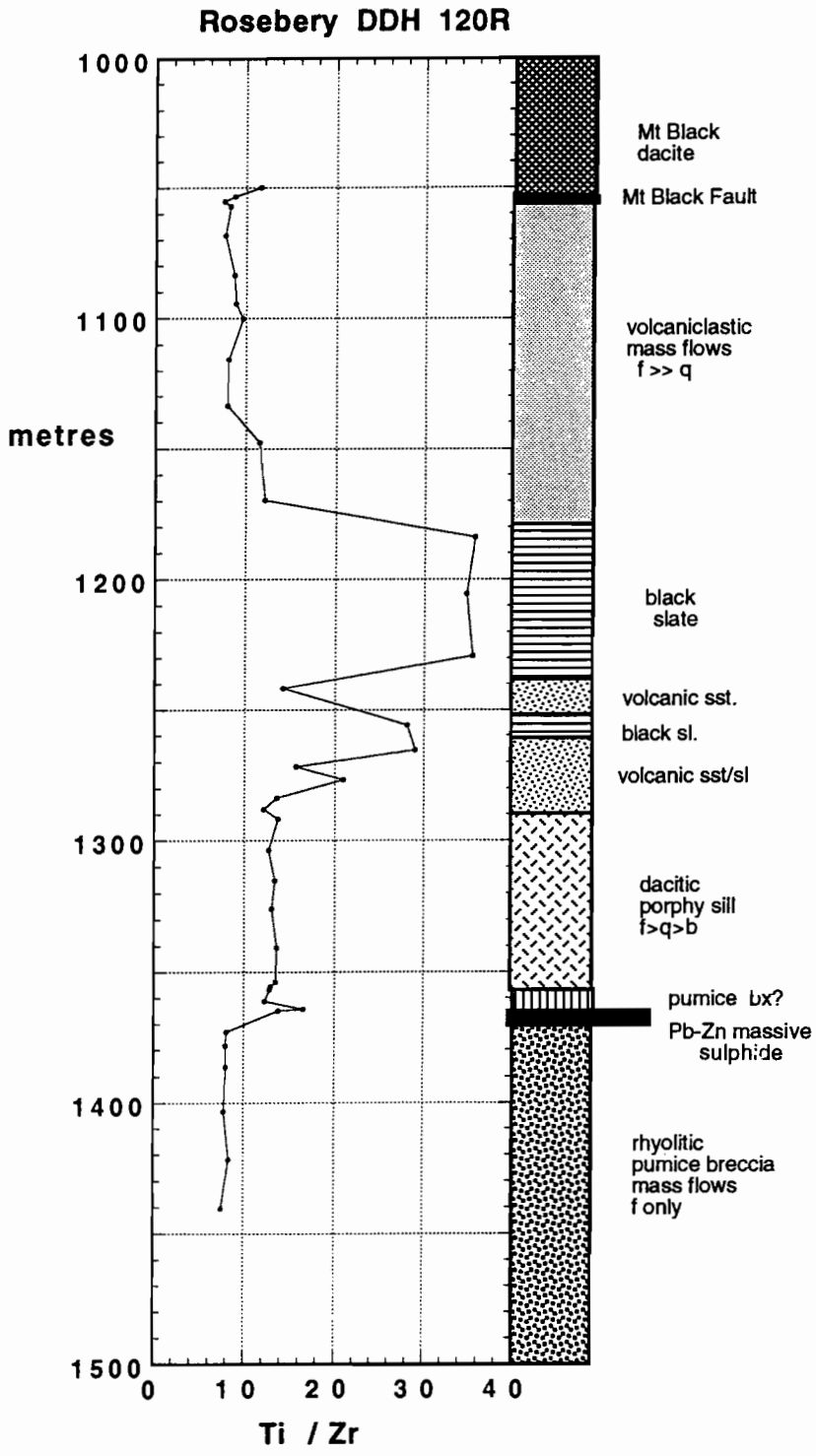

Figure 2. DDH 120R chemostratigraphy Ti/Zr ratio. Note the steps in Ti/Zr ratio at the major stratigraphic boundaries.

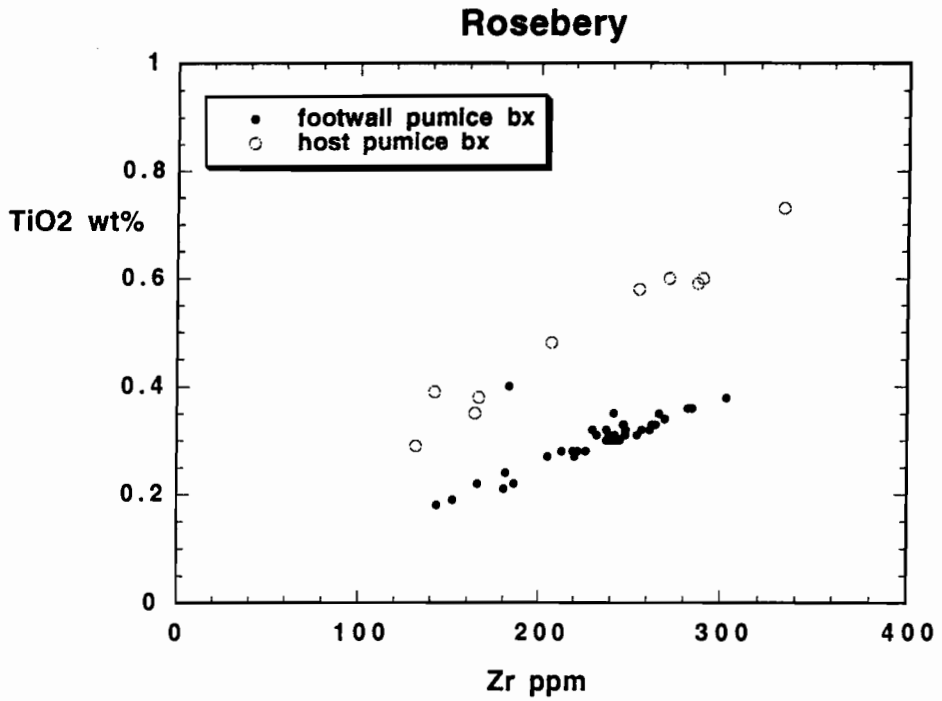

Figure 3a. Relationship between TiO_2 and Zr for the pumice breccias at Rosebery. This graph indicates two compositional types; the host pumice breccia has a higher Ti/Zr ratio (indicative of a dacitic composition) relative to the footwall pumice breccia.

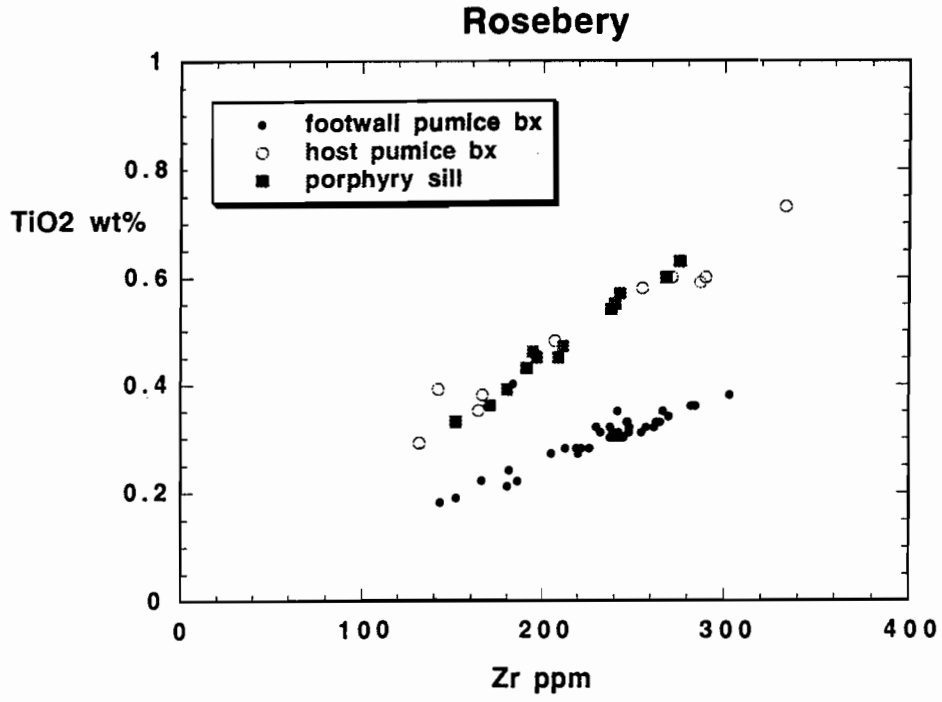

Figure 3b. Samples from the quartz porphyry sill plot on an identical trend to the host pumice breccia. This indicates the porphyry sill and dacitic host pumice breccia are comagmatic and probably unrelated to the rhyolitic footwall pumice breccias.

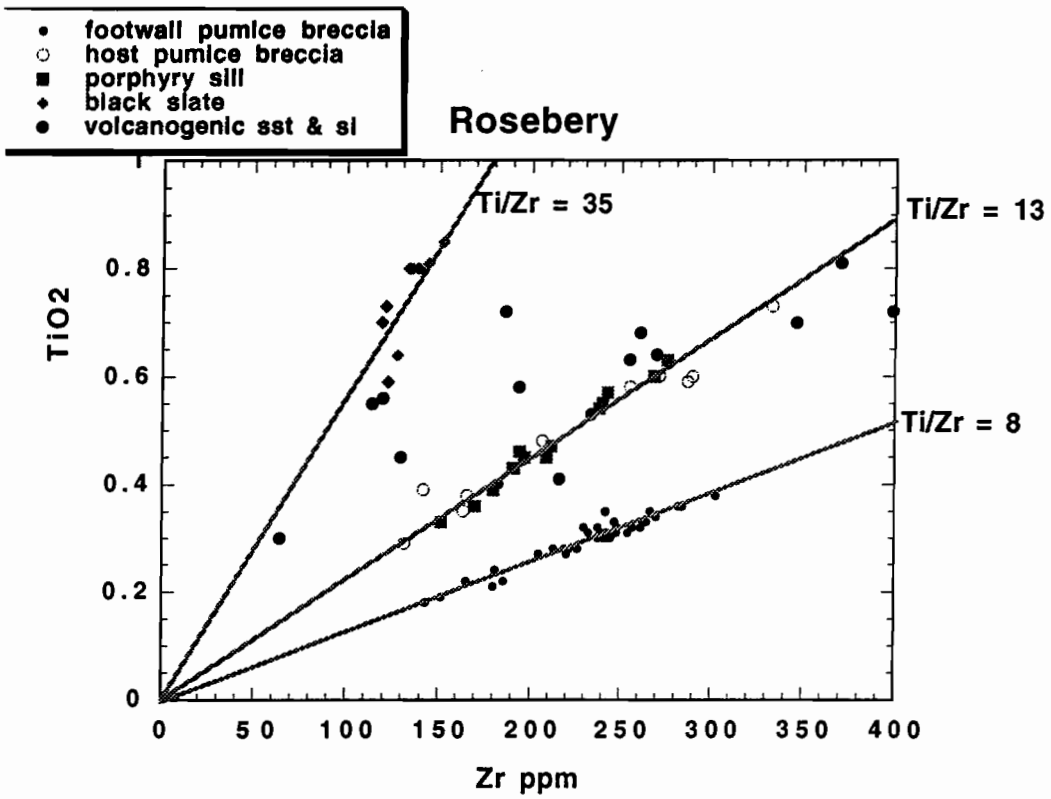

Figure 3c. The black slate forms a separate linear trend with a Ti/Zr=35, indicative of mafic volcanic source rocks. The volcanic sandstones and siltstones have variable Ti/Zr ratios indicative of mixing, with contributions from both felsic and mafic source rocks.

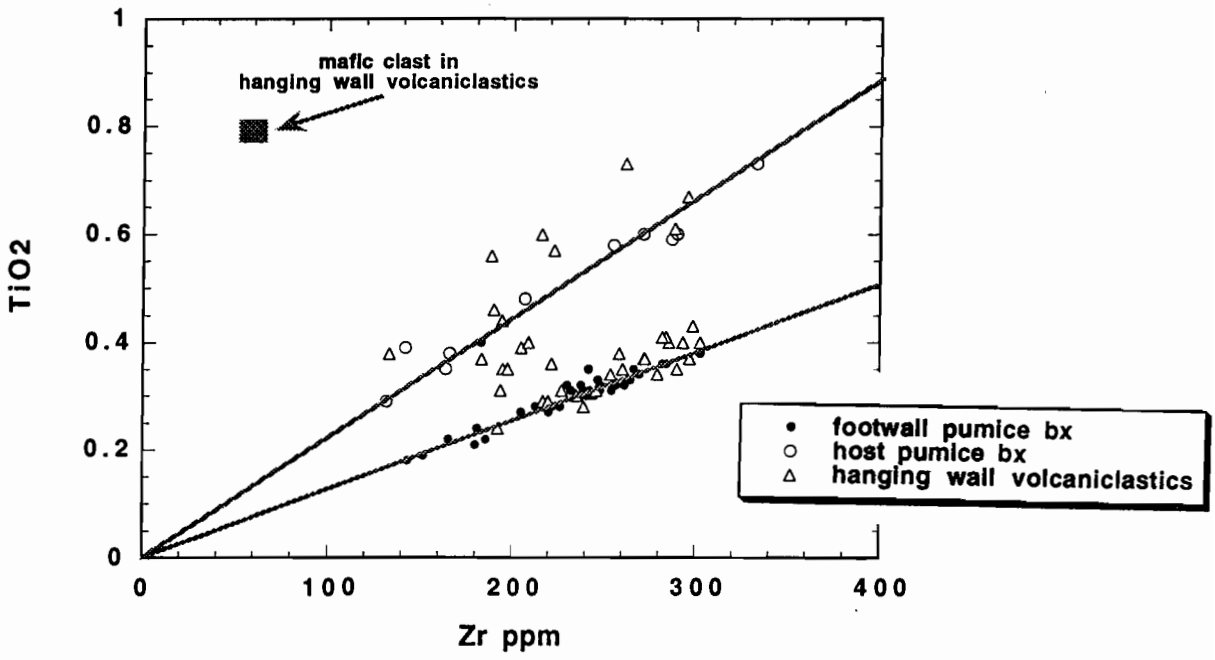

Figure 3d. About 50% of the hangingwall volcaniclastic mass flows plot along the same trend as the footwall rhyolitic mass flows. The remainder exhibit mixing between the rhyolitic end member and a mafic end member most probably represented by the mafic clast composition shown. Mafic clasts are common in the coarse base to the mass flows units (Allen et al. 1996).

- The hangingwall volcaniclastic mass flow units have variable Ti/Zr ratios probably due to physical fractranation of dense and less dense components during deposition.
- The hangingwall Black Slate has a high Ti/Zr ratio (35) due either to a sedimentary fractionation process or to derivation from mafic volcanic rocks.

Alteration geochemistry in DDH 120R

DDH 120R intersected a 3 m thickness of high grade Pb-Zn massive sulphide mineralisation in K-lens 1250 m below surface at 1400N. The hole gives a complete section of the Rosebery stratigraphy extending from the Mt Black Fault (1053 mbc) to the ore horizon (1366 mbc), finishing in the footwall pumice breccia (1445 mbc). A series of down-hole lithochemical plots are shown in Appendix A.

Significant trends in the data which relate to the alteration halo development are described below.

Zinc lead and copper

These three ore metals show a fairly tight concentration around the ore position with no distinct halo extending into the hangingwall. Anomalous values of >1000ppm Zn, >100ppm Pb and >100ppm Cu are confined to within 25m of the ore horizon. Scattered zones of disseminated sphalerite and galena recorded by Allen et al. (1996a) occur in the footwall and in the hangingwall mass flows up to 280m stratigraphically above the ore horizon. These zones result in anomalous Zn and Pb from 100 to 1000ppm.

The black slate exhibits elevated background values of Cu (plus Ni and Cr) consistent with derivation from a mafic volcanic source.

Manganese

Background values of MnO are around 0.1 wt% throughout the drill hole. MnO values over 10 wt% occur as $MnCO_3$ alteration within the dacitic pumice breccia directly above the ore lens. No Mn halo extends into the hangingwall lithologies, but a distinct increase in MnO occurs in the footwall rhyolitic pumice breccia over a distance of 50 m approaching the ore lens. This probably relates to an increase in the Mn content of carbonate (and chlorite?) approaching the ore. Moderate spot highs in MnO occur in the hangingwall and relate to pre-cleavage carbonate impregnations and bleached sericite-carbonate haloes around syntectonic carbonate veinlets.

Sodium and potassium

Sodium exhibits strong depletion to values less than 0.1 wt% Na_2O in the dacitic pumice breccia and in the rhyolitic footwall pumice breccia, due to feldspar destruction associated with serite, chlorite and carbonate alteration. Sodium depletion extends to 50 m below the ore horizon but only 11m above the ore, including only 2 m into the dacitic quartz porphyry sill. Hangingwall lithologies generally contain 2 to 4 wt% Na_2O, although the black slate has < 1 wt% Na_2O, a common feature for most shales.

Potassium displays elevated values from 2.5 to 5.5 wt% in the lithologies encompassing the ore position over 140 m of stratigraphy, including the immediate footwall pumice breccia, dacitic pumice breccia and the dacitic quartz porphyry sill. K_2O values in the upper hangingwall lithologies are generally less than 3 wt%, except for the weakly mineralized zone around 1070 to 1100 m.

Ishikawa alteration index

The AI reaches values of greater than 80 in two locations down hole:

- One sample at 1053 m in the Mt Black Fault.
- Four samples over the 40 m interval in the immediate footwall of the ore lens.

Erratic AI values from 30 to 70 occur in the carbonate altered dacitic pumice breccia overlying the ore and a spot high occurs in the volcanic sandstone overlying the dacite porphyry (1288.3 m).

Chl/carb/py Index

This index was previously defined by Large et al. (1996) as:

$$CI = \frac{(MgO + FeO)100}{(MgO + FeO + K_2O + Na_2O)}$$

The index is partly controlled by primary composition, with more mafic volcanics displaying higher CI values than felsic volcanics. However its greatest value is in outlining zones with chlorite, Mg-carbonate and pyrite enrichment.

In DDH 120R the CI index increases systematically towards the ore position from the footwall side from background values around 20 to maximum alteration values of around 80. Except for the basal 2 m section, the dacitic quartz porphyry has low AI and CI values indicating very little alteration. This observation is supported by the petrography (Allen et al. 1996a). The volcanic sandstone and black slate above the porphyry have elevated chlorite and carbonate contents, leading to CI values of 60 to 75.

Carbonate

Allen et al. (1996b) recorded a complex range of carbonate alteration styles in the drill holes at Rosebery; varying from nodular and spots alteration, to massive patches, veins and limestone beds.

The down hole CO_2 analyses (Appendix A) confirm that the maximum carbonate concentration is within the dacitic pumice breccia overlying the ore lens, where values exceed 10% CO_2, as $MnCO_3$. The other zones of carbonate concentration are within the black slate (as veins and thin beds), within the volcanic sandstones (as abundant impregnations and veins), and locally within the hangingwall mass flow units (as patchy impregnations and veins).

Thallium, antimony and arsenic

Smith and Huston (1992) previously reported significant Tl and Hg halos surrounding the ore lens at Rosebery, however their sampling was limited and the full extent of the halos was not defined.

In DDH 120R thallium exhibits an amazingly systematic pattern, defining a halo at least 270 m across stratigraphy surrounding the ore position. The main features of the Tl halo are:

- The halo of Tl in the hangingwall units (porphyry sill, volcanic sandstone and black slate) varies systematically from 10 ppm down to 1 ppm over a distance of 200 m, passing away from the ore body.
- The footwall halo is less extensive, but penetrates at least 70m below the ore lens.
- A second Tl peak occurs at the upper contact of the porphyry sill/volcanic sandstone suggesting a second ore horizon at this stratigraphic level (this mineralised position is confirmed in DDH 128R).

The full extent of the Tl halo is still not resolved with this data, due to the fact that the detection limit for Tl of 0.5 ppm is above the background and maybe within the limits of the halo. Further analytical work at the CSL is continuing to attempt to reduce the Tl detection limit to below 0.1 ppm and thus test the full halo extent.

Antimony shows a similar distribution to thallium with values above 2 ppm extending over 250 m above the ore and 70 m below the ore. The relationship between Tl and Sb for DDH 120R compared with the regional traverse data is shown in Figure 5. The background box on this diagram is fairly conservative and should be reduced in size when better detection limits for both Tl and Sb are achieved.

Arsenic has been analysed by both XRF (Geology Department) and ICP-MS (Analabs). Analabs provides a lower level of detection of 1ppm and is the preferred data set. Arsenic peaks occur both below and above the dacitic porphyry, marking the two ore positions. However the As pattern is more erratic than shown by Tl and Sb and therefore considered less useful. Also As is known to be associated with the Devonian granite-related mineralising event and may not be diagnostic of Cambrian VHMS environments.

Thorium/uranium ratio

Stolz et al. (1996) and Large (1996) outlined the potential of the Th/U ratio to define proximal and distal ore positions along the Hall Rivulet Canal and

the Hercules traverses. At Hercules the altered volcanics in the host horizon are characterised by Th/U < 3.

In DDH 120R, the Th/U ratio generally varies from 3 to 4 with two zones of values < 3:

- The strongly upper part of the carbonate altered dacitic pumice breccia. and the base of the dacitic quartz porphyry sill, directly above the ore zone.
- The moderately sericite-quartz-carbonate altered volcanic sandstones above the dacitic porphyry.

In this hole, at least, the Th/U ratio appears to effectively discriminate the ore horizon, and point to a second position at the top of the hangingwall dacitic sill. This second position, supported by the Tl, Sb and As data and the AI data, is known to contain Pb-Zn mineralisation in DDH 128R. Both the main and second ore positions, the most anomalous Th/U ratio (1–3) occurs several metres stratigraphically above the actual ore position, and consequently appears to be a lower hangingwall alteration effect.

Rubidium/strontium ratio

In volcanic rocks Rb substitutes for the K in K-feldspar and muscovite, while Sr substitutes for Ca in plagioclase and carbonates. The Rb/Sr ratio is therefore a good measure of muscovite enrichment and plagioclase depletion. In DDH 120R the Rb/Sr ratio shows a virtually identical pattern to the Ishikawa alteration index.

Preliminary assessment of lithochemical halo based on other drill holes

Due to lack of complete data it is not possible, at this time, to make a full assessment of the alteration lithochemical halo related to the A-B and K lens. However some preliminary comments are provided based on the data presented for drill holes R4452, 131R, 113R and 109R (Appendices B to E).

- **DDH 131R** — is located 150–100 m west outside the ore limits of K lens, and about 300m west of DDH 120R
  - less than 3 m of dacitic pumice breccia host horizon was intersected below the quartz porphyry sill
  - the lithochemical patterns for Cu, Pb, Zn, Mn, Na_2O, K_2O, AI, Tl, Sb and As are very similar to those recorded in DDH 120R
  - the Tl anomaly extends at least 160 m in the hangingwall and 100m into the footwall
  - the Sb anomaly may be traced over 300 m into the hangingwall sequence

- **DDH R 4452, 113R and 109R** — provide information on the lateral extent of the alteration halo passing 400m north along strike from the margin of A-B lens, and will be discussed in detail in the next report. Preliminary assessment indicates the following:
  - The dacitic pumic breccia that hosts the ore in R4452 and directly overlies ore 120R in horizon thins considerably, from 30m to less than 3m passing north along strike from R 4452 to 109R.
  - Although the base metals and Mn show limited dispersion along the ore position, other vectors including visible bleaching associated with sericite-quartz-carbonate-pyrite alteration, and AI and the S/Na_2O ratio can be traced over the 400m interval away from A-B lens.
  - Carbonate and Mn alteration are concentrated above or below the ore, or both, mainly in the dacitic pumice breccia and base of the dacitic quartz porphyry sill. All three (CO_2, Mn and dacite) thin along strike passing away from ore.
  - Tl and Sb form a major halo of 50–150 m stratigraphic thickness surrounding the ore position in all drill holes tested.

AI–Cl box plots

Our previous work on the Hercules–Mt Read regional traverse (Large, 1996) indicated that the AI–CI box plot was useful in classifying the CVC volcanics according to their position relative to potential VHMS mineralisation, into the following groups:

- Least altered
- Weakly altered (hangingwall type).
- Footwall altered.
- Ore horizon alteration.

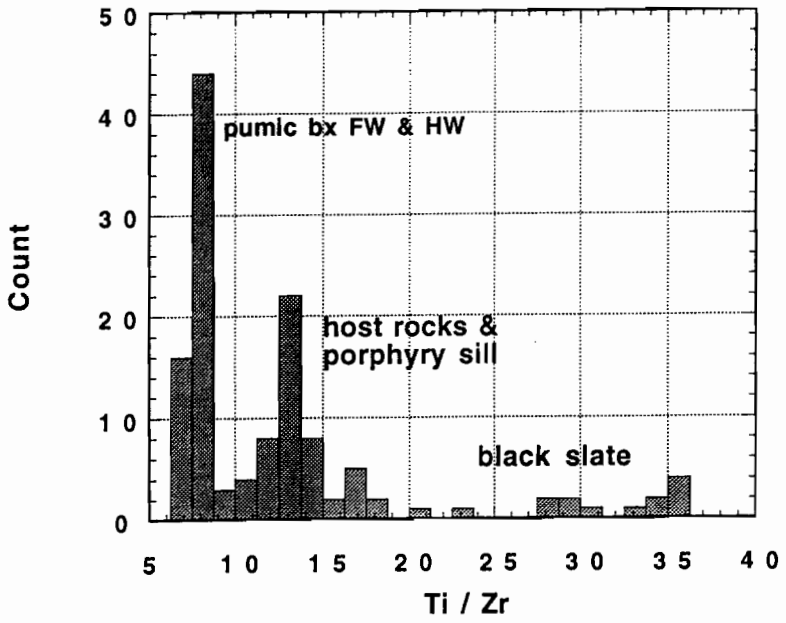

Figure 4. Histogram of Ti/Zr values for the volcanic stratigraphy at Rosebery, showing the peaks at 7–9 representing the rhyolitic footwall pumice breccias and at 12–14 representing the dacitic pumice breccias and quartz porphyry sill.

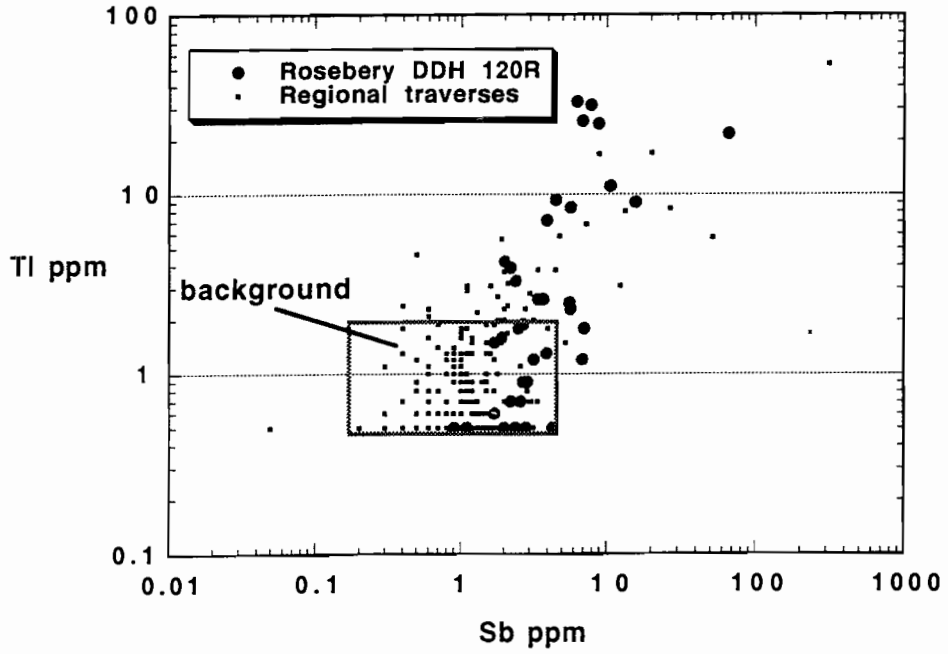

Figure 5. Relationship between Tl and Sb for DDH 120R and the regional traverse samples. The trend of increasing Tl >2ppm and Sb>5ppm is characteristic of the Rosebery and Hercules host rocks.

This classification is shown in Figure 6. Data from the five north-end drill holes have been plotted to test this classification scheme, at Rosebery. Figure 7 is a modified plot showing a revised classification based on data from the Rosebery footwall pumice breccia and the dacitic pumice breccia. The field for the ore related alteration (host horizon) has been expanded compared with the previous plot, to include all samples of the dacitic package. Note that in Figure 8, although most samples from the dacitic porphyry sill plot in the "least altered" box, as to be expected, the altered margins of the sill plot in the "ore horizon" field.

The hangingwall volcanic sandstones and Black Slate (Fig. 9) plot outside the "least altered" box due to higher CI and variable AI values. The volcanic sandstones show moderate hangingwall alteration. However, the black slates probably should not be included in this type of alteration classification, as they give misleading results when grouped with the primary reworked volcanics.

Conclusions

The following preliminary conclusions are drawn from the comparison of the lithochemical data and volcanic facies at Rosebery north-end:

- The Pb-Zn ore lenses (K and A-B) are enclosed by, or overlain by a pumice breccia unit that is texturally to the rhyolitic footwall pumice breccia, and mineralogically similar but which has a distinctly more dacitic Ti/Zr ratio. The overlying quartz porphyry sill has the same dacitic Ti/Zr ratio.

- The dacitic volcanics were either derived from a different magma body to the rhyolitic footwall pumice breccias, or they reflect eruption of a deeper level in the one zoned (chemically and physically stratified) magma chamber.

- The ore lenses are closely associated with the dacitic volcanic package, suggesting a genetic connection between dacite eruption and mineralisation, or .that the emplacement of the dacitic package and the mineralization, were both controlled by the same synvolcanic fault pattern and associated sea floor topography (grabens, half grabens).

- Elevated Ti/Zr, Cu, Ni and Cr in the black slate suggests it may have been derived by erosion of mafic volcanics.

- Variable Ti/Zr ratios in the hangingwall volcanic relate to variable reworking and mixing of felsic and subordinate mafic components. Variable Ti/Zr ratios in the hangingwall mass flow units probably reflect physical fractionation of dense and less dense components during deposition, and the occurrence of mafic lithic clasts in the base of one unit.

- The base metals (Cu, Pb and Zn) show limited dispersion either across strike or along strike from the ore lenses.

- Manganese and carbonate alteration is concentrated in the dacitic pumice breccia either just above or below the ore, or both, but also occurs as local less intense zones in the footwall and hangingwall.

- Na_2O depletion and K_2O enrichment characterise the proximal ore environment.

- The Ishikawa alteration index, Chl/carb/py index, Rb/Sr ratio, and S/Na_2O ratios provide good vectors to mineralisation from the footwall side.

- Thallium and antimony provide excellent vectors to ore in all directions — hangingwall, footwall and along strike.

- The Tl and Sb halos extend up to 200 m into the HW sequence and up to 100 m into the footwall volcanics.

- The AI-CI box plot has been modified, based on the data from both Hercules and Rosebery, and allows a method of classifying alteration related to VHMS ores of the Rosebery-Hercules type.

References

Allen, R.L., Duhig, N., Large, R.R., 1996a, Rosebery alteration study: AMIRA project P439, Report 2: May 1996, 95–118.

Allen, R.L., and Large, R.R., 1996b, Rosebery alteration study: AMIRA project P439, Report 3, October 1996, 143–152.

Barrett, T.J., and MacLean, W.H., 1994, Chemostratigraphy and hydrothermal alteration in exploration for VHMS deposits in greenstones and younger rocks in alteration and alteration processes associated with ore-forming systems. Edited by D.R. Lentz *Geol. Assoc. Can. short course notes* , 11, 433–467.

Berry, R.F., 1992, Geochemical evidence for the structure of the Rosebery deposit: AMIRA project P291 Report ?, 51–66.

Large, R.R., Stolz, A.J., and Duhig, N., 1996, Preliminary assessment of MRV geochemical databases in terms of possible vectors to ore: AMIRA project P439, Report 2: May 1996, P197–209.

Large, R.R., 1996. The Hercules-Mt Read traverse relationships between volcanic mineralogy alteration and geochemistry: AMIRA project P439, Report 3: October 1996, P153–234.

Reid, L.G., 1993. Aspects of north end mineralisation, Rosebery Mine, Western Tasmania: unpub. Master of Econ. Geol. thesis, CODES, University of Tasmania: 82.

Smith, R.N., Huston, D.L., 1992. Distribution and association of selected trace elements at the Rosebery deposit, Tasmania: *Economic Geology* 87: 706–719.

Stolz, A.J., Allen, R., Grifkins, C., Davidson, G., McPhie, J. & Blake, M., 1996. Petrographic and geochemical characteristics of alteration from the Hall Rivulet Canal-Mt Read-Red Hills-Anthony Dam traverse, Mt Read volcanic belt: AMIRA report 3, October 1996, 379–424.

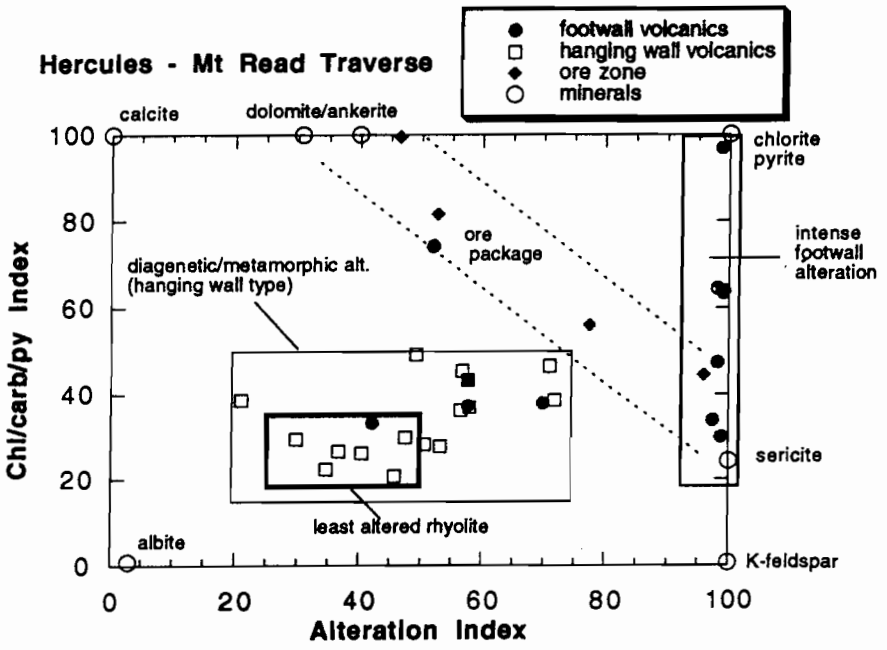

Figure 6. AI-CI box plot based on the Hercules-Mt Read regional traverse (Large, 1996). The footwall altered rocks plot along the sericite-chlorite/pyrite boundary, whereas the ore package alteration occurs in a corridor between sericite and dolomite/ankerite.

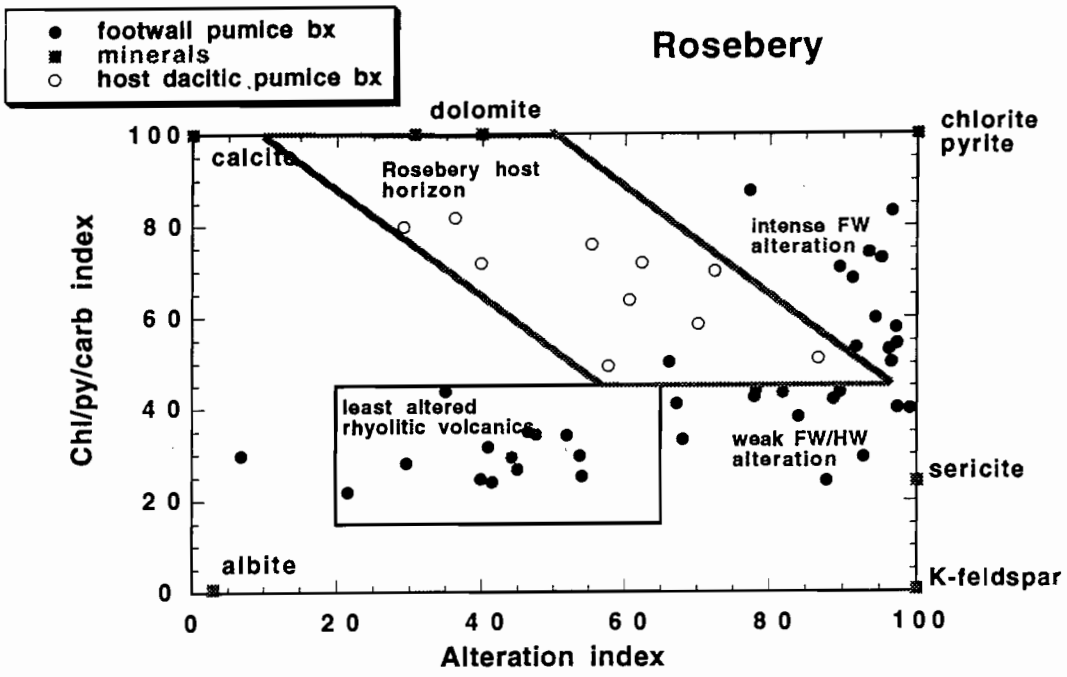

Figure 7. AI-CI box plot for the Rosebery north-end samples. This plot enables the pumice breccias to be classified into the various alteration types shown, relative to the stratiform ore lens.

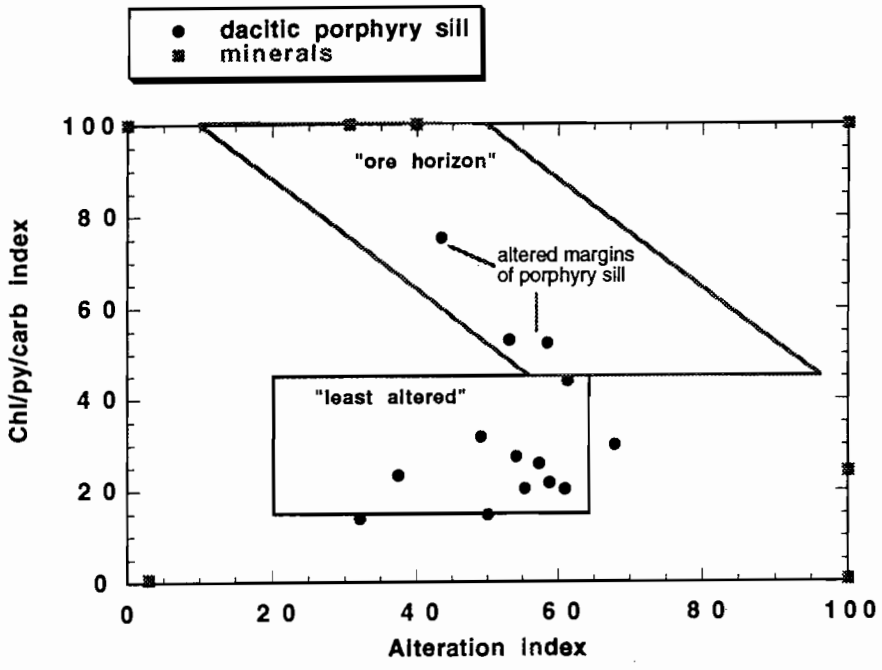

Figure 8. Alteration characteristics of the dacitic quartz porphyry. Most of the samples plot in the "least altered" box. However altered samples from the margins of the porphyry plot in the "ore-horizon" field.

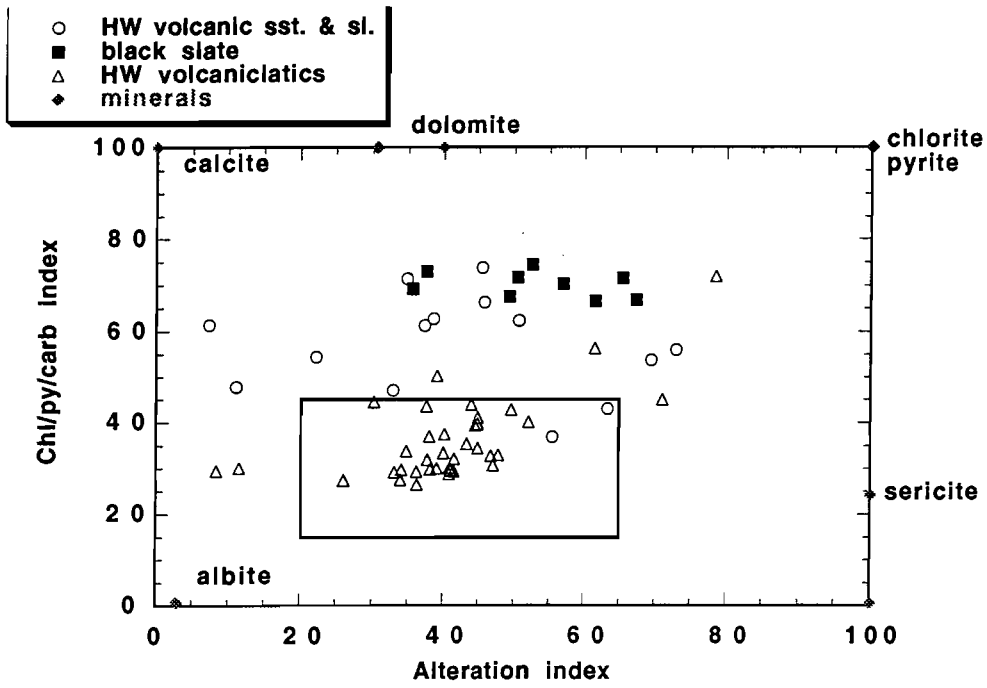

Figure 9. Due to chemical changes during erosion and reworking, volcanic sediments should not be plotted on the AI-CI box plot. Many of the volcanic sandstones and black slates samples plot in the "ore-horizon" field causing misleading interpretation of the data.

Appendix A

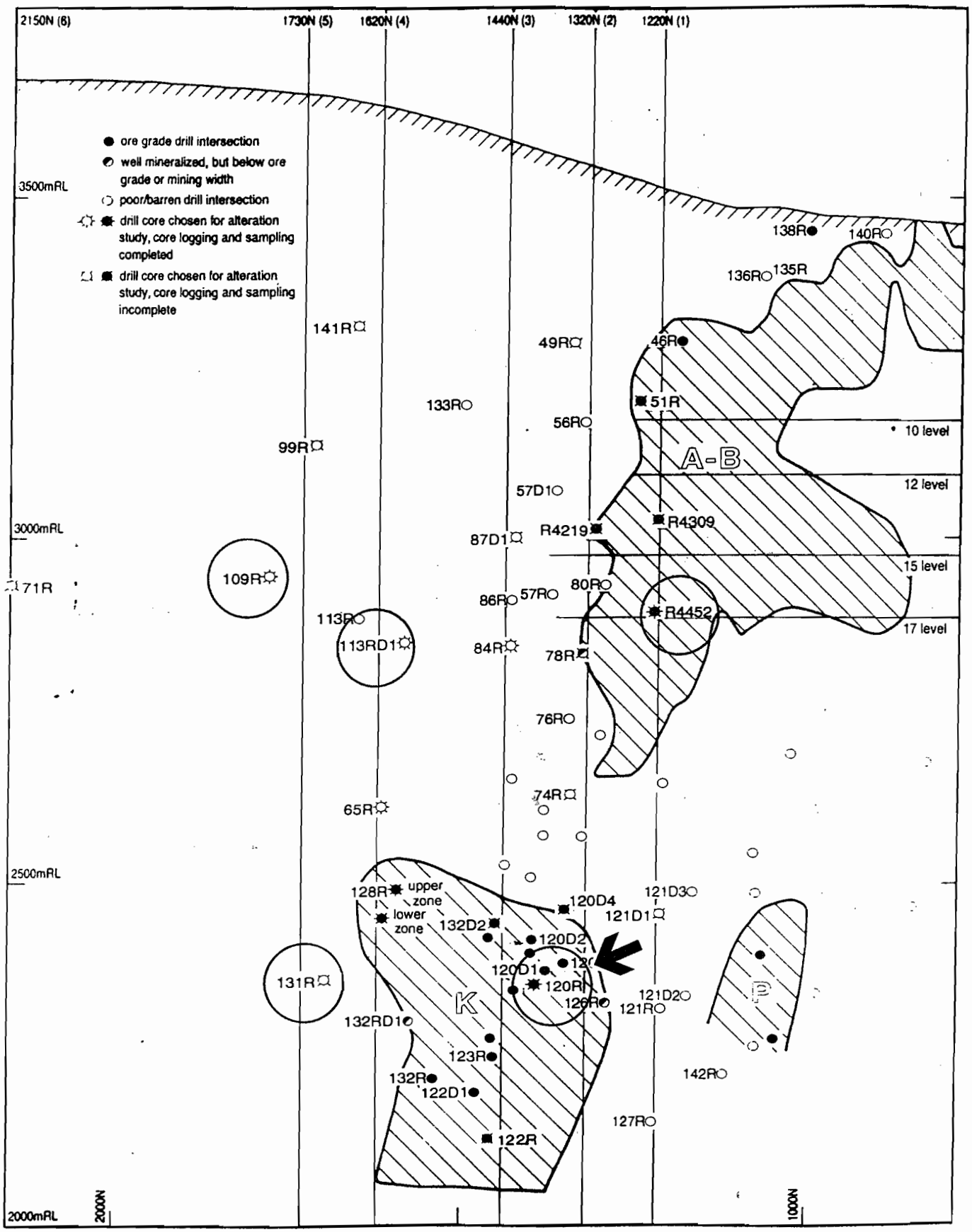

Figure 1: Longitudinal section of the north end of Rosebery mine showing the location of A-B, K and P ore lenses, drill core intersections of the ore stratigraphic position, drill cores selected for this study, and six cross sections designed to compile results (1220 mN, 1320 mN, 1440 mN, 1620 mN, 1730 mN and 2150 mN).

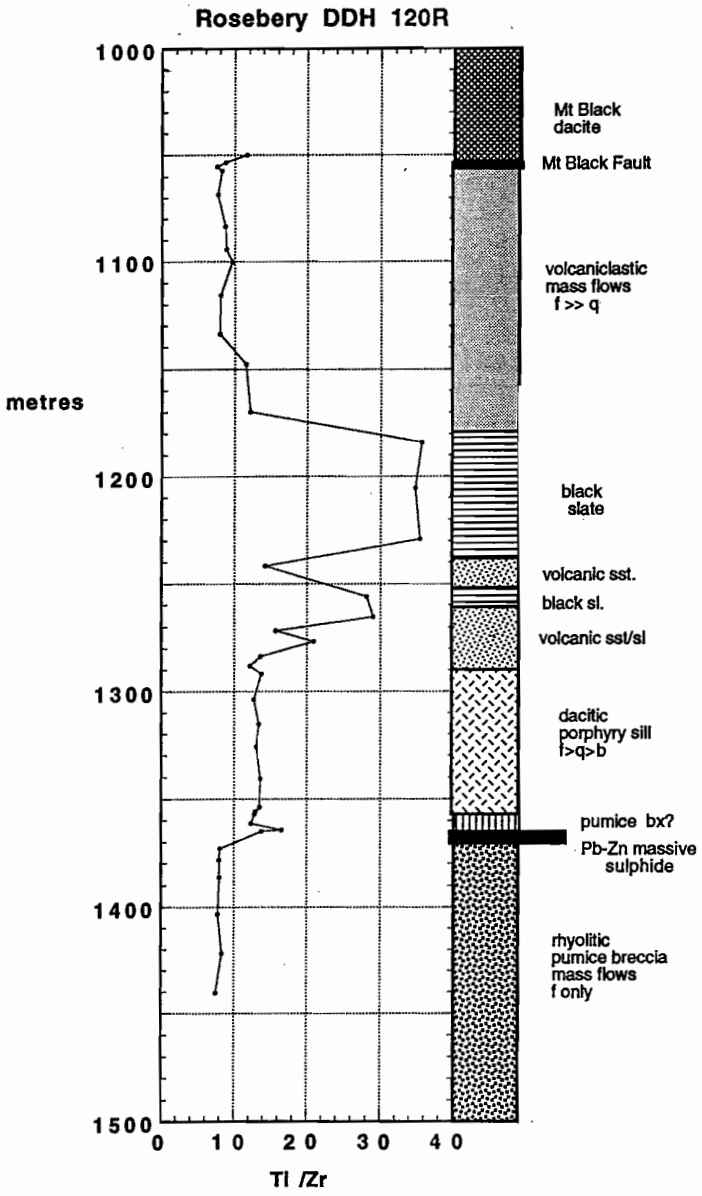
Rosebery DDH 120R
1000
1100
1200
1300
1400
1500
metres
0
10
20
30
40
Tl /Zr
Mt Black dacite
Mt Black Fault
volcaniclastic mass flows f >> q
black slate
volcanic sst.
black sl.
volcanic sst/sl
dacitic porphyry sill f>q>b
pumice bx?
Pb-Zn massive sulphide
rhyolitic pumice breccia mass flows f only

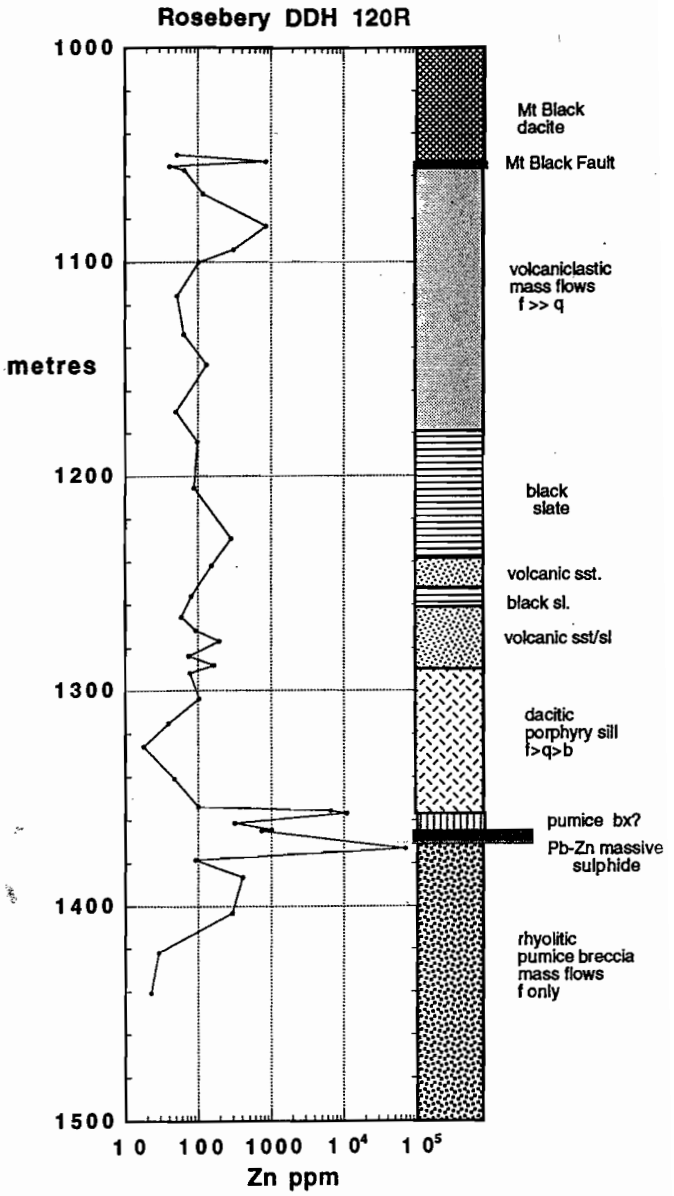
Rosebery DDH 120R
1000
1100
1200
1300
1400
1500
metres
10
100
1000
10⁴
10⁵
Zn ppm
Mt Black dacite
Mt Black Fault
volcaniclastic mass flows f >> q
black slate
volcanic sst.
black sl.
volcanic sst/sl
dacitic porphyry sill f>q>b
pumice bx?
Pb-Zn massive sulphide
rhyolitic pumice breccia mass flows f only

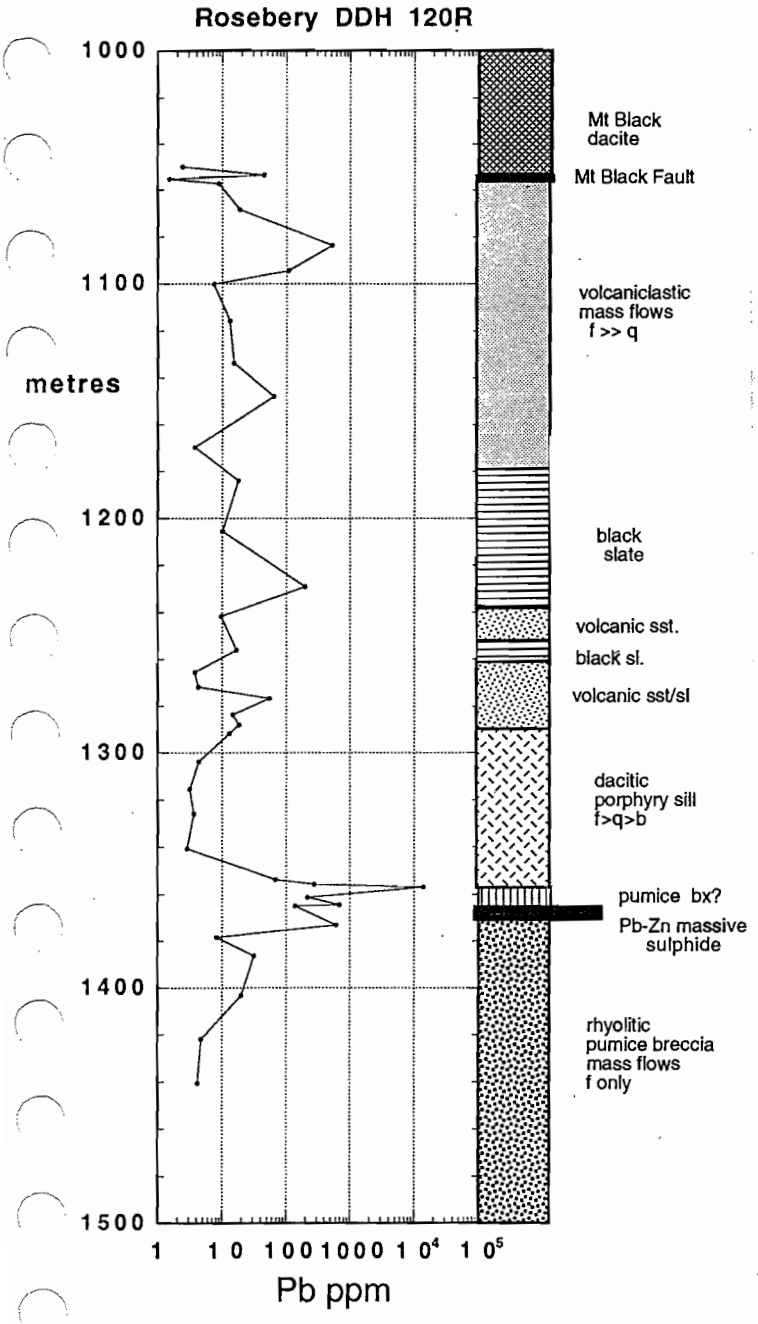
Rosebery DDH 120R
1000
1100
1200
1300
1400
1500
metres
1 10 100 1000 10⁴ 10⁵
Pb ppm
Mt Black dacite
Mt Black Fault
volcaniclastic mass flows f >> q
black slate
volcanic sst.
black sl.
volcanic sst/sl
dacitic porphyry sill f>q>b
pumice bx?
Pb-Zn massive sulphide
rhyolitic pumice breccia mass flows f only

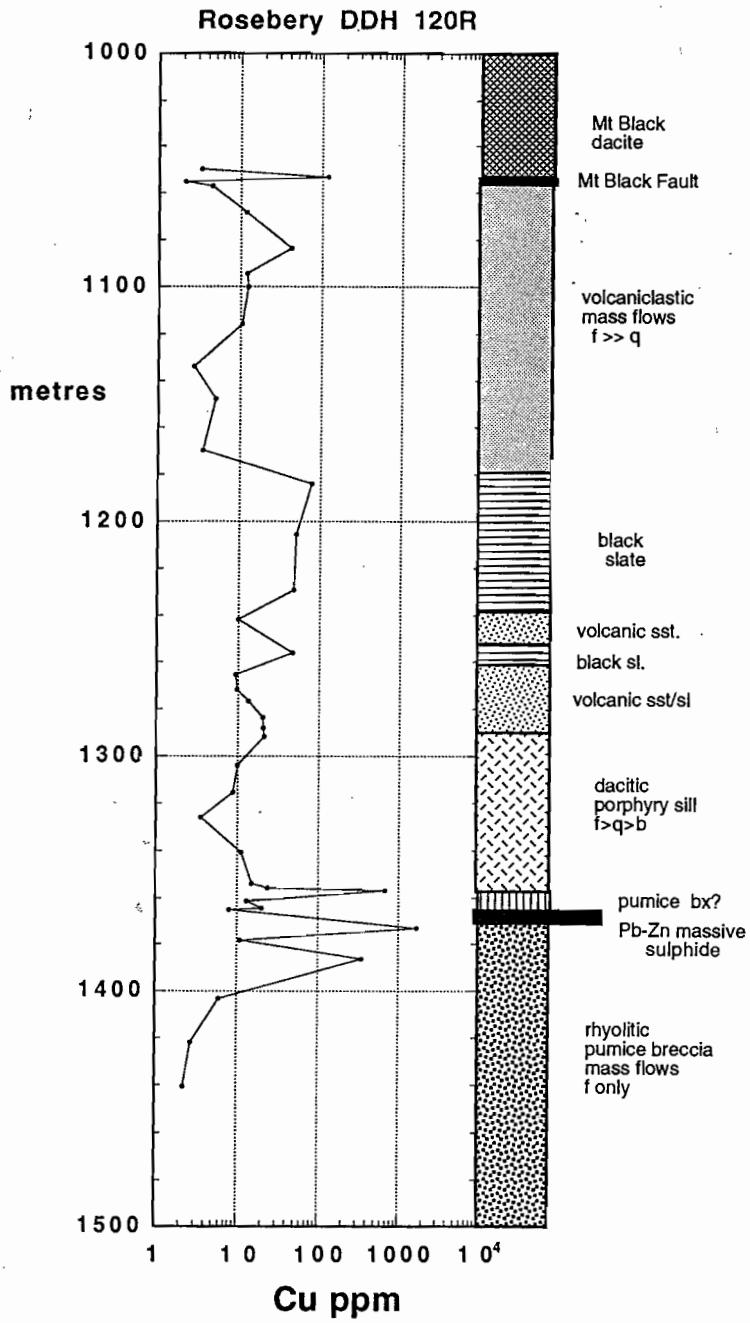
Rosebery DDH 120R
1000
1100
1200
1300
1400
1500
metres
1 10 100 1000 10⁴
Cu ppm
Mt Black dacite
Mt Black Fault
volcaniclastic mass flows f >> q
black slate
volcanic sst.
black sl.
volcanic sst/sl
dacitic porphyry sill f>q>b
pumice bx?
Pb-Zn massive sulphide
rhyolitic pumice breccia mass flows f only

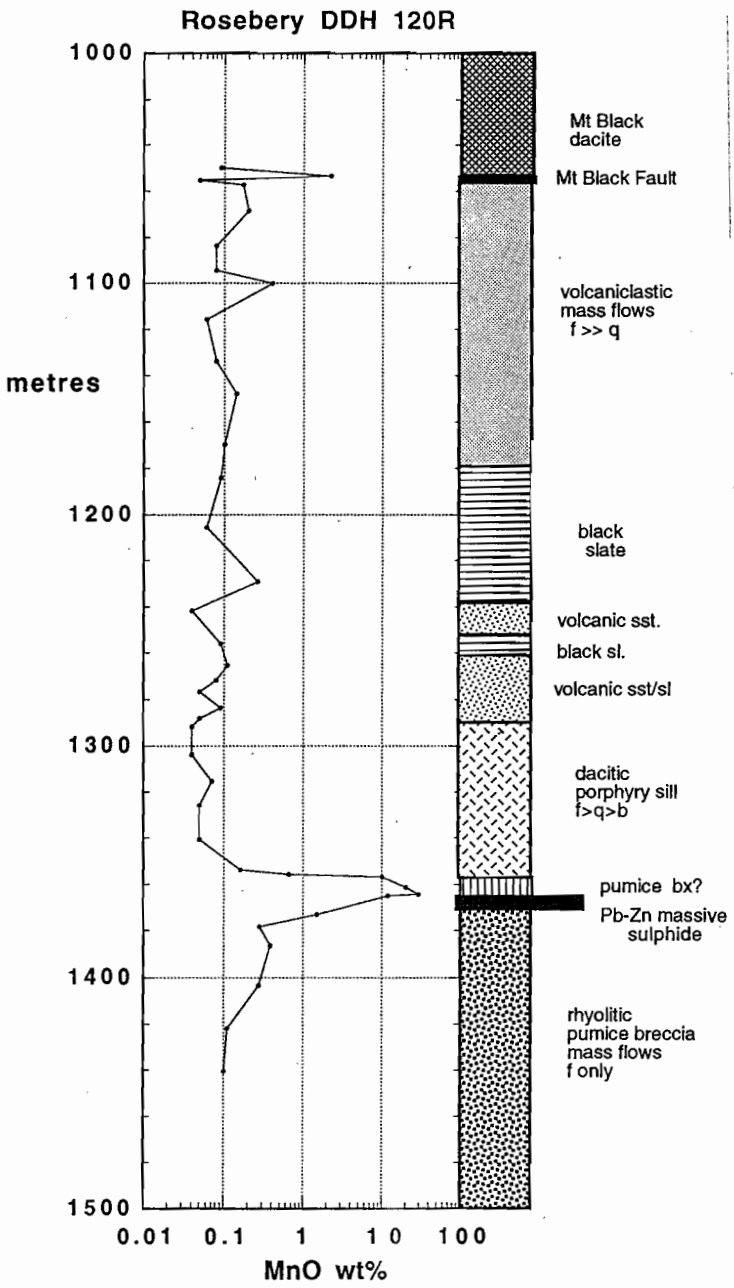
Rosebery DDH 120R
1000
1100
1200
1300
1400
1500
metres
0.01
0.1
1
10
100
MnO wt%
Mt Black dacite
Mt Black Fault
volcaniclastic mass flows f >> q
black slate
volcanic sst.
black sl.
volcanic sst/sl
dacitic porphyry sill f>q>b
pumice bx?
Pb-Zn massive sulphide
rhyolitic pumice breccia mass flows f only

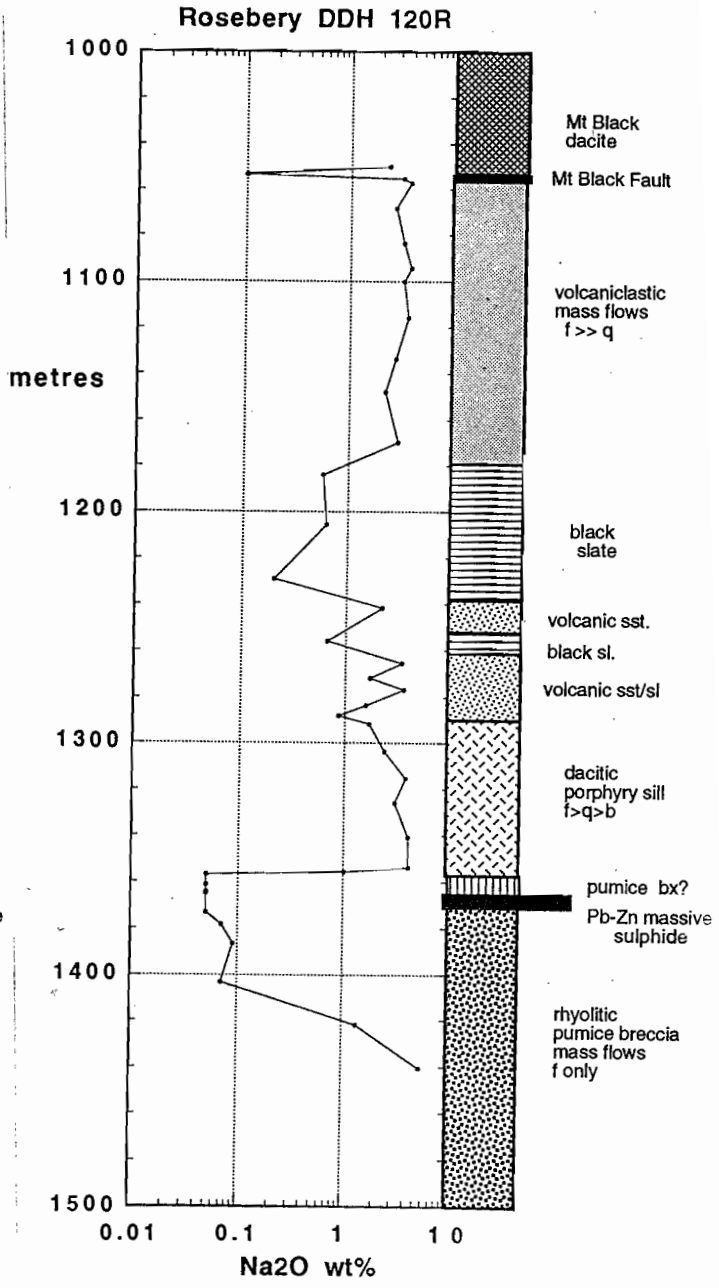
Rosebery DDH 120R
1000
1100
1200
1300
1400
1500
metres
0.01
0.1
1
10
Na2O wt%
Mt Black dacite
Mt Black Fault
volcaniclastic mass flows f >> q
black slate
volcanic sst.
black sl.
volcanic sst/sl
dacitic porphyry sill f>q>b
pumice bx?
Pb-Zn massive sulphide
rhyolitic pumice breccia mass flows f only

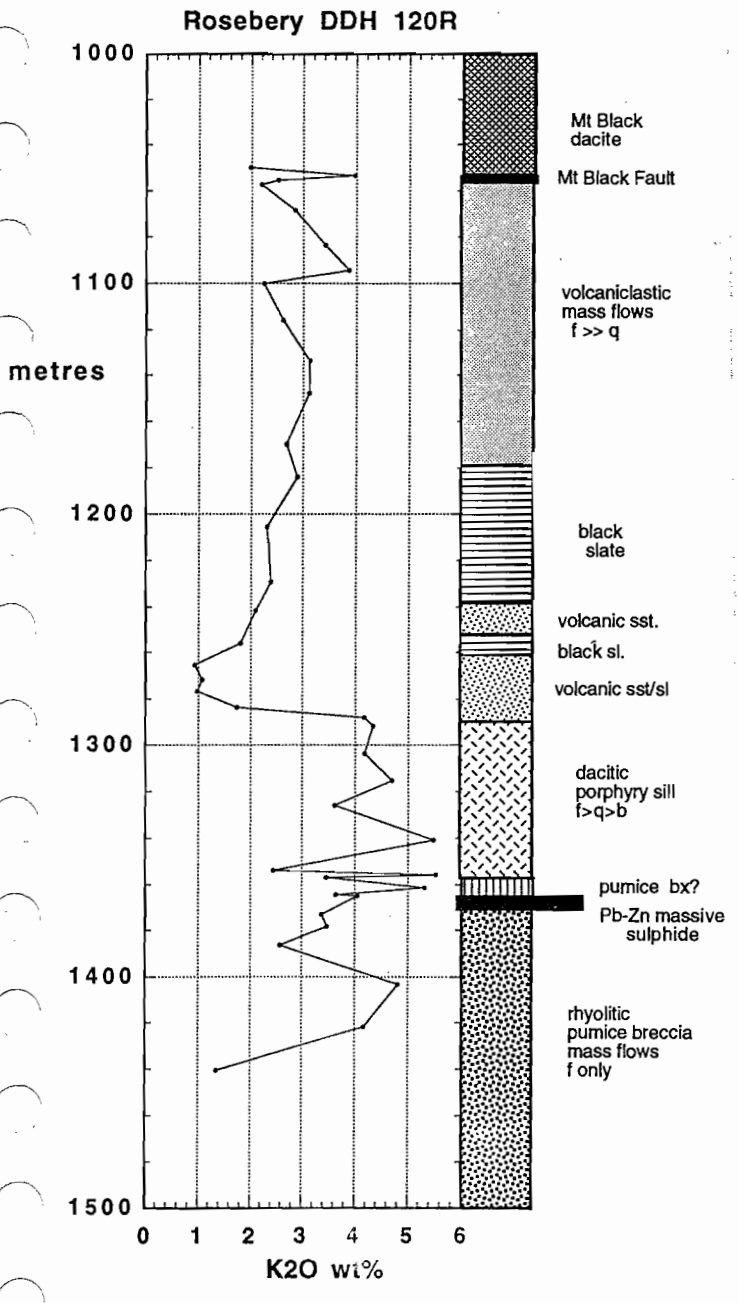
Rosebery DDH 120R
1000
1100
1200
1300
1400
1500
metres
0 1 2 3 4 5 6
K2O wt%
Mt Black dacite
Mt Black Fault
volcaniclastic mass flows f >> q
black slate
volcanic sst.
black sl.
volcanic sst/sl
dacitic porphyry sill f>q>b
pumice bx?
Pb-Zn massive sulphide
rhyolitic pumice breccia mass flows f only

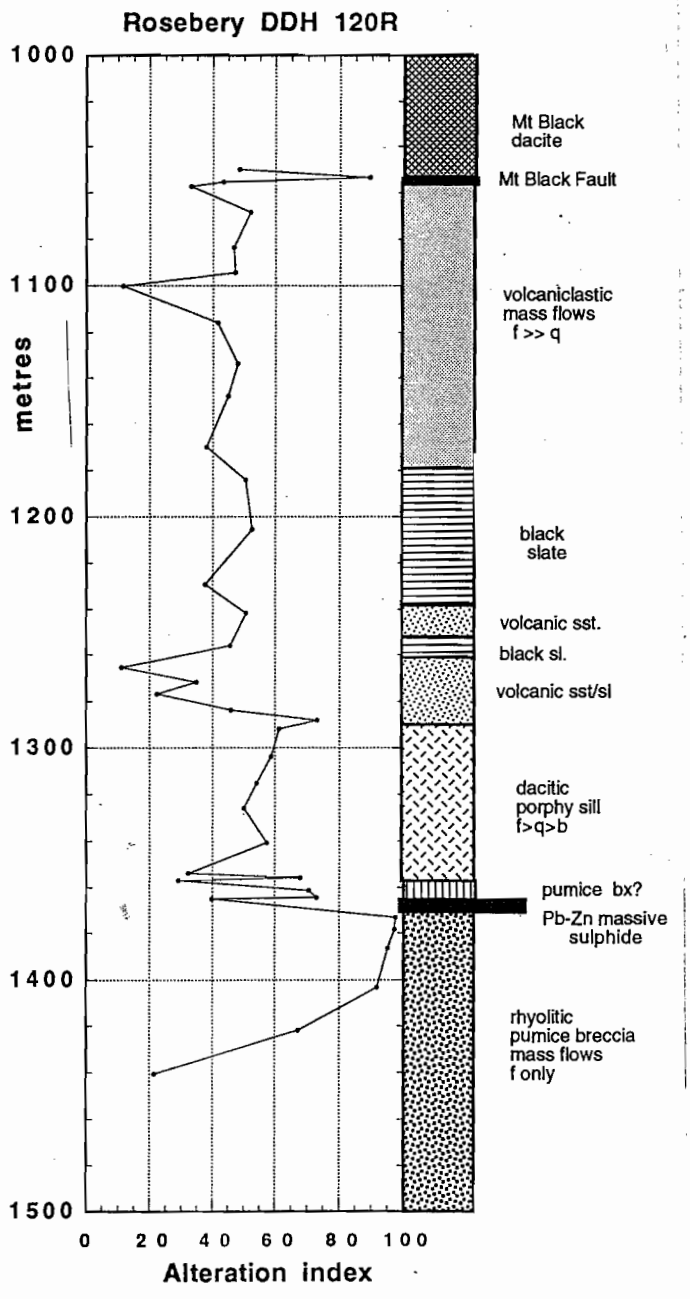
Rosebery DDH 120R
1000
1100
1200
1300
1400
1500
metres
0 20 40 60 80 100
Alteration index
Mt Black dacite
Mt Black Fault
volcaniclastic mass flows f >> q
black slate
volcanic sst.
black sl.
volcanic sst/sl
dacitic porphy sill f>q>b
pumice bx?
Pb-Zn massive sulphide
rhyolitic pumice breccia mass flows f only

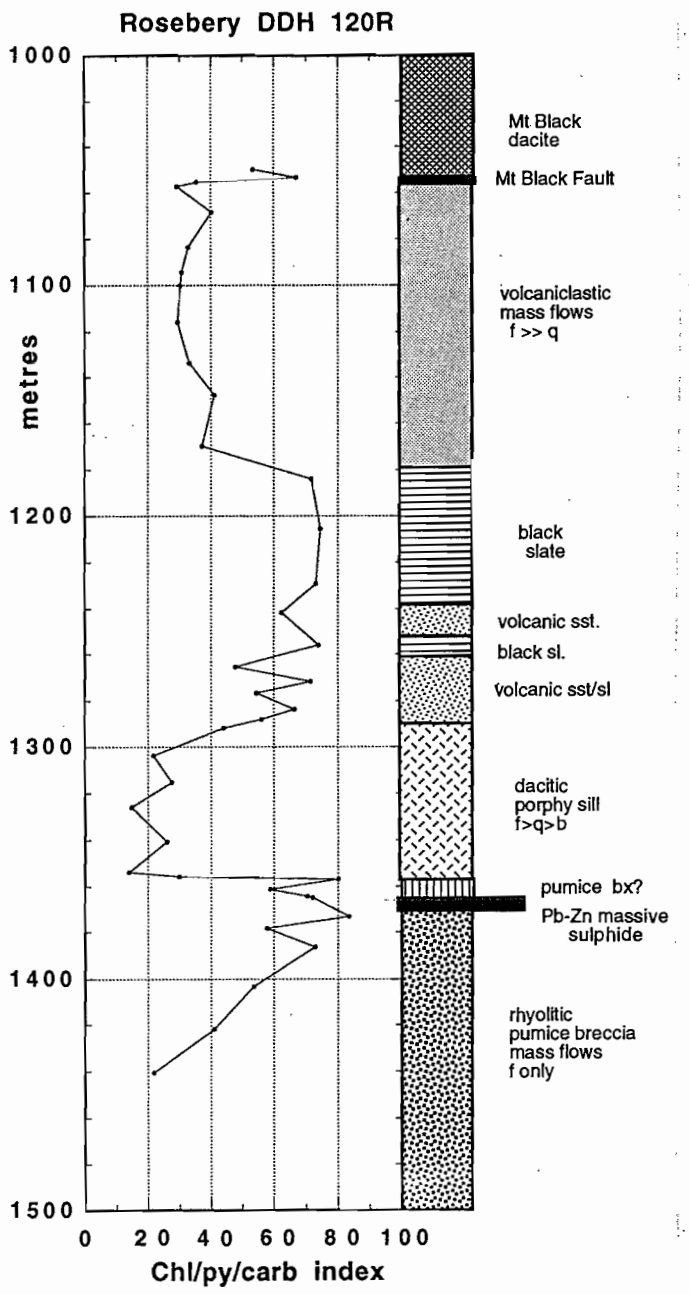
Rosebery DDH 120R
1000
1100
1200
1300
1400
1500
metres
0 20 40 60 80 100
Chl/py/carb index
Mt Black dacite
Mt Black Fault
volcaniclastic mass flows f >> q
black slate
volcanic sst.
black sl.
volcanic sst/sl
dacitic porphy sill f>q>b
pumice bx?
Pb-Zn massive sulphide
rhyolitic pumice breccia mass flows f only

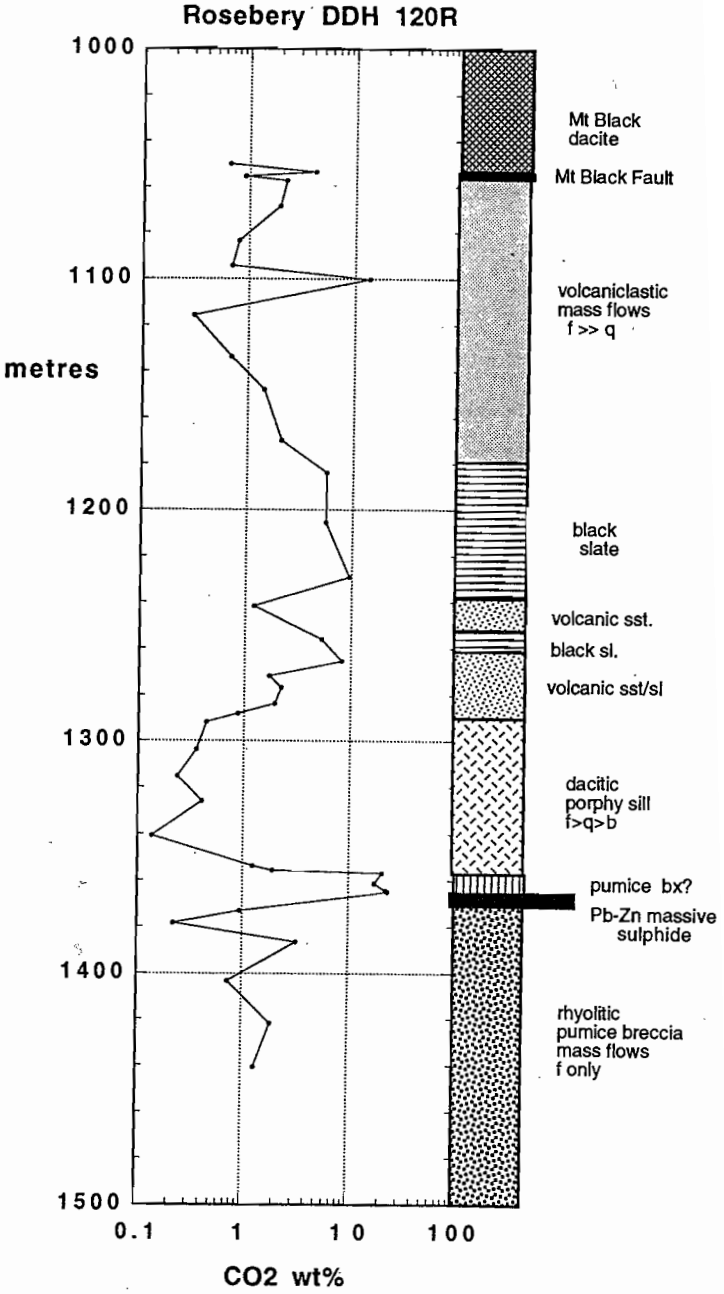
Rosebery DDH 120R
1000
1100
1200
1300
1400
1500
metres
0.1 1 10 100
CO2 wt%
Mt Black dacite
Mt Black Fault
volcaniclastic mass flows f >> q
black slate
volcanic sst.
black sl.
volcanic sst/sl
dacitic porphy sill f>q>b
pumice bx?
Pb-Zn massive sulphide
rhyolitic pumice breccia mass flows f only

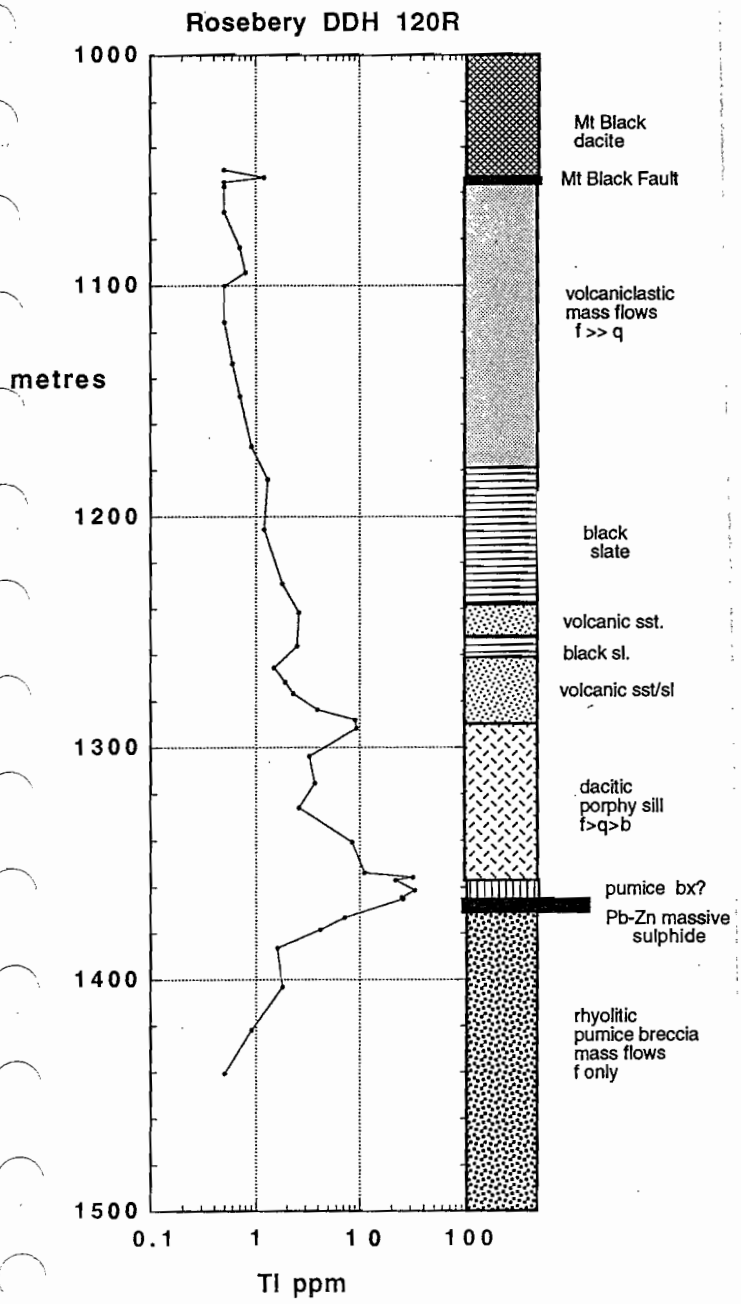
Rosebery DDH 120R
1000
1100
1200
1300
1400
1500
metres
0.1
1
10
100
Tl ppm
Mt Black dacite
Mt Black Fault
volcaniclastic mass flows f >> q
black slate
volcanic sst.
black sl.
volcanic sst/sl
dacitic porphy sill f>q>b
pumice bx?
Pb-Zn massive sulphide
rhyolitic pumice breccia mass flows f only

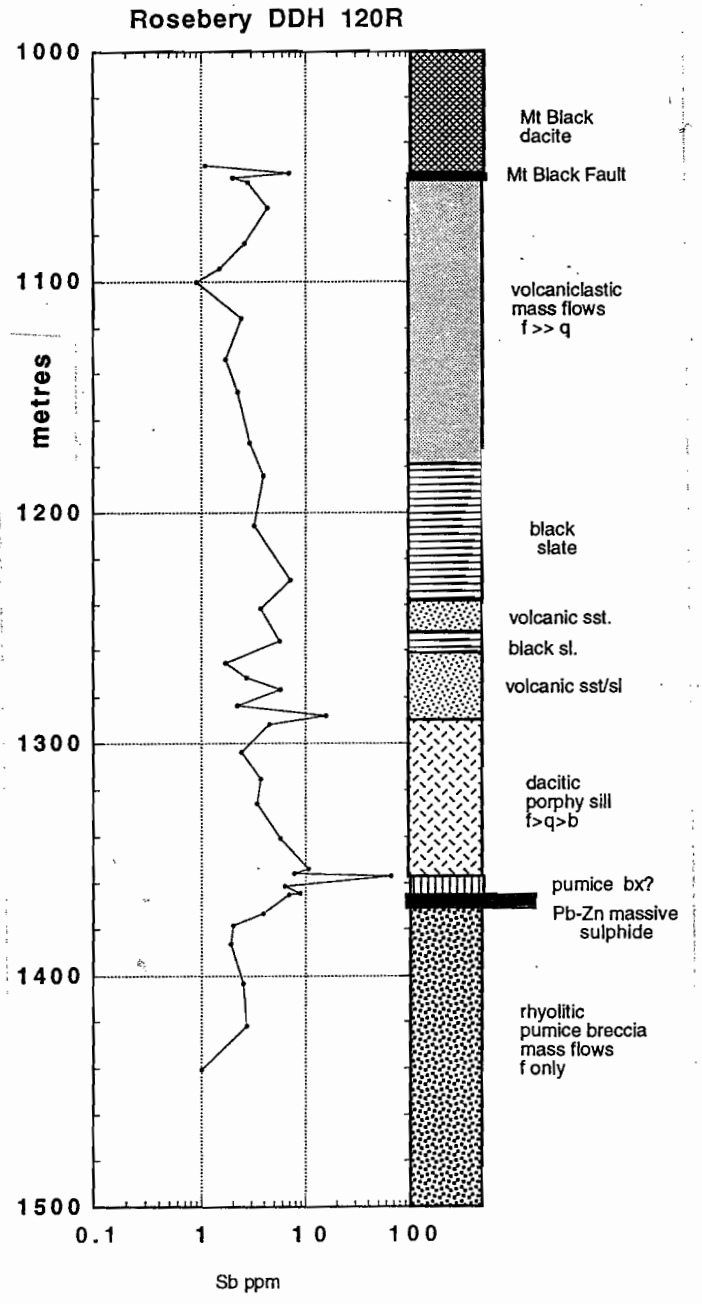
Rosebery DDH 120R
1000
1100
1200
1300
1400
1500
metres
0.1
1
10
100
Sb ppm
Mt Black dacite
Mt Black Fault
volcaniclastic mass flows f >> q
black slate
volcanic sst.
black sl.
volcanic sst/sl
dacitic porphy sill f>q>b
pumice bx?
Pb-Zn massive sulphide
rhyolitic pumice breccia mass flows f only

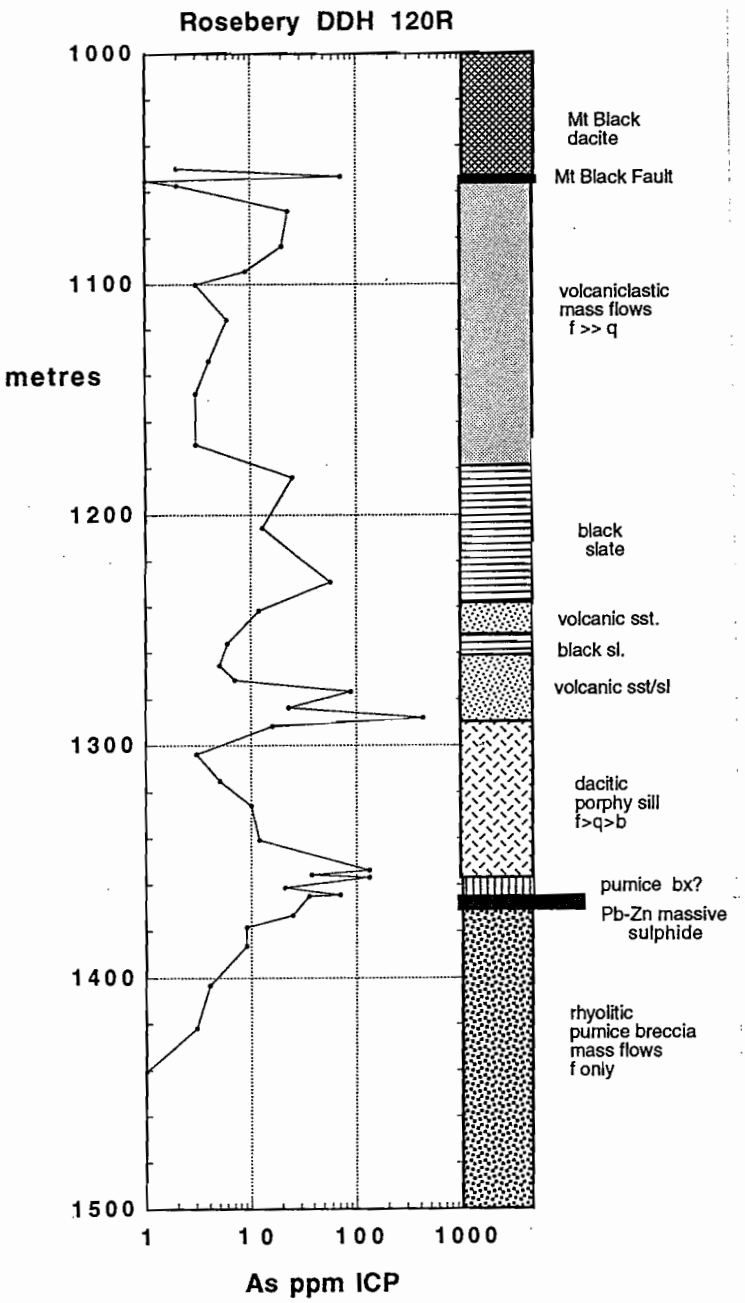
Rosebery DDH 120R
1000
1100
1200
1300
1400
1500
metres
1
10
100
1000
As ppm ICP
Mt Black dacite
Mt Black Fault
volcaniclastic mass flows f >> q
black slate
volcanic sst.
black sl.
volcanic sst/sl
dacitic porphy sill f>q>b
pumice bx?
Pb-Zn massive sulphide
rhyolitic pumice breccia mass flows f only

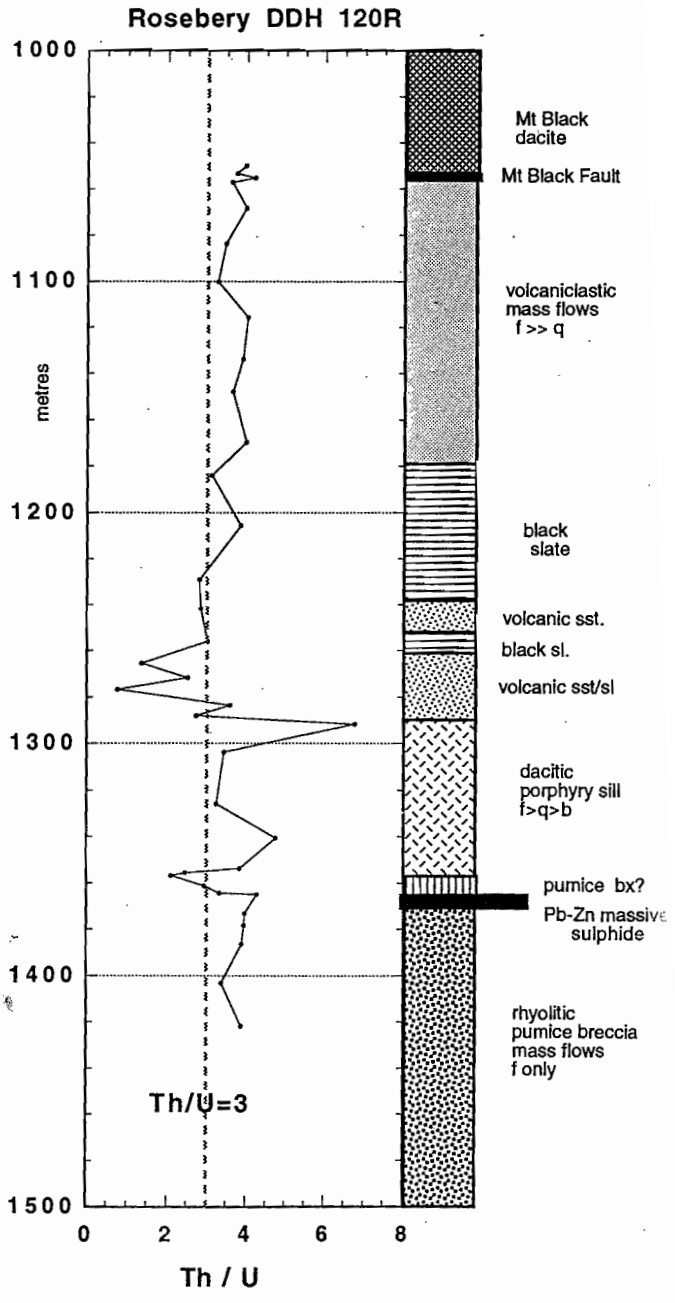
Rosebery DDH 120R
1000
1100
1200
1300
1400
1500
metres
0
2
4
6
8
Th / U
Th/U=3
Mt Black dacite
Mt Black Fault
volcaniclastic mass flows f >> q
black slate
volcanic sst.
black sl.
volcanic sst/sl
dacitic porphyry sill f>q>b
pumice bx?
Pb-Zn massive sulphide
rhyolitic pumice breccia mass flows f only

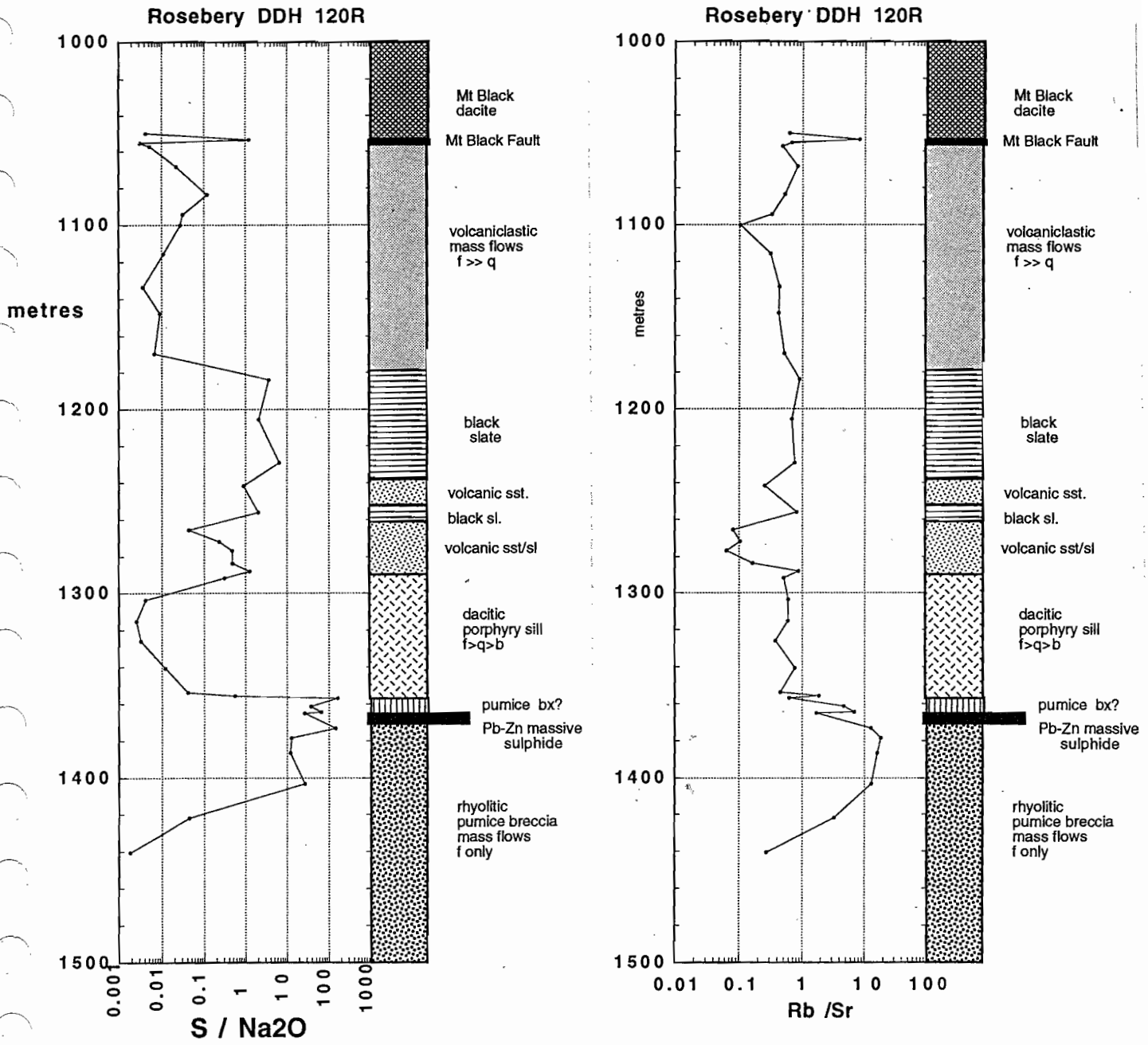
Rosebery DDH 120R
1000
1100
1200
1300
1400
1500
metres
Mt Black dacite
Mt Black Fault
volcaniclastic mass flows f >> q
black slate
volcanic sst.
black sl.
volcanic sst/sl
dacitic porphyry sill f>q>b
pumice bx?
Pb-Zn massive sulphide
rhyolitic pumice breccia mass flows f only
0.001
0.01
0.1
1
10
100
1000
S / Na2O
Rosebery DDH 120R
0.01
0.1
1
10
100
Rb /Sr

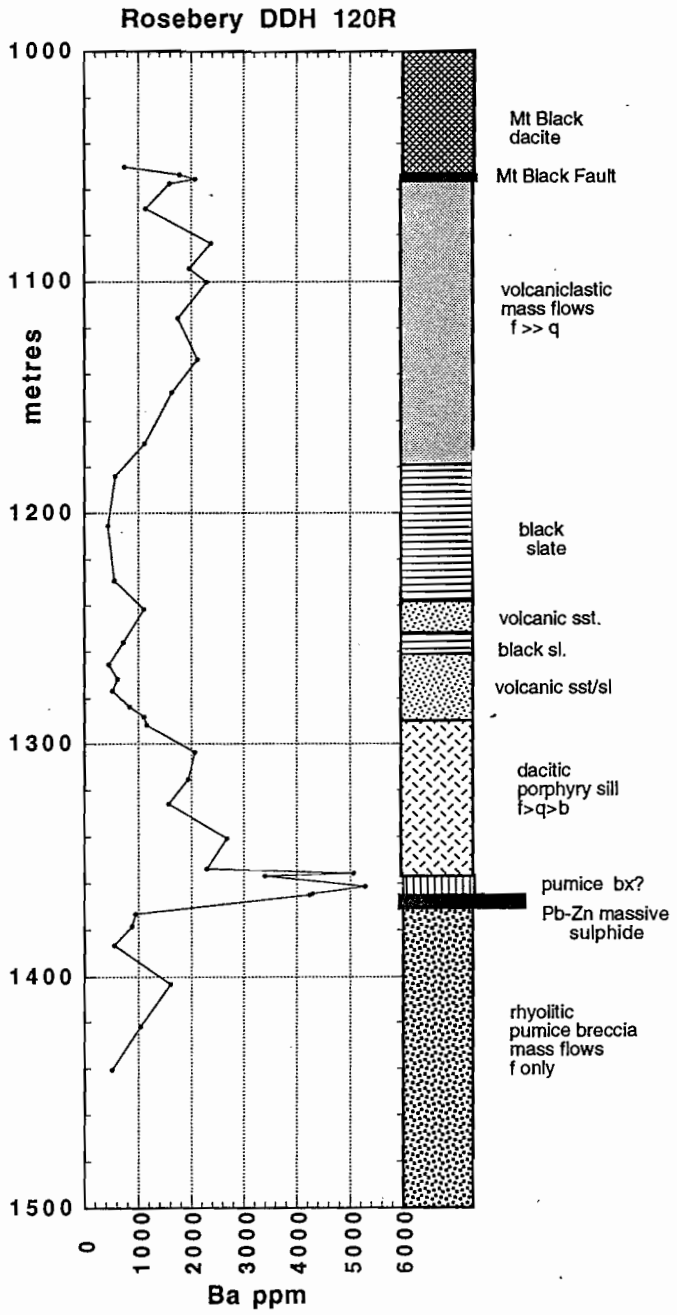
Rosebery DDH 120R
1000
1100
1200
1300
1400
1500
metres
0
1000
2000
3000
4000
5000
6000
Ba ppm
Mt Black dacite
Mt Black Fault
volcaniclastic mass flows f >> q
black slate
volcanic sst.
black sl.
volcanic sst/sl
dacitic porphyry sill f>q>b
pumice bx?
Pb-Zn massive sulphide
rhyolitic pumice breccia mass flows f only

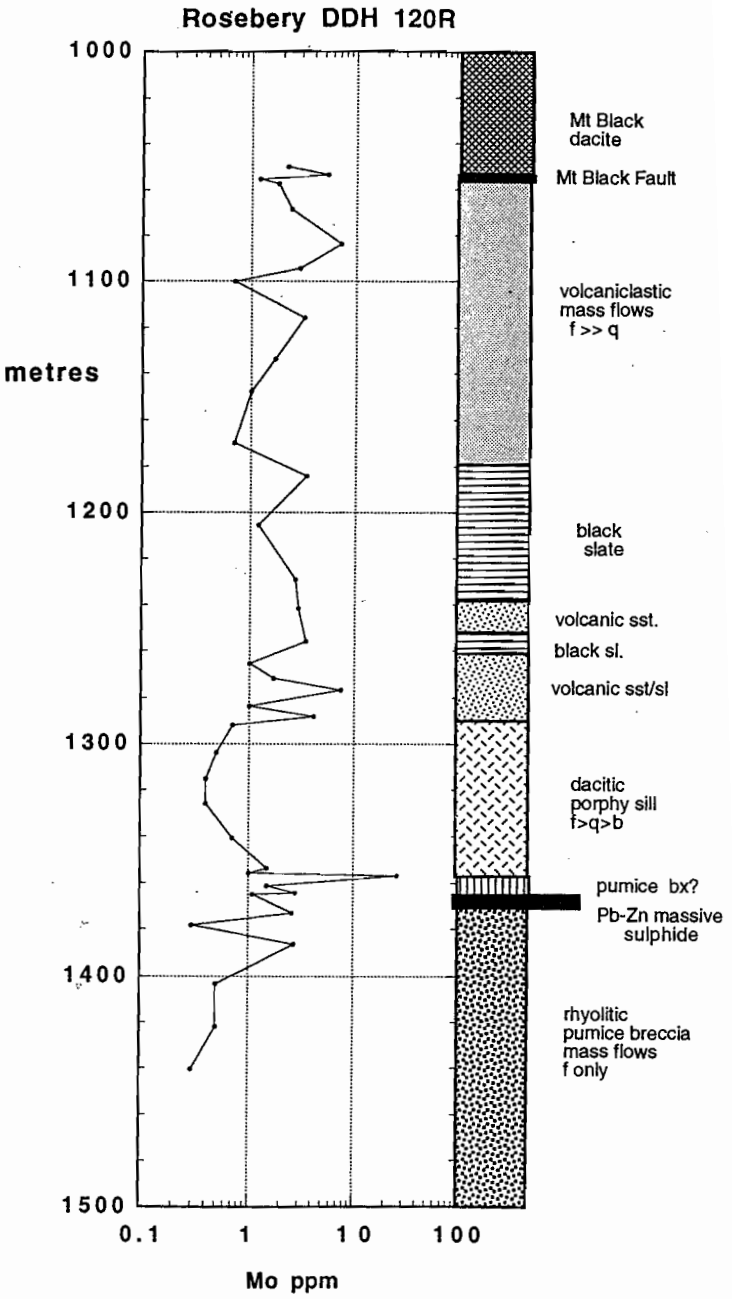
Rosebery DDH 120R
1000
1100
1200
1300
1400
1500
metres
0.1
1
10
100
Mo ppm
Mt Black dacite
Mt Black Fault
volcaniclastic mass flows f >> q
black slate
volcanic sst.
black sl.
volcanic sst/sl
dacitic porphy sill f>q>b
pumice bx?
Pb-Zn massive sulphide
rhyolitic pumice breccia mass flows f only

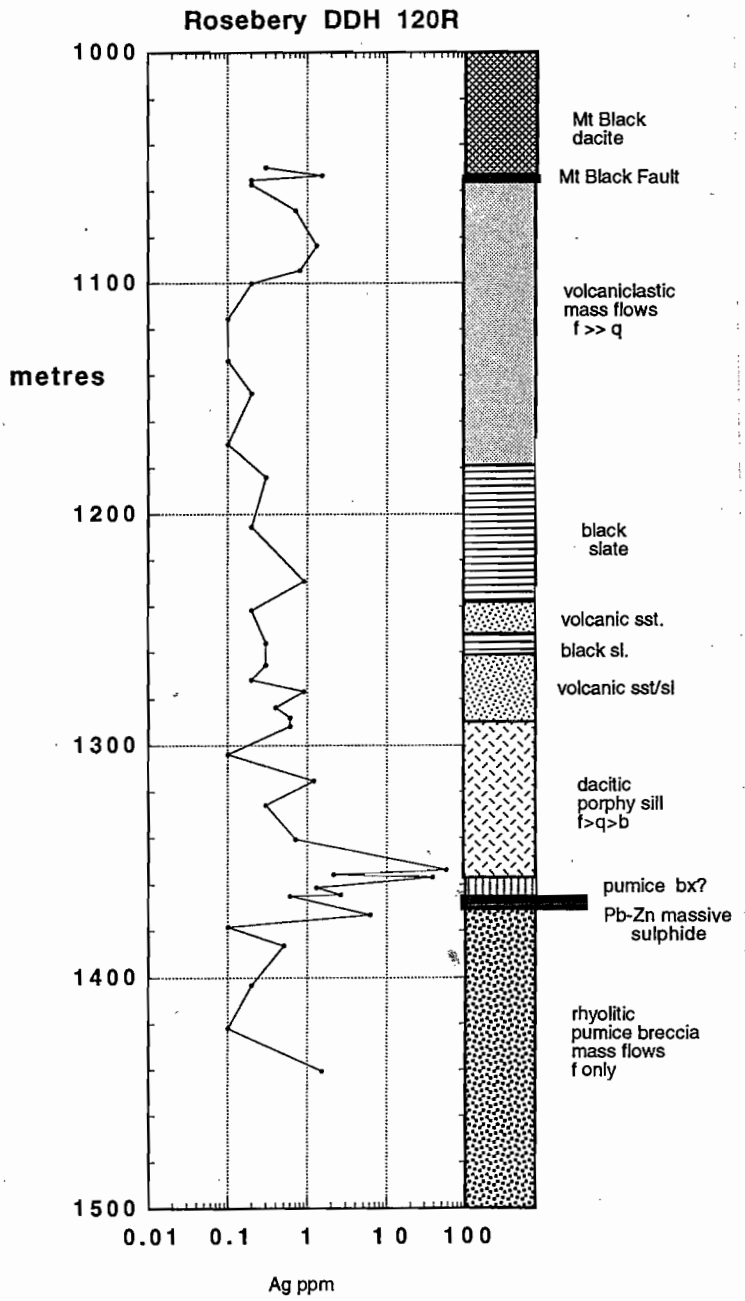
Rosebery DDH 120R
1000
1100
1200
1300
1400
1500
metres
0.01
0.1
1
10
100
Ag ppm
Mt Black dacite
Mt Black Fault
volcaniclastic mass flows f >> q
black slate
volcanic sst.
black sl.
volcanic sst/sl
dacitic porphy sill f>q>b
pumice bx?
Pb-Zn massive sulphide
rhyolitic pumice breccia mass flows f only

Appendix B

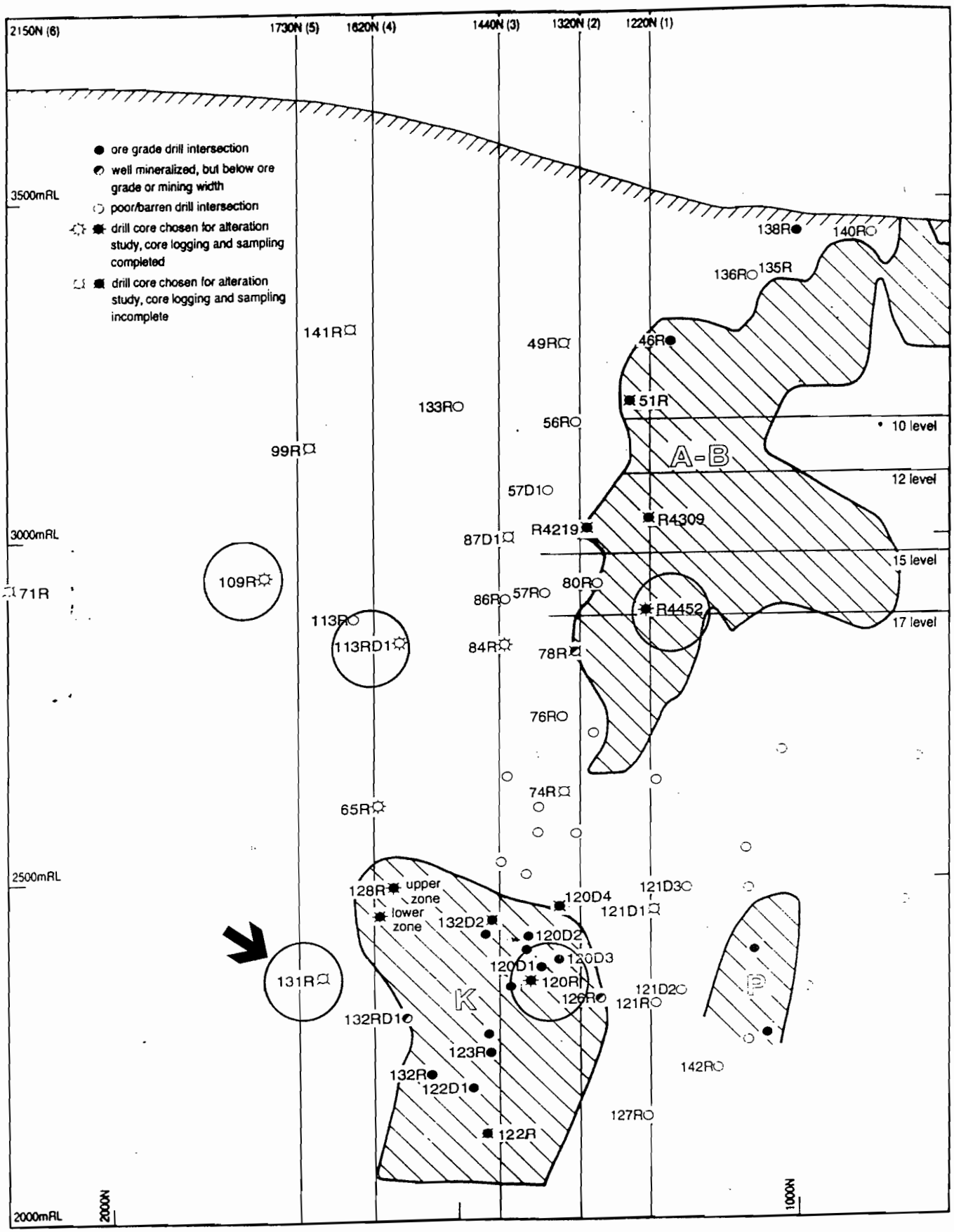

Figure 1: Longitudinal section of the north end of Rosebery mine showing the location of A-B, K and P ore lenses, drill core intersections of the ore stratigraphic position, drill cores selected for this study, and six cross sections designed to compile results (1220 mN, 1320 mN, 1440 mN, 1620 mN, 1730 mN and 2150 mN).

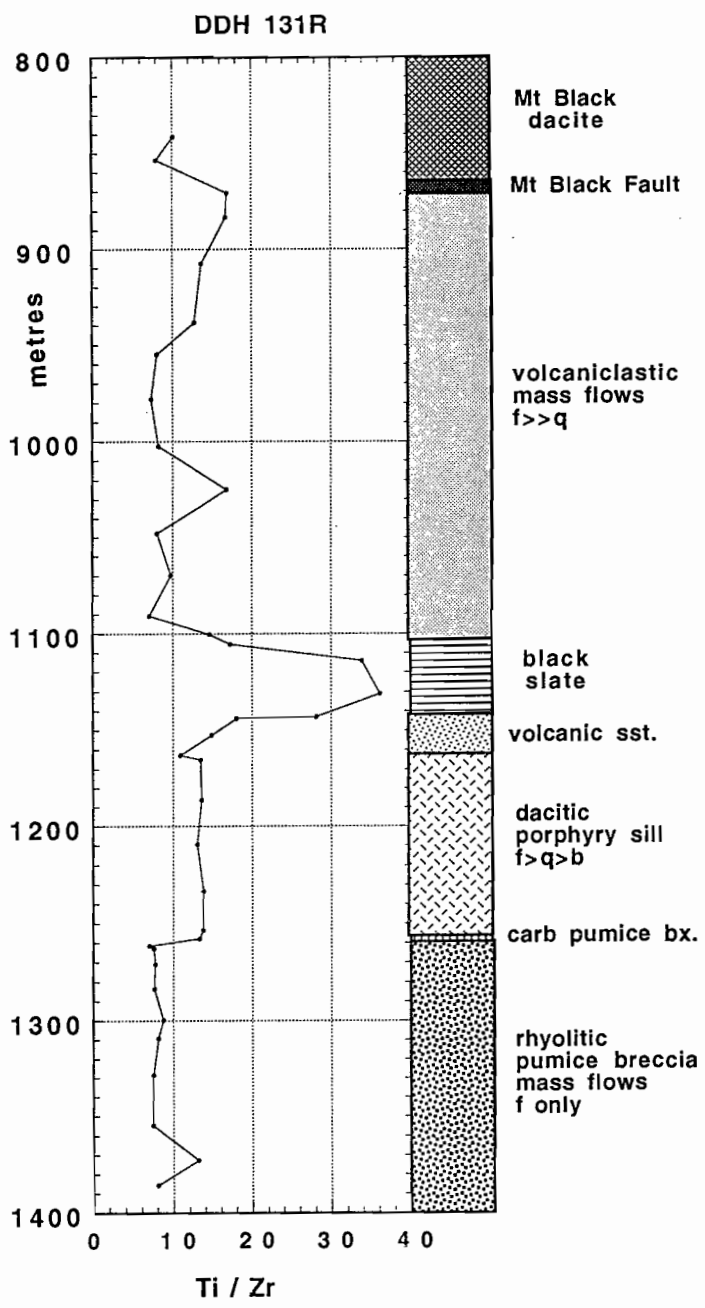
DDH 131R
800
900
1000
1100
1200
1300
1400
metres
0
10
20
30
40
Ti / Zr
Mt Black dacite
Mt Black Fault
volcaniclastic mass flows f>>q
black slate
volcanic sst.
dacitic porphyry sill f>q>b
carb pumice bx.
rhyolitic pumice breccia mass flows f only

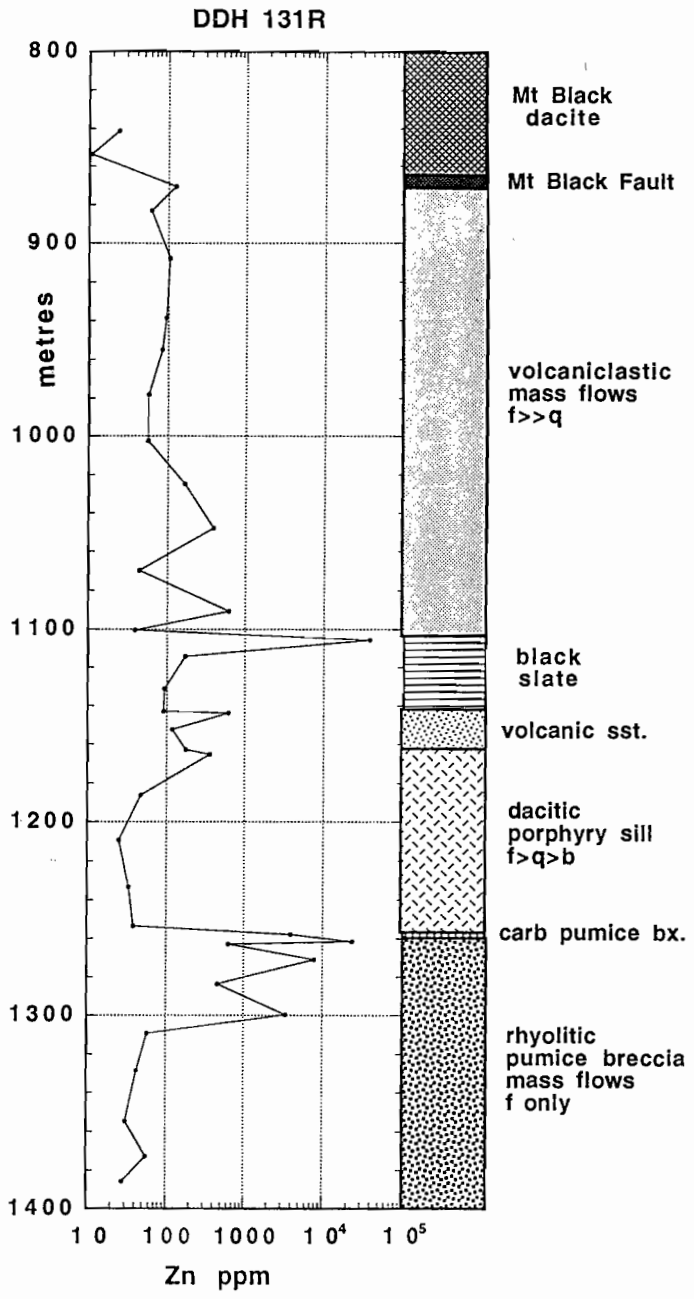
DDH 131R
800
900
1000
1100
1200
1300
1400
metres
10
100
1000
10⁴
10⁵
Zn ppm
Mt Black dacite
Mt Black Fault
volcaniclastic mass flows f>>q
black slate
volcanic sst.
dacitic porphyry sill f>q>b
carb pumice bx.
rhyolitic pumice breccia mass flows f only

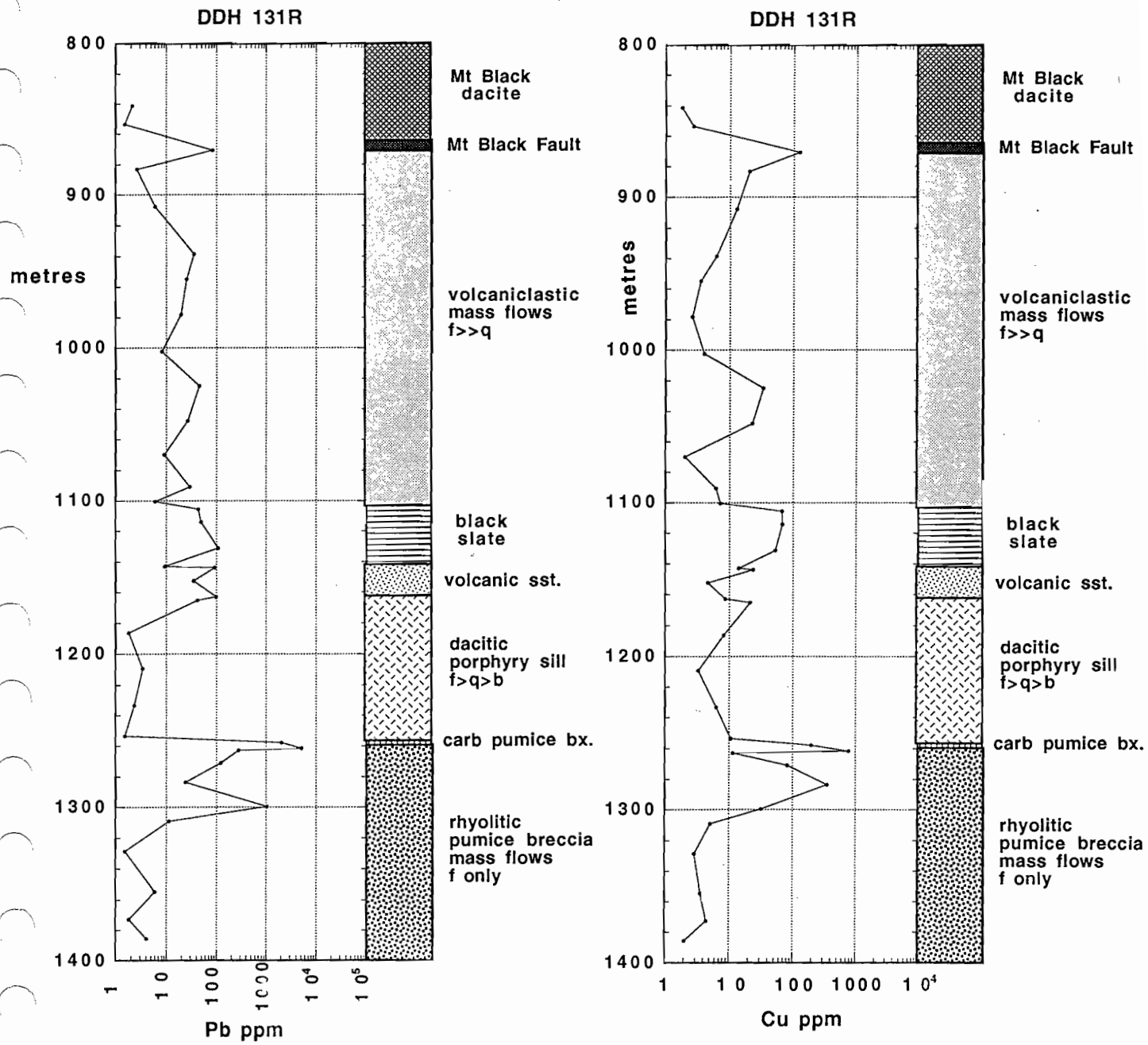
DDH 131R
800
900
1000
1100
1200
1300
1400
metres
Mt Black dacite
Mt Black Fault
volcaniclastic mass flows f>>q
black slate
volcanic sst.
dacitic porphyry sill f>q>b
carb pumice bx.
rhyolitic pumice breccia mass flows f only
1
10
100
1000
10⁴
10⁵
Pb ppm
DDH 131R
800
900
1000
1100
1200
1300
1400
metres
Mt Black dacite
Mt Black Fault
volcaniclastic mass flows f>>q
black slate
volcanic sst.
dacitic porphyry sill f>q>b
carb pumice bx.
rhyolitic pumice breccia mass flows f only
1
10
100
1000
10⁴
Cu ppm

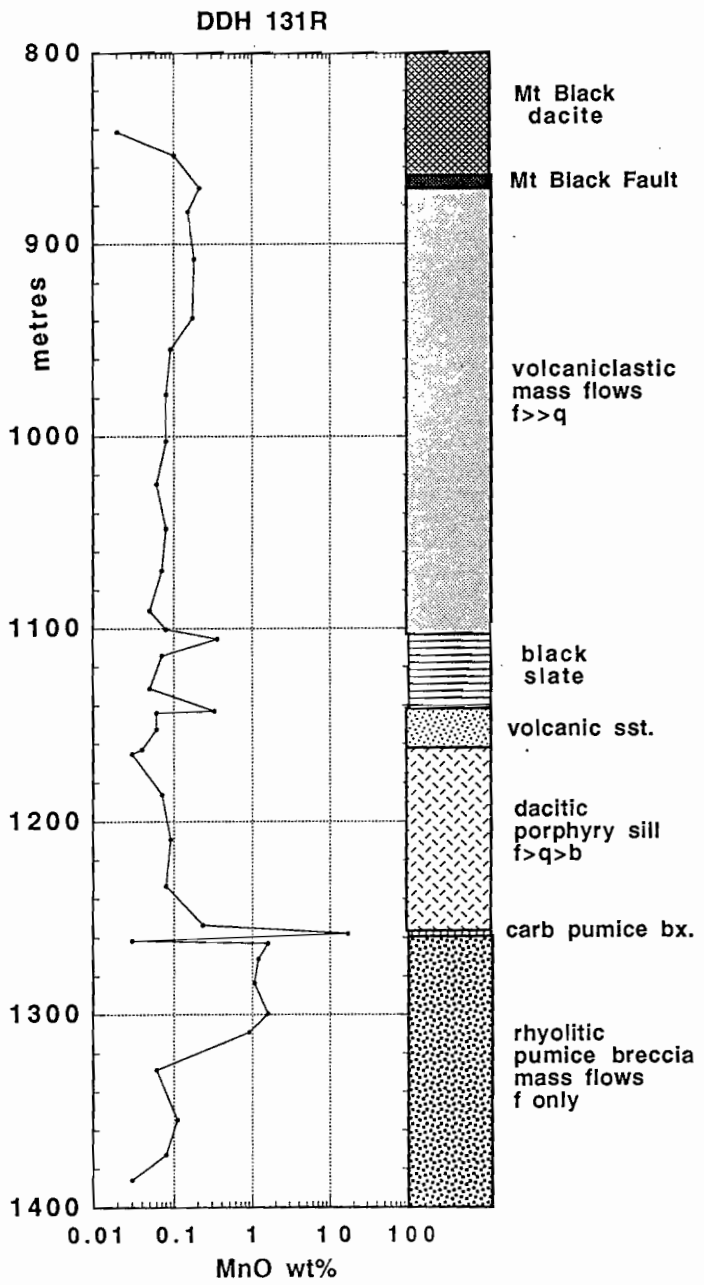
DDH 131R
800
900
1000
1100
1200
1300
1400
metres
0.01
0.1
1
10
100
MnO wt%
Mt Black dacite
Mt Black Fault
volcaniclastic mass flows f>>q
black slate
volcanic sst.
dacitic porphyry sill f>q>b
carb pumice bx.
rhyolitic pumice breccia mass flows f only

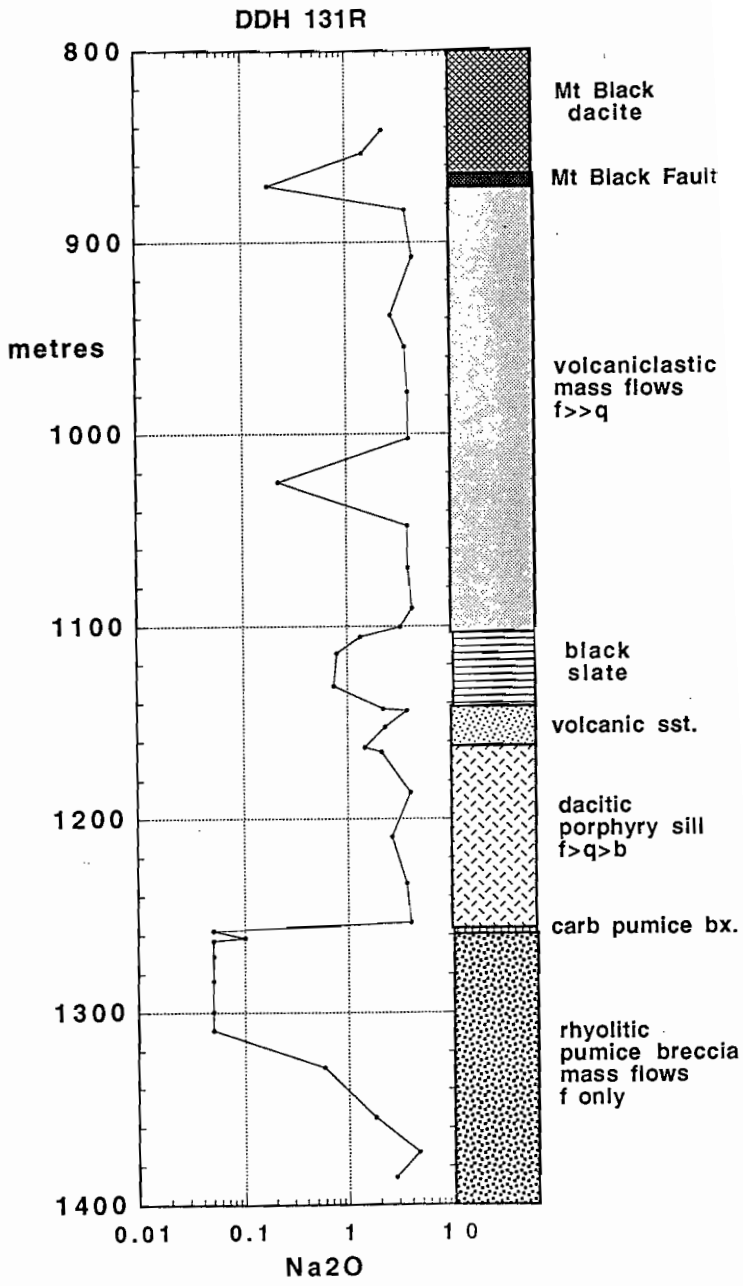
DDH 131R
800
900
1000
1100
1200
1300
1400
metres
0.01
0.1
1
10
Na2O
Mt Black dacite
Mt Black Fault
volcaniclastic mass flows f>>q
black slate
volcanic sst.
dacitic porphyry sill f>q>b
carb pumice bx.
rhyolitic pumice breccia mass flows f only

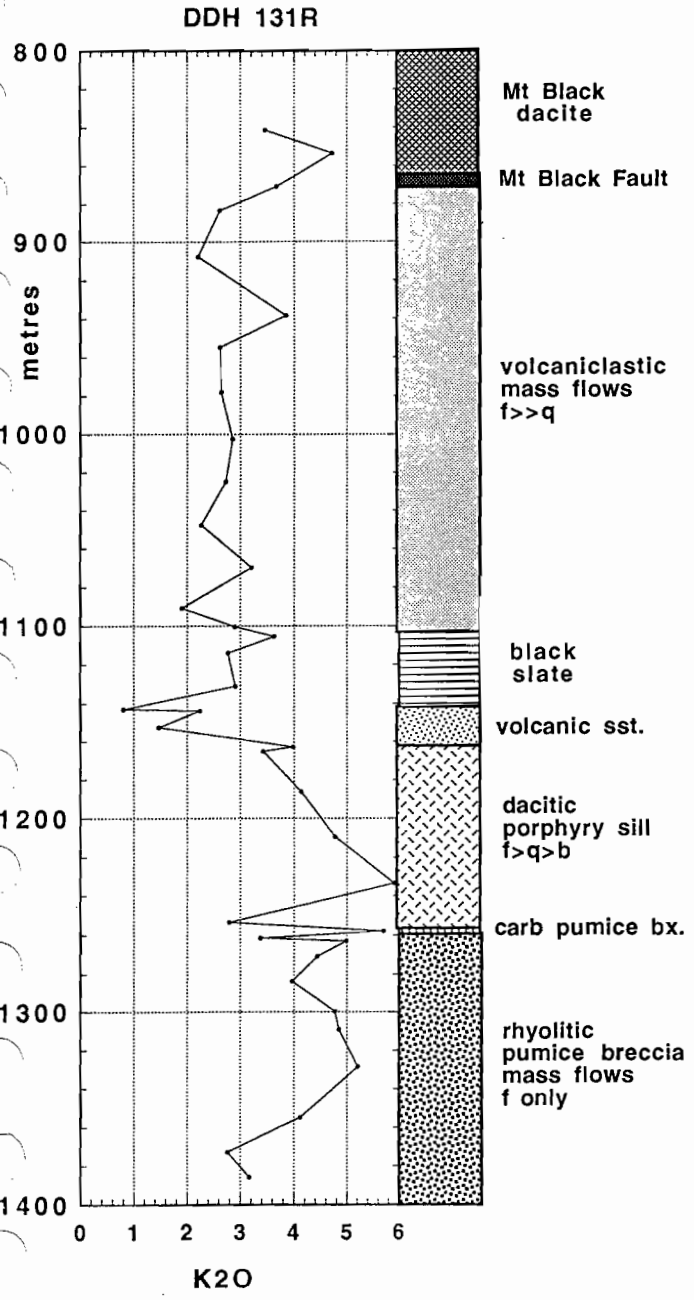
DDH 131R
800
900
1000
1100
1200
1300
1400
metres
Mt Black dacite
Mt Black Fault
volcaniclastic mass flows f>>q
black slate
volcanic sst.
dacitic porphyry sill f>q>b
carb pumice bx.
rhyolitic pumice breccia mass flows f only
0 1 2 3 4 5 6
K2O

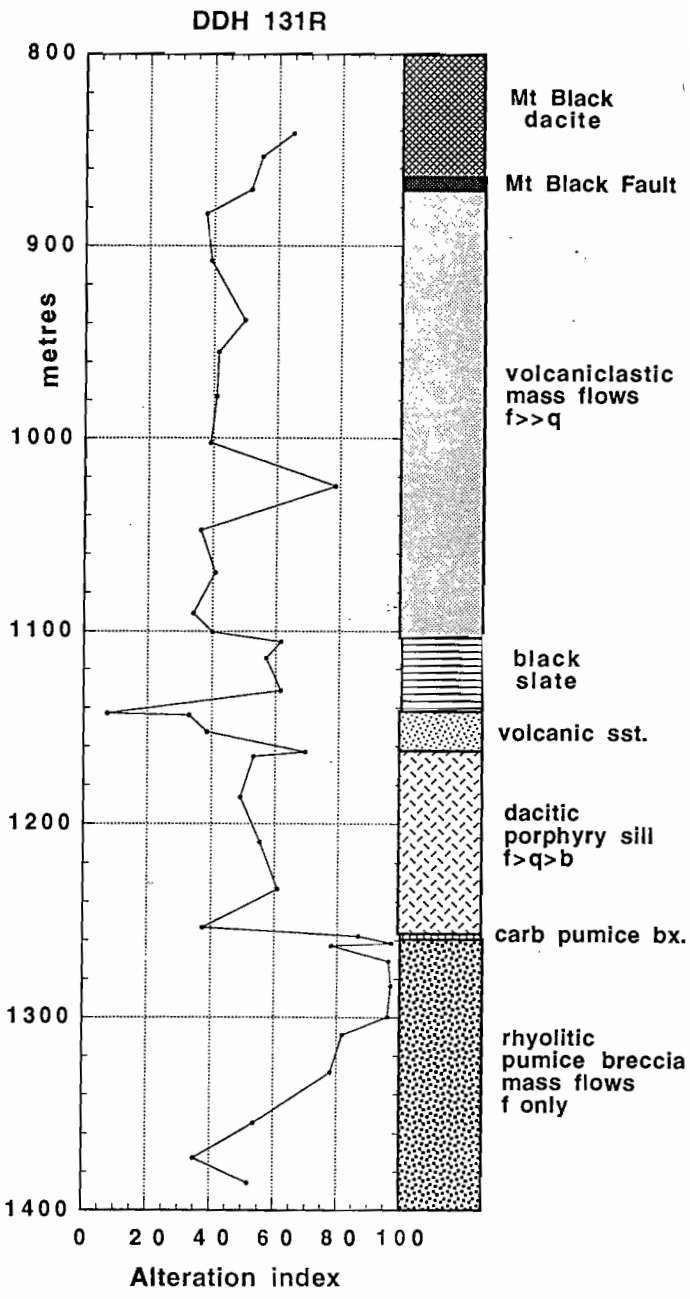
DDH 131R
800
900
1000
1100
1200
1300
1400
metres
Mt Black dacite
Mt Black Fault
volcaniclastic mass flows f>>q
black slate
volcanic sst.
dacitic porphyry sill f>q>b
carb pumice bx.
rhyolitic pumice breccia mass flows f only
0 20 40 60 80 100
Alteration index

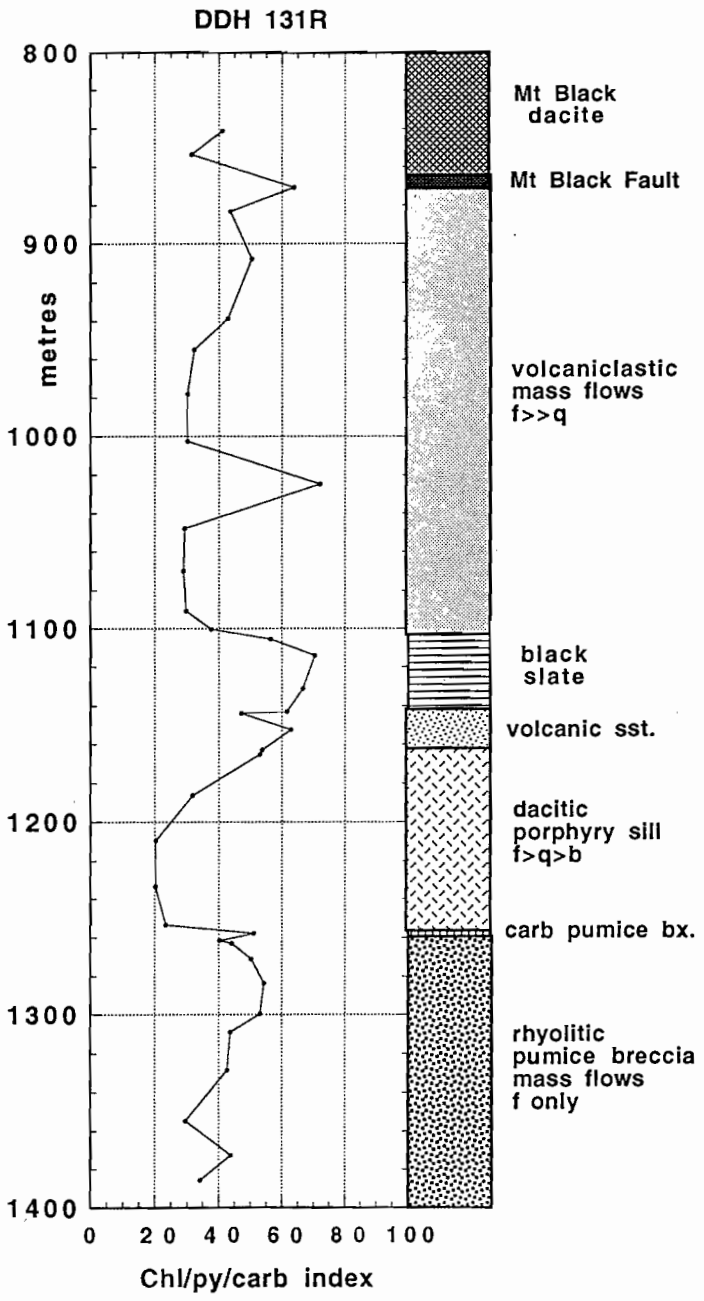
DDH 131R
800
900
1000
1100
1200
1300
1400
metres
0 20 40 60 80 100
Chl/py/carb index
Mt Black dacite
Mt Black Fault
volcaniclastic mass flows f>>q
black slate
volcanic sst.
dacitic porphyry sill f>q>b
carb pumice bx.
rhyolitic pumice breccia mass flows f only

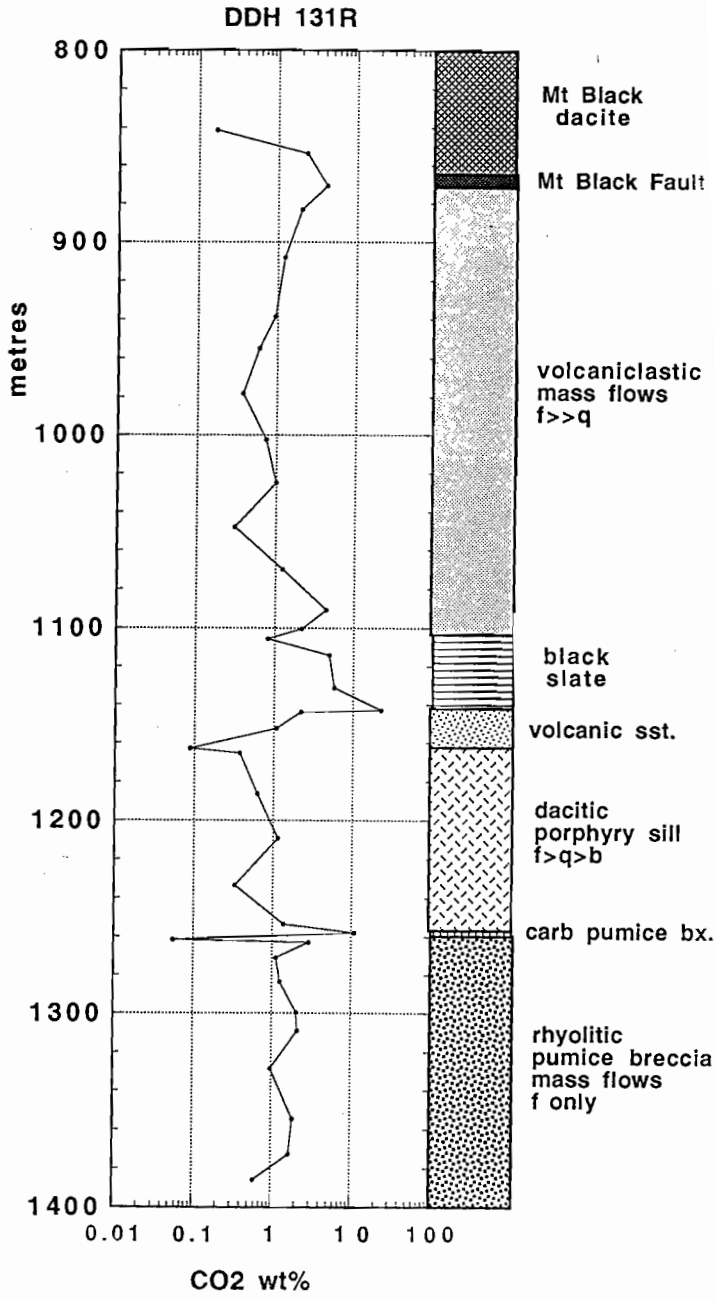
DDH 131R
800
900
1000
1100
1200
1300
1400
metres
0.01 0.1 1 10 100
CO2 wt%
Mt Black dacite
Mt Black Fault
volcaniclastic mass flows f>>q
black slate
volcanic sst.
dacitic porphyry sill f>q>b
carb pumice bx.
rhyolitic pumice breccia mass flows f only

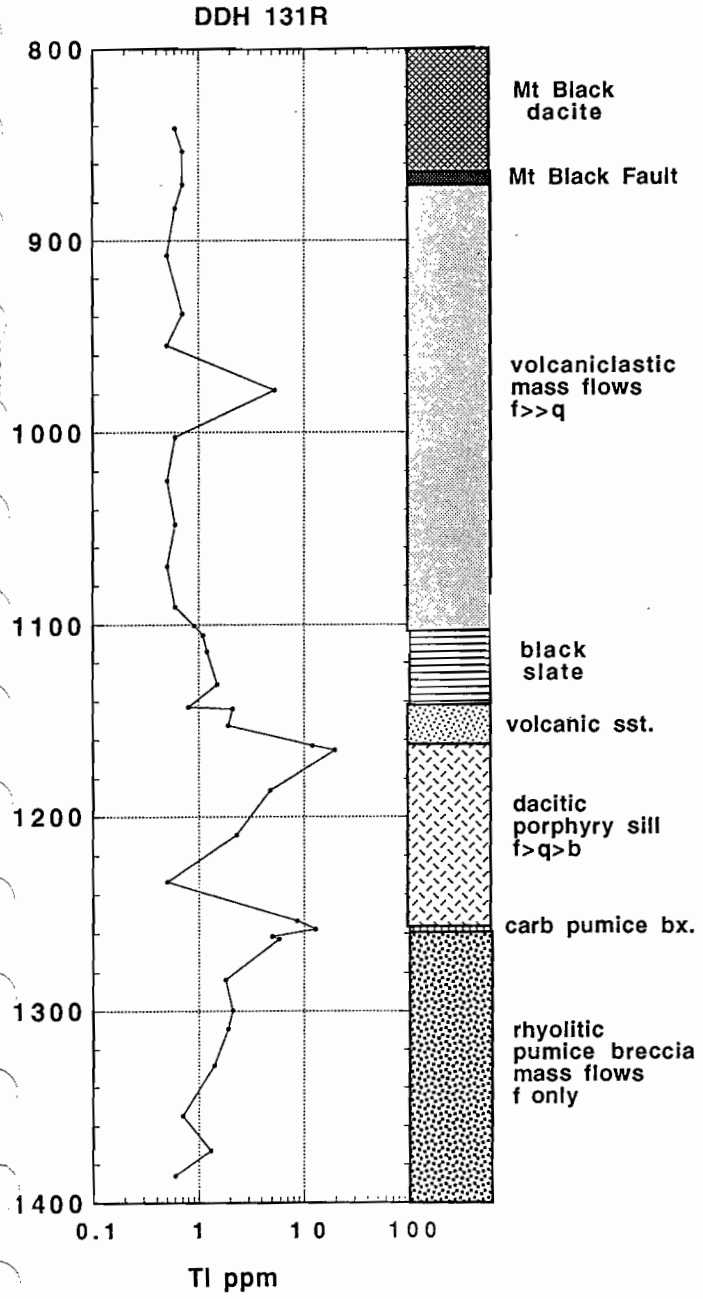
DDH 131R
800
900
1000
1100
1200
1300
1400
met.
0.1
1
10
100
Tl ppm
Mt Black dacite
Mt Black Fault
volcaniclastic mass flows f>>q
black slate
volcanic sst.
dacitic porphyry sill f>q>b
carb pumice bx.
rhyolitic pumice breccia mass flows f only

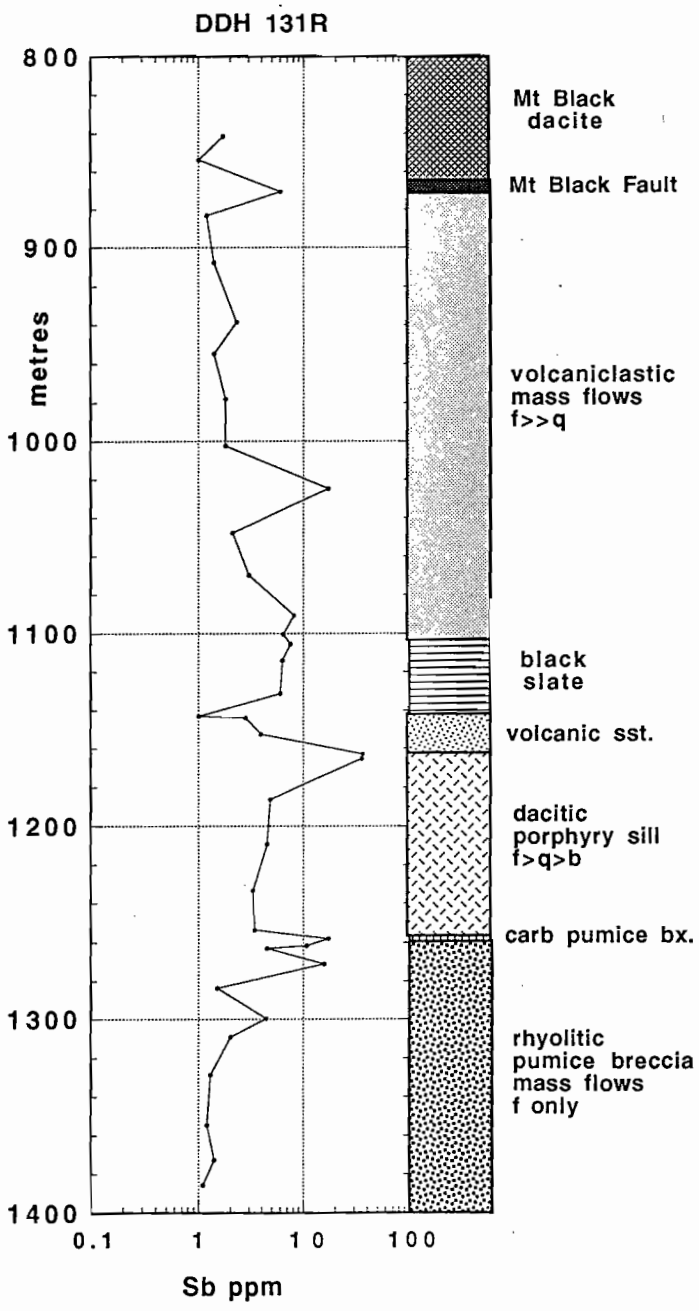
DDH 131R
800
900
1000
1100
1200
1300
1400
metres
0.1
1
10
100
Sb ppm
Mt Black dacite
Mt Black Fault
volcaniclastic mass flows f>>q
black slate
volcanic sst.
dacitic porphyry sill f>q>b
carb pumice bx.
rhyolitic pumice breccia mass flows f only

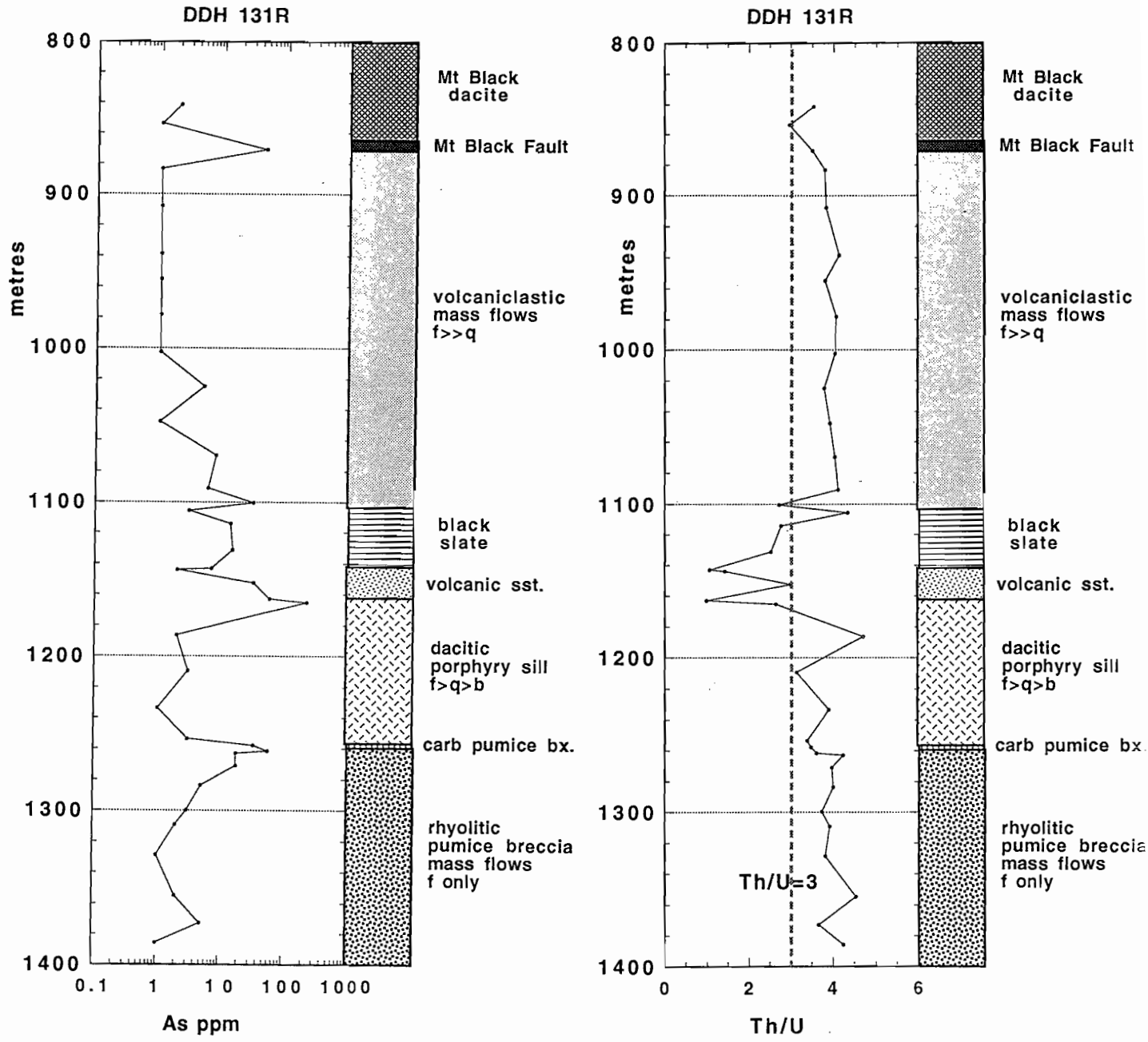
DDH 131R
800
900
1000
1100
1200
1300
1400
metres
0.1
1
10
100
1000
As ppm
Mt Black dacite
Mt Black Fault
volcaniclastic mass flows f>>q
black slate
volcanic sst.
dacitic porphyry sill f>q>b
carb pumice bx.
rhyolitic pumice breccia mass flows f only
DDH 131R
Th/U=3
0
2
4
6
Th/U
Mt Black dacite
Mt Black Fault
volcaniclastic mass flows f>>q
black slate
volcanic sst.
dacitic porphyry sill f>q>b
carb pumice bx.
rhyolitic pumice breccia mass flows f only

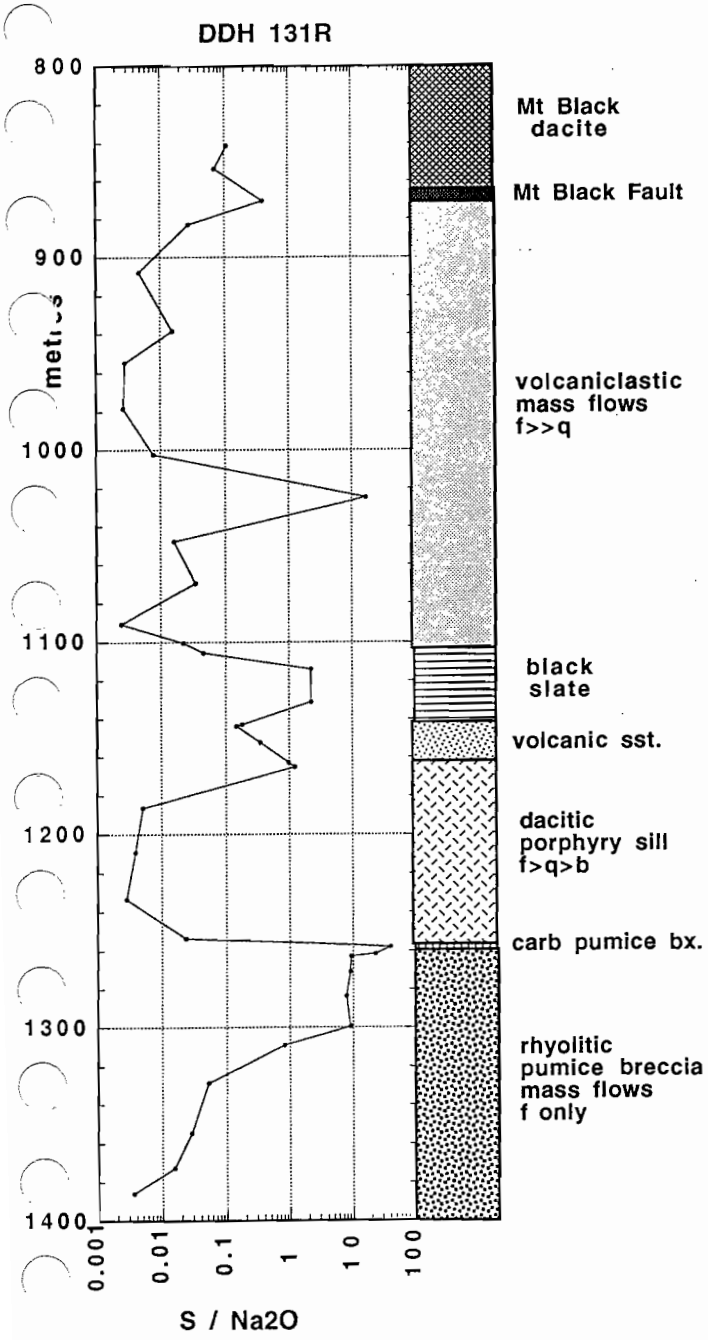
DDH 131R
800
900
1000
1100
1200
1300
1400
metres
Mt Black dacite
Mt Black Fault
volcaniclastic mass flows f>>q
black slate
volcanic sst.
dacitic porphyry sill f>q>b
carb pumice bx.
rhyolitic pumice breccia mass flows f only
0.001
0.01
0.1
1
10
100
S / Na2O

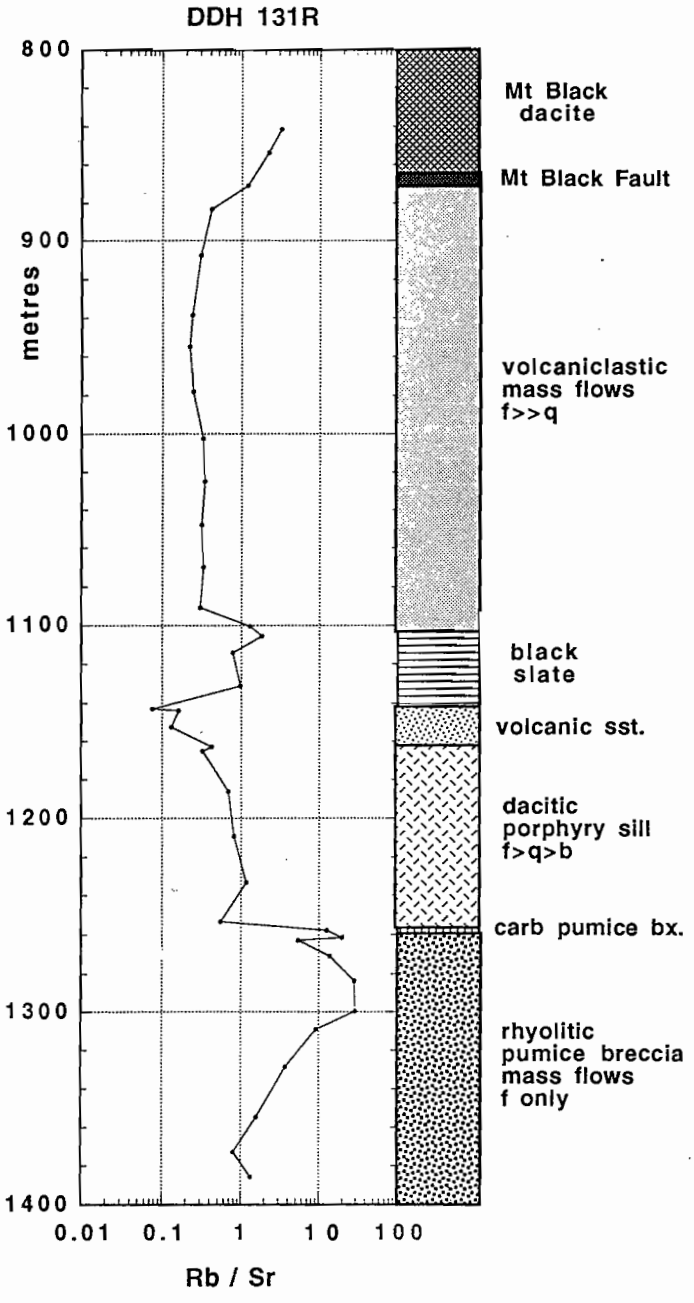
DDH 131R
800
900
1000
1100
1200
1300
1400
metres
Mt Black dacite
Mt Black Fault
volcaniclastic mass flows f>>q
black slate
volcanic sst.
dacitic porphyry sill f>q>b
carb pumice bx.
rhyolitic pumice breccia mass flows f only
0.01
0.1
1
10
100
Rb / Sr

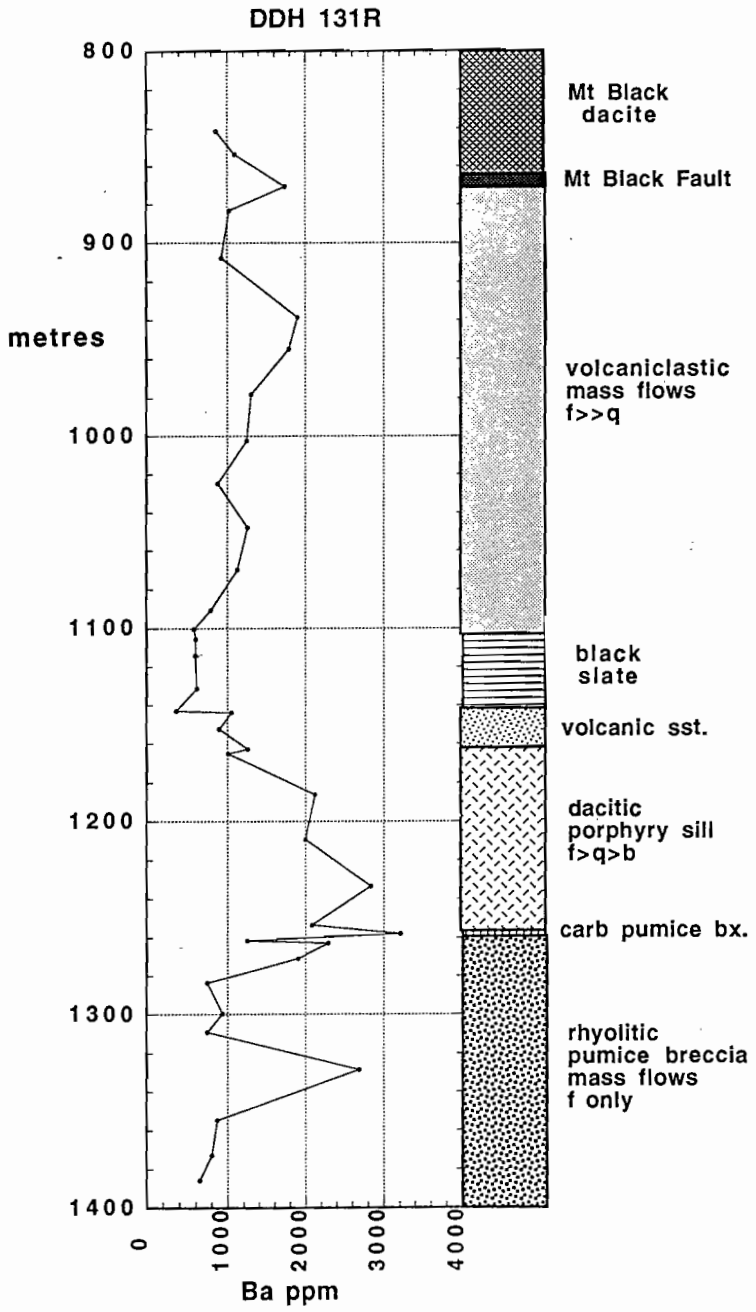
DDH 131R
800
900
1000
1100
1200
1300
1400
metres
0
1000
2000
3000
4000
Ba ppm
Mt Black dacite
Mt Black Fault
volcaniclastic mass flows f>>q
black slate
volcanic sst.
dacitic porphyry sill f>q>b
carb pumice bx.
rhyolitic pumice breccia mass flows f only

Appendix C

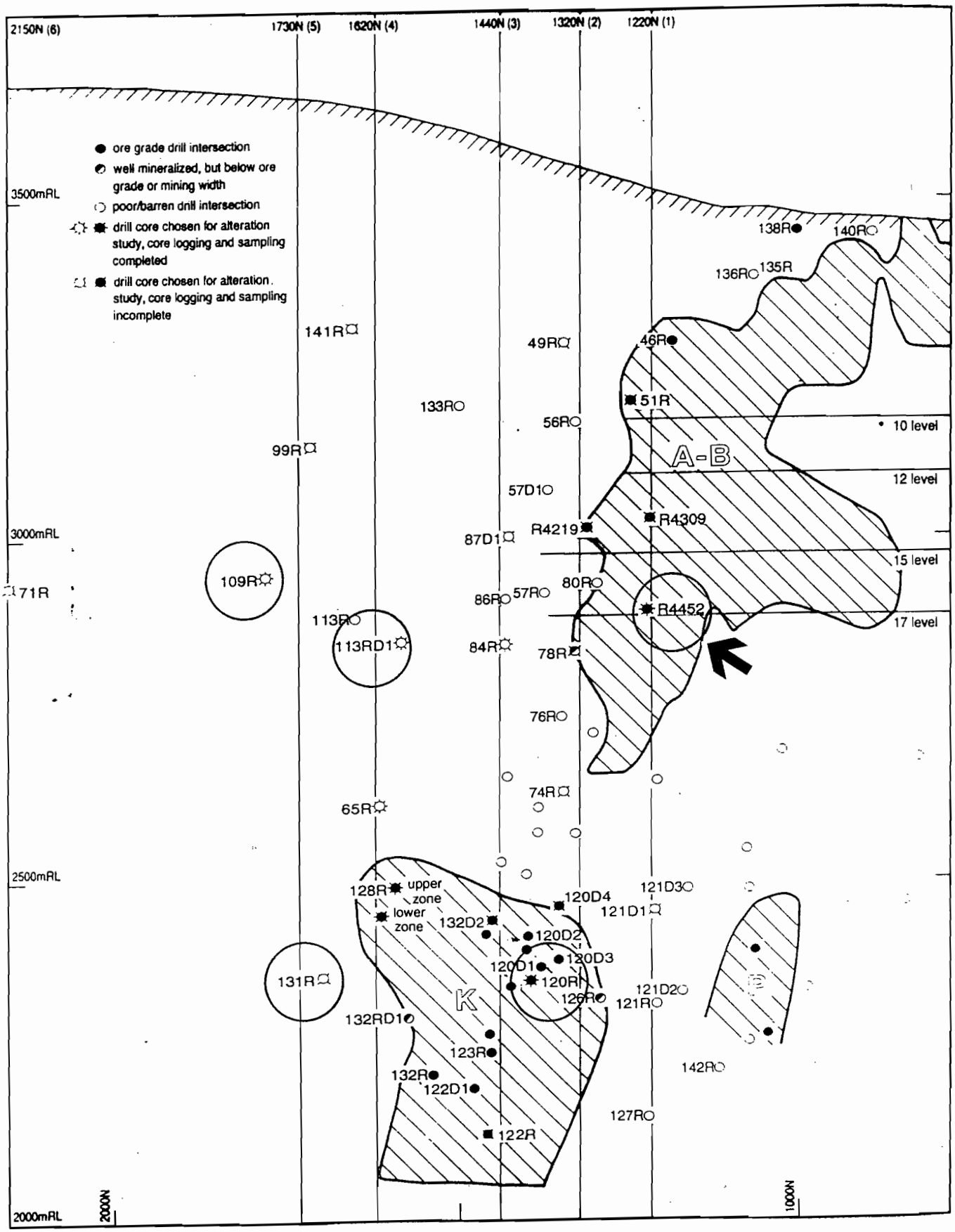

Figure 1: Longitudinal section of the north end of Rosebery mine showing the location of A-B, K and P ore lenses, drill core intersections of the ore stratigraphic position, drill cores selected for this study, and six cross sections designed to compile results (1220 mN, 1320 mN, 1440 mN, 1620 mN, 1730 mN and 2150 mN).

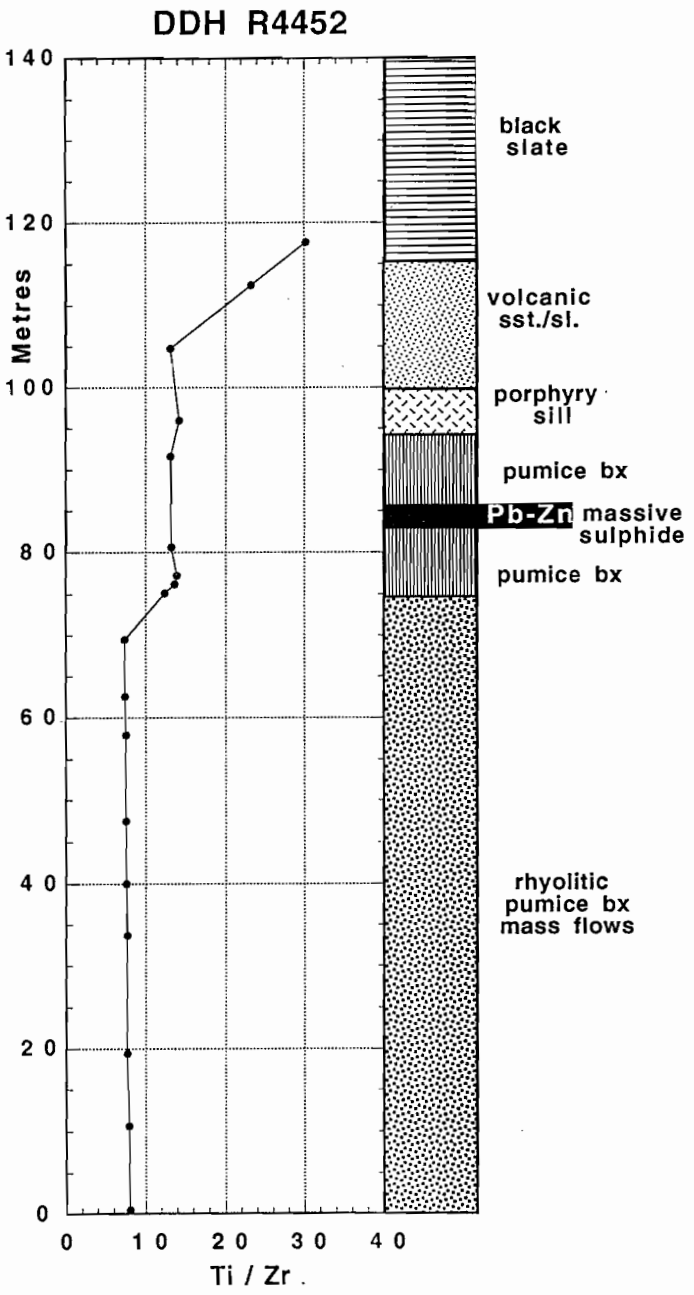
DDH R4452
140
120
100
80
60
40
20
0
Metres
0
10
20
30
40
Ti / Zr
black slate
volcanic sst./sl.
porphyry sill
pumice bx
Pb-Zn massive sulphide
pumice bx
rhyolitic pumice bx mass flows

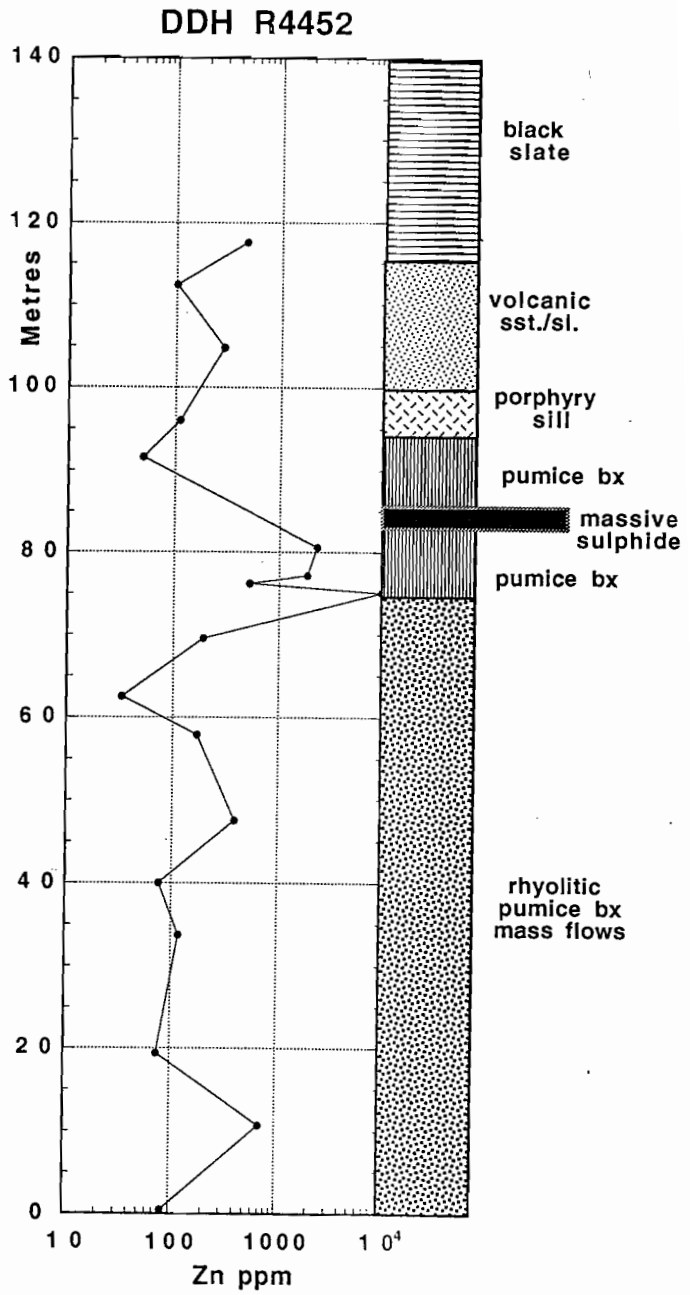
DDH R4452
140
120
100
80
60
40
20
0
Metres
10
100
1000
10⁴
Zn ppm
black slate
volcanic sst./sl.
porphyry sill
pumice bx
massive sulphide
pumice bx
rhyolitic pumice bx mass flows

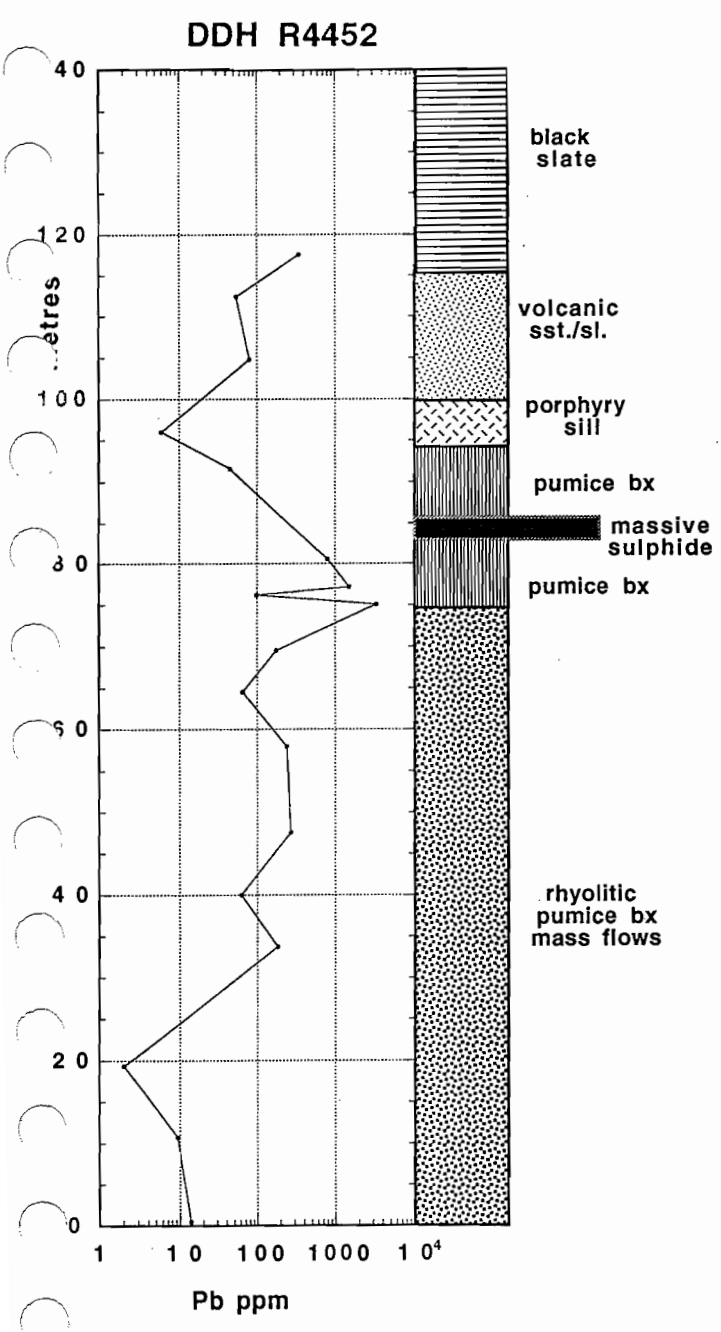
DDH R4452
metres
40
120
100
80
60
40
20
0
1
10
100
1000
10⁴
Pb ppm
black slate
volcanic sst./sl.
porphyry sill
pumice bx
massive sulphide
pumice bx
rhyolitic pumice bx mass flows

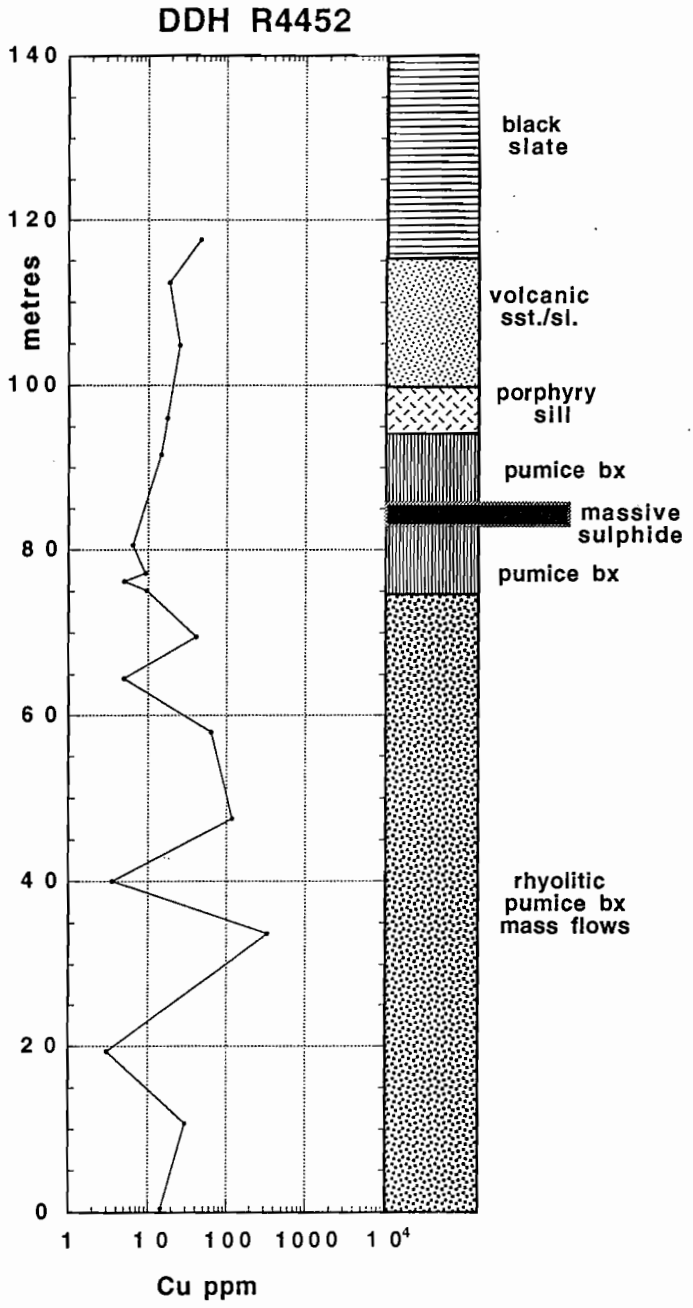
DDH R4452
metres
140
120
100
80
60
40
20
0
1
10
100
1000
10⁴
Cu ppm
black slate
volcanic sst./sl.
porphyry sill
pumice bx
massive sulphide
pumice bx
rhyolitic pumice bx mass flows

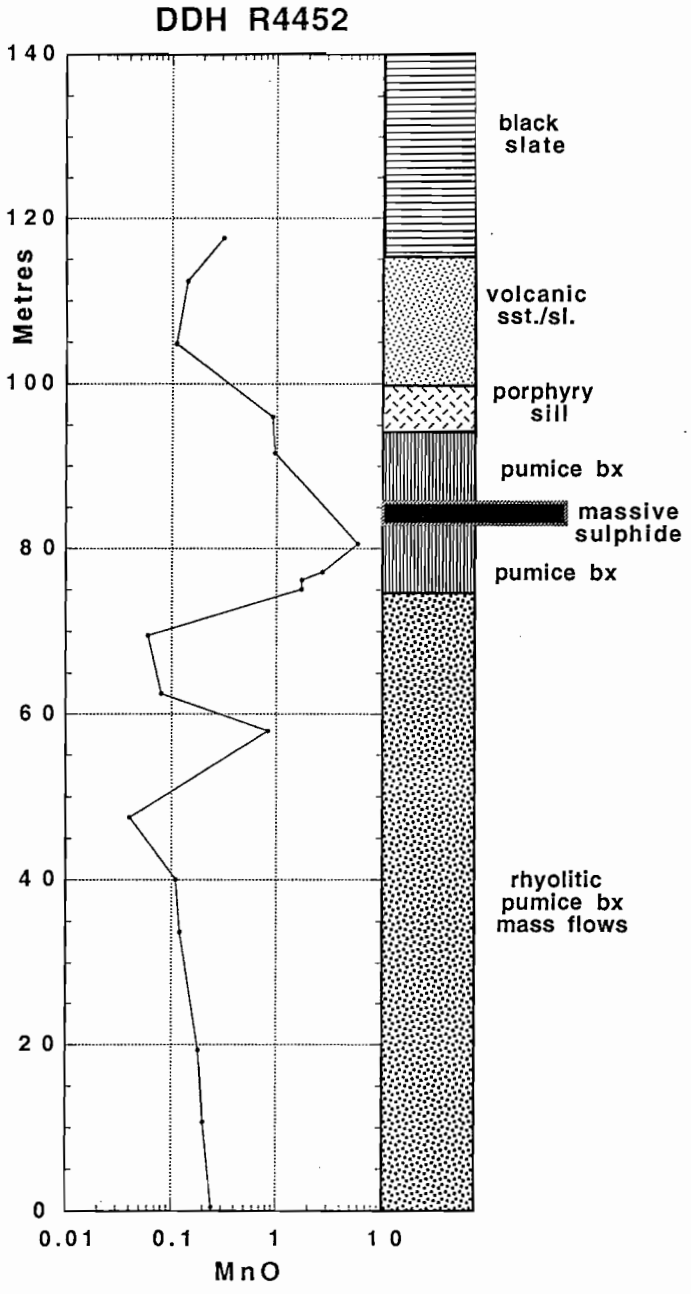
DDH R4452
140
120
100
80
60
40
20
0
Metres
black slate
volcanic sst./sl.
porphyry sill
pumice bx
massive sulphide
pumice bx
rhyolitic pumice bx mass flows
0.01
0.1
1
10
MnO

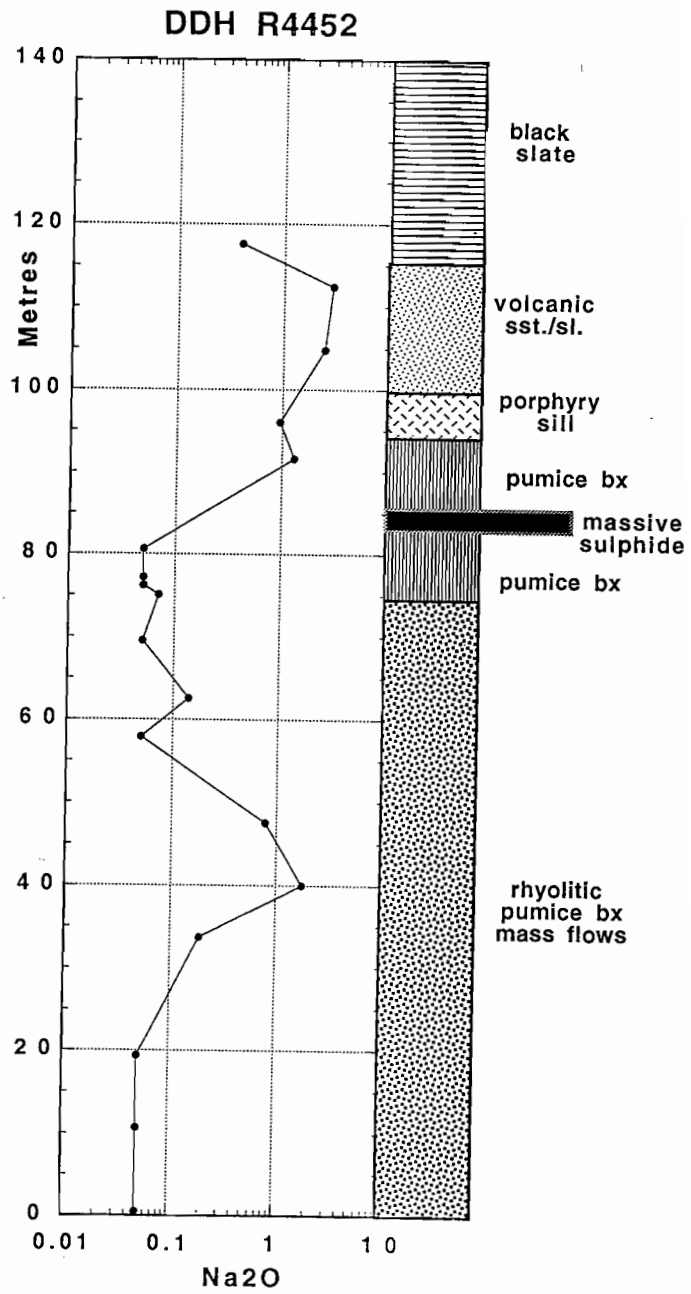
DDH R4452
140
120
100
80
60
40
20
0
Metres
black slate
volcanic sst./sl.
porphyry sill
pumice bx
massive sulphide
pumice bx
rhyolitic pumice bx mass flows
0.01
0.1
1
10
Na2O

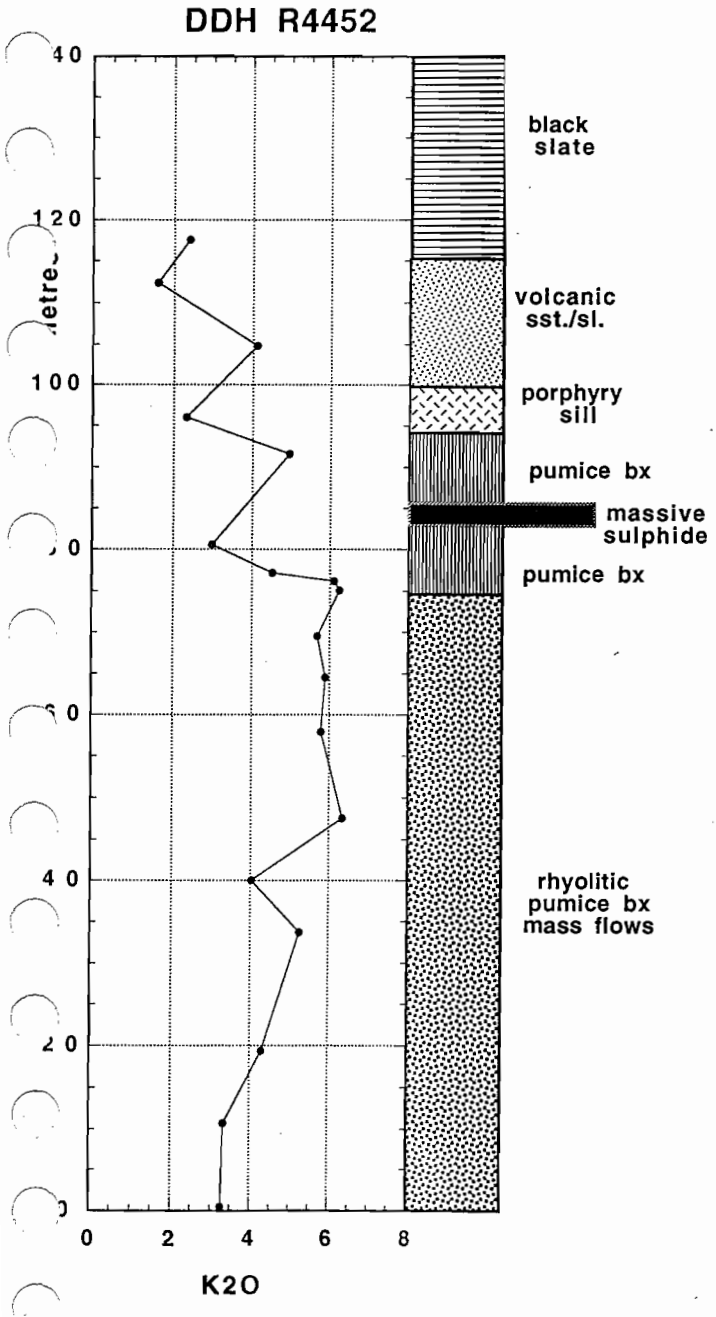
DDH R4452
40
120
100
0
0
40
20
0
0
2
4
6
8
K2O
black slate
volcanic sst./sl.
porphyry sill
pumice bx
massive sulphide
pumice bx
rhyolitic pumice bx mass flows

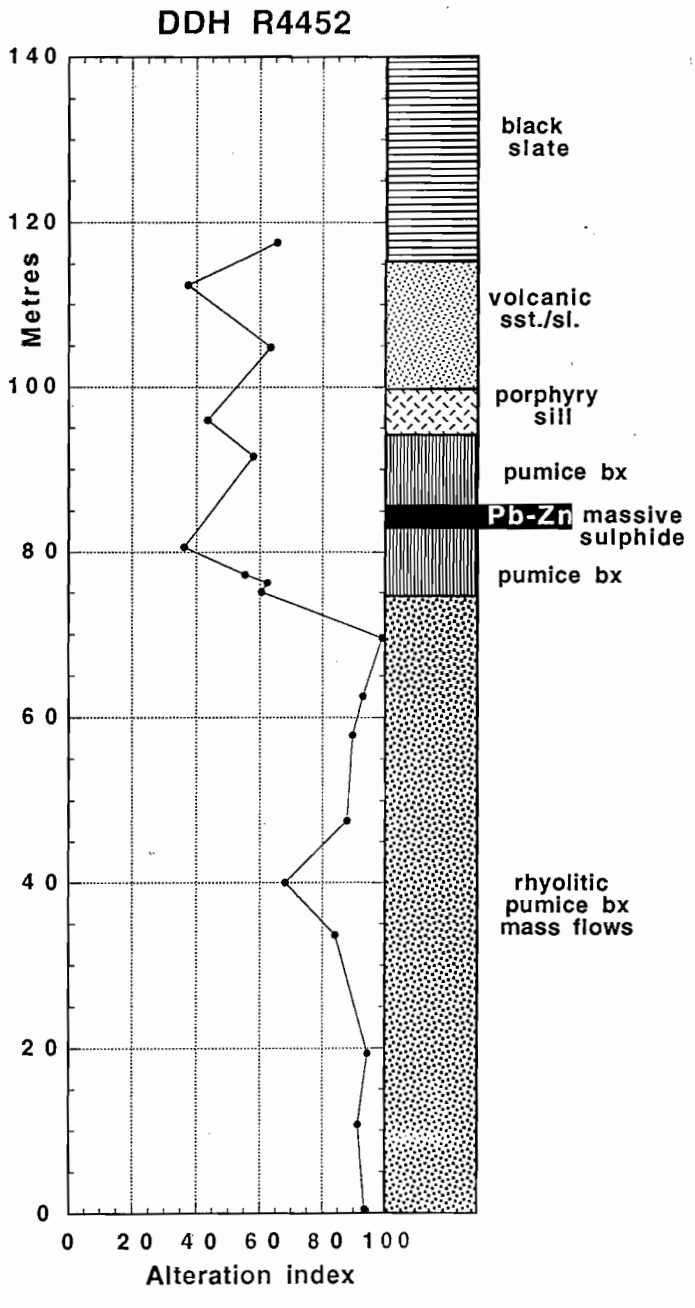
DDH R4452
140
120
100
80
60
40
20
0
Metres
0 20 40 60 80 100
Alteration index
black slate
volcanic sst./sl.
porphyry sill
pumice bx
Pb-Zn massive sulphide
pumice bx
rhyolitic pumice bx mass flows

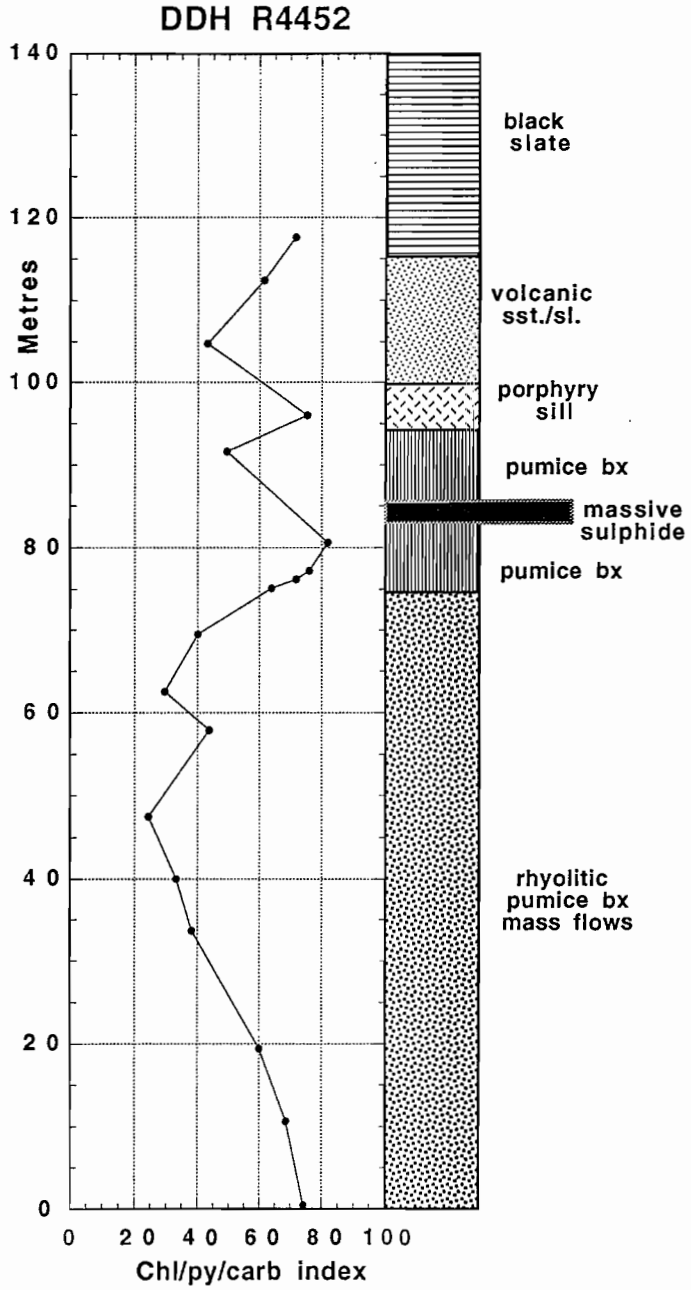
DDH R4452
140
120
100
80
60
40
20
0
Metres
black slate
volcanic sst./sl.
porphyry sill
pumice bx
massive sulphide
pumice bx
rhyolitic pumice bx mass flows
0 20 40 60 80 100
Chl/py/carb index

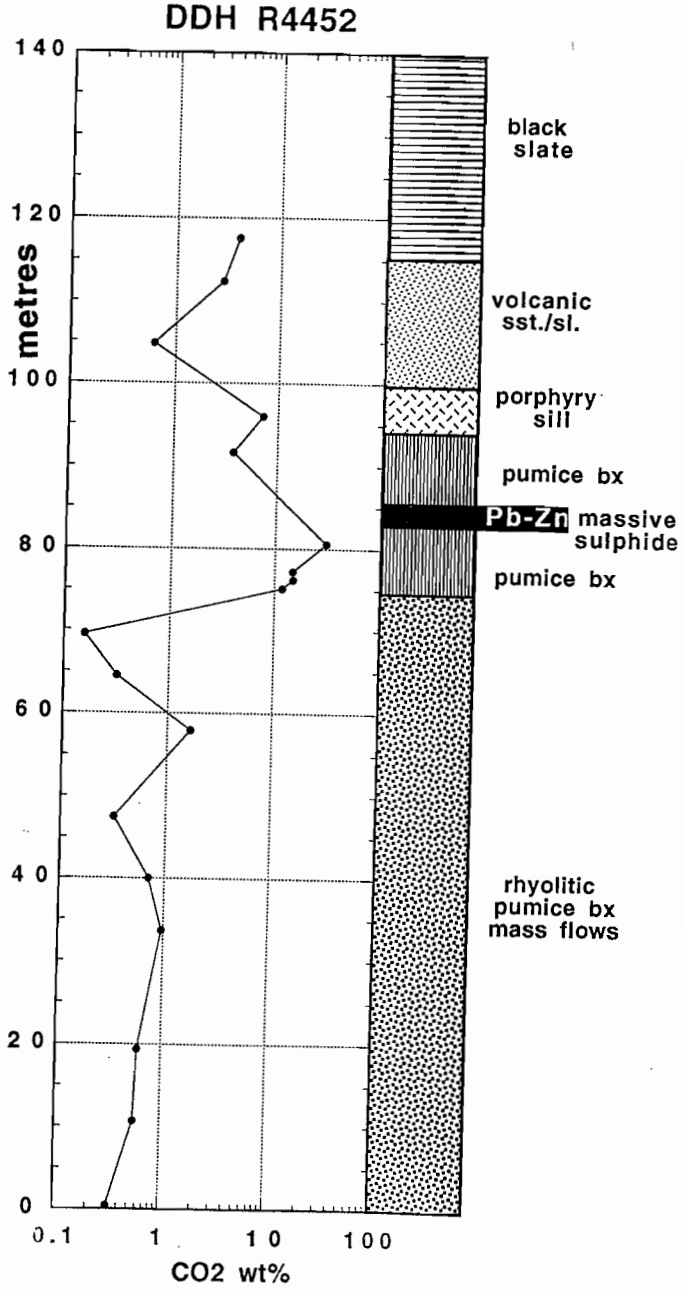
DDH R4452
140
120
100
80
60
40
20
0
metres
black slate
volcanic sst./sl.
porphyry sill
pumice bx
Pb-Zn massive sulphide
pumice bx
rhyolitic pumice bx mass flows
0.1 1 10 100
CO2 wt%

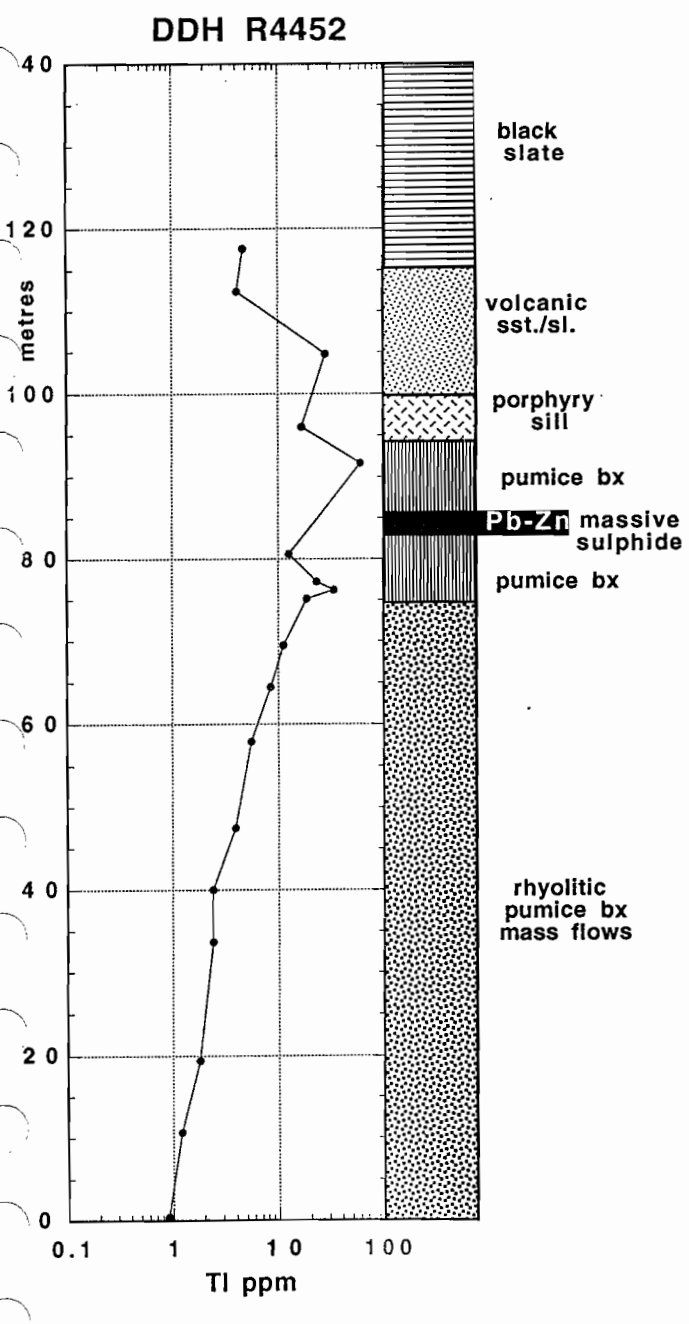
DDH R4452
metres
40
120
100
80
60
40
20
0
0.1
1
10
100
Tl ppm
black slate
volcanic sst./sl.
porphyry sill
pumice bx
Pb-Zn massive sulphide
pumice bx
rhyolitic pumice bx mass flows

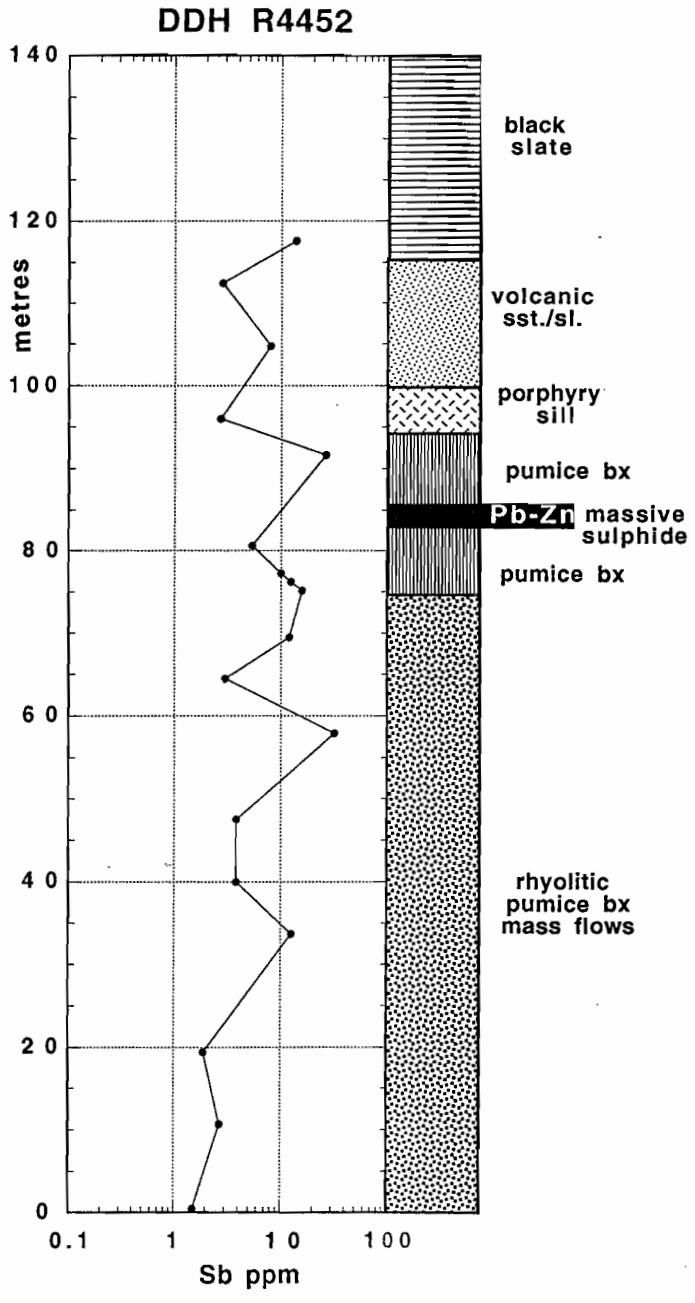
DDH R4452
metres
140
120
100
80
60
40
20
0
0.1
1
10
100
Sb ppm
black slate
volcanic sst./sl.
porphyry sill
pumice bx
Pb-Zn massive sulphide
pumice bx
rhyolitic pumice bx mass flows

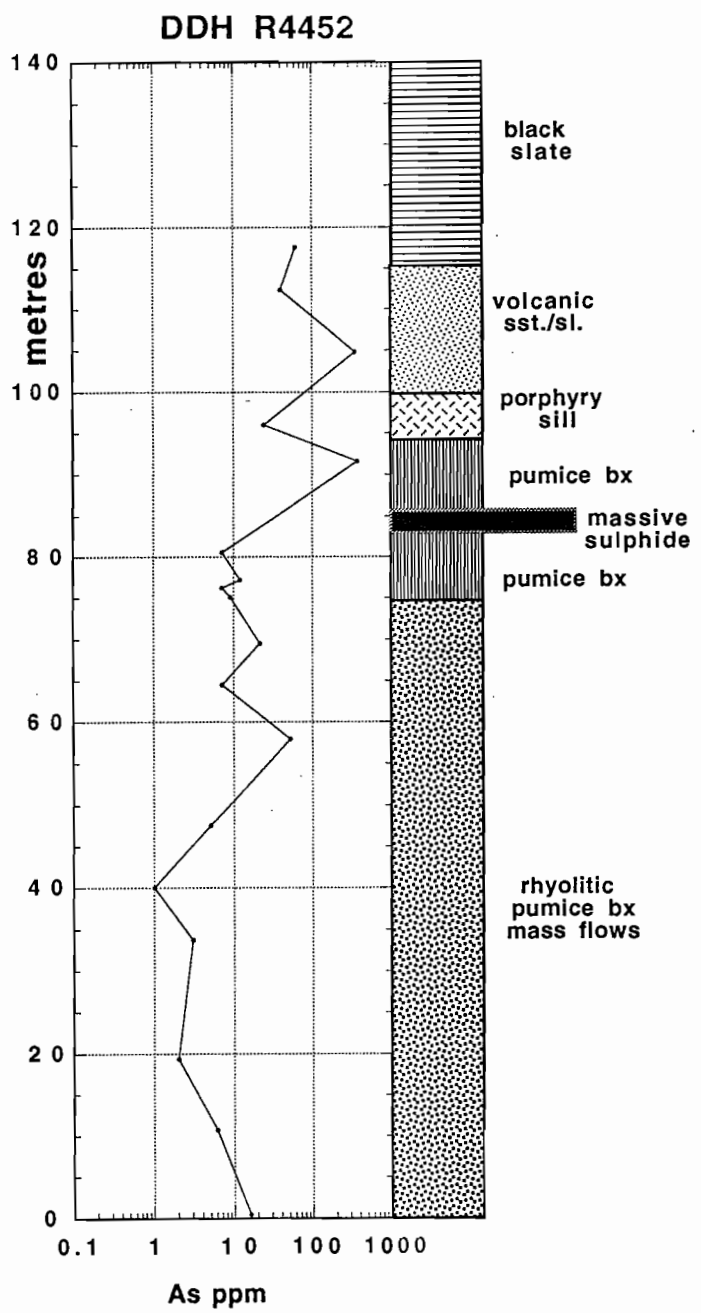
DDH R4452
140
120
100
80
60
40
20
0
metres
0.1
1
10
100
1000
As ppm
black slate
volcanic sst./sl.
porphyry sill
pumice bx
massive sulphide
pumice bx
rhyolitic pumice bx mass flows

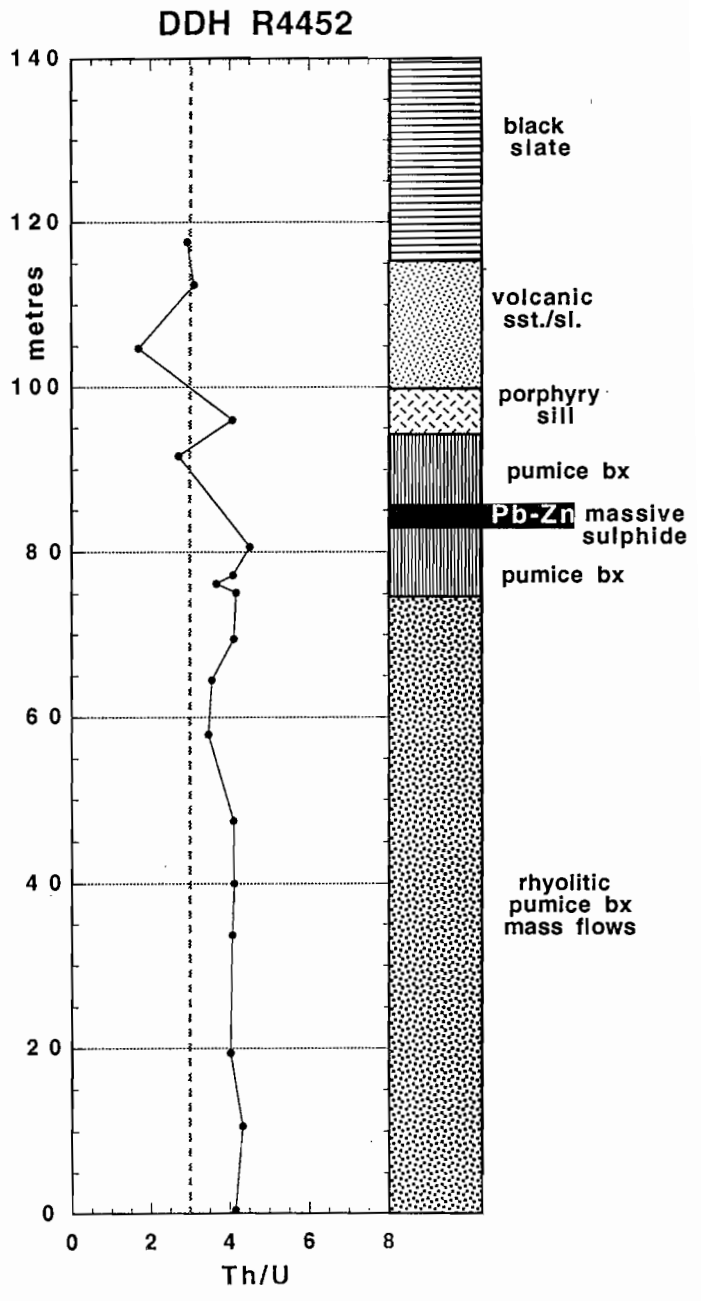
DDH R4452
140
120
100
80
60
40
20
0
metres
0
2
4
6
8
Th/U
black slate
volcanic sst./sl.
porphyry sill
pumice bx
Pb-Zn massive sulphide
pumice bx
rhyolitic pumice bx mass flows

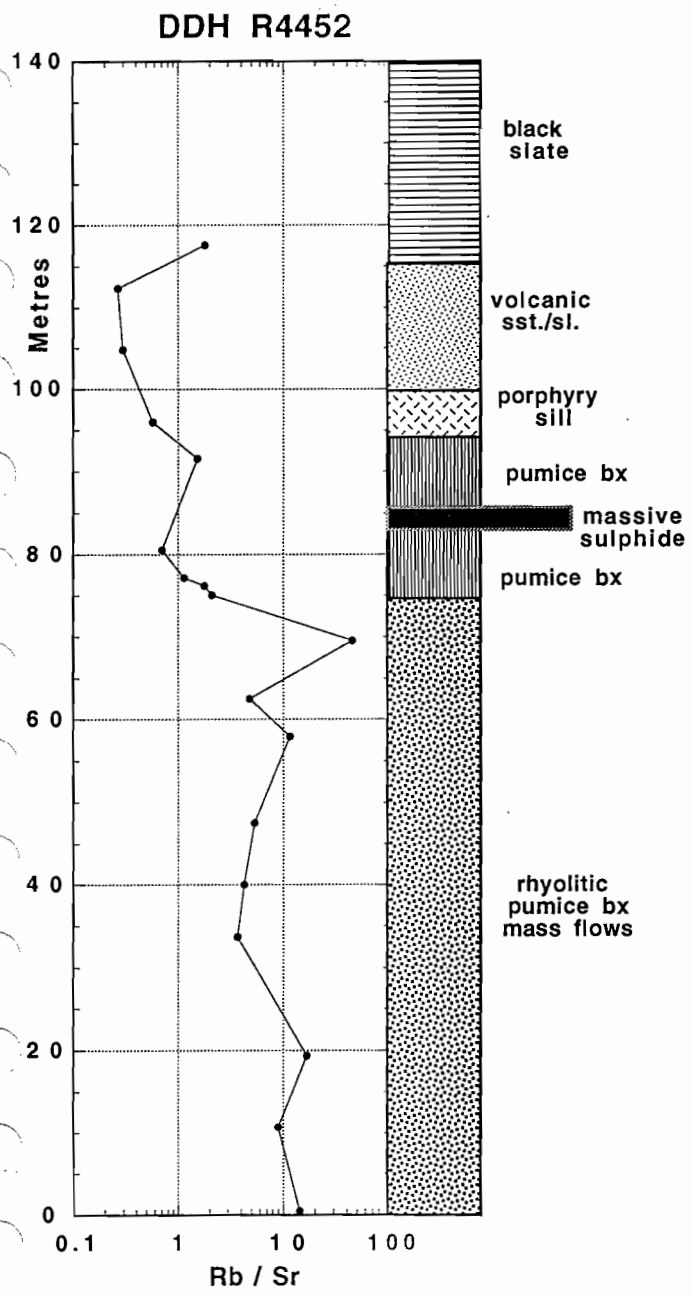
DDH R4452
140
120
100
80
60
40
20
0
Metres
0.1
1
10
100
Rb / Sr
black slate
volcanic sst./sl.
porphyry sill
pumice bx
massive sulphide
pumice bx
rhyolitic pumice bx mass flows

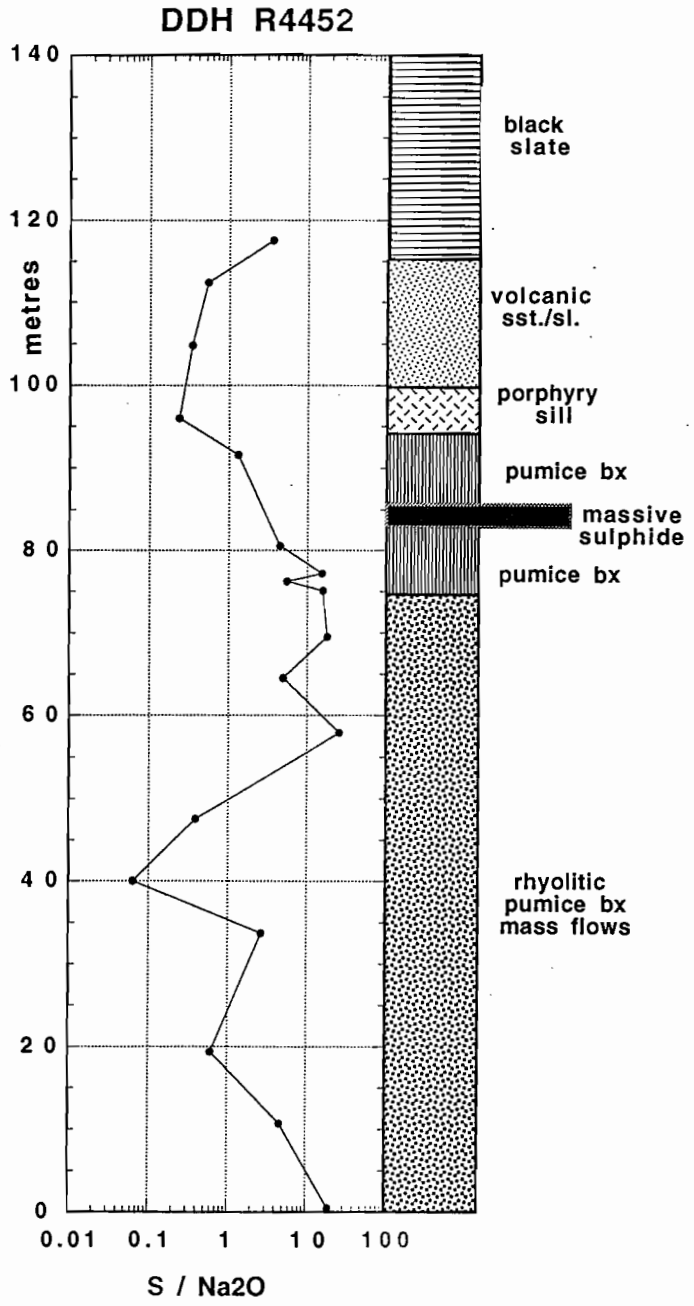
DDH R4452
140
120
100
80
60
40
20
0
metres
0.01
0.1
1
10
100
S / Na2O
black slate
volcanic sst./sl.
porphyry sill
pumice bx
massive sulphide
pumice bx
rhyolitic pumice bx mass flows

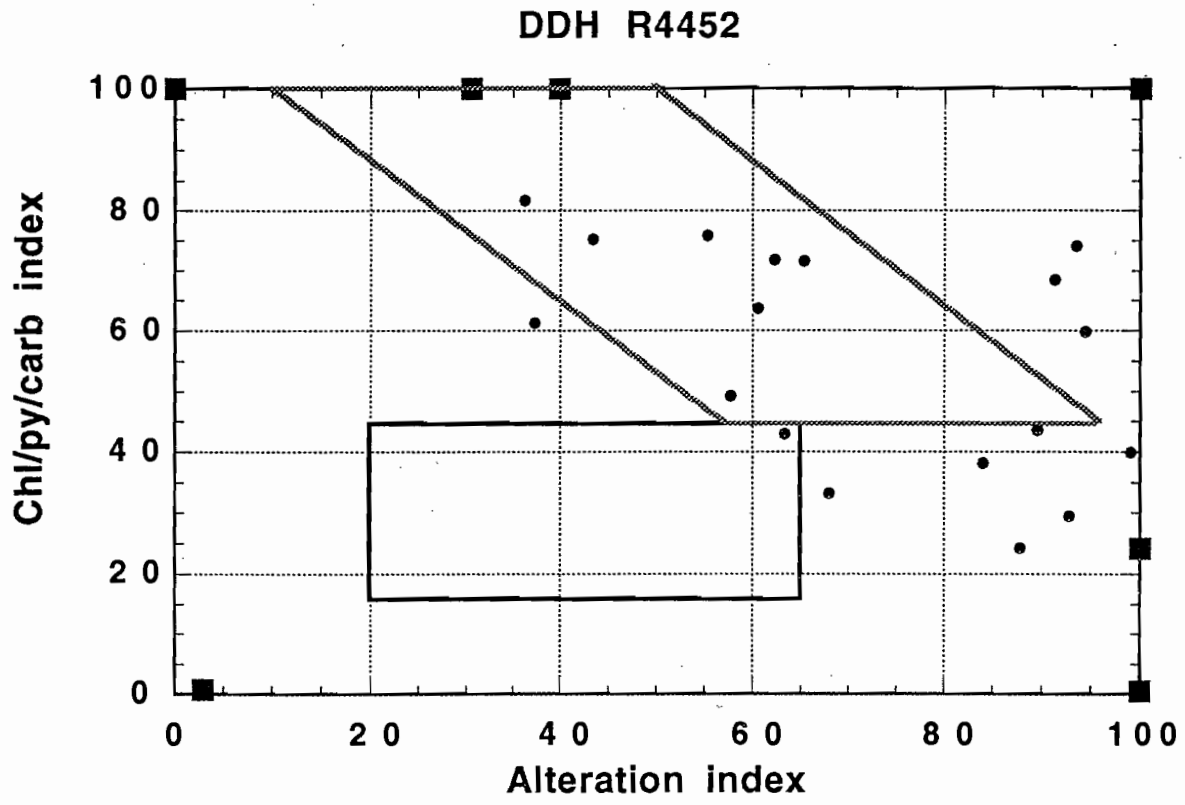
DDH R4452
Chl/py/carb index
100
80
60
40
20
0
0
20
40
60
80
100
Alteration index

Appendix D

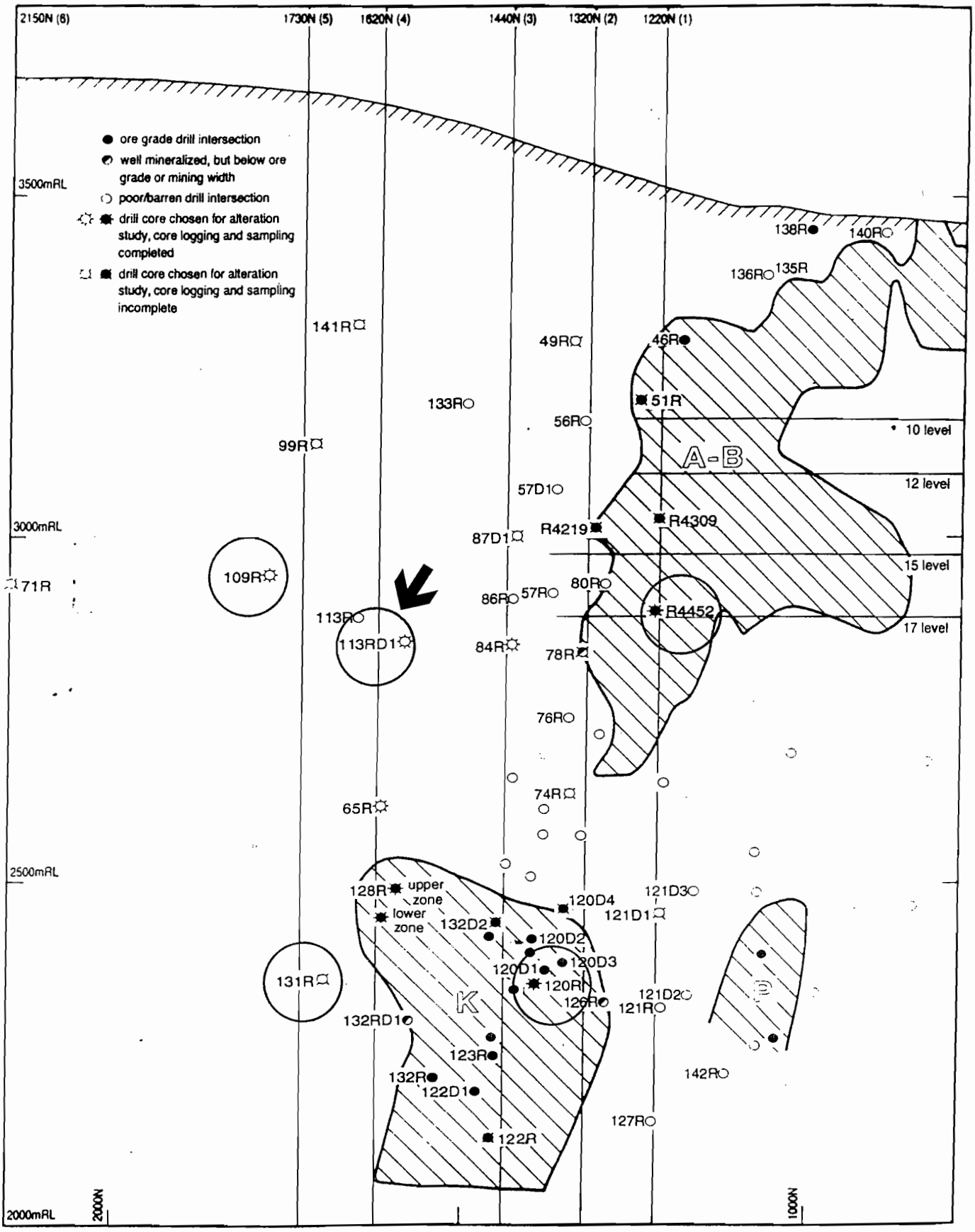

Figure 1: Longitudinal section of the north end of Rosebery mine showing the location of A-B, K and P ore lenses, drill core intersections of the ore stratigraphic position, drill cores selected for this study, and six cross sections designed to compile results (1220 mN, 1320 mN, 1440 mN, 1620 mN, 1730 mN and 2150 mN).

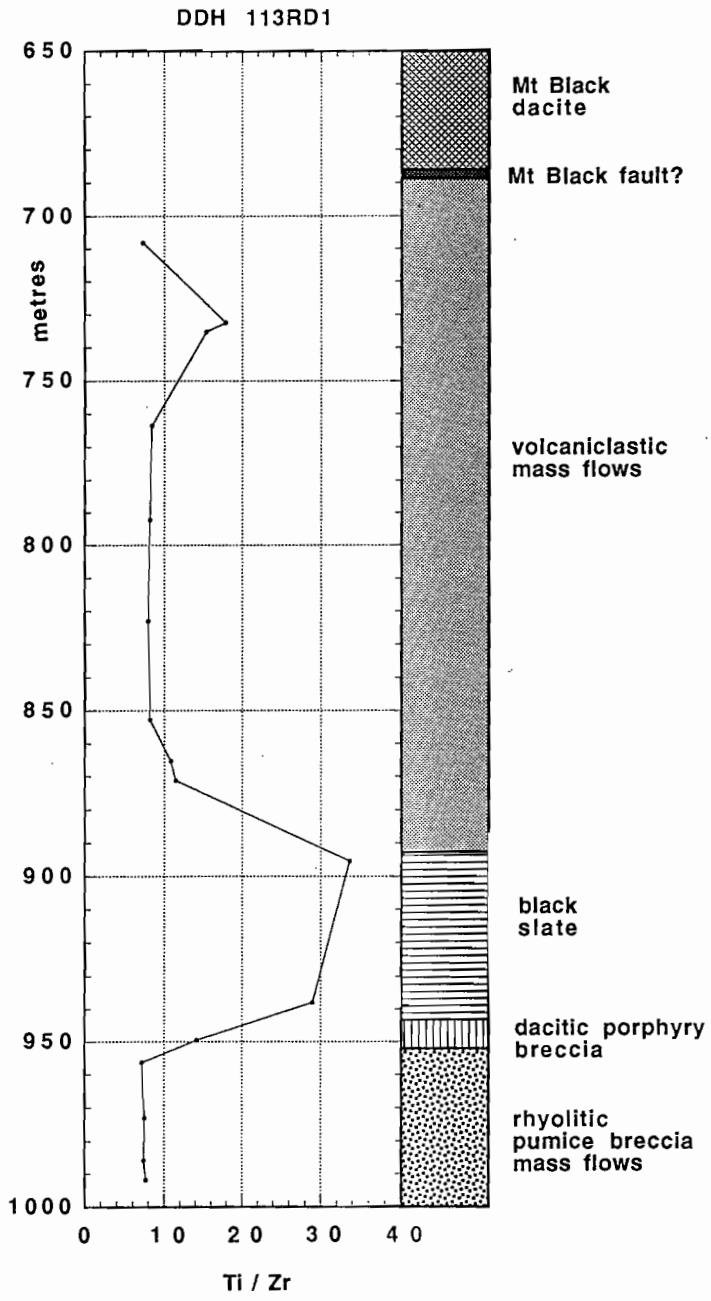
DDH 113RD1
650
700
750
800
850
900
950
1000
metres
0
10
20
30
40
Ti / Zr
Mt Black dacite
Mt Black fault?
volcaniclastic mass flows
black slate
dacitic porphyry breccia
rhyolitic pumice breccia mass flows

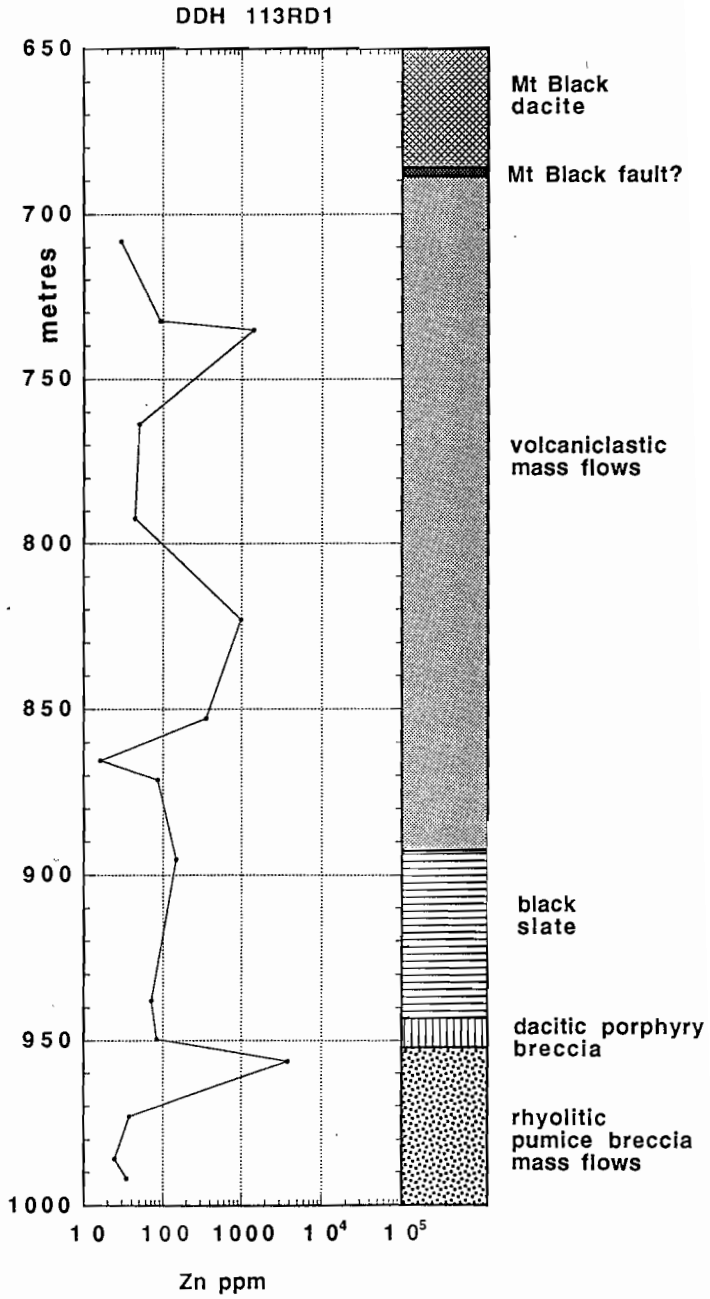
DDH 113RD1
650
700
750
800
850
900
950
1000
metres
10
100
1000
10⁴
10⁵
Zn ppm
Mt Black dacite
Mt Black fault?
volcaniclastic mass flows
black slate
dacitic porphyry breccia
rhyolitic pumice breccia mass flows

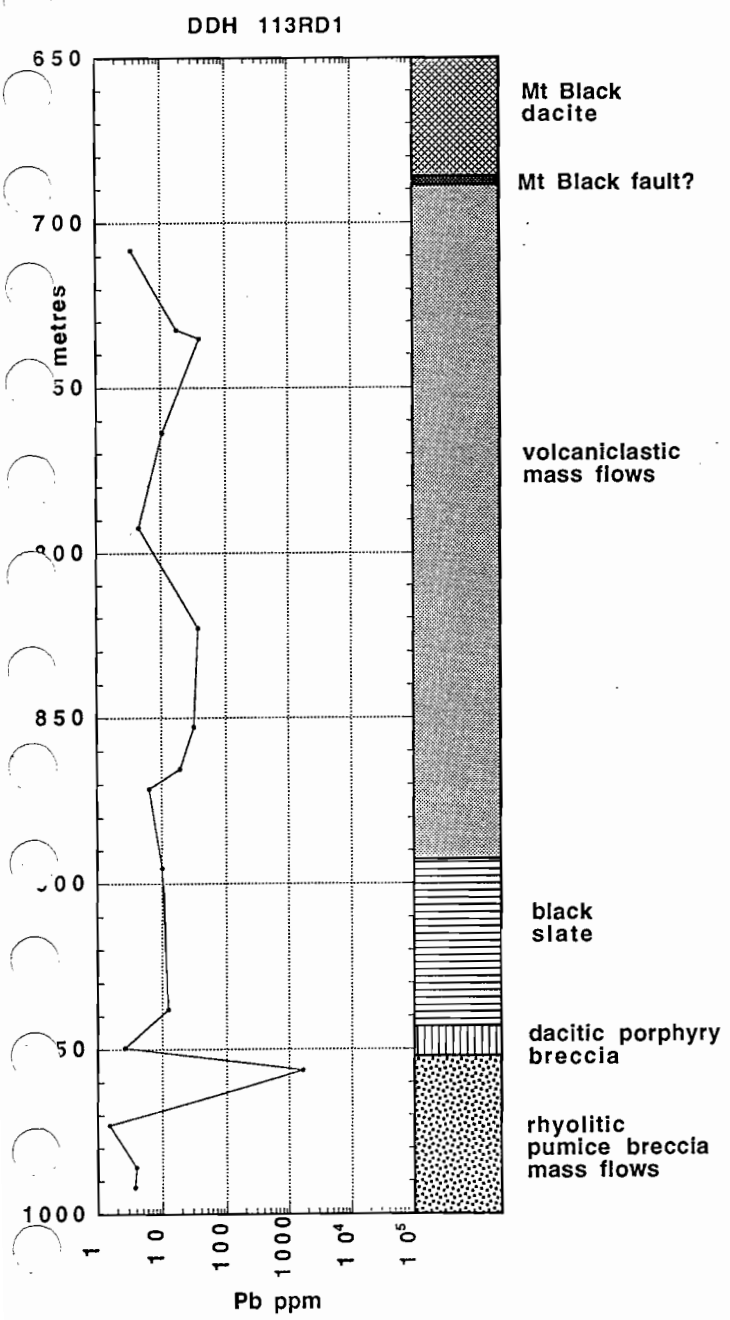
DDH 113RD1
650
700
750
800
850
900
950
1000
metres
Mt Black dacite
Mt Black fault?
volcaniclastic mass flows
black slate
dacitic porphyry breccia
rhyolitic pumice breccia mass flows
1
10
100
1000
10⁴
10⁵
Pb ppm

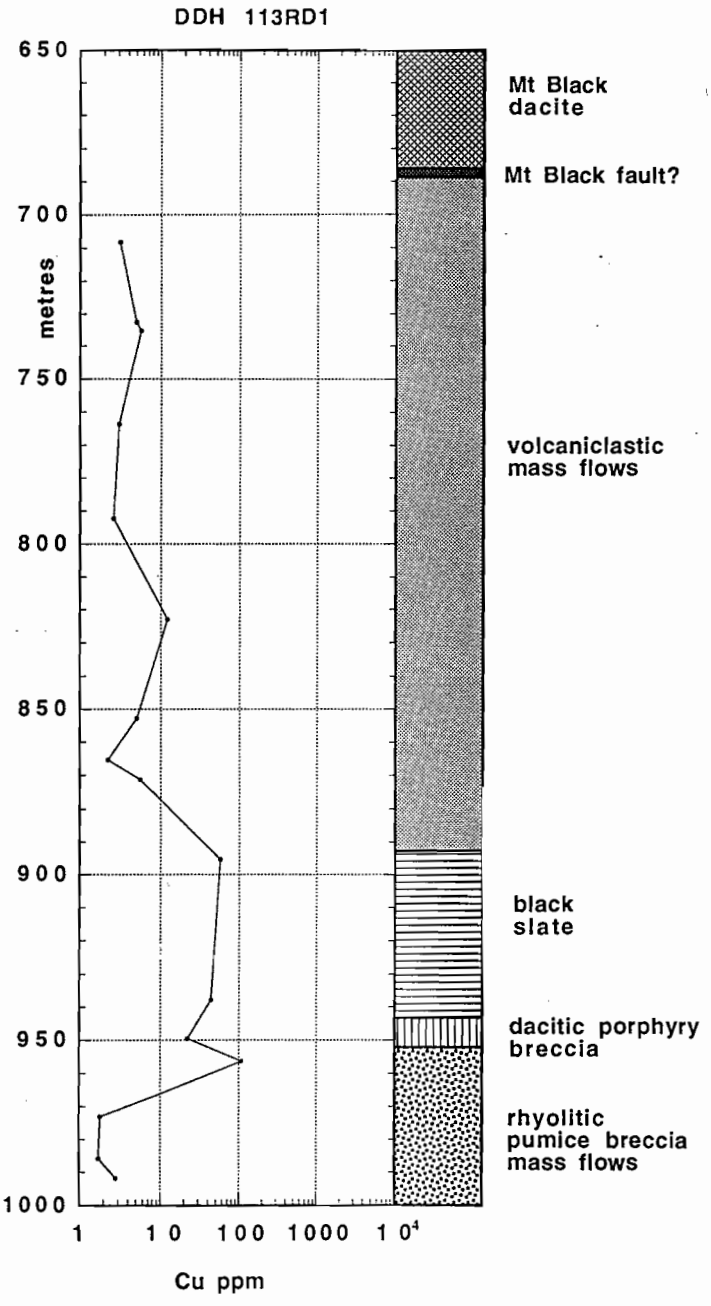
DDH 113RD1
650
700
750
800
850
900
950
1000
metres
Mt Black dacite
Mt Black fault?
volcaniclastic mass flows
black slate
dacitic porphyry breccia
rhyolitic pumice breccia mass flows
1
10
100
1000
10⁴
Cu ppm

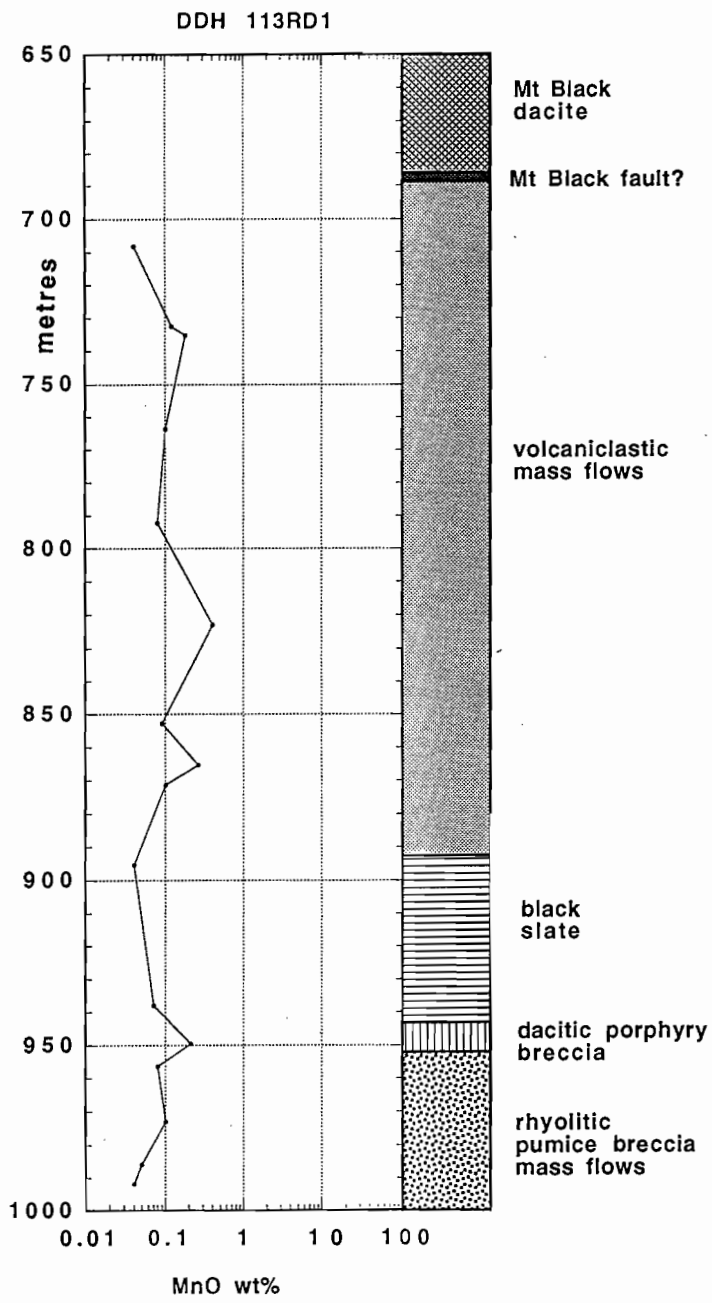
DDH 113RD1
650
700
750
800
850
900
950
1000
metres
0.01
0.1
1
10
100
MnO wt%
Mt Black dacite
Mt Black fault?
volcaniclastic mass flows
black slate
dacitic porphyry breccia
rhyolitic pumice breccia mass flows

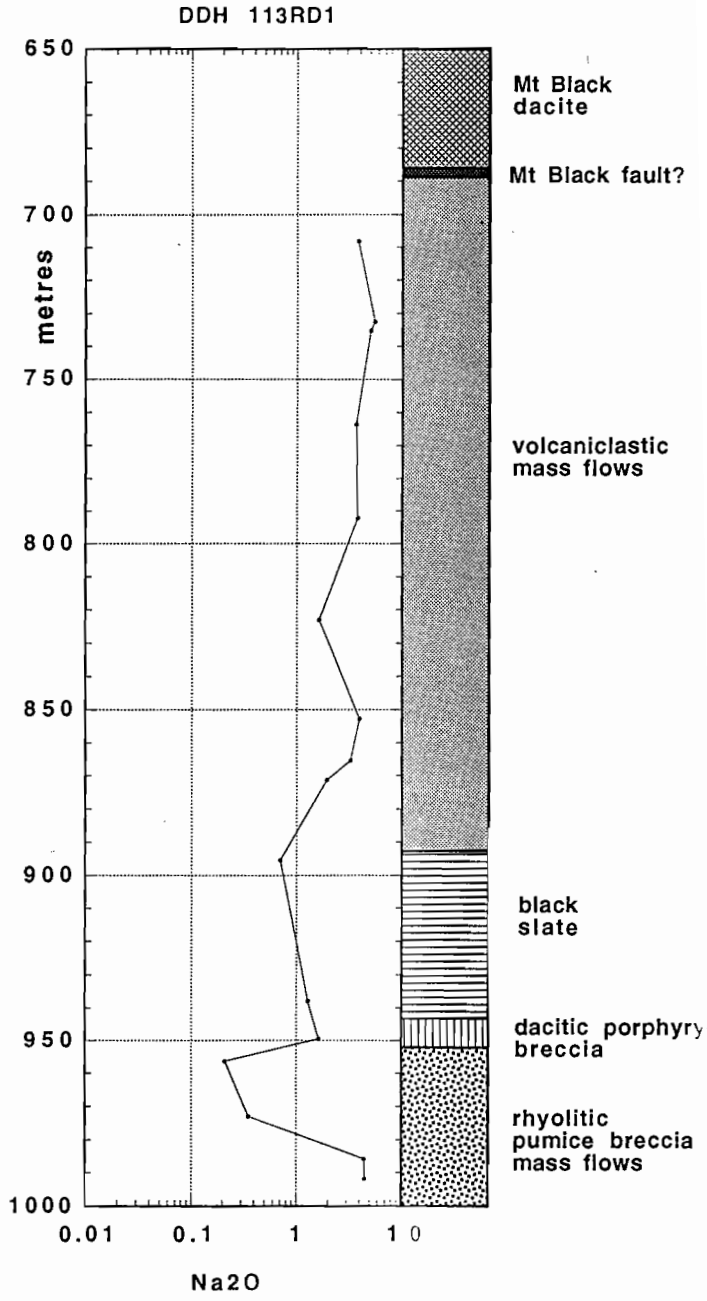
DDH 113RD1
650
700
750
800
850
900
950
1000
metres
0.01
0.1
1
10
Na2O
Mt Black dacite
Mt Black fault?
volcaniclastic mass flows
black slate
dacitic porphyry breccia
rhyolitic pumice breccia mass flows

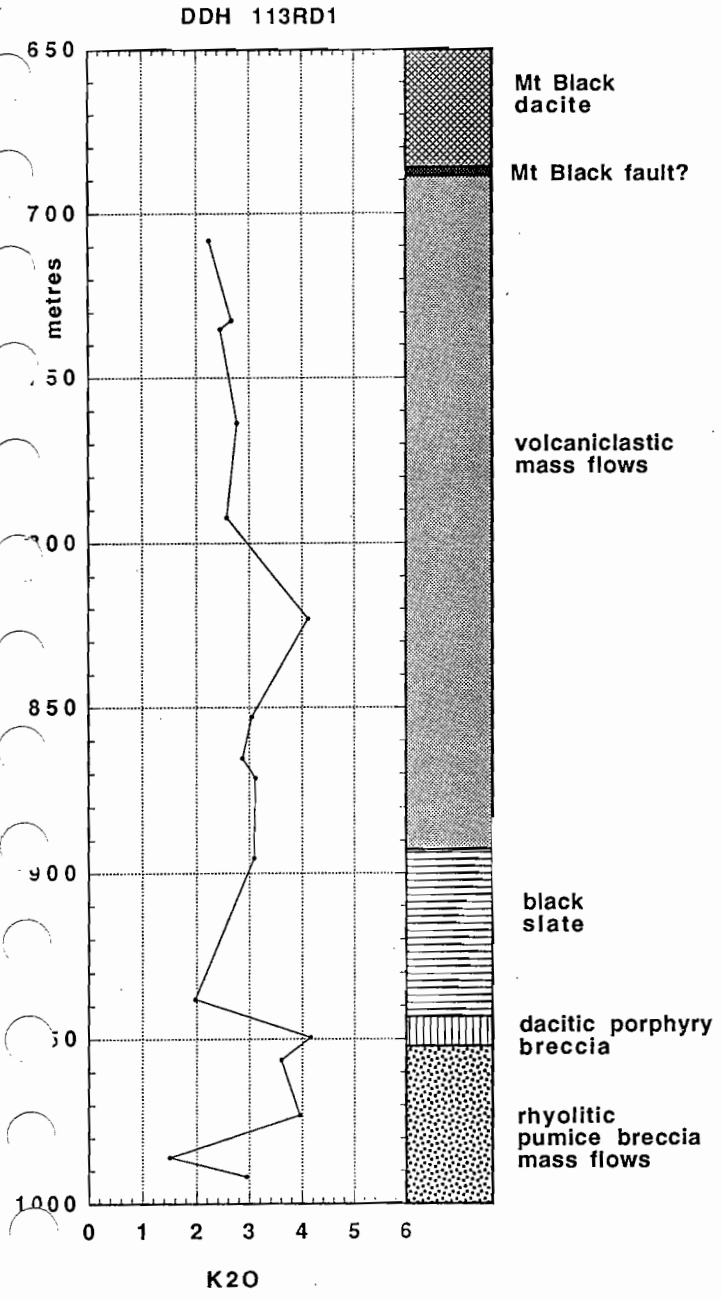
DDH 113RD1
650
700
750
800
850
900
950
1000
metres
0 1 2 3 4 5 6
K2O
Mt Black dacite
Mt Black fault?
volcaniclastic mass flows
black slate
dacitic porphyry breccia
rhyolitic pumice breccia mass flows

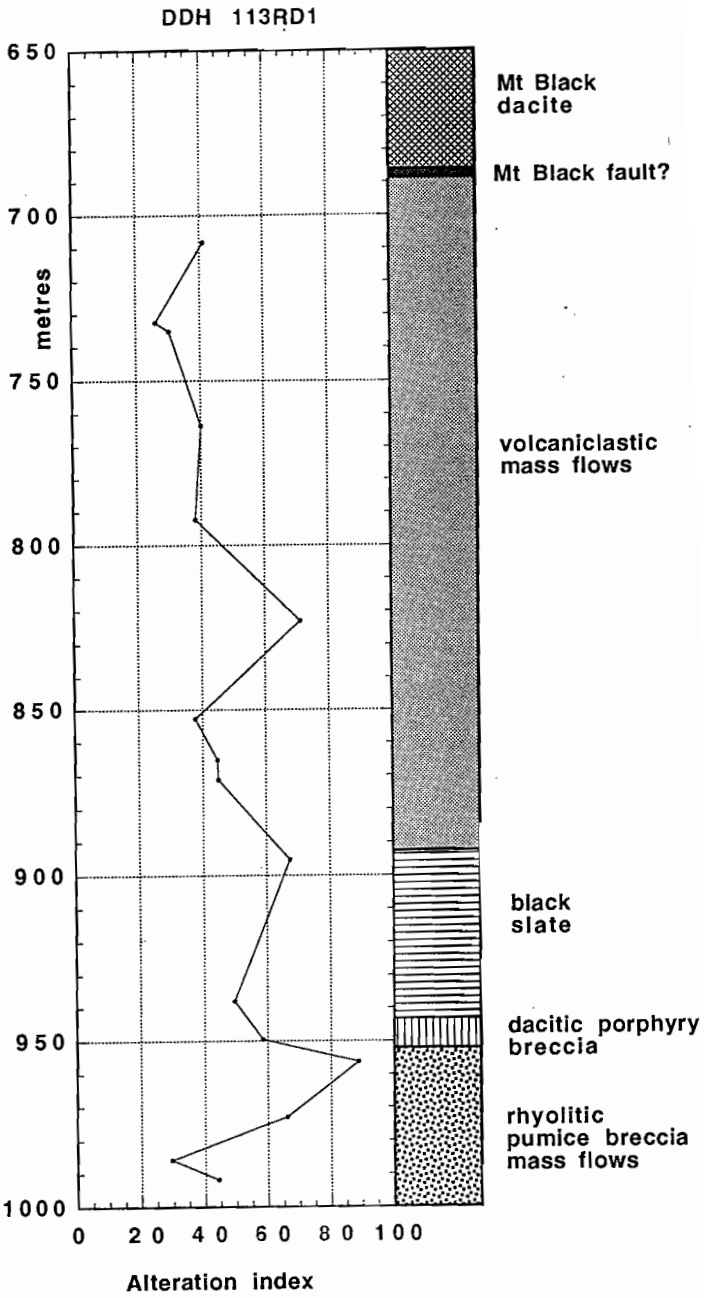
DDH 113RD1
650
700
750
800
850
900
950
1000
metres
0 20 40 60 80 100
Alteration index
Mt Black dacite
Mt Black fault?
volcaniclastic mass flows
black slate
dacitic porphyry breccia
rhyolitic pumice breccia mass flows

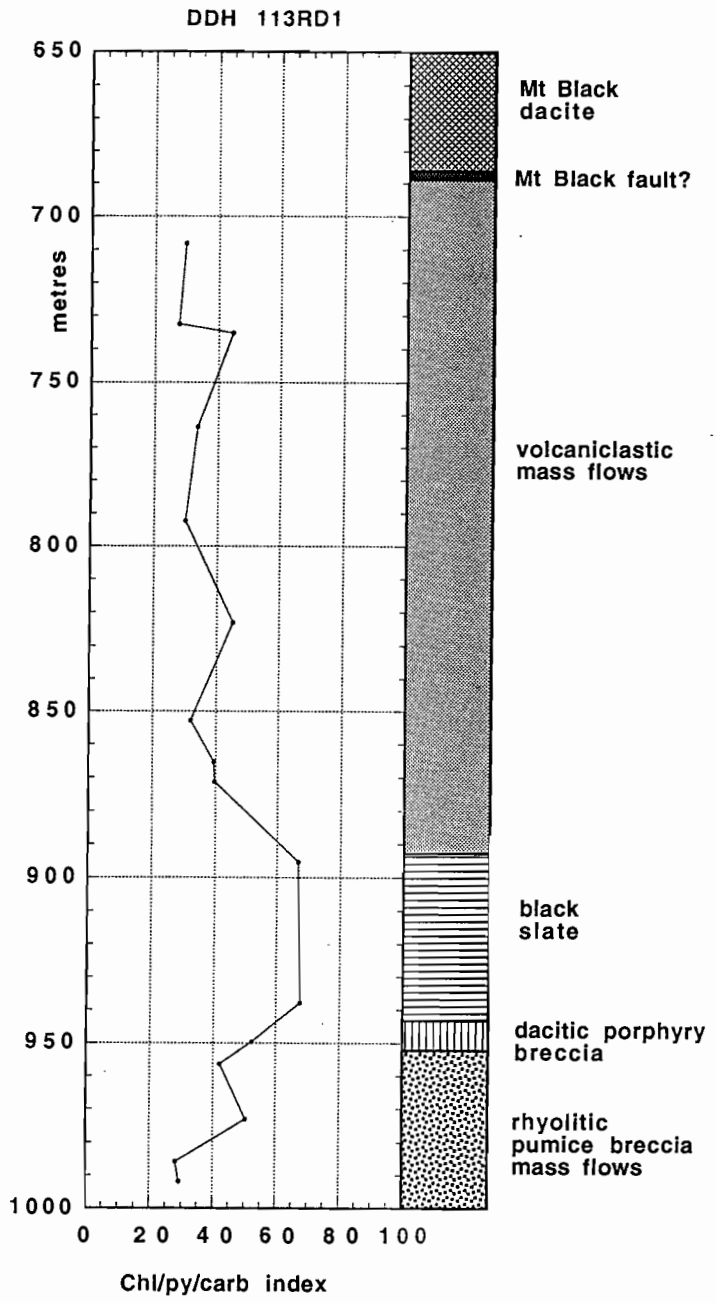
DDH 113RD1
650
700
750
800
850
900
950
1000
metres
0 20 40 60 80 100
Chl/py/carb index
Mt Black dacite
Mt Black fault?
volcaniclastic mass flows
black slate
dacitic porphyry breccia
rhyolitic pumice breccia mass flows

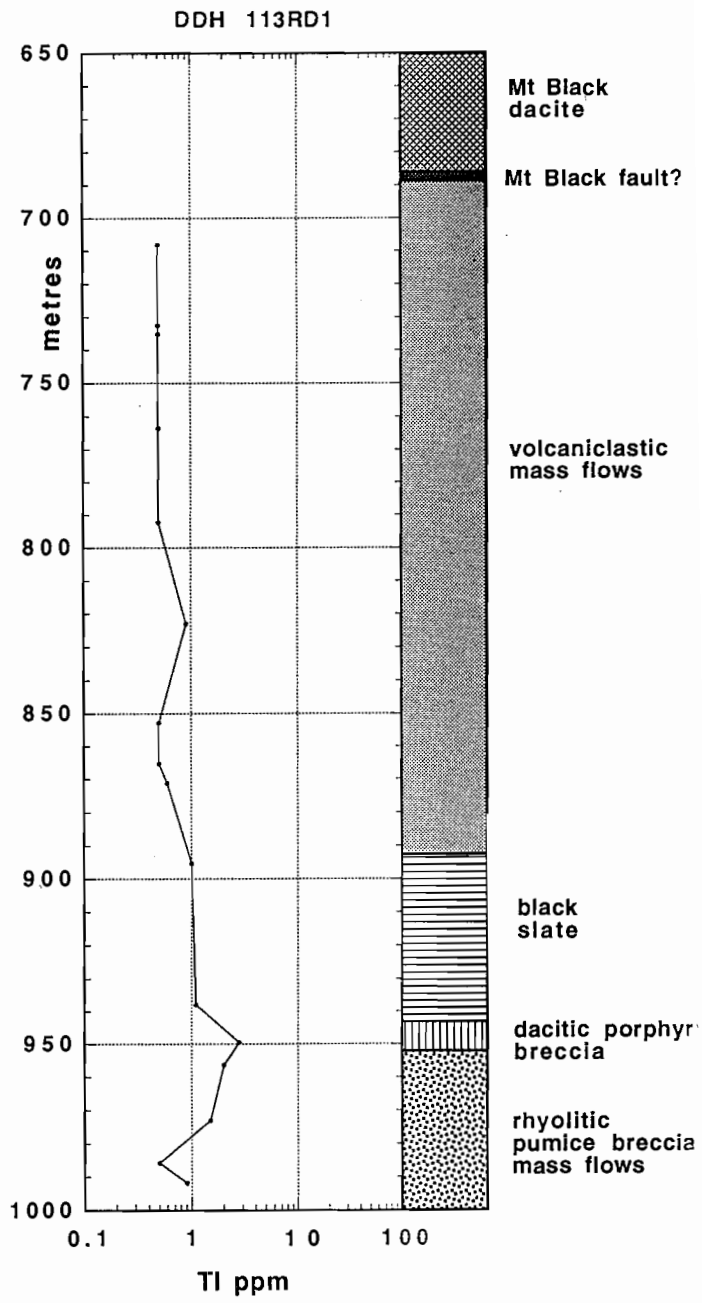
DDH 113RD1
650
700
750
800
850
900
950
1000
metres
0.1 1 10 100
Tl ppm
Mt Black dacite
Mt Black fault?
volcaniclastic mass flows
black slate
dacitic porphyr
breccia
rhyolitic pumice breccia mass flows

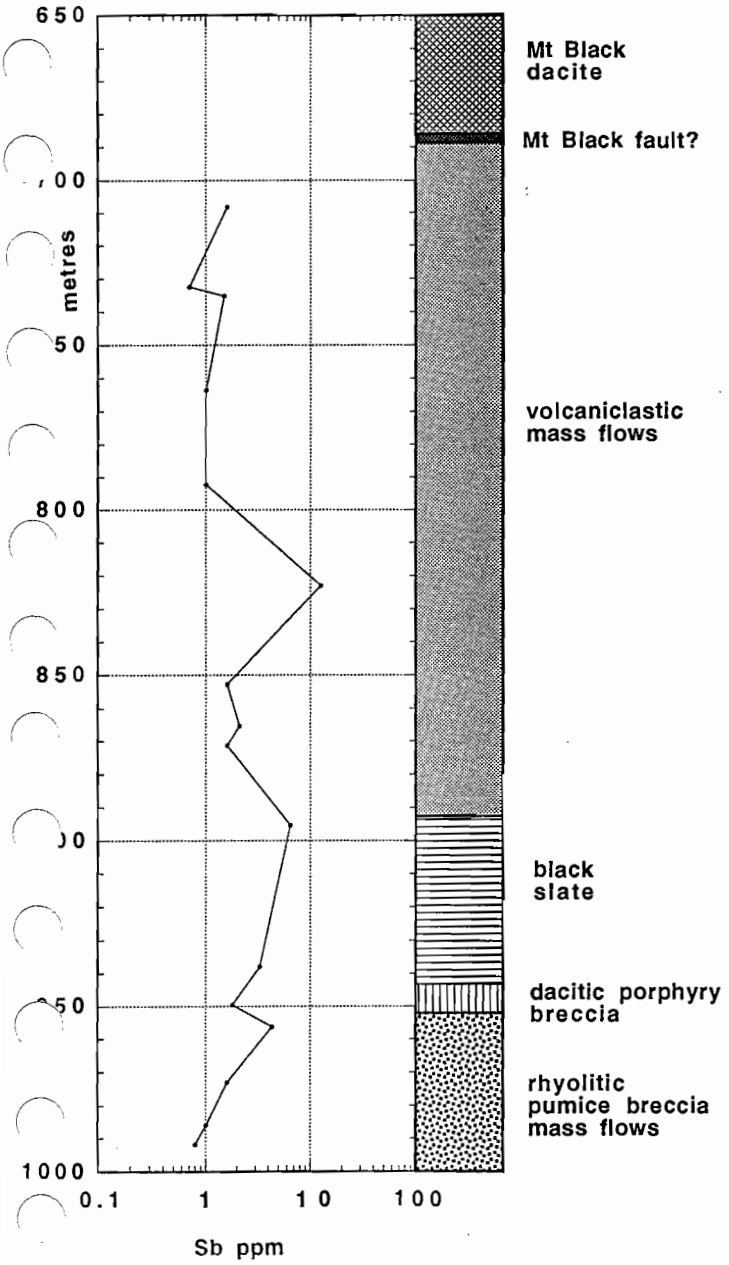
DDH 113RD1
650
700
750
800
850
900
950
1000
metres
0.1
1
10
100
Sb ppm
Mt Black dacite
Mt Black fault?
volcaniclastic mass flows
black slate
dacitic porphyry breccia
rhyolitic pumice breccia mass flows

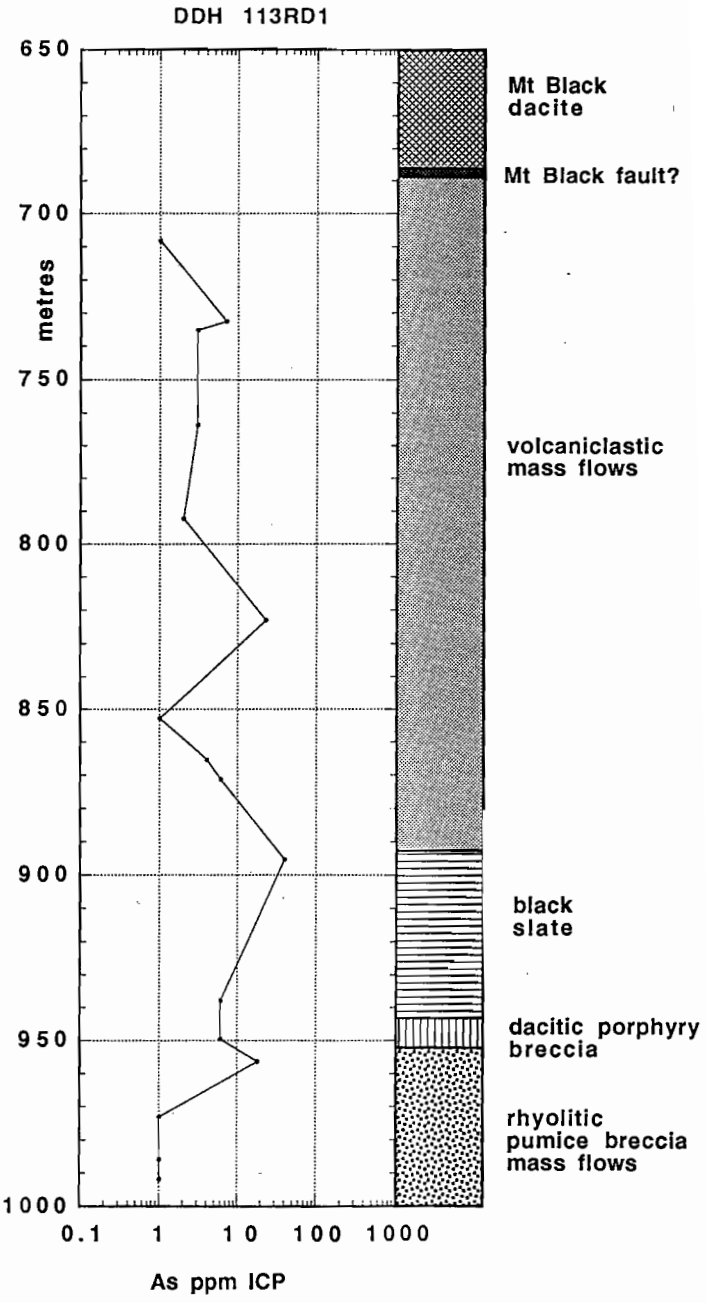
DDH 113RD1
650
700
750
800
850
900
950
1000
metres
0.1
1
10
100
1000
As ppm ICP
Mt Black dacite
Mt Black fault?
volcaniclastic mass flows
black slate
dacitic porphyry breccia
rhyolitic pumice breccia mass flows

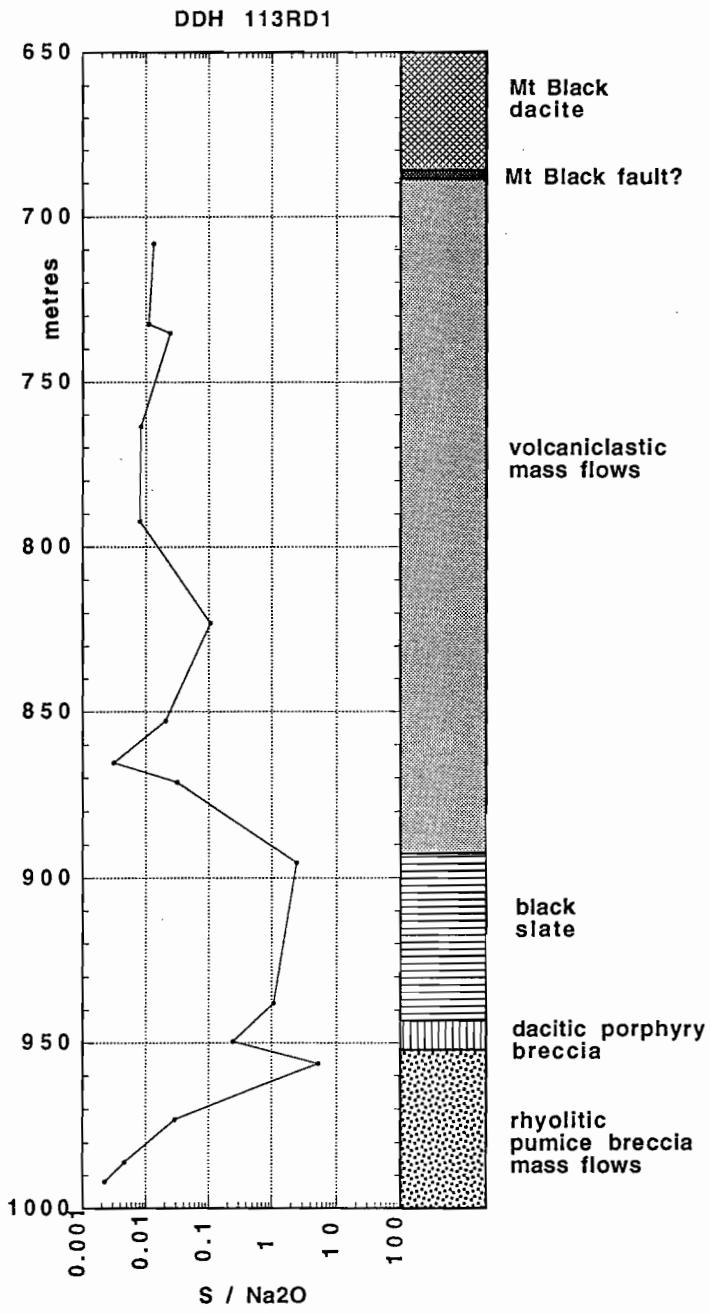
DDH 113RD1
650
700
750
800
850
900
950
1000
metres
0.001
0.01
0.1
1
10
100
S / Na2O
Mt Black dacite
Mt Black fault?
volcaniclastic mass flows
black slate
dacitic porphyry breccia
rhyolitic pumice breccia mass flows

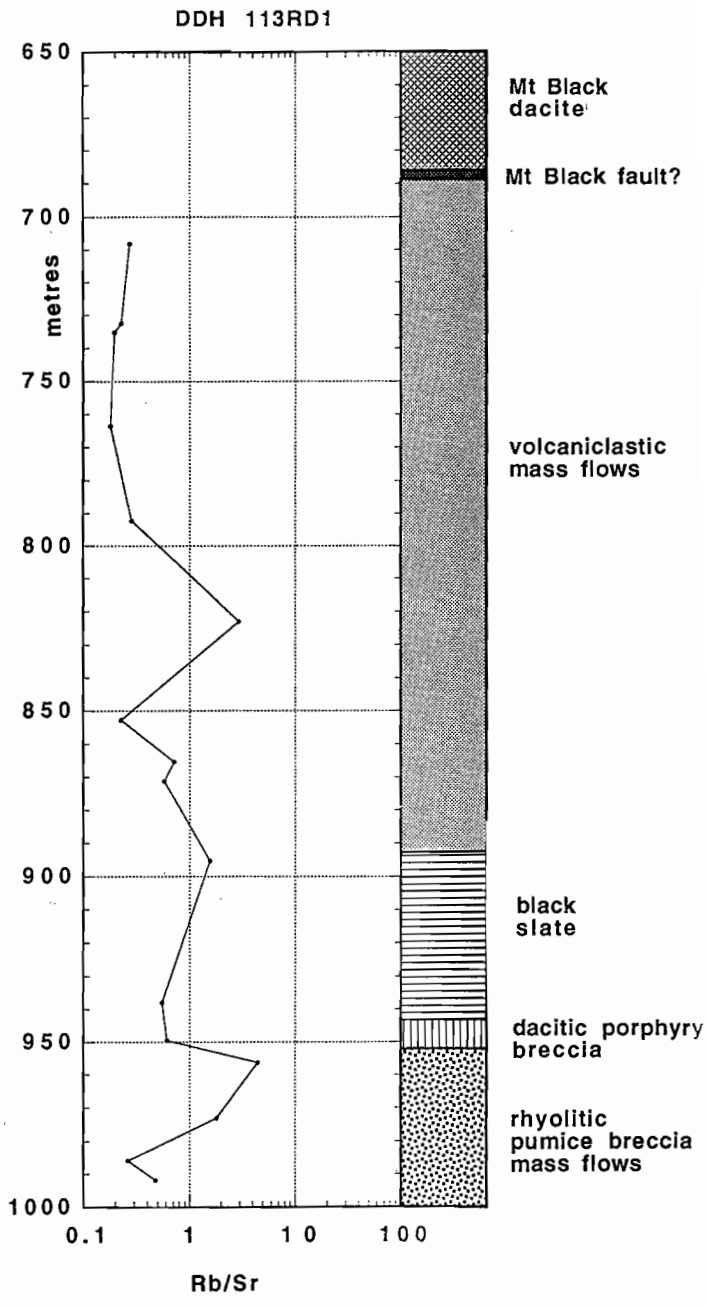
DDH 113RD1
650
700
750
800
850
900
950
1000
metres
0.1
1
10
100
Rb/Sr
Mt Black dacite
Mt Black fault?
volcaniclastic mass flows
black slate
dacitic porphyry breccia
rhyolitic pumice breccia mass flows

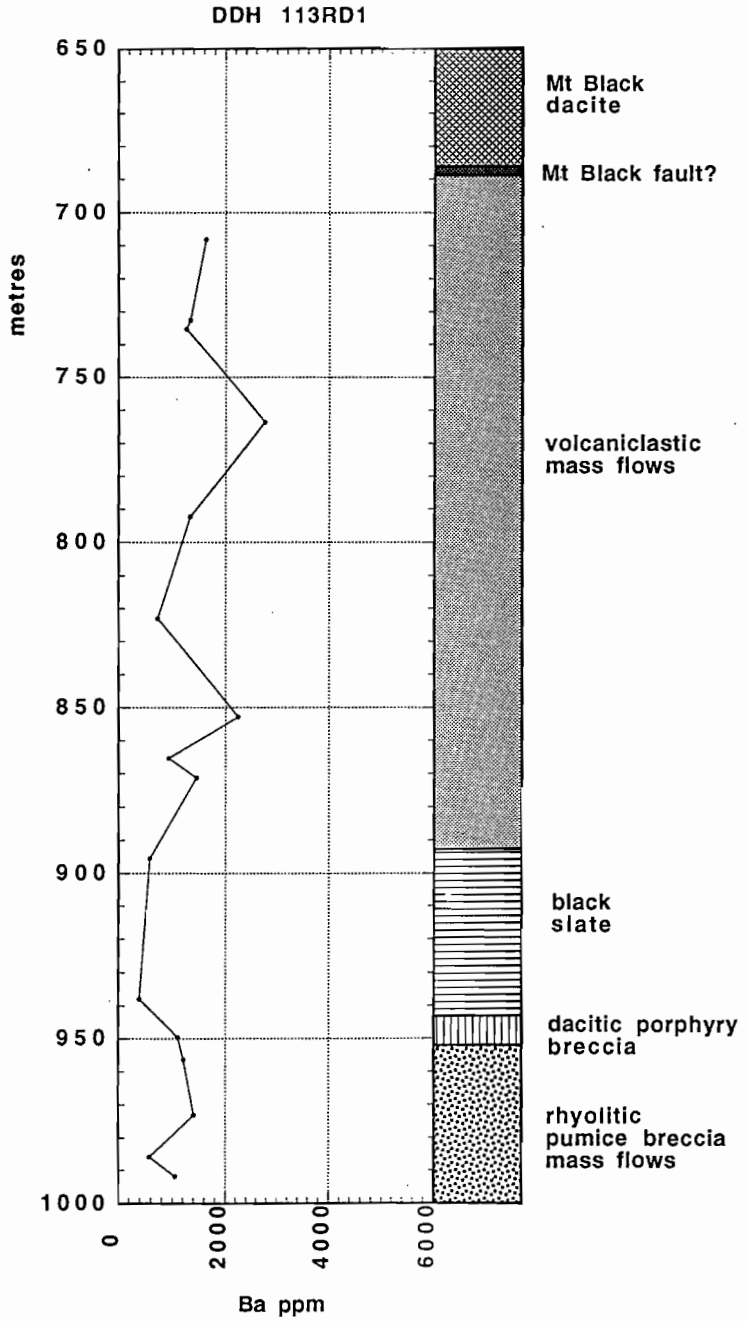
DDH 113RD1
650
700
750
800
850
900
950
1000
metres
0
2000
4000
6000
Ba ppm
Mt Black dacite
Mt Black fault?
volcaniclastic mass flows
black slate
dacitic porphyry breccia
rhyolitic pumice breccia mass flows

Appendix E

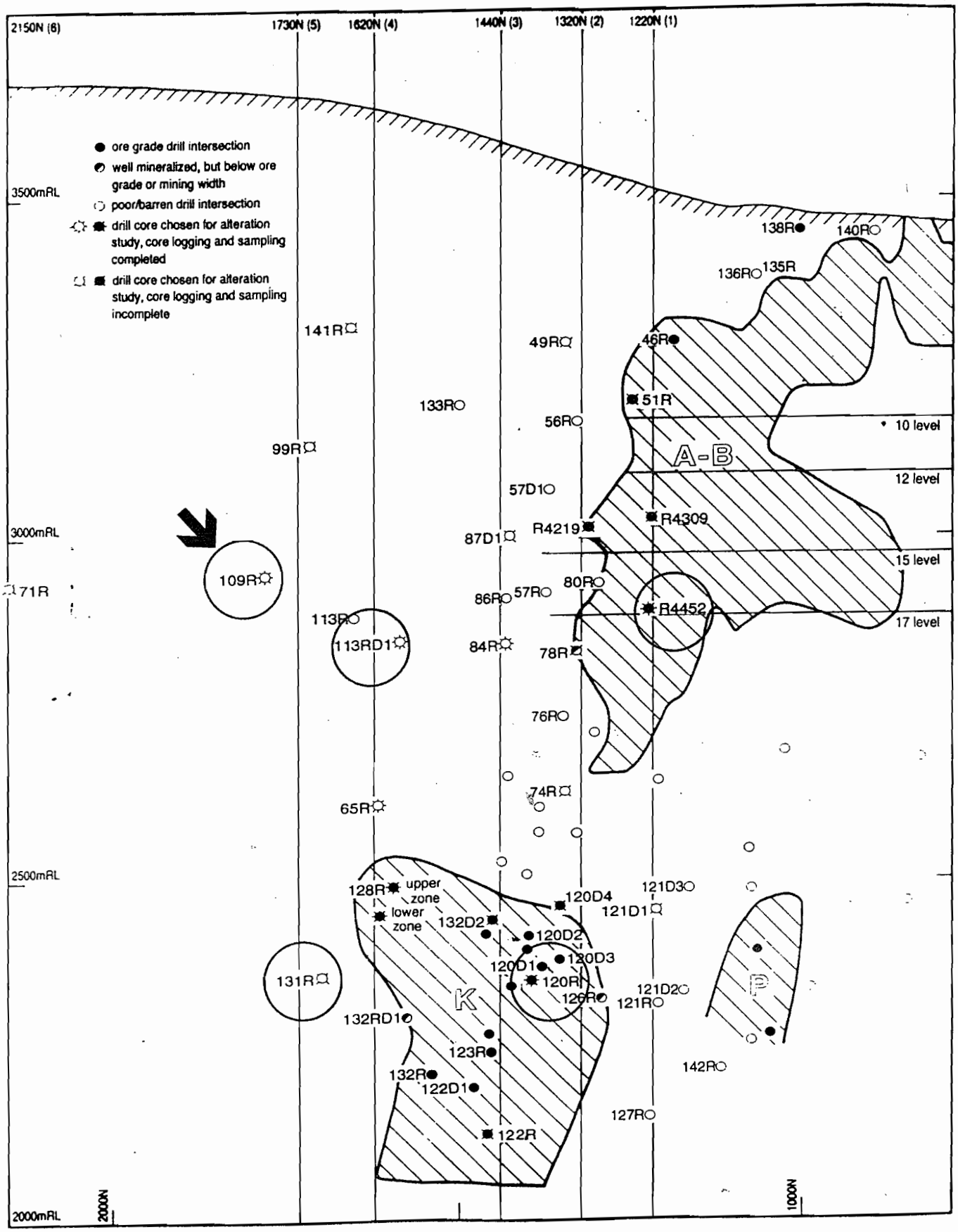

Figure 1: Longitudinal section of the north end of Rosebery mine showing the location of A-B, K and P ore lenses, drill core intersections of the ore stratigraphic position, drill cores selected for this study, and six cross sections designed to compile results (1220 mN, 1320 mN, 1440 mN, 1620 mN, 1730 mN and 2150 mN).

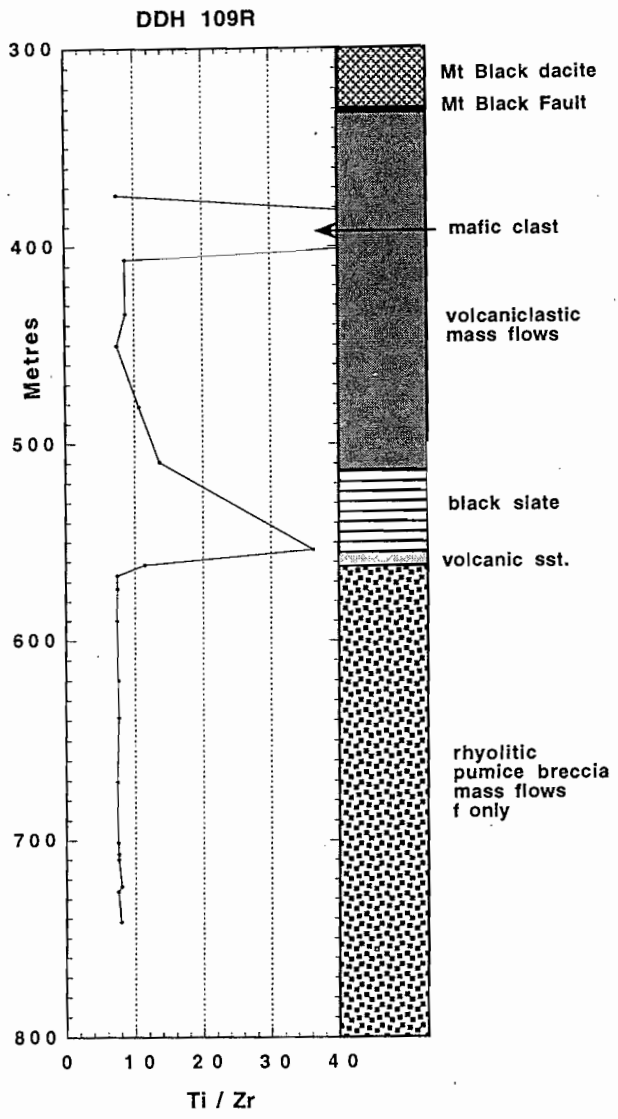
DDH 109R
300
400
500
600
700
800
Metres
0
10
20
30
40
Ti / Zr
Mt Black dacite
Mt Black Fault
mafic clast
volcaniclastic mass flows
black slate
volcanic sst.
rhyolitic pumice breccia mass flows f only

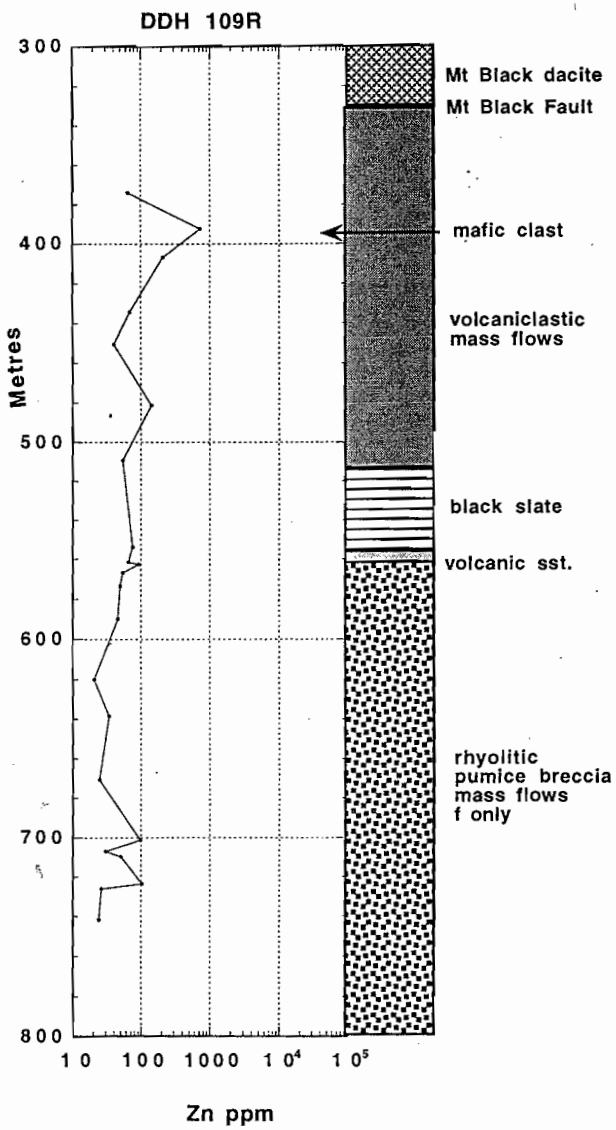
DDH 109R
300
400
500
600
700
800
Metres
10
100
1000
10⁴
10⁵
Zn ppm
Mt Black dacite
Mt Black Fault
mafic clast
volcaniclastic mass flows
black slate
volcanic sst.
rhyolitic pumice breccia mass flows f only

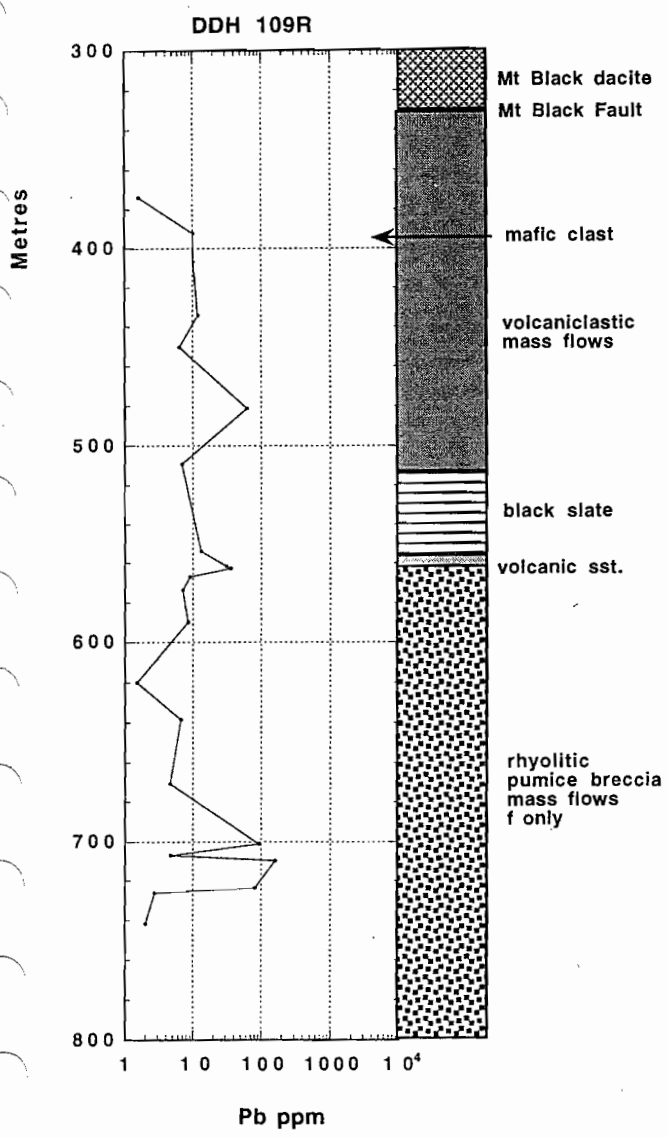
DDH 109R
Metres
300
400
500
600
700
800
1
10
100
1000
10⁴
Pb ppm
Mt Black dacite
Mt Black Fault
mafic clast
volcaniclastic mass flows
black slate
volcanic sst.
rhyolitic pumice breccia mass flows f only

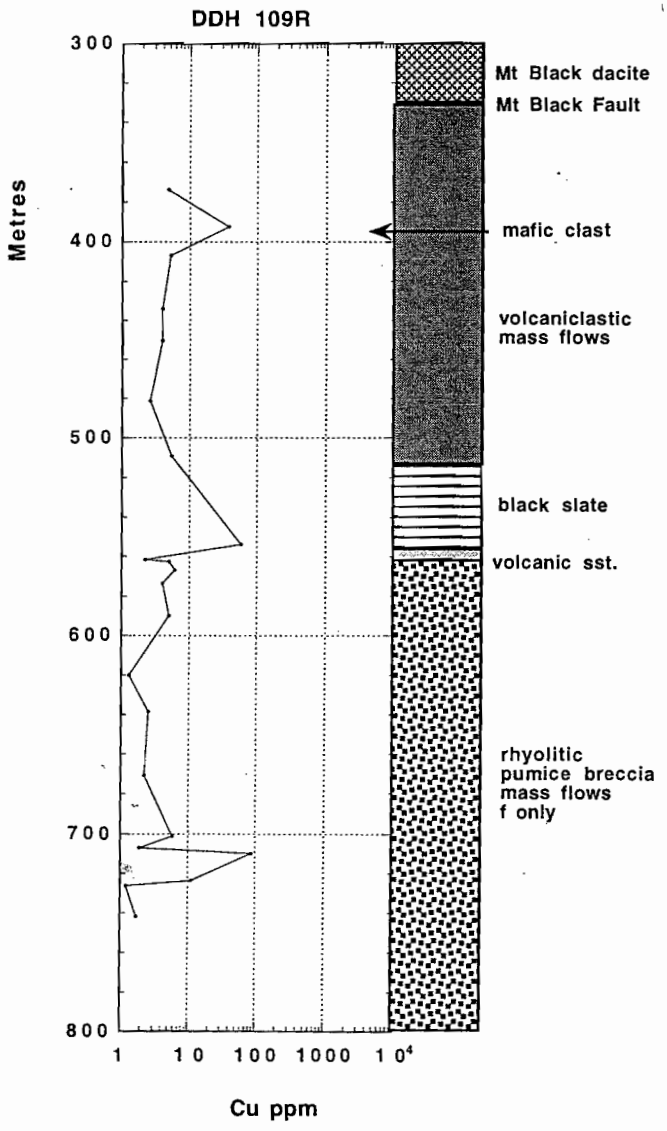
DDH 109R
Metres
300
400
500
600
700
800
1
10
100
1000
10⁴
Cu ppm
Mt Black dacite
Mt Black Fault
mafic clast
volcaniclastic mass flows
black slate
volcanic sst.
rhyolitic pumice breccia mass flows f only

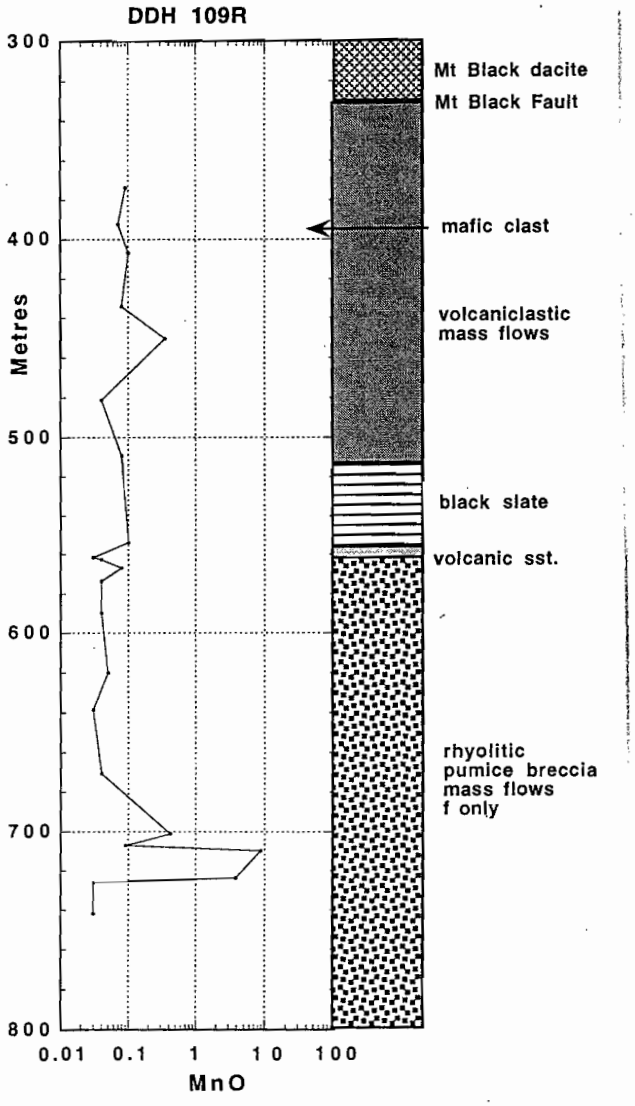
DDH 109R
300
400
500
600
700
800
Metres
0.01
0.1
1
10
100
MnO
Mt Black dacite
Mt Black Fault
mafic clast
volcaniclastic mass flows
black slate
volcanic sst.
rhyolitic pumice breccia mass flows f only

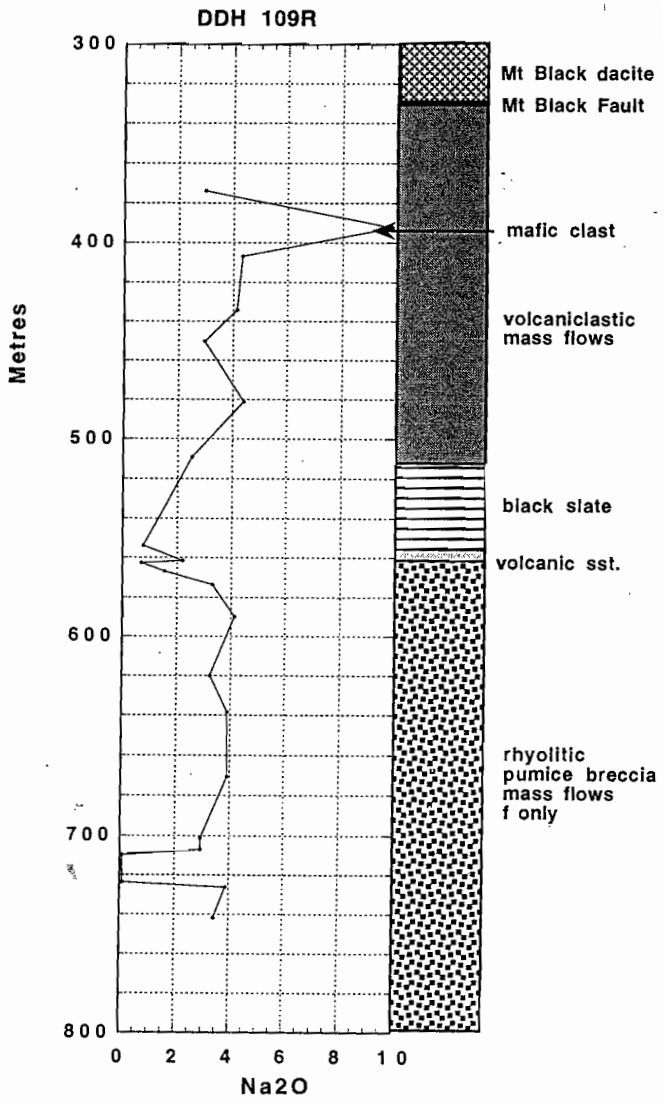
DDH 109R
300
400
500
600
700
800
Metres
0
2
4
6
8
10
Na2O
Mt Black dacite
Mt Black Fault
mafic clast
volcaniclastic mass flows
black slate
volcanic sst.
rhyolitic pumice breccia mass flows f only

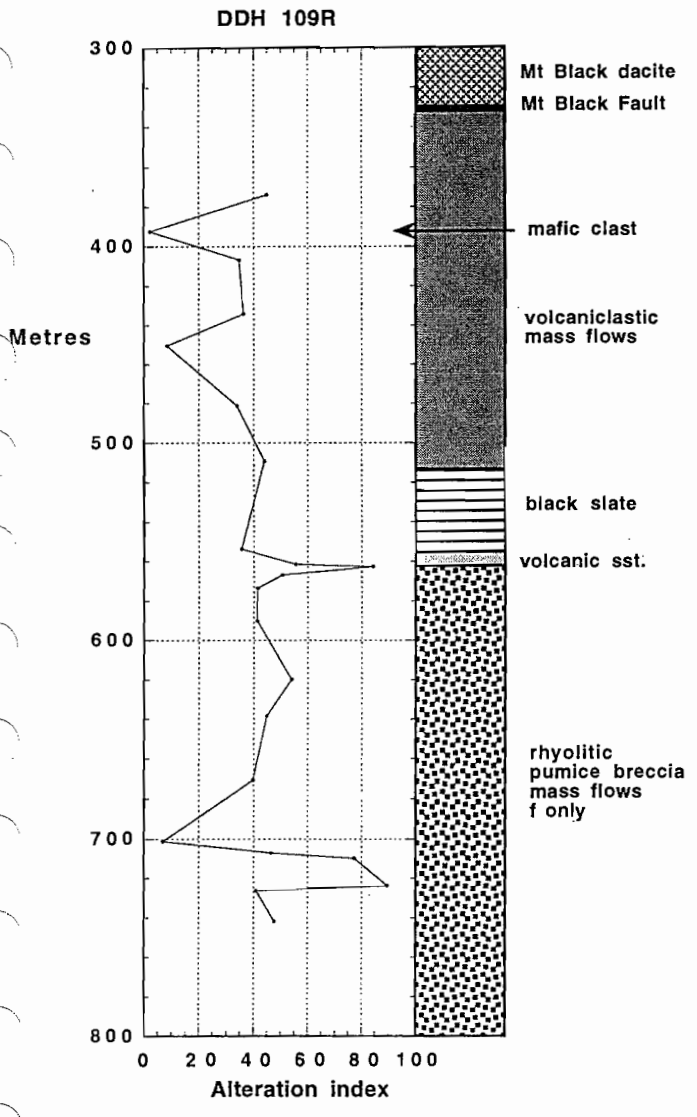
DDH 109R
300
400
500
600
700
800
Metres
0 20 40 60 80 100
Alteration index
Mt Black dacite
Mt Black Fault
mafic clast
volcaniclastic mass flows
black slate
volcanic sst.
rhyolitic pumice breccia mass flows f only

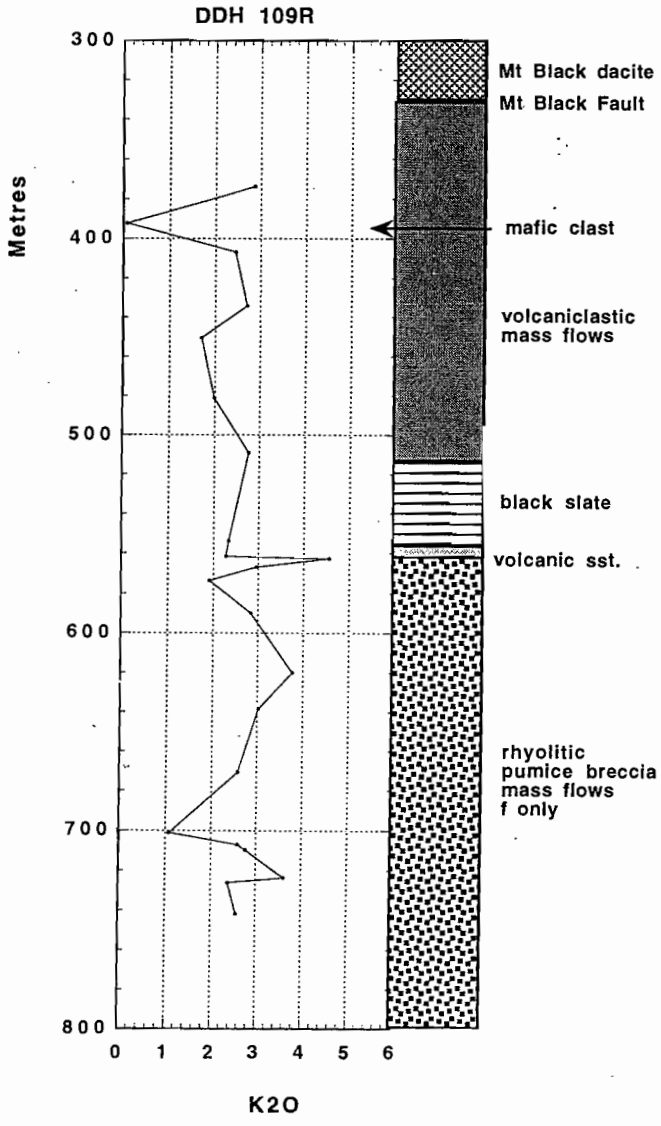
DDH 109R
300
400
500
600
700
800
Metres
0 1 2 3 4 5 6
K2O
Mt Black dacite
Mt Black Fault
mafic clast
volcaniclastic mass flows
black slate
volcanic sst.
rhyolitic pumice breccia mass flows f only

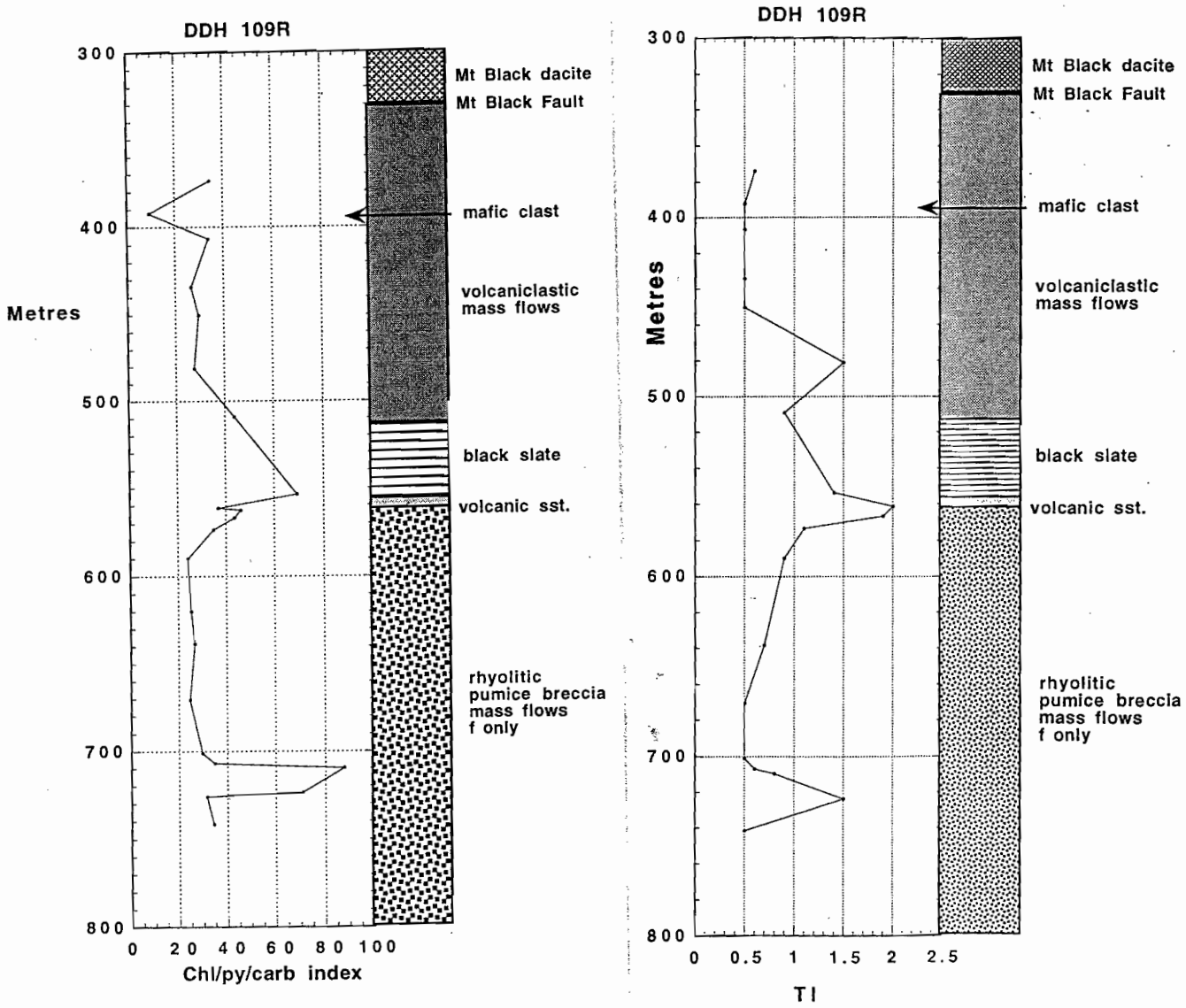
DDH 109R
Metres
300
400
500
600
700
800
0 20 40 60 80 100
Chl/py/carb index
Mt Black dacite
Mt Black Fault
mafic clast
volcaniclastic mass flows
black slate
volcanic sst.
rhyolitic pumice breccia mass flows f only
DDH 109R
Metres
0 0.5 1 1.5 2 2.5
TI
Mt Black dacite
Mt Black Fault
mafic clast
volcaniclastic mass flows
black slate
volcanic sst.
rhyolitic pumice breccia mass flows f only

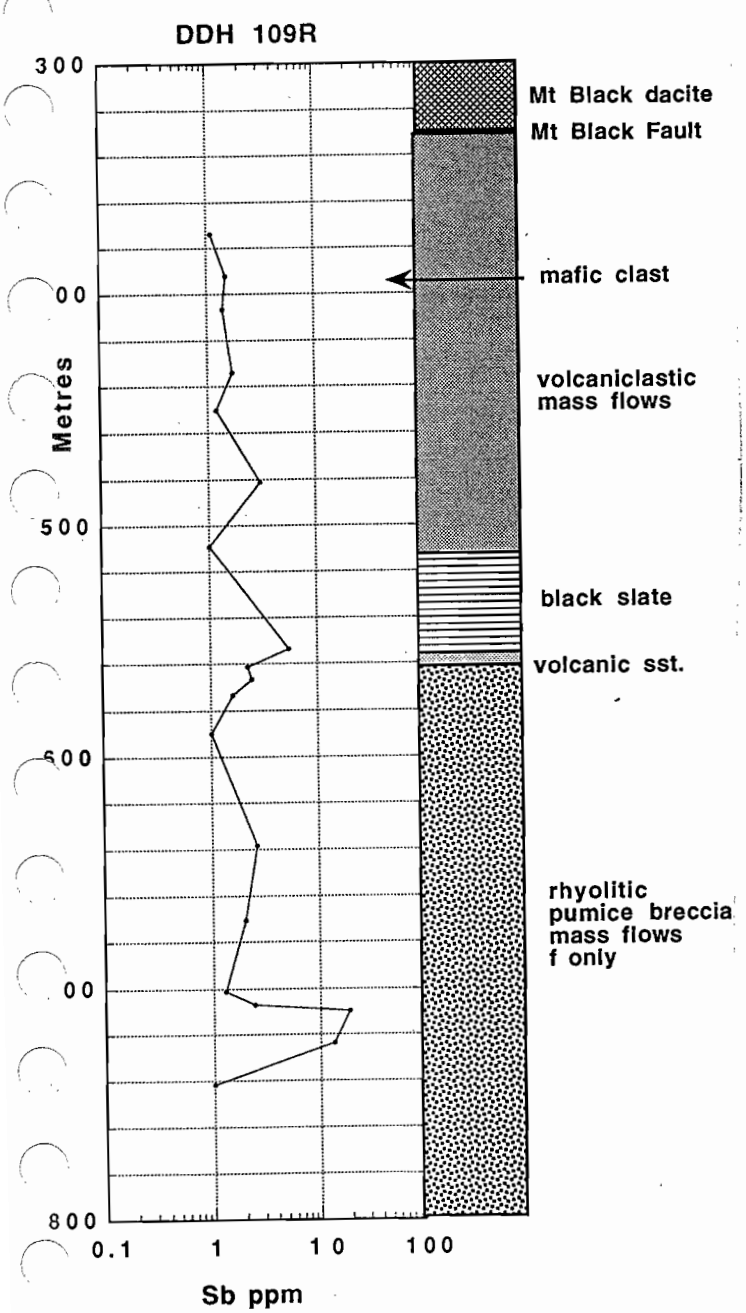
DDH 109R
300
00
500
600
00
800
Metres
0.1
1
10
100
Sb ppm
Mt Black dacite
Mt Black Fault
mafic clast
volcaniclastic mass flows
black slate
volcanic sst.
rhyolitic pumice breccia mass flows f only

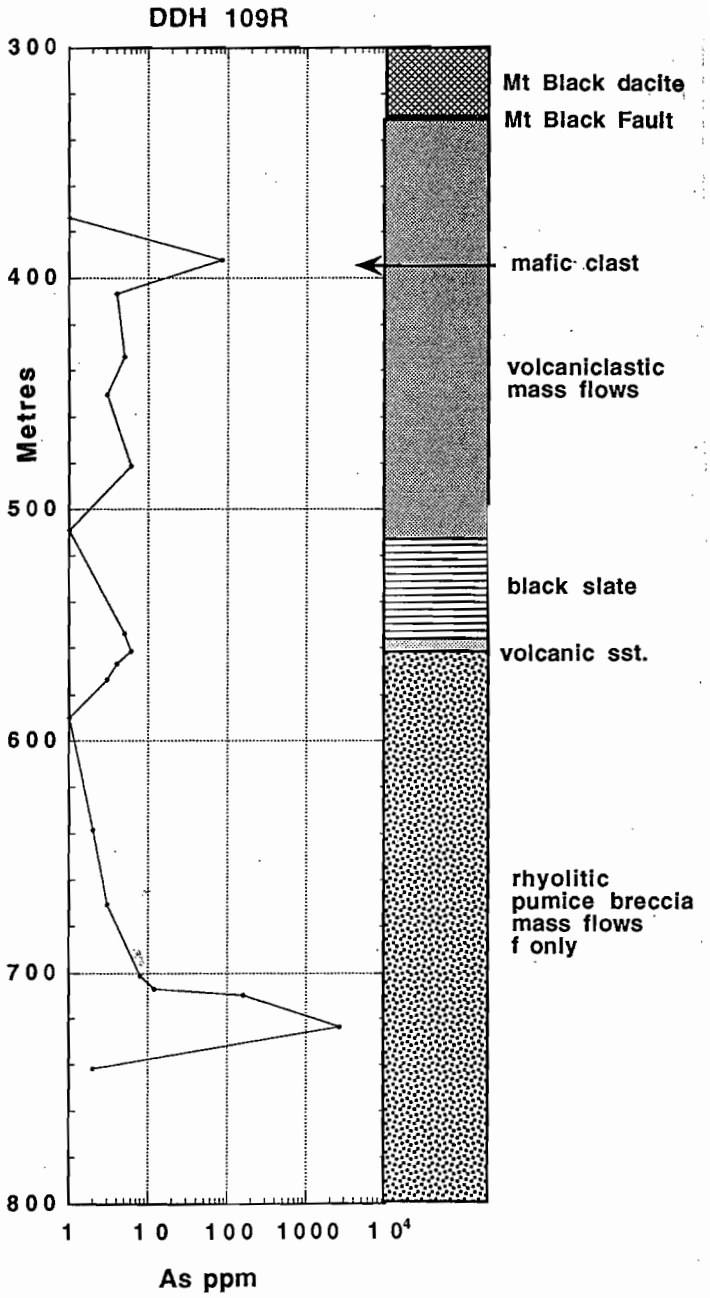
DDH 109R
300
400
500
600
700
800
Metres
1
10
100
1000
10⁴
As ppm
Mt Black dacite
Mt Black Fault
mafic clast
volcaniclastic mass flows
black slate
volcanic sst.
rhyolitic pumice breccia mass flows f only

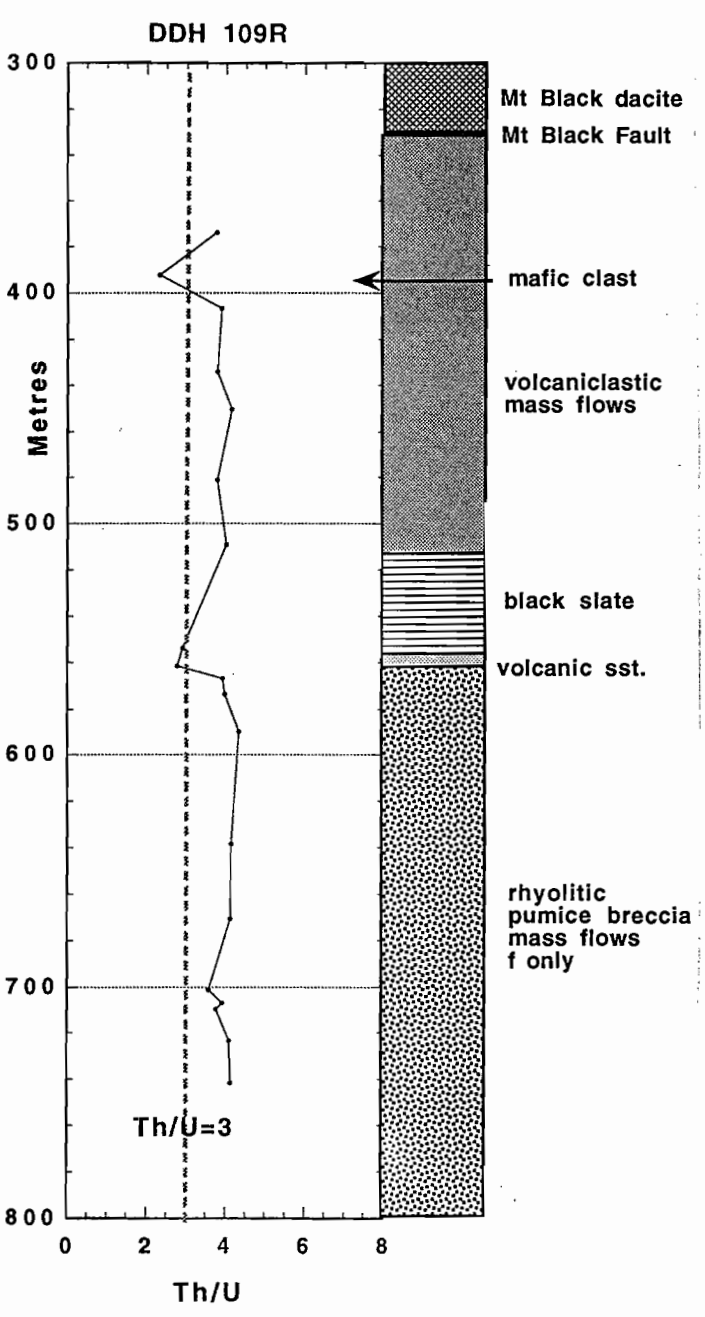
DDH 109R
300
400
500
600
700
800
Metres
Th/U=3
0
2
4
6
8
Th/U
Mt Black dacite
Mt Black Fault
mafic clast
volcaniclastic mass flows
black slate
volcanic sst.
rhyolitic pumice breccia mass flows f only

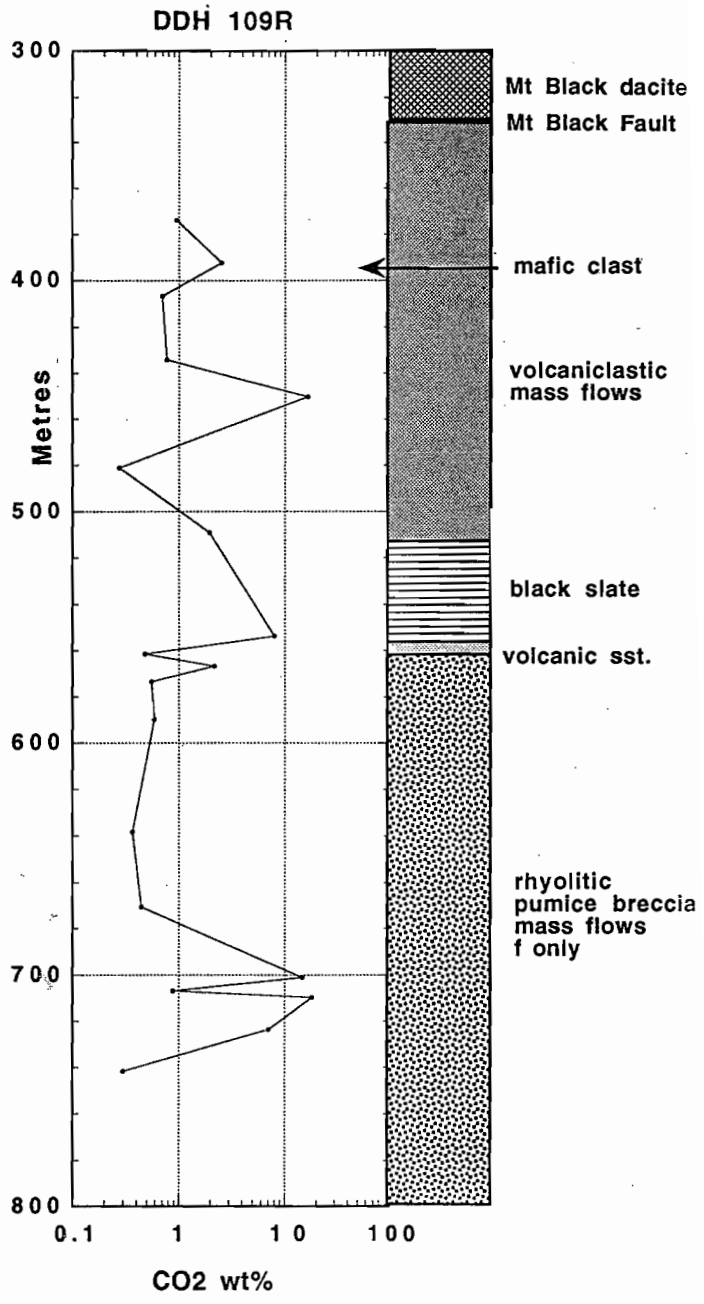
DDH 109R
300
400
500
600
700
800
Metres
0.1
1
10
100
CO2 wt%
Mt Black dacite
Mt Black Fault
mafic clast
volcaniclastic mass flows
black slate
volcanic sst.
rhyolitic pumice breccia mass flows f only

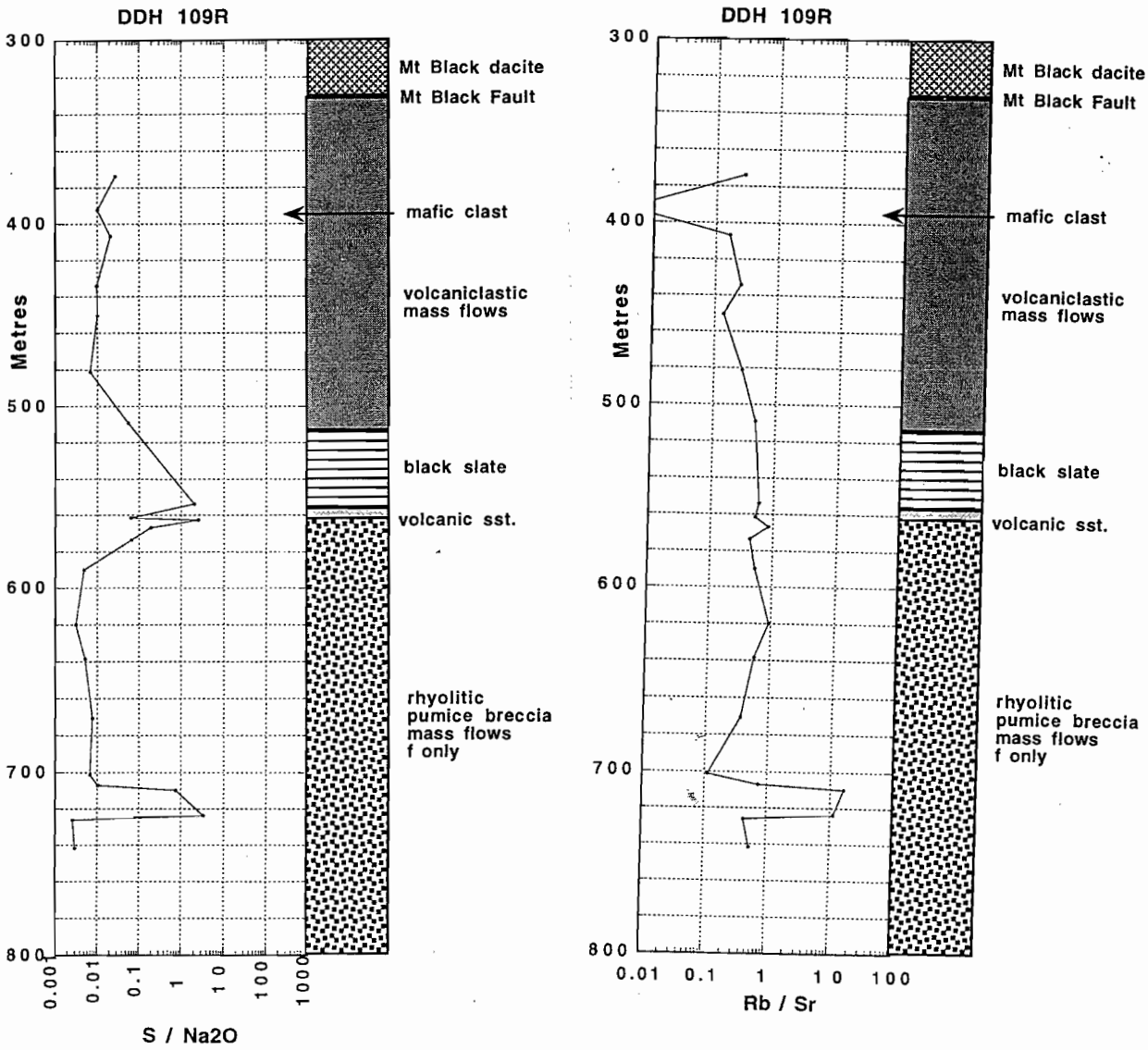
DDH 109R
300
400
500
600
700
800
Metres
0.001
0.01
0.1
1
10
100
1000
S / Na2O
Mt Black dacite
Mt Black Fault
mafic clast
volcaniclastic mass flows
black slate
volcanic sst.
rhyolitic pumice breccia mass flows f only
DDH 109R
300
400
500
600
700
800
Metres
0.01
0.1
1
10
100
Rb / Sr
Mt Black dacite
Mt Black Fault
mafic clast
volcaniclastic mass flows
black slate
volcanic sst.
rhyolitic pumice breccia mass flows f only

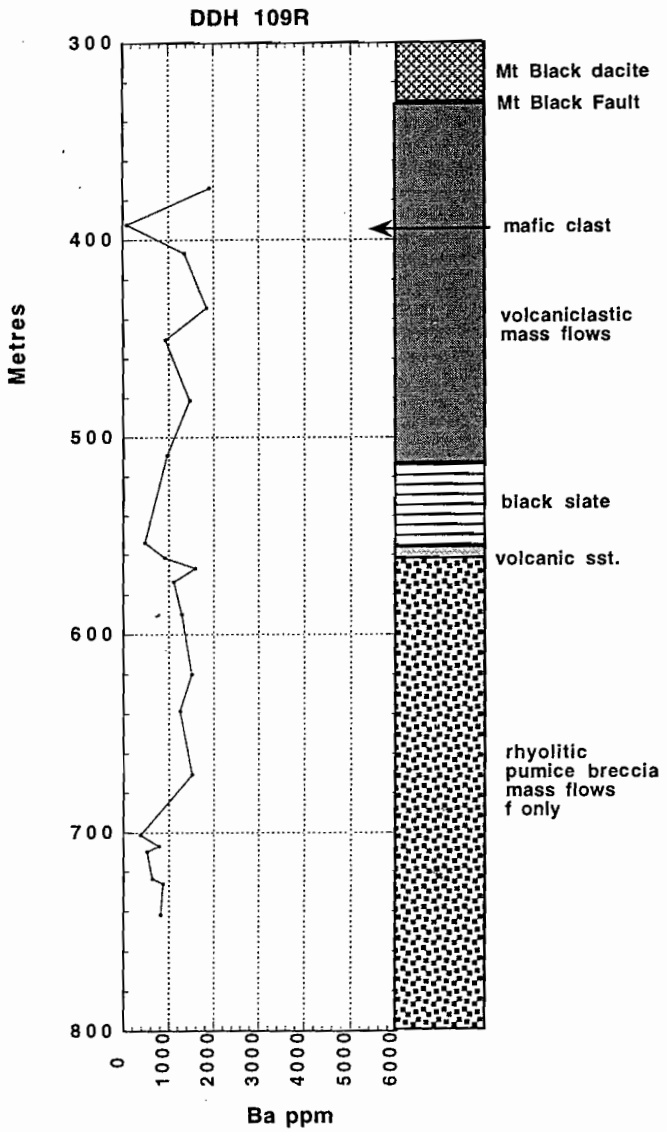
DDH 109R
300
400
500
600
700
800
Metres
0
1000
2000
3000
4000
5000
6000
Ba ppm
Mt Black dacite
Mt Black Fault
mafic clast
volcaniclastic mass flows
black slate
volcanic sst.
rhyolitic pumice breccia mass flows f only

Appendix F

	DDH/metres	SiO2	TiO2	Al2O3	Fe2O3	FeO tot	MnO	MgO	CaO	Na2O	K2O	P2O5	S	Y	Rb
0	120R-1050	74.80	0.38	11.27	4.2	3.8	0.09	1.18	1.02	2.34	1.98	0.08	0.01	25.8	76.5
1	120R-1053	64.00	0.32	12.93	7.8	7.1	2.2	1.18	0.52	0.1	3.97	0.07	0.12	37.5	197.1
2	120R-1055	73.10	0.31	13.56	2.5	2.3	0.05	0.88	1.25	3.2	2.52	0.05	0.01	26.3	94.4
3	120R-1057	72.10	0.31	12.88	2.1	1.9	0.17	0.59	1.84	3.79	2.19	0.04	0.02	33.9	82.9
4	120R-1068	73.00	0.3	12.85	3.3	3	0.2	0.79	0.63	2.72	2.84	0.04	0.06	28.5	108.9
5	120R-1083	69.50	0.41	14.89	2.8	2.5	0.08	0.77	1.5	3.27	3.41	0.06	0.39	48.5	115.4
6	120R-1094	68.80	0.38	15.61	2.8	2.6	0.08	0.84	1.44	3.85	3.86	0.06	0.12	42.1	120.5
7	120R-1100	44.90	0.31	11.63	2	1.8	0.4	0.59	18.58	3.3	2.24	0.05	0.09	41.4	62.3
8	120R-1115	74.30	0.29	13.15	2.3	2.1	0.06	0.55	0.83	3.64	2.61	0.03	0.04	36.8	86.9
9	120R-1133	73.90	0.29	13.23	2.5	2.3	0.08	0.6	1.29	2.77	3.12	0.04	0.01	37.6	102.6
10	120R-1147	68.70	0.4	14.82	3.2	2.9	0.14	0.84	2.63	2.23	3.11	0.08	0.02	34.1	107.5
11	120R-1169	69.30	0.37	14.28	2.8	2.5	0.1	0.79	2.7	2.96	2.68	0.07	0.02	28.2	89.6
12	120R-1184dupl.	63.80	0.8	12.2	7.4	6.7	0.09	2.02	4.25	0.57	2.89	0.15	2.06	25.2	110.5
13	120R-1205	63.00	0.8	11.92	6.1	5.5	0.06	3.01	4.19	0.62	2.31	0.22	1.28	25.5	99.3
14	120R-1229dupl.	58.50	0.7	11.06	4.9	4.5	0.26	2.54	8.01	0.2	2.39	0.12	1.27	27.2	125
15	120R-1241	61.70	0.64	17.22	5.6	5	0.04	2.09	1.87	2.21	2.09	0.14	1.97	33.1	100.1
16	120R-1256dupl.	66.30	0.56	10.72	4.8	4.3	0.09	2.6	4.61	0.66	1.8	0.1	1.32	26.9	75.1
17	120R-1265dupl.	50.80	0.55	16.03	3.2	2.9	0.11	1.13	13.2	3.5	0.93	0.11	0.15	24.3	35.4
18	120R-1271	61.70	0.68	18.83	4.9	4.5	0.08	2.51	4.98	1.73	1.07	0.14	0.4	34.7	42.4
19	120R-1276	55.70	0.45	19.96	3.9	3.5	0.05	2.03	6.89	3.67	0.98	0.15	1.71	31.3	38.8
20	120R-1283	62.70	0.53	16.49	4.2	3.8	0.09	2.71	3.68	1.58	1.74	0.13	0.76	34.5	68.4
21	120R-1288	60.50	0.7	19.36	3.3	3	0.05	3.38	1.92	0.87	4.16	0.13	1.08	52.3	142.8
22	120R-1291	59.10	0.63	21.85	2.2	1.9	0.04	2.8	2.81	1.71	4.33	0.18	0.52	43.7	149
23	120R-1303	75.00	0.36	12.86	1.6	1.5	0.04	0.34	0.74	2.43	4.17	0.1	0.01	22.7	105.9
24	120R-1315	68.60	0.47	15.89	2.9	2.6	0.07	0.61	0.6	3.9	4.69	0.13	0.01	21.2	127.2
25	120R-1326	77.70	0.33	11.53	1	0.9	0.05	0.24	0.76	3.08	3.61	0.09	0.01	27.8	78.4
26	120R-1340	65.00	0.54	18.38	2.9	2.6	0.05	0.72	0.43	4.19	5.47	0.14	0.05	25.2	150.6
27	120R-1353	72.20	0.43	14.21	0.7	0.7	0.16	0.41	1.83	4.2	2.44	0.12	0.17	20.9	87.7
28	120R-1355	62.80	0.45	17.43	1.8	1.6	0.65	1.15	2.16	1.01	5.52	0.12	0.55	28	237.6
29	120R-1356dupl.	18.00	0.35	9.31	12.9	11.6	9.96	2.44	14.33	0.1	3.46	0.1	8.06	0	149.8
30	120R-1361ABdupl.	25.60	0.59	15.57	5.7	5.1	20.02	2.48	3.22	0.1	5.31	0.08	1.85	40.6	246.9
31	120R-1364ABdupl.	16.80	0.39	10.73	7.5	6.8	29.36	1.97	2.04	0.1	3.64	0.13	3.24	20.4	182.9
32	120R-1365ABdupl.	18.40	0.38	11.86	5.1	4.6	11.84	5.91	14.98	0.1	4.04	0.14	1.29	26	205
33	120R-1373dupl.	44.20	0.33	14.48	16.6	14.9	1.49	2.22	0.1	0.1	3.37	0.06	7.18	35.4	174.2
34	120R-1378	75.80	0.27	11.26	4.4	3.9	0.28	0.9	0.06	0.07	3.47	0.04	0.89	36.6	177

	Bi	DDH/metres	Th	Pb ppm	As ppm	Zn ppm	Cu ppm	Ni ppm	Nb ppm	Zr ppm	Sr ppm	Cr ppm	Ba ppm
0	2	120R-1050	15.4	2.4	3	51.4	3.3	3.3	10.8	195.5	125.6	4.6	743.3
1	2	120R-1053	17.2	44.4	51	848.9	117.3	2.9	11.8	221	24.4	10.5	1780.7
2	2	120R-1055	20.3	1.5	3	41.2	2.1	1.9	12.8	245.8	143	2.4	2077.5
3	2	120R-1057	17.8	8.7	3	65.5	4.4	2.1	11.7	227	174.9	5.5	1587.7
4	2	120R-1068	12.7	18.3	13	117.2	11.6	2.9	11.2	235.1	132.8	2.6	1144.7
5	2	120R-1083	17	515.3	15	846.2	41.6	3.1	15.4	283.9	224.2	3.9	2369.3
6	2	120R-1094	20	107.2	8	303.6	12	3.1	13.2	258.5	374	9.4	1967.3
7	2	120R-1100	7.2	7.4	3	101.3	12.3	2.9	10	193.6	610	3.5	2296.7
8	2	120R-1115	17.5	13	5	51.6	10.4	1.5	11.2	216.8	284.6	2.4	1748.4
9	2	120R-1133	19.3	15	3	64	2.7	2.1	12	219.6	245.7	1.9	2112.7
10	2	120R-1147	13	62.9	3	129.9	5	1.9	9.6	208.7	263	2.9	1629.5
11	2	120R-1169	12.9	3.7	3	50.3	3.5	2.7	9.5	183.3	177.8	2.9	1110.1
12	2	120R-1184dupl.	18.8	17.6	15	97.9	77.4	47.2	13	134.8	123.3	152.1	566.8
13	2	120R-1205	9.7	10	8	88.1	50.1	35.5	13.1	138.3	149.2	150.7	432.7
14	2	120R-1229dupl.	10.9	195.3	45	282.2	47.4	71.8	11	118.7	169	134.7	548.7
15	2	120R-1241	16.8	9.5	7	150.9	9.8	3.2	13	269.8	399.6	9.4	1109.6
16	2	120R-1256dupl.	11.7	16.6	3	81	45.9	34.3	12.4	119.6	93.2	104.7	715.7
17	2	120R-1265dupl.	8.7	3.7	3	59.5	9.3	11.6	7.9	113.8	439.6	100	450.9
18	2	120R-1271	17.2	4.2	3	93.4	9.6	16.6	13	260.4	412.2	37.3	609.5
19	2	120R-1276	6.5	54.9	62	194.4	13.3	14.1	9.2	129.2	607.8	23.1	520.8
20	2	120R-1283	15.1	14.3	16	74.1	20.1	6.9	11.3	233.8	422.9	40.7	837.3
21	2	120R-1288	28.8	18.1	266	164	20.4	16	17.9	346.1	166.7	36.6	1103.6
22	2	120R-1291	30.1	12.9	12	77.7	20.9	2.4	15.7	275.6	301.8	8	1161.6
23	2	120R-1303	18	4.3	3	102.4	9.9	0.9	10.2	170.1	181	3.8	2069.9
24	2	120R-1315	19.3	3.1	3	38.8	8.7	2	12.3	211.4	219.5	4.7	1937.2
25	2	120R-1326	15.8	3.8	7	17.8	3.5	1	8.5	151.6	211.2	4.1	1573.2
26	2	120R-1340	26.4	2.8	8	46.7	11.2	2.1	13.6	238.1	200.6	6.3	2668.6
27	2	120R-1353	7.7	67.6	107	100.1	14.9	1.5	11.1	191	198.8	3.7	2290.4
28	2	120R-1355	18.1	272.1	28	6486.9	23.6	4.8	11	208.8	129.7	5.9	5060.9
29	2	120R-1356dupl.	0	13800	112	10900	668.4	1.7	5.9	163.8	243.7	1.8	3392
30	2	120R-1361ABdupl.	10.5	213.4	14	313.5	13	1	15.5	286.9	53.8	1	5285
31	2	120R-1364ABdupl.	18.6	673.7	52	994.7	19.8	2.1	7.2	141.8	27.1	0.8	4297
32	2	120R-1365ABdupl.	11	138	24	727	8	2	7.8	165.8	121.9	0.5	4236
33	12	120R-1373dupl.	22.5	604	16	68200	1677.8	1	12	246.7	13.9	3.7	946
34	2	120R-1378	28.5	8	7	91.7	10.8	1	12.6	204.8	9.6	2.5	879.7

	Mo ppm	Cd ppm	Sb ppm	Cs ppm	Tl ppm	Th ppm	U ppm	toal carbon %	CO2 wt%	DDH/metres
0	2.20	0.30	1.10	2.37	0.50	17.30	4.38	0.18	0.66	120R-1050
1	5.30	2.80	6.90	8.25	1.20	19.90	5.33	1.14	4.18	120R-1053
2	1.20	0.30	2.00	2.50	0.50	21.70	5.17	0.25	0.92	120R-1055
3	1.80	0.40	2.80	2.21	0.50	17.60	4.87	0.61	2.24	120R-1057
4	2.40	1.10	4.30	3.62	0.50	17.90	4.52	0.53	1.95	120R-1068
5	7.10	3.20	2.60	2.60	0.70	20.30	5.88	0.22	0.81	120R-1083
6	2.90	1.20	1.50	3.49	0.80	18.20	4.90	0.19	0.70	120R-1094
7	0.70	0.50	0.90	1.32	0.50	14.50	4.46	3.72	13.65	120R-1100
8	3.20	0.40	2.40	2.03	0.50	20.20	5.03	0.08	0.30	120R-1115
9	1.70	0.40	1.70	2.41	0.60	20.60	5.30	0.19	0.70	120R-1133
10	1.00	0.60	2.20	2.81	0.70	14.20	3.91	0.39	1.43	120R-1147
11	0.70	0.30	2.90	3.24	0.90	13.20	3.32	0.57	2.09	120R-1169
12	3.40	0.50	3.90	4.36	1.30	11.50	3.71	1.54	5.65	120R-1184dupl.
13	1.20	0.30	3.20	4.61	1.20	11.10	2.89	1.52	5.58	120R-1205
14	2.70	1.20	7.10	4.79	1.80	11.00	3.93	2.58	9.47	120R-1229dupl.
15	2.90	0.70	3.70	5.60	2.60	17.10	6.05	0.33	1.21	120R-1241
16	3.40	0.40	5.60	3.44	2.50	13.60	4.54	1.44	5.28	120R-1256dupl.
17	1.00	0.30	1.70	2.47	1.50	8.71	6.44	2.22	8.15	120R-1265dupl.
18	1.70	0.40	2.70	3.72	1.90	18.50	7.37	0.47	1.72	120R-1271
19	7.40	0.90	5.70	3.28	2.30	8.13	10.80	0.61	2.24	120R-1276
20	1.00	0.40	2.20	9.32	3.90	17.30	4.83	0.53	1.95	120R-1283
21	4.10	0.80	15.70	5.34	9.00	31.50	11.60	0.24	0.88	120R-1288
22	0.70	0.40	4.50	5.81	9.30	32.60	4.82	0.12	0.44	120R-1291
23	0.50	0.50	2.40	3.31	3.30	19.00	5.55	0.10	0.36	120R-1303
24	0.40	0.10	3.70	5.91	3.70	22.10	4.40	0.06	0.23	120R-1315
25	0.40	0.30	3.40	2.27	2.60	17.20	5.32	0.11	0.40	120R-1326
26	0.70	0.40	5.70	6.15	8.40	26.00	5.47	0.04	0.14	120R-1340
27	1.50	0.60	10.60	1.78	11.10	19.90	5.19	0.34	1.25	120R-1353
28	1.00	14.60	7.80	4.75	31.50	20.60	8.39	0.52	1.91	120R-1355
29	26.00	22.50	65.90	2.80	21.60	11.80	5.59	5.59	20.52	120R-1356dupl.
30	1.50	0.90	6.30	4.70	32.70	21.00	7.14	4.76	17.47	120R-1361ABdupl.
31	2.80	2.50	8.80	3.59	24.60	14.30	4.31	6.06	22.24	120R-1364ABdupl.
32	1.10	2.50	6.90	7.67	25.60	13.70	3.21	6.33	23.23	120R-1365ABdupl.
33	2.60	163.00	3.90	4.31	7.10	25.40	6.40	0.26	0.95	120R-1373dupl.
34	0.30	0.20	2.00	2.47	4.20	17.90	4.54	0.06	0.22	120R-1378

	Sc ppm	V ppm	La ppm	Ce ppm	Nd ppm	Ti / Zr	Alteration index	Chl/py/carb index	DDH/metres	Ag ppm	As ppm	Bi ppm
0	9.2	35.2	43.3	92.7	38	11.7	48.5	53.4	120R-1050	0.3	2.00	0.20
1	7.1	26.9	58.2	115.6	44.6	8.7	89.3	66.9	120R-1053.4	1.5	72.00	3.50
2	4.2	9.2	44.4	101.8	38.7	7.6	43.3	35.4	120R-1055.3	0.2	1.00	0.20
3	6.8	15.7	26.2	58.1	23.6	8.2	33.1	29.2	120R-1057.3	0.2	2.00	0.30
4	6.9	12.5	29.9	65.4	27.9	7.7	52	40.2	120R-1068.5	0.7	23.00	0.60
5	9	17.2	42.2	99.5	40.2	8.7	46.7	32.8	120R-1083.7	1.3	20.00	2.60
6	8.8	19	42.2	95.5	39.8	8.8	47	30.7	120R-1094.5	0.8	9.00	0.30
7	4.8	19.3	30.4	71.8	29.3	9.6	11.5	30.2	120R-1100.3	0.2	3.00	0.10
8	6.4	14.5	39.6	89.3	34	8	41.4	29.4	120R-1115.9	0.1	6.00	0.20
9	6.9	15.1	38.5	85.4	29.9	7.9	47.8	33	120R-1133.8	0.1	4.00	0.30
10	10.8	35.1	31	68.1	29.2	11.5	44.8	41.1	120R-1147.8	0.2	3.00	0.30
11	9.3	31.4	27.7	58.1	26	12.1	38	37	120R-1169.7	0.1	3.00	0.20
12	20.2	239.3	34.6	61.5	26.5	35.6	50.5	71.6	120R-1184	0.3	25.00	0.90
13	20.1	137.6	21.1	51.1	20.2	34.7	52.5	74.4	120R-1205.5	0.2	13.00	0.50
14	18.9	294.1	22.2	48.7	20.1	35.4	37.5	73	120R-1229.3	0.9	57.00	0.90
15	17	109.1	44.3	96.9	39.5	14.2	50.6	62.3	120R-1241.8	0.2	12.00	2.50
16	13.4	228.2	32.2	70	27	28.1	45.5	73.8	120R-1256	0.3	6.00	0.30
17	14.4	141.3	23.1	57.5	26.8	29	11	47.8	120R-1265.5	0.3	5.00	0.20
18	16.5	139.8	31.8	77.5	32.7	15.7	34.8	71.3	120R-1271.8	0.2	7.00	0.40
19	9	53	24.5	57.6	24	20.9	22.2	54.3	120R-1276.8	0.9	88.00	0.30
20	13.3	47.1	31.6	72.5	31.5	13.6	45.8	66.3	120R-1283.8	0.4	23.00	0.20
21	14.6	55.2	52.9	129.9	53	12.1	73	56	120R-1288.3	0.6	421.00	0.20
22	13.7	93.1	52.3	117.5	47.5	13.7	61.2	44	120R-1291.8	0.6	16.00	0.20
23	3.8	44.8	31.7	71.8	25.8	12.7	58.7	21.7	120R-1303.8	0.1	3.00	0.10
24	9	67.4	35.1	81.1	32.1	13.3	54.1	27.4	120R-1315.4	1.2	5.00	0.10
25	4.2	35	30.3	66.6	23.4	13.1	50.1	14.7	120R-1326	0.3	10.00	0.10
26	12.9	72.8	43.7	101.2	34.7	13.6	57.3	25.9	120R-1340.7	0.7	12.00	0.20
27	5.4	44.5	39.2	85	30.7	13.5	32.1	13.9	120R-1353.8	57.5	132.00	0.30
28	21.9	152.8	51.8	128	48.5	12.9	67.8	29.9	120R-1355.9	2.1	38.00	0.20
29	9.8	31.8	65	157	59	12.8	29	79.8	120R-1356.9	38.1	132.00	0.40
30	13.2	41.1	3.1	0		12.3	70.1	58.5	120R-1361.4	1.3	21.00	0.20
31	7.9	27.7	32.3	0		16.5	72.4	70	120R-1364.4	2.6	70.00	0.20
32	11.2	32.6	27.5	62	23	13.8	39.8	71.8	120R-1365.4	0.6	36.00	0.20
33	2	9	45.8	98	38	8	96.5	83.2	120R-1373	6.1	25.00	13.30
34	3.7	7.2	30.9	71.4	28.8	7.9	97.1	57.7	120R-1378.3	0.1	9.00	4.10

	Mo ppm	Cd ppm	Sb ppm	Cs ppm	Tl ppm	Th ppm	U ppm	toal carbon %	CO2 wt%	DDH/metres
35	2.70	0.90	1.90	1.94	1.60	15.30	3.93	0.88	3.23	120R-1386
36	0.50	0.90	2.50	4.33	1.80	17.80	5.28	0.20	0.73	120R-1403
37	0.50	0.10	2.70	4.88	0.90	17.00	4.39	0.51	1.87	120R-1421
38	0.30	0.20	1.00	1.92	0.50	17.80	4.22	0.36	1.32	120R-1440
39										
40	9.90	0.20	1.70	2.05	0.60	22.80	6.48	0.05	0.17	131R-841
41	1.60	0.20	1.00	2.24	0.70	16.80	5.68	0.62	2.28	131R-853
42	3.90	0.60	6.00	2.94	0.70	14.70	4.21	1.13	4.15	131R-870
43	0.60	0.40	1.20	2.33	0.60	13.50	3.56	0.54	1.98	131R-883
44	2.60	0.20	1.40	1.97	0.50	16.10	4.22	0.33	1.21	131R-907
45	1.60	0.30	2.30	2.61	0.70	17.20	4.18	0.25	0.92	131R-938
46	1.20	0.40	1.40	1.94	0.50	15.50	4.09	0.16	0.59	131R-955
47	0.80	0.20	1.80	2.03	0.50	20.00	4.93	0.10	0.37	131R-978
48	0.50	0.20	1.80	2.40	0.60	15.30	3.80	0.20	0.73	131R-1002
49	1.10	1.20	17.00	2.40	0.60	17.30	4.58	0.27	0.99	131R-1105dupl.
50	2.20	0.30	2.10	1.66	0.50	20.30	5.20	0.08	0.30	131R-1025
51	0.70	2.40	3.00	2.77	0.60	16.20	4.02	0.33	1.21	131R-1047
52	0.80	0.30	8.10	3.05	0.90	13.40	3.27	1.20	4.40	131R-1069
53	5.20	119.00	6.40	3.43	1.10	10.90	4.01	0.59	2.17	131R-1090
54	1.90	0.70	7.50	1.57	0.50	18.30	4.24	0.22	0.81	131R-1100
55	6.80	0.70	6.30	3.61	1.20	11.40	4.12	1.33	4.88	131R-1114dupl.
56	6.00	0.60	6.00	3.84	1.50	10.70	4.25	1.55	5.69	131R-1131dupl.
57	1.00	0.30	1.00	1.37	0.80	3.84	3.64	6.13	22.50	131R-1143.0dupl.
58	2.20	2.30	2.80	3.61	2.10	12.40	8.78	0.59	2.17	131R-1143Bdupl.
59	1.70	0.40	3.90	2.41	1.90	15.80	5.30	0.29	1.06	131R-1152
60	17.60	0.80	36.20	4.94	11.90	31.70	32.40	0.02	0.09	131R-1163
61	3.20	0.60	35.50	4.06	19.40	26.60	10.10	0.10	0.37	131R-1165
62	0.90	0.20	4.80	9.68	4.80	21.50	4.59	0.17	0.62	131R-1186
63	0.30	0.50	4.50	2.93	2.30	16.80	5.37	0.31	1.14	131R-1209
64	0.60	0.20	3.30	3.04	5.30	24.90	6.41	0.09	0.33	131R-1233
65	0.60	0.50	3.40	2.54	8.60	19.30	5.72	0.37	1.36	131R-1253
66	0.90	8.20	17.10	4.09	12.70	19.50	5.62	2.93	10.75	131R-1258abdupl.
67	1.80	59.50	10.70	3.15	5.00	16.00	4.45	0.01	0.06	131R-1261
68	0.40	1.80	4.50	4.24	5.80	22.30	5.28	0.77	2.83	131R-1263
69	0.50	21.00	15.70	4.27	4.20	21.80	5.51	0.30	1.10	131R-1271

	Sc ppm	V ppm	La ppm	Ce ppm	Nd ppm	Ti / Zr	Alteration index	Chl/py/carb index	DDH/metres	Ag ppm	As ppm	Bi ppm
35	3.1	6.7	34.2	75	29.3	8	95.1	72.8	120R-1386.5	0.5	9.00	6.70
36	4.1	11.1	44.7	98.3	39.8	7.8	91.7	53.4	120R-1399.5	0.2	4.00	1.50
37	5.3	13	38	83.2	36.1	8.4	67.1	41.1	120R-1421.8	0.1	3.00	0.60
38	5.4	6.4	56.6	108.9	45.4	7.5	21.4	21.8	120R-1440.5	1.5	1.00	0.10
39	0	0	0	0	0							
40	8.8	30.3	40.2	85.8	35.5	10.1	64.4	41.1	131R-841.4	0.2	2.00	0.40
41	7.1	15.3	50.6	101.7	42.1	8	54.7	31.4	131R-853.6	0.1	1.00	0.40
42	15.9	101.2	31.4	71.2	26.8	16.9	51.3	63.5	131R-870.7	1.2	46.00	5.00
43	16.7	54.7	37.2	84.3	35.1	16.7	37.6	43.5	131R-883.2	0.5	1.00	0.40
44	16.3	53.9	31.3	66.6	30.2	13.6	39	50.3	131R-907.7	0.8	1.00	0.20
45	13.6	44.8	44.2	98.5	39.6	12.7	49.6	42.7	131R-938.5	0.6	1.00	0.40
46	7.2	13.1	42.7	92.4	37.8	8	41.5	32.2	131R-955	0.5	1.00	0.70
47	8.4	12.1	51.2	113	48.1	7.3	40.8	30.1	131R-978.3	0.8	1.00	0.50
48	8.4	13.7	40.4	87.7	38.2	8.2	39.1	30.1	131R-1002.5	0.4	1.00	0.40
49	7.2	12.8	43.8	97.1	42.1	16.7	78.5	71.9	131R-1025.1	0.7	5.00	0.70
50	8	14.2	40.6	84	36.5	8.1	36.2	29.3	131R-1047.9	0.7	1.00	0.40
51	5.5	11	41.4	89.4	33.1	9.8	40.7	28.8	131R-1069.9	0.3	8.00	0.20
52	9.9	37	29.8	69.2	27.5	7	34.1	29.7	131R-1090.8	0.8	6.00	0.30
53	11.7	38.3	43.1	83	34.4	14.5	40.1	37.5	131R-1100.5	1.7	32.00	1.30
54	17.5	148.6	63.6	123.1	51.5	17.2	61.4	56.3	131R-1105.7	0.7	3.00	0.30
55	21.7	219.6	26.1	52.8	23.8	33.8	56.9	70.3	131R-1114.2	0.9	14.00	1.40
56	20.1	142.3	22.1	51.9	22.7	36.1	61.5	66.5	131R-1131.3	1.4	15.00	0.90
57	4.3	84.4	13	30.3	13	28.1	7.3	61.4	131R-1143	1.2	7.00	0.20
58	19.9	185.4	36	80.5	32	18	32.9	47	131R-1143.9	0.9	2.00	0.40
59	15.3	106.6	36.3	87.1	36.4	14.8	38.5	62.8	131R-1152.6	0.7	33.00	0.70
60	16.4	52.2	47.9	114.4	49.4	10.8	69.4	53.6	131R-1163	1.0	59.00	0.50
61	13.9	76.9	51.8	118.5	49.2	13.4	53.1	53	131R-1165.3	1.1	226.00	0.30
62	7.5	62	35.2	82.1	29.5	13.5	49	31.7	131R-1186.4	1.2	2.00	0.20
63	8	48.9	39.4	87.9	32.5	13	55.2	20.3	131R-1209.4	1.3	3.00	0.20
64	14	67.7	38.4	91.3	31	13.7	60.8	20.1	131R-1233.4	0.8	1.00	0.20
65	8.8	57.2	42.5	90.8	35.5	13.7	37.4	23.3	131R-1253.6	0.7	3.00	0.30
66	13.7	46.7	54			13.3	86.7	51	131R-1256	4.5	34.00	0.40
67	3.4	6	41.8	97.6	35.5	7	97.3	40.1	131R-1261.7	5.9	57.00	4.40
68	4.6	8.7	42.7	96	37	7.6	78.1	44	131R-1263.9	1.0	18.00	0.20
69	3.5	6.9	48	107	40	7.7	96.5	50.2	131R-1271	1.3	18.00	1.40

	Bl	DDH/metres	Th	Pb ppm	As ppm	Zn ppm	Cu ppm	Ni ppm	Nb ppm	Zr ppm	Sr ppm	Cr ppm	Ba ppm
35	6	120R-1386	14.2	31.2	6	398.1	343.6	1.3	9	165.4	8.4	2.3	548.6
36	4	120R-1403	17.6	19.6	3	290	6	1.7	13.8	239.2	19.5	2.9	1599.8
37	2	120R-1421	19.4	4.7	3	28.6	2.7	1.7	12.6	229.9	56	2.2	1042.5
38	2	120R-1440	16.4	4.1	3	22.5	2.2	1.1	12.2	240.6	195.4	1.9	506.2
39									0	0	0	0	0
40	2	131R-841	21.5	2.1	3	23.4	1.8	2.3	11.8	208.9	42	3.9	853.9
41	2	131R-853	17.7	1.5	3	10.5	2.7	1.3	18.4	284.7	80.3	2.6	1090.7
42	4	131R-870	13.2	83.5	44	123.1	122.6	45.4	10.4	181.4	114.6	100.2	1733.1
43	2	131R-883	11.5	2.6	3	60.3	19.8	4.3	10.5	215.8	230.3	6.8	1020.6
44	2	131R-907	15.9	6	3	104.1	12.6	4.5	12	295.6	261.9	4.6	923.1
45	2	131R-938	16.3	35	3	94.7	6.1	3.4	12.2	288.5	496.7	4.6	1894.5
46	2	131R-955	17	24.9	3	83.7	3.5	1.3	12.7	253.7	407.1	5.1	1780.4
47	2	131R-978	19.4	19.5	3	56.7	2.6	1.1	13.8	279.3	376.2	3.1	1299.3
48	2	131R-1002	14.6	6.1	3	55.6	4	1.6	11.9	293.1	296.1	3.3	1239.9
49	2	131R-1105dupl.	18.5	44.9	3	164.1	32.8	2.5	13.4	261.6	241.7	7.5	878.2
50	2	131R-1025	17.4	26.1	4	384.6	22.3	1.7	13	260.3	318.4	3.7	1253.1
51	2	131R-1047	19.8	9	3	43.5	2	1.6	11.5	221.5	196	1.8	1124.3
52	2	131R-1069	15.6	28.9	3	609.2	6.1	1.4	10.7	239.1	341.1	2.5	785.4
53	2	131R-1090	12.2	6	3	38.9	7.1	3	9.2	189.7	97.9	3	581.1
54	2	131R-1100	11.2	43	22	37800	65.9	77	11.6	132.8	56.6	133.5	603.2
55	2	131R-1114dupl.	10.7	48.1	8	169.2	67.1	57.4	13.7	143.9	138.8	151.2	597.6
56	2	131R-1131dupl.	10.1	107	11	92.9	51.4	44.6	12.8	133	119.6	147.8	613.4
57	2	131R-1143.0dupl.	3.2	9.2	5	90.5	13.8	9.2	4.2	64.1	409.1	92.7	360.3
58	2	131R-1143Bdupl.	11.4	90.5	3	609.6	23.1	17.1	11.6	193.7	561.4	83.6	1044.9
59	2	131R-1152	16.5	34.7	29	116.6	4.6	4.5	12.8	254.9	425.4	10.2	895.3
60	2	131R-1163	30.9	97.6	50	175.7	8.5	17	21.9	398.3	345.6	16.2	1256
61	2	131R-1165	29.1	41.5	189	354	21.1	4.4	16.1	268.3	376.9	6	1006.4
62	2	131R-1186	20.3	1.8	3	46.8	8.2	2.8	11.2	190.6	183.3	5.6	2114.5
63	2	131R-1209	18.1	3.4	3	24.9	3.3	1.6	11.2	179.9	153.5	4.5	1995.1
64	2	131R-1233	25.3	2.3	3	33.1	6.3	1.7	14.7	240	144.7	5.7	2827.9
65	2	131R-1253	19.4	1.5	3	38.1	10.5	1.5	11.7	196.7	195	4	2080.8
66	2	131R-1258abdupl.	21.7	2020	25	3933.5	195.8	2.8	14.4	271.3	18.4	2.4	3210
67	5	131R-1261	17.9	5100	46	23500	774	0.9	10.2	179.9	7.9	2.3	1249.5
68	2	131R-1263	22.3	280.6	14	632.5	11.4	1	15.1	269.6	44.6	1	2289.1
69	2	131R-1271	20.7	122.5	11	7800	81.5	1	14.2	248	16.6	1.9	1899.3

	DDH/metres	SiO2	TiO2	Al2O3	Fe2O3	FeO tot	MnO	MgO	CaO	Na2O	K2O	P2O5	S	Y	Rb
35	120R-1386	75.50	0.22	9.79	6.5	5.9	0.38	1.29	0.11	0.09	2.58	0.04	1.09	23.7	132.9
36	120R-1403	69.60	0.31	13.09	4.4	4	0.27	1.62	0.51	0.07	4.81	0.06	1.85	31.3	249.6
37	120R-1421	71.50	0.32	12.93	2.4	2.2	0.11	1.65	1.49	1.36	4.16	0.06	0.06	31.8	181.8
38	120R-1440	73.80	0.3	12.7	1.4	1.3	0.1	0.63	1.69	5.58	1.35	0.05	0.01	31.8	52.3
39															
40	131R-841	73.50	0.35	13.78	3.3	3	0.02	0.96	0.19	2.25	3.46	0.07	0.24	18.5	133.4
41	131R-853	67.60	0.38	15.45	2.3	2	0.1	0.77	3.11	1.44	4.72	0.07	0.1	30.5	173.4
42	131R-870	63.00	0.51	13.02	5	4.5	0.21	2.18	5.37	0.18	3.67	0.12	0.07	35	135
43	131R-883	65.90	0.6	14.86	3.9	3.5	0.15	1.32	2.86	3.67	2.61	0.12	0.1	40.7	94.4
44	131R-907	64.10	0.67	16.02	5.4	4.8	0.18	1.74	1.88	4.29	2.21	0.13	0.02	39	78.9
45	131R-938	66.70	0.61	15.6	3.8	3.5	0.17	1.38	2.65	2.66	3.84	0.12	0.04	40.9	116.3
46	131R-955	73.40	0.34	13.4	2.3	2.1	0.09	0.87	1.3	3.61	2.61	0.04	0.01	38.9	88.3
47	131R-978	73.60	0.34	13.68	2.2	2	0.08	0.84	1.2	3.85	2.64	0.04	0.01	41.9	91
48	131R-1002	71.30	0.4	14.21	2.3	2	0.08	0.86	1.89	3.9	2.85	0.06	0.03	41.7	95
49	131R-1105dupl.	64.90	0.73	11.19	6.4	5.8	0.06	1.73	1	0.22	2.72	0.15	3.7	39.9	82.1
50	131R-1025	74.40	0.35	12.76	2.1	1.9	0.08	0.63	1.35	3.76	2.27	0.05	0.06	38.6	98.2
51	131R-1047	71.30	0.36	14.31	2.5	2.2	0.07	0.61	1.73	3.81	3.2	0.05	0.13	39.5	64.1
52	131R-1069	75.80	0.28	12.72	2.2	1.9	0.05	0.62	0.71	4.17	1.9	0.03	0.01	27.7	100.9
53	131R-1090	67.10	0.46	16.47	3.1	2.8	0.08	0.85	2.38	3.2	2.89	0.08	0.07	34.2	124.5
54	131R-1100	65.60	0.38	14.42	6.2	5.6	0.35	0.81	1.45	1.33	3.62	0.08	0.06	34.2	103
55	131R-1114dupl.	63.70	0.81	12.45	6.5	5.9	0.07	2.55	3.23	0.79	2.76	0.16	1.74	27.1	107.7
56	131R-1131dupl.	66.10	0.8	11.97	5.4	4.9	0.05	2.34	2.54	0.74	2.9	0.16	1.61	27.8	115.6
57	131R-1143.0dupl.	27.70	0.3	9.66	3.5	3.1	0.32	1.64	28.97	2.18	0.8	0.14	0.39	15.1	30.7
58	131R-1143Bdupl.	56.60	0.58	20.28	3.9	3.5	0.06	1.77	4.49	3.69	2.24	0.11	0.54	28.4	89.9
59	131R-1152	63.30	0.63	17.12	4.3	3.9	0.06	2.44	3.98	2.27	1.47	0.14	0.78	32.9	55.5
60	131R-1163	58.10	0.72	22.09	3.4	3.1	0.04	3.2	1.73	1.44	3.98	0.15	1.39	48.2	143.1
61	131R-1165	58.20	0.6	20.42	4.4	4	0.03	2.21	2.89	2.09	3.42	0.17	2.51	44.7	120.3
62	131R-1186	68.90	0.43	15.18	3.4	3.1	0.07	0.66	1.07	3.91	4.13	0.11	0.02	20.5	124.1
63	131R-1209	72.10	0.39	13.61	1.6	1.5	0.09	0.41	1.58	2.62	4.77	0.1	0.01	33.3	123.1
64	131R-1233	65.90	0.55	18.49	2	1.8	0.08	0.62	0.6	3.6	5.9	0.14	0.01	25.3	166.4
65	131R-1253	70.50	0.45	14.69	1.5	1.4	0.23	0.67	1.88	3.91	2.79	0.11	0.09	24.8	106.9
66	131R-1258abdupl.	34.40	0.6	17.06	4.8	4.3	16.62	1.64	1.08	0.05	5.7	0.16	2	46.3	229.4
67	131R-1261	77.20	0.21	9.85	1.9	1.7	0.03	0.58	0.01	0.1	3.37	0.03	2.3	23.8	154.3
68	131R-1263	65.90	0.34	14.98	2.2	2	1.57	1.99	1.91	0.05	4.99	0.05	0.46	33.3	239.6
69	131R-1271	69.80	0.32	13.77	2.4	2.1	1.19	2.39	0.2	0.05	4.43	0.05	0.45	23.3	225

	DDH/metres	SiO2	TiO2	Al2O3	Fe2O3	FeO tot	MnO	MgO	CaO	Na2O	K2O	P2O5	S	Y	Rb
70	131R-1283	72.70	0.28	12.08	3.9	3.5	1.06	1.23	0.1	0.05	3.96	0.04	0.39	30	224.9
71	131R-1299dupl.	67.70	0.35	13.22	4.6	4.2	1.58	1.26	0.19	0.05	4.77	0.06	0.45	34.4	263.9
72	131R-1309	69.90	0.32	13.52	2.4	2.1	0.9	1.62	1.39	0.05	4.84	0.05	0.04	34.6	265.2
73	131R-1328	69.20	0.33	14.82	2.8	2.6	0.06	1.72	1.39	0.58	5.21	0.05	0.03	35.2	221.1
74	131R-1354dupl.	71.90	0.3	12.74	1.9	1.7	0.11	0.74	2.41	1.77	4.11	0.05	0.05	34.3	148.3
75	131R-1372	66.40	0.4	14.18	5.3	4.7	0.08	1	2.34	4.65	2.75	0.11	0.07	35.9	123.7
76	131R-1385	74.50	0.33	13.44	2.5	2.3	0.03	0.82	0.88	2.81	3.16	0.06	0.01	30.9	120.1
77															
78	R4452-0.5	68.80	0.31	12.68	8.7	7.8	0.24	1.62	0.29	0.05	3.26	0.05	0.96	34.3	150.2
79	R4452-10.7	72.50	0.28	12.08	5.6	5	0.2	2.31	0.49	0.05	3.33	0.05	0.23	36.1	165.6
80	R4452-19.4	70.90	0.31	13.94	5	4.5	0.18	1.96	0.32	0.05	4.29	0.05	0.03	25.8	211.2
81	R4452-33.7	74.20	0.28	12.26	2.9	2.6	0.12	0.72	0.95	0.19	5.26	0.04	0.5	33.5	208.1
82	R4452-40	74.10	0.3	13.5	2.1	1.9	0.11	1.01	0.61	1.76	4.01	0.04	0.11	28.8	196.7
83	R4452-47.5	73.80	0.31	13.95	1.6	1.4	0.04	0.84	0.22	0.78	6.33	0.05	0.3	30.3	227.9
84	R4452-57.9	67.20	0.33	14.9	4	3.6	0.83	0.91	0.73	0.05	5.78	0.05	1.28	31.2	266.4
85	R4452-64.5	74.60	0.28	13.04	2	1.8	0.08	0.66	0.37	0.14	5.88	0.04	0.69	29.1	207.4
86	R4452-69.5	70.20	0.31	15.43	2.9	2.6	0.06	1.23	0.02	0.05	5.68	0.04	0.89	37.7	258.9
87	R4452-75.1	35.20	0.6	17.64	5.2	4.7	1.7	6.4	8.17	0.07	6.23	0.14	1.1	46.3	293
88	R4452-76.2	30.10	0.58	16.15	5.8	5.2	1.73	10.41	9.97	0.05	6.1	0.14	0.27	36.2	334.6
89	R4452-77.2dupl.	33.60	0.48	13.5	6.6	5.9	2.69	8.45	10.43	0.05	4.52	0.12	0.76	34.9	224.2
90	R4452-80.6dupl.	14.10	0.29	8.04	5	4.5	5.86	8.98	21.01	0.05	2.96	0.08	0.22	20.7	135.3
91	R4452-91.6a.b	52.00	0.73	20.02	3.6	3.4	0.96	2.68	4.28	1.31	4.94	0.18	1.69	42.8	199.4
92	R4452-96dupl.	50.70	0.46	14.64	5.7	5.2	0.91	4.72	8.23	0.95	2.31	0.14	0.22	38.8	88.9
93	R4452-104.8	56.20	0.81	24.34	2.9	2.6	0.11	2.34	1.27	2.47	4.1	0.18	0.84	36.5	168.3
94	R4452-112.4	62.80	0.72	13.91	5.2	4.7	0.14	2.42	3.86	2.91	1.6	0.15	1.55	27	70.4
95	R4452-117.6	68.20	0.64	11.63	4.9	4.4	0.31	2.57	2.23	0.4	2.39	0.12	1.41	25.6	120.4
96															

	Bi	DDH/metres	Th	Pb ppm	As ppm	Zn ppm	Cu ppm	Ni ppm	Nb ppm	Zr ppm	Sr ppm	Cr ppm	Ba ppm
70	4	131R-1283	17	24	3	455.8	349.8	1.3	12	221.7	7.9	2.7	745.5
71	2	131R-1299dupl.	19.5	1028.4	3	3400	31.2	2.2	12.3	241.8	9.1	3.2	932.1
72	2	131R-1309	19.2	11.1	3	57.9	5.1	0.9	12.6	237.6	29.3	2.4	740.4
73	2	131R-1328	21.4	1.5	3	42.4	2.9	1.9	14.9	264.4	60.2	2.7	2684
74	2	131R-1354dupl.	18.8	5.9	3	30.5	3.6	2.6	12.9	242.5	95.6	2.5	863.1
75	2	131R-1372	19.9	1.8	3	55.6	4.4	4.4	10.6	183	156.8	5	799.6
76	2	131R-1385	19.4	4	3	27.8	2	1.1	12.9	246.9	92.3	3	643.9
77									0	0	0	0	0
78	2	R4452-0.5	22	13.7	10	83.2	14.4	1.4	13	232.4	10.5	2.9	487.2
79	2	R4452-10.7	19	9.3	3	692	29.3	1.8	12.5	212.7	18.5	3.2	662.2
80	2	R4452-19.4	20.6	2	3	74.4	3	1	14.3	242.4	12.7	3.5	892.5
81	10	R4452-33.7	17.9	179.7	3	116.4	330.3	1.6	12.9	219	56.8	1.8	1650.1
82	2	R4452-40	21	62.1	3	75.1	3.5	0.7	13.8	238.3	46.6	1.9	851.5
83	3	R4452-47.5	19.9	266.2	3	388.1	116.4	1.4	13.6	247.4	43.1	1.2	2664.7
84	3	R4452-57.9	20.6	239.5	40	168.7	63.1	1.8	13.8	262.5	23.1	1.7	1599.9
85	2	R4452-64.5	19.8	64.3	5	33.1	4.9	1.3	12.8	226.3	43.7	1.7	3184
86	4	R4452-69.5	27.5	174.8	16	190.9	40.8	1.6	16.3	254.3	5.8	1.5	2194.9
87	2	R4452-75.1	21.9	3300	6	9500	9.6	2.7	13.9	289.7	140.3	2.5	2868.8
88	2	R4452-76.2	16.7	97.1	4	518.5	5	1.7	13.2	255.1	189.3	2.6	2364.8
89	2	R4452-77.2dupl.	15.1	1479.4	7	1854.6	9.2	2.4	10.8	206.5	198.6	2.2	2081.9
90	2	R4452-80.6dupl.	9.4	788.8	3	2278.1	6.4	0.8	6.3	131.5	194.3	1.8	1353
91	2	R4452-91.6a.b	22.4	44.3	257	50.3	14.3	2.3	17.8	332.9	131.7	2.8	7218.6
92	2	R4452-96dupl.	20.1	5.9	10	109.9	17.3	3.2	11.5	194.3	155.7	4.7	3054.9
93	2	R4452-104.8	25.7	78.6	220	284.8	25	4.5	21.2	370.2	572.2	22.5	3993.9
94	2	R4452-112.4	10.3	53.6	36	101.4	18.4	8.9	9.6	186.1	265.1	43.6	755
95	2	R4452-117.6	12.3	341.9	45	459.5	46	39	13	127.3	67.6	113.4	668.2
96									0	0	0	0	0

	Sc ppm	V ppm	La ppm	Ce ppm	Nd ppm	Ti / Zr	Alteration index	Chl/py/carb index	DDH/metres	Ag ppm	As ppm	Bi ppm
70	3.1	9.4	44.7	92	38	7.6	97.2	54.3	131R-1283.9	1.6	5.00	3.60
71	5.5	13.8	37.7	90	37	8.7	96.2	53	131R-1299.7	1.4	3.00	0.50
72	5.6	14.4	44.7	97	39	8.1	81.8	43.5	131R-1309.3	0.2	2.00	0.30
73	4.6	8.5	37.2	89.1	33.1	7.5	77.9	42.5	131R-1328.7	0.6	1.00	0.30
74	5.2	8.6	34.6	76.4	31.2	7.4	53.7	29.6	131R-1354.7	0.5	2.00	0.50
75	13	60.2	39.4	79.6	32.3	13.1	34.9	43.7	131R-1372.7	0.6	5.00	0.40
76	4.5	13.6	40.2	85.1	37.1	8	51.9	34.2	131R-1385.7	0.5	1.00	0.30
77	0	0	0	0	0							
78	3.3	10	51	113	46.3	8	93.5	74.1	R4452-0.5	0.8	16.00	1.60
79	4.2	8.5	38.9	84	34.2	7.9	91.3	68.4	R4452-10.7	0.5	6.00	2.90
80	4.2	9.1	28.2	61	26.1	7.7	94.4	59.8	R4452-19.4	0.2	2.00	0.70
81	3.2	7.6	44.8	99.6	39.8	7.7	84	38.1	R4452-33.7	3.6	3.00	11.20
82	4.6	7.4	40.9	94	36.6	7.6	67.9	33.2	R4452-40	0.3	1.00	0.40
83	3.9	7.1	40.3	94.8	33.7	7.5	87.8	24.2	R4452-47.5	1.1	5.00	1.80
84	5	8.6	32	76	31	7.5	89.6	43.6	R4452-57.9	2.1	52.00	3.00
85	3.9	7	36.5	90.8	34.3	7.4	92.8	29.4	R4452-64.5	0.4	7.00	2.10
86	3.3	5	49.7	110.2	42.5	7.3	99	39.9	R4452-69.5	3.0	21.00	4.40
87	15.5	43.7	51	123	49	12.4	60.5	63.7	R4452-75.1	4.9	9.00	0.40
88	13.8	43.2	48.7	105	39	13.6	62.2	71.8	R4452-76.2	0.6	7.00	0.40
89	12.7	30.2	43.3	99	39	13.9	55.3	75.9	R4452-77.2	1.3	12.00	0.30
90	5.1	20.3	28.5	55	23	13.2	36.2	81.8	R4452-80.6	0.8	7.00	0.20
91	17.1	52	47.4	128	47	13.2	57.7	49.3	R4452-91.6	1.1	372.00	2.90
92	10.5	60.3	37.1	86	32	14.2	43.4	75.2	R4452-96	0.3	24.00	0.40
93	21.8	86.2	33.3	93.3	33.3	13.1	63.3	43	R4452-104.8	0.5	349.00	0.30
94	21.3	145.5	23	54.6	24.4	23.2	37.3	61.3	R4452-112.4	0.4	39.00	0.20
95	16.6	110.8	25.3	54.2	21.4	30.2	65.3	71.5	R4452-117.6	1.5	61.00	0.40
96	0	0	0	0	0							

	Mo ppm	Cd ppm	Sb ppm	Cs ppm	Tl ppm	Th ppm	U ppm	toal carbon %	CO2 wt%	DDH/metres
70	0.40	1.90	1.50	3.33	1.80	19.80	4.96	0.34	1.25	131R-1283
71	0.40	8.40	4.40	4.85	2.10	20.00	5.37	0.55	2.02	131R-1299dupl.
72	0.30	0.30	2.00	3.77	1.90	19.50	4.99	0.57	2.09	131R-1309
73	0.50	0.30	1.30	7.66	1.40	23.20	6.09	0.26	0.95	131R-1328
74	0.90	0.30	1.20	2.73	0.70	18.30	4.05	0.50	1.84	131R-1354dupl.
75	0.90	0.20	1.40	7.78	1.30	19.70	5.38	0.45	1.65	131R-1372
76	0.80	0.20	1.10	3.35	0.60	20.20	4.77	0.16	0.59	131R-1385
77										
78	0.20	0.20	1.50	2.52	0.90	19.90	4.80	0.09	0.31	R4452-0.5
79	0.80	2.10	2.70	2.97	1.20	19.20	4.44	0.15	0.55	R4452-10.7
80	8.20	0.30	1.90	3.95	1.80	22.80	5.68	0.16	0.59	R4452-19.4
81	2.00	0.70	12.50	4.40	2.40	21.20	5.22	0.26	0.95	R4452-33.7
82	0.50	0.60	3.80	5.50	2.40	23.50	5.73	0.19	0.70	R4452-40
83	1.20	1.70	3.80	4.12	3.90	23.30	5.71	0.09	0.32	R4452-47.5
84	2.00	0.90	32.10	5.49	5.50	21.20	6.14	0.45	1.65	R4452-57.9
85	22.10	0.40	3.00	3.69	8.50	20.70	5.85	0.09	0.32	R4452-64.5
86	10.30	1.30	12.00	5.89	11.20	26.90	6.57	0.04	0.15	R4452-69.5
87	11.10	28.40	15.80	12.70	18.60	23.60	5.68	3.25	11.93	R4452-75.1
88	0.70	1.50	12.40	25.80	33.10	21.30	5.83	4.08	14.97	R4452-76.2
89	3.80	6.40	9.90	14.30	22.80	17.30	4.25	4.04	14.83	R4452-77.2dupl.
90	1.10	6.90	5.30	8.18	12.60	11.50	2.56	8.24	30.24	R4452-80.6dupl.
91	1.20	0.40	26.20	5.73	60.00	23.00	8.52	1.02	3.74	R4452-91.6a.b
92	0.60	0.30	2.70	3.74	16.60	22.40	5.52	1.96	7.19	R4452-96dupl.
93	14.90	1.20	7.90	6.58	27.80	27.30	16.20	0.17	0.62	R4452-104.8
94	1.50	0.40	2.80	2.30	4.10	9.89	3.20	0.76	2.79	R4452-112.4
95	4.50	1.70	13.70	3.81	4.70	13.60	4.65	1.07	3.93	R4452-117.6
96										

	MnO/CaO	DDH/metres	Ag	As	Bi	Mo	Cd	Sb	Cs	Tl	Th	U	Total C	Th/U	CO2 wt%
0	0.05	109R-373.9	0.1	1.00	0.30	0.50	0.30	1.10	1.92	0.60	17.70	4.72	0.26	3.75	1.0
1	0.01	109R-392.2	0.1	83.00	0.10	0.40	2.40	1.50	0.32	0.50	0.97	0.42	0.69	2.31	2.5
2	0.05	109R-406.8	0.1	4.00	0.30	0.40	0.80	1.40	1.40	0.50	13.20	3.40	0.19	3.88	0.7
3	0.05	109R-434.2	0.1	5.00	0.20	0.40	0.30	1.70	1.48	0.50	14.50	3.85	0.21	3.77	0.8
4	0.02	109R-450.3	0.1	3.00	0.30	0.30	0.20	1.20	1.27	0.50	13.30	3.22	4.41	4.13	16.2
5	0.07	109R-481	0.2	6.00	0.40	1.20	0.50	3.00	1.85	1.50	15.20	4.04	0.08	3.76	0.3
6	0.03	109R-509.2	0.1	1.00	0.10	1.70	0.20	1.00	2.75	0.90	10.20	2.55	0.53	4.00	1.9
7	0.01	109R-553.8	0.2	5.00	0.30	3.30	0.30	5.40	2.93	1.40	10.10	3.49	2.17	2.89	8.0
8	0.04	109R-561.5	0.1	6.00	0.20	1.30	0.30	2.20	3.12	2.00	16.60	6.03	0.13	2.75	0.5
9	0.08														
10	0.03	109R-566.8	0.1	4.00	0.30	0.40	0.20	2.40	2.79	1.90	20.10	5.14	0.59	3.91	2.2
11	0.04	109R-573.6	0.1	3.00	0.20	0.30	0.20	1.60	1.99	1.10	20.00	5.05	0.15	3.96	0.6
12	0.05	109R-590.8	0.1	1.00	0.20	0.20	0.20	1.00	3.15	0.90	22.30	5.15	0.16	4.33	0.6
13	0.09														
14	0.04	109R-638.4	0.1	2.00	0.20	0.30	0.20	2.60	3.18	0.70	24.50	5.92	0.10	4.14	0.4
15	0.05	109R-670.6	0.1	3.00	0.20	0.30	0.20	2.00	2.71	0.50	20.00	4.86	0.12	4.12	0.4
16	0.02	109R-701.3	0.2	8.00	0.10	0.20	0.60	1.30	1.32	0.50	12.70	3.57	3.95	3.56	14.5
17	0.08	109R-707.8	0.1	12.00	0.20	0.30	0.20	2.40	2.97	0.60	19.90	5.09	0.24	3.91	0.9
18	7.57	109R-709.7	1.6	158.00	7.00	0.20	0.20	19.00	3.28	0.80	12.80	3.41	4.91	3.75	18.0
19	8.41	109R-723.5	0.4	2630.00	1.00	0.20	0.50	13.50	7.21	1.50	16.00	3.91	1.90	4.09	7.0
20	0.03	109R-726													
21	0.04	109R-741.8	0.1	2.00	0.20	0.30	0.20	1.00	2.72	0.50	23.60	5.73	0.08	4.12	0.3
22															
23															

	metres	Sr ppm	Cr ppm	Ba ppm	Sc ppm	V ppm	La ppm	Ce ppm	Nd ppm	Ti / Zr	Alteration index	Chl/py/carb index	Rb / Sr
0	373.9	388	3.2	1912.2	9.2	15	49.7	109.4	45.3	7.5	44.9	34.4	0.282
1	392.2	316.3	156.9	85.2	34.6	151.8	16.6	35.4	17.3	87.3	2.2	9.1	0.004
2	406.8	444.8	13.6	1356.6	9.6	22.4	36.8	83.2	35.2	8.6	34.7	33.8	0.166
3	434.2	308.5	11.3	1846.7	8.8	17.2	44.7	94.6	41.1	8.7	36.2	26.5	0.257
4	450.3	347.4	1.7	931.2	4	8.9	26.9	63.3	27.8	7.5	8.4	29.6	0.137
5	481.0	260.5	3.2	1471.5	6	20.2	35.7	77.8	32.2	10.6	33.9	27.5	0.286
6	509.2	197.5	3.5	961.2	9.5	42.7	25.7	56.3	23.5	13.6	43.9	43.9	0.486
7	553.8	167.2	132.6	470.1	18.3	194.5	25.5	49.2	24.1	36.2	35.6	69.3	0.584
8	561.5	211.6	1.8	910.8	8.9	19.3	27.4	61.9	26.7	11.4	55.4	36.9	0.519
9	562.6										84.3	46.1	
10	566.8	152	2	1591	4	8	41	96	39	7.4	50.6	43.7	0.850
11	573.6	196	2	1115	3	8	42	94	36	7.4	41.4	34.9	0.430
12	590.0	236.9	1.8	1290.8	4.4	8.3	43.1	95.1	36.5	7.3	41.3	24.0	0.534
13	620.0	179.3	1.9	1506.8	4.7	8.7	40.7	95	40.8	7.5	53.9	25.3	0.917
14	638.4	238.3	3.3	1253.7	5.8	10.1	46.8	102.8	43.9	7.6	44.8	26.7	0.561
15	670.6	278.6	2.2	1520.1	4.1	8.3	46.4	100.4	38.8	7.4	39.7	24.6	0.358
16	701.3	439.1	2.1	375.7	2	5.3	22.9	50.5	20.8	7.5	6.7	29.7	0.111
17	707.0	188.2	2	772.1	4.1	7.1	42.3	89.4	37	7.6	46.3	34.8	0.728
18	709.7	13.5	3.1	515	2.2	6.3	27.6	53	22	7.6	77.2	87.8	16.126
19	723.5	22.2	2.3	636	2.3	7	35.3	92	30	8	89.5	70.8	11.144
20	726.0	256.6	3	865.8	4.5	9.7	37.9	88	37.2	7.5	40.8	31.5	0.429
21	741.8	236.5	3.4	822.3	4	9.4	39.9	90.1	37.2	7.9	47.5	34.2	0.541
22													
23													

	S	DDH/metrs	Y	Rb	Bi	Th	Pb ppm	As ppm	Zn ppm	Cu ppm	Ni ppm	AK	Y	Nb ppm	Zr ppm
0	0.08	109R-373.9	40.5	109.4	2	19.4	1.6	3	64.2	4.8	2.4	109	109	13.9	296.7
1	0.1	109R-392.2	41.7	1.3	2	1	10.2	85	728.7	37.3	17	109	109	2.7	54.3
2	0.09	109R-406.8	39	73.9	2	14.8	10.1	4	208.6	5.2	2.7	109	109	11.5	298.3
3	0.04	109R-434.2	40.4	79.4	2	15.4	11.9	3	69.1	3.9	2.2	109	109	12.1	281.9
4	0.03	109R 450.3	34.9	47.7	2	12.8	6.4	3	40.1	3.9	0.8	109	109	8.8	192.2
5	0.03	109R 481.0	32.7	74.6	2	14.9	62.3	4	141.5	2.6	1.7	109	109	10.8	197.4
6	0.14	109R 509.2	22.6	96	2	9.8	6.9	3	53.8	5.4	2.1	109	109	9.6	194.2
7	1.49	109R 553.8	21.5	97.6	2	10.3	13.1	3	75	57.7	51.4	109	109	12.2	120.9
8	0.14	109R 561.5	26	109.8	2	16.2	30.7	5	65.7	2.2	0.8	109	109	13.3	215.8
9	1.68	562.6	34	224	2	25	36	143	92	5	2				
10	0.29	566.8	38	129	2	20	9	3	54	6	1			14.4	258
11	0.22	573.6	29	84	2	19	7	3	49	4	1			12.8	234
12	0.02	109R 590	34.8	126.4	2	22.7	8.4	3	45.3	5	1	109	109	14.7	261.4
13	0.01	109R 620	38.5	164.5	2	25.4	1.5	3	20.3	1.3	0.8	109	109	16.1	302.5
14	0.02	109R 638.4	37	133.8	2	24.7	6.6	3	34	2.5	1.5	109	109	15.6	284.1
15	0.03	109R 670.6	31.3	99.6	2	20.3	4.6	3	24.5	2.2	1.4	109	109	14.2	244.7
16	0.02	109R 701.3	24.4	48.8	2	11.9	92.3	3	96.8	5.8	1	109	109	7.4	151.8
17	0.03	109R 707	31.4	137.1	2	20	4.7	3	30.3	1.9	1.3	109	109	12.9	237.7
18	0.06	109R 709.7	37.1	217.7	2	14.3	158.6	133	51	87.4	1.3	109	109	6.7	143
19	0.3	109R 723.5	32.6	247.4	2	16	80.9	2153	102.2	11	1.6	109	109	10.1	180.9
20	0.01	109R 726	33.3	110.2	2	22.7	2.7	3	26.1	1.2	1.3	109	109	14.2	256.9
21	0.01	109R 741.8	38.9	127.9	2	24.8	2	3	23.8	1.7	1.6	109	109	15.6	266.5
22															
23												0			

	Ident	Metres	lithology	Ti / Zr	SiO2	TiO2	Al2O3	Fe2O3	FeO tot	MnO	MgO	CaO	Na2O	K2O	P2O5
0	109R-373	373.9	h	7.5	71.89	0.37	13.99	2.25	2.03	0.09	1.03	1.81	2.97	2.86	0.05
1	109R-392	392.2	mafic clast in h	87.3	62	0.79	17.51	0.83	0.75	0.07	0.25	4.9	9.83	0.08	0.27
2	109R-406	406.8	h	8.6	70	0.43	14.72	2.88	2.59	0.1	0.87	1.88	4.34	2.44	0.06
3	109R-434	434.2	h	8.7	71.98	0.41	13.9	2.04	1.84	0.08	0.63	1.74	4.14	2.71	0.06
4	109R-450	450.3	h	7.5	45.09	0.24	9.4	1.65	1.49	0.35	0.47	20.81	2.96	1.7	0.02
5	109R-481	481.0	h	10.6	74.4	0.35	14.34	2.06	1.86	0.04	0.57	0.58	4.41	1.99	0.05
6	109R-509	509.2	h	13.6	67.97	0.44	14.58	3.05	2.75	0.08	1.38	2.77	2.51	2.76	0.07
7	109R-553	553.8	bs	36.2	59.68	0.73	11.2	5.14	4.63	0.1	2.29	7.63	0.74	2.33	0.15
8	109R-561	561.5	t	11.4	76.53	0.41	12.25	1.25	1.13	0.03	1.49	0.84	2.19	2.28	0.09
9	562.6	562.6	t		67.82	0.39	16.52	3.12	2.84	0.04	1.65	0.48	0.68	4.56	0.06
10	566.8	566.8	t	7.4	69.83	0.32	13.81	2.05	1.86	0.08	1.63	2.95	1.53	2.96	0.04
11	573.6	573.6	f	7.4	75.16	0.29	12.74	1.9	1.71	0.04	1.09	0.93	3.31	1.91	0.04
12	109R-590	590.0	f	7.3	72.63	0.32	14.65	1.71	1.54	0.04	0.66	0.84	4.13	2.84	0.04
13	109R-620	620.0	f	7.5	71.91	0.38	15.27	1.87	1.68	0.05	0.68	0.57	3.23	3.77	0.05
14	109R-638	638.4	f	7.6	71.55	0.36	15.15	2.01	1.81	0.03	0.71	0.71	3.89	3.03	0.05
15	109R-670	670.6	f	7.4	74.09	0.3	13.28	1.73	1.56	0.04	0.56	0.85	3.91	2.58	0.04
16	109R-701	701.3	f	7.5	49.93	0.19	8.35	1.36	1.23	0.42	0.47	18.51	2.94	1.08	0.03
17	109R-707	707.0	f	7.6	74.2	0.3	12.88	2.24	2.02	0.09	0.94	1.15	2.94	2.59	0.04
18	109R-709dupl.	709.7	f	7.6	38.7	0.18	7.95	21.1	19.01	8.71	1.4	1.15	0.08	2.76	0.03
19	109R-723dupl.	723.5	f	8	60.85	0.24	11.07	8.75	7.88	3.87	1.07	0.46	0.09	3.61	0.04
20	109R-726	726.0	f	7.5	73.26	0.32	14.13	2.11	1.9	0.03	0.97	0.99	3.87	2.38	0.04
21	109R-741	741.8	f	7.9	71.9	0.35	14.39	2.14	1.93	0.03	1.2	0.7	3.45	2.56	0.05
22															
23															

	Mo ppm	Cd ppm	Sb ppm	Cs ppm	Tl ppm	DDH/metres	Th ppm	U ppm	toal carbon %	CO2 wt%	Rb/Sr	S/Na2O	Th / U
0	0.1	0.2	1.6	1.8	0.5	113R-708	22.2	5.4	0.1		0.3	0.0	4.08
1	0.6	0.4	0.7	2.0	0.5	113R-732	9.3	2.8	0.8		0.2	0.0	3.25
2	0.5	6.2	1.5	1.9	0.5	113R-735	12.7	3.3	0.8		0.2	0.0	3.81
3	0.3	0.2	1.0	2.0	0.5	113R-763	15.3	3.8	0.2		0.2	0.0	4.05
4	0.4	0.2	1.0	1.5	0.5	113R-792	18.4	4.4	0.2		0.3	0.0	4.22
5	0.5	3.4	12.5	5.8	0.9	113R-823	21.0	4.9	0.6		2.9	0.1	4.26
6	0.5	1.5	1.6	3.7	0.5	113R-852	17.1	4.7	0.3		0.7	0.0	3.62
7	1.6	0.2	2.1	3.3	0.5	113R-865	15.9	4.0	0.8		0.6	0.0	3.95
8	0.9	0.3	1.6	3.3	0.6	113R-871	15.6	3.9	0.5		1.6	2.4	4.03
9	4.3	0.6	6.4	4.3	1.0	113R-895	11.9	4.2	0.8		0.5	1.1	2.85
10	0.7	0.2	3.3	2.7	1.1	113R-938dupl.	12.7	3.4	1.2		0.6	0.2	3.71
11	0.2	0.2	1.8	5.9	2.8	113R-949	25.8	6.2	0.6		0.2	0.0	4.19
12	9.0	10.7	4.3	4.2	2.0	113R-956	18.8	4.8	0.8		4.5	5.2	3.93
13	0.2	0.2	1.6	5.0	1.5	113R-973	22.0	5.9	0.6		1.8	0.0	3.72
14	0.3	0.2	1.0	2.0	0.5	113R-985	18.4	3.8	0.1		0.3	0.0	4.89
15	0.2	0.2	0.8	5.4	0.9	113R-991	21.7	5.1	0.0		0.5	0.0	4.26
16													
17													

	Sc ppm	V ppm	DDH/metres	La ppm	Ce ppm	Nd ppm	Ti / Zr	Alteration index	Chl/py/carb index	Ag ppm	As ppm	Bi ppm
0	6.9	10.6	113R-708	40.6	93.8	37	7.2	41	29.6	2.5	1.0	0.1
1	18.3	80.9	113R-732	25.2	55.4	24.9	17.8	26.1	27.4	1.3	7.0	0.4
2	22.1	155.9	113R-735	36.3	74.6	30.1	15.4	30.3	44.5	0.5	3.0	0.4
3	8.8	16.1	113R-763	40.4	93.5	36.5	8.4	40	33.4	0.4	3.0	0.2
4	8.2	12	113R-792	48.8	103.3	43.6	8.1	38.1	29.9	0.4	2.0	0.1
5	8.9	15.3	113R-823	48.3	104.2	43.4	7.9	71	45	0.6	23.0	0.3
6	7.9	14.5	113R-852	52.1	116.5	46.5	8.2	37.7	31.9	0.7	1.0	0.2
7	8.2	21.4	113R-865	33.5	72.8	28.8	10.8	44.5	39.4	0.2	4.0	0.
8	11.7	28.1	113R-871	31.4	69.8	26.6	11.4	44.8	39.6	0.3	6.0	0.
9	21.8	166	113R-895	29	55	24.8	33.6	67.3	66.7	1.6	40.0	0.5
10	16	125.1	113R-938dupl.	28	56.9	24.9	28.9	49.3	67.6	0.4	6.0	0.1
11	13.5	81	113R-949	38.6	84	32.8	14.1	58.4	52.3	0.3	6.0	0.1
12	3.5	5	113R-956	47.3	105.3	38.2	7.1	88.7	42	2.4	18.0	0.6
13	4.6	8.1	113R-973	40.6	91.7	35.3	7.5	66.1	50.3	0.8	1.0	0.1
14	3.2	6.2	113R-985	36.4	79.8	33.5	7.4	29.5	28.1	0.3	1.0	0.1
15	4.5	10.8	113R-991	48.8	104.6	42.3	7.7	44.1	29.3	0.3	1.0	0.1
16												
17												

	Rb	DDH/metres	Bi	Th	Pb ppm	As ppm	Zn ppm	Cu ppm	Ni ppm	Nb ppm	Zr ppm	Sr ppm	Cr ppm	Ba ppm
0	89.6	113R-708	2	21.9	3.5	3	29.5	3.1	2.3	16.2	290	330	2	1627.2
1	77.9	113R-732	2	8.3	17.5	7	91.9	4.9	4.7	8.1	188.5	344.5	63.6	1336.8
2	63	113R-735	2	12.7	39.0	3	1400.8	5.6	8.8	9.8	222.6	320.7	57.3	1261.7
3	81.9	113R-763	2	15.5	10.5	3	49.7	3	2.7	12.4	285.4	457.8	9.4	2753.1
4	77.7	113R-792	2	19.3	4.5	3	43.5	2.6	1.5	13.5	272.4	273.7	2.7	1332.1
5	186.3	113R-823	2	21.1	37.2	19	969	12	1.5	15.7	302.6	63.8	4.4	723.4
6	93.9	113R-852	2	16.5	31.5	3	351	5	2.3	12.6	271.9	418.5	4.7	2243.4
7	110.6	113R-865	2	14.3	19.1	4	16	2.2	2.2	11	194.8	156.1	2.7	928.8
8	107.9	113R-871	2	14.4	6.3	6	85	5.5	1.7	10.5	204.7	187.5	2.5	1452
9	114.3	113R-895	2	10.6	9.9	33	145.7	56.8	47.8	14.6	151.9	73.5	155.3	572.4
10	77.3	113R-938dupl.	2	12.4	12.2	5	70.7	43.2	33	12.3	122.4	141.6	114.2	382
11	170.3	113R-949	2	26.6	2.6	4	82.8	21.6	2.9	13	242.8	278.8	6	1099.8
12	160.7	113R-956	2	20.4	1632.0	15	3768	107.4	0.8	12.2	185.5	36.1	2.3	1202.1
13	166.8	113R-973	2	21.1	1.5	3	37.1	1.8	0.9	14.3	247.9	92.5	1.6	1396.4
14	73.8	113R-985	2	19.6	3.9	3	24.1	1.7	1	11.9	220	284.6	2.7	564.8
15	144.3	113R-991	2	22.1	3.7	3	34.2	2.8	1.1	14.4	281.9	305.9	3.3	1044.5
16														
17														

	DDH/metres	metres	SiO2	TiO2	Al2O3	Fe2O3	FeO tot	MnO	MgO	CaO	Na2O	K2O	P2O5	S	Y
0	113R-708	708.3	74.2	0.35	13.6	1.9	1.7	0.04	0.8	0.58	3.8	2.24	0.04	0.05	44.5
1	113R-732	732.6	62.5	0.56	16.33	2.4	2.2	0.12	0.89	4.59	5.48	2.66	0.13	0.06	41.4
2	113R-735	735.3	59.7	0.57	15.96	4.7	4.3	0.18	1.71	4.6	4.99	2.45	0.12	0.12	44.6
3	113R-763	763.7	71.3	0.4	14.33	2.5	2.3	0.1	0.92	1.87	3.65	2.76	0.05	0.03	41
4	113R-792	792.3	74.1	0.37	12.95	2.3	2	0.08	0.66	1.46	3.78	2.57	0.05	0.03	47
5	113R-823	823.1	67.7	0.4	15.56	4.5	4	0.4	0.67	0.34	1.61	4.11	0.06	0.17	39.8
6	113R-852	852.8	68.4	0.37	15.46	2.8	2.5	0.09	0.78	2.37	3.94	3.04	0.06	0.08	44.7
7	113R-865	865.4	68.7	0.35	14.26	3.5	3.2	0.26	0.76	1.28	3.24	2.86	0.05	0.01	29.2
8	113R-871	871.3	69.7	0.39	14.3	2.8	2.5	0.1	0.79	2.88	1.92	3.11	0.06	0.06	33
9	113R-895	895.4	67.0	0.85	13.02	6.5	5.9	0.04	1.7	1.62	0.7	3.08	0.17	1.68	27.1
10	113R-938dupl.	938.0	67.6	0.59	11.38	4.7	4.2	0.07	2.56	3.38	1.27	1.97	0.18	1.34	27.5
11	113R-949	949.7	57.6	0.57	19.23	3.6	3.2	0.21	3.09	3.54	1.61	4.15	0.15	0.39	38.4
12	113R-956	956.4	77.4	0.22	11.31	1.9	1.7	0.08	1.02	0.38	0.21	3.6	0.03	1.09	27.9
13	113R-973	973.1	68.8	0.31	13.91	2.1	1.9	0.1	2.49	2.96	0.35	3.95	0.04	0.01	35
14	113R-985	985.9	76.4	0.27	12.32	1.7	1.6	0.05	0.75	0.95	4.43	1.5	0.04	0.02	27.7
15	113R-991	991.8	71.9	0.36	15.5	2.3	2.1	0.04	0.96	0.48	4.47	2.94	0.05	0.01	38.1
16															
17															

Research program and preliminary results of alteration studies at the Western Tharsis deposit, Mt Lyell field

David L. Huston
Australian Geological Survey, G.P.O. Box 378, Canberra, ACT 2601

Summary

To determine alteration patterns around Cu-rich, disseminated pyrite-chalcopyrite deposits in the Mt Lyell field, a research program involving core logging, surface traversing, whole rock geochemistry, isotope geochemistry, mineral chemistry and petrography has begun at the Western Tharsis deposit. The first stage of field activity has been completed, and geochemical analyses have begun. Results from the field program indicate that: (1) the Western Tharsis ore zone occurs in felsic fragmental rocks, which are overlain and underlain by fragmental, mafic volcanic rocks with ~20%, intercalated sills or lavas, (2) the ore zone is most closely associated with a quartz-chlorite-bearing alteration zone, which is surrounded by a quartz-sericite alteration zone, and by a more distal chlorite-bearing, but quartz-free, alteration zone, and (3) the orebody occurs within the centre of a pyritic zone, which is surrounded by a distal siderite zone, with hematitic zones along the contact between these two zones. Future research at Western Tharsis will involve whole rock geochemical analyses, petrography, REE analyes, PIMA scans, electron and proton microprobe studies and isotopic analyses. In addition, the use of surface traversers should determine the effect of weathering on alteration halos determined from drill core studies. A final report is anticipated for the October 1997 meeting.

Introduction

To date AMIRA project P439 has concentrated mainly on documenting alteration zonation about Zn-rich and relatively Cu-poor, massive sulfide deposits. However, Cu-rich and Zn-poor massive to dissminated deposits also are potential exploration targets in submarine volcanic provinces such as the Mt Read and Mt Windsor volcanic belts. The best example of such targets are Cu-rich orebodies of the Mt Lyell field in the southern Mt Read Volcanics. At the time RGC ceased mining in 1995, the Mt Lyell field had produced 113 Mt of ore grading 1.23% Cu, 6.81 g/t Ag and 0.40 g/t Au (Wills, 1996).

Historically, three general types of sulfide orebodies have been recognised in the Mt Lyell field: (1) massive sulfide lenses, such as Iron Blow and South Lyell, that contain pyrite and chalcopyrite as the principal ore minerals, (2) strataform, disseminated sulfide lenses, such as Prince Lyell and Western Tharsis, that are also dominated by pyrite and chalcopyrite, and (3) irregular, disseminated to massive sulfide lenses characterised by the presence of abundant bornite (Walshe and Solomon, 1981). Of these ore types, most production came from the disseminated ores.

As the composition of these ores differs from that of other studied deposits, it is likely that the alteration mineralogy and element dispersion halos also differ. Hence, a program to document alteration zonation, geochemistry and element dispersion has began at

the Western Tharsis orebody at Mt Lyell. Western Tharsis is the only known Mt Lyell deposits deposit that does not outcrop at surface. In addition, with a total resource of 12.4 Mt at 1.3% Cu (GMA annual reports), it is the only major undeveloped deposit in the Mt Lyell field. The purpose of this project is to document deposit-scale mineralogical and geochemical zonation within the alteration zone associated with the Western Tharsis deposit, and to use these data to establish deposit-scale vectors to ore about disseminated pyrite-chalcopyrite-type orebodies within the Mt Lyell field.

Research plan

After discussions with other members of the P439 research team and geologists at Copper Mines of Tasmania, a research program was designed to document deposit scale (i.e. within 1 km of the deposit) variations in alteration mineralogy and geochemistry. This program involves three stages: (1) core logging, surface traversing and sample collection, (2) collection of geochemical, mineralogical and isotopic data, and (3) data interpretation, development of vectors to ore and reporting. At this writing, stage 1 is approximately 70% complete, and stage 2 is underway.

Stage 1–Core logging, surface traversing and sample collection

Three cross sections were chosen for detailed study during this reseach program. Selection of cross sections was governed by abundance and availability of diamond drill holes for logging. One section, section 8850 mN, was selected as it passed through the centre of the Western Tharsis deposit and it contained a number of long drill holes that passed through a thick stratigraphic section both in the footwall and in the hanging wall of the deposit. Two other sections (8600 mN and 9100 mN) were selected as they occur 100–150 m to the south and north of the orebody margins and do not contain extensive ore grade intersections. Eleven holes, totalling almost 5 km, were selected for logging and sampling (Table 1). In addition surface traverses along all three section lines were planned. Provision was made for the collection of 200–400 samples.

Stage 2–Collection of geochemical, mineralogical and isotopic data

Based on previous experience and discussions with Joe Stolz, an analytical program involving whole rock geochemistry and a number of isotopic and spectrometric techniques has been developed. Approximately 200 samples will be submitted for whole rock geochemistry, and subsets of these samples will be submitted for the other analytical techniques.

A suite including of elements, including major elements, S, total C, CO_2, Sc, V, Ni, Cu, Zn, As, Rb, Sr, Y, Zr, Mo, Ag, Sb, Cs, Ba, La, Ce, Nd, Tl, Pb, Bi, Th, U, Sn, Co and Se, will be determined using XRF and ICP-MS techniques. Approximately fifty of these samples will also be analyzed for rare-earth elements.

Mineralogical studies, including petrography, PIMA (Portable Infrared Mineral Analyser), XRD, electron and proton microprobe analysis, and laser Raman analysis, will be undertaken to determine variations in the abundance and composition of alteration minerals and pyrite. PIMA analysis (supported by XRD analysis) will be conducted on all 200 samples submitted for whole rock geochemical analysis.

Thin sections will be cut and examined for ~50 samples. Electron microprobe studies will be undertaken on phyllosilicate minerals from these samples to quantify variations in composition. These analyses will be supplemented with laser Raman studies to determine TiO_2 polymorphs (this technique has proven to have potential in the porphyry-epithermal environment). An etching and proton microprobe study will be undertaken on pyrite from ~20 samples in hole WT0077D (previous studies at Mt Lyell and other volcanic hosted massive sulfide deposits have indicated the potential of these techniques).

Limited isotopic studies (oxygen, sulfur and carbon) will be undertaken on WT0077D to determine if systematic variations can be recognised in the

Table 1. Summary of core logging and sampling, Western Tharsis research program.

Hole	Interval logged (m)	Total samples collected	Samples collected for geochemistry	Samples collected for thin sections
Section 8600 mN				
WT0037	0-258	11	11	0
Section 8850 mN				
WT0025	0-256	12	11	0
WT0038	0-295	12	12	0
WT0050	3-707	36	32	26
WT0055	0-314	13	13	0
WT0056	7-274	11	10	0
WT0066	0-418	19	18	0
WT0077D	607-1269	62	38	27
95WTD0090	0-574	19	18	1
95WTD0091	0-533	19	18	0
Section 9100 mN				
WT0048	0-496	29	20	0
Totals	4777	243	201	54

alteration zones. These studies will be very limited unless they successfully give vectors to ore. Previous oxygen and sulfur isotope studies by Manning (1990) and Raymond (1992) were limited to the immediate ore environment. A programme of ~20 whole rock $\delta^{18}O$ and 20–30 laser ablation $\delta^{34}S$ analyses from samples away from the orebody, combined with existing analyses, should test the viability of oxygen and sulfur isotopes as vectors to ore. Although siderite is a significant alteration mineral at Western Tharsis, no $\delta^{13}C$ and $\delta^{18}O$ data for this mineral exist for Western Tharsis. Analysis of 10–20 samples from WT0077D should indicate if this technique has exploration usefulness.

Stage 3–Data interpretation, development of vectors to ore and reporting

This research program will comprehensively test a number of geochemical and mineral techniques as vectors to ore at the Western Tharsis deposit. These results will serve as an excellent comparison to the Zn-rich deposits that are presently being studied as part of this AMIRA project.

The major results of this program will be reported to the October 1997 meeting. This report will summarise the results of these geochemical and mineralogical studies, suggest potential ore vectors for Western Tharsis-type Cu-Au deposits, and discuss potential differences in exploration vectors for Zn-rich volcanic-hosted *massive* sulfide deposits and Cu-rich volcanic-hosted *disseminated* sulfide deposits.

Work completed

All eleven drill holes selected for this study have been logged with emphasis on alteration assemblages. A total of 243 samples have been collected, of which 201 have been submitted for geochemical analysis and 54 have been submitted for thin sectioning. Table 1 summarises the core logging and sampling completed.

Cross sections for section 8850 mN have been constructed showing lithology, silicate alteration assemblages and Fe-O-S-C mineral assemblages (Figs 1 to 3).

Preliminary results

Based on observations made during core logging and from Figures 1 to 3, several very preliminary observations can be made:

1. Although not always distinguishable because of overprinting alteration assemblages, six distinctive rock types are present within the Western Tharsis area (Fig. 1):
   (a) Coarse, aphyric to sparsely quartz-phyric, felsic fragmental rocks, which are characterised by ash to lapilli-sized, rhyolitic fragments. This rock type forms a unit approximately 200–300 m wide that hosts the dissiminated sulfide mineralisation. Massive felsic volcanic rocks occur in the mafic sequence to the east of the ore lens.
   (b) Aphyric to feldspar-phyric, mafic fragmental rocks, which are characterised by ash-sized mafic fragments. This rock type forms 100–300 m thick units that underlie and overlie the ore-hosting felsic fragmental units.
   (c) Aphyric to feldspar-phyric, coherent mafic rocks that commonly contain siderite-filled amygdales. This rock type comprises approximately 20% of the mafic rocks and occurs in strataforms sills or flows that vary in thickness from 2 to 30 m thick.
   (d) Volcanogenic sandstones, siltstones and shales up to 50 m in true thickness that occur with the mafic fragmentals in the footwall to the ore position.
   (e) Quartz-phyric, rhyolitic volcanic rock, which is characterised by up to 5% 1–2 mm quartz phenocrysts. This unit is restricted to an approximately 3 m thick unit along the contact between the volcanic sequence and the Owen Conglomerate.
   (f) Hematitic, clast- and matrix-supported, pebble-cobble conglomerate, with sub-angular to rounded, polymict clasts in a hematitic sandy matrix. This unit, the Owen Conglomerate, was intersected at the bottom of holes WT0048, WT0050 and WT0077D.

2. Based on silicate minerals, four major alteration assemblages are recognised (Fig. 2):
   (a) Chlorite-bearing assemblages that lack quartz (e.g. chlorite, chlorite-sericite and sericite-chlorite) which are best developed distal to the ore zone and occur mainly in mafic rocks.
   (b) Quartz- and chlorite-bearing assemblages (e.g. quartz-chlorite, quartz-chlorite-sericite and quartz-sericite-chlorite) that affect fragmental felsic rock types largely within the ore zone.
   (c) Quartz- and sericite-bearing assemblages (e.g. quartz-sericite and siliceous quartz-sericite assemblages), which generally occur in felsic fragmental rocks between the proximal quartz-chlorite-bearing assemblages and the distal chlorite-bearing assemblages. Some ore also occurs in chlorite-free, quartz-sericite altered zones.
   (d) Weak quartz-sericite-bearing assemblages, which occur in the stratigraphic footwall some 200–300 m west of the orebody.
   With very few exceptions (Fig. 2), the alteration at Western Tharsis is feldspar-destructive. Strongly sericitically altered zones are generally associated with late shear zones or with late quartz-siderite-bearing veins.

3. In addition to variations in silicate assemblages, Fe-S-C-O minerals are also distributed symmetrically about the ore zone at Western Tharsis (Fig. 3):
   (a) Pyrite forms an inner halo (> 1% by volume) that extends up to 100 m stratigraphically above and below the orebody. Within this halo, pyrite occurs as disseminated grains, irregular 1–20 mm stringers, and planar 2–50 mm veins. Outside of this halo, pyrite content rarely exceeds 0.5%.
   (b) Siderite forms an outer halo in both the hanging wall and the footwall distal to the pyritic inner halo. It occurs in late, 1–30 mm veins, as early, 1–5 mm, irregular veins, and as 1–10 mm, lenticular nodules after clasts and/or feldspar phenocrysts. Siderite forms a halo around, but not within the orebody. The siderite halo generally fades out when the pyrite content exceeds 1–2%.

(c) Hematite occurs as disseminated, visible grains, and as a fine dusting that gives units a purplish tinge. Hematite occurs mainly within mafic rocks in a zone up to 50 m thick around the contact between the pyritic inner halo and the sideritic outer halo. Although the hematitic zone is best developed in the stratigraphic footwall, hematite is also present in the hanging wall in drill hole WT0077D. Although verification is required, hematitic zones appear to thicken around the thickest part of the ore zone.

These observations must be considered very preliminary, and are subject to change as more data is collected and geochemical analyses become available. However, they serve as a guide to the direction the research is proceeding.

Forward program

Results to date have demonstrated that alteration mineralogy varies systematically and symmetrically about the Western Tharsis orebody. The next step in the program, whole rock geochemical analyses to establish geochemical halos about the ore zone, is presently under way. Geochemical results are expected in July or August. After these results are obtained, a the author will return to Mt Lyell to undertake surface traverses and complete the logging of hole WT0077, which penetrates approximately 700 m into the stratigraphic footwall of the Western Tharsis deposit. The purpose of these field activities are to determine the effect of weathering on any geochemical halo and to extend the study into "unaltered" rocks underlying the deposit. Approximately 50–70 samples will be collected in this second field trip.

Addtional analytical work to include petrography, REE analyes, PIMA scans, electron and proton microprobe studies and isotopic analyses will be undertaken between July and October in time for the October meeting.

Acknowledgements

The author's involvement in this project is with permission and support from the Australian Geological Survey Organisation. Discussion with Peter Benjamin, Paul Harbon, Joe Stolz and Ross Large are acknowledged in setting up the research program. Bruce Kilgour of AGSO captured the geologic interpretation into digital form.

References

Manning, C.G. 1990. The geology and mineralisation of the Western Tharsis copper deposit, Mt. Lyell, Tasmania. Unpub. B.Sc. Hons. thesis, Univ. Tasmania. 98 p.

Raymond, O.L. 1992. Geology and mineralisation of the southern Prince Lyell deeps, Queenstown, Tasmania. Unpub. M.Sc. thesis, Univ. Tasmania. 161 p.

Walshe, J.L. and Solomon, M. 1981. An investigation into the environment of formation of the volcani-hosted Mt. Lyel copper deposits using geology, mineralogy, stable isotopes and a six-component chlorite solid solution model. Econ. Geol. 76, 246–284.

Wills, K.J.A. 1996. A synthesis of Mount Lyell geology and exploration. Unpub. report to Copper Mines of Tasmania.

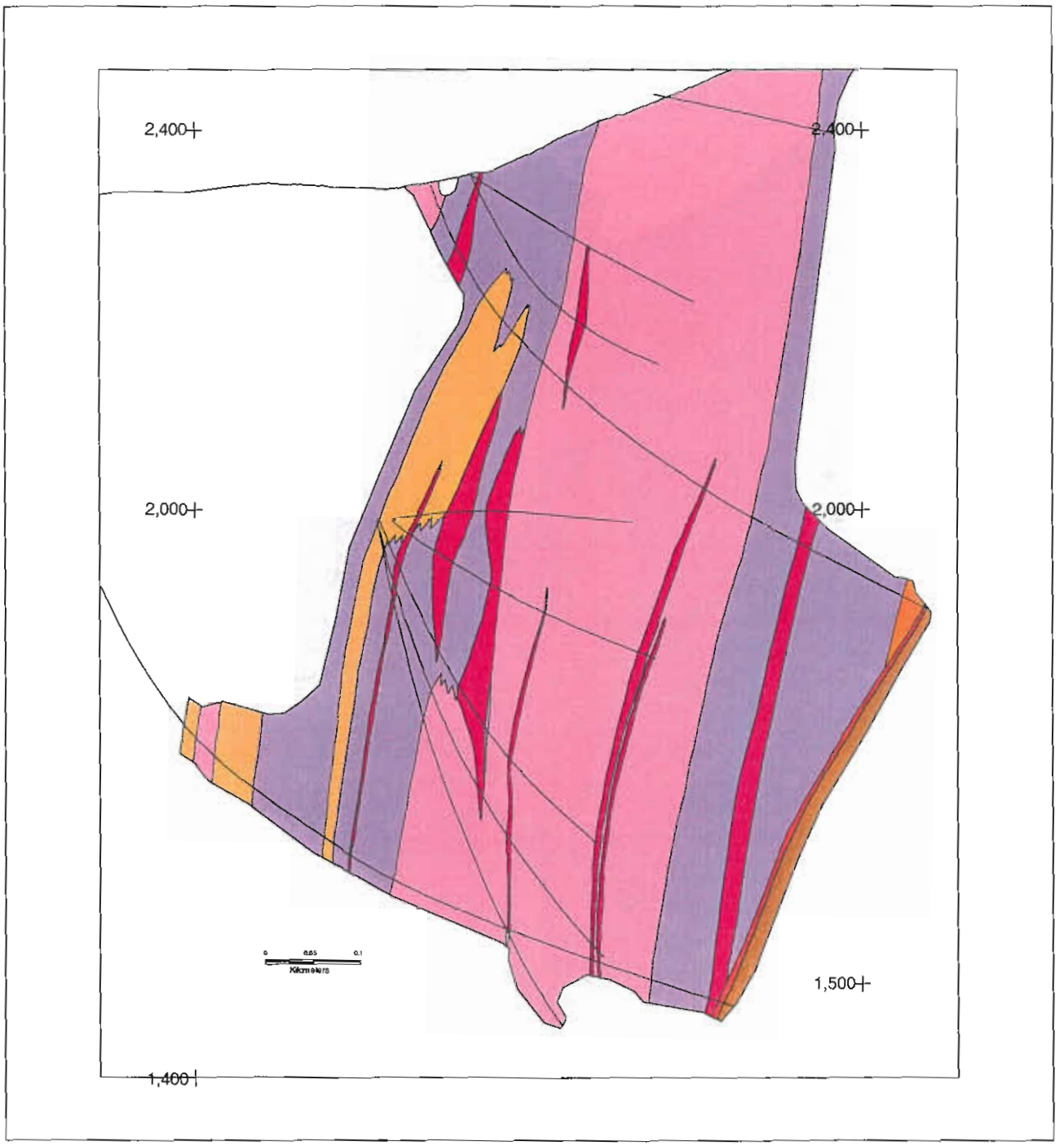

Figure 1. Cross section 8850 mN, Western Tharsis deposit, showing lithological variations.

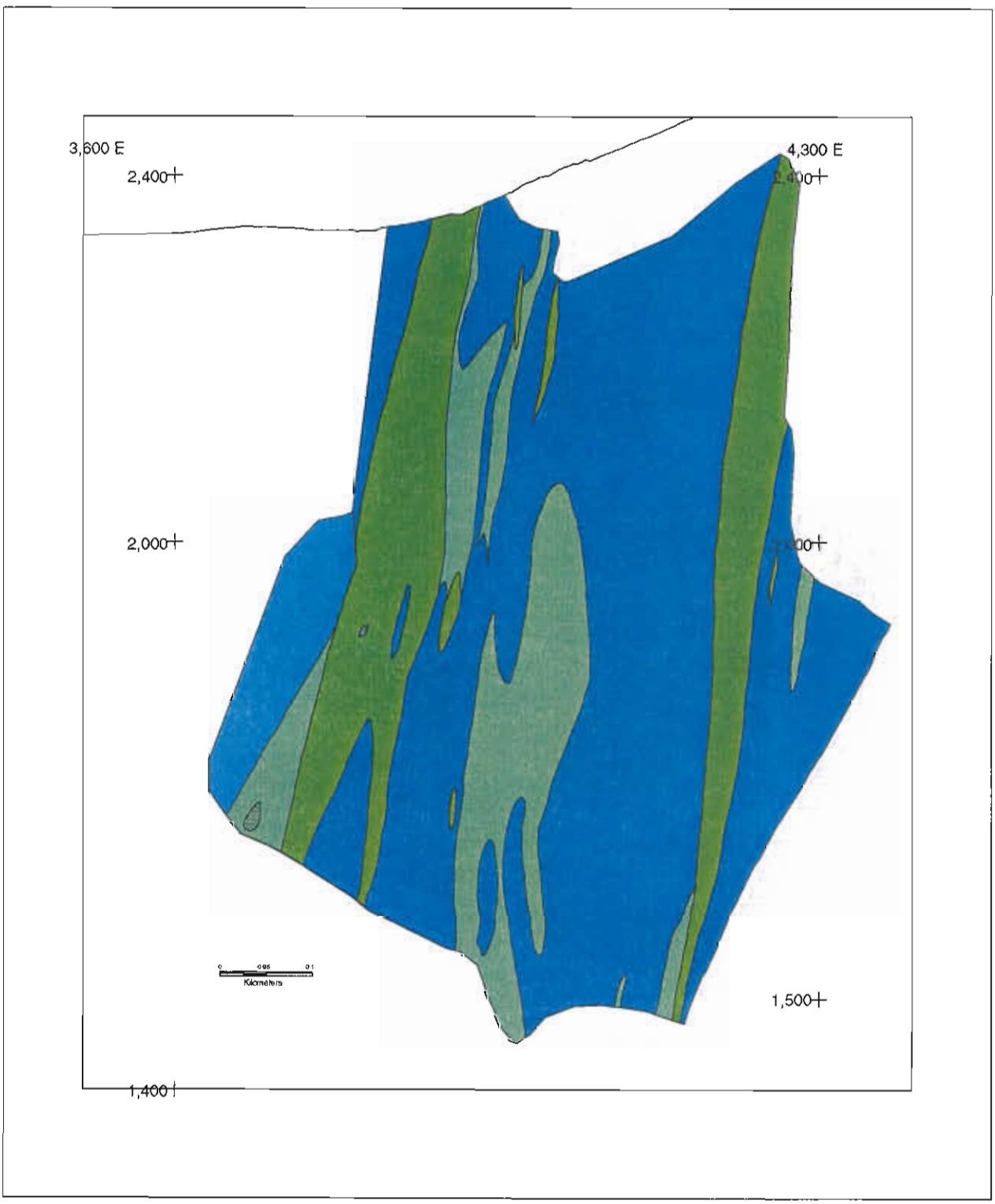

Figure 2. Cross section 8850 mN, Western Tharsis deposit, showing variations in silicate alteration mineralogy.

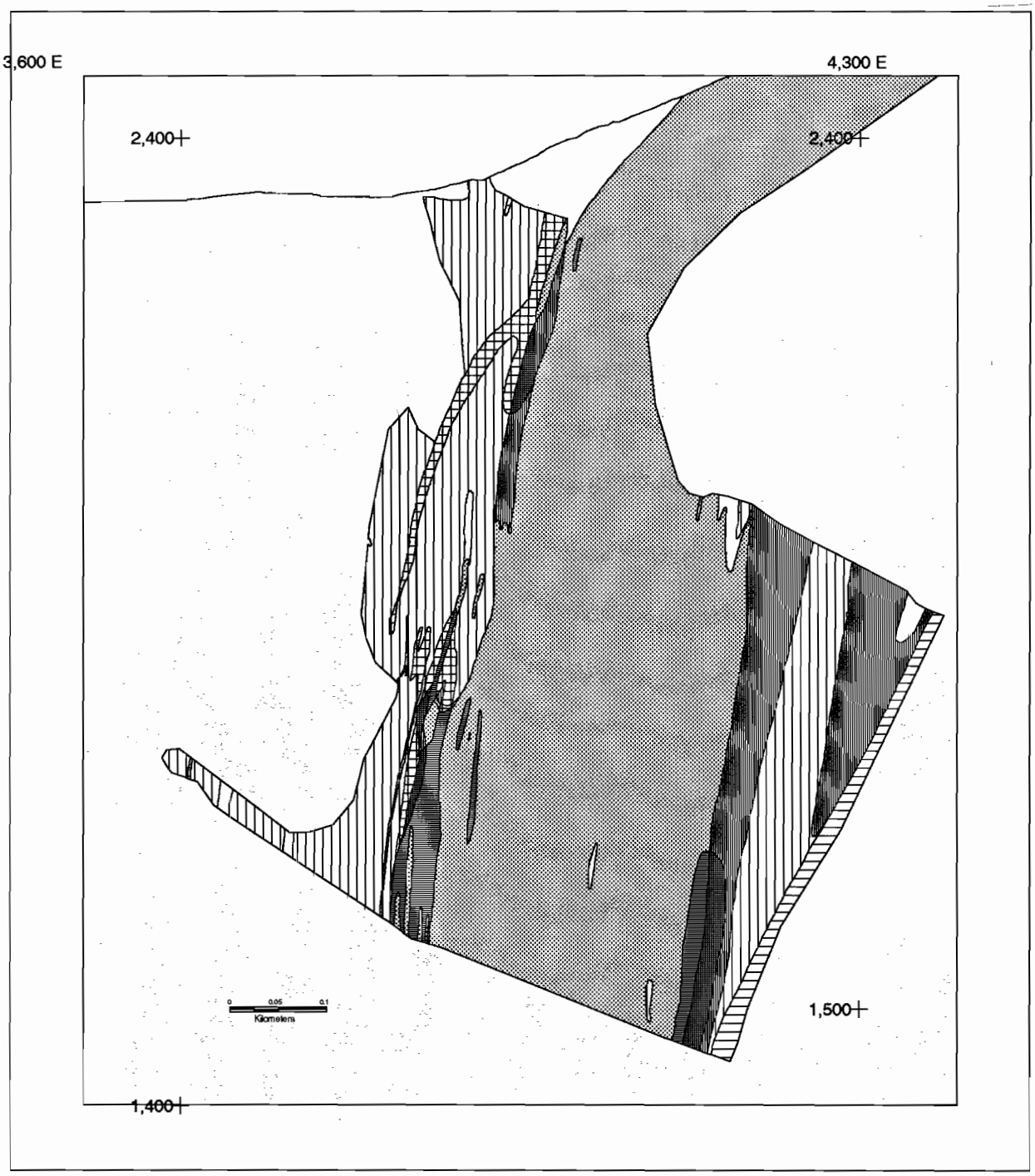

Western Tharsis Section 8850mN (+/- 100m)
Fe-S-O-C Mineral Assemblages

- >1% Pyrite (by volume)
- Hematite
- Hematite/ >1% Pyrite (by volume)
- Hematite/Siderite
- Hematite/Siderite/ >1% Pyrite (by volumne)
- no alteration
- no data
- Siderite
- Siderite/ >1% Pyrite (by volume)

Figure 3. Cross section 8850 mN, Western Tharsis deposit, showing variations in Fe-S-C-O mineralogy.

AMIRA /ARC Project P439: Meeting 26th May 1997

Dobson Creek–White Spur area "step-out" traverses: preliminary report

Rod Allen, Jocelyn McPhie, Cathryn Gifkins, Michael Blake

Introduction

Mapping and sampling along the Hall Rivulet Canal - Hercules - Mount Read - Red Hills - Anthony Dam regional traverse revealed important geochemical anomalies (Th/U ratio, Tl abundance) coincident with the White Spur Formation–Central Volcanic Complex contact and contrasts in alteration style and intensity between the two lithostratigraphic units (Stolz et al. 1996; Large 1996; McPhie et al. 1996). Volcaniclastic mass-flow units at the base of the White Spur Formation (WSF) north of Hall Rivulet Canal locally include massive sulfide clasts (e.g. in outcrop on Howards Road; in the Mines Department DDH MR 1; Corbett and Lees 1987). The White Spur Formation–Central Volcanic Complex contact is also of importance because the quartz-bearing volcaniclastic units in the hangingwall to the Hercules massive sulfide mineralisation (hosted by the top of very thick Central Volcanic Complex pumice breccia units; Allen 1994) could be facies equivalents of the WSF (McPhie and Allen 1992). In order to test the extent of the apparent anomaly and further document alteration and facies relationships across the White Spur Formation–Central Volcanic Complex contact, four short sampling and mapping traverses have been completed focussing on the contact in the Dobson Creek–White Spur area between Hall Rivulet Canal and Hercules.

Traverse locations

The traverse positions were chosen to provide good coverage of the area between existing traverse lines but constrained by the availability of grid lines and tracks. The four traverses comprise (Fig. 1): (1) east-west along Grid 62500N; (2) mainly east-west along Grid 64000; (3) north-south along a track branching from White Spur; (4) east-west along White Spur track. These traverse lines crossed the White Spur Formation–Central Volcanic Complex contact several times. In each case, samples were collected either side of, and as close as possible to, the contact.

Lithofacies and contact relationships

A total of 46 samples - 23 in the WSF and 23 in the Central Volcanic Complex (CVC) - were obtained for geochemistry and petrography. Most of the samples from the CVC are feldspar-phyric pumice breccias, with variations in feldspar abundance (5% to 25%), feldspar size (<1 mm to 2 mm) and pumice clast size (<1 cm to 3–4 cm). The pumice breccia units are evidently non-stratified and very thick (> several metres). The CVC also includes coherent, massive or flow-banded, feldspar>quartz-phyric porphyry.

The WSF mainly comprises variably crystal-rich pumice breccias distinguished by the presence of both quartz and feldspar. Total crystal abundance ranges from about 15% to in excess of 60%, with feldspar being in general twice more abundant than quartz. Other components are felsic volcanic clasts, mudstone clasts and in one instance (WS 97-20), sulfide clasts. The units are very thick (several metres) and graded from lithic clast-rich coarse bases to pumiceous or crystal-rich middle and upper portions. This facies dominates the base of the WSF close to contacts with the CVC. Other facies present higher in the WSF are tuffaceous mudstone–siltstone, black mudstone and micaceous sandstone. These facies occur in laminated to medium bedded intervals generally only a few metres in thickness.

Relationships between the WSF and CVC where encountered by the traverse lines varied. In some cases (e.g. WS 97-17–18, 21–22, 23–24, 42–43), the contact coincides with intense cleavage and is likely to be faulted. In other cases, the contact is unsheared and apparently conformable (e.g. WS 97-19–20, WS 97-33–34). Where exposure near the contact is poor (e.g. WS 97-6), relationships are unresolved.

Alteration

Alteration of the CVC pumice breccia is typically moderate, pervasive or patchy–mottled and involves combinations of feldspar, sericite, chlorite, quartz, carbonate, epidote, leucoxene and magnetite. The patchy–mottled alteration comprises pinkish, feldspar-rich domains and green or grey, sericite and/or chlorite-rich domains (e.g. WS 97-12). Feldspar phenocrysts within relic pumice clasts are commonly weakly to moderately sericite-carbonate altered. Pervasive, moderate to strong quartz-sericite±carbonate alteration occurs in some places close to the contact with the WSF (e.g. WS 97-33, 42).

Alteration of the WSF quartz-bearing volcaniclastic units is mainly weak, pervasive and dominated by sericite and carbonate. Black mudstone is unaltered or weakly silicified and micaceous sandstone units are very weakly sericite-carbonate altered. Tuffaceous mudstone–siltstone units are silicified and some show bedding-parallel, weak, banded feldspar versus

sericite-chlorite alteration (e.g. WS 97-40). On one section (1), intense silicification together with minor sulfides (pyrite>galena) occur in WSF pumice breccia (WS 97-34) just above the contact with the CVC.

The alteration mineralogy and textures encountered in the WSF and CVC in the White Spur–Dobson Creek area are comparable with those encountered on the Hall Rivulet Canal traverse. In the CVC, feldspar alteration appears to be widespread and pervasive and has been locally overprinted by sericite-chlorite±quartz. Alteration in the WSF is generally weak and dominated by sericite-carbonate±quartz.

Future work

Samples have been submitted for thin-section preparation. Following petrographic studies, whole rock major element and trace element analyses, and mineral analyses will be undertaken.

References

Allen RL 1994 Volcanic facies analysis indicates large pyroclastic eruptions, sill complexes, synvolcanic grabens and subtle thrusts in the Cambrian "Central volcanic complex" volcanic centre, western Tasmania. In "Contentious Issues in Tasmanian Geology: A symposium". Geological Society of Australia, Tasmania Division, Abstracts 31-33.

Corbett KD and Lees T 1987 Stratigraphic and structural relationships and evidence for Cambrian deformation at the western margin of the Mt Read Volcanics, Tasmania. Australian Journal of Earth Sciences 34: 45-67.

Large RL 1996 The Hercules–Mount Read traverse: Relationships between volcanic mineralogy, alteration and geochemistry. AMIRA/ARC Project 439, Report 3, 153-233.

McPhie J and Allen RL 1992 Facies architecture of mineralised submarine volcanic sequences: Cambrian Mount Read volcanics, western Tasmania. Economic Geology 87: 587-596.

McPhie J, Allen R, Stolz J, Gifkins C, Davidson G, Duhig N 1996 Hall Rivulet Canal–Hercules–Mount Read–Red Hills–Anthony Dam. AMIRA/ARC Project 439, Report 3, 19-28.

Stolz J, Allen R, Gifkins C, Davidson G, McPhie J, Blake M 1996 Petrographic and geochemical characteristics of alteration from the Hall Rivulet Canal–Mt Read–Red Hills–Anthony Dam traverse, Mt Read Volcanic Belt. AMIRA/ARC Project 439, Report 3, 379-413.

WESTERN TASMANIA

Fig. 1. Dobson Creek - White Spur Traverses - Sample Locations

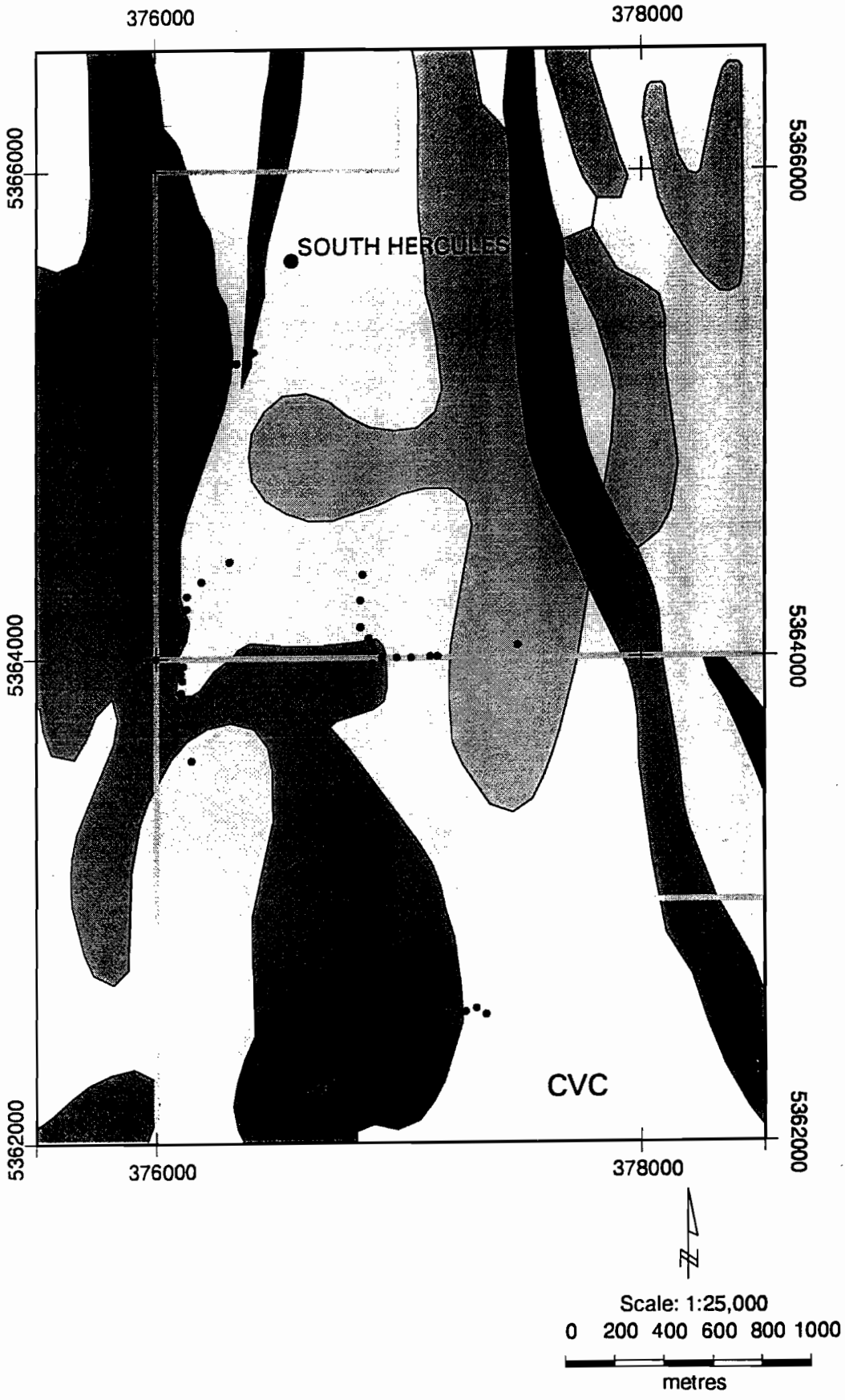

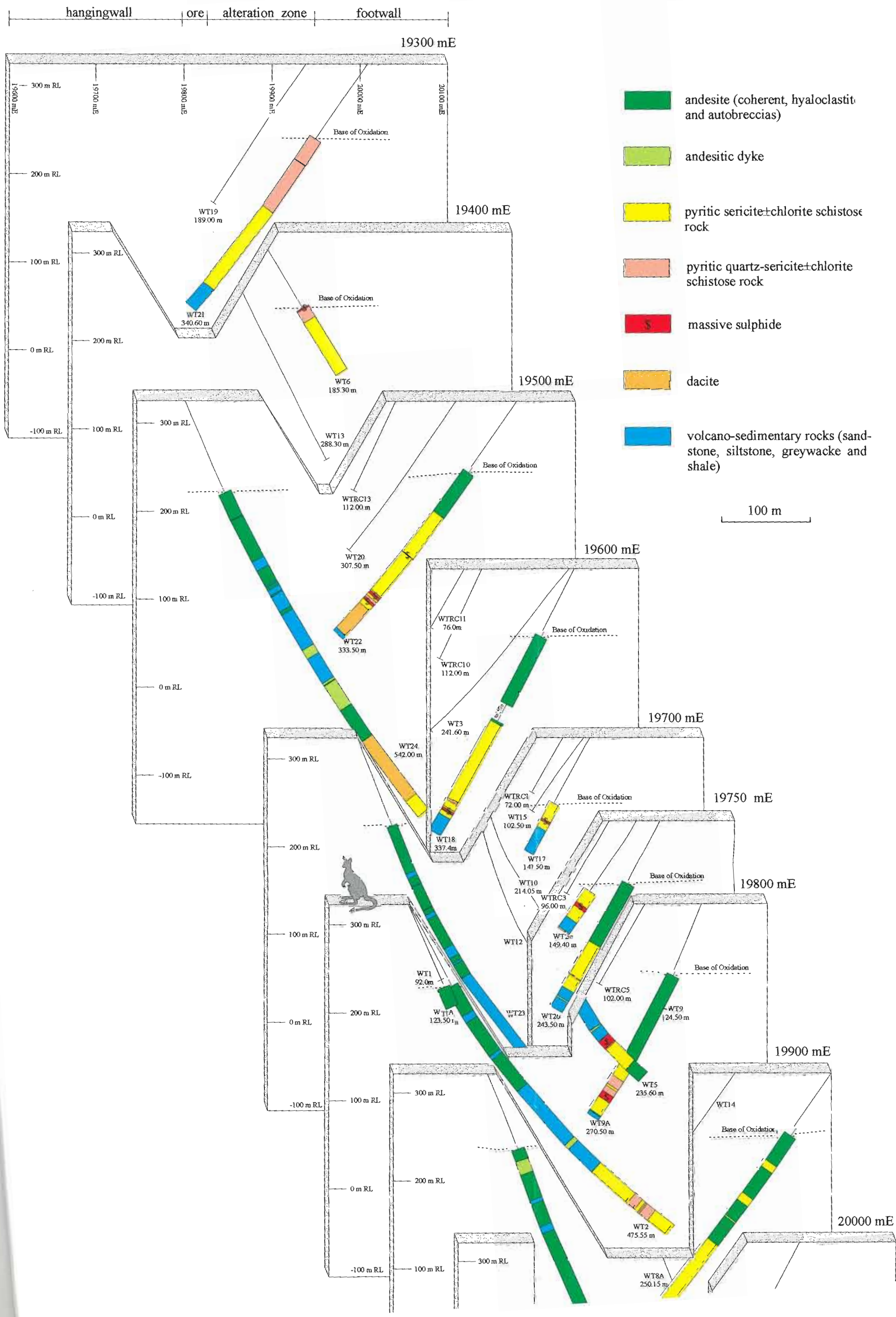
hangingwall
ore
alteration zone
footwall
19300 mE
19400 mE
19500 mE
19600 mE
19700 mE
19750 mE
19800 mE
19900 mE
20000 mE
19600 mE
19700 mE
19800 mE
19900 mE
20000 mE
300 m RL
200 m RL
100 m RL
0 m RL
-100 m RL
Base of Oxidation
WT19
189.00 m
WT21
340.60 m
WT6
185.30 m
WT13
288.30 m
WTRC13
112.00 m
WT20
307.50 m
WT22
333.50 m
WTRC11
76.0m
WTRC10
112.00 m
WT3
241.60 m
WT24
542.00 m
WTRC1
72.00 m
WT15
102.50 m
WT18
337.4m
WT17
147.50 m
WT10
214.05 m
WTRC3
96.00 m
WT12
WT1
92.0m
WT1A
123.50 m
WT23
WT26
243.50 m
WTRC5
102.00 m
WT9
124.50 m
WT5
235.60 m
WT9A
270.50 m
WT14
WT2
475.55 m
WT8A
250.15 m
andesite (coherent, hyaloclastit and autobreccias)
andesitic dyke
pyritic sericite±chlorite schistose rock
pyritic quartz-sericite±chlorite schistose rock
massive sulphide
dacite
volcano-sedimentary rocks (sandstone, siltstone, greywacke and shale)
100 m

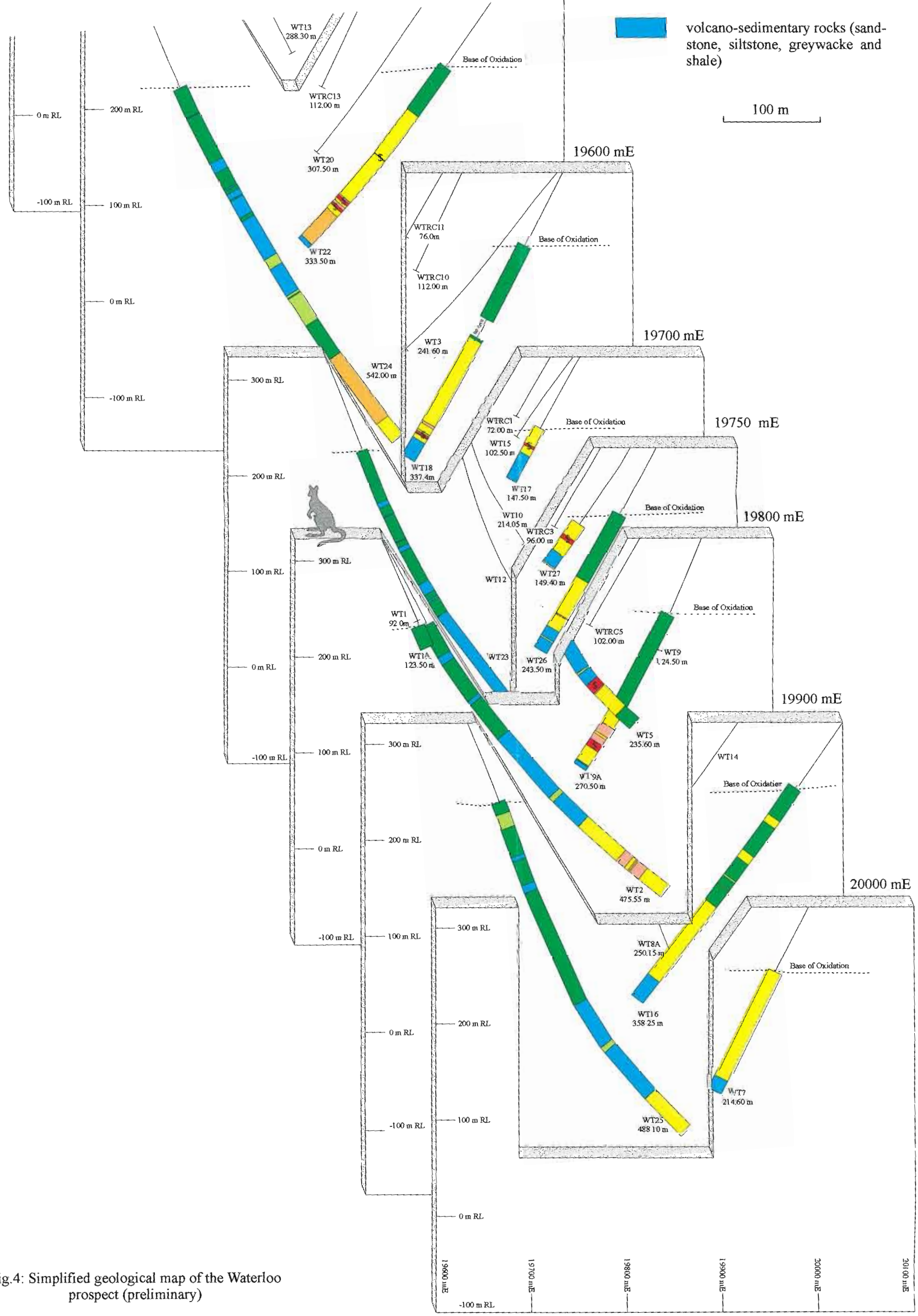

Fig.4: Simplified geological map of the Waterloo prospect (preliminary)

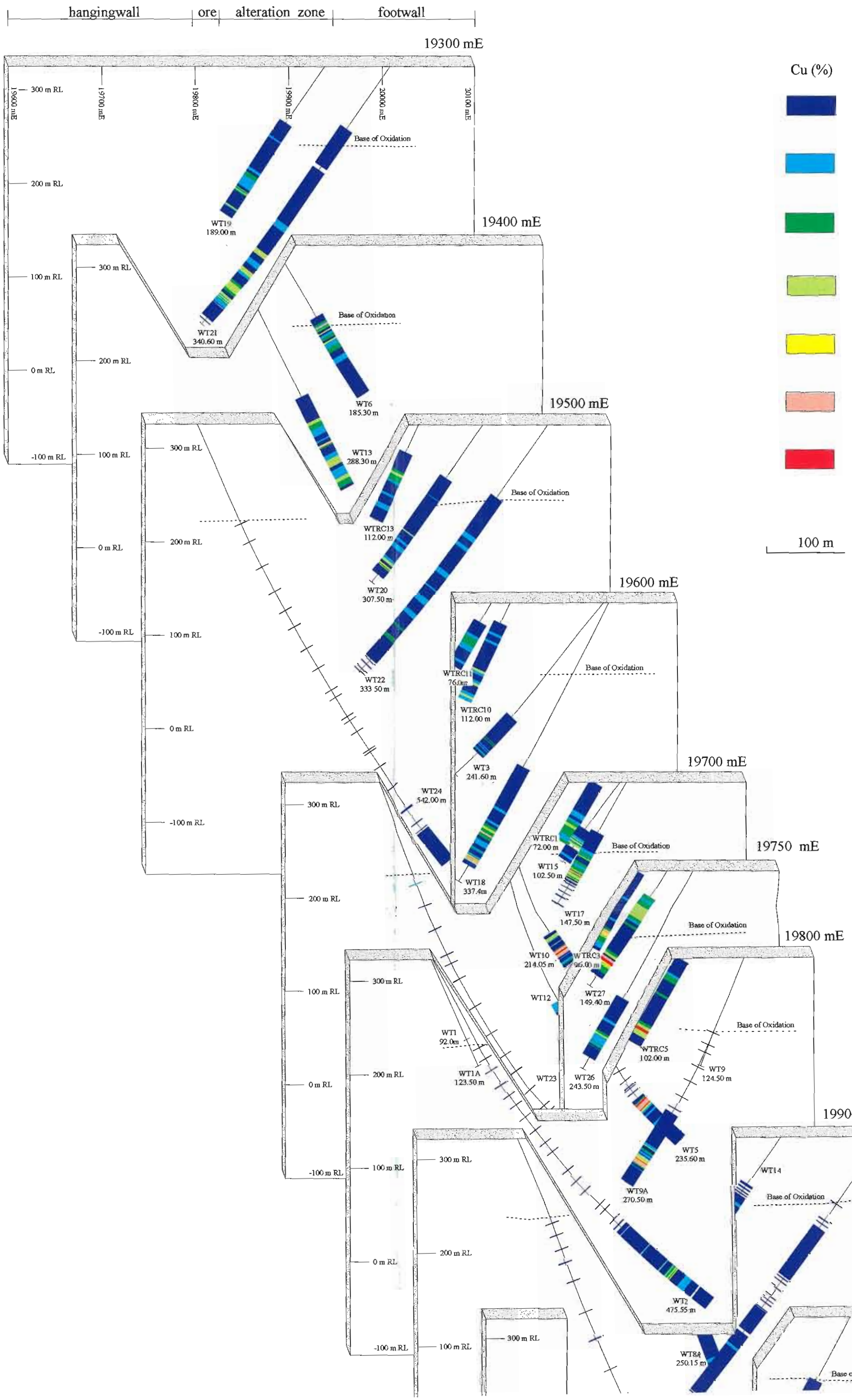
hangingwall
ore
alteration zone
footwall
19300 mE
19400 mE
19500 mE
19600 mE
19700 mE
19750 mE
19800 mE
19906
19600 mE
19700 mE
19800 mE
19900 mE
20000 mE
20100 mE
300 m RL
200 m RL
100 m RL
0 m RL
-100 m RL
Base of Oxidation
WT19
189.00 m
WT21
340.60 m
WT6
185.30 m
WT13
288.30 m
WTRC13
112.00 m
WT20
307.50 m
WT22
333 50 m
WTRC11
76.0m
WTRC10
112.00 m
WT3
241.60 m
WT24
542.00 m
WT18
337.4m
WTRC1
72.00 m
WT15
102.50 m
WT17
147.50 m
WT10
214.05 m
WTRC3
96.0 m
WT27
149.40 m
WT12
WT1
92.0m
WT1A
123.50 m
WT23
WT26
243.50 m
WTRC5
102.00 m
WT9
124.50 m
WT5
235.60 m
WT9A
270.50 m
WT14
WT2
475.55 m
WT8A
250.15 m
Cu (%)
100 m

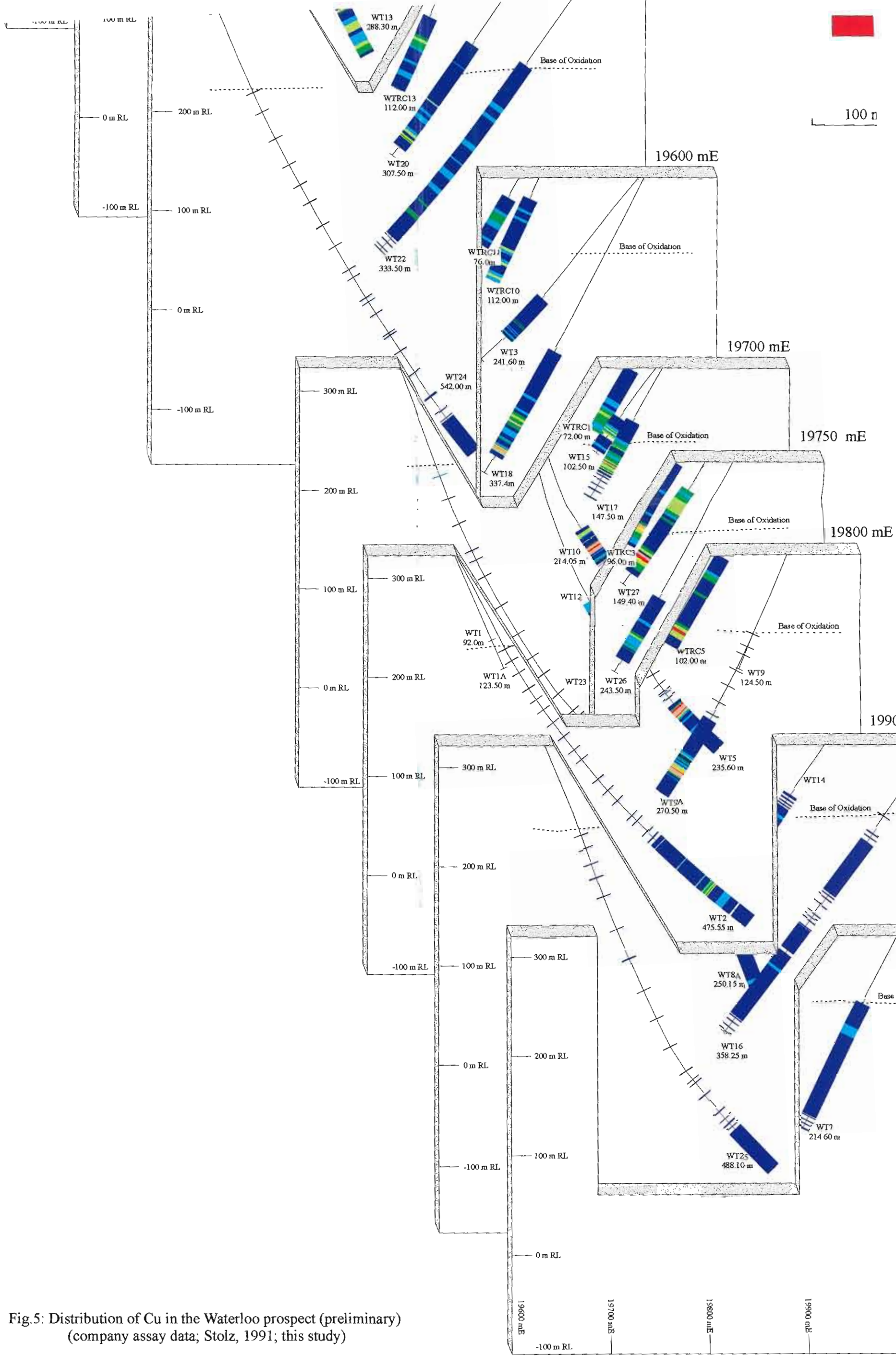

Fig.5: Distribution of Cu in the Waterloo prospect (preliminary)
(company assay data; Stolz, 1991; this study)

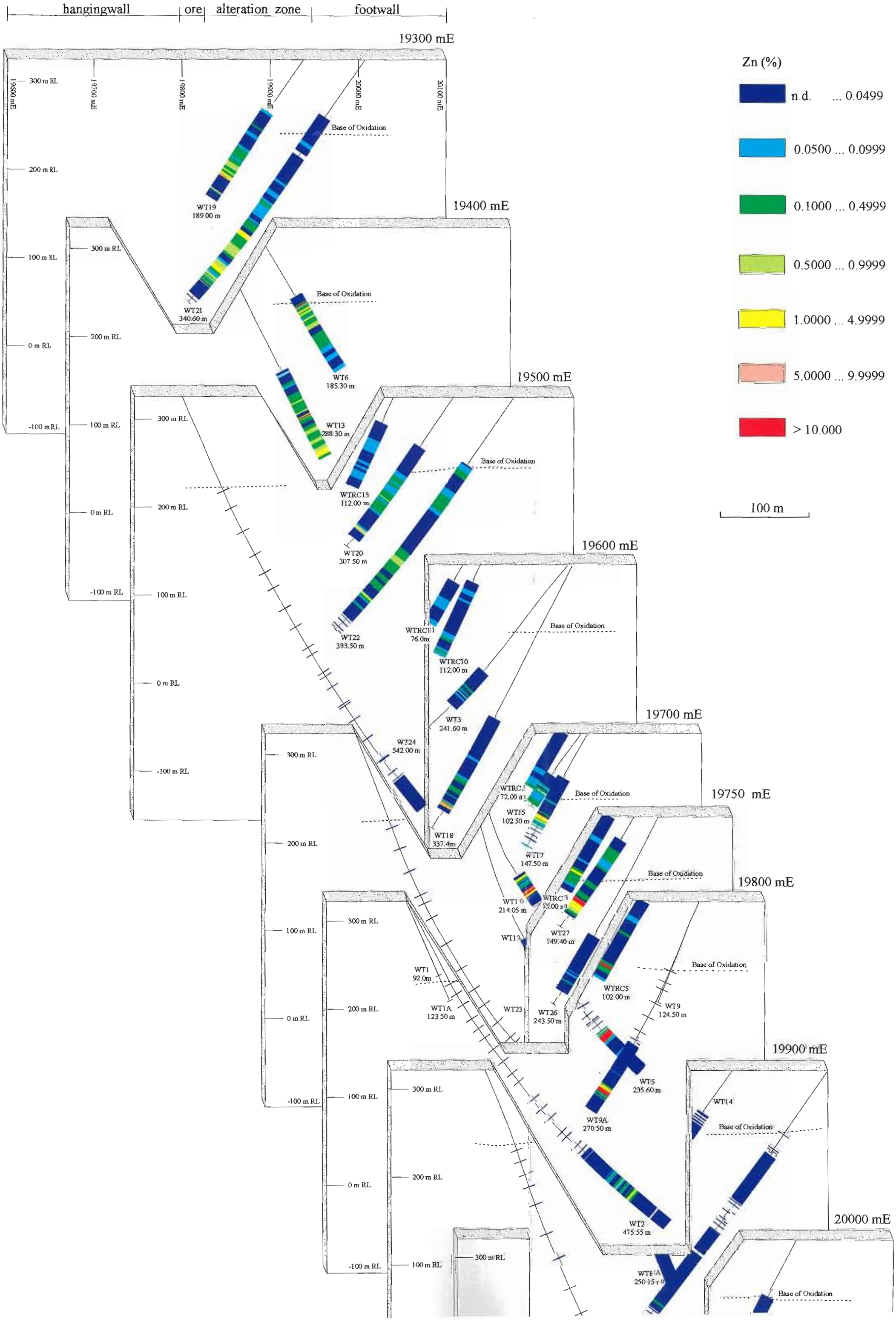
hangingwall
ore
alteration zone
footwall
19300 mE
19400 mE
19500 mE
19600 mE
19700 mE
19750 mE
19800 mE
19900 mE
20000 mE
19600 mE
19700 mE
19800 mE
19900 mE
20000 mE
300 m RL
200 m RL
100 m RL
0 m RL
-100 m RL
Base of Oxidation
WT19
189.00 m
WT21
340.60 m
WT6
185.30 m
WT13
288.30 m
WTRC13
112.00 m
WT20
307.50 m
WT22
333.50 m
WTRC11
76.0m
WTRC10
112.00 m
WT3
241.60 m
WT24
542.00 m
WT18
337.4m
WTRC7
72.00 m
WT15
102.50 m
WT17
147.50 m
WT16
214.05 m
WTRC6
95.00 m
WT27
149.40 m
WT12
WT1
92.0m
WT1A
123.50 m
WT23
WT26
243.50 m
WTRC5
102.00 m
WT9
124.50 m
WT5
235.60 m
WT9A
270.50 m
WT14
WT2
475.55 m
WT8A
250.15 m
Zn (%)
n.d. ... 0.0499
0.0500 ... 0.0999
0.1000 ... 0.4999
0.5000 ... 0.9999
1.0000 ... 4.9999
5.0000 ... 9.9999
> 10.000
100 m

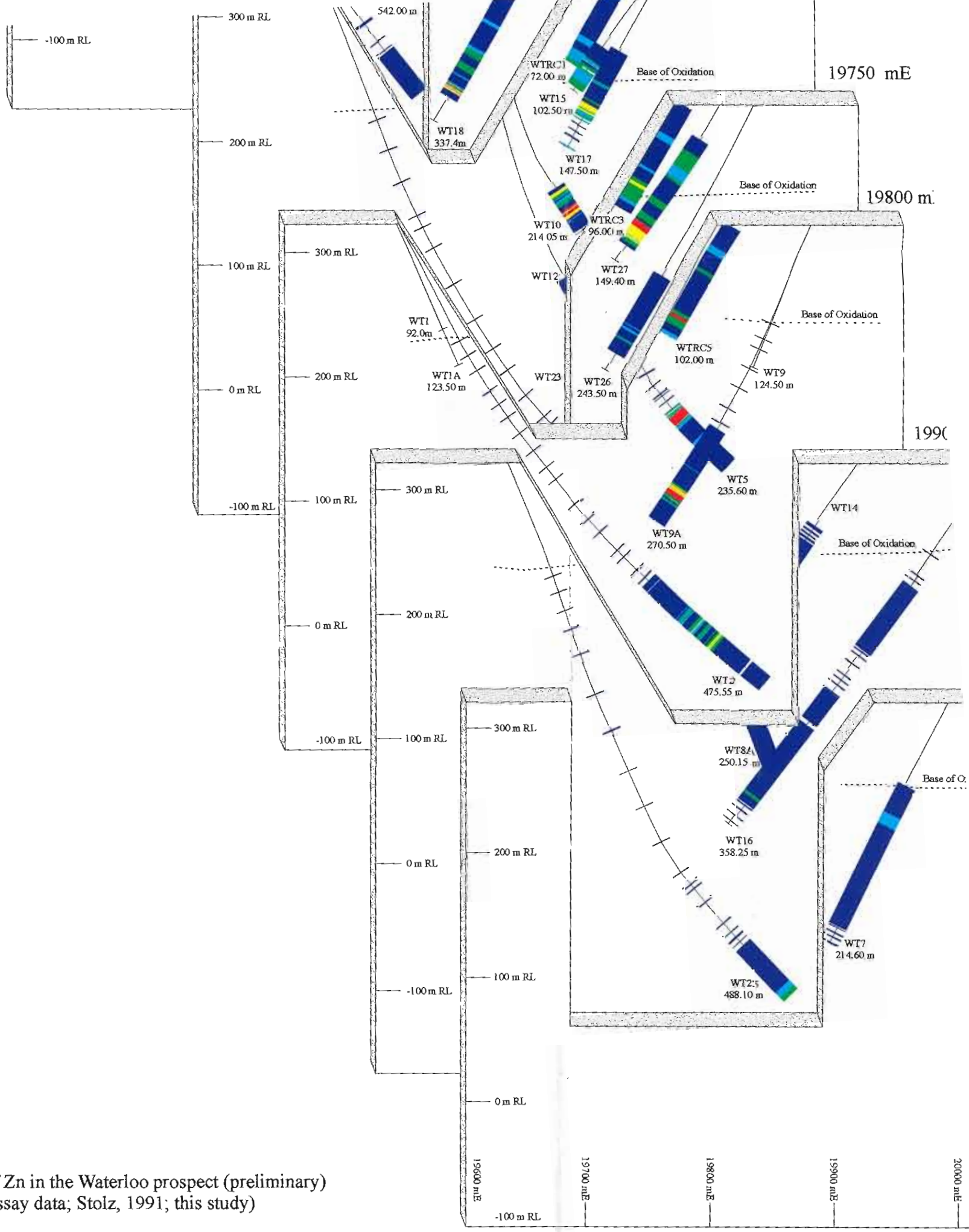

Fig.6: Distribution of Zn in the Waterloo prospect (preliminary)
(company assay data; Stolz, 1991; this study)

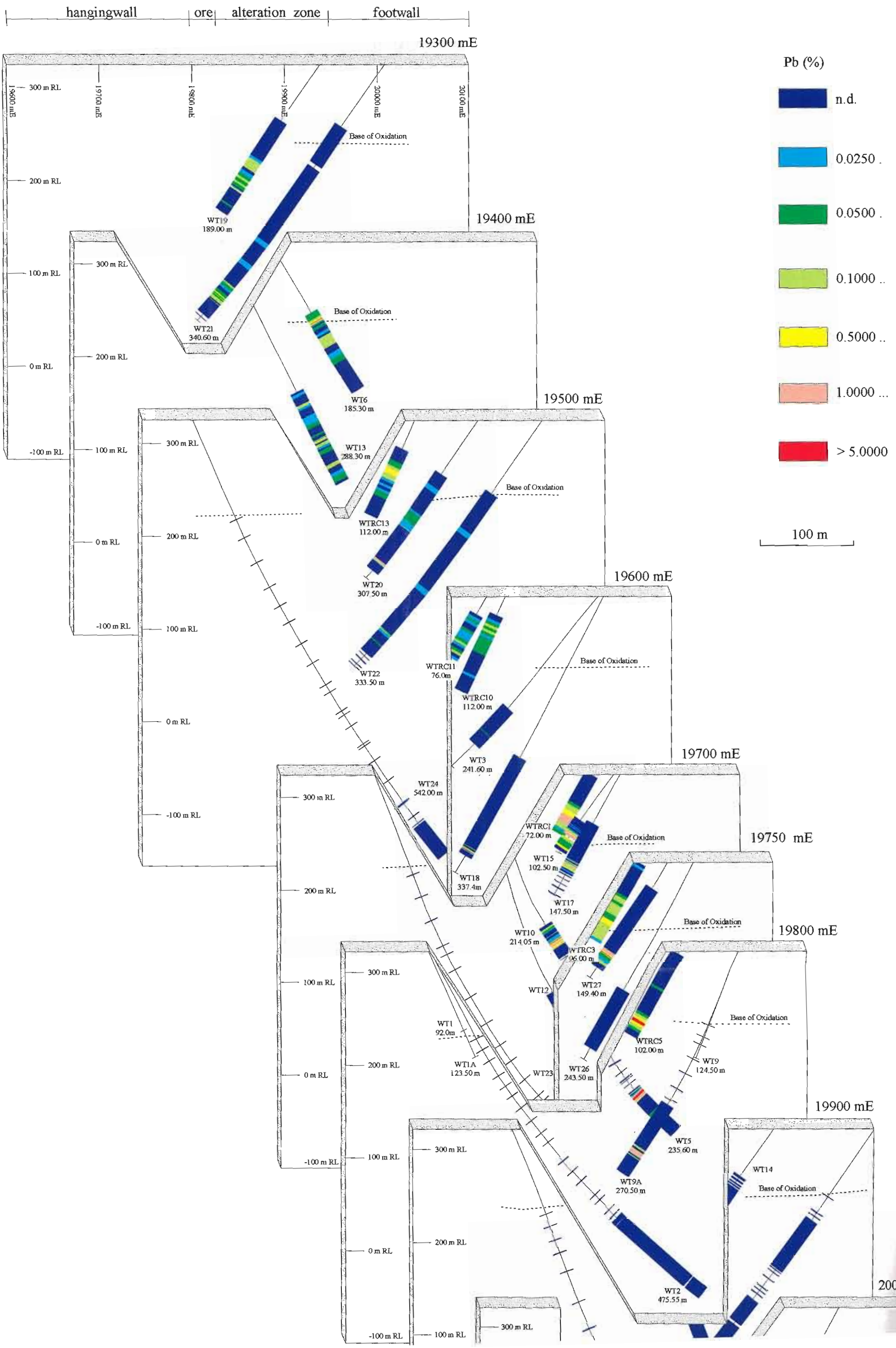
hangingwall
ore
alteration zone
footwall
19300 mE
19400 mE
19500 mE
19600 mE
19700 mE
19750 mE
19800 mE
19900 mE
19600 mE
19700 mE
19800 mE
19900 mE
300 m RL
200 m RL
100 m RL
0 m RL
-100 m RL
Base of Oxidation
WT19
189.00 m
WT21
340.60 m
WT6
185.30 m
WT13
288.30 m
WTRC13
112.00 m
WT20
307.50 m
WT22
333.50 m
WTRC11
76.0m
WTRC10
112.00 m
WT3
241.60 m
WT24
542.00 m
WTRC1
72.00 m
WT15
102.50 m
WT18
337.4m
WT17
147.50 m
WT10
214.05 m
WTRC3
96.00 m
WT27
149.40 m
WT12
WT1
92.0m
WT1A
123.50 m
WT23
WT26
243.50 m
WTRC5
102.00 m
WT9
124.50 m
WT5
235.60 m
WT9A
270.50 m
WT14
WT2
475.55 m
Pb (%)
n.d.
0.0250 .
0.0500 .
0.1000 ..
0.5000 ..
1.0000 ...
> 5.0000
100 m

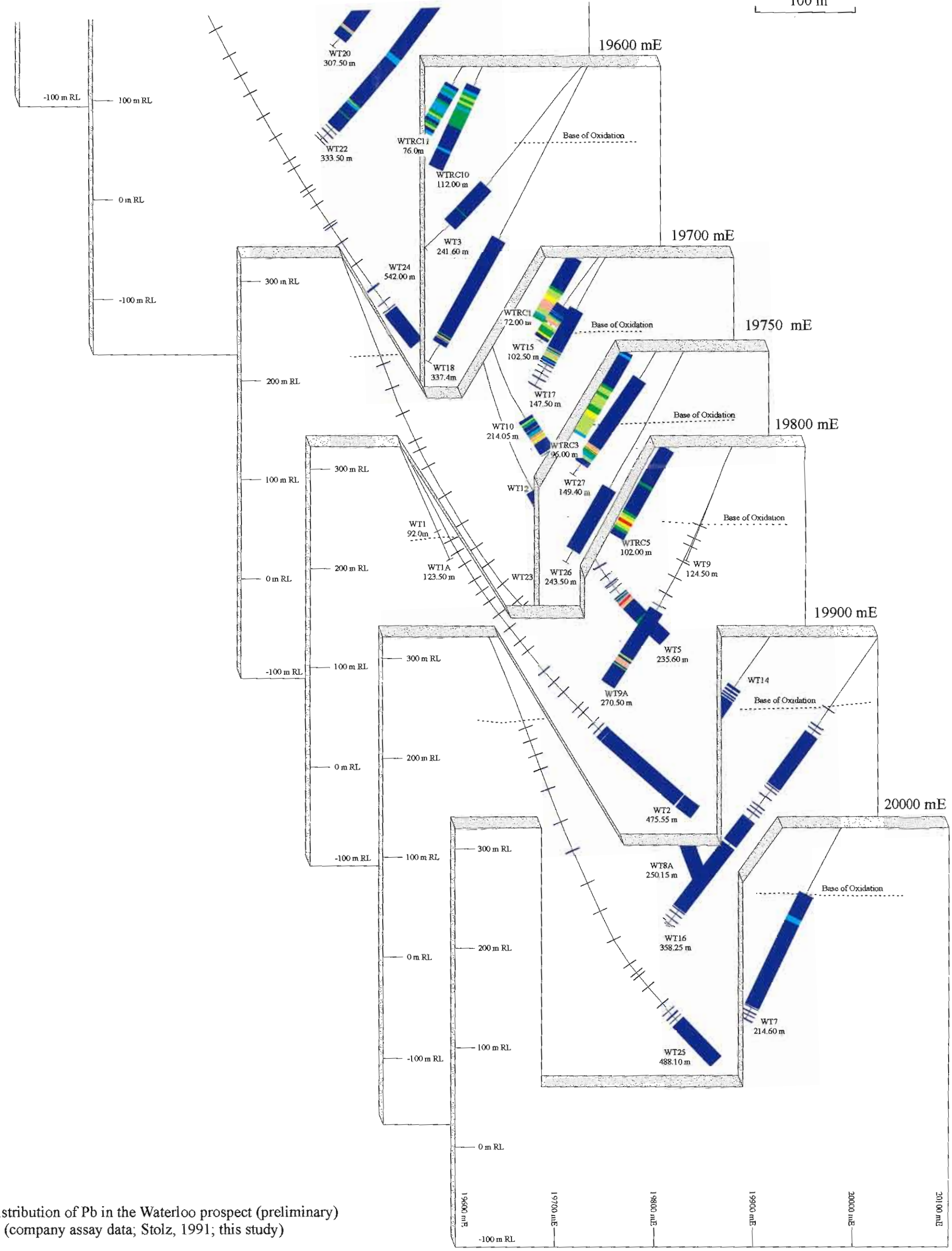

Fig.7:Distribution of Pb in the Waterloo prospect (preliminary)
(company assay data; Stolz, 1991; this study)